Introducing selected variations in architecture, linker and ligand composition of glycooligo(amides) targeting non-enveloped viruses

Inaugural-Dissertation

To obtain the academic degree

Doctor rerum naturalium

Submitted to the Faculty of Mathematics and Natural Sciences

of the Heinrich Heine University of Düsseldorf

by

Mischa Baier

From Unna, Germany

Düsseldorf, February 2019

The work presented in this thesis was accomplished in a period between November 2014 and March 2018 at the Chair of Macromolecular Chemistry at the Institute of Organic and Macromolecular Chemistry at the Heinrich Heine University of Düsseldorf under supervision of Prof. Dr. Laura Hartmann.

Printed with permission of the
Faculty of Mathematics and Natural Sciences of the
Heinrich Heine University of Düsseldorf

1st Reviewer: Prof. Dr. Laura Hartmann
2nd Reviewer: Prof. Dr. Thomas J. J. Müller
Day of oral exam: May 13th, 2019

Eidesstattliche Versicherung

Ich, Herr Mischa Baier, versichere an Eides statt, dass die vorliegende Dissertation von mir selbstständig und ohne unzulässige fremde Hilfe unter Beachtung der „Grundsätze zur Sicherung guter wissenschaftlicher Praxis an der Heinrich-Heine-Universität Düsseldorf" erstellt worden ist.

Statutory declaration

I, Mr. Mischa Baier, assure on oath that this dissertation has been written by me independently and without any unauthorized foreign assistance in compliance with the "Principles for securing good scientific practice at the Heinrich Heine University of Düsseldorf".

Düsseldorf, den 25. Februar 2019 _____
                                                             Unterschrift / Signature

Per nonna

„Wir neigen viel zu sehr dazu, Dingen,
die das Ergebnis vieler Ursachen sind,
einer einzigen zuzuschreiben.“

Justus Freiherr von Liebig (1803 – 1873)

Table of Contents

Abstract

In the presented work fundamental questions are investigated, which arise from the structure of the glycocalyx, a dense layer of carbohydrates which decorates almost all kind of cells, and its interaction with non-enveloped viruses. One of the important underlying questions is on how viral surface proteins and, ultimately, entire viruses communicate with cell surfaces and thus infect cells using carbohydrates. The often very low affinities of individual carbohydrates to receptor proteins of viral surfaces are overcome by multivalent effects in the so-called cluster glycoside effect resulting in an overall increase of avidity. However, the analysis of the structure and composition of the glycocalyx poses a barrier due to structural complexity. One way to elucidate fundamental processes of virus-carbohydrate interactions is the synthesis of simplified, multivalent glycomimetics composed of an artificial scaffold with carbohydrate side chains and their use as model compounds in binding assays.

In this work the solid phase polymer synthesis was used to obtain monodisperse sequence-defined oligoamides as highly defined scaffolds for the multivalent presentation of carbohydrate ligands. Through the stepwise assembly of tailor-made building blocks site selective introduction of different functional groups within the scaffold is achieved that can then be used for further functionalization with carbohydrate ligands. The major goal of this work was to explore whether the avidity of multivalent glycomimetics can generally be influenced, ideally increased, by changing and adapting selected structural parameters (**Figure 1**): In the first part, the synthesis of branched glycomimetics was developed to allow for systematic comparison with their linear counterparts. In the second part of the thesis mono- and trisaccharide ligands are attached to a scaffold via different hydrophobic linkers. In the third part of the thesis different types of carbohydrate ligands are combined to realize heteromultivalency.

Abstract

A: Solid phase synthesis of glycomacromolecules assembled from tailor-made building blocks and carbohydrates

B: Strategy: Introducing branches for higher avidity;

Method: Solid phase synthesis assisted split & combine approach.

linear vs. branched

2 branches vs. 3 branches

C: Strategy: Different combinations of ligand type and aromatic linkers;

Method: Solid phase synthesis by applying different building blocks and carbohydrates.

vs.

Comparison of different ligand & linker combinations

D: Strategy: Targeting heteromultivalent receptors with heteromultivalent ligands;

Method: Solid phase synthesis of glycooligo-(amidoamines) and coupling thereof with heparin fragments.

Coupling of Fondaparinux® with two glycooligo-(amidoamines)

E: Carbohydrate legend

Mannose   Sialic acid   3'-Sialyllactose   Fondaparinux®

Figure 1: Overview of the three parts of the work presented. **A**: General principle of solid phase synthesis with tailor-made building blocks and functionalized carbohydrates; **B**: Comparison of linear and branched molecules; with varying number of branches, made *via* a *split & combine* approach; **C**: Comparison of equivalent glycomacromolecules with different ligand and linker combinations; **D**: Synthesis of structure-defined, macromolecular conjugates of heparin fragments and sialylated glycans using solid phase synthesis; **E**: Legend of carbohydrates used.

In the first part of the work, (Baier *et al.*, *Chem. Eur. J.* **2018**, *24*, 1619-1630), a series of linear and branched mannose-functionalized glycooligo(amidoamines) was obtained by means of a "*split-and-combine*"-approach thereby combining solid phase synthesis-derived branches of different sugar-valencies with different scaffolds on solid phase. For this purpose, the new, azide-functionalized building block BADS was developed. The building block was obtained in high quantities of more than 20 g out of one batch in an overall yield of 34 % over seven reaction steps. BADS was used in the solid phase synthesis of four linear and six branched glycomacromolecules, all of them differing in valency and degree of branching. Binding to model system Con A was determined *via* a direct binding assay in surface plasmon resonance (SPR). The obtained results suggest that not only a higher valency of the investigated molecules causes an increase in affinity, but also the degree of branching with higher degrees of branching giving higher affinities.

In the second part of the work, (Baier *et al.*, manuscript submitted) a focus is put on sialic acid (Neu5Ac), which was used as propargyl- and azide-functionalized monosaccharide as well as part of the sialyllactose trisaccharide in the solid phase synthesis of multivalent glycooligo(amides) for the first time. Structures were designed to target the outer capsid of the *Trichodysplasia spinulosa*-associated polyomavirus (TSPyV). Furthermore, it has been shown for similar sugar-recognizing proteins that binding affinity can be increased using secondary interactions by incorporation of aromatic linkers. The combination of both elements results in the synthesis of sequence- and structure-defined, divalent, sialylated glycooligomers, in which the ligand as well as the linker are varied systematically. The structures were then tested for their ability to interact with capsid proteins-pentamers (VP1) of the TSPyV by co-crystallisation experiments. Crystal structures were only obtained for oligomers based on a longer, aromatic linker with both, sialic acid as well as sialyllactose where for the monosaccharide also parts of the linker, up to the phenyl motif, were detectable in the x-ray structure. In case of the sialyllactose-derivative, the structure of the whole trisaccharide could be revealed. Thus, it could be shown that sialic acid with an appropriate linker, in this case consisting of a triazole and a phenyl motif, can occupy the same sites in the crystal as sialyllactose.

In the third part of the thesis, (Baier *et al.*, *Chem. Commun.* **2018**, *54*, 10487 – 10490) the synthesis of highly-controlled carbohydrate-polymer based hybrid compounds consisting of heparin fragments, sialic acid derivatives and solid phase polymer synthesis-derived oligo(amidoamines) is presented. One strategy for generating binding selectivity is to combine different sugars in heterogeneous systems to exploit multivalent effects to increase binding affinity. Previously it has been shown that Merkel cell polyomavirus (MCPyV) capsids bind to two distinct classes of carbohydrates, namely 3'-sialyllactose and heparin fragments. Using the oligo(amidoamine) platform, both sugar classes are chemically linked to test whether they are jointly involved in the binding event. Three macromolecular conjugates were obtained by combining heparin fragments of different length with sialic acid or sialyllactose ligands in solid phase synthesis. The obtained molecules were tested in first saturation transfer difference NMR

(STD-NMR) experiments against the MCPyV capsid showing that both types of carbohydrate ligands still bind when attached to an oligo(amidoamine) scaffold. However, when combining both types of ligands covalently only binding of sialyllactose was detectable.

Overall this thesis extends the platform of solid phase polymer synthesis to obtain a variety of glycomimetic structures that allow for systematic structure-property studies. Special focus was devoted to develop high affinity ligands binding to capsid proteins of non-enveloped viruses. The first generation of glycomimetics in this work revealed a number of critical parameters to realize high affinity such as the introduction of aromatic linker motifs and use of branched scaffolds. Based on the findings of this work, next generation glycomimetics will be developed in the future to also address full virus capsids and potentially be used as inhibitors of viral adhesion and thereby infection.

Kurzzusammenfassung

Die vorliegende Arbeit beschäftigt sich mit grundlegenden Fragestellungen, die sich aus der Struktur der Glykokalyx, einer Zellen umhüllenden Schicht von Kohlenhydraten, und ihrer Wechselwirkung mit unbehüllten Viren ableiten. Eine der wichtigen zugrundeliegenden Fragestellungen ist, wie virale Oberflächenproteine und letztendlich ganze Viren mit Zelloberflächen kommunizieren und zu einer Infektion der Zelle mittels Kohlenhydraten führen. Die oft sehr geringen Affinitäten einzelner Kohlenhydrate, wie zum Beispiel jener der Glykokalyx zu Rezeptorproteinen, werden beim sogenannten Cluster-Glykosideffekt durch multivalente Effekte überwunden. Leider stellt die Analyse der Glykokalyx, aufgrund ihrer komplexen Struktur, eine Hürde dar, sodass eine Vereinfachung dieser Strukturen angestrebt wird. So sollen grundlegende Erkenntnisse über das Zusammenspiel von Kohlenhydrat-Liganden und Rezeptor-Proteinen gesammelt werden. Ein Weg, diese grundlegenden Prozesse aufzuklären, ist die Synthese multivalenter Glykomimetika bestehend aus einem künstlichen Gerüst mit Kohlenhydrat-Seitenketten und deren Verwendung als Modellverbindungen in Bindungsexperimenten.

In dieser Arbeit wurde die sogenannte Festphasen-Polymersynthese verwendet, um monodisperse sequenzdefinierte Oligoamide als hoch definierte Gerüste für die multivalente Präsentation von Kohlenhydratliganden zu erhalten. Durch die stufenweise Aneinanderreihung maßgeschneiderter Bausteine wird eine ortsspezifische Einführung verschiedener funktioneller Gruppen innerhalb des Gerüsts erreicht, welche dann zur weiteren Funktionalisierung mit Kohlenhydratliganden genutzt werden können. Das Hauptziel dieser Arbeit war es zu untersuchen, wie die Avidität multivalenter Glykomimetika im Allgemeinen durch Ändern und Anpassen ausgewählter Strukturparameter beeinflusst, idealerweise erhöht, werden kann (**Abbildung 1**): Im ersten Teil dieser Arbeit wird die Synthese von verzweigten Glykomimetika gezeigt, um einen systematischen Vergleich dieser mit ihren linearen Pendants zu ermöglichen. Im zweiten Teil werden Mono- und Trisaccharid-Liganden über verschiedene hydrophobe Linker an ein Gerüst gebunden. Im dritten Teil der Arbeit werden verschiedene Arten von Kohlenhydratliganden kombiniert um Heteromultivalenz zu realisieren.
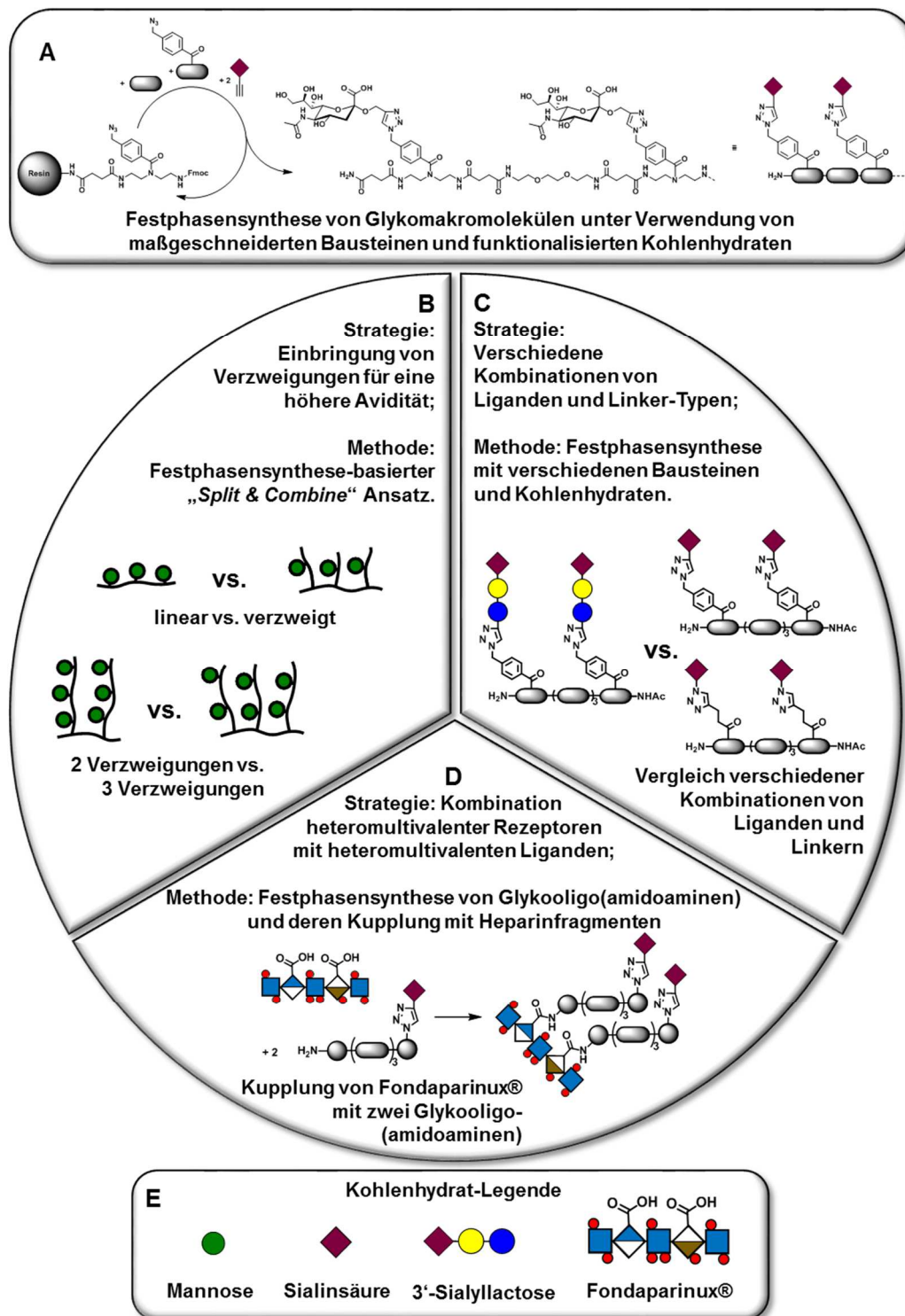
Abbildung 1: Überblick über die drei Teile der vorgestellten Arbeit. **A**: Darstellung des generellen Prinzips der Festphasensynthese mit maßgeschneiderten Bausteinen und funktionalisierten Kohlenhydraten; **B**: Vergleich von linearen und verzweigten Molekülen, mit mehr und weniger Verzweigungen, hergestellt durch einen *Split & Combine* Ansatz; **C**: Vergleich von gleichvalenten Glykomakromolekülen mit unterschiedlichen Kombinationen von Ligand und Linker; **D**: Synthese von strukturdefinierten, makromolekularen Konjugaten aus Heparinfragmenten und sialylierten Glykanen mittels Festphasensynthese; **E**: Legende der eingesetzten Kohlenhydrate.

Im ersten Teil der Arbeit (Baier *et al.*, *Chem. Eur. J.* **2018**, *24*, 1619-1630) wurde eine Reihe von linearen und verzweigten Mannose-funktionalisierten Glykooligoamiden mittels eines „*Split-and-Combine*"-Ansatzes (Aufteilung und Kombination) erhalten. Hierzu wurden lineare Arme unterschiedlicher Zuckervalenz auf dem Festphasenharz mit verschiedenen Rückgraten kombiniert. Zu diesem Zweck wurde der neue, Azid-funktionalisierte Baustein BADS entwickelt. Der Baustein konnte in Mengen über 20 g aus einem Ansatz in einer Gesamtausbeute von 34% verteilt über sieben Reaktionsschritte gewonnen werden. BADS wurde in der Festphasensynthese von vier linearen und sechs verzweigten Glykomakromolekülen verwendet, die sich alle in ihrer Valenz und ihrem Verzweigungsgrad unterscheiden. Die Bindung an das Modellsystem Con A wurde über ein Direktbindungsexperiment mittels Oberflächenplasmonenresonanz (SPR) bestimmt. Die erhaltenen Ergebnisse legen nahe, dass nicht nur eine höhere Valenz der untersuchten Moleküle eine Erhöhung der Affinität bewirkt, sondern auch der Verzweigungsgrad, wobei ein höherer Verzweigungsgrad ebenfalls zu einer Erhöhung der Affinität führt.

Im zweiten Teil der Arbeit (Baier *et al.*, Manuskript eingereicht) wird ein Schwerpunkt auf Sialinsäure (Neu5Ac) gelegt, die als Propargyl- und Azid-funktionalisiertes Monosaccharid und als Teil des Trisaccharids Sialyllactose zum ersten Mal in der Festphasensynthese von multivalenten Glykooligoamiden eingesetzt wurde. Die Molekülstrukturen wurden so gewählt, dass diese an das Kapsid des *Trichodysplasia spinulosa*-assoziierten Polyomavirus (TSPyV) binden. Für ähnliche zuckererkennende Proteine wurde bereits gezeigt, dass die Bindungsaffinität durch sekundäre Wechselwirkungen durch den Einbau aromatischer Linker erhöht werden kann. Die Kombination beider Elemente führt zur Synthese einer Reihe von sequenz- und strukturdefinierten, zweiwertigen sialylierten Glykooligomeren, in denen sowohl der Ligand als auch der Linker systematisch variiert wurden. Die Strukturen wurden dann auf ihre Fähigkeit getestet, in Co-Kristallisationsexperimenten mit Kapsidprotein-Pentameren (VP1) des TSPyV zu interagieren. Kristallstrukturen wurden jedoch nur für Oligomere auf der Basis eines längeren aromatischen Linkers sowohl mit Sialinsäure als auch mit Sialyllactose erhalten. Während für das Monosaccharid auch Teile des Linkers bis hin zum Phenylmotiv in der Röntgenstruktur nachweisbar waren, konnte im Falle des Sialyllactose-Derivats sogar die Struktur des gesamten Trisaccharids aufgezeigt werden. Es konnte so gezeigt werden, dass Sialinsäure mit einem geeigneten Linker, in diesem Fall bestehend aus einem Triazol- und einem Phenylmotiv, die gleichen Stellen im Kristall wie Sialyllactose besetzen kann.

Im dritten Teil der Arbeit (Baier *et al.*, *Chem. Commun.* **2018**, *54*, 10487 - 10490) wurde die Synthese von hochkontrollierten Kohlenhydrat-Polymer-Hybridverbindungen bestehend aus Heparin-fragmenten, Sialinsäure-Derivaten und festphasenpolymersynthese-basierter Oligo(amidoamine) vorgestellt. Eine Strategie zur Erzeugung der Bindungsselektivität kann darin bestehen, verschiedene Zucker in heterogenen Systemen zu kombinieren, um so multivalente Effekte zur Erhöhung der Bindungsaffinität zu nutzen. Bisher wurde gezeigt, dass das Merkelzell-

Polyomavirus (MCPyV) - Kapsid an zwei unterschiedliche Kohlenhydratklassen bindet. Diese sind 3'-Sialyllactose- und Heparinfragmente. Unter Verwendung der Oligo(amidoamin)-Plattform wurden beide Zuckerklassen chemisch kovalent miteinander verbunden, um zu testen, ob diese gemeinsam binden. Drei makromolekulare Konjugate wurden durch Kombination von Heparinfragmenten unterschiedlicher Länge mit Sialinsäure- und Sialyllactose-Liganden mittels Festphasensynthese erhalten. Die erhaltenen Moleküle wurden in ersten Sättigungs-übertragungsdifferenz-NMR (STD-NMR) Experimenten gegen das MCPyV-Kapsid getestet, was zeigte, dass beide Arten von Kohlenhydratliganden immer noch binden, wenn sie an ein Oligo(amidoamin)-Gerüst gebunden sind. Wenn allerdings beide Arten von Liganden kovalent miteinander verbunden vorliegen, konnte nur die Bindung der Sialyllactose nachgewiesen werden.

Insgesamt erweitert die vorliegende Dissertation die Plattform der Festphasen-Polymersynthese um eine Vielzahl von glykomimetischen Strukturen, welche die systematische Untersuchung von Struktur-Wirkungs-Beziehungen ermöglichen. Ein besonderer Schwerpunkt lag auf der Entwicklung hochaffiner Liganden, die an Kapsidproteine von unbehüllten Viren binden. Die erste Generation von Glykomimetika in dieser Arbeit offenbarte eine Reihe kritischer Parameter zum Erhalt einer hohen Affinität, wie beispielsweise die Einführung aromatischer Linker-Motive und die Verwendung von verzweigten Gerüsten. Basierend auf den Erkenntnissen dieser Arbeit sollen zukünftig Glykomimetika der nächsten Generation entwickelt werden, welche auch an vollständige Viruskapside binden und möglicherweise als Inhibitoren der Virusadhäsion und damit der Infektion eingesetzt werden können.

List of publications

Publications included in this thesis

Split-and-Combine Approach Towards Branched Precision Glycomacromolecules and their Lectin Binding Behavior

Mischa Baier, Markus Giesler and Laura Hartmann

Chemistry – A European Journal, **2018**, *24*, 1619 – 1630.

Divalent Sialylated Precision Glycooligomers Binding to Polyomaviruses and the Effect of Different Linkers

Mischa Baier, Nils H. Rustmeier, Joachim Harr, Norbert Cyrus, Guido J. Reiss, Andrea Grafmüller, Bärbel S. Blaum, Thilo Stehle and Laura Hartmann

Macromolecular Bioscience, **2019**, *19*, 1800426.

Synthesis of highly controlled carbohydrate–polymer based hybrid structures by combining heparin fragments and sialic acid derivatives, and solid phase polymer synthesis

Mischa Baier, Jana L. Ruppertz, Moritz M. Pfleiderer, Bärbel S. Blaum and Laura Hartmann

Chemical Communications, **2018**, *54*, 10487 – 10490.

Publications not included in this thesis

Cu Elimination from Cu-Coordinating Macromolecules

Morten F. Ebbesen, Dana Itskalov, **Mischa Baier** and Laura Hartmann

ACS Macro Letters, **2017**, *6* (4), 399 – 403.

Oral presentations

Solid phase assisted split & combine approach towards branched precision glycomacromolecules

Mischa Baier, Markus Giesler and Laura Hartmann

Abstracts of Papers of The American Chemical Society (254th National Meeting & Exposition, **2017**, Abstract No. 619).
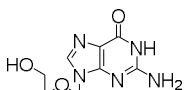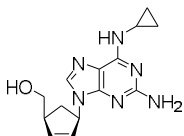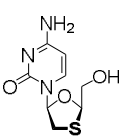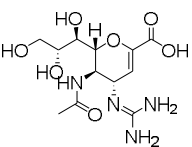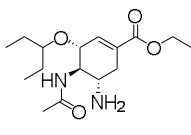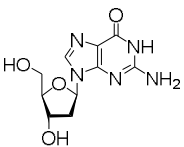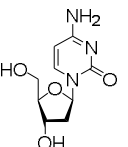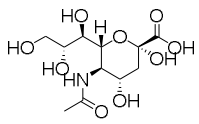
Publisher: Amer. Chemical Soc., 1155 16th St, NW, Washington, DC 20036 USA

1. General introduction

Infectious organisms and toxins are called pathogens, which in turn are all capable, in their own way, of damaging the affected organism. Pathogens include in ascending complexity parasitic prions, transponsons, viroids and viruses as well as higher evolved bacteria, fungi and parasites.[1] Whereas prions and transponsons cause deadly diseases,[2, 3] but have also been proven to have a non-self-beneficial biological benefit,[4-8] viroids and viruses are self-serving and only carry information of their own replication, to which these turn cells into machines of their own replication.

Fungal infections can be treated by default with antimycotics and bacterial infections with antibiotics; however, the treatment of diseases caused by non-self-reproducing pathogens like viruses is still in its early stages for a variety of reasons. The inability to break a lifecycle in a virus makes it necessary to explore new routes. Effective methods of combating viral infections are so far mainly vaccinations, so the acquaintance of an organism with the virus to allow this a faster response to the intruder. Second, antimetabolite drugs such as Aciclovir® [9, 10] or Abacavir® and Lamivudine®,[11, 12] which, in their phosphorylated form, for Herpes Simplex Virus (HSV) and Human Immunodeficiency Virus (HIV) serve as nucleotides and are incorporated into the genome of the virus and lead to its inactivation are in use. Third, the treatment or prophylaxis of e.g. Influenza virus infections with neuraminidase inhibitors such as Zanamivir® [13] or Oseltamivir®,[14] represents a currently pursued treatment possibility.

Table 1 : Guanosine and cytidine-mimicking antimetabolite drugs and sialic acid-like neuraminidase inhibitors as examples of drugs used against viral infections. In the lower line the naturally occurring analogon is shown.

1.1. Viruses and glycans

In 1892, Dmitri Ivanovsky first described a non-bacterial pathogen infecting tobacco plants, which was later identified as the tobacco mosaic virus by Martinus Beijerinck.[15, 16] The first virus was thus discovered. This was the starting point for the emergence of a new science: Virology.

Viruses are small infectious agents, which can be found in almost every ecosystem on Earth. They spread outside of cells by transmission, but multiply only within a suitable host cell. The program for their own propagation is inherent to viruses. They are not able to replicate by themselves, do not possess any own metabolism and are therefore dependent on the metabolism of the host cell. Viruses are therefore generally not counted as living beings, but, even not independently, show the ability to replicate.

Independent Virus particles outside of cells are called virions, these are particles that consist of nucleic acids, either deoxyribonucleic acids (DNA) or ribonucleic acids (RNA), and mostly a protein shell, termed capsid. In addition, some virions are surrounded by a lipid bilayer interspersed with viral membrane proteins called the viral envelope. The replication cycle of a virus generally begins with the adsorption of a virion to surface proteins on a host cell that are used by the virus as receptors. This initial contact is based on an interaction of surface proteins of the capsid with glycans of the cell surface, which are part of the so-called glycocalyx.[17, 18]

1.1.1. Viruses bind to glycans

Of the four fundamental building blocks of life, proteins, carbohydrates, lipids and nucleic acids, probably carbohydrates are the least well understood and the most underappreciated.[18, 19] Glycans append to a wide variety of biological molecules and are found almost everywhere in Biology. Besides energy storage and contribution to physical and structural integrity, where their function is well understood, they are involved into extracellular matrix formation, signal transduction, protein folding, information exchange between cells, and pathogen uptake.[20, 21] They are found on cell surfaces as *N*- and *O*-linked glycans, as well as sphingolipids, glycosaminoglycans (GAGs), and glycophospholipids.[20, 22, 23] However, we know little about many of these functions because glycans are difficult to synthesize, to analyze and to work with. Unlike nucleic acids and proteins, they cannot be cloned and sequenced, are not always commercially available and information about their biological behavior is limited. Furthermore, in an aqueous medium, glycans take on a variety of different conformations, of which in most cases only one shows biological activity.[24] Due to the low affinity of glycans for specifically binding proteins, the so-called lectins as well as glycosaminoglycan-binding

proteins, Nature makes use of the principle of multivalency.[25, 26] Lectins exclusively bind to terminal mono- or oligosaccharides,[27, 28] whereas glycosaminoglycan-binding proteins bind to acidic, sulfated side chains of the disperse polysaccharides.[19] Adequate avidity is achieved only by the multiple presentation of the same binding motif. [28]

The lack of knowledge about glycan structure and function contrasts with their importance for biological processes; this is particularly obvious when investigating the life cycle of a virus.[29-31] Attachment is a key determinant of this cycle, as it helps to regulate the entry pathway used by the virus. First, a virus must attach to one or several receptors at the host cell surface. **Figure 2** shows a simplified cell surface with attached glycans to which a virus approach. Sialic acid-terminated glycans as well as heparan sulfate are known to act as initial receptors for viruses and are most relevant for the initial virus-host cell interaction for a great number of the studied viruses. Viral glycan ligands such as sialic-acid containing carbohydrates [25, 32-36] and glycosaminoglycans [37-40] are often negatively charged, but neutral glycans such as histo-blood group antigens (HBGAs) are also known to mediate cell attachment *e.g* in the case of noroviruses.[41, 42] However, little is known about affinities between a virus and its counterpart glycan receptor, as current technologies are often limited for determining critical parameters such as dissociation constants of weak affinity interactions. Moreover, densities and distribution patterns of glycans on cell surfaces are not well understood.
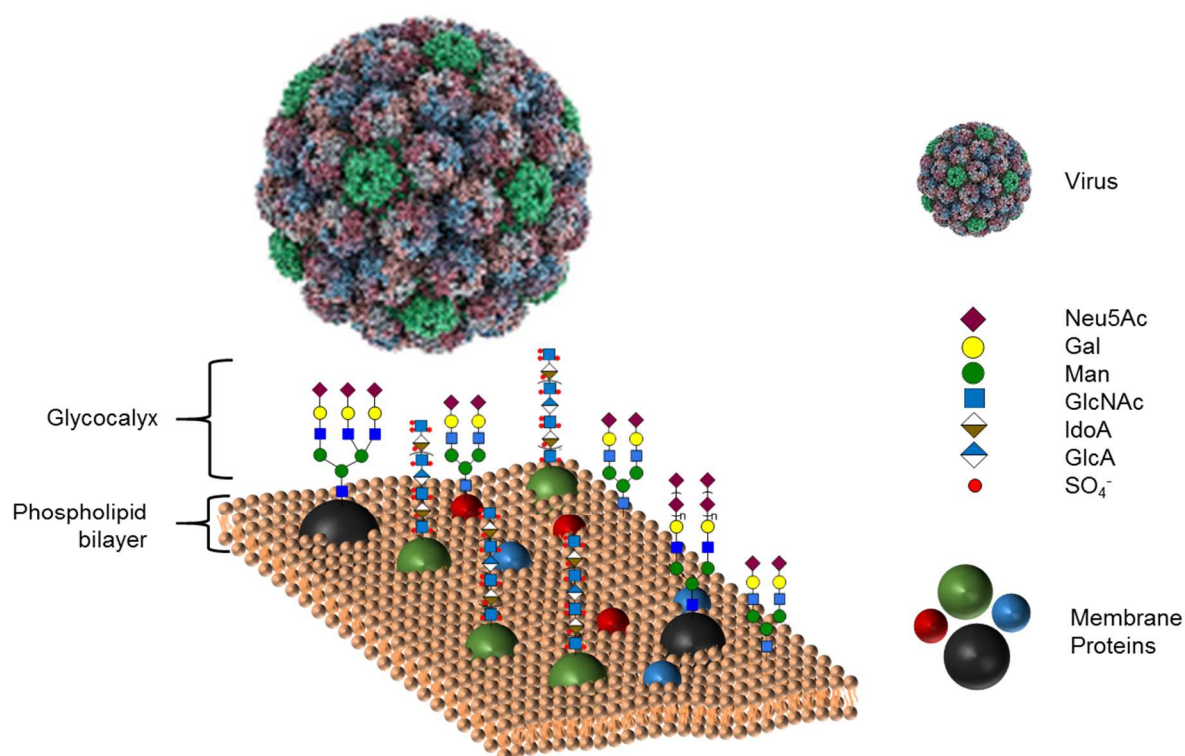
Figure 2: Simplified cell surface with attached glycans to which a virus approach. Above all, sialic acid-terminated glycans and heparan sulfate are known to act as initial receptors for viruses.

1.1.2. First contact - Sialic acids in virus-cell interaction

Sialic acid has first been discovered and characterized in the early 1940's and short after it became clear that *N*-acetylneuraminic acid (Neu5Ac) is the major member of a family of differently substituted compounds.[43] Until now, still *N*-acetylneuraminic acid and sialic acid are used synonymously. Sialic acid is a 9-carbon carboxylated sugar and generally occurs as terminal monosaccharide of many different animal cell surface glycans.[20, 44] Sialic acids are ubiquitously expressed in higher vertebrates and are attached at terminal ends of *N*- and *O*-glycans as well as glycolipids and glycoproteins.[43] In **Figure 3** the structure of sialic acid (Neu5Ac) is shown in its α-form highlighting positions on which variations can occur in yellow. Furthermore, common mammalian sialylated *N*- and *O*-glycans are presented. Studies show that each cell carries up to several million sialic acids and their high hydrophilicity as well as their high negative net charge cause cell repellence and morphological stabilization of these cells.[45-47] Moreover, Neu5Ac is involved in key interactions between cells and many different viruses as well as other pathogens at various points in their infection and transmission life cycle. A great number of viruses, as well as bacteria, specifically bind to host sialic acids and use them as primary receptors for infection,[48-51] where they are involved in cell-cell adhesion and cell signalling.[18, 52, 53] Usually, interactions of virus surface proteins with single sialylated glycans are of low affinity and thus strongly make use of multivalent effects in order to increase avidity.[25, 26] Neu5Ac is most common in humans, but various modifications such as acetylation,
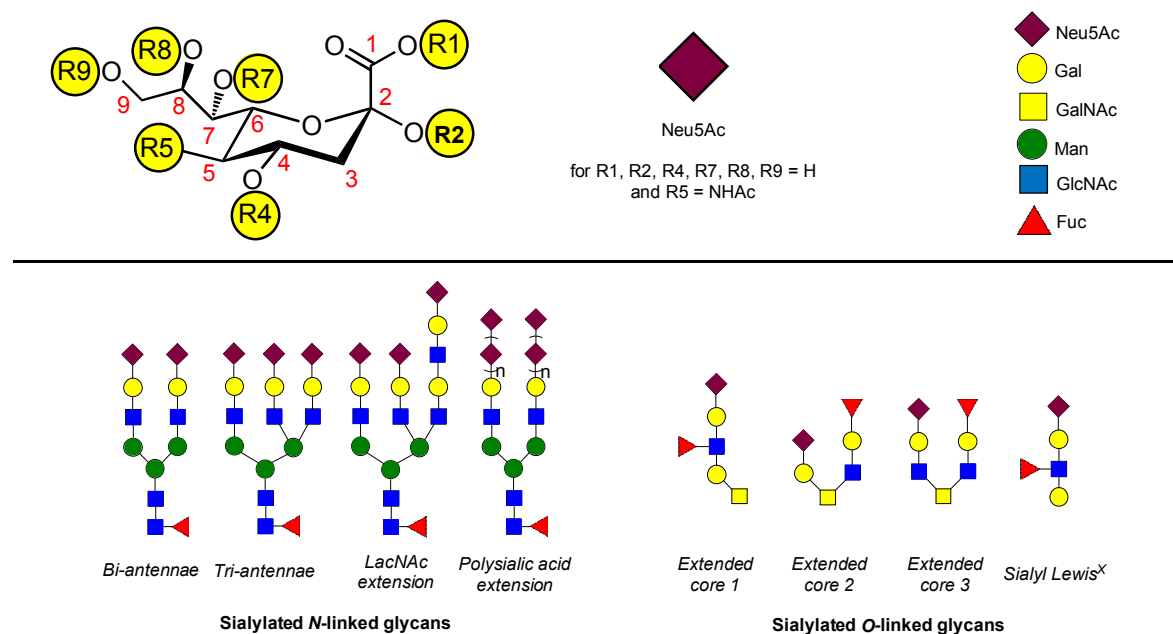
Figure 3: Sialic acid (Neu5Ac) modifications and chemical structures of common mammalian sialylated *N*- and *O*-glycans. The nine-carbon backbone common to all known sialic acids is shown in the α configuration. Variations can occur at the carbon positions highlighted in yellow (Figure modified from Varki *et al.* [20]). The chemical structures of mammalian sialylated *N*- and *O*-glycans are adapted from Thaysen-Andersen *et al.* [54])

methylation or sulfation at C4, C5, C7, C8 and C9 give rise to more than 50 different sialic acid variants (**Figure 3**), not all of which occur in all species.[44, 50, 55, 56] Sialic acids are usually connected *via* α2,3- or α2,6-glycosidic linkages to galactose (Gal) or *N*-acetylgalactosamine (GalNAc) so that functional groups such as carboxylate, glycerol, *N*-acetyl and hydroxyl groups in the case of Neu5Ac are easily accessible for engagement.[36, 53, 57] Furthermore, two sialic acid resiudues can be connected one to another *via* α2,8- or α2,9-linkages, and thus sialic acids can also occupy internal positions within glycoconjugates. For example, di- and tri-sialic acid motifs are common in the context of human b- and c-series gangliosides.[58] Even longer chains of sialic acids, so-called polysialic acids or colominic acids, can modify proteins such as neural cell adhesion molecules (NCAM) and are expressed divergently in tumors.[59-63]

The biology of sialic acids is complex, but so is their synthesis.[64] Problems arise from the particular 9-cabon form, the relative acid instability of the glycosidic bond, the base instability *e.g.* of the amide at the 5-position as well as in the instability of various modifications. Chemical sialylation is probably one of the most elaborate and challenging glycosylation, due to difficulties in accessing the anomeric center, the presence of the electron-withdrawing carboxyl group at the anomeric center, and the lack of a directing vicinal group.[50] Nevertheless, structural modifications at every position within the sialic acid corpus have successfully been elaborated.[65, 66]

In the following, possibilities for the glycosylation of sialic acids will be discussed, which provide 2-substituted derivatives, as they are predominantly found terminally on human cells glycans. Except for the cytidine-5'-monophospho-Neu5Ac (CMP-Neu5Ac), the activated form of Neu5Ac used by sialyltransferases, all naturally occurring sialic acids are bound α-glycosidically.[67-69] In addition to the already mentioned problem of a missing directing group at C3, the carboxylate on C2 makes sialic acid very sensitive to 2,3-eliminations. For glycosylation, sialyltransferases can generally be used.[70] The advantages here are the specificity with respect to an α2,3- or α2,6-linkage and that no protective groups are required. The possibility to convert ManNAc chemoenzymatically into Neu5Ac, which in turn can be converted into CMP-Neu5Ac chemoenzymatically, makes this route appealing.[70]

For the chemical preparation of *O*-sialosides, the choice of the activating group at C2 is crucial.[70] In analogy to the CMP-Neu5Ac, phosphites [70-72], xanthates [73, 74], thio-compounds [75, 76] and the 2-chloro-derivative of sialic acid are used in particular.[77, 78] The latter is the easiest to synthesize, the least hazardous and offers, if used in large quantities, no odor nuisance compared to sulphur-containing molecules. High yields, high selectivity as well as high reactivities are generally aimed. Sialic acid modifications at C1 and C3 have therefore led to selective and highly reactive compounds, but, in turn, are associated with more synthesis steps and a greater synthetic effort.[70, 79, 80] In this way, oligosaccharides, all kind of sialylated biomolecules but also functionalizations of sialic acid with alkyne- or azide-derivatives, which can be used in so-called click reactions have been accomplished.[77,

[81] In addition to the *O*-glycosidic sialosides, especially *N*, *S*, and *C* modifications to C2 are common and offer the advantage of being resistant to enzymatic degradation.[77, 82] The use of an azide as the nucleophile allows straightforward access to a "clickable" azido-sialic acid derivative.[77, 83-86]

Click reactions are one of the most commonly used reactions to attach carbohydrates, whether mono- or oligosaccharides, to previously built molecular scaffolds. Click reactions are generally classified as high yield-reactions, they are stereospecific, provide no or well-separable side-products, do not require harsh conditions and have been applied extensively *e.g.* for the synthesis of carbohydrate-peptide-conjugates.[87-90] Probably the most important of all click reactions up to date is the copper(I)-catalyzed alkyne azide cycloaddition (CuAAC), which affords 1,4-substituted 1, 2, 3-triazoles as conjugation pattern and which is based on the 1,3-dipolar cycloaddition reported by Huisgen.[91-95] Other representatives of the click reactions include the strain-promoted alkyne-azide cycloaddition (SPAAC),[96-98] Staudinger ligations,[99-102] thiol-ene [103-106], thiol-yne [107-109] and thiol-Michael reactions,[105] oxime [110, 111] and thiazolidine ligations,[112-114] as well as all types of Diels-Alder cycloadditions.[115-118] **Scheme 1** shows the biologically activated form of the sialic acid: β-CMP-Neu5Ac, possible functionalizations starting from unfunctionalized sialic acid and, *e.g.*, two functionalized sialic acids which later can be used in copper-click reactions.
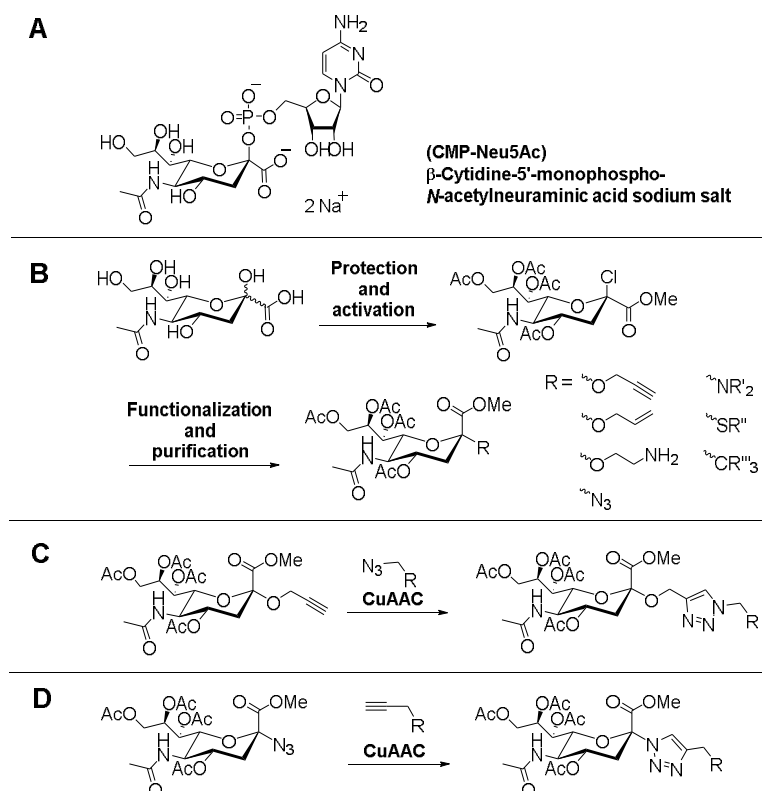
Scheme 1: **A**: The biologically activated form of the sialic acid: β-CMP-Neu5Ac. **B**: Possible functionalizations starting from unfunctionalized sialic acid and. **C** and **D**: Two functionalized sialic acids for later click reactions.

1.1.3. Heparan sulfate mediating viral infections

Heparan sulfate (HS) belongs to the class of glycosaminoglycans (GAGs), it is found as glycan strands on the plasma membrane of all animal cells and is attached to the protein backbone of proteoglycans, where it reaches molecular weights of up to 50 kDa with an average of 30 kDa.[119, 120] HS is a linear polysaccharide consisting of heterogeneously *N*-acetylated and / or *N*-sulfated glucosamines as well as uronic acids, which form the disaccharide-repeating unit.[121-124] These modifications give rise to domains with high acetylation and low sulfation content ('NA-domains') and highly sulfated domains ('S-domains').[125, 126] Generally, it is believed that interactions of heparan sulfate with proteins are strongly dependant on the degree of sulfation in the different domains and the orientation of the carboxyl groups.[127-129] An omnipresent topic is the electrostatic interaction of the HS chains with protein ligands, which affects metabolism, transport, information transfer, support and regulation in all organ systems.[19, 130] A distinction must be made between heparan sulfate and heparin at this point, the latter showing a similar sulfation pattern but which does not occur in the plasma membrane and is formed and stored by mast cells.[124] However, difficulties in evaluating the role of heparin and heparan sulfate *in vivo* may be ascribed to a lack of information of the detailed structure and sequence of these polysaccharides. One of the best-studied examples of heparin-activity is the activation of the serine protease inhibitor antithrombin by a specific pentasaccharide sequence.[131, 132] This pentasaccharide, which specifically binds to positively charged amino acids in the protein, is nowadays accessed synthetically and used as an anticoagulant named Fondaparinux®.[133-137] Binding results in a conformational change of the protein, which affects coagulation *e.g.* in the case of factors IIa and Xa. **Figure 4** shows the chemical structure of heparan sulfate and the synthetic pentasaccharide Fondaparinux® for comparison.
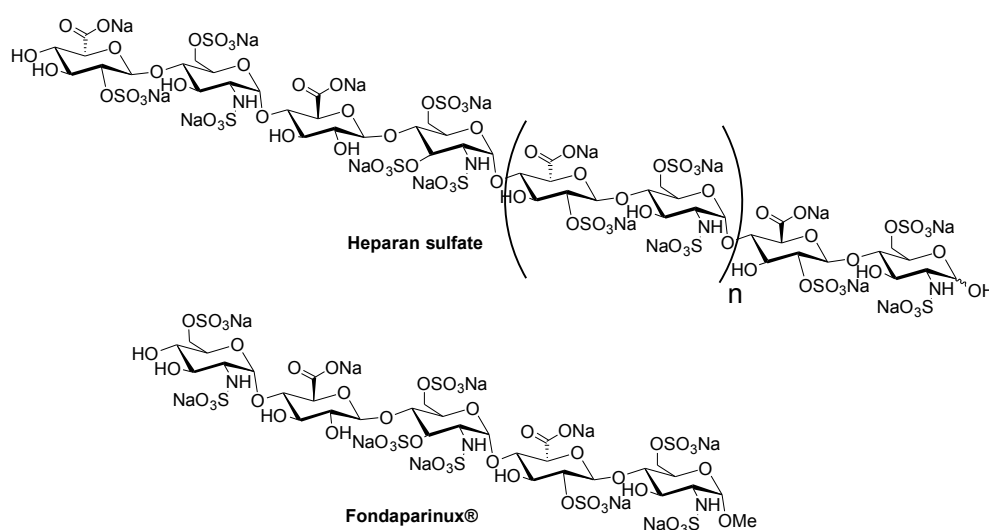

Figure 4: Chemical structures of heparan sulfate and of the synthetic pentasaccharide Fondaparinux®.

Since HS is found on the surface of most mammalian tissues, its involvement in viral binding and entry mechanisms is not surprising.[125, 130, 138] Docking to sulfated GAGs such as heparin is a strategy shared by a wide variety of pathogens such as viruses, bacteria, parasites, and fungi as already discussed above.[139] They use GAGs to promote their attachment and invasion of host cells, movement from one cell to another, and to protect themselves from immune attack. First studies showed that human blood inhibits Herpes Simplex Virus infection.[138, 140] Later on this effect could be attributed to heparin, which is found in human blood.[138] In another example evidence has been found that heparin has multiple anti-HIV activities.[141, 142] This activity was clearly attributed to the presence of sulfates by desulfation experiments.[143] The minimum-sized heparin fragment involved in specific binding was identified as a hexasaccharide in this case, but binding affinity increases with increasing oligosaccharide size up to 18 saccharide residues required to reach heparin affinity.[144] Similar circumstances have been identified so far in case of Flaviviruses, members of which are yellow fever virus, west Nile virus and dengue fever virus.[145] Papillomaviruses,[146, 147] of which the member HPV16 (Human papillomavirus Virus type 16) is well-known favouring the occurrence of cervical cancer. Furthermore, the Merkel cell polyomavirus (MCPyV),[148-152] which is the unique member in the family of Polyomaviruses that requires highly sulfated glycosaminoglycans such as heparan sulfate for infection and is a presumable cause for the occurrence of Merkel cell carcinoma, in which it was first found.[153, 154]

To approach specific interactions between GAGs and complementary receptor proteins, complexity of this polysaccharides needs to be broken down. This is one way to gain deeper insights into structure-activity relationships for findings that later might pave the way for the development of drugs or therapeutic approaches.[124] Here, the possibilities of enzymatically degraded oligosaccharide fragments or the use of defined GAG fragments as in the case of Fondaparinux® are given.[40, 155-157] Both methods are very complex and provide the desired products only in small amounts, but both ways remain the only accesses to this special class of carbohydrates.[112, 158-160]

While it is already complicated to isolate GAG-fragments, it is even more challenging to convert them into glycoconjugates. There are four ways to perform couplings on them. These include binding to the non-reducing and reducing end [161-163] as well as the conversion of the carboxylic acids of the uronic acids or the amines of the glucosamine-residues.[161, 164-167] Binding to the non-reducing end is for example achieved *via* ozonolysis followed by oxidative or reductive work-up, binding to the reducing end typically is performed *via* reductive amination. Both approaches will not be further discussed here. Possible coupling methods are shown in **Scheme 2.** Amide bond formation with the carboxylic acids or with the amines particularly demands special characteristics on the coupling reagent used. Due to the high number of sulfates and the associated exclusive solubility of the GAG-fragments in water or aqueous solutions, the coupling reagents must tolerate aqueous media as a fundamental prerequisite. The only two common representatives are EDC / NHS and DMTMM.[166, 168-170] 1-Ethyl-3-(3-dimethylaminopropyl)carbodiimide (EDC) is a water-soluble carbodiimide-representative and is first
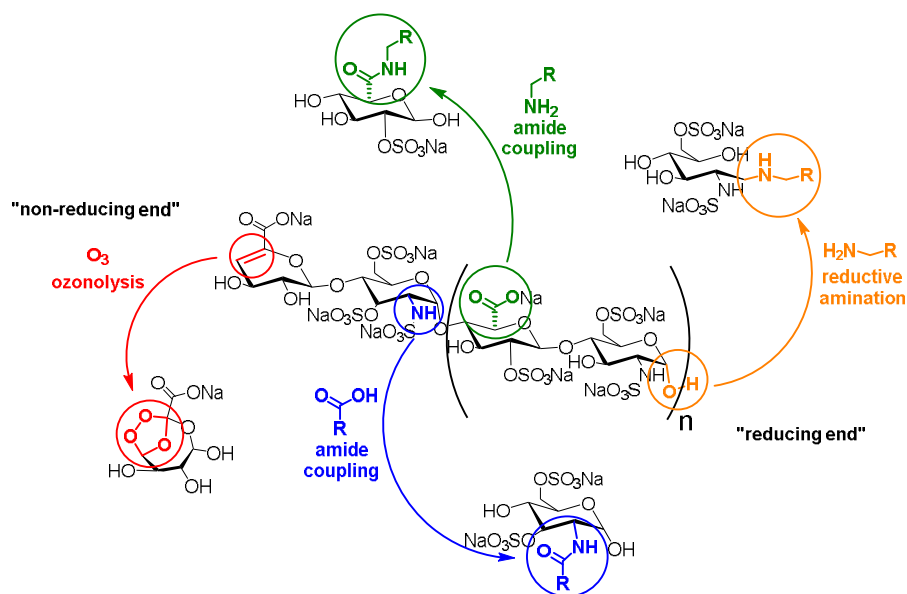
Scheme 2: Enzymatically degraded heparan sulfate and possible ways of functionalization.

converted to *O*-acylisourea with a carboxylic acid, before this intermediate is further converted to the NHS-ester by replacement with *N*-hydroxysuccinimide (NHS). Thereby urea is formed. In the last step, the NHS-active ester is converted to the amide by release of *N*-hydroxysuccinimide. DMTMM (4-(4,6-dimethoxy-1,3,5-triazin-2-yl)-4-methyl-morpholinium chloride), in turn, first reacts by forming an active ester and release of one molecule of *N*-methylmorpholine. The triazine-active ester is then attacked by the amine yielding the desired amide and one molecule of 4,6-dimethoxy-1,3,5-triazin-2-ol. Both methods have shown to be suitable for the synthesis of GAG-conjugates. However, DMTMM provides slightly better results.[166, 168-170] The amide coupling mechanisms of both EDC / NHS as well as DMTMM mediated coupling are presented in **Scheme 3** exemplarily based on the example of glucuronic acid, to which an amine is coupled. Both ways provide the same the desired glucuronic acid amide, but DMTMM as coupling reagent requires less reaction steps and is therefore easier to handle with regards to the reaction conditions.
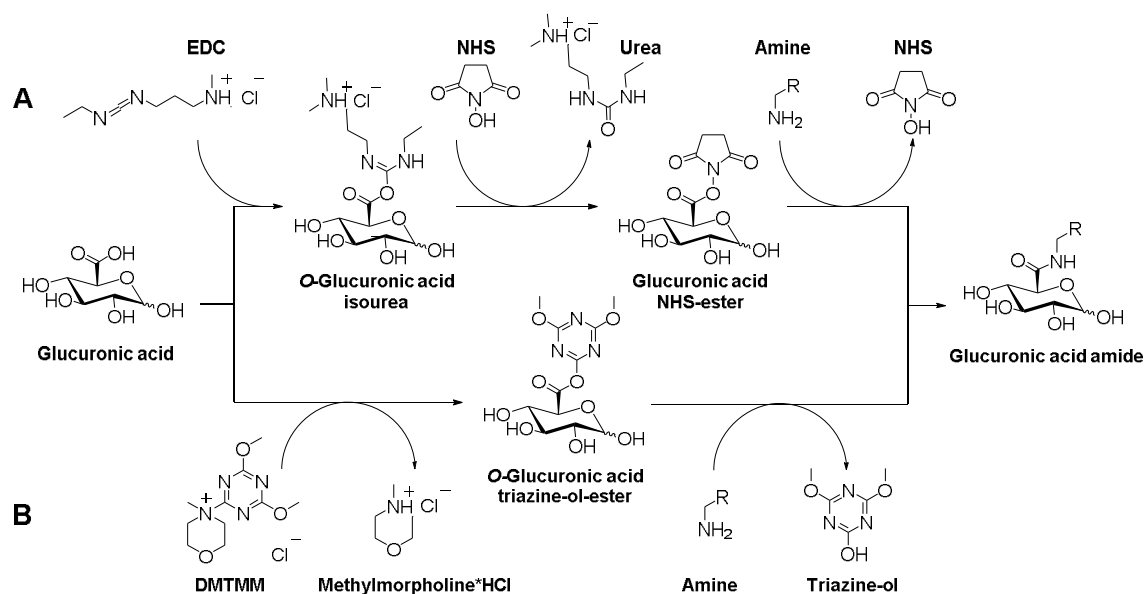
Scheme 3: Exemplary glucuronic acid amide forming *via* two ways: **A**: EDC / NHS mediated coupling. **B**: DMTMM mediated coupling.

1.2. Multivalent glycomimetics

1.2.1. Basic principles of glycomimetics and multivalency effects

To gain basic knowledge from the interplay of the glycocalyx and the receptor protein counterpart, one major idea is to simplify the complexity of the glycocalyx to the essentials. Thus, it is possible to derive fundamental structure-activity relationships and mechanistic insights from the research with artificial glycan-carrying structures, so-called glycomimetics, for which the glycocalyx is far too complicated to work with because of its structural complexity.[171-174] For this purpose, it is used that lectins, proteins that bind specifically bind to carbohydrates, typically bind only to a certain type of carbohydrates, usually a single terminal mono- or short oligosaccharide. The smallest possible unit to which binding is still possible is named the minimum binding epitope. This binds to the carbohydrate recognition domain (CRD) of the lectin typically in a shallow cavity which allows the carbohydrate easily to unbind when displaced by competing binders such as additional carbohydrates or solvent molecules. Glycan mimetics are designed in a way so that glycan binding epitopes are presented on an artificial scaffold, either mono- as well as multivalently, homo- as well as heterogeneously as both cases shown exemplarily in **Figure 5**.[21]
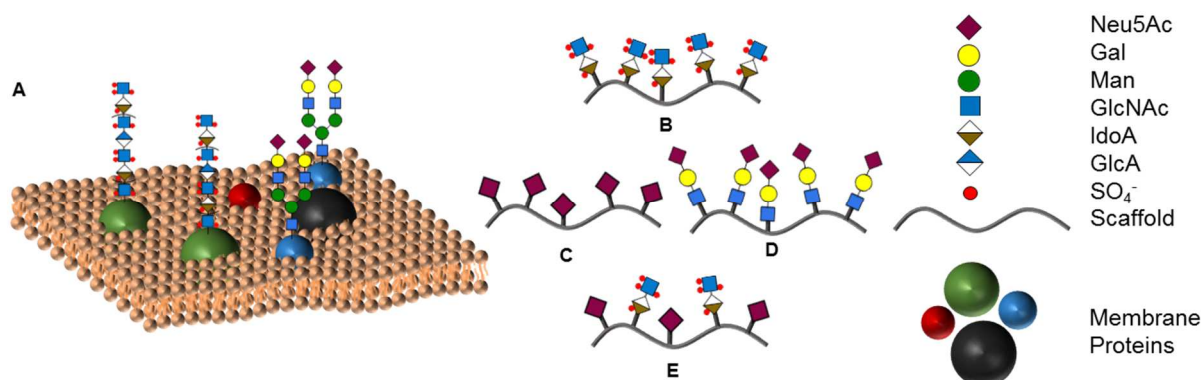
Figure 5: Glycan mimetics based on Glycans displayed on a random cell surface (**A**). Different sugar types can be presented homo- as well as heterogeneously on artificial scaffolds, such as GAG-fragments (**B**), terminal mono-or oligosaccharides (**C** and **D**) as well as a combination of both types (**E**).

Taking into account today's knowledge about multivalent binding modes, four major multivalent binding mechanisms of glycosylated compounds can be distinguished in the binding of multivalent constructs to receptors.[175-181] These four multivalent binding mechanisms are chelation, statistical rebinding, clustering and steric shielding as exemplarily shown in **Figure 6** for a trivalent ligand binding which binds to a trivalent receptor.
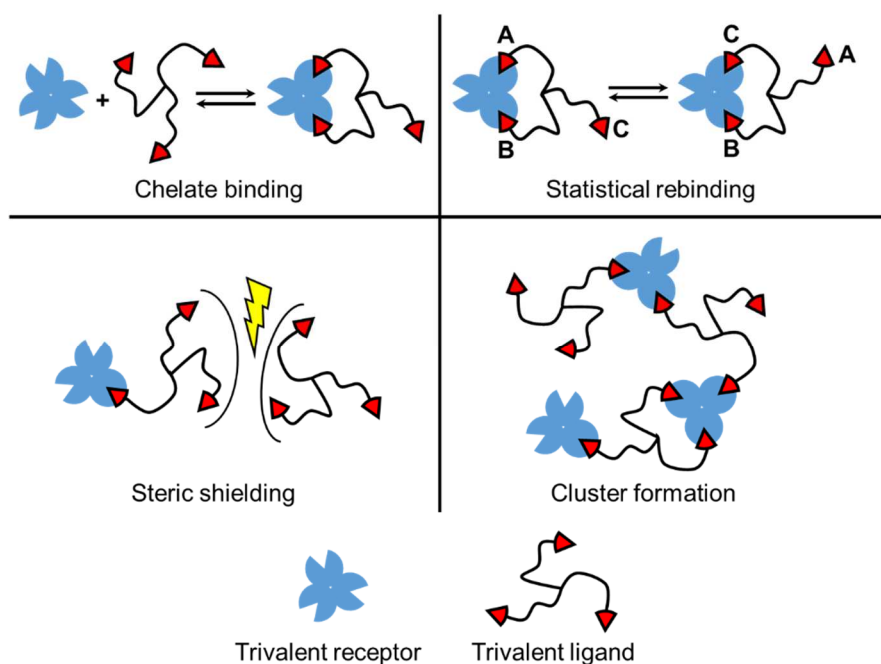
Figure 6: Multivalency effects visualized for a trivalent ligand binding to a trivalent receptor.

Chelation refers to the multiple binding of a multivalent ligand to a multivalent receptor. The advantage of this binding is that ligand and receptor have already been brought into contact and translational and rotational entropic losses must be paid only once.[182, 183] But this strictly only holds true for ligands

based on rigid scaffolds. Considering ligands with flexible linkers and scaffolds equal entropic losses have to be paid for every individual ligand as investigated by Whitesides *et al.*[184] Aspects such as the distance and the accessibility of the binding motifs or the binding pockets, respectively, strongly influence avidity.[185, 186] Statistical rebinding refers to the reversible binding of binding motifs to binding pockets. This phenomenon happens because sugar-protein interactions are usually weak so that individual carbohydrates are not tightly bound. Another binding carbohydrate in close proximity to the formerly bound moiety can displace the previously bound binding partner, thereby increasing the total binding strength.[183, 187] Furthermore, binding sites are typically shallow depressions and highly accessible for solvent molecules. Clustering is the common aggregation of multivalently bound compounds. Depending on the concentrations of ligand and receptor, these form agglomerates. Steric shielding describes the case that unbound parts of a partially bound multivalent construct are able to shield the previously formed carbohydrate-lectin complex from competing ligands, thereby conserving and stabilizing the original state.[175, 177, 188, 189]

The appearance of each of these multivalency effects usually results in an increase in binding affinity by up to several orders of magnitude, but multivalent effects do not necessarily occur cooperatively.[177] Negative cooperativity has been described for numerous receptor-ligand pairs as in the early case of binding of insulin to its counterpart receptor,[190] but is hardly detectable for receptor-carbohydrate-ligand pairs due to low affinities. However, Dam *et al.* reported evidence of negative cooperativity of the investigated mannose-carrying small dendrimers and the receptor lectins Con A and *Dioclea grandiflora* lectin (DGL) when investigated in isothermal titration calorimetry assays (ITC) and Hill-plotting.[191] Apart from the sheer number of binding partners, their distance, density, the nature of the linker and the scaffold, even the compounds architecture, play a crucial role. Furthermore, it is of importance in which medium or in which form the binding partners occur. Here, it makes a difference whether both binding partners are both dissolved, or only one and the other is suspended or dispersed, or whether one of the partners has been covalently immobilized on a surface such as in the natural glycocalyx for example.

From a synthetic point of view, different classes of glycomimetics need to be differentiated depending on the scaffold used to attach the glycan epitopes. In the following, four classes of multivalent glycomimetics will be discussed exemplary with respect to their synthesis, structure and properties, highlighting selected examples from literature. Specifically, glycopolymers will be discussed as well as glycopeptides, glycodendrimers and sequence-defined glycooligo(amidoamines).

1.2.2. Glycopolymers

Glycopolymers are generally based on the principle of carbohydrate-functionalized side chains on a polymeric backbone.[192-194] Glycopolymers are characterized by a rather simple synthesis, a great variability and by their high availability, but also show intrinsic disadvantages. Classical polymers are always disperse, are homogeneously linked in the rarest cases and, in contrast to biological macromolecules such as DNA or proteins, typically form random coils in solution and do not take over defined superstructures.[195, 196] Biological activity must always be considered in the context of the three-dimensional structure of the investigated molecules, whether a defined structure or a random coil. Although the synthesis of homopolymers from glycofunctionalized monomers results in precise knowledge of the sequence, it usually provides over-functionalized polymers having a too high density of sugars for appropriate binding. These tend to interfere with one another in inter- and intramolecular clustering rather than resulting in an increase in avidity as shown in the case of mannose in its interplay with Concanavalin A (Con A).[197-202] Lower densities of sugars, higher molecular weights and variable functionalities are achieved by running copolymers-approaches. However, copolymers create further intrinsic problems such as a lack of knowledge on the exact sequence of different monomer units incorporated. **Figure 7** gives a short view on glycopolymers exemplary based on acrylic acid or acrylic amide on three ways. The possibility of using highly developed polymerization methods, which lead,
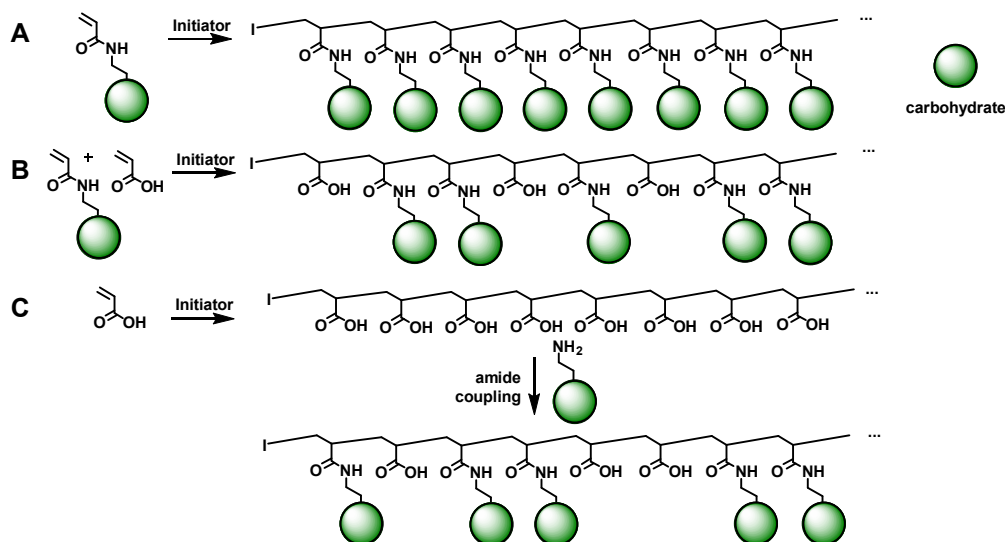
Figure 7: Exemplary visualization of acrylic acid / acrylic amide-based glycopolymer-synthesis *via* three ways. **A**: Glyco-homopolymer synthesis *via* the *grafting-through* method using a glycofunctionalized monomer. **B**: Statistical glyco-copolymer synthesis using a glycofunctionalized and a non-functionalized monomer resulting in a random copolymer. **C**: Polymer analogous synthesis of a Glyco-copolymer *via* the *grafting-to* method by amide coupling of an amino-functional carbohydrate to poly acrylic acid. Also, here a statistical copolymer is obtained.

for example, to low dispersities or controlled sequences remain unaffected, moreover, also graft polymers appear a promising approach,[203-205] nowadays even using 'green chemistry'.[206] However, neither chain-growth, nor step-growth nor graft polymers allow for a total structure and sequence-control. Generally, the number and distance of the incorporated sugars, their density, their position on the backbone and the nature of the linker determine the ability of glycopolymers to bind to lectins.[207, 208] Glycopolymers have for example been applied in numerous therapeutical applications as has recently been reviewed by Spain *et al*.[209] The synthesis and application of glycopolymers have been described in detail from Becer *et al*.,[210] selected examples of sialic acid based glycopolymers are given by Suzuki *et al*. [211] and Totani *et al*. [212] Glycosaminoglycans have been used in Glycopolymers as well, what has been reviewed by Miura *et al*.[213]

1.2.3. Glycopeptides

Synthetic glycopeptides offer the opportunity to present glycan epitopes in many ways due to the synthetic flexibility of assembling peptide scaffolds. Parameters such as the architecture of the scaffold, the structure of the linker, and the type of sugar can be adjusted in a rather simple way.[214] For example, natural *N*- or *O*-glycosidic linkages can be used as well as non-natural linkages as *e.g.* a result from click chemistry approaches. However, a distinction must be made between different ways to synthesize these macromolecules, which in turn strongly influences their properties. Short, defined sequences can *e.g.* be produced by solid phase synthesis and either can be glycofunctionalized by incorporation of glyco-functionalized amino acids, they can be glycosylated either resin-bound or after cleavage, respectively.[215, 216] Thus, it is possible to isolate both homo- and heteromultivalent constructs by iterative, step-wise coupling and functionalization or by making use of orthogonal protecting group strategies, but this research area still is in its infancy.[21] Longer sequences can be obtained, for example, by cloning protein domains or by chain growth polymerization of amino acid *N*-carboxyanhydrides, [217-219] but glycofunctionalizations of these structures is not complete because of their polymer analogy. In principle, there is also the possibility of targeting a secondary structure such as α-helices or β-sheets,[220-223] which, in turn may also occur unintentionally. Just a precisely defined secondary of glycopeptides can serve for the targeted presentation of glycans, the unwanted, accidental formation of superstructures would significantly influence interactions.[224, 225] Furthermore, synthetic glycoproteins are always risky with respect to the organism response. Most-likely, these structures will be digested by the organism and / or lead to an immune response of the organism when tested *in vivo*.[226, 227] In selected applications, such as in the research and testing of drug-delivery systems or in the field of synthetic vaccines, this is desirable and limits to use of glycoproteins in general.[228-233]

1.2.4. Glycodendrimers

A unique class of multivalent molecules, more specifically multivalent glycofunctionalized molecules, are glycodendrimers. The structure of each dendrimer resembles a tree in which the trunk and the inner, supporting branches represent the framework of the dendrimer and the outer branches represent the attached glycans. The divergent synthesis progresses by the stepwise attachment of multiple layers to a core molecule, which is typically associated with the use of protecting groups or at least two 2 functional group pairs. These need to be installed alternately, ultimately the synthesis ends with the decoration of the terminal functional groups with sugar moieties. In the convergent synthesis, functional glycoclusters, here called glycodendrons, are synthesized first. In the last step, these are bound to a multifunctional core molecule. While dendrimers are highly functional, they are often limited in their three-dimensional structure resulting in mainly globular shapes. In **Figure 8**, both the divergent as well as the convergent reation route are visualized.
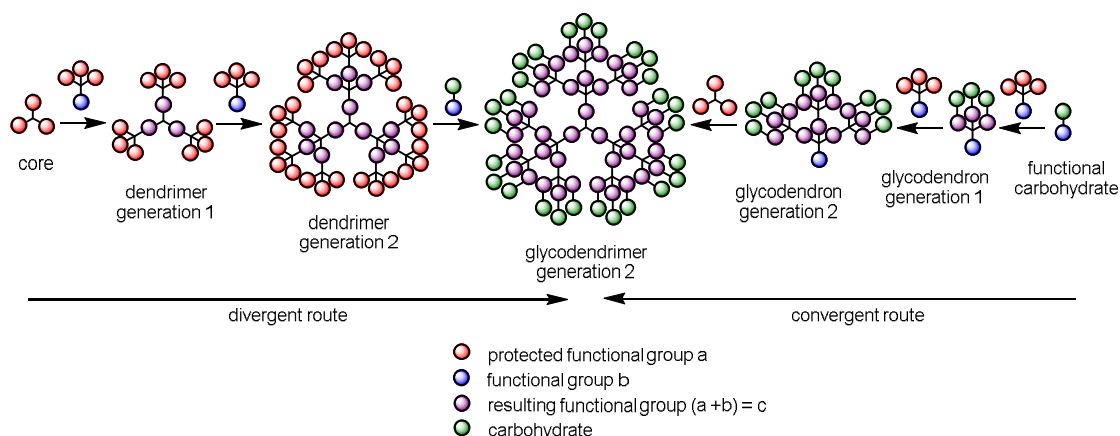
Figure 8: Glycodendrimer synthesis *via* the divergent and the convergent route. Every new generation requires previous activation of functional group **a** and subsequent coupling of **b** to **a** resulting in functionality **c**. Figure modified from Carlmark *et al.*[234]

The high degree of functional groups has proven advantageous in numerous applications. When looking at glycomimetics presenting sialic acid motifs, important examples on the use of a dendritic scaffold were presented by Rene Roy and coworkers. Examples are here the synthesis of hyperbranched glycodendrimers using α-thiosialosides based on a gallic acid core,[235] or a 3,3'-iminobis(propylamine)-core,[236] respectively, which were then tested for their binding behavior towards a specific sialic acid-binding lectin from *Limax Flavus* revealing an increase in inhibitory potency with increasing valency.[237] Likewise, dendritic sialic acid macromolecules were also synthesized based on solid phase synthesis.[238] Further results were gained by evaluating the ability of sialic acid-functionalized carbosilane dendrimers to act as influenza neuraminidase inhibitors.[239] Furthermore, Dominguez-Rodriguez *et al.* e.g. reported glycosaminoglycan-based dendrimers.[240] They synthesized dendritic Chondroitin sulfate mimetics and tested them against growth factor midkine.

1.2.5. Monodisperse, sequence-defined Glycooligo(amidoamines)

A very special class of multivalent glycomimetics, namely the glycofunctionalized oligo(amidoamines), in short glycooligo(amidoamines) will be emphasized in detail below. Glycooligo(amidoamines) have several advantages compared to the classes of compounds discussed so far. Poly(amidoamines), from which oligo(amidoamines) derive, are classically of dendritic type but also linear approaches have been elaborated.[241-243] Like dendrimers, they can be prepared both divergently and convergently. In both cases, at least bifunctional building blocks are used, which give a polymer consisting of amides as well as free amines in the backbone and thus have generally a basic character. Poly(amidoamines) show high biocompatibility and have been and are being used, for example, as drug delivery agents or in gene therapy approaches.[241, 242, 244-246]

Oligo(amidoamines) are a hybrid class of macromolecular compounds that combine the advantages of poly(amidoamines) with those of polypeptides.[247, 248] They are characterized by a defined sequence of the building blocks and they are aimed to be monodisperse. Unlike poly(amidoamines), they are not built up like dendrimers, but rather linearly using peptide solid phase synthesis (SPS) as introduced by Merrifield in the early 60'ies.[249] Glyco-functionalization of oligo(amidoamines) is achieved either by coupling functionalized carbohydrates to solid-phase-compatible building blocks prior to their use, or to resin-bound, macromolecular constructs, or by coupling them to already cleaved oligomers. Following this approach, homo- as well as heterogeneous glycooligo(amidoamines) can be obtained.

1.2.5.1. Solid phase synthesis

The technique of solid phase synthesis (SPS) makes it possible to grow an arbitrarily large number (usually not more than 40-50 units) of, like Merrifield did, amino acids, iteratively as pearls on a string, thus isolating the ready oligopeptide as a sequentially and structurally defined entity after cleavage from solid support. Merrifield's first publication in this regard dealt with the synthesis of a synthetic tetrapeptide.[249]

Generally, solid phase synthesis requires a functional resin to which molecules are iteratively coupled by activation, coupling and deprotection reaction sequences to finally obtain a macromolecular entity of high purity after cleavage from the resin. In particular, solid phase synthesis is characterized by nearly quantitative conversion in every step due to the use of high excesses of reagents and spatial separation of the functional groups on the functionalized resin, what, in turn, precludes aggregation. Excess starting materials, degradation products of the activating reagents and catalysts are easily

removed by washing the resin without time-consuming and yield-lowering chromatographic purification or extraction processes. Likewise, solvents can be changed by simple rinsing. In this way, high molecular weight, structure and sequence-defined, ideally almost pure products are obtained, nowadays even fully automated using peptide synthesizers.

The resins used in the solid phase synthesis must be stable and inert to standard synthesis conditions and towards the building blocks, reagents, catalysts and solvents used; they must also have adequate pore size and swelling capacity so that the reagents can diffuse unhindered and quantitative coupling of the building blocks is achieved. Typically, as already used by Merrifield, poly(styrene-co-divinylbenzene) copolymer resins are used today.[249] So-called linkers, sometimes with an additional spacer, are grafted to remaining vinyl-groups, which serve to attach the first building block onto the resin. The spacer determines whether rather hydrophobic or hydrophilic building blocks can be coupled particularly well and thus influences the yield and purity of the target structure. Furthermore, an additional spatial separation is thereby achieved. The linker, in turn, determines the cleavage conditions. Linkers are designed so that the desired product is obtained either by acidic, basic, hydrogenolytic, enzymatic, palladium-catalyzed, photochemical or oxidative and reductive treatment. Special types of linkers are traceless- and safety-catch-linkers.

Today, the field of solid phase synthesis has developed enormously. By choosing a suitable resin with an appropriate linker, the cleavage conditions, but also the resulting end-group functionality of the cleavage group are specified. Furthermore, spacers allow for the reduction of steric hindrance and the adaption of hydrophilic and hydrophobic properties. The use of newly developed protecting groups and coupling reagents, with appropriate adaptation of the synthesis conditions, allow for the resin-bound synthesis of complex linear as well as non-linear, complex organic molecules such as peptides, oligonucleotides, oligosaccharides or drugs. Solid phase synthesis was thus elevated to a universal tool, which goes far beyond the synthesis of peptides, although originally intended for this purpose.[250-255] **Scheme 4** depicts the general principle of solid phase synthesis giving access to highly pure macromolecules.
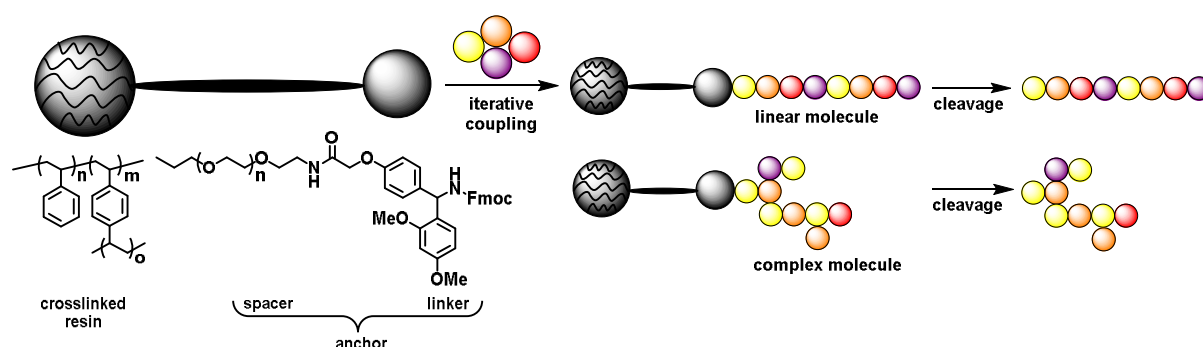
Scheme 4: General principle of solid phase synthesis allowing for the synthesis of complex molecules. Exemplary a TentaGel® S RAM resin is shown which is made up of a crosslinked poly(styrene-co-divinylbenzene) resin, a polyethylene glycol spacer and a rink-amide- linker allowing for cleavage under acidic conditions.

Nowadays, solid phase synthesis is predominantly based on Fluorenylmethoxycarbonyl (Fmoc) protecting groups along the main chain. This was introduced by Carpino *et al*.[256, 257] Fmoc as main chain protection strategy successfully pushed through for several reasons. Initially it tolerates the use of non-nucleophilic bases to activate coupling in every step and is itself particularly labile to secondary amines. The use of the latter, after successful coupling of the Fmoc-protected building block, cleaves off the Fmoc-group. This allows for the activation of the carboxylic acids of the building blocks in excess in- as well as outside the reactor with highly evolved coupling reagents with which then the free amine of the peptide sequence is reacted. Therefore, primarily acid-labile linker systems were developed. To what extent which development has affected another resembles the question of the chicken and the egg. Parallel development of protecting groups, coupling reagents and linkers of the resins used makes it possible to run the synthesis of extremely complex organic macromolecules today.

The process of building up a peptide on the solid phase occurs in three repetitive steps. Activation of the carboxylic acid, coupling of the resulting active ester to the resin-bound, free amine, and deprotection of the newly introduced N-terminus. Finally, the resulting product must be cleaved from the solid phase. As coupling reagents, carbodiimides such as DCC (dicyclohexyl carbodiimide), DIC (di*iso*propyl carbodiimide) or EDC (1-ethyl-3-(3-dimethylaminopropyl) carbodiimide) are used. Nowadays, however, mainly cationic conjugates of hydroxybenzotriazole (HOBt), hydroxyazabenzotriazole (HOAt) and ethyl (hydroxyimino) cyanoacetate (OxymaPure®) on the one hand and tripyrrolidinophosphine or tetramethydiaminomethane on the other hand, together with a non-nucleophilic counterion such as hexafluorophosphate are used. Common representatives are PyBOP (benzotriazol-1-yl-oxytripyrrolidinophosphonium hexafluorophosphate), HATU (1-[Bis(dimethylamino)methylene]-1H-1,2,3-triazolo[4,5-b]pyridinium 3-oxid hexafluorophosphate) or PyOxim (Ethyl cyano(hydroxyimino)acetate-O^2]tri-1-pyrrolidinylphosphonium hexafluorophosphate). These usually couple without racemization of amino acids, faster, more efficiently and are less toxic then carbodiimides. Recent developments include triazine-based coupling reagents such as DMTMM (4-(4,6-dimethoxy-1,3,5-triazin-2-yl)-4-methyl-morpholinium chloride), which couple equally well and allow for the use of aqueous media.

Hartmann *et al*. introduced the solid phase assisted synthesis of oligo(amidoamines), similarly to the solid phase synthesis reported by Merrifield. These compounds are synthesized by stepwise coupling of tailor-made building blocks to a functional polystyrene resin and final cleavage of the assembled macromolecule. Early work was done with the resin-bound synthesis of poly(amidoamines) for example for gene therapy approaches by alternating incorporation of linear multi-amine-functional building blocks and succinic acid elements.[247, 258, 259] Subsequent work dealt with the further development of the synthesis of poly(amidoamines) to sequentially and structurally defined oligo(amidoamines), in which diamine and succinic acid building blocks were pre-condensated, Fmoc-protected and further

functionalized before coupling to solid support.[199, 201, 260-263] Various tailor-made building blocks were developed in succession, the synthesis of which will be described in detail in the next sub-chapter.

1.2.5.2. Tailor-made building blocks for the synthesis of glycooligo(amidoamines)

The building blocks for the synthesis of glycooligo(amidoamines) can be subdivided into spacer and functional building blocks. Both types are based on linear, diamino-functional, and in the case of functional building blocks, linear triamino-functional molecules. These are converted into their final, free carboxy- and Fmoc-protected amino-group carrying form in multistep syntheses. One of the most commonly used spacer building blocks is called EDS ((*E*thylene*d*ioxy)bis(ethylamine) *s*uccinic acid amide), which incorporates a short, flexible and amphiphilic diethylene glycol unit. In a 4-step synthesis, 2,2'-(ethylenedioxy)bis(ethylamine) is first protected on one amine using trityl chloride before the second amine is reacted with Fmoc-Cl. The initially trityl-protected amine is subsequently deprotected with dilute trifluoroacetic acid before the resulting free amine is reacted under basic conditions with succinic anhydride in a ring-opening reaction. After protonation of the resulting carboxylate, the desired building block EDS is thereby obtained *via* crystallization from ethyl acetate. Initially, the synthesis was reported by Ponader *et al.*,[199] but using the Boc instead of the Trt protecting group. Further development of the synthesis, now using the Trt protecting group, was published by Ebbesen *et al.*[264] Further spacer building blocks used within the Hartmann group are SDS (*S*hort ethylene*d*iamine *s*uccinic acid amide) and ODS (*O*ctane*d*iamine *s*uccinic acid amide), in which the diamine used in the EDS synthesis are replaced by ethylenediamine or octanediamine, respectively.[265]

The synthesis of functional building blocks typically occurs in a linear 7-step sequence. Diethylenetriamine is first selectively protected by using trityl chloride on one primary amine before the remaining primary amine is converted to the corresponding trifluoroacetamide using ethyl trifluoroacetate. The remaining, central, free, secondary amine is then reacted with a functional, short-chained carboxylic acid using either a coupling reagent such as PyBOP (Benzotriazol-1-yl-oxytripyrrolidinophosphonium hexafluorophosphate) or by making use of the corresponding acid chloride. Thereafter, in a 2-step sequence, the trifluoroacetimidate is first replaced by the Fmoc protecting group, before the trityl group is replaced by succinic acid in a final 2-step sequence in analogy to the EDS synthesis. Up to date, a series of functional building blocks have been elaborated and published in this way. Examples are TDS [199] (*t*riple bond-functionalized *d*iethylenetriamine *s*uccinic acid amide), DDS [262] (*d*ouble bond-functionalized *d*iethylenetriamine *s*uccinic acid amide), MDS [266] (*M*ethylsuccinyl *d*iethylenetriamine *s*uccinic acid amide), BDS and ADS [260, 261] (*B*oc (*tert*-butyloxycarbonyl) and *A*lloc (allyloxycarbonyl)-functionalized *d*iethylenetriamine *s*uccinic acid

amide). In this order, access is gained to terminal alkynes, alkenes, carboxylic acids and, in the case of BDS and ADS, to free backbone amines in two different ways. TDS and MDS allow to link azide-functionalized carbohydrates either *via* a copper(I)-catalyzed alkyne azide cycloaddition (CuAAC) or *via* a Staudinger ligation, respectively.[266] DDS, in turn, gives access to thiol-ene click-approaches of thiol-modified carbohydrates. BDS and ADS carry a Boc and an Alloc protecting group on the central, secondary amine, thus allowing orthogonal access to free amines in the backbone. The discussed spacer as well as functional building blocks are shown in **Figure 9**.
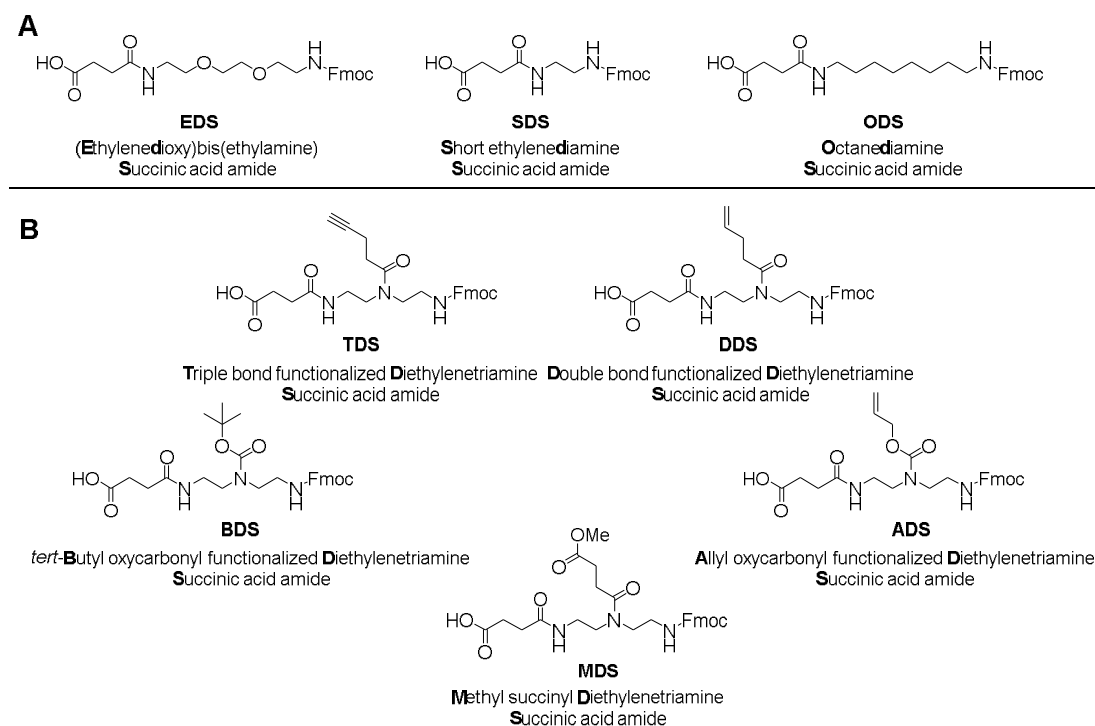
Figure 9: Spacer (**A**) and functional (**B**) building blocks developed and applied within the Hartmann's group for solid phase synthesis purposes of oligo(amidoamines).

1.2.5.3. Solid phase polymer synthesis of oligo(amidoamines)

In the following, the typical synthesis of an oligo(amidoamine) scaffold will briefly be described as shown in **Scheme 5**. The first building block is to be bound to the amine-functionalized resin by means of an amide linkage. In case of PyBOP-mediated coupling, which serves as an example here, the activation of the carboxylic acid of the first building block occurs first by deprotonation with the Hünig's base DIPEA (diisopropylethylamine), before the resulting carboxylate attacks the positively charged phosphorus of PyBOP and releases the hydroxybenzotriazolate. The resulting carboxylic acid-phosphoric acid anhydride now reacts in an aminolysis either with release of the tripyrrolidino phosphine oxide with the free amine of the resin, or alternatively previously reacts with the first released

hydroxybenzotriazolate to the corresponding activated ester. This, in turn, also reacts in an aminolysis to the desired amide. Hydroxybenzotriazole and the salt of the Hünig's base and hexafluorophosphoric acid are released. The deprotection of the N-terminus in case of Fmoc-based SPS is carried out with dilute piperidine solution. Piperidine deprotonates the fluorene at the non-aromatic ring-carbon, resulting in aromatization, which represents the driving force here. In an $E1_{CB}$-mechanism-initiated cascade, carbon dioxide and 9-methylene fluorene are released, the latter of which is trapped by excess piperidine in a Michael-like electrophilic addition reaction. After renewed intensive washing, the next building block can be coupled. In **Scheme 5** the exemplary solid phase coupling- and Fmoc-deprotection mechanism circle for the functional building block TDS is shown using PyBOP and Hünig's base as coupling reagents and piperidine as Fmoc deprotection agent.
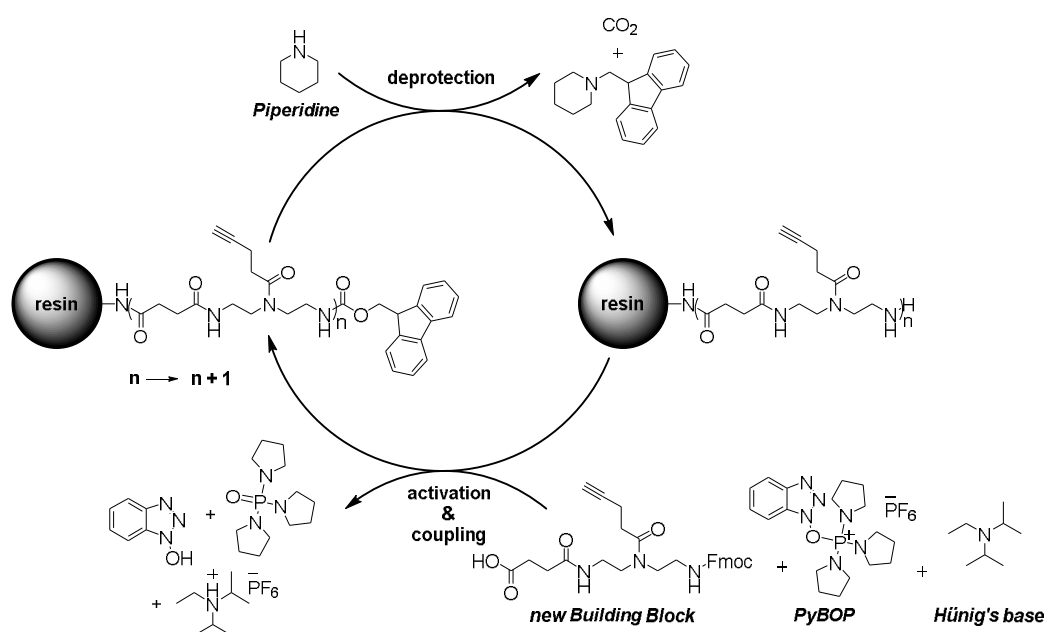
Scheme 5: Exemplary TDS building block coupling mechanism with PyBOP as coupling agent.

The cleavage from the resin is discussed with reference to a Rink Amide linker. Usually a mixture of trifluoroacetic acid in dichloromethane is used for cleavage of amides, amines or carboxylates. The linker bears the initial, Fmoc-protected amine to which, after prior deprotection, the first building block is coupled, at a central carbon, which is activated with two substituents, 2,4-dimethoxyphenyl and 4-methoxyphenol, *via* the latter the linker is grafted to the resin as depicted above in **Scheme 4**. Cleavage releases the aimed macromolecule and leaves the cationic, conjugated linker with trifluoroacetate as counterion. To avoid reacting the cationic linker with nucleophilic groups of the macromolecule, a hydride-donating scavenger such as triisopropylsilane is used. This reduces the carbocation and further reacts in a second step with the trifluoroacetate anion to unreactive trifluoroacetic acid triisopropylsilyl ester.

1.2.5.4. Glycooligo(amidoamines) as glycan mimetics

The first examples for glycooligo(amidoamines) were predominantly based on the two previously presented functional building blocks TDS and DDS, a series of spacer building blocks, but mostly EDS, and the three monosaccharides mannose, glucose and galactose. These glycooligo(amidoamines) all have in common that they are linearly built up and that they were primarily synthesized to test their binding behavior to the tetrameric plant lectin Concanavalin A.[199, 201, 208, 261-263, 266] This lectin is isolated from the jack bean and binds selectively to mannose and glucose in different intensities and explicitly not to galactose.

An azide-functionalized mannose was the first carbohydrate derivative to multivalently be coupled in solid phase polymer synthesis to TDS-containing oligo(amidoamines). Part of the compounds were tested in an SPR assay against Con A showing higher affinity for higher functionalization-degrees.[199] It turned out that these compounds non-linearly bind better the more sugar moieties they contain, compared to methyl-α-D-mannopyranoside and that the type of backbone and sugar density are of significant importance. On the one hand, following publications revealed that multivalent, alkene-functionalized oligomers can be fully reacted with a thiol-functionalized monosaccharide in a photochemical thiol-ene reaction in a continuous-flow reactor.[261, 262] On the other hand, not only homo-multivalent glycooligo(amidoamines) were synthesized, but also hetero-multivalent representatives in applying the above-mentioned three monosaccharides mannose, glucose and galactose. These were coupled in a defined number and position along the backbone and the resulting glycomacromolecules again tested in their binding behavior towards Con A.[201] Surprisingly it was found in SCP-RICM (*S*oft *c*olloidal *p*robe *r*eflection *i*nterference *c*ontrast *m*icroscopy) experiments that heteromultivalent compounds with combinations of Man and poor binding sugars Glc and Gal can bind better than homomultivalent representatives, which exclusively carry the best binding sugar mannose. Furthermore, evidence was found in dynamic light scattering (DLS) studies that glycooligo(amidoamines) can cluster lectins. Further research has led to the development of azabenzene-based photo switchable precision glycooligomers, which, depending on their configuration, exhibit a differential binding behavior towards lectins thus proving the architecture of the macromolecules, independently from size and valency, to influence binding affinity .[263] Recent studies focused on the effects of varying interligand spacing and linker functionalities on the binding behavior of mannosylated glycomacromolecules to Con A using isothermal titration calorimetry (ITC) [208] and the bacterial lectin Fim H. Recently, orthogonal access to sequence-defined, monodisperse and heteromultivalent glycomacromolecules on solid support was examined using Staudinger ligation and copper(I)-catalysed click reactions.[266]

In a collaborative project with glycobiologists, glycooligo(amidoamines) could be shown to mimic cell surface polysaccharides of the bacterium *Clostridium Difficile* and to provoke an immune response in mice.[233] The disaccharide rhamnose α1->3 glucose, which is found in three variants on the surface of the above-mentioned bacterium, was pentavalently presented on an oligo(amidoamine) *via* standardized protocols. In the context of this study, the isolated molecule was injected into mice. Thus, when naturally occurring disaccharides are compared with the artificial pentavalent oligo(amidoamine), antibody avidity as a measure of antigenicity increases by about five orders of magnitude. **Figure 10** gives an overview on selected glycooligo(amidoamines) taken from the discussed publications.
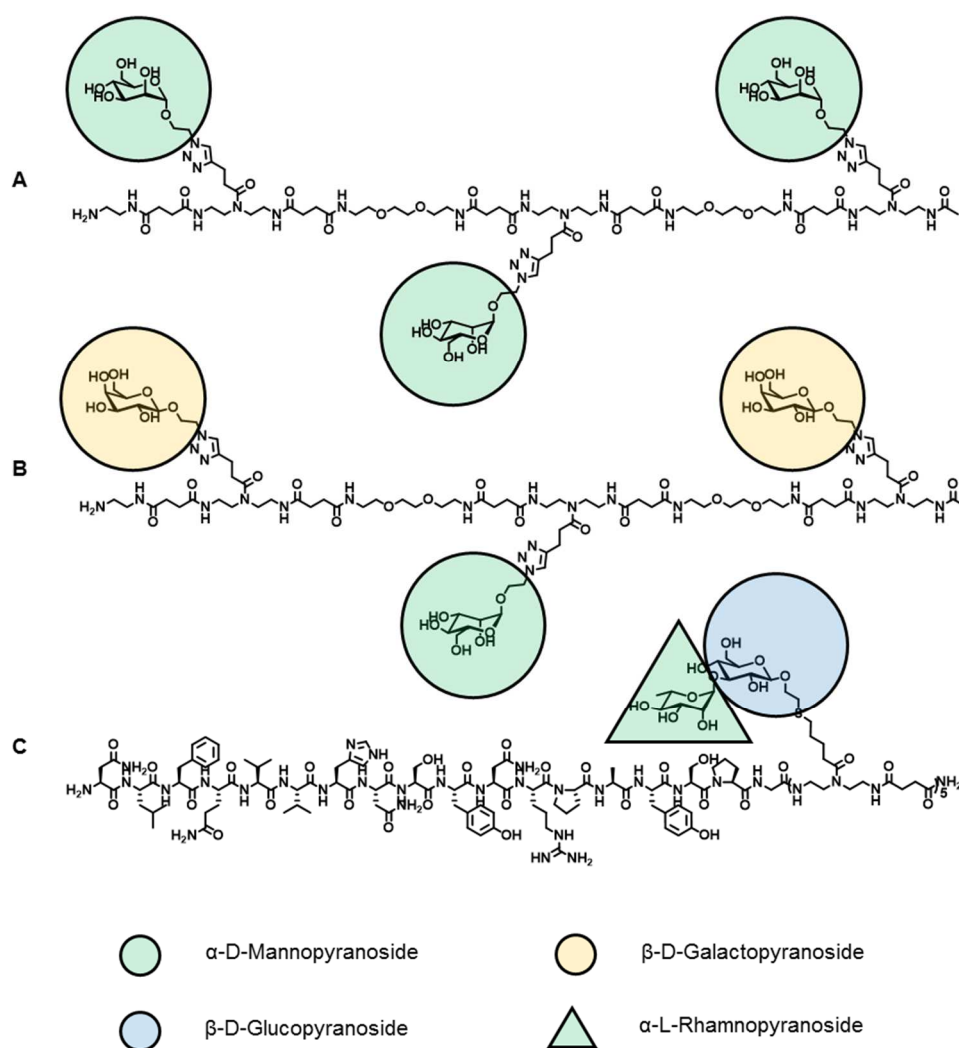
Figure 10: Three examples of glycooligo(amidoamines). **A**: Homotrivalent α-D-mannopyranoside macromolecule;[201] **B**: Heterotrivalent β-D-galacto- and α-D-mannopyranoside macromolecule;[199] **C**: Both oligopeptide and pentavalent rhamnose-α1->3-glucopypanoside disaccharide containing glycomacromolecule.[233]

Using glycooligo(amidoamines) derived from solid phase, recently, Hartmann and co-workers have shown different bottom-up approaches to derive more complex glycofunctionalized materials. For example, Gerke *et al*. synthesized di-cysteine-functionalized glycooligo(amidoamines) and then reacted them with di-alkene-functionalized oligomers in a poly-thiol-ene-reaction yielding sequence-controlled glycopolymers.[202] The resulting mannose-bearing polymers were tested for their binding behavior investigating the effect of sequence-controlled copolymers with alternating binding and non-binding blocks on lectin-binding in precipitation as well as surface plasmon resonance assays. It turned out here, that at a certain level of ligand valency a further increase in receptor clustering cannot be achieved by an increase in sugar valency. Furthermore, when keeping valency constant, an increase in ligand size does not increase binding affinity. A second example is given by Boden *et al*.[265] Here, the authors use cysteine-functionalized glycooligo(amidoamines) to coat gold nanoparticles to test the effect of hydrophobicity of the backbone of the oligomers-coated nanoparticles on the binding intensity to Con A by applying UV-Vis, dynamic light scattering as well as surface plasmon resonance experiments. Carbohydrate-coated gold nanoparticles showed increased binding compared to free ligands as well as an impact of the backbone-properties. Examplary glycooligo(amidoamine)- macromolecules of both publications are shown in **Figure 11**.
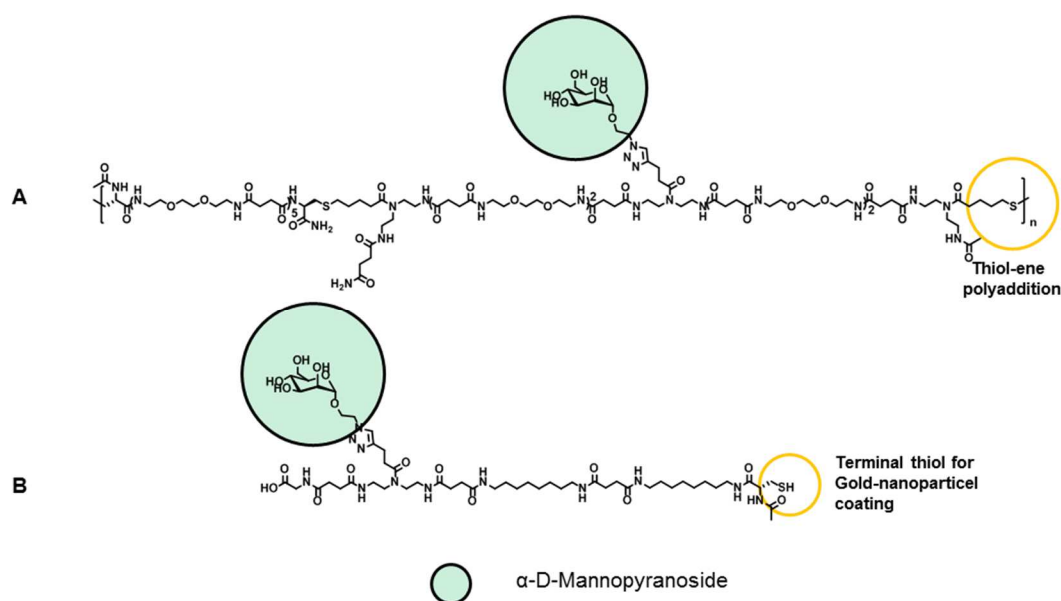
Figure 11: Two examples for advanced glycooligo(amidoamines). **A**: Sequence-controlled block-glycopolymer via step-growth thiol-ene polyaddition.[202] **B**: Precision glycomacromolecule for gold-nanoparticle coating.[265]

2. Aims and Outline

In the group of Hartmann, glycooligo(amidoamines) were developed as glycan mimetics to study fundamental aspects of multivalency and develop novel bioactive polymeric materials. Glycooligo(amidoamines) are derived via solid phase synthesis giving monodisperse and sequence-defined scaffolds that allow for controlled sugar composition, sugar valency, sugar distance and sugar density using different coupling strategies. So far glycooligo(amidoamines) have been mainly tested for their binding to model lectin Con A and for targeting bacterial lectins. However, it is well known that also viruses use glycans as attachment factors. Therefore, in this thesis, glycooligomers targeting viral lectins should be synthesized and characterized in terms of their lectin binding properties.

First, attachment of glycan and glycan fragments relevant for targeting viral lectins must be realized to the oligomer scaffold. However, so far mainly azide-functionalized sugars were used and attached to an established alkyne-functionalized building block. Especially for more complex sugars like sialic acid or short sialylated oligosaccharides such as 3'-sialyllactose, it is much easier to introduce an alkyne on the sugar. Therefore, in order to stay with the well-developed use of CuAAC, a novel azide-displaying building block should be developed. Another important class of glycans involved in viral interactions are glycosaminoglycans (GAGs). Thus, methods should be developed to attach GAG fragments onto oligomeric scaffolds. Here, the use of the GAGs carboxylic acids appears promising as point of attachment by applying amide-formation strategies. The possibility of synthesizing hetero-multivalent glycooligo(amides) incorporating both sialic acid derivatives as well as heparin fragments should be investigated against the background that both sugar classes, as demonstrated in case of the Merkel cell polyomavirus, influence viral entry.

In previous studies looking at the binding of glycooligomers to Con A, the influence of the type, number and position of glycan fragment have been shown. It is known from literature that such effects also take place when targeting viral lectins. However, what is less known, are the effects of linker chemistry and scaffold architecture. Work on glycooligomers targeting bacterial lectins have shown that the introduction of hydrophobic moieties can engage in secondary binding close to the carbohydrate binding domain leading to an increase in affinity. Therefore, the effect of selectively changing the linker composition should be tested in this work. It was shown that the architecture of the scaffold also contributes significantly to the binding properties of the compounds. Above all, branched structures seem to bind better to lectins than linear ones. This serves as the basis for the development of branched systems. Here, it is necessary to develop a solid-phase-compatible approach for the synthesis of

branched glycooligo(amides) and to quantify the binding properties of the resulting molecules with suitable assays.

Together with collaboration partners from virology, the derived glycooligomers should then be tested for their binding to non-enveloped viruses such as polyomaviruses and papillomaviruses to gain first insights into the design of glycooligo(amides) targeting viral lectins. Powerful analytical techniques such as X-ray diffraction of receptor-ligand co-crystals as well as STD NMR measurements will give first insights into the binding mechanisms of viral lectins to glycan mimetics.

3. Conclusion

The overarching goal of this work was the development of glycooligo(amides) targeting non-enveloped viruses such as polyoma- and papillomaviruses.

In the first part, special focus was devoted to the synthesis of branched glyco(oligoamidoamines) to investigate the effect of scaffold architecture on receptor affinity. Therefore, a novel azide-functionalized building block was developed. The synthesis-sequence proceeded analogously to the TDS synthesis as previously described by Ponader *et al*[202] but reversing the two-stage deprotection and functionalization sequences in their order to avoid isomerization as shown in **Scheme 6**. BADS was obtained in an overall yield of 34% in amounts up to 20 g per batch and excellent purities greater than 98% by recrystallization from acetone after successful conversion in the last step of the synthesis. When following the original synthesis sequence for the azide building block, the constitutional isomer *Iso*BADS was obtained. In the latter case, the central, secondary amine ultimately bears the Fmoc protecting group and the functional side chain decorates one of the primary amines of the diethylenetriamine-backbone. Coupling efficiency studies revealed a coupling efficiency of 98% of the BADS building block when applying PyBOP- and DIPEA-mediated coupling in dimethylformamide and using five equivalents of the building block as well as the coupling agent.
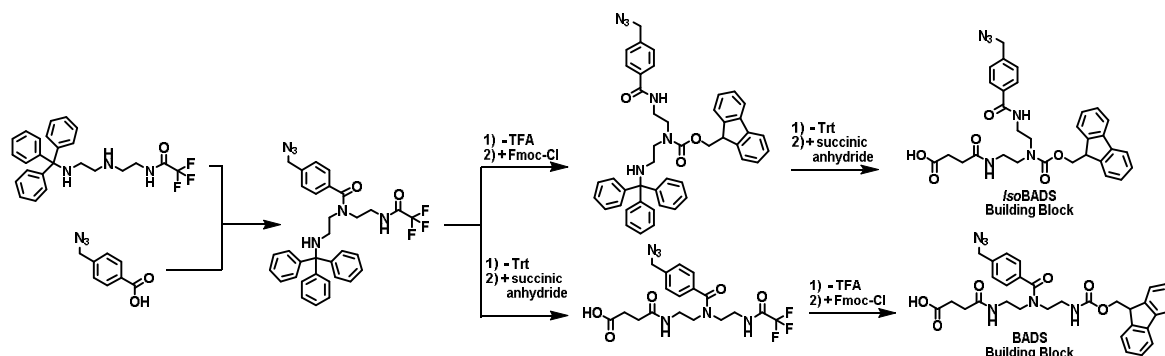
Scheme 6: Synthesis routes of both azide-containing building blocks BADS and *Iso*BADS, respectively. Only an inversion of the former for the functional TDS building block published route leads to the desirerd BADS building block. Otherwise *Iso*BADS is obtained due to an isomerization within the synthesis sequence.

Both building blocks, BADS and *Iso*BADS, were successfully applied in solid phase polymer synthesis to gain access to branched glycomacromolecules as well as for the introduction of alkyne-functionalized sialic acid derivatives. Applying the newly developed BADS building block in solid phase polymer synthesis, a series of linear and branched precision glycomacromolecules were synthesized by means

of a split-and-combine approach. Here, multiple azide-functionalized oligo(amides) are built up iteratively on solid support, and this approach is divided into two parts prior to functionalization with propargyl-functionalized α-D-mannopyranoside. One part, the so-called backbone, is end capped and serves to later couple the arm. The other part, the so-called arm, is glyco- and end-functionalized, cleaved from the resin and purified before being coupled to the previously separated backbone. The exemplary synthesis of compound 2X2 is shown in **Scheme 7**. In this case a divalent framework is first built up, which after partial functionalization with mannose is coupled twice to the corresponding backbone, so that finally a tetravalent structure is formed. In the second step, this approach allows for a straightforward combination of different backbones and arms.

In the synthesis of the branched glycomacromolecules, it turned out that certain limitations in terms of size and purity must be taken in consideration and thus limit applicability of this approach. While the smallest arm with only one mannose unit per macromolecule could be coupled quantitatively to a trivalent backbone, the divalent arm could only be quantitatively combined with a divalent backbone thus limiting yield and making chromatographic purification necessary. In general, it was found that factors such as the choice of solvent, the number of equivalents used, the concentration of the arms as well as the reaction time tremendously affect conversion, whereas the equivalents of the catalyst used in case of the applied copper-click reaction showed no effect.

The obtained linear and branched glycomacromolecules were then measured for their binding affinities to immobilized Con A in a surface plasmon resonance direct binding assay (**Figure 12**). The obtained results indicate that not only higher valency contributes to higher binding affinities, but also the degree of branching. On a macromolecular scaffold terminal sugars can act most likely free from spatial constriction and shielding, compared to sugars in the midst of a linear, multivalent compound. The introduction of the concept of an effective valence seems meaningful and expedient, which expresses how many sugars are effectively involved in a binding event. Absolutely, the hexavalent molecule 3X2 binds best, in which six mannose units are distributed over three branching arms. Above all, this molecule binds better than compound 2X3, where 6 mannose units are attached to 2 arms. The binding constants normalized to the number of mannoses per molecule are the highest for compounds 2X2 and 3X2, both better than compounds arm3 and 2X3, both molecules with less points of branching. The obtained results are in line with already published results that cautiously perceive the degree of branching at constant valency as enhancing binding strength.[267]
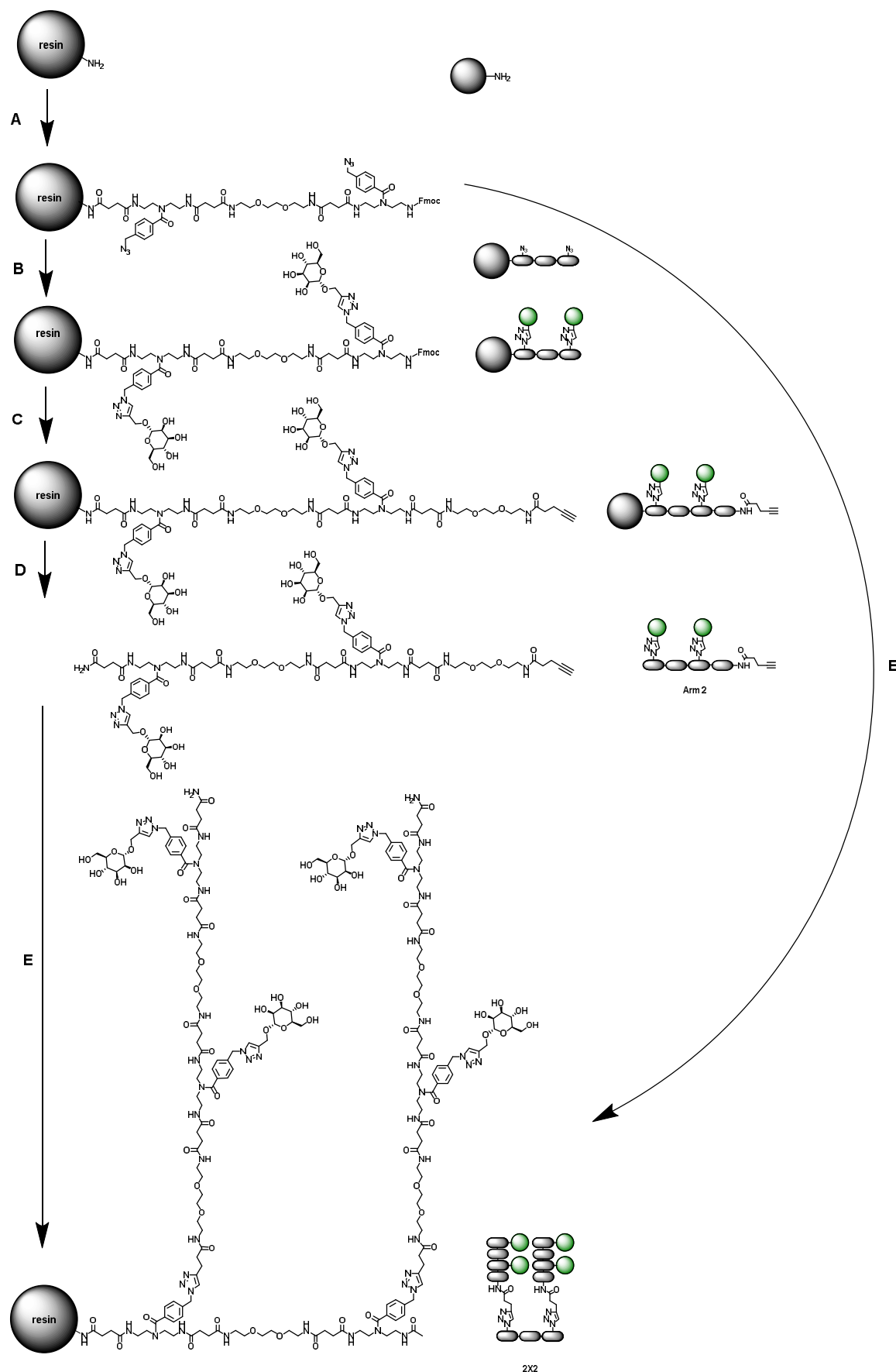
Scheme 7: Exemplary synthesis of compound 2X2 by means of a split & combine approach. **A**: Solid phase peptide synthesis; **B**: Glycofunctionalization via CuAAC; **C**: Endfunctionalization via SPPS; **D**: Cleavage of the arm from solid support; **E**: Combination of backbone and arms via CuAAC on solid support.
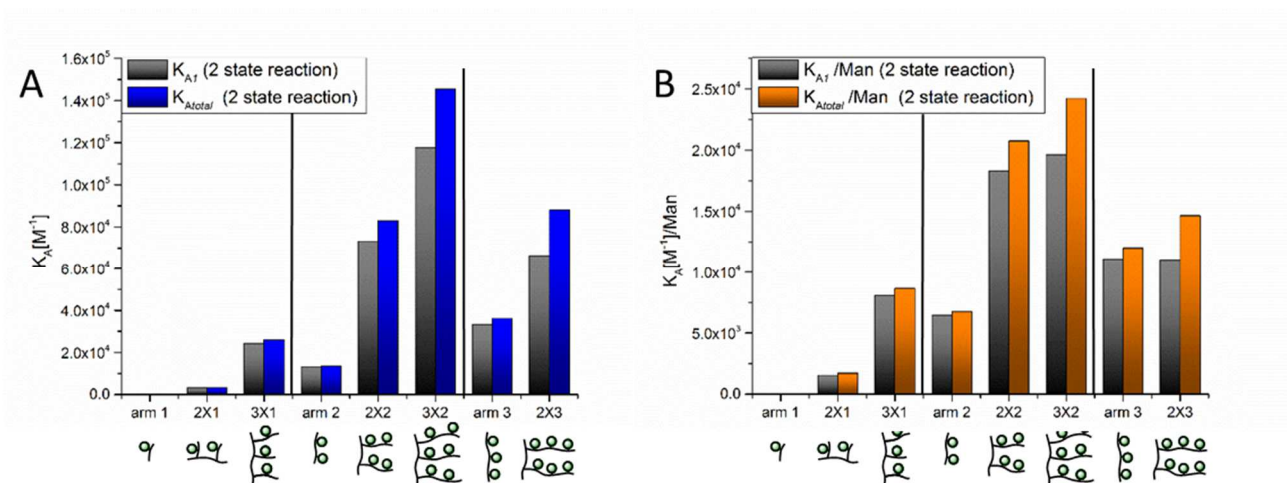
Figure 12: Binding constants obtained from a SPR-direct binding assay with multivalent glycomacromolecules in the mobile phase and immobilized tetrameric receptor protein Con A. (**A**) K_{A1} values (black bars) and K_{Atotal} values (blue bars) obtained from the two-state reaction for all analyzed compounds. (**B**) Mannose normalized K_{A1} values (black bars) and K_{Atotal} values (orange bars) obtained from the two-state reaction for all analyzed compounds. Constructs of higher valency bind multivalently better than constructs of lower valency; constructs with more branches are relatively superior to compound with less branches. Figure taken from Baier *et al., Chem. Eur. J.* **2018**, *24*, 1619-1630.

In a second part of this thesis, the BADS building block as well as its isoform *Iso*BADS were also used to attach glycan fragments onto the oligoamide scaffold. Here, special focus was devoted to sialic acid and 3'-sialyllactose as glycan fragments and previously identified minimal binding epitopes of clinically relevant *Trichodysplasia spinulosa*-associated polyomavirus (TSPyV). TSPyV was first discovered in 2010 and is associated with the occurrence of *Trichodysplasia spinulosa,* a rare skin disease occurring in immunocompromised individuals.[268] TSPyV binds both sialic acid itself in its α-form, as well as 3'- and 6'-sialylated glycans such as 3'-sialyllactose and 6'-sialyllactose.[269] The TSPyV virus capsid consists of 72 VP1 pentamers of which each presents five carbohydrate binding sites that have been shown to undergo multivalent binding. In this work, a first generation of divalent glycomacromolecules targeting VP1 pentamer was synthesized explicitly not looking at maximizing multivalency effects but rather at the structural impact of selectively changing the linker composition and glycan fragment by X-ray crystallography of the ligand-protein complex. Applying solid phase polymer synthesis, four divalent glycooligomers differing in their combination of ligand and linker were synthesized (**Figure 13**).

Two of the macromolecules were synthesized using propargylated sialic acid and differ in the use of different building blocks for coupling of the carbohydrate derivative. One was synthesized using previously discussed BADS and the other with *Iso*BADS, thereby extending the distance to the backbone by one moiety of ethylene. A third macromolecule was synthesized using the established,
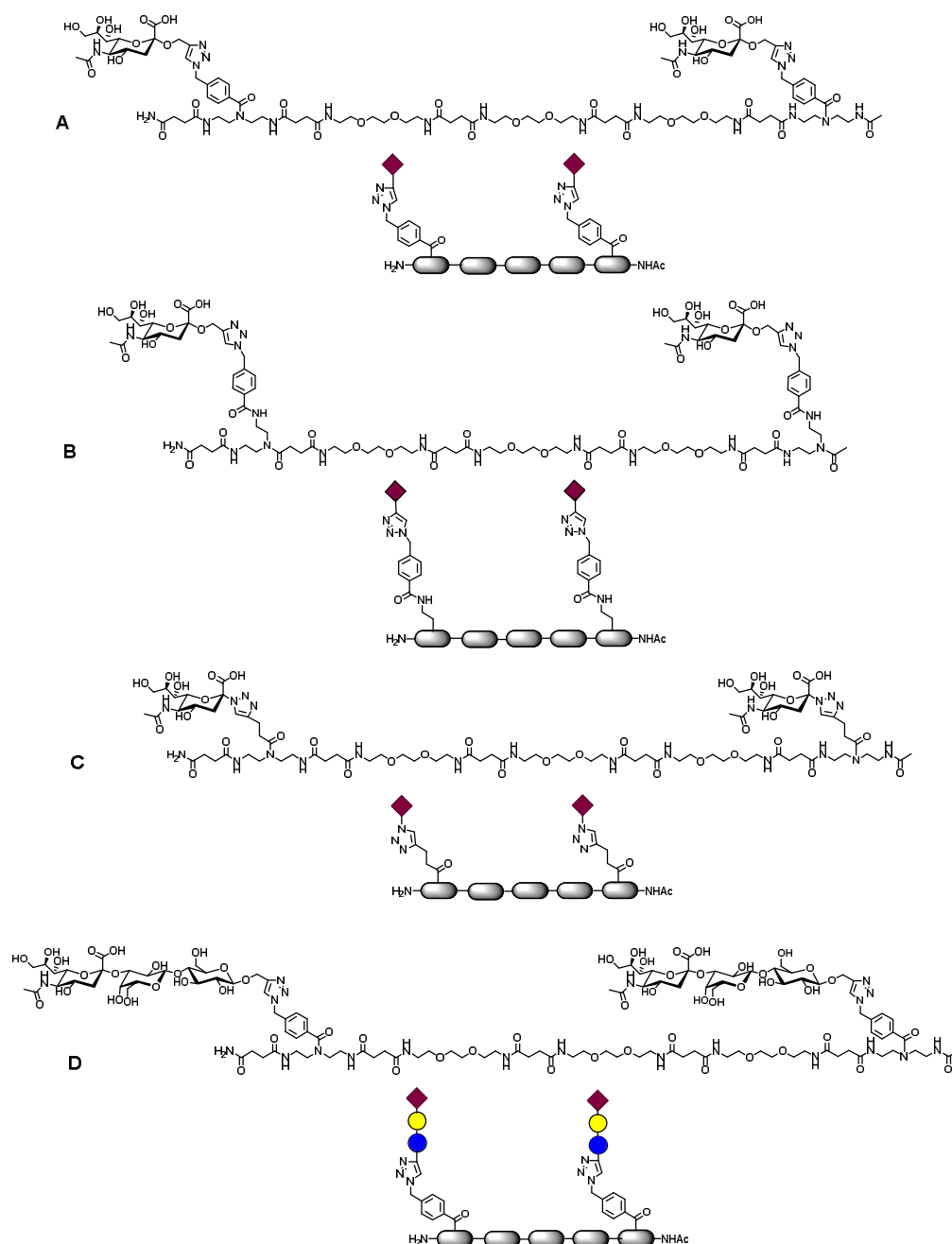
Figure 13: Exemplary structures of sialylated divalent glycooligomers intended for crystal soaking experiments with the VP1 of *Trichodysplasia spinulosa*-associated polyomavirus (TSPyV). **A**: Linker made up of propargylated sialic acid and BADS; **B**: Linker made up of propargylated sialic acid and *Iso*BADS; **C**: Linker made up of azido-sialic acid and TDS; **D**: Two propargylated 3'-SL trisaccharide-residues connected to BADS.

alkyne-displaying building block TDS and complementary, azide-functionalized sialic acid. Since the azide in this, easier to synthesize sialic acid, is connected directly to the anomeric carbon, coupling of the carbohydrate to TDS *via* CuAAC leads to the formation of a 1, 2, 3-triazole, which is directly bound to the sugar. Here, the linker, in comparison to the above-described compound, shortens. Moreover, most likely the whole structure loses flexibility. The last of the four compounds was prepared using the

propargylated 3'-SL derivative and BADS which are both known from previous parts of the work. Combination of the latter results in an artificially linked construct but with the naturally occurring trisaccharide as linker. Single crystal structure analyses of both the propargylated and the azide-carrying sialic acid derivatives were obtained by X-ray diffraction thereby verifying their absolute configuration.

Two of the three molecules studied in crystallization studies provided high-resolution co-crystal structures. These are shown in **Figure 14**. The combination of propargylated sialic acid and BADS provided a crystal structure in which not only the terminal sialic acid could be solved, but also the triazole and phenyl ring-containing linker up to the backbone. This clearly demonstrates the linker being involved in the binding. The second molecule that provided a crystal structure was the 3'-sialyllactose-bearing structure connected to the BADS building block. Here, the entire trisaccharide, but without linker, could be resolved. The glycomacromolecule, which was formed from the combination of azidated sialic acid and TDS, did not give any co-crystal structure. Either the triazole on the sugar is sterically too bulky or too inflexible for occupation of the binding site, alternatively the entire linker is too short for a stable bond. Furthermore, electronic reasons cannot be ruled out since the triazole shifts the electron density of the sugar appreciably. ^{1}H NMR spectra also hint at such effects, where a pronounced downfield shift for both hydrogens at sialic acid-C3 compared to propargylated sialic acid-derivative were observed. The sialic acids carboxylic acid, which is involved in binding to the protein as it can be seen in the crystal structures, thus is likely to change in its electronic properties. All in all, these results clearly indicate that linker in general, but above all the examined artificial ones consisting of 1, 2, 3-triazoles and/or phenyl rings, are able to replace parts of naturally occurring oligosaccharides.

Molecular dynamics (MD) simulations and dynamic light scattering (DLS) experiments revealed distances of the terminal sialic acids of 15-27 Å in the examined glycomacromolecules, which is smaller than the distance between two neighboring sialic acid binding pockets in the investigated TSPyV-VP1 pentamers of 35 Å. Therefore, no multivalent binding for these structures can be expected but based on the findings concerning the role of linker and glycan fragment, higher valent glycomacromolecules can be synthesized in the future and should then also be tested for the affinity towards VP1 e.g. by establishing and performing suitable SPR assays.

In the third part of this thesis, ligands addressing another important non-enveloped virus, the Merkel cell polyomavirus (MCPyV), were developed.[148, 150, 270] MCPyV is a non-enveloped virus related to the occurrence of highly aggressive Merkel cell carcinoma in immunocompromised individuals, in which it was first found in 2008.[153, 271] The virus outer capsid consists of 72 VP1 protein pentamers, each of which exhibits five shallow binding sites for sialylated glycans, notably 3'-sialyllactose.[148, 270] In addition, binding sites for highly sulfated heparin/heparan sulfate lie in the canyons between the VP1 pentamers, thus making the whole capsid a receptor for the latter discussed carbohydrate class, but not for individual VP1.
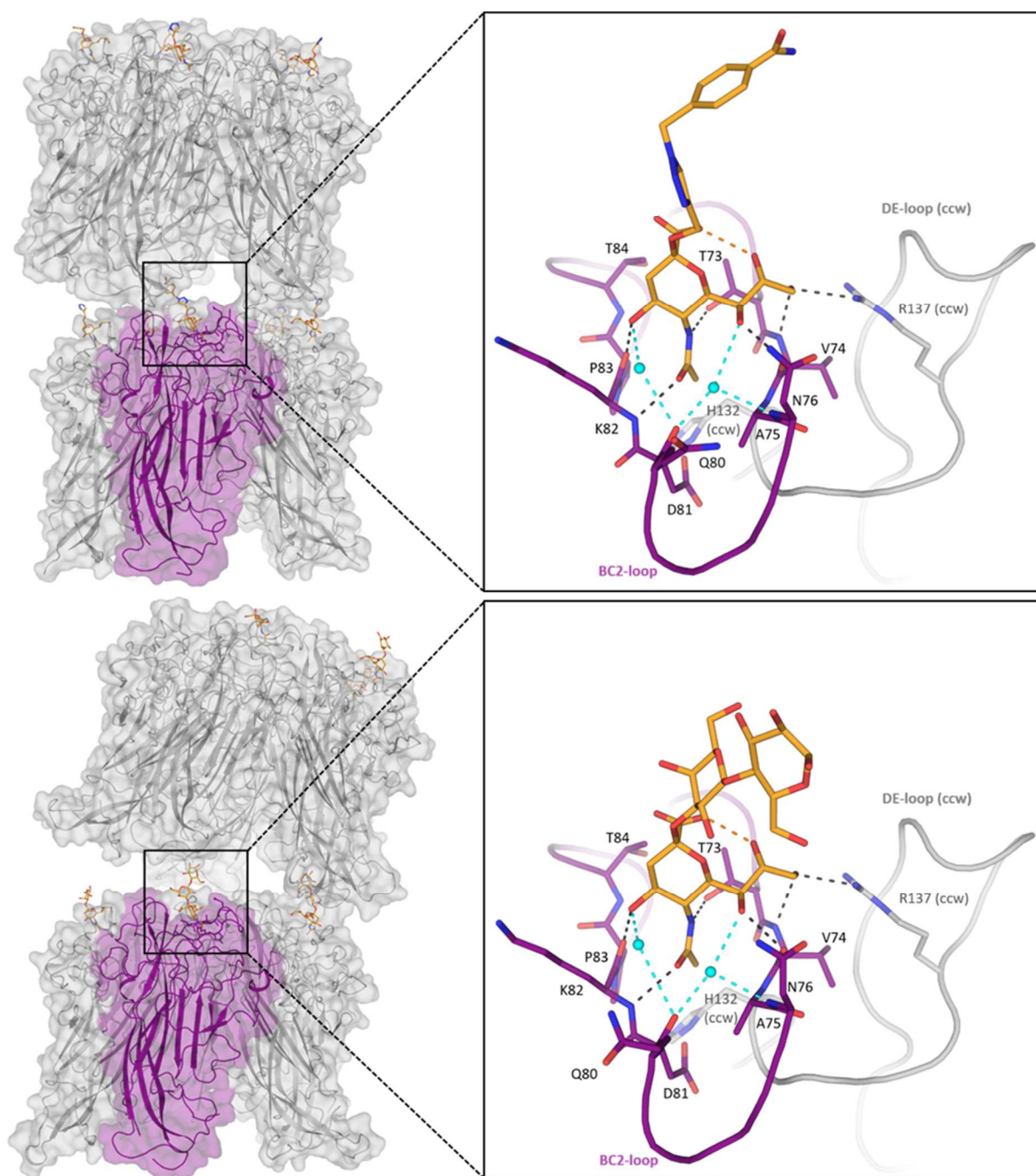
Figure 14: Structure of the glycooligomer - TSPyV VP1 complexes. Models on the top refer to the complexed **O1**, the lower ones to **O4**. Left: The structure of the bound ligand is shown in the context of the crystallographic asymmetric unit, with VP1 depicted in cartoon representation and as a transparent surface, with one chain colored in purple. Glycooligomer moieties are drawn as sticks with carbon atoms colored in orange, nitrogen in blue and oxygen in red. Right: Close-up view of the binding sites. In both cases the Neu5Ac part of the glycooligomer is recognized by residues of the VP1 surface loops BC2 and DE (ccw). Hydrogen bonds, here represented as dashed lines, between the compounds and protein residues are colored in dark grey, between the compounds and water (cyan spheres) in cyan and within the compounds in orange.

Conclusion

These circumstances make the MCPyV generally an excellent model for the study of homo- and heteromultivalent effects.[180, 181, 272, 273] In this work, special focus was devoted to developing strategies to directly attach GAG fragments to the olioamide scaffolds without the need for further functionalization of the glycan fragment prior to conjugation. This is especially relevant for GAG fragments as their site-selective sulfation should be maintained but is known to be instable e.g. under too harsh acidic conditions. Furthermore, for the first time, heteromultivalent constructs covalently linking both GAG fragments and sialic acid ligands were synthesized giving the opportunity to investigate the role of both carbohydrate motifs simultaneously in binding to MCPyV.

For this purpose, the two propargyl-functionalized sialic acid derivatives discussed above were applied, and two heparin fragments were used. The heparin-disaccharide dp2 was obtained *via* enzymatic degradation of heparin provided from a co-worker and the synthetic pentasaccharide Fondaparinux® was chosen. The latter is used postoperatively under the trade name Arixtra® as an anticoagulant.

Three hybrid, structurally defined glycomacromolecules were obtained by coupling previously synthesized, glycosylated as well as non-glycosylated oligo(amidoamines) to heparin fragments in solution-phase. DMTMM was used as the coupling agent, thus allowing for coupling in aqueous mixtures. One of these glycomacromolecules carries two heparin-dp2 fragments connected by an oligo(amidoamine) chain. The other two compounds are composed of Fondaparinux®, to which two free carboxylic acids coupling of sialylated oligo(amidoamines) was achieved. These hybrid structures were obtained in yields of up to 86% and in relative purities of 98% based on integration of spectra from RP-HPLC and SAX-HPLC measurements. Mass spectrometry proved that the sulfates of the heparin fragments do not hydrolyze and remain intact during both the coupling as well as purification protocols. All obtained hybrid glycomacromolecules and their synthesis are shown in **Scheme 8**. Two of them were finally screened using saturation transfer difference NMR (STD NMR) experiments for their ability to bind to the MCPyV outer capsid. The latter has been shown before to bind both the unmodified dp2 fragment as well as Fondaparinux®, and the 3'siallyllactose epitope. For the dp2-functionalized glycomacromolecule, binding of the dp2-fragments to the capsid was shown as well as binding to the exposed 3'-SL epitopes in the 3'-SL bearing construct. In the latter case, however, no binding of the Fondaparinux®-scaffold was observed. A conclusive reason why both sugar classes do not bind simultaneously cannot yet be drawn. Further studies, especially with the help of further binding assays and systematic variation of selected parameters such as linker type and linker length would be required. An important finding is that heparin dp2-fragments seem to be able to bind to the MCPyV capsid when bound to a macromolecular scaffold. Previous studies suggested that only longer GAG fragments can bind in their free form. Furthermore, simple methylation experiments of the Fondaparinux® carboxylic acids and subsequent binding experiments could give insights if these functional groups are required for binding or if the sulfates provide enough affinity.
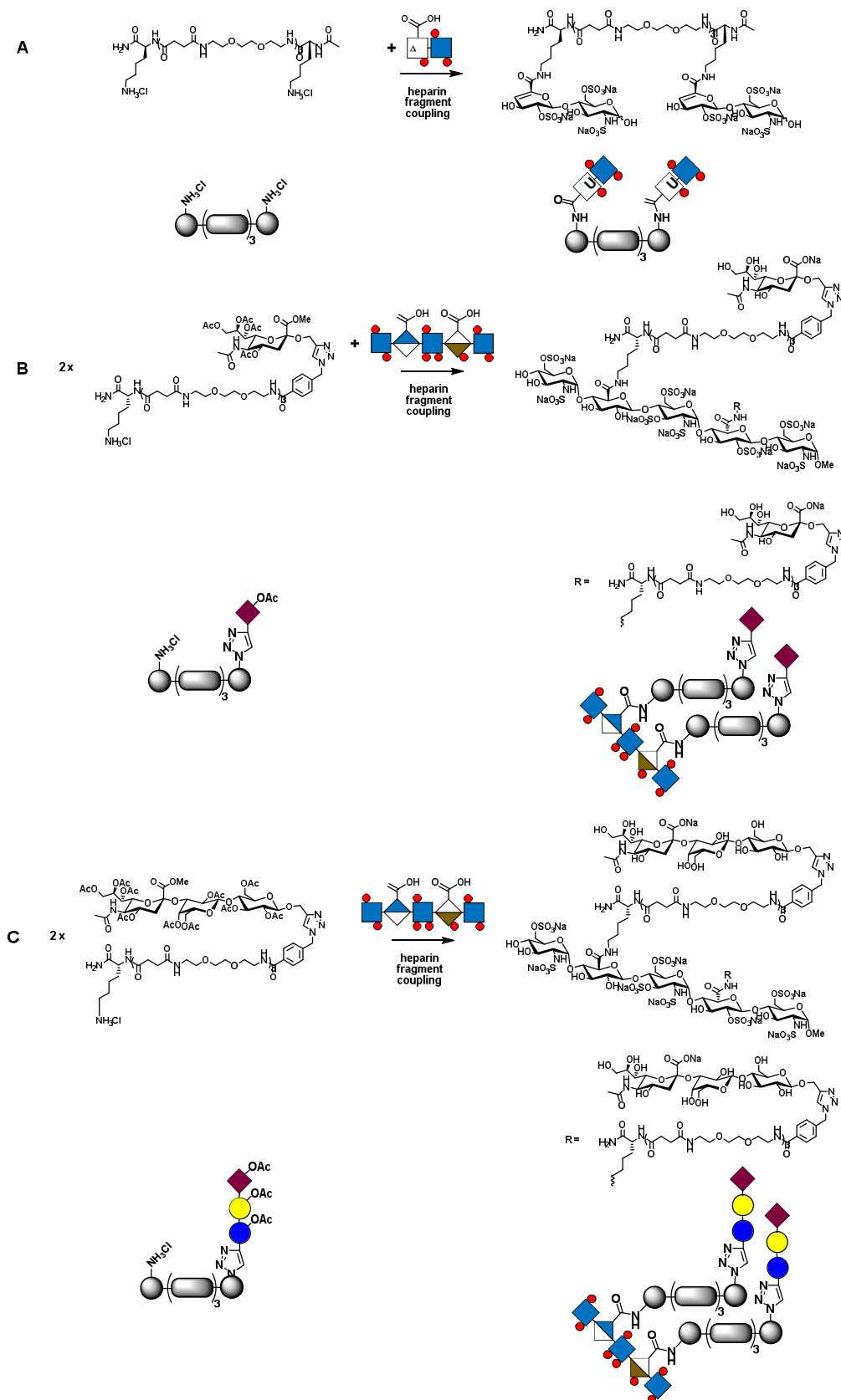
Scheme 8: Exemplary synthesis and structures of hybrid glycomacromolecules made up of oligo(amidoamines), heparin fragments as well as sialic acid or propargylated 3'-sialyllactose. **A**: Two heparin dp2-fragments are connected to a di-lysin-functionalized oligo(amidoamin); **B**: Two sialic acid-functionalized glycooligo(amidoamines) are connected to Fondaparinux®; **C**: Two 3'-SL-functionalized glycooligo(amidoamines) are connected to Fondaparinux®.

Interestingly, the conjugated dp2-fragments bind to the capsid although the carboxylic acid moieties are converted to amides. Co-crystallization experiments potentially would give further insights on how the carbohydrates are involved in the binding event. When both examined compounds are compared, only terminal carbohydrates show binding, whereas Fondaparinux®, in its function as backbone, remains inactive in the STD NMR experiment. Overall, these results would support results from the first part of the thesis, where terminal carbohydrates are believed to participate easier in binding due to less sterical restraints.

Looking at all three parts of this thesis, one lesson learned is that the type of presentation of sugar-ligands is of crucial importance. There are three aspects to be distinguished, all of which make their contribution in this field. First, it matters whether sugars are placed terminally on an oligo(amidoamine) scaffold or in the middle of the construct. Thus, of the investigated branched compounds, those with the most branching bind best. Secondly, the chemical nature of the linker to which a sugar is covalently bound, and which links it to the scaffold plays another important role. Hereby, aromatic linkers have the advantage that, as especially studied for bacterial lectins in detail, they contribute in affinity in secondary binding modes and thus lead to a better binding. This principle could here be applied to viral lectins and, above all, aromatic linkers were able to replace natural linkers consisting of additional sugar units as shown in the case of 3'-silalyllactose. A third finding is that binding sugars, as in the case of the Fondaparinux®, can become non-binding when chemically conjugated, raising the general question of whether ligands can always be attached to a linker without losing binding specificity and/or affinity.

In addition to initial success in the synthesis and evaluation of the aimed molecules towards their potential to bind to virus surface proteins, in future work, well-known concepts should be combined to give the best binding ligands for viruses. One possibility would be the synthesis of branched sialylated oligo(amidoamines) and their use as inhibitors ultimately also *in vitro* and *in vivo* experiments. Additionally, further research is needed to investigate the effect of differently sized GAG fragments on their binding properties when connected to an amidoamine scaffold. A chemically challenging approach would be the attachment of differently sized GAG fragments to oligo(amidoamines). For example, four dp2 fragments on one scaffold could be compared with two dp4 fragments, each consisting of a tetrasaccharide, on another scaffold and both could be compared with a dp8 octasaccharide. In brief, four disaccharides vs. two tetrasaccharides vs. one octasaccharide all of them linked covalently.

Overall this work has demonstrated the use of solid phase polymer synthesis to develop glycomimetic ligands addressing viral lectins. Based on this first generation of glycooligo(amidoamines) ongoing development has the potential to derive high affinity and selective ligands to then act as inhibitors of viral adhesion.

4. References

[1] L. A. Pirofski, A. Casadevall, Q and A: What is a pathogen? A question that begs the point, *BMC Biol.* **2012**, *10*, 6.

[2] A. Aguzzi, M. Nuvolone, C. Zhu, The immunobiology of prion diseases, *Nat. Rev. Immunol.* **2013**, *13*, 888.

[3] B. Chenais, Transposable elements in cancer and other human diseases, *Curr. Cancer Drug Targets* **2015**, *15*, 227-242.

[4] C. Feschotte, The contribution of transposable elements to the evolution of regulatory networks, *Nat. Rev. Genet.* **2008**, *9*, 397-405.

[5] L. Welberg, A protective role for prions, *Nat. Rev. Neurosci.* **2010**, *11*, 151.

[6] M. Muñoz-López, J. L. García-Pérez, DNA Transposons: Nature and Applications in Genomics, *Curr. Genomics* **2010**, *11*, 115-128.

[7] A. Küffer, A. K. K. Lakkaraju, A. Mogha, S. C. Petersen, K. Airich, C. Doucerain, R. Marpakwar, P. Bakirci, A. Senatore, A. Monnard, C. Schiavi, M. Nuvolone, B. Grosshans, S. Hornemann, F. Bassilana, K. R. Monk, A. Aguzzi, The prion protein is an agonistic ligand of the G protein-coupled receptor Adgrg6, *Nature* **2016**, *536*, 464.

[8] J. B. Rayman, E. R. Kandel, Functional Prions in the Brain, *Cold Spring Harb. Perspect. Biol.* **2017**, *9*.

[9] A. J. Wagstaff, D. Faulds, K. L. Goa, Aciclovir. A reappraisal of its antiviral activity, pharmacokinetic properties and therapeutic efficacy, *Drugs* **1994**, *47*, 153-205.

[10] Y.-C. Jiang, H. Feng, Y.-C. Lin, X.-R. Guo, New strategies against drug resistance to herpes simplex virus, *Int. J. Oral Sci.* **2016**, *8*, 1.

[11] C. M. Perry, D. Faulds, Lamivudine. A review of its antiviral activity, pharmacokinetic properties and therapeutic efficacy in the management of HIV infection, *Drugs* **1997**, *53*, 657-680.

[12] T. M. Dando, L. J. Scott, Abacavir plus lamivudine: a review of their combined use in the management of HIV infection, *Drugs* **2005**, *65*, 285-302.

[13] C. J. Dunn, K. L. Goa, Zanamivir: a review of its use in influenza, *Drugs* **1999**, *58*, 761-784.

[14] K. McClellan, C. M. Perry, Oseltamivir: a review of its use in influenza, *Drugs* **2001**, *61*, 263-283.

[15] A. van Kammen, in *100 Years of Virology: The Birth and Growth of a Discipline* (Eds.: C. H. Calisher, M. C. Horzinek), Springer Vienna, Vienna, **1999**, pp. 1-8.

[16] H. Lecoq, [Discovery of the first virus, the tobacco mosaic virus: 1892 or 1898?], *C. R. Acad. Sci. III* **2001**, *324*, 929-933.

[17] A. Rambourg, C. P. Leblond, Electron microscope observations on the carbohydrate-rich cell coat present at the surface of cells in the rat, *J. Cell Biol.* **1967**, *32*, 27-53.

[18] A. Varki, Glycan-based interactions involving vertebrate sialic-acid-recognizing proteins, *Nature* **2007**, *446*, 1023-1029.

[19] J. R. Bishop, M. Schuksz, J. D. Esko, Heparan sulphate proteoglycans fine-tune mammalian physiology, *Nature* **2007**, *446*, 1030-1037.

[20] A. Varki, R. D. Cummings, J. D. Esko, H. H. Freeze, P. Stanley, C. R. Bertozzi, G. W. Hart, M. E. Etzler, in *Essentials of Glycobiology*, Cold Spring Harbor Laboratory Press, Cold Spring Harbor (NY), **2009**.

[21] A. Bernardi, J. Jimenez-Barbero, A. Casnati, C. De Castro, T. Darbre, F. Fieschi, J. Finne, H. Funken, K. E. Jaeger, M. Lahmann, T. K. Lindhorst, M. Marradi, P. Messner, A. Molinaro, P. V. Murphy, C. Nativi, S. Oscarson, S. Penades, F. Peri, R. J. Pieters, O. Renaudet, J. L. Reymond, B. Richichi, J. Rojo, F. Sansone, C. Schaffer, W. B. Turnbull, T. Velasco-Torrijos, S. Vidal, S. Vincent, T. Wennekes, H. Zuilhof, A. Imberty, Multivalent glycoconjugates as anti-pathogenic agents, *Chem. Soc. Rev.* **2013**, *42*, 4709-4727.

[22] K. Ohtsubo, J. D. Marth, Glycosylation in cellular mechanisms of health and disease, *Cell* **2006**, *126*, 855-867.

[23] M. E. Taylor, K. Drickamer, *Introduction to glycobiology*, Oxford university press, **2011**.

[24] J. P. Carver, S. W. Michnick, A. Imberty, D. A. Cumming, Oligosaccharide-protein interactions: a three-dimensional view, *Ciba Found Symp.* **1989**, *145*, 6-18; discussion 18-26.

[25] E. S. Barton, J. L. Connolly, J. C. Forrest, J. D. Chappell, T. S. Dermody, Utilization of sialic acid as a coreceptor enhances reovirus attachment by multistep adhesion strengthening, *J. Biol. Chem.* **2001**, *276*, 2200-2211.

[26] L. L. Kiessling, T. Young, T. D. Gruber, K. H. Mortell, in *Glycoscience: Chemistry and Chemical Biology* (Eds.: B. O. Fraser-Reid, K. Tatsuta, J. Thiem), Springer Berlin Heidelberg, Berlin, Heidelberg, **2008**, pp. 2483-2523.

[27] K. Drickamer, M. E. Taylor, Identification of lectins from genomic sequence data, *Methods Enzymol.* **2003**, *362*, 560-567.

[28] N. Sharon, H. Lis, History of lectins: from hemagglutinins to biological recognition molecules, *Glycobiology* **2004**, *14*, 53r-62r.

[29] J. E. Stencel-Baerenwald, K. Reiss, D. M. Reiter, T. Stehle, T. S. Dermody, The sweet spot: defining virus–sialic acid interactions, *Nat. Rev. Microbiol.* **2014**, *12*, 739-749.

[30] T. Stehle, Z. M. Khan, Rules and exceptions: sialic acid variants and their role in determining viral tropism, *J. Virol.* **2014**, *88*, 7696-7699.

[31] B. R. Wasik, K. N. Barnard, C. R. Parrish, Effects of Sialic Acid Modifications on Virus Binding and Infection, *Trends Microbiol.* **2016**, *24*, 991-1001.

[32] G. Rogers, J. Paulson, R. Daniels, J. Skehel, I. Wilson, D. Wiley, Single amino acid substitutions in influenza haemagglutinin change receptor binding specificity, *Nature* **1983**, *304*, 76.

[33] J. D. Chappell, V. L. Gunn, J. D. Wetzel, G. S. Baer, T. S. Dermody, Mutations in type 3 reovirus that determine binding to sialic acid are contained in the fibrous tail domain of viral attachment protein sigma1, *J. Virol.* **1997**, *71*, 1834-1841.

[34] J. D. Chappell, J. L. Duong, B. W. Wright, T. S. Dermody, Identification of Carbohydrate-Binding Domains in the Attachment Proteins of Type 1 and Type 3 Reoviruses, *J. Virol.* **2000**, *74*, 8472-8479.

[35] B. Tsai, J. M. Gilbert, T. Stehle, W. Lencer, T. L. Benjamin, T. A. Rapoport, Gangliosides are receptors for murine polyoma virus and SV40, *Embo J.* **2003**, *22*, 4346-4355.

[36] U. Neu, J. Bauer, T. Stehle, Viruses and sialic acids: rules of engagement, *Curr. Opin. Virol.* **2011**, *21*, 610-618.

[37] C. L. Gardner, G. D. Ebel, K. D. Ryman, W. B. Klimstra, Heparan sulfate binding by natural eastern equine encephalitis viruses promotes neurovirulence, *Proc. Natl. Acad. Sci. U.S.A.* **2011**, *108*, 16026-16031.

[38] V. Tiwari, E. Maus, I. M. Sigar, K. H. Ramsey, D. Shukla, Role of heparan sulfate in sexually transmitted infections, *Glycobiology* **2012**, *22*, 1402-1412.

[39] C. L. Gardner, J. Choi-Nurvitadhi, C. Sun, A. Bayer, J. Hritz, K. D. Ryman, W. B. Klimstra, Natural variation in the heparan sulfate binding domain of the eastern equine encephalitis virus E2 glycoprotein alters interactions with cell surfaces and virulence in mice, *J. Virol.* **2013**, *87*, 8582-8590.

[40] L. A. Silva, S. Khomandiak, A. W. Ashbrook, R. Weller, M. T. Heise, T. E. Morrison, T. S. Dermody, A single-amino-acid polymorphism in Chikungunya virus E2 glycoprotein influences glycosaminoglycan utilization, *J. Virol.* **2014**, *88*, 2385-2397.

[41] L. Hu, S. E. Crawford, R. Czako, N. W. Cortes-Penfield, D. F. Smith, J. Le Pendu, M. K. Estes, B. V. Prasad, Cell attachment protein VP8* of a human rotavirus specifically interacts with A-type histo-blood group antigen, *Nature* **2012**, *485*, 256-259.

[42] Y. Liu, P. Huang, B. Jiang, M. Tan, A. L. Morrow, X. Jiang, Poly-LacNAc as an Age-Specific Ligand for Rotavirus P[11] in Neonates and Infants, *PLoS One* **2013**, *8*, e78113.

[43] A. Varki, Diversity in the sialic acids, *Glycobiology* **1992**, *2*, 25-40.

[44] C. Traving, R. Schauer, Structure, function and metabolism of sialic acids, *Cell Mol. Life Sci.* **1998**, *54*, 1330-1349.

[45] U. Rutishauser, Polysialic acid at the cell surface: Biophysics in service of cell interactions and tissue plasticity, *J. Cell. Biochem.* **1998**, *70*, 304-312.

[46] B. E. Collins, O. Blixt, A. R. DeSieno, N. Bovin, J. D. Marth, J. C. Paulson, Masking of CD22 by cis ligands does not prevent redistribution of CD22 to sites of cell contact, *Proc. Natl. Acad. Sci. U.S.A.* **2004**, *101*, 6104-6109.

[47] B. Byrne, G. G. Donohoe, R. O'Kennedy, Sialic acids: carbohydrate moieties that influence the biological and physical properties of biopharmaceutical proteins and living cells, *Drug Discov. Today* **2007**, *12*, 319-326.

[48] L. Svennerholm, Interaction of cholera toxin and ganglioside G(M1), *Adv. Exp. Med. Biol.* **1976**, *71*, 191-204.

[49] G. N. Rogers, T. J. Pritchett, J. L. Lane, J. C. Paulson, Differential sensitivity of human, avian, and equine influenza A viruses to a glycoprotein inhibitor of infection: selection of receptor specific variants, *Virol.* **1983**, *131*, 394-408.

[50] M. J. Kiefel, M. von Itzstein, Recent advances in the synthesis of sialic acid derivatives and sialylmimetics as biological probes, *Chem. Rev.* **2002**, *102*, 471-490.

[51] K. Reiss, J. E. Stencel, Y. Liu, B. S. Blaum, D. M. Reiter, T. Feizi, T. S. Dermody, T. Stehle, The GM2 Glycan Serves as a Functional Coreceptor for Serotype 1 Reovirus, *PLoS Pathog.* **2012**, *8*, e1003078.

[52] C. R. Bertozzi, Kiessling, L. L., Chemical Glycobiology, *Science* **2001**, *291*, 2357-2364.

[53] M. Schwarzkopf, K.-P. Knobeloch, E. Rohde, S. Hinderlich, N. Wiechens, L. Lucka, I. Horak, W. Reutter, R. Horstkorte, Sialylation is essential for early development in mice, *Proc. Natl. Acad. Sci. U.S.A.* **2002**, *99*, 5267-5270.

[54] M. Thaysen-Andersen, M. R. Larsen, N. H. Packer, G. Palmisano, Structural analysis of glycoprotein sialylation - Part I: pre-LC-MS analytical strategies, *RSC Adv.* **2013**, *3*, 22683-22705.

[55] R. Schauer, Achievements and challenges of sialic acid research, *Glycoconj. J.* **2000**, *17*, 485-499.

[56] T. Angata, A. Varki, Chemical Diversity in the Sialic Acids and Related α-Keto Acids: An Evolutionary Perspective, *Chem. Rev.* **2002**, *102*, 439-470.

[57] A. Harduin-Lepers, R. Mollicone, P. Delannoy, R. Oriol, *The animal sialyltransferases and sialyltransferase-related genes: A phylogenetic approach, Vol. 15*, **2005**.

[58] R. K. Yu, Y. T. Tsai, T. Ariga, M. Yanagisawa, Structures, biosynthesis, and functions of gangliosides--an overview, *J. Oleo. Sci.* **2011**, *60*, 537-544.

[59] J. Roth, C. Zuber, P. Wagner, D. J. Taatjes, C. Weisgerber, P. U. Heitz, C. Goridis, D. Bitter-Suermann, Reexpression of poly(sialic acid) units of the neural cell adhesion molecule in Wilms tumor, *Proc. Natl. Acad. Sci. U.S.A.* **1988**, *85*, 2999-3003.

[60] H. Hildebrandt, C. Becker, S. Gluer, H. Rosner, R. Gerardy-Schahn, H. Rahmann, Polysialic acid on the neural cell adhesion molecule correlates with expression of polysialyltransferases and promotes neuroblastoma cell growth, *Cancer Res.* **1998**, *58*, 779-784.

[61] M. Mühlenhoff, M. Eckhardt, R. Gerardy-Schahn, Polysialic acid: three-dimensional structure, biosynthesis and function, *Current Opinion in Structural Biology* **1998**, *8*, 558-564.

[62] R. Seidenfaden, A. Krauter, F. Schertzinger, R. Gerardy-Schahn, H. Hildebrandt, Polysialic Acid Directs Tumor Cell Growth by Controlling Heterophilic Neural Cell Adhesion Molecule Interactions, *Mol. Cell. Biol.* **2003**, *23*, 5908-5918.

[63] C. Sato, K. Kitajima, Disialic, oligosialic and polysialic acids: distribution, functions and related disease, *J. Biochem.* **2013**, *154*, 115-136.

[64] X. Chen, A. Varki, Advances in the Biology and Chemistry of Sialic Acids, *ACS Chem. Biol.* **2010**, *5*, 163-176.

[65] H. Ogura, A. Hasegawa, *Carbohydrates: synthetic methods and applications in medicinal chemistry*, Wiley-VCH, **1992**.

[66] S. Ogawa, Z. Witczak, K. Nieforth, *Carbohydrates in Drug Design*, Dekker: New York, **1997**.

[67] M. P. Deninno, The synthesis and glycosidation of N-acetylneuraminic acid, *Synthesis* **1991**, *1991*, 583-593.

[68] A. Varki, Biological roles of oligosaccharides: all of the theories are correct, *Glycobiology* **1993**, *3*, 97-130.

[69] R. Schauer, S. Kelm, G. Reuter, P. Roggentin, L. Shaw, in *Biology of the sialic acids*, Springer, **1995**, pp. 7-67.

[70] G. J. Boons, A. V. Demchenko, Recent advances in o-sialylation, *Chem. Rev.* **2000**, *100*, 4539-4566.

[71] T. J. Martin, R. R. Schmidt, Efficient sialylation with phosphite as leaving group, *Tetrahedron Lett.* **1992**, *33*, 6123-6126.

[72] H. Kondo, Y. Ichikawa, C. H. Wong, .beta.-Sialyl phosphite and phosphoramidite: synthesis and application to the chemoenzymic synthesis of CMP-sialic acid and sialyl oligosaccharides, *J. Am. Chem. Soc* **1992**, *114*, 8748-8750.

[73] U. Greilich, R. Brescello, K. H. Jung, R. R. Schmidt, Glycosyl Imidates, 74. Synthesis of Ganglioside GM1 via a GM3 Intermediate, *Liebigs Ann.* **1996**, *1996*, 663-672.

[74] V. Martichonok, G. M. Whitesides, Stereoselective α-Sialylation with Sialyl Xanthate and Phenylsulfenyl Triflate as a Promotor, *J. Org. Chem.* **1996**, *61*, 1702-1706.

[75] O. Kanie, M. Kiso, A. Hasegawa, Glycosylation using methylthioglycosides of N-acetylneuraminic acid and dimethyl (methylthio) sulfonium triflate, *J. Carbohyd. Chem.* **1988**, *7*, 501-506.

[76] P. Kováč, *Synthetic Oligosaccharides: Indispensable Probes for the Life Sciences*, ACS Publications, **1994**.

[77] M. Weiwer, C. C. Chen, M. M. Kemp, R. J. Linhardt, Synthesis and Biological Evaluation of Non-Hydrolyzable 1,2,3-Triazole-Linked Sialic Acid Derivatives as Neuraminidase Inhibitors, *Eur. J. Org. Chem.* **2009**, 2611-2620.

[78] R. Šardzík, G. T. Noble, M. J. Weissenborn, A. Martin, S. J. Webb, S. L. Flitsch, Preparation of aminoethyl glycosides for glycoconjugation, *Beilstein J. Org. Chem.* **2010**, *6*, 699-703.

[79] J. M. Haberman, D. Y. Gin, A new C (1)-auxiliary for anomeric stereocontrol in the synthesis of α-sialyl glycosides, *Org. Lett.* **2001**, *3*, 1665-1668.

[80] X.-S. Ye, X. Huang, C.-H. Wong, Conversion of the carboxy group of sialic acid donors to a protected hydroxymethyl group yields an efficient reagent for the synthesis of the unnatural beta-linkage, *Chem. Commun.* **2001**, 974-975.

[81] R. Caraballo, M. Saleeb, J. Bauer, A. M. Liaci, N. Chandra, R. J. Storm, L. Frangsmyr, W. X. Qian, T. Stehle, N. Arnberg, M. Elofsson, Triazole linker-based trivalent sialic acid inhibitors of adenovirus type 37 infection of human corneal epithelial cells, *Org. Biomol. Chem.* **2015**, *13*, 9194-9205.

[82] Y. Suzuki, K. Sato, M. Kiso, A. Hasegawa, New ganglioside analogs that inhibit influenze virus sialidase, *Glycoconj. J.* **1990**, *7*, 349-356.

[83] F. D. Tropper, F. O. Andersson, S. Braun, R. Roy, Phase Transfer Catalysis as a General and Stereoselective Entry into Glycosyl Azides from Glycosyl Halides, *Synthesis* **1992**, 618-620.

[84] M. Llinares, R. Roy, Multivalent neoglycoconjugates: solid-phase synthesis of N-linked alpha-sialodendrimers, *Chem. Commun.* **1997**, 2119-2120.

[85] W. Michel, C. Chi-Chang, K. M. M., L. R. J., Synthesis and Biological Evaluation of Non-Hydrolyzable 1,2,3-Triazole-Linked Sialic Acid Derivatives as Neuraminidase Inhibitors, *Eur. J. Org. Chem.* **2009**, *2009*, 2611-2620.

[86] F. Amblard, J. H. Cho, R. F. Schinazi, The Cu(I)-catalyzed Huisgen azide-alkyne 1,3-dipolar cycloaddition reaction in nucleoside, nucleotide and oligonucleotide chemistry, *Chem. Rev.* **2009**, *109*, 4207-4220.

[87] H. C. Kolb, M. G. Finn, K. B. Sharpless, Click-Chemie: diverse chemische Funktionalität mit einer Handvoll guter Reaktionen, *Angew. Chem.* **2001**, *113*, 2056-2075.

[88] H. C. Kolb, M. G. Finn, K. B. Sharpless, Click Chemistry: Diverse Chemical Function from a Few Good Reactions, *Angew. Chem. Int. Ed.* **2001**, *40*, 2004-2021.

[89] W. Tang, M. L. Becker, "Click" reactions: a versatile toolbox for the synthesis of peptide-conjugates, *Chem. Soc. Rev.* **2014**, *43*, 7013-7039.

[90] D. Lim, M. A. Brimble, R. Kowalczyk, A. J. Watson, A. J. Fairbanks, Protecting-Group-Free One-Pot Synthesis of Glycoconjugates Directly from Reducing Sugars, *Angew. Chem. Int. Edit.* **2014**, *126*, 12101-12105.

[91] R. Huisgen, G. Szeimies, L. Möbius, 1.3-Dipolare Cycloadditionen, XXXII. Kinetik der Additionen organischer Azide an CC-Mehrfachbindungen, *Eur. J. Inorg. Chem.* **1967**, *100*, 2494-2507.

[92] A. Padwa, 1, 3-Dipolar cycloaddition chemistry, *New York* **1984**.

[93] R. Huisgen, Kinetics and reaction mechanisms: selected examples from the experience of forty years, *Pure Appl. Chem.* **1989**, *61*, 613-628.

[94] V. V. Rostovtsev, L. G. Green, V. V. Fokin, K. B. Sharpless, A stepwise huisgen cycloaddition process: copper (I)-catalyzed regioselective "ligation" of azides and terminal alkynes, *Angew. Chem.* **2002**, *114*, 2708-2711.

[95] Z.-J. Zheng, D. Wang, Z. Xu, L.-W. Xu, Synthesis of bi- and bis-1,2,3-triazoles by copper-catalyzed Huisgen cycloaddition: A family of valuable products by click chemistry, *Beilstein J. Org. Chem.* **2015**, *11*, 2557-2576.

[96] N. E. Mbua, J. Guo, M. A. Wolfert, R. Steet, G.-J. Boons, Strain-Promoted Alkyne-Azide Cycloadditions (SPAAC) Reveal New Features of Glycoconjugate Biosynthesis, *ChemBioChem* **2011**, *12*, 1912-1921.

[97] J. D. Thomas, H. Cui, P. J. North, T. Hofer, C. Rader, T. R. Burke, Application of Strain-Promoted Azide-Alkyne Cycloaddition and Tetrazine Ligation to Targeted Fc-Drug Conjugates, *Bioconjug. Chem.* **2012**, *23*, 2007-2013.

[98] J. Dommerholt, F. P. J. T. Rutjes, F. L. van Delft, Strain-Promoted 1,3-Dipolar Cycloaddition of Cycloalkynes and Organic Azides, *Top. Curr. Chem.* **2016**, *374*, 16.

[99] M. Kohn, R. Breinbauer, The Staudinger ligation-a gift to chemical biology, *Angew. Chem. Int. Ed.* **2004**, *43*, 3106-3116.

[100] F. L. Lin, H. M. Hoyt, H. van Halbeek, R. G. Bergman, C. R. Bertozzi, Mechanistic Investigation of the Staudinger Ligation, *J. Am. Chem. Soc.* **2005**, *127*, 2686-2695.

[101] C. I. Schilling, N. Jung, M. Biskup, U. Schepers, S. Brase, Bioconjugation via azide-Staudinger ligation: an overview, *Chem. Soc. Rev.* **2011**, *40*, 4840-4871.

[102] S. S. van Berkel, M. B. van Eldijk, J. C. van Hest, Staudinger ligation as a method for bioconjugation, *Angew. Chem. Int. Ed.* **2011**, *50*, 8806-8827.

[103] C. E. Hoyle, C. N. Bowman, Thiol–Ene Click Chemistry, *Angew. Chem. Int. Ed.* **2010**, *49*, 1540-1573.

[104] A. B. Lowe, Thiol-ene "click" reactions and recent applications in polymer and materials synthesis: a first update, *Polym. Chem.* **2014**, *5*, 4820-4870.

[105] D. P. Nair, M. Podgórski, S. Chatani, T. Gong, W. Xi, C. R. Fenoli, C. N. Bowman, The Thiol-Michael Addition Click Reaction: A Powerful and Widely Used Tool in Materials Chemistry, *Chem Mater.* **2014**, *26*, 724-744.

[106] P. M. Kharkar, M. S. Rehmann, K. M. Skeens, E. Maverakis, A. M. Kloxin, Thiol–ene click hydrogels for therapeutic delivery, *ACS Biomater. Sci. Eng.* **2016**, *2*, 165-179.

[107] A. B. Lowe, C. E. Hoyle, C. N. Bowman, Thiol-yne click chemistry: A powerful and versatile methodology for materials synthesis, *Journ. Mat. Chem.* **2010**, *20*, 4745-4750.

[108] A. B. Lowe, Thiol-yne 'click'/coupling chemistry and recent applications in polymer and materials synthesis and modification, *Polymer* **2014**, *55*, 5517-5549.

[109] L. J. Macdougall, V. X. Truong, A. P. Dove, Efficient In Situ Nucleophilic Thiol-yne Click Chemistry for the Synthesis of Strong Hydrogel Materials with Tunable Properties, *ACS Macro Lett.* **2017**, *6*, 93-97.

[110] A. Dirksen, P. E. Dawson, Rapid Oxime and Hydrazone Ligations with Aromatic Aldehydes for Biomolecular Labeling, *Bioconjug. Chem.* **2008**, *19*, 2543-2548.

[111] U. Sébastien, B. Didier, M. Alberto, R. Olivier, D. Pascal, Oxime Ligation: A Chemoselective Click-Type Reaction for Accessing Multifunctional Biomolecular Constructs, *Chem. Eur. J.* **2014**, *20*, 34-41.

[112] F. Damien, B. Didier, D. Eric, L. Jean, D. Pascal, Highly Efficient Synthesis of Peptide–Oligonucleotide Conjugates: Chemoselective Oxime and Thiazolidine Formation, *Chem. Eur. J.* **2001**, *7*, 3976-3984.

[113] E. C. B. Johnson, S. B. H. Kent, Insights into the Mechanism and Catalysis of the Native Chemical Ligation Reaction, *J. Am. Chem. Soc.* **2006**, *128*, 6640-6646.

[114] C. S. McKay, M. G. Finn, Click Chemistry in Complex Mixtures: Bioorthogonal Bioconjugation, *Chem. Biol.* **2014**, *21*, 1075-1101.

[115] M. A. Tasdelen, Diels-Alder "click" reactions: recent applications in polymer and material science, *Polym. Chem.* **2011**, *2*, 2133-2145.

[116] C. M. Nimmo, S. C. Owen, M. S. Shoichet, Diels−Alder Click Cross-Linked Hyaluronic Acid Hydrogels for Tissue Engineering, *Biomacromolecules* **2011**, *12*, 824-830.

[117] T. Reiner, B. M. Zeglis, The inverse electron demand Diels-Alder click reaction in radiochemistry, *J. Labelled. Comp. Radiopharm.* **2014**, *57*, 285-290.

[118] M. Gregoritza, F. P. Brandl, The Diels-Alder reaction: A powerful tool for the design of drug delivery systems and biomaterials, *Eur. J. Pharm. Biopharm.* **2015**, *97*, 438-453.

[119] C. C. Griffin, R. J. Linhardt, C. L. Van Gorp, T. Toida, R. E. Hileman, R. L. Schubert, 2nd, S. E. Brown, Isolation and characterization of heparan sulfate from crude porcine intestinal mucosal peptidoglycan heparin, *Carbohydr. Res.* **1995**, *276*, 183-197.

[120] B. Casu, A. Naggi, G. Torri, Re-visiting the structure of heparin, *Carbohydr. Res.* **2015**, *403*, 60-68.

[121] W. D. Comper, *Heparin (and Related Polysaccharides): Structural and Functional Properties, Vol. 7*, Gordon & Breach Publishing Group, **1981**.

[122] B. Casu, Structure and biological activity of heparin, *Adv. Carbohydr. Chem. Biochem.* **1985**, *43*, 51-134.

[123] J. A. Marcum, William Henry Howell and Jay McLean: the experimental context for the discovery of heparin, *Perspect. Biol. Med.* **1990**, *33*, 214-230.

[124] I. Capila, R. J. Linhardt, Heparin - Protein interactions, *Ang. Chem. Int. Ed.* **2002**, *41*, 391-412.

[125] J. T. Gallagher, J. E. Turnbull, M. Lyon, Heparan sulphate proteoglycans: molecular organisation of membrane--associated species and an approach to polysaccharide sequence analysis, *Adv. Exp. Med. Biol.* **1992**, *313*, 49-57.

[126] J. D. Esko, S. B. Selleck, Order out of chaos: assembly of ligand binding sites in heparan sulfate, *Annu. Rev. Biochem.* **2002**, *71*, 435-471.

[127] B. Casu, Heparin structure, *Haemost.* **1990**, *20 Suppl 1*, 62-73.

[128] B. Mulloy, R. J. Linhardt, Order out of complexity--protein structures that interact with heparin, *Curr. Opin. Struct. Biol.* **2001**, *11*, 623-628.

[129] C. I. Gama, S. E. Tully, N. Sotogaku, P. M. Clark, M. Rawat, N. Vaidehi, W. A. Goddard, A. Nishi, L. C. Hsieh-Wilson, Sulfation patterns of glycosaminoglycans encode molecular recognition and activity, *Nature Chem. Biol.* **2006**, *2*, 467-473.

[130] M. Bernfield, M. Gotte, P. W. Park, O. Reizes, M. L. Fitzgerald, J. Lincecum, M. Zako, Functions of cell surface heparan sulfate proteoglycans, *Annu. Rev. Biochem.* **1999**, *68*, 729-777.

[131] R. D. Rosenberg, P. S. Damus, The purification and mechanism of action of human antithrombin-heparin cofactor, *J. Biol. Chem.* **1973**, *248*, 6490-6505.

[132] J. Huntington, Mechanisms of glycosaminoglycan activation of the serpins in hemostasis, *J. Thromb. Haemost.* **2003**, *1*, 1535-1549.

[133] J. Choay, M. Petitou, J. C. Lormeau, P. Sinaÿ, B. Casu, G. Gatti, Structure-activity relationship in heparin: A synthetic pentasaccharide with high affinity for antithrombin III and eliciting high anti-factor Xa activity, *Biochem. Biophys. Res. Commun.* **1983**, *116*, 492-499.

[134] K. A. Bauer, D. W. Hawkins, P. C. Peters, M. Petitou, J.-M. Herbert, C. A. A. van Boeckel, D. G. Meuleman, Fondaparinux, a Synthetic Pentasaccharide: The First in a New Class of Antithrombotic Agents — The Selective Factor Xa Inhibitors, *Cardiovasc. Drug Rev.* **2002**, *20*, 37-52.

[135] H. Bounameaux, T. Perneger, Fondaparinux: a new synthetic pentasaccharide for thrombosis prevention, *Lancet* **2002**, *359*, 1710-1711.

[136] M. Petitou, P. Duchaussoy, J.-M. Herbert, G. Duc, M. El Hajji, J.-F. Branellec, F. Donat, J. Necciari, R. Cariou, J. Bouthier, E. Garrigou, The Synthetic Pentasaccharide Fondaparinux: First in the Class of Antithrombotic Agents that Selectively Inhibit Coagulation Factor Xa, *Semin. Thromb. Hemost.* **2002**, *28*, 393-402.

[137] J. M. Walenga, W. P. Jeske, F. X. Frapaise, R. L. Bick, J. Fareed, M. M. Samama, Fondaparinux: a synthetic heparin pentasaccharide as a new antithrombotic agent, *Expert Opin. Investig. Drugs* **2002**, *11*, 397-407.

[138] R. S. Aquino, P. W. Park, Glycosaminoglycans and infection, *Front. Biosci.* **2016**, *21*, 1260-1277.

[139] R. R. Dinglasan, M. Jacobs-Lorena, Insight into a Conserved Lifestyle: Protein-Carbohydrate Adhesion Strategies of Vector-Borne Pathogens, *Infect. Immun.* **2005**, *73*, 7797-7807.

[140] J. Akhtar, D. Shukla, Viral entry mechanisms: cellular and viral mediators of herpes simplex virus entry, *FEBS J.* **2009**, *276*, 7228-7236.

[141] D. S. Newburg, R. J. Linhardt, S. A. Ampofo, R. H. Yolken, Human milk glycosaminoglycans inhibit HIV glycoprotein gp120 binding to its host cell CD4 receptor, *J. Nutr.* **1995**, *125*, 419-424.

[142] C. C. Rider, The potential for heparin and its derivatives in the therapy and prevention of HIV-1 infection, *Glycoconjugate J.* **1997**, *14*, 639-642.

[143] C. C. Rider, D. R. Coombe, H. A. Harrop, E. F. Hounsell, C. Bauer, J. Feeney, B. Mulloy, N. Mahmood, A. Hay, C. R. Parish, Anti-HIV-1 activity of chemically modified heparins: correlation between binding to the V3 loop of gp120 and inhibition of cellular HIV-1 infection in vitro, *Biochemistry* **1994**, *33*, 6974-6980.

[144] M. Rusnati, G. Tulipano, D. Spillmann, E. Tanghetti, P. Oreste, G. Zoppetti, M. Giacca, M. Presta, Multiple interactions of HIV-I Tat protein with size-defined heparin oligosaccharides, *J. Biol. Chem.* **1999**, *274*, 28198-28205.

[145] Y. Chen, T. Maguire, R. E. Hileman, J. R. Fromm, J. D. Esko, R. J. Linhardt, R. M. Marks, Dengue virus infectivity depends on envelope protein binding to target cell heparan sulfate, *Nat. Med.* **1997**, *3*, 866-871.

[146] C. Cerqueira, Y. Liu, L. Kuhling, W. G. Chai, W. Hafezi, T. H. van Kuppevelt, J. E. Kuhn, T. Feizi, M. Schelhaas, Heparin increases the infectivity of Human Papillomavirus Type 16 independent of cell surface proteoglycans and induces L1 epitope exposure, *Cell. Microbiol.* **2013**, *15*, 1818-1836.

[147] P. M. Day, M. Schelhaas, Concepts of papillomavirus entry into host cells, *Curr. Opin. Virol.* **2014**, *4*, 24-31.

[148] R. M. Schowalter, D. V. Pastrana, C. B. Buck, Glycosaminoglycans and Sialylated Glycans Sequentially Facilitate Merkel Cell Polyomavirus Infectious Entry, *PLoS Pathog.* **2011**, *7*, e1002161.

[149] T. Dalianis, H. H. Hirsch, Human polyomaviruses in disease and cancer, *Virology* **2013**, *437*, 63-72.

[150] W. Liu, R. Yang, A. S. Payne, R. M. Schowalter, M. E. Spurgeon, P. F. Lambert, X. Xu, C. B. Buck, J. You, Identifying the target cells and mechanisms of Merkel cell polyomavirus infection, *Cell Host Microbe* **2016**, *19*, 775-787.

[151] E. M. Geoghegan, D. V. Pastrana, R. M. Schowalter, U. Ray, W. Gao, M. Ho, G. T. Pauly, D. M. Sigano, C. Kaynor, E. Cahir-McFarland, B. Combaluzier, J. Grimm, C. B. Buck, Infectious Entry and Neutralization of Pathogenic JC Polyomaviruses, *Cell Rep.* **2017**, *21*, 1169-1179.

[152] S. Bhattacharjee, S. Chattaraj, Entry, infection, replication, and egress of human polyomaviruses: an update, *Can. J. Microbiol.* **2017**, *63*, 193-211.

[153] H. C. Feng, M. Shuda, Y. Chang, P. S. Moore, Clonal integration of a polyomavirus in human Merkel cell carcinoma, *Science* **2008**, *319*, 1096-1100.

[154] M. E. Spurgeon, P. F. Lambert, Merkel Cell Polyomavirus: A Newly Discovered Human Virus with Oncogenic Potential, *Virology* **2013**, *435*, 118-130.

[155] C. Zong, A. Venot, O. Dhamale, G.-J. Boons, Fluorous Supported Modular Synthesis of Heparan Sulfate Oligosaccharides, *Org. Lett.* **2013**, *15*, 342-345.

[156] O. P. Dhamale, C. Zong, K. Al-Mafraji, G.-J. Boons, New glucuronic acid donors for the modular synthesis of heparan sulfate oligosaccharides, *Org. Biomol. Chem.* **2014**, *12*, 2087-2098.

[157] P. Liu, L. Chen, J. K. C. Toh, Y. L. Ang, J.-E. Jee, J. Lim, S. S. Lee, S.-G. Lee, Tailored chondroitin sulfate glycomimetics via a tunable multivalent scaffold for potentiating NGF/TrkA-induced neurogenesis, *Chem. Sci.* **2015**, *6*, 450-456.

[158] R. J. Linhardt, K. G. Rice, Y. S. Kim, D. L. Lohse, H. M. Wang, D. Loganathan, Mapping and quantification of the major oligosaccharide components of heparin, *Biochem. J.* **1988**, *254*, 781-787.

[159] D. Ruhela, K. Riviere, F. C. Szoka, Efficient synthesis of an aldehyde functionalized

hyaluronic acid and its application in the preparation of hyaluronan-lipid conjugates, *Bioconjugate Chem.* **2006**, *17*, 1360-1363.

[160] A. Bisio, A. Mantegazza, E. Urso, A. Naggi, G. Torri, C. Viskov, B. Casu, High-performance liquid chromatographic/mass spectrometric studies on the susceptibility of heparin species to cleavage by heparanase, *Semin. Thromb. Hemost.* **2007**, *33*, 488-495.

[161] M. Funahashi, I. Matsumoto, N. Seno, Preparation of three types of heparin-Sepharose and their binding activities to thrombin and antithrombin III, *Anal. Biochem.* **1982**, *126*, 414-421.

[162] S. Masuko, K. Higashi, Z. Wang, U. Bhaskar, A. M. Hickey, F. Zhang, T. Toida, J. S. Dordick, R. J. Linhardt, Ozonolysis of the double bond of the unsaturated uronate residue in low-molecular-weight heparin and K5 heparosan, *Carbohyd. Res.* **2011**, *346*, 1962-1966.

[163] Z. Q. Wang, C. Shi, X. R. Wu, Y. J. Chen, Efficient access to the non-reducing end of low molecular weight heparin for fluorescent labeling, *Chem. Commun.* **2014**, *50*, 7004-7006.

[164] Y. Inoue, K. Nagasawa, Selective N-desulfation of heparin with dimethyl sulfoxide containing water or methanol, *Carbohydr. Res.* **1976**, *46*, 87-95.

[165] L. Huang, R. J. Kerns, Diversity-oriented chemical modification of heparin: Identification of charge-reduced N-acyl heparin derivatives having increased selectivity for heparin-binding proteins, *Bioorganic Med. Chem.* **2006**, *14*, 2300-2313.

[166] E. Gemma, A. N. Hulme, A. Jahnke, L. Jin, M. Lyon, R. M. Muller, D. Uhrin, DMT-MM mediated functionalisation of the non-reducing end of glycosaminoglycans, *Chem. Commun.* **2007**, 2686-2688.

[167] D. Tebbe, R. Thull, U. Gbureck, Influence of spacer length on heparin coupling efficiency and fibrinogen adsorption of modified titanium surfaces, *Biomed. Eng. Online* **2007**, *6*, 31.

[168] W.-C. Shieh, Z. Chen, S. Xue, J. McKenna, R.-M. Wang, K. Prasad, O. Repič, Synthesis of sterically-hindered peptidomimetics using 4-(4,6-dimethoxy-1,3,5-triazine-2-yl)-4-methyl-morpholinium chloride, *Tetrahedron Lett.* **2008**, *49*, 5359-5362.

[169] P. Farkas, A. Cizova, S. Bekesova, S. Bystricky, Comparison of EDC and DMTMM efficiency in glycoconjugate preparation, *Int. J. Biol. Macromol.* **2013**, *60*, 325-327.

[170] M. D'Este, D. Eglin, M. Alini, A systematic analysis of DMTMM vs EDC/NHS for ligation of amines to Hyaluronan in water, *Carbohydr. Polym.* **2014**, *108*, 239-246.

[171] T. K. Lindhorst, in *Host-Guest Chemistry: Mimetic Approaches to Study Carbohydrate Recognition* (Ed.: S. Penadés), Springer Berlin Heidelberg, Berlin, Heidelberg, **2002**, pp. 201-235.

[172] A. Imberty, Y. M. Chabre, R. Roy, Glycomimetics and glycodendrimers as high affinity microbial anti-adhesins, *Chem. Eur. J.* **2008**, *14*, 7490-7499.

[173] O. Renaudet, R. Roy, Multivalent scaffolds in glycoscience: an overview, *Chem. Soc. Rev.* **2013**, *42*, 4515-4517.

[174] S. Cecioni, A. Imberty, S. Vidal, Glycomimetics versus Multivalent Glycoconjugates for the Design of High Affinity Lectin Ligands, *Chem. Rev.* **2015**, *115*, 525-561.

[175] L. L. Kiessling, N. L. Pohl, Strength in numbers: Non-natural polyvalent carbohydrate derivatives, *Chem. Biol.* **1996**, *3*, 71-77.

[176] R. Roy, Syntheses and some applications of chemically defined multivalent glycoconjugates, *Curr. Opin. Struct. Biol.* **1996**, *6*, 692-702.

[177] M. Mammen, S. K. Choi, G. M. Whitesides, Polyvalent interactions in biological systems: Implications for design and use of multivalent ligands and inhibitors, *Angew. Chem. Int. Edit.* **1998**, *37*, 2755-2794.

[178] S. M. Dimick, S. C. Powell, S. A. McMahon, D. N. Moothoo, J. H. Naismith, E. J. Toone, On the Meaning of Affinity: Cluster Glycoside Effects and Concanavalin A, *J. Am. Chem. Soc.* **1999**, *121*, 10286-10296.

[179] J. J. Lundquist, E. J. Toone, The Cluster Glycoside Effect, *Chem. Rev.* **2002**, *102*, 555-578.

[180] C. Fasting, C. A. Schalley, M. Weber, O. Seitz, S. Hecht, B. Koksch, J. Dernedde, C. Graf, E. W. Knapp, R. Haag, Multivalency as a Chemical Organization and Action Principle, *Angew. Chem. Int. Edit.* **2012**, *51*, 10472-10498.

[181] C. Fasting, C. A. Schalley, M. Weber, O. Seitz, S. Hecht, B. Koksch, J. Dernedde, C. Graf, E.-W. Knapp, R. Haag, Multivalenz als chemisches Organisations- und Wirkprinzip, *Angew. Chem.* **2012**, *124*, 10622-10650.

[182] P. I. Kitov, D. R. Bundle, On the nature of the multivalency effect: a thermodynamic model, *J. Am. Chem. Soc.* **2003**, *125*, 16271-16284.

[183] R. J. Pieters, Maximising multivalency effects in protein-carbohydrate interactions, *Org. Biomol. Chem.* **2009**, *7*, 2013-2025.

[184] E. T. Mack, P. W. Snyder, R. Perez-Castillejos, B. a. Bilgiçer, D. T. Moustakas, M. J. Butte, G. M. Whitesides, Dependence of avidity on linker length for a bivalent ligand–bivalent receptor model system, *J. Am. Chem. Soc.* **2011**, *134*, 333-345.

[185] E. T. Mack, P. W. Snyder, R. Perez-Castillejos, B. Bilgiçer, D. T. Moustakas, M. J. Butte, G. M. Whitesides, Dependence of Avidity on Linker Length for a Bivalent Ligand–Bivalent Receptor Model System, *J. Am. Chem. Soc.* **2012**, *134*, 333-345.

[186] S. André, G.-N. Wang, H.-J. Gabius, P. V. Murphy, Combining glycocluster synthesis with protein engineering: an approach to probe into the significance of linker length in a tandem-repeat-type lectin (galectin-4), *Carbohydr. Res.* **2014**, *389*, 25-38.

[187] T. K. Dam, C. F. Brewer, Effects of clustered epitopes in multivalent ligand-receptor interactions, *Biochemistry* **2008**, *47*, 8470-8476.

[188] W. J. Lees, A. Spaltenstein, J. E. Kingery-Wood, G. M. Whitesides, Polyacrylamides bearing pendant. alpha.-sialoside groups strongly inhibit agglutination of erythrocytes by influenza A virus: multivalency and steric stabilization of particulate biological systems, *J. Med. Chem.* **1994**, *37*, 3419-3433.

[189] G. B. Sigal, M. Mammen, G. Dahmann, G. M. Whitesides, Polyacrylamides bearing pendant α-sialoside groups strongly inhibit agglutination of erythrocytes by influenza virus: the strong inhibition reflects enhanced binding through cooperative polyvalent interactions, *J. Am. Chem. Soc.* **1996**, *118*, 3789-3800.

[190] P. D. Meyts, E. Van Obberghen, J. Roth, A. Wollmer, D. Brandenburg, Mapping of the residues responsible for the negative cooperativity of the receptor-binding region of insulin, *Nature* **1978**, *273*, 504.

[191] T. K. Dam, R. Roy, D. Pagé, C. F. Brewer, Negative Cooperativity Associated with Binding of Multivalent Carbohydrates to Lectins. Thermodynamic Analysis of the "Multivalency Effect", *Biochemistry* **2002**, *41*, 1351-1358.

[192] Y. Miura, Design and synthesis of well-defined glycopolymers for the control of biological functionalities, *Polym. J.* **2012**, *44*, 679.

[193] G. Yilmaz, C. R. Becer, Glycopolymer Code Based on Well-Defined Glycopolymers or Glyconanomaterials and Their Biomolecular Recognition, *Front. Bioeng. Biotechnol.* **2014**, *2*, 39.

[194] R. Narain, *Glycopolymers: Synthesis and Applications*, Smithers Rapra, **2014**.

[195] B. D. Polizzotti, K. L. Kiick, Effects of Polymer Structure on the Inhibition of Cholera Toxin by Linear Polypeptide-Based Glycopolymers, *Biomacromolecules* **2006**, *7*, 483-490.

[196] K. Yu, B. F. L. Lai, J. H. Foley, M. J. Krisinger, E. M. Conway, J. N. Kizhakkedathu, Modulation of Complement Activation and Amplification on Nanoparticle Surfaces by Glycopolymer Conformation and Chemistry, *ACS Nano* **2014**, *8*, 7687-7703.

[197] C. W. Cairo, J. E. Gestwicki, M. Kanai, L. L. Kiessling, Control of Multivalent Interactions by Binding Epitope Density, *J. Am. Chem. Soc.* **2002**, *124*, 1615-1619.

[198] S. R. S. Ting, G. Chen, M. H. Stenzel, Synthesis of glycopolymers and their multivalent recognitions with lectins, *Polym. Chem.* **2010**, *1*, 1392-1412.

[199] D. Ponader, F. Wojcik, F. Beceren-Braun, J. Dernedde, L. Hartmann, Sequence-Defined Glycopolymer Segments Presenting Mannose: Synthesis and Lectin Binding Affinity, *Biomacromolecules* **2012**, *13*, 1845-1852.

[200] G. Yanzi, G. Jin, R. Sarah-Jane, B. James, R. B. C., H. D. M., A detailed study on understanding glycopolymer library and Con A interactions, *J. Polym. Sci. A* **2013**, *51*, 2588-2597.

[201] D. Ponader, P. Maffre, J. Aretz, D. Pussak, N. M. Ninnemann, S. Schmidt, P. H. Seeberger, C. Rademacher, G. U. Nienhaus, L.

Hartmann, Carbohydrate-Lectin Recognition of Sequence-Defined Heteromultivalent Glycooligomers, *J. Am. Chem. Soc.* **2014**, *136*, 2008-2016.

[202] C. Gerke, M. F. Ebbesen, D. Jansen, S. Boden, T. Freichel, L. Hartmann, Sequence-Controlled Glycopolymers via Step-Growth Polymerization of Precision Glycomacromolecules for Lectin Receptor Clustering, *Biomacromolecules* **2017**, *18*, 787-796.

[203] J. Chiefari, Y. K. Chong, F. Ercole, J. Krstina, J. Jeffery, T. P. T. Le, R. T. A. Mayadunne, G. F. Meijs, C. L. Moad, G. Moad, E. Rizzardo, S. H. Thang, Living Free-Radical Polymerization by Reversible Addition−Fragmentation Chain Transfer: The RAFT Process, *Macromolecules* **1998**, *31*, 5559-5562.

[204] G. Moad, E. Rizzardo, S. H. Thang, Radical addition–fragmentation chemistry in polymer synthesis, *Polymer* **2008**, *49*, 1079-1131.

[205] R. T. Mathers, A. J. Magenau, K. Schröder, K. Matyjaszewski, *Overview of Controlled/Living polymerization Methods of Vinyl Monomers*, **2013**.

[206] M. Semsarilar, S. Perrier, 'Green' reversible addition-fragmentation chain-transfer (RAFT) polymerization, *Nat. Chem.* **2010**, *2*, 811.

[207] R. S. Kane, Thermodynamics of Multivalent Interactions: Influence of the Linker, *Langmuir* **2010**, *26*, 8636-8640.

[208] S. Igde, S. Röblitz, A. Müller, K. Kolbe, S. Boden, C. Fessele, T. K. Lindhorst, M. Weber, L. Hartmann, Linear Precision Glycomacromolecules with Varying Interligand Spacing and Linker Functionalities Binding to Concanavalin A and the Bacterial Lectin FimH, *Macromol. Biosci.* **2017**, *17*, 1700198.

[209] S. G. Spain, N. R. Cameron, A spoonful of sugar: the application of glycopolymers in therapeutics, *Polym. Chem.* **2011**, *2*, 60-68.

[210] C. R. Becer, L. Hartmann, *Glycopolymer Code: Synthesis of Glycopolymers and Their Applications*, Royal Society of Chemistry, **2015**.

[211] K. Suzuki, J.-I. Sakamoto, T. Koyama, S. Yingsakmongkon, Y. Suzuki, K. Hatano, D. Terunuma, K. Matsuoka, Synthesis of sialic acid derivatives having a CC double bond substituted at the C-5 position and their glycopolymers, *Bioorganic Med. Chem. Lett.* **2009**, *19*, 5105-5108.

[212] K. Totani, T. Kubota, T. Kuroda, T. Murata, K. I. Hidari, T. Suzuki, Y. Suzuki, K. Kobayashi, H. Ashida, K. Yamamoto, T. Usui, Chemoenzymatic synthesis and application of glycopolymers containing multivalent sialyloligosaccharides with a poly(L-glutamic acid) backbone for inhibition of infection by influenza viruses, *Glycobiology* **2003**, *13*, 315-326.

[213] Y. Miura, T. Fukuda, H. Seto, Y. Hoshino, Development of glycosaminoglycan mimetics using glycopolymers, *Polym. J.* **2015**, *48*, 229.

[214] D. Specker, V. Wittmann, in *Glycopeptides and Glycoproteins*, Springer, **2006**, pp. 65-107.

[215] H. Hojo, Y. Nakahara, Recent progress in the solid-phase synthesis of glycopeptide, *Curr. Protein Pept. Sci.* **2000**, *1*, 23-48.

[216] Y. Nakahara, H. Hojo, in *Experimental Glycoscience: Glycochemistry* (Eds.: N. Taniguchi, A. Suzuki, Y. Ito, H. Narimatsu, T. Kawasaki, S. Hase), Springer Japan, Tokyo, **2008**, pp. 195-199.

[217] K. Aoi, K. Tsutsumiuchi, M. Okada, Glycopeptide Synthesis by an .alpha.-Amino Acid N-Carboxyanhydride (NCA) Method: Ring-Opening Polymerization of a Sugar-Substituted NCA, *Macromolecules* **1994**, *27*, 875-877.

[218] T. J. Deming, Synthesis of Side-Chain Modified Polypeptides, *Chem. Rev.* **2016**, *116*, 786-808.

[219] E. Liarou, S. Varlas, D. Skoulas, C. Tsimblouli, E. Sereti, K. Dimas, H. Iatrou, Smart polymersomes and hydrogels from polypeptide-based polymer systems through α-amino acid N-carboxyanhydride ring-opening polymerization. From chemistry to biomedical applications, *Prog. Polym. Sci.* **2018**.

[220] J. D. Warren, J. S. Miller, S. J. Keding, S. J. Danishefsky, Toward Fully Synthetic Glycoproteins by Ultimately Convergent Routes: A Solution to a Long-Standing Problem, *J. Am. Chem. Soc.* **2004**, *126*, 6576-6578.

[221] B. Meyer, H. Möller, in *Glycopeptides and Glycoproteins*, Springer, **2006**, pp. 187-251.

[222] L. Corcilius, G. Santhakumar, R. S. Stone, C. J. Capicciotti, S. Joseph, J. M. Matthews, R. N. Ben, R. J. Payne, Synthesis of peptides and glycopeptides with polyproline II helical topology as potential antifreeze molecules, *Bioorg. Med. Chem.* **2013**, *21*, 3569-3581.

[223] J. R. Rogers, S. M. McHugh, Y. S. Lin, Predictions for alpha-Helical Glycopeptide Design from Structural Bioinformatics Analysis, *J. Chem. Inf. Model.* **2017**, *57*, 2598-2611.

[224] S. E. O'Connor, B. Imperiali, Modulation of protein structure and function by asparagine-linked glycosylation, *Chem. Biol.* **1996**, *3*, 803-812.

[225] D. Shental-Bechor, Y. Levy, Effect of glycosylation on protein folding: A close look at thermodynamic stabilization, *Proc. Natl. Acad. Sci. U.S.A.* **2008**, *105*, 8256-8261.

[226] U. Westerlind, Synthetic glycopeptides and glycoproteins with applications in biological research, *Beilstein J. Org. Chem.* **2012**, *8*, 804-818.

[227] L.-X. Wang, M. N. Amin, Chemical and Chemoenzymatic Synthesis of Glycoproteins for Deciphering Functions, *Chem. Biol.* **2014**, *21*, 51-66.

[228] Y. Park, K. Y. Kwok, C. Boukarim, K. G. Rice, Synthesis of sulfhydryl cross-linking poly (ethylene glycol)-peptides and glycopeptides as carriers for gene delivery, *Bioconjugate Chem.* **2002**, *13*, 232-239.

[229] J. D. Warren, X. Geng, S. J. Danishefsky, in *Glycopeptides and Glycoproteins*, Springer, **2006**, pp. 109-141.

[230] A. Liakatos, H. Kunz, Synthetic glycopeptides for the development of cancer vaccines, *Curr. Opin. Mol. Ther.* **2007**, *9*, 35-44.

[231] S. Boonyarattanakalin, J. Hu, S. A. Dykstra-Rummel, A. August, B. R. Peterson, Endocytic Delivery of Vancomycin Mediated by a Synthetic Cell Surface Receptor: Rescue of Bacterially-Infected Mammalian Cells and Tissue Targeting In Vivo, *J. Am. Chem. Soc.* **2007**, *129*, 268-269.

[232] J. Claesen, M. A. Fischbach, Synthetic Microbes As Drug Delivery Systems, *ACS Synth. Biol.* **2015**, *4*, 358-364.

[233] F. Broecker, J. Hanske, C. E. Martin, J. Y. Baek, A. Wahlbrink, F. Wojcik, L. Hartmann, C. Rademacher, C. Anish, P. H. Seeberger, Multivalent display of minimal Clostridium difficile glycan epitopes mimics antigenic properties of larger glycans, *Nat. Commun.* **2016**, *7*.

[234] A. Carlmark, E. Malmstrom, M. Malkoch, Dendritic architectures based on bis-MPA: functional polymeric scaffolds for application-driven research, *Chem. Soc. Rev.* **2013**, *42*, 5858-5879.

[235] S. J. Meunier, Q. Wu, S.-N. Wang, R. Roy, Synthesis of hyperbranched glycodendrimers incorporating α-thiosialosides based on a gallic acid core, *Can. J. Chem.* **1997**, *75*, 1472-1482.

[236] D. Zanini, R. Roy, Novel Dendritic α-Sialosides: Synthesis of Glycodendrimers Based on a 3,3'-Iminobis(propylamine) Core, *J. Org. Chem.* **1996**, *61*, 7348-7354.

[237] D. Zanini, R. Roy, Synthesis of new α-thiosialodendrimers and their binding properties to the sialic acid specific lectin from Limax flavus, *J. Am. Chem. Soc.* **1997**, *119*, 2088-2095.

[238] M. Llinares, R. Roy, Multivalent neoglycoconjugates: solid-phase synthesis of N-linked [small alpha]-sialodendrimers, *Chem. Commun.* **1997**, 2119-2120.

[239] J. Sakamoto, T. Koyama, D. Miyamoto, S. Yingsakmongkon, K. I. Hidari, W. Jampangern, T. Suzuki, Y. Suzuki, Y. Esumi, T. Nakamura, K. Hatano, D. Terunuma, K. Matsuoka, Systematic syntheses of influenza neuraminidase inhibitors: a series of carbosilane dendrimers uniformly functionalized with thioglycoside-type sialic acid moieties, *Bioorg. Med. Chem.* **2009**, *17*, 5451-5464.

[240] P. Dominguez-Rodriguez, J. J. Reina, S. Gil-Caballero, P. M. Nieto, J. L. de Paz, J. Rojo, Glycodendrimers as Chondroitin Sulfate Mimetics: Synthesis and Binding to Growth Factor Midkine, *Chemistry* **2017**, *23*, 11338-11345.

[241] R. Esfand, D. A. Tomalia, Poly(amidoamine) (PAMAM) dendrimers: from biomimicry to drug delivery and biomedical applications, *Drug. Discov. Today* **2001**, *6*, 427-436.

[242] E. Mohammadifar, A. Nemati Kharat, M. Adeli, Polyamidoamine and polyglycerol; their linear, dendritic and linear-dendritic architectures as anticancer drug delivery

systems, *J. Mater. Chem. B* **2015**, *3*, 3896-3921.

[243] N. Mauro, P. Ferruti, E. Ranucci, A. Manfredi, A. Berzi, M. Clerici, V. Cagno, D. Lembo, A. Palmioli, S. Sattin, Linear biocompatible glyco-polyamidoamines as dual action mode virus infection inhibitors with potential as broad-spectrum microbicides for sexually transmitted diseases, *Sci. Rep.* **2016**, *6*, 33393.

[244] D. M. Shadrack, E. B. Mubofu, S. S. Nyandoro, Synthesis of Polyamidoamine Dendrimer for Encapsulating Tetramethylscutellarein for Potential Bioactivity Enhancement, *Int. J. Mol. Sci.* **2015**, *16*, 26363-26377.

[245] P. Kesharwani, S. Banerjee, U. Gupta, M. C. I. Mohd Amin, S. Padhye, F. H. Sarkar, A. K. Iyer, PAMAM dendrimers as promising nanocarriers for RNAi therapeutics, *Mater. Today* **2015**, *18*, 565-572.

[246] S. Sanyakamdhorn, D. Agudelo, H. A. Tajmir-Riahi, Review on the targeted conjugation of anticancer drugs doxorubicin and tamoxifen with synthetic polymers for drug delivery, *J. Biomol. Struct. Dyn.* **2017**, *35*, 2497-2508.

[247] L. Hartmann, S. Haefele, R. Peschka-Suess, M. Antonietti, H. G. Borner, Tailor-made poly(amidoamine)s for controlled complexation and condensation of DNA, *Chem. Eur. J.* **2008**, *14*, 2025-2033.

[248] L. Hartmann, Polymers for Control Freaks: Sequence-Defined Poly(amidoamine)s and Their Biomedical Applications, *Macromol. Chem. Phys.* **2011**, *212*, 8-13.

[249] R. B. Merrifield, Solid Phase Peptide Synthesis I. The Synthesis of a Tetrapeptide, *J. Am. Chem. Soc.* **1963**, *85*, 2149-&.

[250] B. Merrifield, Solid phase synthesis, *Science* **1986**, *232*, 341-347.

[251] P. H. Hermkens, H. C. Ottenheijm, D. Rees, Solid-phase organic reactions: a review of the recent literature, *Tetrahedron* **1996**, *52*, 4527-4554.

[252] P. H. Seeberger, W.-C. Haase, Solid-phase oligosaccharide synthesis and combinatorial carbohydrate libraries, *Chem. Rev.* **2000**, *100*, 4349-4394.

[253] M. Weishaupt, S. Eller, P. H. Seeberger, Solid phase synthesis of oligosaccharides, *Methods Enzymol.* **2010**, *478*, 463-484.

[254] P. J. Scott, Solid-phase Organic Synthesis of Drugs and Natural Products, *Stereoselective Synthesis of Drugs and Natural Products* **2013**, 1-50.

[255] J. M. Palomo, Solid-phase peptide synthesis: an overview focused on the preparation of biologically relevant peptides, *RSC Adv.* **2014**, *4*, 32658-32672.

[256] L. A. Carpino, G. Y. Han, The 9-Fluorenylmethoxycarbonyl Function, a New Base-Sensitive Amino-Protecting Group, *J. Am. Chem. Soc.* **1970**, *92*, 5748-5749.

[257] L. A. Carpino, The 9-Fluorenylmethyloxycarbonyl Family of Base-Sensitive Amino-Protecting Groups, *Acc. Chem. Res.* **1987**, *20*, 401-407.

[258] L. Hartmann, E. Krause, M. Antonietti, H. G. Börner, Solid-Phase Supported Polymer Synthesis of Sequence-Defined, Multifunctional Poly(amidoamines), *Biomacromolecules* **2006**, *7*, 1239-1244.

[259] L. Hartmann, S. Häfele, R. Peschka-Süss, M. Antonietti, H. G. Börner, Sequence Positioning of Disulfide Linkages to Program the Degradation of Monodisperse Poly(amidoamines), *Macromolecules* **2007**, *40*, 7771-7776.

[260] F. Wojcik, S. Mosca, L. Hartmann, Solid-Phase Synthesis of Asymmetrically Branched Sequence-Defined Poly/Oligo(amidoamines), *J. Org. Chem.* **2012**, *77*, 4226-4234.

[261] F. Wojcik, S. Lel, A. G. O'Brien, P. H. Seeberger, L. Hartmann, Synthesis of homo- and heteromultivalent carbohydrate-functionalized oligo(amidoamines) using novel glyco-building blocks, *Beilstein J. Org. Chem.* **2013**, *9*, 2395-2403.

[262] F. Wojcik, A. G. O'Brien, S. Gotze, P. H. Seeberger, L. Hartmann, Synthesis of Carbohydrate-Functionalised Sequence-Defined Oligo(amidoamine)s by Photochemical ThiolEne Coupling in a Continuous Flow Reactor, *Chem. Eur. J.* **2013**, *19*, 3090-3098.

[263] D. Ponader, S. Igde, M. Wehle, K. Marker, M. Santer, D. Bleger, L. Hartmann, Photoswitchable precision glycooligomers and their lectin binding, *Beilstein J. Org. Chem.* **2014**, *10*, 1603-1612.

[264] M. F. Ebbesen, C. Gerke, P. Hartwig, L. Hartmann, Biodegradable poly(amidoamine)s with uniform degradation fragments via

sequence-controlled macromonomers, *Polym. Chem.* **2016**, *7*, 7086-7093.

[265] S. Boden, K. Wagner, M. Karg, L. Hartmann, Presenting Precision Glycomacromolecules on Gold Nanoparticles for Increased Lectin Binding, *Polymers* **2017**, *9*, 716.

[266] T. Freichel, S. Eierhoff, N. L. Snyder, L. Hartmann, Toward Orthogonal Preparation of Sequence-Defined Monodisperse Heteromultivalent Glycomacromolecules on Solid Support Using Staudinger Ligation and Copper-Catalyzed Click Reactions, *J. Org. Chem.* **2017**, *82*, 9400-9409.

[267] K. Lin, A. M. Kasko, Effect of Branching Density on Avidity of Hyperbranched Glycomimetics for Mannose Binding Lectin, *Biomacromolecules* **2013**, *14*, 350-357.

[268] E. van der Meijden, R. W. A. Janssens, C. Lauber, J. N. B. Bavinck, A. E. Gorbalenya, M. C. W. Feltkamp, Discovery of a New Human Polyomavirus Associated with Trichodysplasia Spinulosa in an Immunocompromized Patient, *PloS Pathog.* **2010**, *6*.

[269] L. J. Ströh, G. V. Gee, B. S. Blaum, A. S. Dugan, M. C. W. Feltkamp, W. J. Atwood, T. Stehle, Trichodysplasia spinulosa-Associated Polyomavirus Uses a Displaced Binding Site on VP1 to Engage Sialylated Glycolipids, *PLoS Pathog.* **2015**, *11*, e1005112.

[270] U. Neu, H. Hengel, B. S. Blaum, R. M. Schowalter, D. Macejak, M. Gilbert, W. W. Wakarchuk, A. Imamura, H. Ando, M. Kiso, N. Arnberg, R. L. Garcea, T. Peters, C. B. Buck, T. Stehle, Structures of Merkel Cell Polyomavirus VP1 Complexes Define a Sialic Acid Binding Site Required for Infection, *Plos Pathogens* **2012**, *8*.

[271] M. Shuda, H. C. Feng, H. J. Kwun, S. T. Rosen, O. Gjoerup, P. S. Moore, Y. Chang, T antigen mutations are a human tumor-specific signature for Merkel cell polyomavirus, *Proc. Natl. Acad. Sci. U.S.A.* **2008**, *105*, 16272-16277.

[272] J. D. Badjic, A. Nelson, S. J. Cantrill, W. B. Turnbull, J. F. Stoddart, Multivalency and cooperativity in supramolecular chemistry, *Acc. Chem. Res.* **2005**, *38*, 723-732.

[273] L. K. S. von Krbek, C. A. Schalley, P. Thordarson, Assessing cooperativity in supramolecular systems, *Chem. Soc. Rev.* **2017**, *46*, 2622-2637.

References

5. Publications

5.1. Split-and-Combine Approach Towards Branched Precision Glycomacromolecules and Their Lectin Binding Behavior

1st author contribution:

Collaborative design of structures and binding assays. Synthesis of all used building blocks including propargyl-functionalized carbohydrates; development, synthesis optimization and analysis of the azide-displaying BADS building block as well as of its constitutional isomer *Iso*BADS. Optimization of the solid phase synthesis coupling conditions applying the new building block, determination of its coupling efficiency, synthesis, isolation and analysis of all resulting linear and branched precision glycomacromolecules. Joint performance of SPR measurements, visualization and interpretation of the obtained data supported by the co-authors. Collaborative writing of manuscript.

▌Polymer Synthesis

Split-and-Combine Approach Towards Branched Precision Glycomacromolecules and Their Lectin Binding Behavior

Mischa Baier, Markus Giesler, and Laura Hartmann*[a]

Abstract: Previously, monodisperse and sequence-controlled oligo(amidoamine) scaffolds were synthesized based on the step-wise assembly of tailor-made building blocks on a solid support that allow for the multivalent presentation of sugar ligands. Here, we extend on this concept using a split-and-combine approach to gain access to a small library of linear and branched glycomacromolecules. Azide side chains were introduced in the scaffold by the use of a novel building block allowing for copper-mediated azide-alkyne cycloaddition (CuAAC) of readily available propargyl-functionalized glycans. In the first stage, after assembly of the linear scaffold on solid support, the batch was divided into two. One part of the resin-bound oligomers was end-capped and further used as backbone and the other part was functionalized with propargylated α-D-mannopyranoside in the sidechain, end capped with an alkyne functionality and finally cleaved from solid support to give the branching arm. In the second stage, the linear, glycosylated and alkynylated arms were then coupled to the end capped backbone via CuAAC. In this way, branched glycomacromolecules with two and three branches, respectively, have been synthesized carrying from two to six sugar residues per molecule. Both, linear arms and branched glycomacromolecules were then subjected to a lectin binding assay using surface plasmon resonance (SPR) and model lectin Concanavalin A (Con A) showing the effect of branching as well as valency on the binding kinetics.

Introduction

Many important cell processes are regulated by the cell surface, that is, cell–cell communication, pathogen recognition, or cell differentiation.[1] In particular, the glycocalyx, a dense layer of carbohydrates on the cell surface, plays a key role in mediating such interactions. The glycocalyx constitutes a multitude of different carbohydrate structures such as polysaccharides, glycoproteins and glycolipids that can act as binding sites for other biomolecules.[2] Indeed, many cell interactions do not result from addressing a single binding site but rather from the interplay of several ligands and receptors simultaneously. Such multivalency effects especially contribute to the weak interaction of carbohydrates with lectins resulting in the so called cluster-glycoside effect.[3] Here, several carbohydrate ligands or glycans interact with several binding sites leading to an overall increase in avidity. Nature benefits in different ways from the occurrence of multivalency, that is, through the localization of several glycans on the cell surface or on a protein scaffold. In the latter case, several glycans are linked onto a protein backbone leading to a comb-like structure as known

for mucins.[4] This concept not only holds true for the natural constructs, but can also be applied to create biomimetic molecules by attaching glycans to a synthetic, polymeric scaffold.[5] Such polymeric glycomimetics have been used as model compounds to study multivalency effects based on glycan interactions but also give straightforward access to glycomimetics with increased avidity.[3g,i,6] One of the limitations of such polymeric glycomimetics is their intrinsic dispersity stemming from their synthesis through classical polymerization methods. Previously, we have introduced the so-called solid phase polymer synthesis (SPPoS), now giving access to monodisperse, sequence-controlled oligo(amidoamine) scaffolds suitable for the presentation of different carbohydrate ligands.[7] Inspired by the solid phase synthesis (SPS) as introduced by Merrifield in 1963[8] and further developed by Carpino et al.[9] with the introduction of the fluorenylmethoxycarbonyl (Fmoc) protective group, in combination with a library of tailor-made building blocks, we can synthesize scaffolds presenting a defined number of functional groups at defined positions along the main chain allowing for conjugation of carbohydrate ligands.[7,10] Through combination of different conjugation methods, we can also obtain heteromultivalent glycomacromolecules presenting diverse carbohydrate ligands at specific positions within the sequence.[11] Here, we now extend the concept of the so-called precision glycomacromolecules from linear to branched structures. In nature, branched structures are found for various carbohydrates and carbohydrate-conjugates, for example, polysaccharides as well as glycoproteins. Also for glycomimetics, branched structures have been realized

[a] M. Baier, M. Giesler, Prof. Dr. L. Hartmann
Institute of Organic and Macromolecular Chemistry
Heinrich-Heine-University Duesseldorf
Universitaetsstraße 1, 40225 Duesseldorf (Germany)
E-mail: laura.hartmann@hhu.de

and applied as model systems to study the effect of branching on the interactions with carbohydrate recognizing proteins such as lectins.[12] For example, Lin et al.[13] found that the polymer architecture of a mannose glycopolymer strongly affected the mannose binding lectin (MBL) interaction: A branched polymer carrying on average 14 mannose residues showed a 90 times higher avidity than a linear polymer with the same valency. To evaluate the role of the scaffold's architecture more closely, here we present the synthesis of a series of branched precision glycomacromolecules specifically varying the degree of branching, overall valency as well as valency per branch. Therefore, we established a so-called "split-and-combine" approach based on the previously established solid phase polymer synthesis (Figure 1). In the first step, using a novel build-
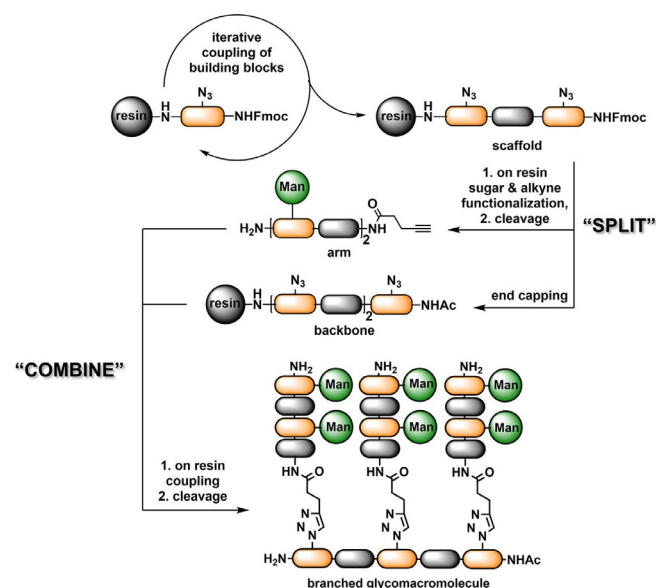
Figure 1. Split-and-combine approach for solid phase synthesis of branched precision glycomacromolecules.

ing block, a scaffold with azide side chains was assembled on solid phase. In the second step, this scaffold was either conjugated with mannose ligands through Cu-mediated azide alkyne cycloaddition (CuAAC) and end-group functionalized with an alkyne group giving the arm of latter branched glycomacromolecule or directly used as the backbone for conjugation of the previously synthesized arm side chains. This approach is similar to the "arm-first" synthesis of dendrimers or mictoarm polymers.[14] Using the presented split-and-combine approach, different arms and backbones can be combined using CuAAC to create branched glycomacromolecules with varying degree of branching and valency. Finally, this series of branched structures was subjected to binding studies using model lectin Con A studying the influence of branching on the lectin-binding behavior.

Results and Discussion

Synthesis of the azide-containing building block

To allow for a split-and-combine approach using CuAAC as the coupling method for both conjugation of the carbohydrate as well as the grafting of the arm onto the backbone, a novel building block carrying an azide group in the side chain was developed. The choice of an aromatic side chain can be explained by the following reasons. Firstly, dealing with low molecular weight azides is not trivial and the molecule to be synthesized should not be below a certain C:N ratio for safety reasons.[15] First attempts towards a building block with an aliphatic linker showed difficulties during purification of the final building block (data not shown), whereas the aromatic linker was readily installed. Secondly, several studies have shown hydrophobic areas in the vicinity of the carbohydrate binding site of Con A, which favor the binding of sugars with hydrophobic, especially aromatic linkers resulting in higher affinities.[16]

The azide containing building block *p*-(azidomethyl)benzoyl diethylenetriamine succinic acid (BADS) was synthesized following a general protocol previously established in our group (Scheme 1)[7] starting from key intermediate **1**, a triphenylmethyl- (Trt) and trifluoroacetamide- (TFA) protected diethylenetriamine (Scheme 1). The free, secondary amine of **1** was used to couple the 4-(azidomethyl) benzoic acid through an amide bond formation. Here, two reaction conditions showed comparable results regarding the yield: one condition implements the conversion of 4-(azidomethyl) benzoic acid (**2**) to the corresponding acid chloride by the use of oxalyl chloride and dimethylformamide as catalyst. The acid chloride was then coupled to the free amine. The alternative route makes use of the well-established coupling agents benzotriazol-1-yl-oxytripyrrolidinophosphonium hexafluorophosphate (PyBOP) and hydroxybenzotriazole (HOBt) for active ester formation. The azide-functionalized product (**3**) was then subjected to an exchange of protecting groups. Therefore, in a first attempt, following the previously established procedure, the TFA protecting group was removed by using a potassium carbonate solution in a biphasic mixture of methanol and water at room temperature. The reaction was completed after five days, but after the addition of the Fmoc group, a rearrangement within the molecule during the deprotection procedure giving two Fmoc-functionalized isomers (**4** and **4b**) was observed and could not be prevented. Further removal of the trityl group followed by functionalization with succinic anhydride was carried out without problems, but only **5b** could be isolated through multiple recrystallization steps. A likely reason for the observed rearrangement during the deprotection step could be the fast isomerization of the intermediary primary amine: The free primary amine intramolecularly adds to the azide-bearing functional group in an S$_N$2t reaction and, after elimination, leaves the free secondary amine in the center of the molecule. Additionally, the reaction could be favored by the five-membered ring transition state. The previously established TDS building block as described by Ponader et al.[7] reacts more rapidly and the iso-
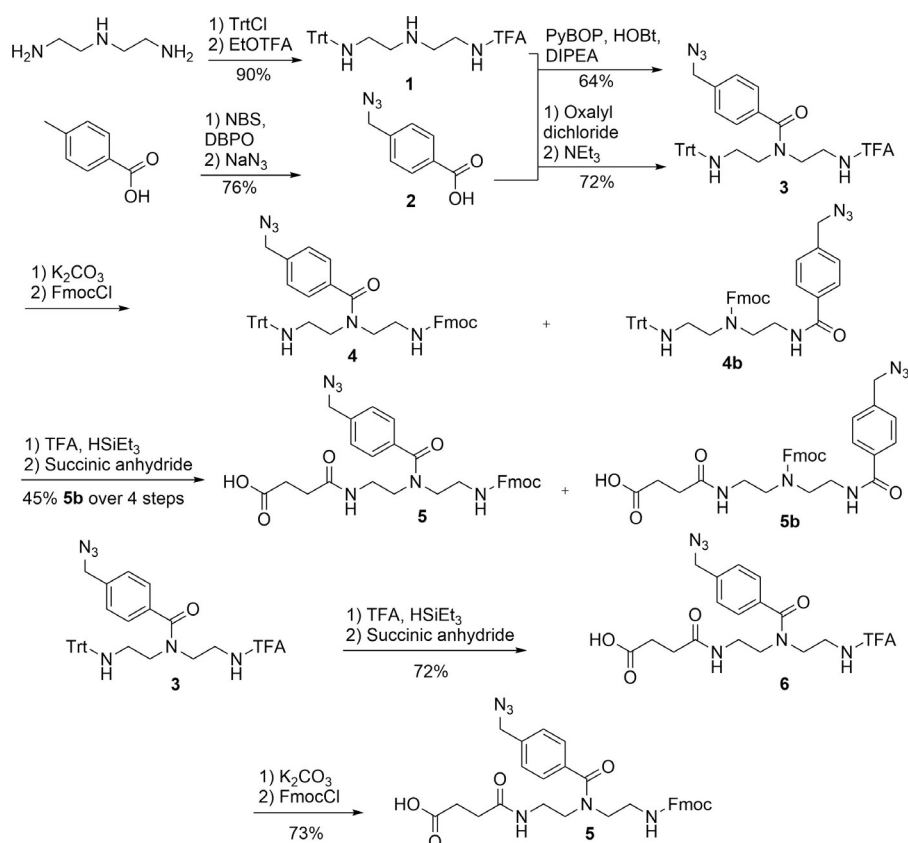
Scheme 1. Synthesis of BADS building block (**5**) for solid-phase synthesis: a) synthesis of the azide-functionalized intermediate **3**; b) first route leading to the rearrangement product **5 b**; c) second route leading to the targeted compound **5**.

merization appears to be less favored. Therefore, the reaction sequence was changed to overcome the isomerization problem. Intermediate **3** was first set to the deprotection of the trityl group and the subsequent functionalization with succinic anhydride. Acid **6** was obtained in high yield and was used for the final TFA deprotection procedure. Due to the fact that compound **6** shows higher hydrophilicity than compound **3**, TFA deprotection in an aqueous potassium carbonate solution was much faster, so that the deprotection was complete after 12 h at room temperature. Furthermore, the reaction could be carried out in a 10% aqueous potassium carbonate solution without any addition of methanol. The desired product **5** was isolated in high yield and high purity after two cycles of recrystallization. ^{1}H NMR, ^{13}C NMR and reversed-phase HPLC (RP-HPLC) confirm the structure of **5** and give no indication for the undesired isomer **5 b** (see the Supporting Information for isomerization kinetics and spectra). The ^{1}H NMR as well as the ^{13}C NMR spectra show a broadening of the signals as well as the appearance of several bands for chemically equivalent protons and carbons in all steps of the building block synthesis that we attribute to the presence of rotational isomers. The ^{1}H NMR spectra were therefore additionally recorded at 100 °C leading to coalescence and signal sharpening (see the Supporting Information for spectra).

Solid phase synthesis of glycomacromolecules

With the new building block BADS (**5**) in hand, a series of precision glycomacromolecules were synthesized following previously established protocols for solid phase polymer synthesis. In addition to the new BADS building block, EDS (**7**) as adapted from Ebbesen et al.[17] (see Supporting Information) was used as spacer building block introducing a short ethylene glycol unit within the scaffold (Scheme 2). All building blocks carry a free carboxylic acid and a Fmoc-protected amine group that allow for stepwise coupling on solid support using standard Fmoc peptide chemistry. In short, activation and coupling of a building block onto the resin followed by on-resin deprotection prior to the activation and coupling of the next building block gives a monodisperse sequence-controlled oligo(amidoamine) scaffold. Depending on the sequence of building blocks during assembly, the number and position of azide groups is controlled. To achieve such control, building blocks have to couple with nearly quantitative yield for every addition step. Therefore, for the new building block BADS, coupling efficiency was evaluated and optimized according to Fmoc coupling protocols using the test sequence BADS-EDS-BADS and three different coupling conditions: PyBOP and *N,N*-diisopropylethylamine (DIPEA); (1-[Bis(dimethylamino)methylene]-1H-1,2,3-triazolo[4,5-b]pyridinium 3-oxid hexafluorophosphate) (HATU) and DIPEA and diisopropylcarbodiimide (DIC) and ethyl (hydroxyimino)cyanoacetate (OxymaPure®), respectively. The
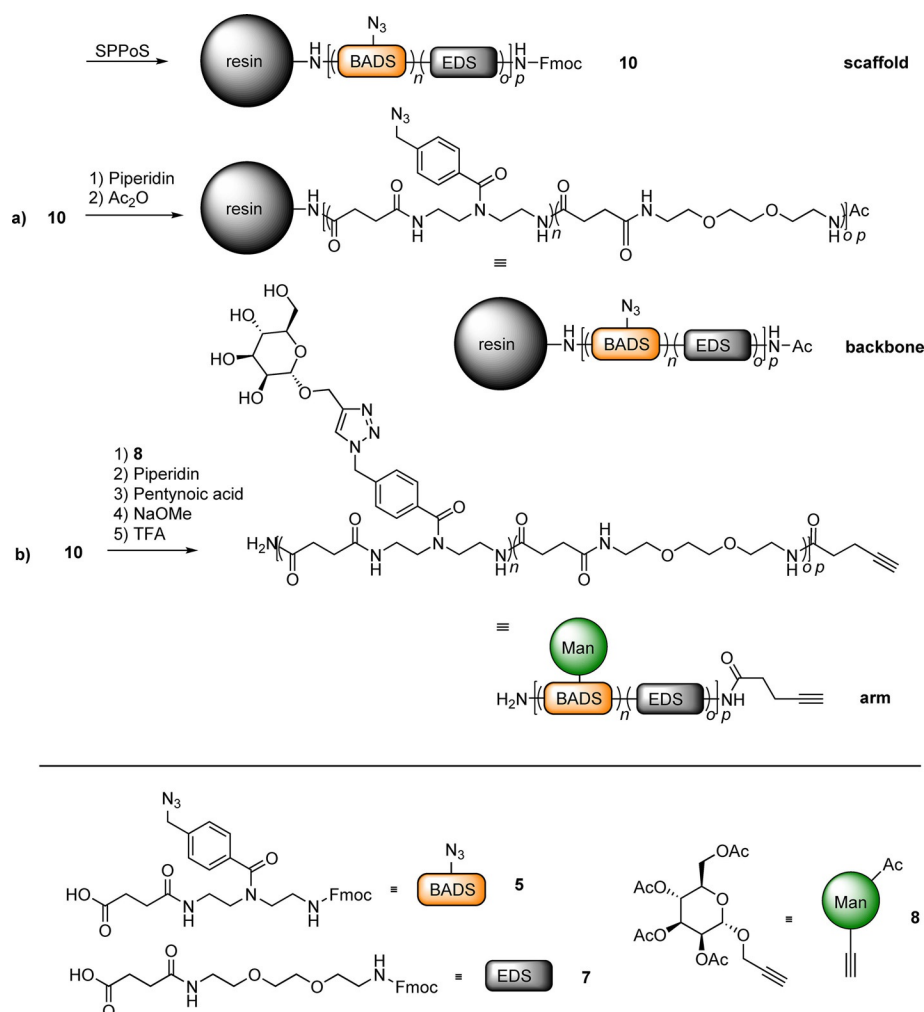
Scheme 2. Schematic representation of the solid phase synthesis of precision glycomacromolecule arms and backbones. a) synthesis of **backbone**; b) synthesis of **arm**.

DIPEA-catalyzed amide coupling using PyBOP or HATU as coupling reagent nowadays is one of the most efficient coupling conditions, whereas the use of DIC represents a more classical approach with a lower expected efficiency.[18] All couplings were performed using 5 equiv. of the respective building block and the coupling reagents along with 20 equiv. of DIPEA regarding the resin loading. PyBOP and HATU showed similarly good results with coupling efficiencies of about 98%. A combination of DIC and OxymaPure® did not exceed 60% coupling efficiency in the first step. For the trimeric test structure based on these coupling efficiencies, a theoretical maximum purity of 93.9% could be achieved and confirmed by RP-HPLC analysis of the oligomer after cleavage from the support (see the Supporting Information for determination of coupling efficiency and chromatograms). Using the optimized coupling conditions, six different oligomers were synthesized varying between 2–6 building blocks in length and introducing 1–3 azide groups (Table 1). The nomenclature of the precision glycomacromolecules follows the previously introduced scheme: A(B)-C-D, in which (A) stands for the introduced side chain functionality and (B) for its position within the oligomer chain. After the first

Table 1. List of all synthesized macromolecular backbones and arms.

Compound	Name	Yield[a] [%]	Purity [%][c]	MW [Da]
backbone 1	N₃(1,3)-3	_[b]	94	878.1
backbone 2	N₃(1,3,5)-5	_[b]	87	1552.7
arm 1	Man(1)-2-PA	51	96	890.0
arm 2	Man(1,3)-4-PA	62	98	1682.8
arm 3	Man(1,3,5)-6-PA	41	96	2475.6
arm 4	Gal(1,3)-4-PA	85	97	1682.8

[a] Yields were determined after preparative RP-HPLC based on the resin loading. [b] Scaffolds were not isolated quantitatively. [c] Purities were determined by RP-HPLC (MeCN in H₂O, linear gradient from 5–50% in 30 min) without (**backbone**) or after preparative purification (**arms**).

hyphen (C), the total length (number of used building blocks) is given and after the second hyphen (D), a potential end functionality is listed. The split-and-combine approach is implemented as follows: in the first stage, after assembly of the linear scaffold on solid support, the resin beads are divided into two parts. One of these parts is end-capped and further

used as resin-bound backbone. The other part is further functionalized with propargylated α-D-mannopyranoside (**8**), which was synthesized adapting a protocol by Bergeron-Brlek et al.,[19] or with propargylated β-D-galactopyranoside (**9**), which was synthesized according to the method described by Spicer et al.[20] (see the Supporting Information). Then the oligomer was end capped introducing a terminal alkyne group and, after catalytic deprotection of all carbohydrate moieties, finally cleaved from solid support to be used as arm. Four alkyne-functionalized glycomacromolecules (**arms 1–4**) were obtained with molecular weights from 0.9 to 2.5 kDa, which were then combined with the **backbones 1–2**. Before grafting of the **arms 1–4**, they were purified by preparative HPLC leading to purities ≥96%. For **arm 1** and **arm 2** after purification, we identified by-products as glycomacromolecules which partially contain the rearranged BADS building block. The previously observed isomerization of the newly developed building block BADS can potentially also take place on solid phase during basic Fmoc deprotection and thus leads to a mixture of molecules with the same m/z ratio but different retention times (see the Supporting Information). For **arm 3**, a deletion sequence was identified as a by-product missing one spacer building block EDS (see the Supporting Information). **Arm 4** partially contains α-galactose side chains as the propargylated β-D-galactopyranoside contained 8% α-anomer.

In the second step, the linear, glycosylated and alkynylated macromolecules were then grafted onto the scaffolds using CuAAC (Scheme 3). Different reaction conditions were tested for the tetravalent compound **14** (**2X2**) to determine the most suitable conditions in terms of conversion and quantity of used material. Solid phase synthesis often requires excess of reagent during the coupling step to assure high conversion. However, to minimize loss of the previously synthesized arms, excess during coupling should be minimized. Overall, the effect of reaction time, catalyst concentration, solvent mixture and excess of reagent (**arms**) was evaluated (Table 2). Reaction times of 24 h and 120 h were compared showing that longer reaction times increased overall conversion. An increase in the catalyst concentration above two equivalents had no effect on the conversion, which is an indication that the catalyst remains active at long reaction times and is not a limiting factor.
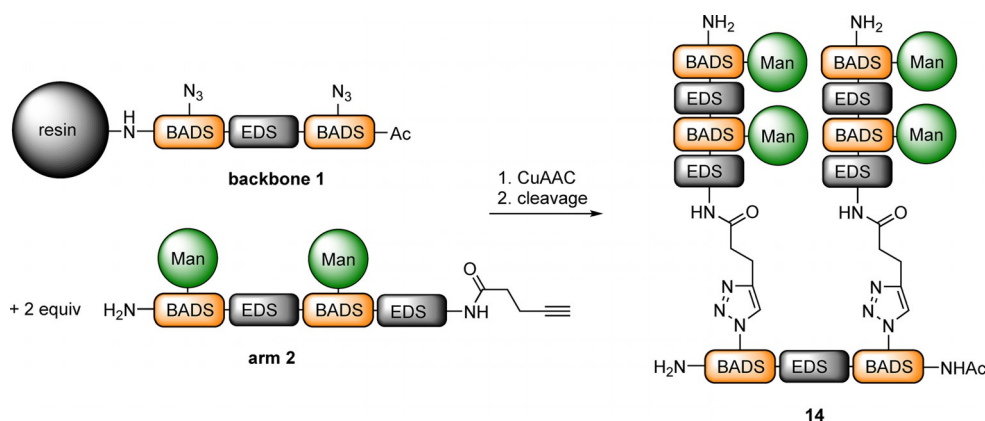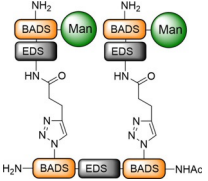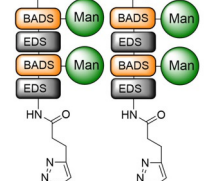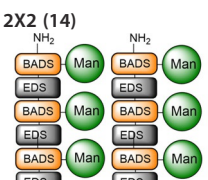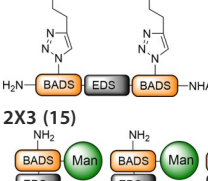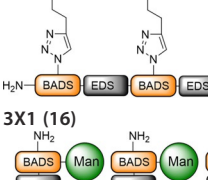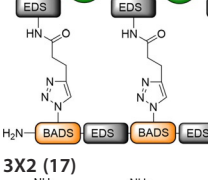
Table 2. Detected ratios of the double-coupled product **A**, the semi-converted product **B**, and the non-converted scaffold **C** after the variation of the following parameters: Reactant concentration, reaction time, catalyst concentration, solvent, and the reactant concentration. All reactions were performed on a 10 μmol scale.

Oligomer [equiv]	Reaction time [h]	Cat. conc.[a] [equiv]	Solvent	Oligomer conc. [mM]	Formed product A/B/C[b] [%]
3	24	2	DMF/H$_2$O = 1:1	2.5	40/7/53
3	24	2	tBuOH/H$_2$O = 1:1	2.5	75/0/25[c]
3	24	2	DMF/H$_2$O/DCM = 2:2:1	2.5	35/3/62
3	24	2	tBuOH/H$_2$O/DCM = 2:2:1	2.5	0/0/100
3	24	2	H$_2$O	2.5	10/8/82
3	24	4	tBuOH/H$_2$O = 1:1	2.5	32/0/68[c]
3	24	4	DMF/H$_2$O = 1:1	2.5	35/4/62
3	120	2	DMF/H$_2$O = 1:1	2.5	72/7/22
3	24	2	DMF/H$_2$O = 1:1	7.5	55/6/39
4	120	2	DMF/H$_2$O = 1:1	2.5	98/0/2
4	120	2	DMF/H$_2$O = 1:1	7.5	100/0/0[d]

[a] CuSO$_4$/sodium ascorbate = 1:1.25. [b] Product ratios were obtained by integration of the absolute RP-HPLC signal intensities (MeCN in H$_2$O, linear gradient from 5–50% in 30 min) of the product after microcleavage. [c] The use of tBuOH led to irreproducible results due to a separation of layers within the syringe reactor. [d] Reaction conditions used for all following solid phase assisted macromolecule couplings.

Four different solvent mixtures were tested: A 1:1 mixture of DMF and water or tBuOH and water, as well as a 2:2:1 mixture of DMF and water or tBuOH and water with DCM. An aprotic and a protic water-miscible solvent were chosen with DMF and tBuOH. DCM was added to increase swelling of the resin. Here, a 1:1 mixture of water and DMF showed the best results in terms of coupling efficiency. An increase of the equivalents of the coupling partner (**arm**) from three to four in conjunction with higher concentrations during coupling by decrease of solvent resulted in complete conversion. Thus, these conditions were then applied for all following macromolecule coupling reactions. Combining the **arms 1–4** and **backbones 1–2**, branched glycomacromolecules **13–18** were synthesized and isolated in yields from 56–77% after purification through preparative HPLC (Table 3). Hexavalent compound **15** was isolated

Scheme 3. Combination of backbone and arms by CuAAC on solid support.

Table 3. List of synthesized branched glycomacromolecules.

Oligomer [#]	Yield[a] [%]	Purity[b] [%]	PDI[c]	MW [Da], found m/z[d] (calc.)
2X1 (13)	68	98	1.03	2758.0 690.3 (690.3)
2X2 (14)	77	94	1.03	4343.7 869.5 (869.6)
2X3 (15)	32	88	1.05	5926.4 989.2 (989.0)
3X1 (16)	58	83	1.04	4222.6 845.5 (845.4)
3X2 (17)	67	96	1.03	6601.1 1101.1 (1100.9)
2X2Gal (18)	56	87	1.06	4343.7 869.7 (869.6)

[a] Yields were determined after preparative RP-HPLC. [b] Purities were determined by RP-HPLC (MeCN in H_2O, linear gradient from 5–50% in 30 min). [c] PDIs were analyzed by GPC-RI-LS. [d] Monoisotopic mass.

in a lower yield of 32% because no quantitative conversion during coupling of the arms was achieved in this case. MS analysis of the final compounds shows the desired products (see the Supporting Information). However, we detect multiple peaks in the HPLC-MS chromatogram giving the same *m/z* in the mass spectrum. We attribute this finding to the presence of side-products that cannot be separated during preparative HPLC: The molecules that contain **arm 1** and **arm 2**, namely **2X1**, **2X2**, **3X1** and **3X2**, contain partially rearranged BADS building block as previously identified for the single arm macromolecules. For the final branched structures, this leads to multiple peaks in the chromatogram with similar *m/z* as determined by HPLC-MS (see Supporting Information). As additional by-products, deletion sequences missing EDS spacer building block were identified stemming from incomplete coupling during scaffold synthesis. For compound **2X3**, 10.2% of the by-products could be assigned to EDS-deletion sequences. EDS is partially missing in both the **arm 3** branches, as well as in the **backbone**, but never more than one unit per glycomacromolecule. Values for purities given in Table 3 only refer to the main peak not including isomers or deletion sequences.

To obtain additional information on the dispersities of branched macromolecules **13**–**18**, these were further analyzed by GPC-RI-LS (gel permeation chromatography with refractive index and light scattering detectors). The obtained GPC elugrams show dispersities for all glycomacromolecules between 1.03 and 1.06 with an estimated error limit of 5% and thus are in good agreement with the data from the HPLC. Overall our data show that the split-and-combine approach has been successfully implemented giving a first series of six branched glycomacromolecules. The purities range from 83–98%, so we do not call these molecules monodisperse. Nevertheless, the degree of branching and overall valency of the obtained molecules is highly controlled and they can be further used for binding studies looking into their structure–property correlations when binding to model lectin Con A.

Lectin binding behavior of linear versus branched glycomacromolecules

All obtained glycofunctionalized compounds, linear arms as well as branched glycomacromolecules, were subjected to a SPR direct binding assay measuring their binding towards model lectin Con A. All glycomacromolecules were measured in the single cycle mode showing binding to the Con A functionalized chip surface to give association constants (K_A; Figure 2A, Table 4). The compounds were subdivided into four groups according to the arm that was used during synthesis.

The Langmuir 1:1 steady state model ($A + B \rightleftharpoons AB$), which is often used to evaluate carbohydrate-lectin interactions[16j, 21] and which we have used in previous work on linear precision glycomacromolecules and -polymers,[10c, 22] does not seem to satisfy the requirements in this case. In the steady state, only the absolute response is of importance, but not the association and dissociation behavior of the compounds. Similarly, Muñoz et al.[23] argue and use a bivalent binding model instead of the steady state analysis for their glycodendrimers. This seems to
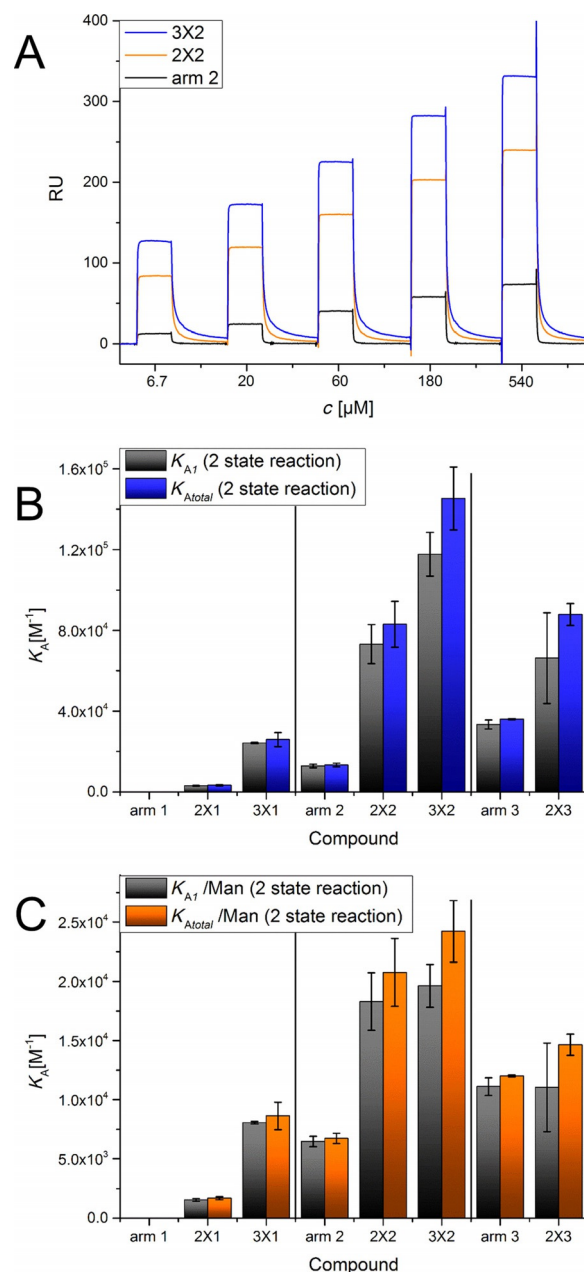
Figure 2. (**A**) Exemplary SPR sensograms of the three selected compounds **arm 2**, **2X2**, and **3X2**; (**B**) K_{A1} values (black bars) and K_{Atotal} values (blue bars) obtained from the two state reaction for all analyzed compounds. (**C**) Mannose normalized K_{A1} values (black bars) and K_{Atotal} values (orange bars) obtained from the two-state reaction for all analyzed compounds.

be particular useful for the investigated compounds, as long as relatively spherical structures are assumed, in which the hydrophilic sugar units decorate the surface and the more hydrophobic framework lies inside.[24] In our case, the association and dissociation behavior of the branched glycomacromolecules also suggests a multi-stage binding behavior. We therefore assume a two-state reaction model for the branched glycomacromolecules (A) binding to Con A (B): $A + B \rightleftharpoons AB \rightleftharpoons AB^*$.[25] All sensograms were fitted accordingly giving K_{A1} and K_{Atotal} for the arms and branched glycomacromolecules (Table 4). For **arm 1**, the monovalent compound, fitting accord-

Table 4. Con A binding of linear and branched glycomacromolecules as determined by direct binding assay using SPR.

Group	Compound	Structure	Valency	K_{A1}[a] $[10^3 \, \text{M}^{-1}]$	K_{Atotal}[a] $[10^3 \, \text{M}^{-1}]$	K_{A1}[a] $[10^3 \, \text{M}^{-1}]$ per Man	K_{Atotal}[a] $[10^3 \, \text{M}^{-1}]$ per Man
	Arm 1		1	–	–	–	–
Arm 1	2X1		2	3.1 ± 0.2	3.4 ± 0.3	1.5 ± 0.1	1.7 ± 0.1
	3X1		3	24.2 ± 3.2	25.9 ± 3.5	8.1 ± 0.1	8.6 ± 1.2
	Arm 2		2	12.9 ± 0.9	13.4 ± 0.9	6.5 ± 0.4	6.7 ± 0.4
Arm 2	2X2		4	73.2 ± 9.7	83.0 ± 11.4	18.3 ± 2.4	20.8 ± 2.8
	3X2		6	117.7 ± 10.8	145.3 ± 15.6	19.6 ± 1.8	24.2 ± 2.6
	Arm 3		3	33.3 ± 2.2	36.0 ± 0.3	11.1 ± 0.8	12.0 ± 0.1
Arm 3	2X3		6	66.2 ± 22.5	87.9 ± 5.4	11.0 ± 3.7	14.7 ± 0.9
	Arm 4		2	n.b.[b]	n.b.	n.b.	n.b.
Gal	2X2Gal		4	n.b.	n.b.	n.b.	n.b.

[a] K_A values obtained from fitting SPR sensograms with a two-state reaction model. Errors were obtained from the deviations of the mean values of two independent measuring series. [b] Galactose-containing molecules did not show any binding in the assay.

ing to a two-step process does not give reproducible values. This makes sense according to the model; for a monovalent compound, no two-step process can occur. As negative control, galactose-containing molecules (**arm 4** and **2X2Gal**) were tested and showed no binding to Con A (Table 4). The highest values in K_{A1} and K_{Atotal} were obtained for branched glycomacromolecule **3X2**. Interestingly, compound **2X3** with the same valency but different degree of branching shows a clear decrease in K_{A1} and K_{Atotal} and rather similar values to compound **2X2**, although the latter one carries less sugar ligands. It seems as if a higher degree of branching affects the observed protein binding more strongly than the absolute valency of the structures. This is in agreement with previous studies[3f,g,26] discussing that depending on the accessibility of the sugar ligands within the construct, the introduction of additional sugar ligands does not lead to a further increase in binding affinity. Our data thus would suggest that an increased valency within the arms does not increase binding due to insufficient accessibility of the ligands for branched glycomacromolecules of our study. Comparing the di- and trivalent arms (**arm 2** and **arm 3**) with the di- and trivalent branched glycomacromolecules (**2X1** and **3X1**), here the non-branched arms show increased K_{A1} and K_{Atotal}. This might point again to a less favorable presentation of the sugar ligands if they are presented within an oligo(amidoamine) side chain and located rather closely to the backbone. To further evaluate the importance of valency versus the effect of branching, all values were normalized for the number of mannose ligands attached to the macromolecules (Table 4). Again, we see that compounds **3X2** and **2X2** give the highest binding values, however, their normalized values are now rather similar. This suggests that sugars in these constructs have a similar accessibility based on the similar structure of the side chains. Similarly, the trivalent arm (**arm 3**) and com-

pound **2X3** presenting the same arm two times on a backbone give similar normalized values. Divalent **arm 2** and trivalent compound **3X1** show similar normalized values with compound **2X1** giving the lowest normalized values, being less favorable in both, branching and valency. Overall our data show that an increase in valency by increasing the branching (e.g., going from **2X2** to **3X2**) leads to higher binding with Con A, whereas an increase in valency by elongating the side chains (e.g., going from **2X2** to **2X3**) does not lead to elevated binding suggesting that the location of sugars within the macromolecule makes them more or less accessible for contact with the protein receptor.

Conclusions

In summary, we were able to establish a split-and-combine approach for solid phase polymer synthesis to give access to branched glycomacromolecules. Firstly, a novel azide-functionalized building block was introduced now allowing for the direct introduction of azide moieties during solid phase polymer synthesis. By combining this new building block with previously established protocols for the synthesis of precision glycomacromolecules, a series of glycofunctionalized arms and backbones of varying length and valency were obtained. Using optimized CuAAC conjugation, arms and backbones were combined giving differently branched glycomacromolecules. These were then subjected to a binding study using model lectin Con A looking at the influence of branching on the protein binding properties. We have seen that a higher degree of branching leads to increased protein binding. However, for glycomacromolecules with similar degree of branching increasing the valency within the arms did not lead to further increase in binding. At this point, we attribute this to a potentially re-

duced accessibility of sugar ligands placed in the arms closer to the backbone. Future studies will extend on this concept creating branched precision glycomacromolecules presenting different carbohydrate ligands at the tip of the arm versus the ligands located closer to the scaffold to further evaluate our findings.

Experimental Section

Surface plasmon resonance (SPR): SPR measurements were performed with a Biacore X100 instrument from GE Healthcare Life Sciences. Con A was immobilized on a CM5 carboxymethyl dextran matrix sensor chip using 1-ethyl-3-(3-dimethylaminopropyl)carbodiimide (EDC) and N-hydroxysuccinimide (NHS) to 4000 response units (RU). The immobilization was performed in acetate buffer with pH 4.5. Sensograms were recorded with the Biacore X100 Control Software and evaluated with the Biacore X100 Evaluation Software. The sensograms were measured in 2 series of 3 cycles, at least one day between the series. Lectin Binding Buffer (LBB, 10 mM HEPES, 50 mM NaCl, 1 mM MnCl$_2$, 1 mM CaCl$_2$, pH 7.4 in MilliQ water) was used as the running buffer. The flow rate was set to 30 µL min^{-1}, and the contact and dissociation times were 105 and 180 s, respectively. After injecting concentration series, the sensor chip was regenerated by injecting 0.8 M α-D-methyl-mannopyranoside in LBB buffer twice at a flow rate of 10 µL min^{-1}, to completely dissociate the bound ligand from the immobilized Con A. The compounds were injected at concentrations of 20, 60, 180, 540, and 1620 µM for **arm 1** and 6.67, 20, 60, 180, 540 µM for all other compounds. Kinetic data of all glycomacromolecules were obtained using a two state reaction model.

General solid phase synthesis amide coupling protocols as well as solid phase assisted glycopyranoside CuAAC protocols are applied from established protocols and provided in the Supporting Information.[7, 17]

General CuAAC protocol for glycomacromolecule coupling: To a syringe reactor was added 20 µmol of the resin bound oligomeric structure **scaffold 1–2**, 30 µmol (1.5 equiv.) of **arms 1–4** per azide group, 10 mg (2 equiv.) of CuSO$_4$, and 10 mg (2.5 equiv.) of sodium ascorbate, all in their dry form. 0.8 mL of a DMF/H$_2$O = 1:1 mixture were drawn up to the syringe and the mixture was shaken for 5 days. Subsequently, the resin was washed extensively with water, a 23 mM solution of sodium diethyldithiocarbamate in DMF/H$_2$O = 1:1, DMF and DCM.

Synthesis of 2,2,2-trifluoro-N-(2-((2-(tritylamino)ethyl)amino)ethyl)-acetamide (1) according to the method described by Ponader et al.:[7] Triphenylmethyl chloride (69.7 g, 250 mmol) was dissolved in dichloromethane (150 mL) and added dropwise to an ice-cooled solution of diethylenetriamine (103.2 g, 1000 mmol) in dichloromethane (250 mL) over a period of 3 h. After complete addition, the solution was allowed to reach room temperature and stirred for additional 3 h. Then the mixture was concentrated to half volume, washed with saturated sodium bicarbonate solution (3×100 mL), brine (100 mL), dried over magnesium sulfate, and concentrated in vacuo. The resulting yellowish gel was used without further purification. The gel-like product was dissolved in tetrahydrofuran (250 mL) and cooled to 0 °C before ethyl trifluoroacetate (39.1 g, 275 mmol) was added in one portion. The mixture was allowed to reach room temperature and stirred for an additional 18 h before all volatiles were removed in vacuo. The resulting white foam was recrystallized from dichloromethane (200 mL), to which one drop of water was added. Compound **1** (99.6 g, 226 mmol, 90%) was isolated in excellent yield as a white powder. m.p. 106–108 °C;

^{1}H NMR (300 MHz, [D$_6$]DMSO): δ = 9.15 (s, 1H, NH-TFA), 7.44–7.13 (m, 15H, $aryl$-H), 3.34 (m, 2H, NH), 3.22 (t, ^3J = 6.5 Hz, 2H, CH_2), 2.63 (t, ^3J = 6.1 Hz, 2H, CH_2), 2.54 (t, ^3J = 6.5 Hz, 2H, CH_2), 2.06 ppm (t, ^3J = 6.1 Hz, 2H, CH_2); ^{13}C NMR (75 MHz, [D$_6$]DMSO): δ = 156.04 (q, ^3J = 35.8 Hz, CO-CF_3), 146.19 (3C), 128.40 (6C), 127.65 (6C), 126.01 (3C) (18C, all $aryl$-C), 117.88 (CF_3), 70.23 (CPh_3), 49.09, 47.49, 43.06, 39.39 ppm (4C, all CH_2); IR (ATR): $\tilde{v}_{max}$ = 3349 (w), 2847 (w), 1705 (s), 1147 (s), 694 cm^{-1} (s); MS for C$_{24}$H$_{26}$F$_3$N$_3$O (ESI, 4 eV) m/z: [M+H$^+$]: 442.2; found: 442.2.

Synthesis of 4-(azidomethyl)benzoic acid (2) according to the method described by Wrobel et al.:[27] P-toluic acid (102 g, 750 mmol), N-bromosuccinimide (133 g, 750 mmol), and benzoyl peroxide (0.24 g, 1.0 mmol) were dissolved in tetrachloromethane (1.5 l), before the mixture was refluxed for 6 h under rigorous stirring and afterwards dried in vacuo. The brominated product was isolated quantitatively after recrystallization from ethanol. This compound was then suspended in dimethylformamide under rigorous stirring (1.0 l), before sodium azide (98.5 g, 1.5 mol) was added in one portion. After 24 h the suspension was dried carefully. **Caution: Azide bearing low molecular weight compounds tend to have explosive properties due to heat and impact sensitivity.** The white solid was dissolved in water (500 mL) and concentrated hydrochloric acid was added dropwise until no white solid precipitated anymore. The white solid was filtered off, washed with hydrochloric acid (0.1 M) and dried in vacuo. Compound **2** (100.4 g, 567 mmol, 76%) was isolated as white granular powder. m.p. 129–131 °C; ^{1}H NMR (600 MHz, [D$_6$]DMSO): δ = 7.95 (d, ^3J = 8.1 Hz, 2H, $aryl$-H), 7.44 (d, ^3J = 8.2 Hz, 2H, $aryl$-H), 5.18 (s, 1H, CO_2H), 4.53 ppm (s, 2H, CH_2-N_3); ^{13}C NMR (151 MHz, [D$_6$]DMSO): δ = 167.61 (CO-Ph), 139.72 (1C), 132.33 (1C), 129.65 (2C), 128.17 (2C) (6C, all $aryl$-C), 53.20 ppm (CH_2-N_3); IR (ATR): $\tilde{v}_{max}$ = 3390 (b), 2550 (m), 2107 (ss), 1675 (ss), 1288 (ss), 750 cm^{-1} (s); GC-MS for C$_8$H$_7$N$_3$O$_2$ (EI, 70 eV) R_t = 7.5 min, m/z (%): 135 (100) [M-N$_3^-$], 148 (99) [M-N$_2$H$^-$], 177 (21) [M^+].

Synthesis of 4-(azidomethyl)-N-(2-(2,2,2-trifluoroacetamido)ethyl)-N-(2-(tritylamino)ethyl)benzamide (3): Compound 3 was synthesized using two different methods.

A: Compound **2** (4.87 g, 27.8 mmol) was suspended in dichloromethane (100 mL) and dimethylformamide (5 mL) with rigorous stirring under nitrogen atmosphere. A solution of oxalyl chloride (3.83 g, 30.3 mmol) in dichloromethane (5 mL) was carefully added dropwise into the solution of **2**. Meanwhile, compound **1** was dissolved in dichloromethane (100 mL) and triethylamine (10 mL) and cooled in an ice bath to 0 °C, to which the crude mixture of **2** was added dropwise using a dropping funnel over a period of 1 h. After complete addition, the ice bath was removed and the mixture was stirred for one more hour at room temperature. The reaction was quenched by the addition of saturated sodium bicarbonate solution (200 mL) before the organic layer was washed with water (3×100 mL), saturated sodium bicarbonate solution (100 mL) and brine (100 mL), dried over magnesium sulfate and concentrated in vacuo. The crude product (12.2 g, 20.2 mmol, 81%) was obtained after column chromatography (EtOAc/nHex = 1:1, R_f = 0.80) as a white foam and further recrystallized from diethylether. Pure compound **3** (10.8 g, 18.0 mmol, 72%) was isolated as a white powder. m.p. 111–113 °C; ^{1}H NMR (600 MHz, [D$_6$]DMSO, 100 °C): δ = 9.14 (s, 1H, NH-TFA), 7.52–7.10 (m, 19H, $aryl$-H), 4.51 (s, 2H, CH_2-N_3), 3.57–3.50 (m, 2H, $alkyl$-CH_2), 3.46–3.36 (m, 4H, 2 $alkyl$-CH_2), 3.00 (s, 1H, NH-Trt), 2.25 ppm (s, 2H, $alkyl$-CH_2); ^{13}C NMR (75 MHz, [D$_6$]DMSO): δ = 170.95 (CO-Ph), 156.36 (q, ^3J = 35.8 Hz, CO-CF_3), 145.85 (3C), 136.55 (2C), 128.17 (8C), 127.70 (6C), 126.84 (2C), 126.10 (3C) (24C, all $aryl$-C), 117.88 (CF_3), 70.28 (CPh_3), 53.21 (CH_2-N_3), 49.17, 44.07, 42.66, 37.17 ppm (4C, all CH_2); IR (ATR): $\tilde{v}_{max}$ =

3262 (m), 3100 (w), 2840 (w), 2097 (m), 1724 (s), 1625 (s), 1183 (s), 1142 (s), 707 cm^{-1} (s); HRMS for $C_{33}H_{31}F_3N_6O_2$ (ESI-TOF) m/z: [M+H$^+$]: 601.2533; found: 601.2547; elemental analysis calc.d (%) for $C_{33}H_{31}F_3N_6O_2$: C 65.99, H 5.20, N 13.99; found: C 66.07, H 5.45, N 13.98.

B: Compound **1** (11.0 g, 25.0 mmol) and **2** (4.84 g, 27.8 mmol), PyBOP (14.4 g, 27.8 mmol), and hydroxybenzotriazole (0.37 g, 2.8 mmol) were dissolved in dimethylformamide (200 mL) before diisopropylethylamine (13 mL, 75 mmol) was added in one portion. After complete conversion (18 h, the reaction progress was monitored by thin layer chromatography; EtOAc/nHex = 1:1, $R_f = 0.80$) the mixture was poured into water (400 mL) and the solvents were decanted off. The resulting white residue was dissolved in ethyl acetate (100 mL) and water (100 mL). The organic layer was washed with water (2×100 mL) and brine (100 mL), dried over magnesium sulfate, concentrated in vacuo and redissolved in diethylether (100 mL). The resulting white crystals (tripyrrolidinium-phosphoxide) were filtered off and the remaining solution was concentrated in vacuo, purified using column chromatography and recrystallized from diethylether. Compound **3** (10.3 g, 17.1 mmol, 69%) was isolated as white powder.

Synthesis of (9H-fluoren-9-yl)methyl (2-(4-(azidomethyl)-N-(2-(tritylamino)ethyl)benzamido)ethyl)carbamate and (9H-fluoren-9-yl)methyl (2-(4-(azidomethyl)benzamido)ethyl)(2-(tritylamino)ethyl)-carbamate (4 and 4b): Compound **3** (13.2 g, 21.9 mmol) was dissolved in methanol (200 mL) and an aqueous potassium carbonate solution (30 g, 220 mmol) in deionized water (20 mL) was added in one portion under rigorous stirring. The complete conversion of the starting material was confirmed by TLC after 5 days (EtOAc/nHex = 1:1), at which point all solvents were removed in vacuo and the resulting white foam was dissolved in a mixture of tetrahydrofuran (200 mL) and water (100 mL). Fmoc-chloride (5.95 g, 23.0 mmol) was added in one portion and the mixture was stirred for 1 h at room temperature. After complete conversion, as monitored by TLC, tetrahydrofuran was removed in vacuo and ethyl acetate (200 mL) was added. The organic layer was washed with water (3×100 mL) and brine (100 mL), dried over magnesium sulfate and concentrated in vacuo. **4** and **4b** were obtained quantitatively as a crude mixture as a slightly yellow foam and were used without further purification.

Synthesis of 7-(4-(azidomethyl)benzoyl)-1-(9H-fluoren-9-yl)-3,11-dioxo-2-oxa-4,7,10-triazatetradecan-14-oic acid (5)

6→5: Compound **6** was dissolved in potassium carbonate solution (6.0 g, 43 mmol) in water (60 mL). The reaction progress was monitored by RP-HPLC (linear gradient from 0–50% eluent B in 12 min at 25 °C). The reaction was stopped after 12 h at room temperature or after 2.5 h at 40 °C, when all starting material was consumed and almost no rearrangement product could be observed. Then tetrahydrofuran (180 mL) was added to the crude mixture before Fmoc-chloride (3.70 g, 14.3 mmol) was added in one portion. The mixture was then stirred for 4 h. Once the reaction was completed (monitored by TLC, EtOAc/nHex = 1:1) a 20% citric acid solution was added until pH 3–5 was reached. The product was then extracted with ethyl acetate (3×100 mL) and the organic phase was washed with brine (100 mL), dried over magnesium sulfate and concentrated in vacuo. After recrystallization from acetone, compound **5** (5.57 g, 9.5 mmol, 73%) was obtained as a white powder. m.p. 119–121 °C; ^{1}H NMR (600 MHz, [D$_6$]DMSO, 100 °C): δ = 11.59 (s, 1H, -CO$_2$H), 7.86 (d, ^3J = 7.5 Hz, 2H, Fmoc-H), 7.66 (d, ^3J = 7.4 Hz, 2H, Fmoc-H), 7.63 (s, 1H, NH-Fmoc), 7.41 (t, ^3J = 7.5 Hz, 2H, Fmoc-H), 7.39–7.34 (m, 4 aryl-H), 7.34–7.30 (t, ^3J = 7.4 Hz, 2H, Fmoc-H), 6.99 (s, 1H, NH-CO), 4.47 (s, 2H, CH$_2$-N$_3$), 4.30 (d, ^3J = 6.5 Hz, 2H, Fmoc-CH$_2$), 4.21 (t, ^3J = 6.6 Hz, 1H, Fmoc-CH), 3.41 (m, 4H, 2x alkyl-

CH$_2$), 3.26 (m, 2H, alkyl-CH$_2$), 3.19 (m, 2H, alkyl-CH$_2$), 2.44 (t, ^3J = 7.0 Hz, 2H, succinyl-CH$_2$), 2.34 ppm (t, ^3J = 7.0 Hz, 2H, succinyl-CH$_2$); ^{13}C NMR (75 MHz, [D$_6$]DMSO): δ = 173.85 (CO$_2$H), 170.68 (2C, CO, CO-Ph), 156.40 (carbamate-C), 143.92 (2C), 140.76 (2C), 136.66, 128.12 (2C), 128.04, 127.62 (2C), 127.06 (2C), 126.95 (2C), 125.13 (2C), 120.12 (2C) (18C, all aryl-C), 65.39 (Fmoc-CH), 53.21 (CH$_2$-N$_3$), 48.56 (CH$_2$), 46.69 (Fmoc-CH$_2$), 44.60 (CH$_2$), 38.46 (CH$_2$), 36.37 (CH$_2$), 30.07 (succinyl-CH$_2$), 29.09 ppm (succinyl-CH$_2$); IR (ATR): $\tilde{\nu}_{max}$ = 3290 (m), 3067 (w), 2953 (w), 2098 (m), 1730 (m), 1683 (m), 1604 (s), 1540 (m), 1276 (s), 1170 (s), 732 cm^{-1} (s); HRMS for $C_{31}H_{32}N_6O_6$ (ESI-TOF) m/z: [M+H$^+$] calcd: 585.2456; found: 585.2457; elemental analysis calcd (%) for $C_{31}H_{32}N_6O_6$: C 63.69, H 5.52, N 14.38; found: C 63.90, H 5.77, N 14.05; RP-HPLC (linear gradient from 0–75% eluent B in 30 min at 25° C): t_R = 18.9 min. Determined purity: 98%.

Synthesis of 4-((2-((((9H-fluoren-9-yl)methoxy)carbonyl)(2-(4-(azido-methyl)benzamido)ethyl)-amino)ethyl)amino)-4-oxobuta-noic acid (5b)

4 and 4b→5b: The crude mixture of **4** and **4b** and triethylsilane (3.9 mL, 24.6 mmol) was dissolved in dichloromethane (200 mL) and cooled to 0 °C before trifluoroacetic acid (20 mL) was added dropwise. The mixture was allowed to warm to room temperature and stirred for additional 2 h. Toluene (20 mL) was added and all volatiles were removed in vacuo. The resulting yellow-brown slurry was dissolved in dichloromethane (100 mL) and precipitated in diethylether (400 mL). The resulting yellow solid was filtered off and dried in vacuo to obtain the ammonium salt intermediate, which was dissolved in a solution of trimethylamine (9.3 mL, 67.2 mmol) and dichloromethane (200 mL) before succinic anhydride (2.47 g, 24.5 mmol) was added in one portion. The reaction was complete after 1 h (Ninhydrin test on TLC). Once the reaction was completed, a 10% citric acid solution was added until pH 3–5 was reached. Then the product was extracted with ethyl acetate (2×100 mL), washed with brine (100 mL), dried over magnesium sulfate and concentrated in vacuo. The raw product was purified using column chromatography (DCM/MeOH = 1:1, R_f = 0.9) and subsequent recrystallization from acetone. Compound **5b** (5.93 g, 10.1 mmol, 45%) was isolated as a white powder, **5** was not obtained and washed away. m.p. 150–152 °C; ^{1}H NMR (600 MHz, [D$_6$]DMSO): δ = 12.03 (s, 1H, -CO$_2$H), 8.72–8.49 (m, 1H, NH-Fmoc), 7.87 (t, ^3J = 6.6 Hz, 2H, Fmoc-H), 7.83 (t, ^3J = 8.3 Hz, 2H, Fmoc-H), 7.67 (dd, ^3J = 7.5, 5.2 Hz, 2H, Fmoc-H), 7.50–7.34 (m, 5H, NH-CO, Fmoc-H, aryl-H), 7.34–7.29 (m, 2H, aryl-H), 4.54–4.49 (m, 2H, CH$_2$-N$_3$), 4.30 (dd, ^3J = 12.0, 7.0 Hz, 2H, Fmoc-CH$_2$), 4.21 (t, ^3J = 7.0 Hz, 1H, Fmoc-CH), 3.46–3.31 (m, 6H, 3x 2 alkyl-CH$_2$), 3.21–3.11 (m, 2H, alkyl-CH$_2$), 2.59 (t, ^3J = 6.7 Hz, 1H, succinyl-CH), 2.55 (t, ^3J = 6.7 Hz, 1H, succinyl-CH), 2.45–2.40 ppm (m, 2H, succinyl-CH$_2$); ^{13}C NMR (151 MHz, [D$_6$]DMSO): δ = 173.98 (CO$_2$H), 171.29 (CO), 165.95 (CO-Ph), 156.26 (carbamate-C), 143.87 (2C), 140.73 (2C), 138.66, 133.93, 128.17 (2C), 127.58 (2C), 127.55 (2C), 127.04 (2C), 125.08 (2C), 120.09 (2C) (18C, all aryl-C), 65.45 (Fmoc-CH), 53.11 (CH$_2$-N$_3$), 47.15 (CH$_2$), 46.73 (Fmoc-CH$_2$), 45.60 (CH$_2$), 38.85 (CH$_2$), 37.45 (CH$_2$), 29.27 (succinyl-CH$_2$), 27.40 ppm (succinyl-CH$_2$); IR (ATR): $\tilde{\nu}_{max}$ = 3286 (m), 3153 (w), 2951 (m), 2101 (m), 1730 (s), 1697 (s), 1624 (s), 1218 (s), 739 cm^{-1} (s); HRMS for $C_{31}H_{32}N_6O_6$ (ESI-TOF) m/z: [M+H$^+$]: 585.2456; found: 585.2461; elemental analysis calcd (%) for $C_{31}H_{32}N_6O_6$: C 63.69, H 5.52, N 14.38; found: C 63.61, H 5.62, N 14.25.

Synthesis of 4-((2-(4-(azidomethyl)-N-(2-(2,2,2-trifluoroacetami-do)-ethyl)benzamido)ethyl)amino)-4-oxobutanoic acid (6): Compound **3** (10.8 g, 18.0 mmol) was dissolved in dichloromethane (100 mL) and triethylsilane (4.3 mL, 27.0 mmol) and cooled to 0 °C before trifluoroacetic acid (20 mL) was added dropwise. The reaction was allowed to reach room temperature and stirred for additional 2 h. After complete conversion the mixture was poured onto

diethylether (200 mL) in which the desired product settled down at 4 °C overnight. All solvents were decanted off and the resulting brown gel was dissolved in a mixture of trimethylamine (7.5 mL, 54.0 mmol) and dichloromethane (100 mL) before succinic anhydride (1.98 g, 19.8 mmol) was added in one portion. The reaction was complete after 1 h (Ninhydrin test on TLC). Upon completion of the reaction, a 10 % aqueous citric acid solution was added until pH 3–5 was reached. The product was extracted with ethyl acetate (2×100 mL), washed with brine (100 mL), dried over magnesium sulfate and concentrated in vacuo. The raw product was purified by recrystallization from ethyl acetate. Compound **6** (5.94 g, 13.0 mmol, 72 %) was isolated as a white powder. m.p. 127–129 °C; ^{1}H NMR (600 MHz, [D$_6$]DMSO, 100 °C): δ = 11.51 (s, 1H, -CO$_2$H), 9.20 (s, 1H, NH-TFA), 7.67 (s, 1H, NH-CO), 7.41 (d, ^3J = 8.1 Hz, 2H, aryl-H), 7.38 (d, ^3J = 7.9 Hz, 2H, aryl-H), 4.51 (s, 2H, CH$_2$-N$_3$), 3.54 (m, 2H, alkyl-CH$_2$), 3.41 (m, 4H, 2x alkyl-CH$_2$), 3.25 (m, 2H, alkyl-CH$_2$), 2.43 (t, ^3J = 7.1 Hz, 2H, succinyl-CH$_2$), 2.33 ppm (t, ^3J = 7.0 Hz, 2H, succinyl-CH$_2$); ^{13}C NMR (75 MHz, [D$_6$]DMSO): δ = 173.93 (CO), 173.90 (CO), 170.88 (CO-Ph), 156.40 (CO-CF$_3$), 136.60, 136.41, 128.21, 126.86 (6C, all aryl-C), 117.96 (CF$_3$), 53.20 (CH$_2$-N$_3$), 48.14, 43.40, 37.06, 36.94 (4C, all CH$_2$), 29.90 (succinyl-CH$_2$), 29.04 ppm (succinyl-CH$_2$); IR (ATR): $\tilde{\nu}_{max}$ = 3299 (m), 3084 (w), 2955 (w), 2104 (m), 1730 (m), 1701 (s), 1610 (s), 1160 cm^{-1} (s); HRMS for C$_{18}$H$_{21}$F$_3$N$_6$O$_5$ (ESI-TOF) m/z: [M+H$^+$] calcd: 459.1598; found: 459.1601; elemental analysis calcd (%) for C$_{18}$H$_{21}$F$_3$N$_6$O$_5$: C 47.16, H 4.62, N 18.33; found: C 46.87, H 4.59, N 17.94.

EDS (**7**),[17] α-D-propargyl-mannopyranoside (**8**)[19] and β-D-propargyl-galactopyranoside (**9**)[20] were synthesized according to previously described procedures.

Acknowledgements

Keywords: biomimetic synthesis · glycoconjugates · multivalency · precision glycomacromolecules · solid-phase synthesis

[1] a) K. Drickamer, M. E. Taylor, Annu. Rev. Cell Biol. **1993**, 9, 237–264; b) A. Varki, Glycobiology **1993**, 3, 97–130; c) C. R. Bertozzi, L. L. Kiessling, Science **2001**, 291, 2357–2364; d) M. Ambrosi, N. R. Cameron, B. G. Davis, Org. Biomol. Chem. **2005**, 3, 1593–1608.

[2] a) A. R. Pries, T. W. Secomb, P. Gaehtgens, Pflugers Arch. **2000**, 440, 653–666; b) S. Reitsma, D. W. Slaaf, H. Vink, M. van Zandvoort, M. Egbrink, Pflugers Arch. **2007**, 454, 345–359; c) S. Weinbaum, J. M. Tarbell, E. R. Damiano in Annual Review of Biomedical Engineering, Vol. 9, Annual Reviews, Palo Alto, **2007**, pp. 121–167.

[3] a) L. L. Kiessling, N. L. Pohl, Chem. Biol. **1996**, 3, 71–77; b) R. Roy, Curr. Opin. Struct. Biol. **1996**, 6, 692–702; c) D. A. Mann, M. Kanai, D. J. Maly, L. L. Kiessling, J. Am. Chem. Soc. **1998**, 120, 10575–10582; d) M. Mammen, S. K. Choi, G. M. Whitesides, Angew. Chem. Int. Ed. **1998**, 37, 2754–2794; Angew. Chem. **1998**, 110, 2908–2953; e) C. W. Cairo, J. E. Gestwicki, M. Kanai, L. L. Kiessling, J. Am. Chem. Soc. **2002**, 124, 1615–1619; f) J. E. Gestwicki, C. W. Cairo, L. E. Strong, K. A. Oetjen, L. L. Kiessling, J. Am. Chem. Soc. **2002**, 124, 14922–14933; g) C. A. Hunter, H. L. Anderson, Angew. Chem. Int. Ed. **2009**, 48, 7488–7499; Angew. Chem. **2009**, 121, 7624–7636; h) B. Voit, D. Appelhans, Macromol. Chem. Phys. **2010**, 211, 727–735; i) G. Ercolani, L. Schiaffino, Angew. Chem. Int. Ed. **2011**, 50, 1762–1768; Angew. Chem. **2011**, 123, 1800–1807; j) C. Fasting, C. A. Schalley, M. Weber, O. Seitz, S. Hecht, B. Koksch, J. Dernedde, C. Graf, E. W. Knapp, R. Haag, Angew. Chem. Int. Ed. **2012**, 51, 10472–10498; Angew. Chem. **2012**, 124, 10622–10650.

[4] a) N. Jentoft, Trends Biochem. Sci. **1990**, 15, 291–294; b) J. Perez-Vilar, R. L. Hill, J. Biol. Chem. **1999**, 274, 31751–31754.

[5] a) A. Imberty, Y. M. Chabre, R. Roy, Chem. Eur. J. **2008**, 14, 7490–7499; b) O. Renaudet, R. Roy, Chem. Soc. Rev. **2013**, 42, 4515–4517; c) G. Yilmaz, C. R. Becer, Front. Bioeng. Biotechnol. **2014**, 2, 39.

[6] a) T. K. Dam, C. F. Brewer, Chem. Rev. **2002**, 102, 387–429; b) T. K. Dam, R. Roy, D. Page, C. F. Brewer, Biochemistry **2002**, 41, 1359–1363; c) T. K. Dam, R. Roy, D. Page, C. F. Brewer, Biochemistry **2002**, 41, 1351–1358; d) J. J. Lundquist, E. J. Toone, Chem. Rev. **2002**, 102, 555–578; e) T. K. Dam, C. F. Brewer, Methods Enzymol. **2004**, 379, 107–128; f) M. Ambrosi, N. R. Cameron, B. G. Davis, S. Stolnik, Org. Biomol. Chem. **2005**, 3, 1476–1480; g) T. K. Dam, H. J. Gabius, S. Andre, H. Kaltner, M. Lensch, C. F. Brewer, Biochemistry **2005**, 44, 12564–12571; h) T. K. Dam, S. Oscarson, R. Roy, S. K. Das, D. Page, F. Macaluso, C. F. Brewer, J. Biol. Chem. **2005**, 280, 8640–8646; i) T. K. Dam, C. F. Brewer, Biochemistry **2008**, 47, 8470–8476; j) T. K. Dam, T. A. Gerken, C. F. Brewer, Biochemistry **2009**, 48, 3822–3827; k) V. Wittmann, Curr. Opin. Chem. Biol. **2013**, 17, 982–989; l) A. Bernardi, J. Jimenez-Barbero, A. Casnati, C. De Castro, T. Darbre, F. Fieschi, J. Finne, H. Funken, K. E. Jaeger, M. Lahmann, T. K. Lindhorst, M. Marradi, P. Messner, A. Molinaro, P. V. Murphy, C. Nativi, S. Oscarson, S. Penades, F. Peri, R. J. Pieters, O. Renaudet, J. L. Reymond, B. Richichi, J. Rojo, F. Sansone, C. Schaffer, W. B. Turnbull, T. Velasco-Torrijos, S. Vidal, S. Vincent, T. Wennekes, H. Zuilhof, A. Imberty, Chem. Soc. Rev. **2013**, 42, 4709–4727; m) S. Cecioni, A. Imberty, S. Vidal, Chem. Rev. **2015**, 115, 525–561; n) C. Lavilla, G. Yilmaz, V. Uzunova, R. Napier, C. R. Becer, A. Heise, Biomacromolecules **2017**, 18, 1928–1936.

[7] D. Ponader, F. Wojcik, F. Beceren-Braun, J. Dernedde, L. Hartmann, Biomacromolecules **2012**, 13, 1845–1852.

[8] R. B. Merrifield, J. Am. Chem. Soc. **1963**, 85, 2149–2154.

[9] L. A. Carpino, G. Y. Han, J. Am. Chem. Soc. **1970**, 92, 5748–5749.

[10] a) F. Wojcik, S. Lel, A. G. O'Brien, P. H. Seeberger, L. Hartmann, Beilstein J. Org. Chem. **2013**, 9, 2395–2403; b) F. Wojcik, A. G. O'Brien, S. Gotze, P. H. Seeberger, L. Hartmann, Chem. Eur. J. **2013**, 19, 3090–3098; c) D. Ponader, S. Igde, M. Wehle, K. Marker, M. Santer, D. Bleger, L. Hartmann, Beilstein J. Org. Chem. **2014**, 10, 1603–1612; d) D. Ponader, P. Maffre, J. Aretz, D. Pussak, N. M. Ninnemann, S. Schmidt, P. H. Seeberger, C. Rademacher, G. U. Nienhaus, L. Hartmann, J. Am. Chem. Soc. **2014**, 136, 2008–2016.

[11] T. Freichel, S. Eierhoff, N. L. Snyder, L. Hartmann, J. Org. Chem. **2017**, 82, 9400–9409.

[12] a) B. Ernst, J. L. Magnani, Nat. Rev. Drug Discovery **2009**, 8, 661–677; b) M. Semsarilar, V. Ladmiral, S. Perrier, Macromolecules **2010**, 43, 1438–1443; c) O. Renaudet, G. Dasgupta, I. Bettahi, A. Shi, A. B. Nesburn, P. Dumy, L. BenMohamed, PLoS One **2010**, 5, e11216; d) G. Goti, A. Palmioli, M. Stravalaci, S. Sattin, M. G. De Simoni, M. Gobbi, A. Bernardi, Chem. Eur. J. **2016**, 22, 3686–3691; e) S. Sattin, A. Bernardi, Trends Biotechnol. **2016**, 34, 483–495.

[13] K. Lin, A. M. Kasko, Biomacromolecules **2013**, 14, 350–357.

[14] a) W. B. Turnbull, J. F. Stoddart, Rev. Mol. Biotechnol. **2002**, 90, 231–255; b) Y. M. Chabre, R. Roy, Curr. Top. Med. Chem. **2008**, 8, 1237–1285; c) Y. M. Chabre, R. Roy in Advances in Carbohydrate Chemistry and Biochemistry Vol 63, Vol. 63, (Ed.: D. Horton), Elsevier Academic Press Inc, San Diego, **2010**, pp. 165–393; d) K. Khanna, S. Varshney, A. Kakkar, Polym. Chem. **2010**, 1, 1171–1185; e) R. Roy, T. C. Shiao, K. Rittenhouse-Olson, Braz. J. Pharm. Sci. **2013**, 49, 85–108; f) J. M. Ren, T. G. McKenzie, Q. Fu, E. H. H. Wong, J. T. Xu, Z. S. An, S. Shanmugam, T. P. Davis, C. Boyer, G. G. Qiao, Chem. Rev. **2016**, 116, 6743–6836; g) A. Sharma, R. Sharma, A. Abouelmagd, A. Kakkar in Miktoarm Star Polymers: From Basics of Branched Architecture to Synthesis Self-assembly and Applications, RSC, **2017**, pp. 150–180.

[15] S. Bräse, C. Gil, K. Knepper, V. Zimmermann, Angew. Chem. Int. Ed. **2005**, 44, 5188–5240; Angew. Chem. **2005**, 117, 5320–5374.

[16] a) R. D. Poretz, I. J. Goldstein, Biochem. Pharmacol. **1971**, 20, 2727–2739; b) F. G. Loontiens, J. P. Vanwauwe, R. Degussem, C. K. Debruyne, Carbohydr. Res. **1973**, 30, 51–62; c) R. D. Farina, R. G. Wilkins, Biochim. Biophys. Acta Gen. Subj. **1980**, 631, 428–438; d) N. Sharon, H. Lis, Faseb J. **1990**, 4, 3198–3208; e) D. Loganathan, S. E. Osborne, G. D. Glick, I. J. Goldstein, Arch. Biochem. Biophys. **1992**, 299, 268–274; f) A. Troganis, C. I. Stassinopoulou, Biochim. Biophys. Acta Protein Struct. Mol. Enzymol. **1994**, 1206, 215–224; g) P. N. Kanellopoulos, K. Pavlou, A. Perrakis, B. Agianian, C. E. Vorgias, C. Mavrommatis, M. Soufi, P. A. Tucker, S. J. Ha-

modrakas, *J. Struct. Biol.* **1996**, *116*, 345–355; h) M. W. Jones, L. Otten, S. J. Richards, R. Lowery, D. J. Phillips, D. M. Haddleton, M. I. Gibson, *Chem. Sci.* **2014**, *5*, 1611–1616; i) K. L. Hudson, G. J. Bartlett, R. C. Diehl, J. Agirre, T. Gallagher, L. L. Kiessling, D. N. Woolfson, *J. Am. Chem. Soc.* **2015**, *137*, 15152–15160; j) M. Touaibia, A. Wellens, T. C. Shiao, Q. Wang, S. Sirois, J. Bouckaert, R. Roy, *ChemMedChem* **2007**, *2*, 1190–1201.

[17] M. F. Ebbesen, C. Gerke, P. Hartwig, L. Hartmann, *Polym. Chem.* **2016**, *7*, 7086–7093.

[18] C. Montalbetti, V. Falque, *Tetrahedron* **2005**, *61*, 10827–10852.

[19] M. Bergeron-Brlek, T. C. Shiao, M. C. Trono, R. Roy, *Carbohydr. Res.* **2011**, *346*, 1479–1489.

[20] C. D. Spicer, B. G. Davis, *Chem. Commun.* **2013**, *49*, 2747–2749.

[21] a) M. Touaibia, T. C. Shiao, A. Papadopoulos, J. Vaucher, Q. G. Wang, K. Benhamioud, R. Roy, *Chem. Commun.* **2007**, 380–382; b) C. R. Becer, M. I. Gibson, J. Geng, R. Ilyas, R. Wallis, D. A. Mitchell, D. M. Haddleton, *J. Am. Chem. Soc.* **2010**, *132*, 15130–15132; c) D. Grünstein, M. Maglinao, R. Kikkeri, M. Collot, K. Barylyuk, B. Lepenies, F. Kamena, R. Zenobi, P. H. Seeberger, *J. Am. Chem. Soc.* **2011**, *133*, 13957–13966; d) L. Dehuyser, E. Schaeffer, O. Chaloin, C. G. Mueller, R. Baati, A. Wagner, *Bioconjugate Chem.* **2012**, *23*, 1731–1739; e) X. B. Li, P. X. Wu, S. H. Cheng, X. Lv, *J. Med. Chem.* **2012**, *55*, 2702–2710.

[22] C. Gerke, M. F. Ebbesen, D. Jansen, S. Boden, T. Freichel, L. Hartmann, *Biomacromolecules* **2017**, *18*, 787–796.

[23] a) E. M. Muñoz, J. Correa, E. Fernandez-Megia, R. Riguera, *J. Am. Chem. Soc.* **2009**, *131*, 17765–17767; b) E. M. Muñoz, J. Correa, R. Riguera, E. Fernandez-Megia, *J. Am. Chem. Soc.* **2013**, *135*, 5966–5969.

[24] M. Ballauff, C. N. Likos, *Angew. Chem. Int. Ed.* **2004**, *43*, 2998–3020; *Angew. Chem.* **2004**, *116*, 3060–3082.

[25] N. J. de Mol, M. J. E. Fischer in *Handbook of Surface Plasmon Resonance*, The Royal Society of Chemistry, **2008**, pp. 123–172.

[26] a) E. K. Woller, E. D. Walter, J. R. Morgan, D. J. Singel, M. J. Cloninger, *J. Am. Chem. Soc.* **2003**, *125*, 8820–8826; b) M. L. Wolfenden, M. J. Cloninger, *J. Am. Chem. Soc.* **2005**, *127*, 12168–12169; c) S. L. Mangold, M. J. Cloninger, *Org. Biomol. Chem.* **2006**, *4*, 2458–2465; d) M. L. Wolfenden, M. J. Cloninger, *Bioconjugate Chem.* **2006**, *17*, 958–966.

[27] M. Wrobel, J. Aube, B. Konig, *Beilstein J. Org. Chem.* **2012**, *8*, 1027–1036.

CHEMISTRY
A European Journal

Supporting Information

Split-and-Combine Approach Towards Branched Precision Glycomacromolecules and Their Lectin Binding Behavior

Mischa Baier, Markus Giesler, and Laura Hartmann*[a]

chem_201704179_sm_miscellaneous_information.pdf

Supporting Information

Split & Combine Approach towards Branched Precision Glycomacromolecules and their Lectin Binding Behavior

Mischa Baier,[a] Markus Giesler [a] and Laura Hartmann*[a]

[a]   Institute of Organic and Macromolecular Chemistry
       Heinrich-Heine-University Duesseldorf
       Universitaetsstraße 1, 40225 Duesseldorf (Germany)
       M. Baier, M. Giesler, Prof. Dr. L. Hartmann, E-mail: laura.hartmann@hhu.de

Table of Contents

Materials and Methods

Materials

Diethylenetriamine (99%), 2, 2′-(Ethylenedioxy)bis(ethylamine) (98%), Ethyl trifluoroacetate (99%), Propargyl alcohol (99%), Succinic anhydride (>99%), Triethylsilane (99%), Triisopropylsilane (98%), (+)-Sodium-L-ascorbate (> 99.0%), Manganese (II) chloride tetrahydrate (>99%), 1-Hydroxybenzotriazole hydrate (>97%), HATU (O-(7-Azabenzotriazol-1-yl)-N,N,N',N'-tetramethyluronium-hexafluorphosphat, 97%), Oxyma pure (Ethyl (hydroxyimino)cyanoacetate, 97%) and N-(2-Hydroxyethyl)piperazine-N′-(2-ethanesulfonic acid (HEPES) (>99.5) were purchased from Merck (former Sigma Aldrich). D-(+)-Galactose (>99%), Trityl chloride (98%), p-Toluic acid (98%), Piperidine (99%), copper (II) sulfate (98%), 4-Pentynoic acid (98%) were purchased from Acros Organics. Oxalyl dichloride (98%), p-Toluenesulfonic acid monohydrate (98%), Boron trifluoride diethyl etherate (>98%), β-D-Galactose pentaacetate (98%) and Sodium methoxide (98%) were purchased from Alfa Aesar. N-Bromosuccinimide (99%) was purchased from Merck. Sodium azide (99%), Calcium chloride (≥ 97%) and diethyl dithiocarbamate (99%) were purchased from Applichem. PyBOP (Benzotriazole-1-yl-oxy-tris-pyrrolidino-phosphonium hexafluorophosphat) was obtained from Iris Biotech. Acetic anhydride (99%) was purchased from VWR. D (+)-Mannose (99%) was purchased from Amresco. 9-Fluorenylmethyl chloroformate (Fmoc-Cl, 98%) was purchased from Chempur. N, N-Diisopropylethylamine (99%), was obtained from Roth. Diisopropylcarbodiimide (DIC, 98%) and Trifluoroacetic acid (TFA, 99%) were purchased from Fluorochem. Tentagel S RAM (Rink Amide) resin (Capacity 0.25 mmol/g) was purchased from Rapp Polymere. Peptide synthesis grade N,N-Dimethylformamide was used. All solvents were of $p.a.$ reagent grade.

Instrumentation

Nuclear Magnetic Resonance spectroscopy (NMR)
^{1}H-NMR (300 MHz) spectra were recorded on a Bruker AVANCE III - 300. ^{1}H-NMR (600 MHz) spectra were recorded on a Bruker AVANCE III - 600. Chemical shifts of all NMR spectra were reported in delta (δ) expressed in parts per million (ppm). For ^{1}H-NMR the residual, non-deuterated solvent was used as internal standard. The following abbreviations are used to indicate the multiplicities: s, singlet; d, doublet; t triplet; m multiplet.

Attenuated Total Reflectance Fourier Transform Infrared Spectroscopy (ATR FTIR)
IR spectra were recorded with a Nicolet 6700, attenuated total reflectance Fourier transform infrared spectroscopy (ATR FTIR) spectrometer from Thermo Scientific and spectra analyzed using Omnic software 7.4.

Melting point
Melting points were measured on a BÜCHI Melting Point B – 545 apparatus.

Reversed Phase - High Performance Liquid Chromatography - Mass Spectrometry (RP-HPLC-MS)
Measurements were performed on an Agilent 1260 Infinity instrument coupled to a variable wavelength detector (VWD) (set to 214 nm) and a 6120 Quadrupole LC/MS containing an Electrospray Ionization (ESI) source (operated in positive ionization mode in a m/z range of 200 to 2000). As HPLC column a Poroshell 120 EC-C18 (3.0×50 mm, 2.5 μm) RP column from Agilent was used. The mobile phases A and B were H_2O/ACN (95/5) and H_2O/ACN (5/95), respectively. Both mobile phases contained 0.1% of formic acid. Samples were analyzed at a flow rate of 0.4 mL/min using a linear gradient starting with 100% mobile phase A reaching 50% mobile phase B within 30 min. The temperature of the column compartment was set to 25 °C. UV and MS spectral analysis was done within the OpenLab ChemStation software for LC/MS from Agilent Technologies.

Ultra High Resolution - Mass Spectrometry (UHR-MS)
UHR-MS measurements were performed with a Bruker UHR-QTOF maXis 4G instrument with a direct inlet via syringe pump, an ESI source and a quadrupole followed by a Time Of Flight (QTOF) mass analyzer.

Gel Permeation Chromatography (GPC) analysis
GPC was performed using an Agilent 1200 series HPLC system equipped with three aqueous GPC columns from Polymer Standards Service (PSS) Mainz, Germany (Suprema Lux analytical 8 mm diameter, 5 μm particle size, precolumn of 50 mm, 2 Å ~ 100 Å of 300 mm, 1000 Å of 300 mm). MilliQ water with 50 mM NaH_2PO_4, 150 mM NaCl, 250 ppm NaN_3 and of pH 7 + 30% ACN, filtered through an inline 0.1 μm membrane filter, was used as GPC eluent with a flow rate of 1 mL/min. Multi-angle light scattering- and differential refractive index spectra were recorded using a miniDAWN TREOS and Optilab rEX, respectively, that were both from Wyatt Technologies EU. Data analysis was performed using the Astra 5 software using a measured dn/dc value of 0.156 mL/g for all the glycooligo(amidoamine)s.

Surface Plasmon Resonance (SPR)
SPR measurements were performed with a Biacore X100 instrument from GE Healthcare Life Sciences. Con A was immobilized on a CM5 carboxymethyl dextran matrix sensor chip using 1-ethyl-3-(3-dimethylaminopropyl)carbodiimide (EDC) and N-hydroxysuccinimide (NHS) to 4000 response units (RU). The immobilization was performed in acetate buffer with pH 4.5. Sensograms were recorded with the Biacore X100 Control Software and evaluated with the Biacore X100 Evaluation Software. The sensograms were measured in 2 series of 3 cycles, at least one day between the series. Lectin Binding Buffer (LBB, 10mM Hepes, 50mM NaCl, 1mM $MnCl_2$, 1mM $CaCl_2$, pH 7.4 in MilliQ water) was used as the running buffer. The flow rate was set to

30 μL/min, and the contact and dissociation times were 105 and 180 s, respectively. After injecting concentration series, the sensor chip was regenerated by injecting 0.8 M α-D-methyl-mannopyranoside in LBB buffer at a flow rate of 10 μL/min twice to completely dissociate the bound ligand from the immobilized Con A. The compounds were injected at concentrations of 20, 60, 180, 540 and 1620 μM for **arm 1** and 6.67, 20, 60, 180, 540 μM for all other compounds respectively.

Freeze dryer
The final oligomers were freeze dried with an Alpha 1-4 LD plus instrument from Martin Christ Freeze Dryers GmbH. The main drying method was set to -55 °C and 0.1 mbar.

General Methods

Solid phase synthesis protocols
The batch sizes for synthesizing the oligomers using solid phase synthesis varied from 10 μmol to 500 μmol.

Fmoc cleavage
The Fmoc protecting group of the resin as well as from the coupled building blocks or amino acid were cleaved by the addition of a solution of 25% piperidine in DMF. The deprotection was performed twice for 10 min. After that, the resin was washed thoroughly 10 times with DMF.

General coupling protocol
Commercially available Tentagel S RAM (Rink Amide) resin was used as resin for solid phase synthesis. As an example 200 μmol of the resin were swollen in 10 mL of DCM for 20 min and subsequently washed five times with 10 mL of DMF. The Fmoc protecting group of the Tentagel S RAM resin was removed following the Fmoc cleavage protocol. A building block was coupled to the resin using a mixture of 1 mmol (5 eq.) of building block and 1 mmol PyBOP (5 eq.) dissolved in 4 mL DMF to which 2 mmol (10 eq.) of DIPEA were added. The mixture was shaken for 30 s under a nitrogen stream for activation and subsequently added to the resin. The resin with the coupling mixture was shaken for 1 h. After that, the resin was washed from excessive reagent 5 times with 10 mL of DMF.

Capping of *N*-terminal primary amine
After successful assembly of the desired number of building blocks on solid phase, the *N*-terminal site was capped with an acetyl group. Therefore, 10 mL acetic anhydride were shaken with the resin for 30 min.

General CuAAC protocol
To 200 μmol of the resin loaded with the oligomeric structure, 400 μmol (2 eq.) of acetyl protected propargyl pyranoside **8-9** per azide group, dissolved in 3 mL DMF, were added. 5 mg (0.1 eq.) of $CuSO_4$ per azide and 5 mg (0.125 eq.) of sodium ascorbate per azide were dissolved each in 1 mL of water and also added to the resin. This mixture was shaken overnight and subsequently washed extensively with water, a 23 mM solution of sodium diethyldithiocarbamate in DMF/H_2O = 1:1, DMF and DCM.

General CuAAC protocol for glycomacromolecule coupling
To a syringe reactor exemplary 20 μmol of the resin bound oligomeric structure **scaffold 1-2**, 30 μmol (1.5 eq.) of **arms 1-4** per azide group, 10 mg (2 eq.) of $CuSO_4$ and 10 mg (2.5 eq.) of sodium ascorbate were added in their dry form. 0.8 mL of a DMF/H_2O = 1:1 mixture were drawn up to the syringe and the mixture was shaken for 5 days. Subsequently, the resin was washed extensively with water, a 23 mM solution of sodium diethyldithiocarbamate in DMF/H_2O = 1:1, DMF and DCM.

On resin acetyl deprotection
In order to remove the acetyl protective groups of the carbohydrate moieties, 10 mL of a 0.2 M solution of sodium methanolate in methanol were added to the resin and shaken for 1 h. Subsequently the resin was washed 5 times with 10 mL of DMF.

Cleavage from solid phase
13 mL of a mixture of 95% TFA, 2.5% of TIPS and 2.5% of DCM were added to the resin and shaken for 1 h. The filtrate was poured into 60 mL cold diethyl ether. The resin was washed with an additional 5 mL of the cleavage mixture which were also added to the cold ether. The resulting precipitate was centrifuged three times and the ether decanted. The crude product was dried over a stream of nitrogen, dissolved in 6 mL of H_2O and lyophilized twice.

General preparative purification protocol of the oligomers
The oligomers were all purified by preparative Reversed Phase - High Performance Liquid Chromatography on an Agilent 1260 Infinity instrument coupled to a variable wavelength detector (VWD) (set to 214 nm). As HPLC column a UG80 C18 (20mmI.D.×250 mm, 5 μm) RP column from Shiseido was used. The mobile phases A and B were H_2O and ACN, respectively. Samples were purified at a flow rate of 20 mL/min using a linear gradient starting with 100% mobile phase A reaching 50% mobile phase B within 12 min. The temperature of the column compartment was room temperature (18-23° C). UV analysis was done within the OpenLab ChemStation software for LC/MS from Agilent Technologies.

Experimental Data

Spectra of the BADS building block
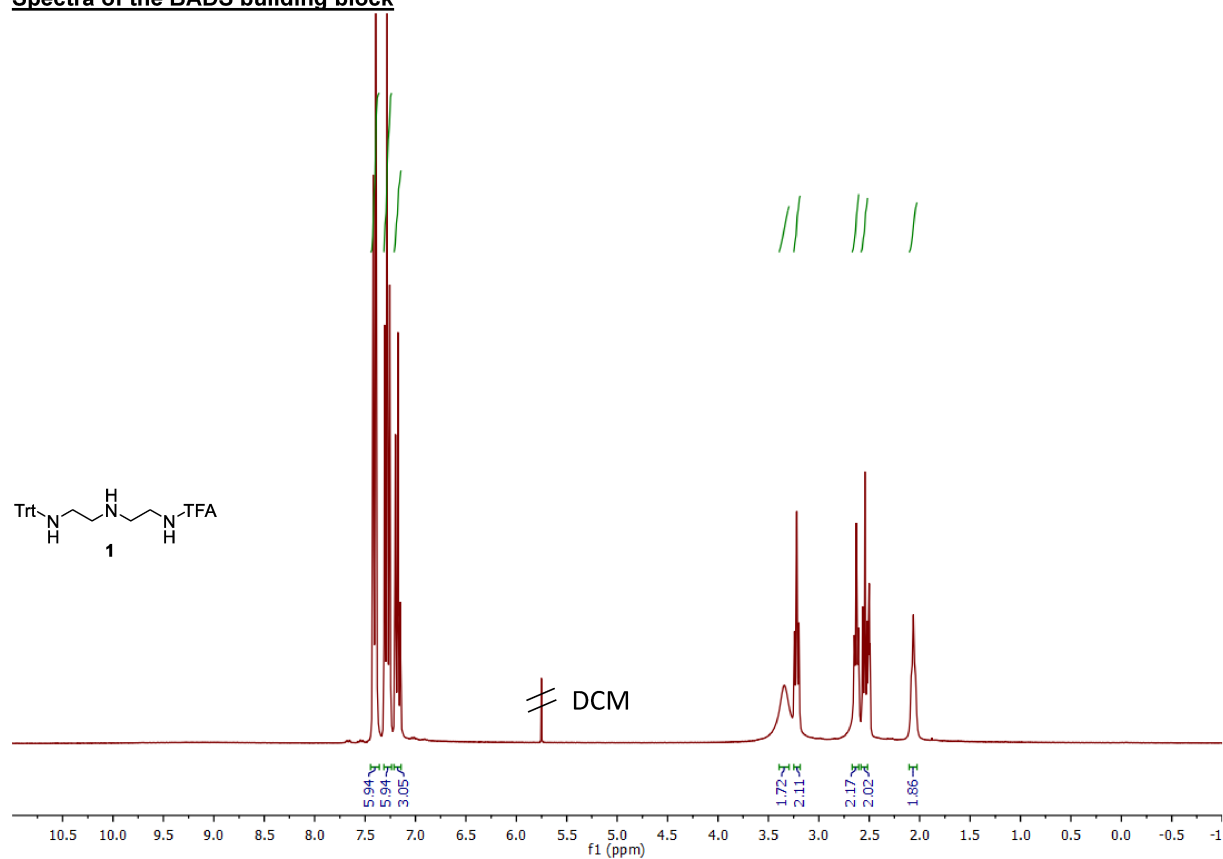
Figure S1: ^{1}H-NMR (300 MHz, DMSO-d_6) of compound **1.**
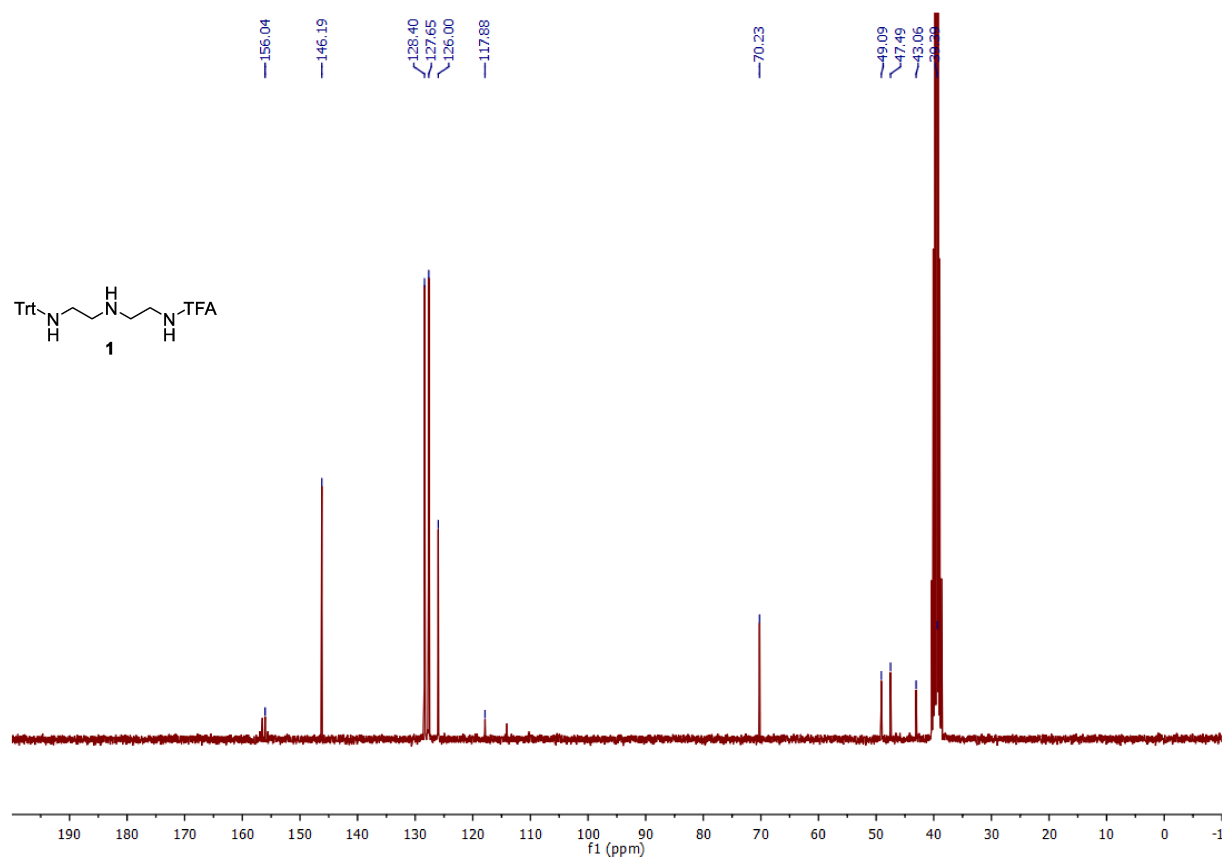
Figure S2: ^{13}C-NMR (75 MHz, DMSO-d_6) of compound **1.**
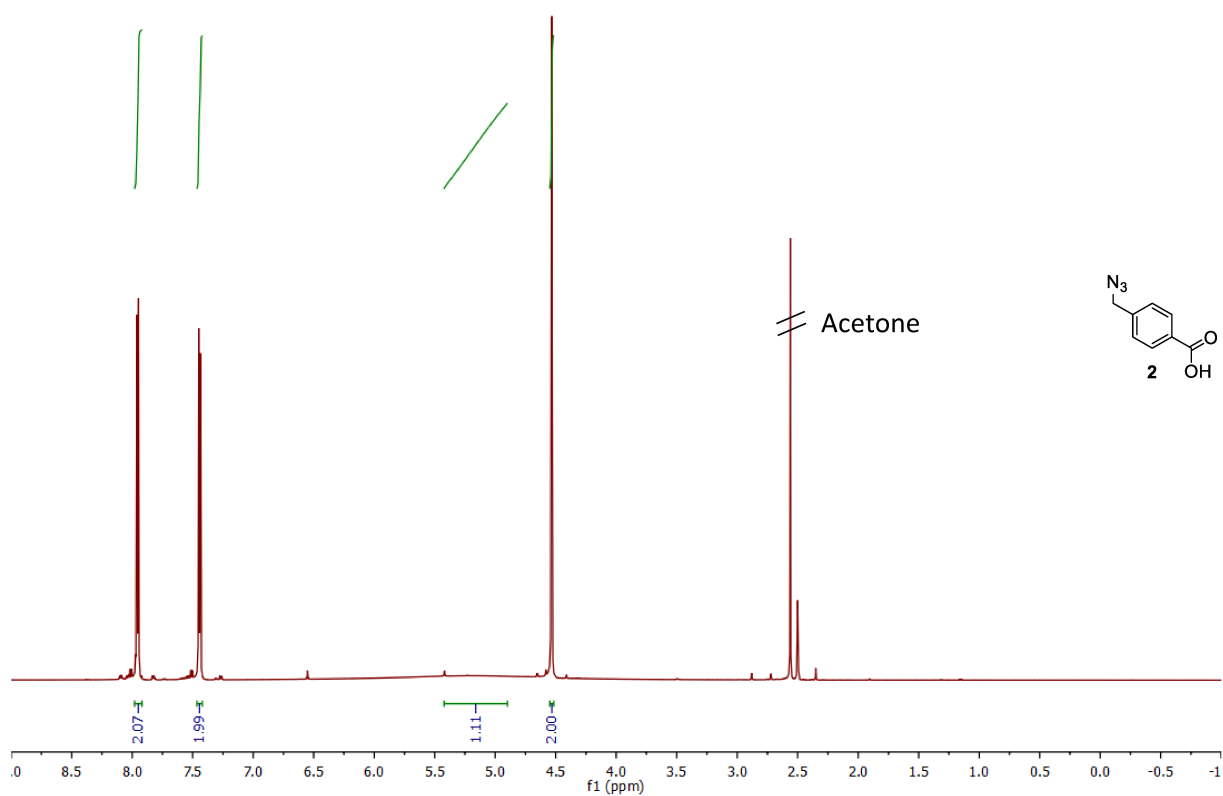
Figure S3: ^{1}H-NMR (600 MHz, DMSO-d_6) of compound **2.**
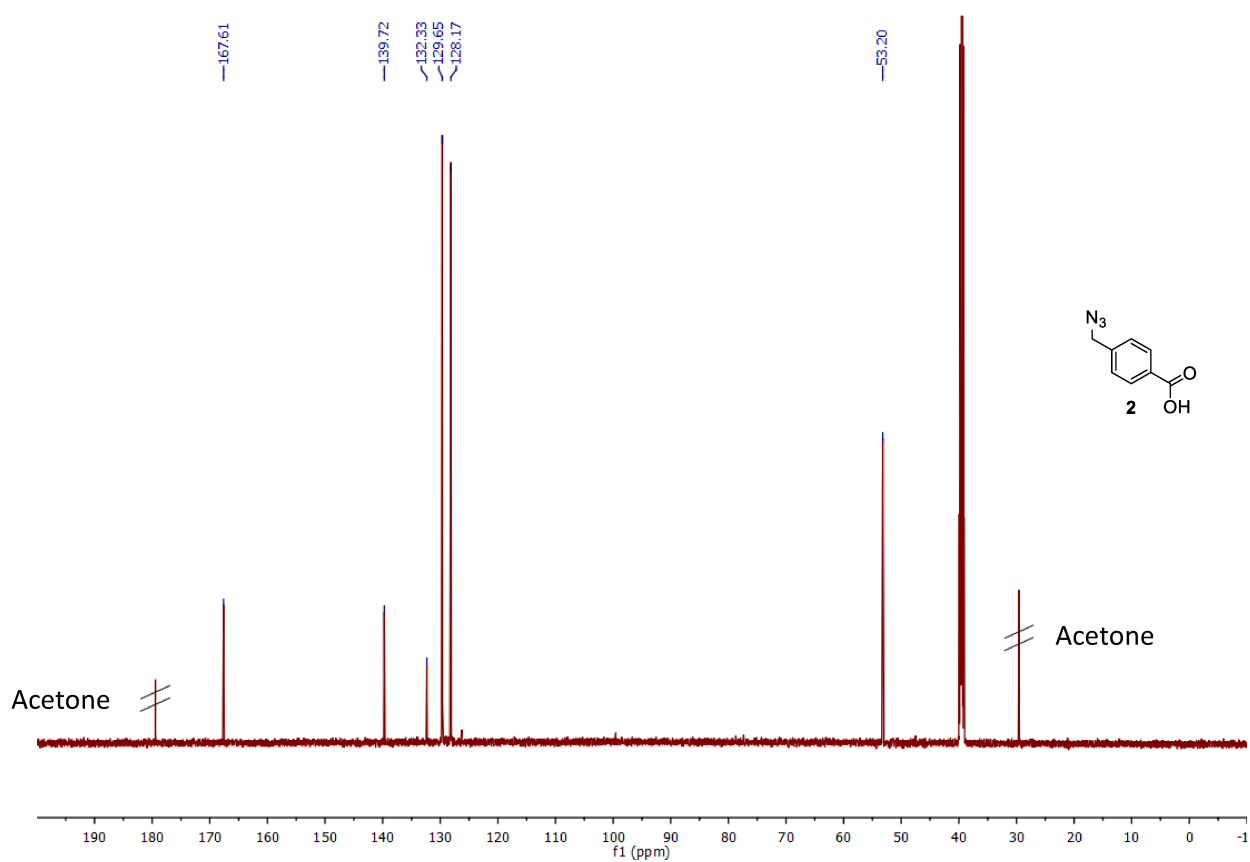
Figure S4: ^{13}C-NMR (151 MHz, DMSO-d_6) of compound **2.**
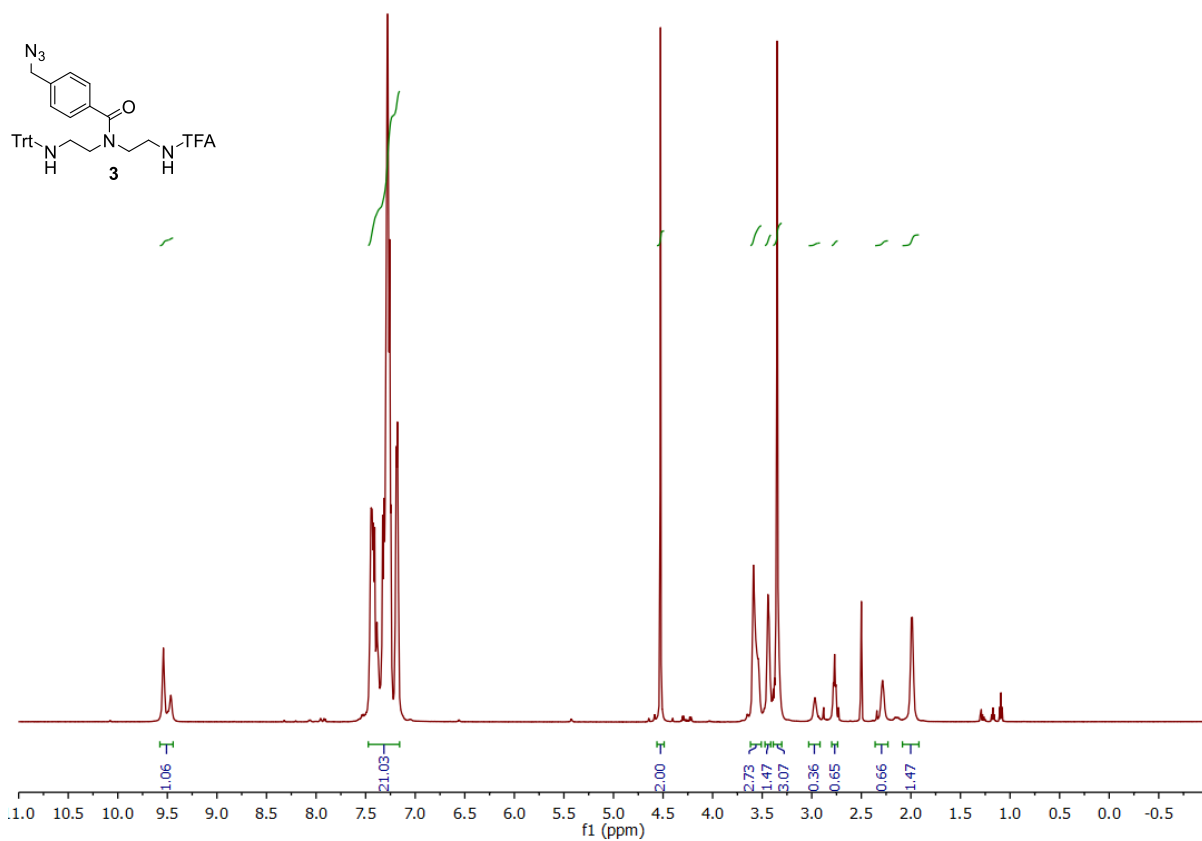
Figure S5: ¹H-NMR (600 MHz, DMSO-d_6) of compound **3** recorded at 25°C.
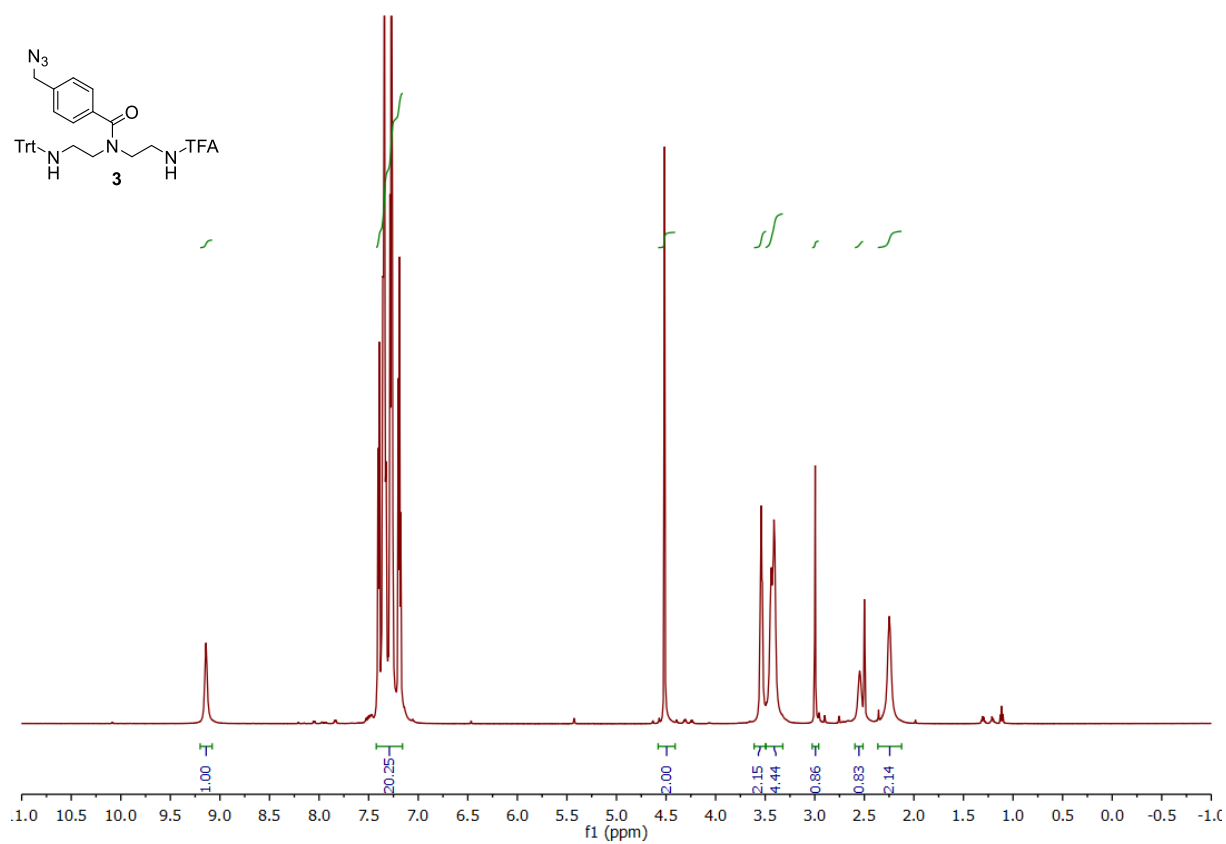
Figure S6: ¹H-NMR (600 MHz, DMSO-d_6) of compound **3** recorded at 100°C.

Figure S7: ^{13}C-NMR (151 MHz, DMSO-d_6) of compound **3** recorded at 25°C.

Figure S8. RP-HPLC (linear gradient from 0 - 75% eluent B in 30 min at 25°C) and HR-MS (ESI+ Q-TOF, positive mode) of compound **3**.
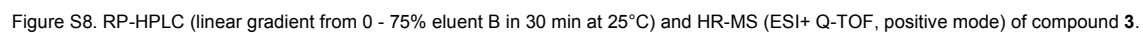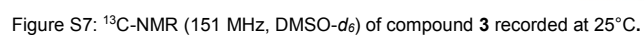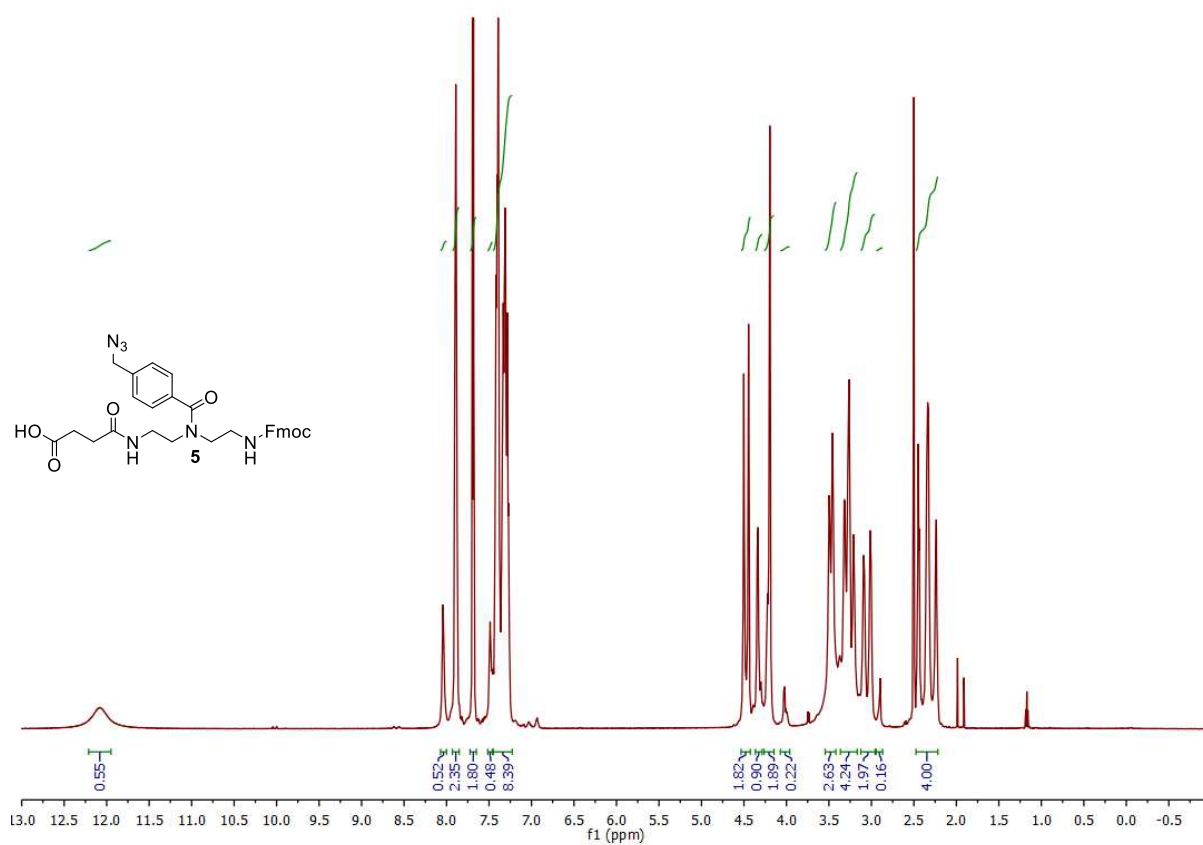
Figure S9: ^{1}H-NMR (600 MHz, DMSO-d_6) of compound **5** recorded at 25°C.
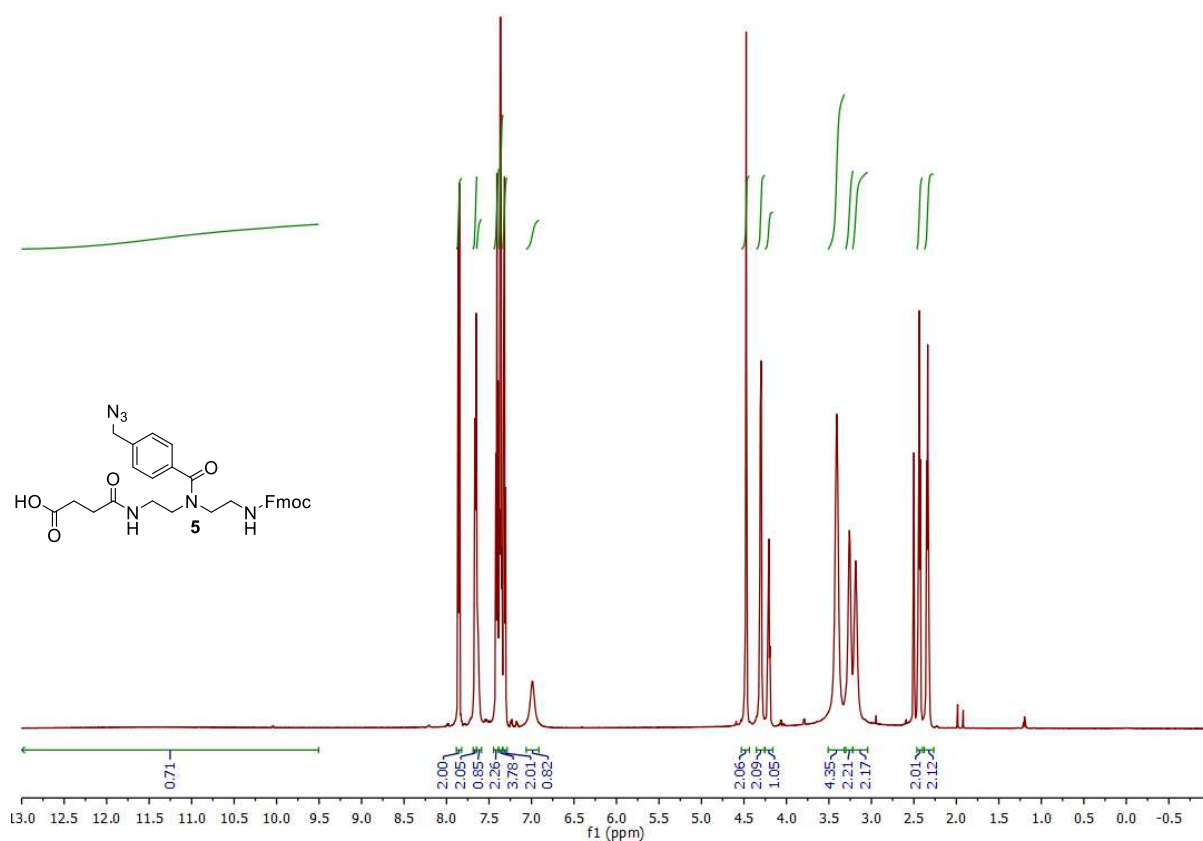
Figure S10: ^{1}H-NMR (600 MHz, DMSO-d_6) of compound **5** recorded at 100°C.
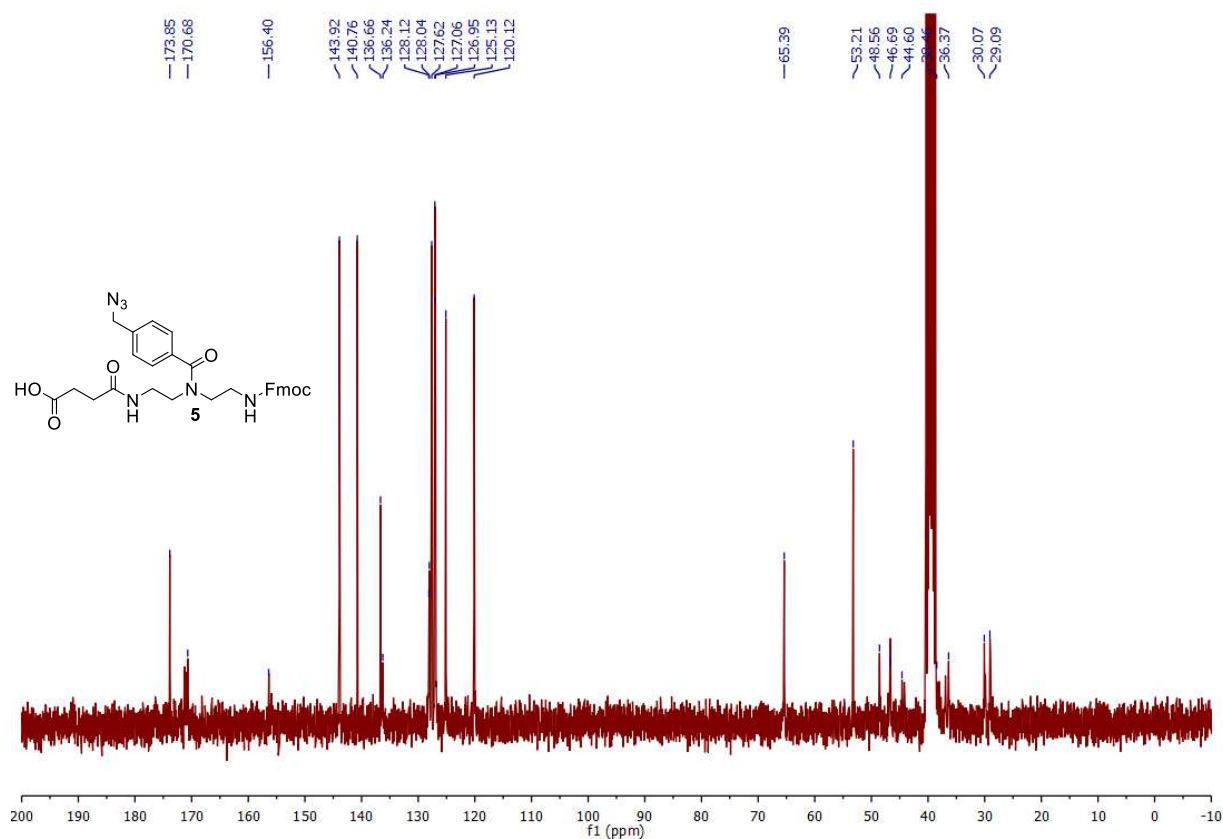
Figure S11: ¹³C-NMR (151 MHz, DMSO-*d₆*) of compound **5** recorded at 25°C.
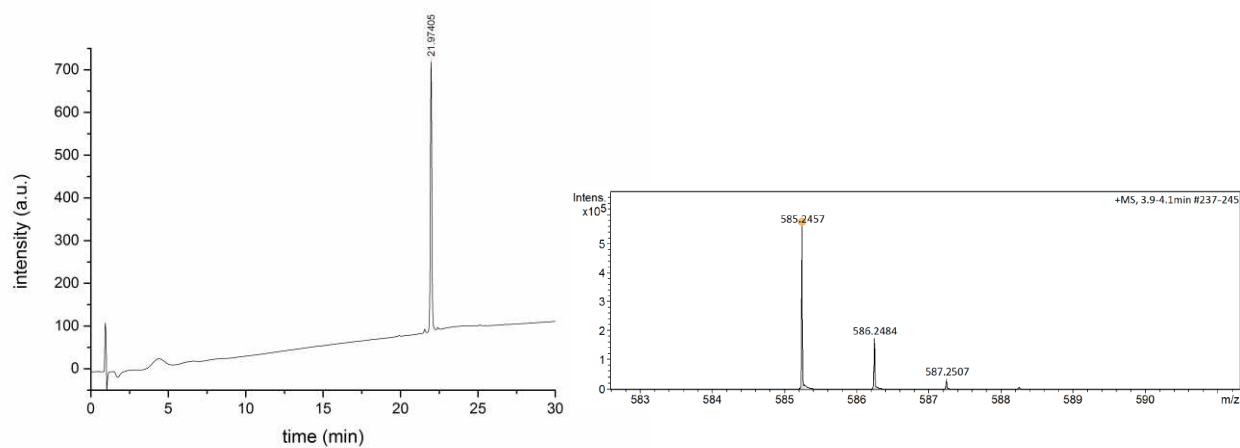
Figure S12. RP-HPLC (linear gradient from 0 - 75% eluent B in 30 min at 25°C) and HR-MS (ESI+ Q-TOF, positive mode) of compound **5**.
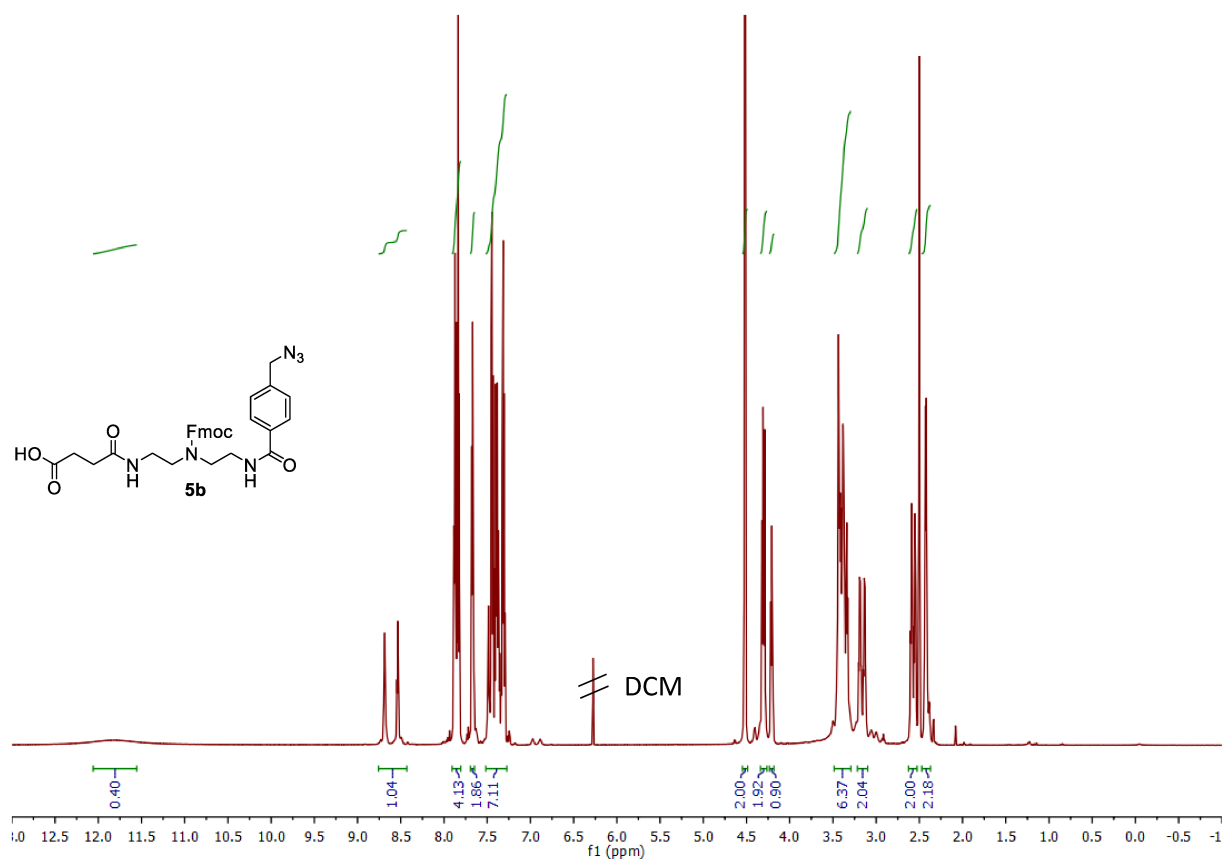
Figure S13: ^{1}H-NMR (600 MHz, DMSO-d_6) of compound **5b** recorded at 25°C.
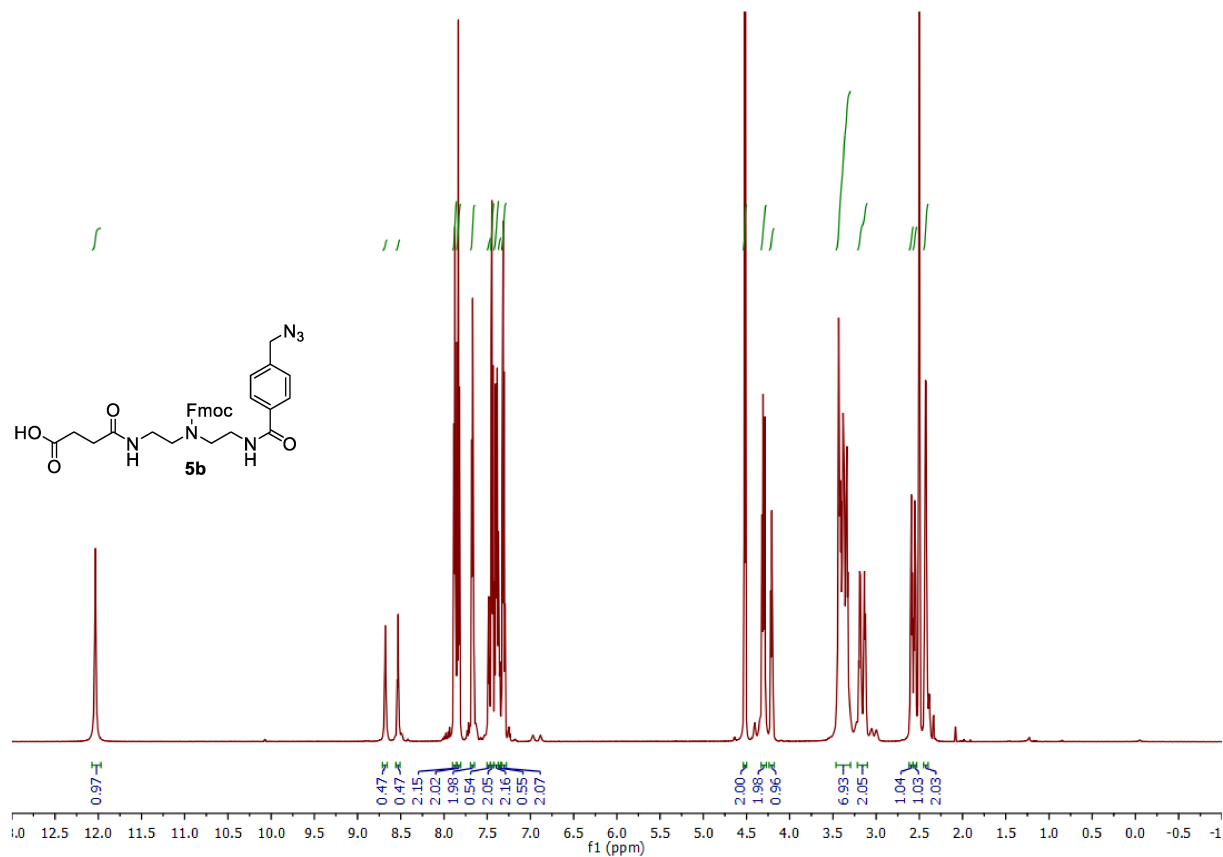
Figure S14: ^{1}H-NMR (600 MHz, DMSO-d_6) of compound **5b** recorded at 100°C.

Figure S15: ^{13}C-NMR (151 MHz, DMSO-d_6) of compound **5b** recorded at 25°C.

Figure S16. RP-HPLC (linear gradient from 0 - 75% eluent B in 30 min at 25°C) and HR-MS (ESI+ Q-TOF, positive mode) of compound **5b**.
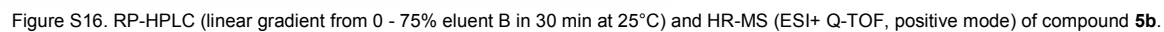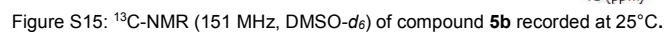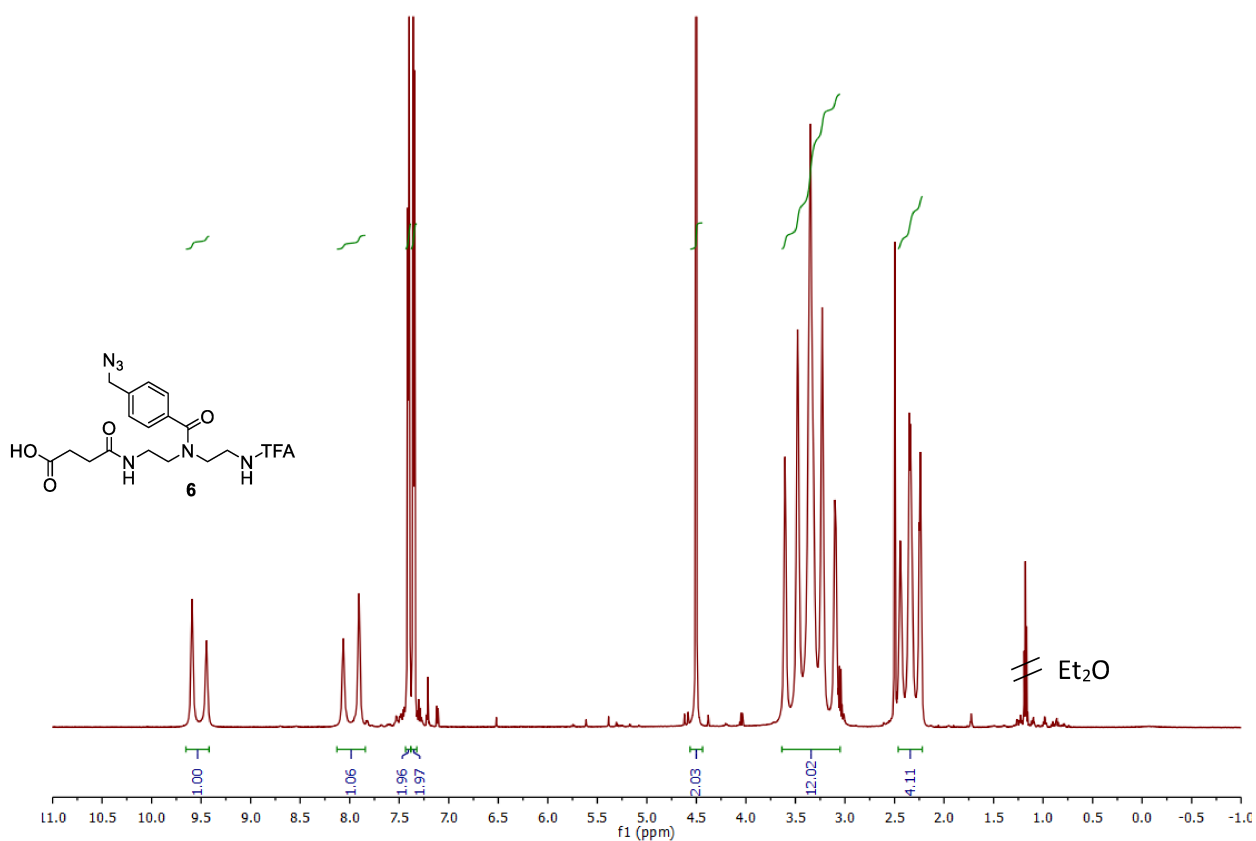
Figure S17: ¹H-NMR (600 MHz, DMSO-*d₆*) of compound **6** recorded at 25°C.
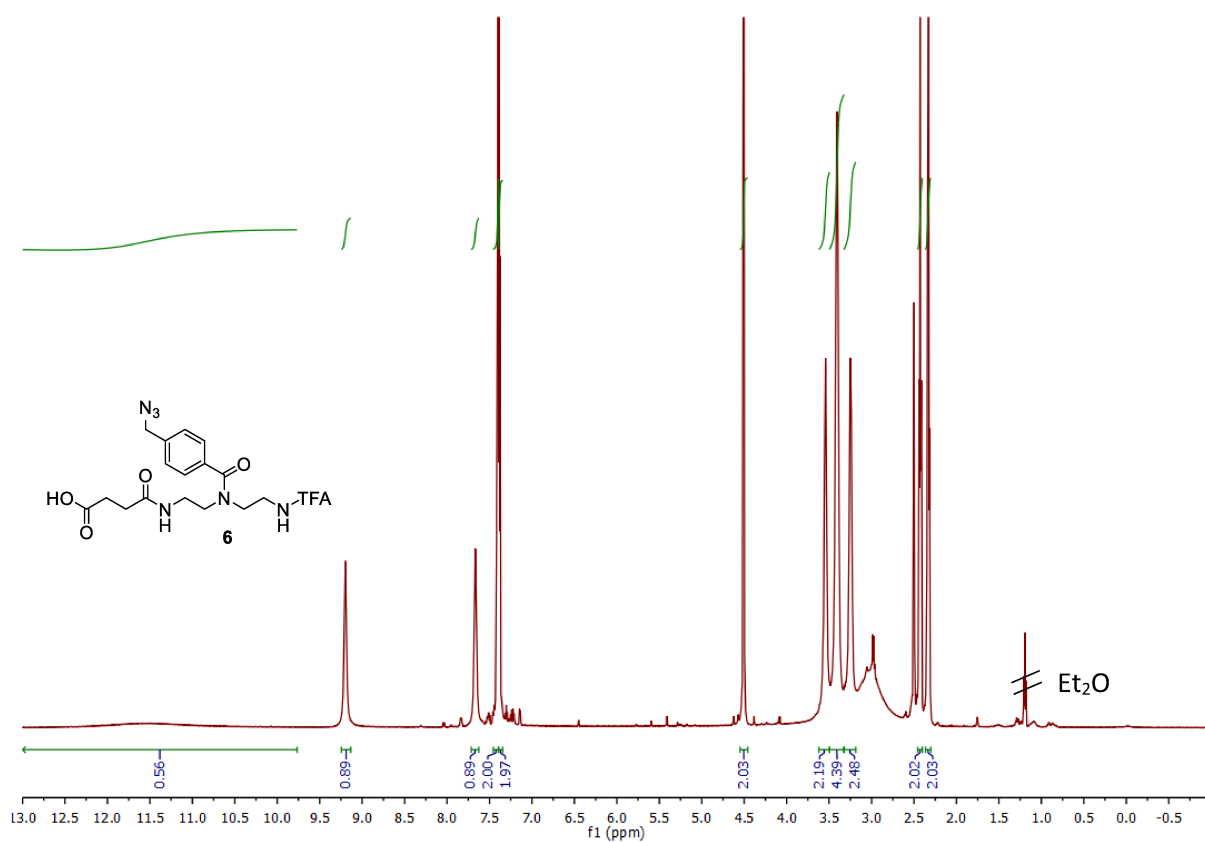
Figure S18: ¹H-NMR (600 MHz, DMSO-*d₆*) of compound **6** recorded at 100°C.
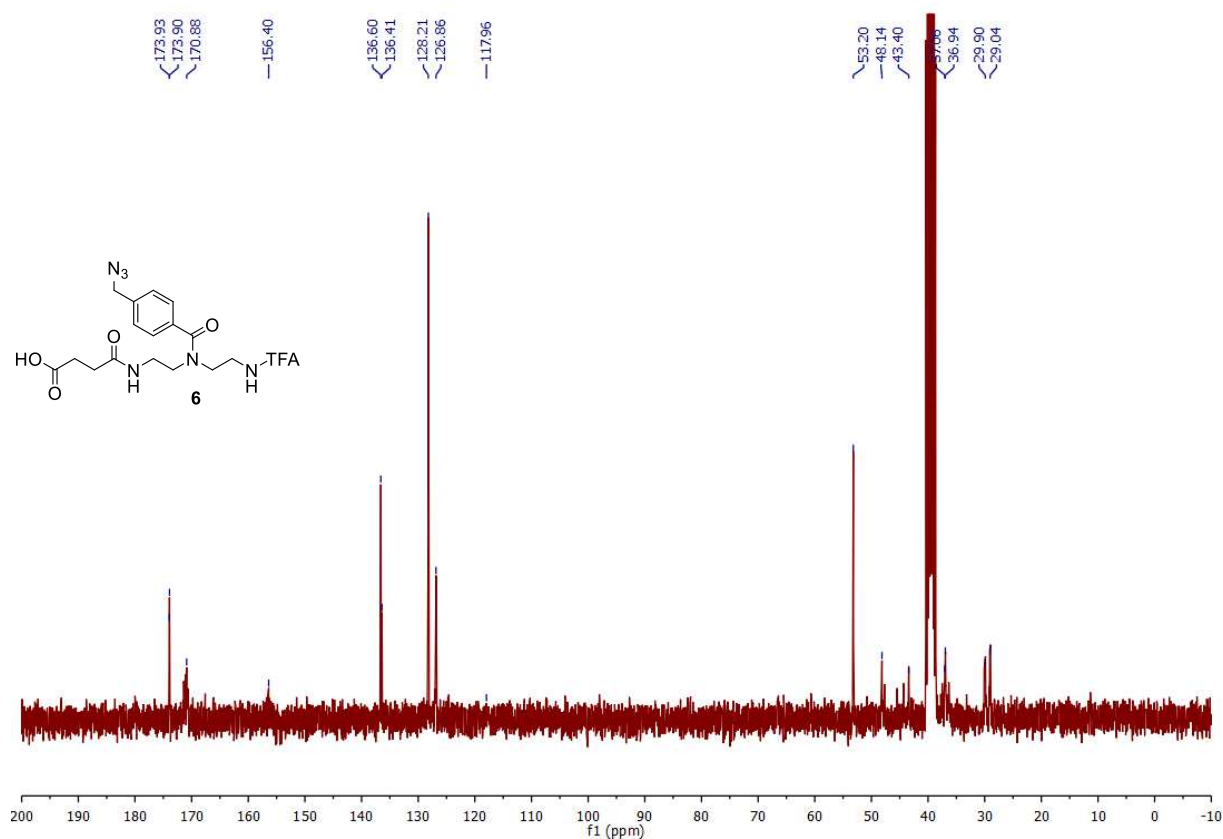
Figure S19: ^{13}C-NMR (151 MHz, DMSO-d_6) of compound **6** recorded at 25° C.
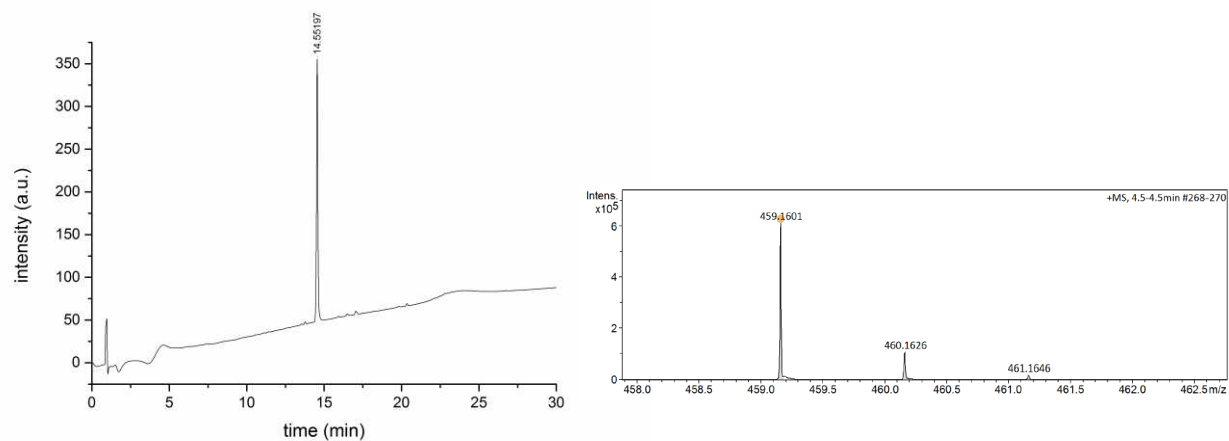
Figure S20. RP-HPLC (linear gradient from 0 - 75% eluent B in 30 min at 25°C) HR-MS (ESI+ Q-TOF, positive mode) of compound **6**.

Spectra of EDS, α-D-propargyl-mannopyranoside and β-D-propargyl-galactopyranoside
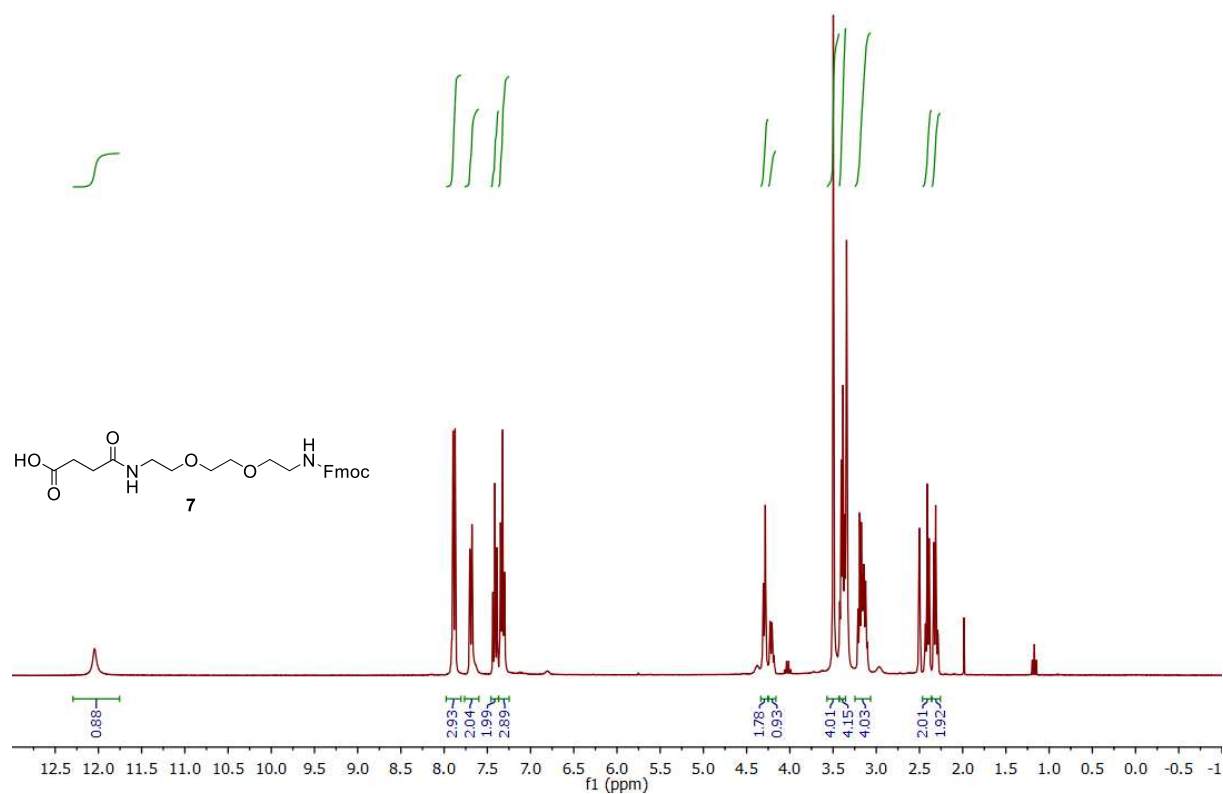
Figure S21: ¹H-NMR (300 MHz, DMSO-d_6) of compound **7.**
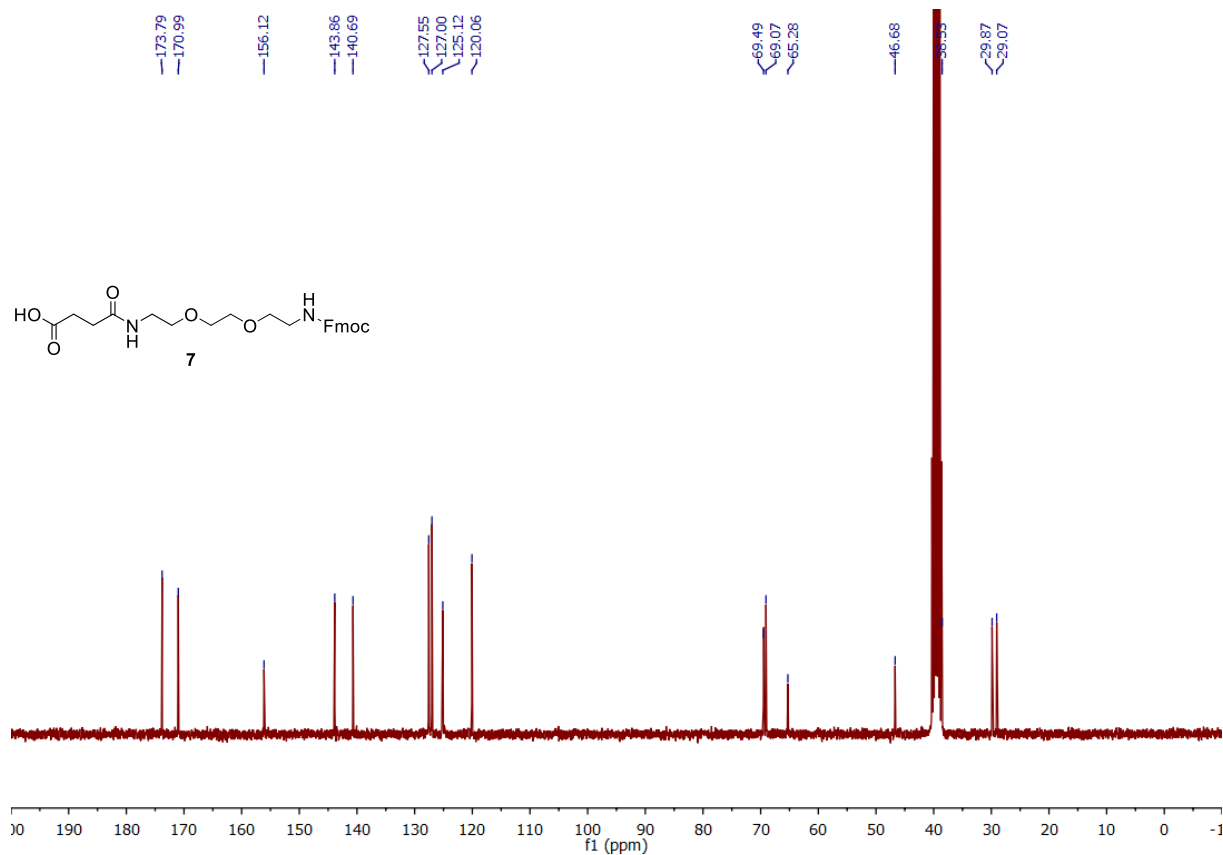
Figure S22: ¹³C-NMR (75 MHz, DMSO-d_6) of compound **7.**
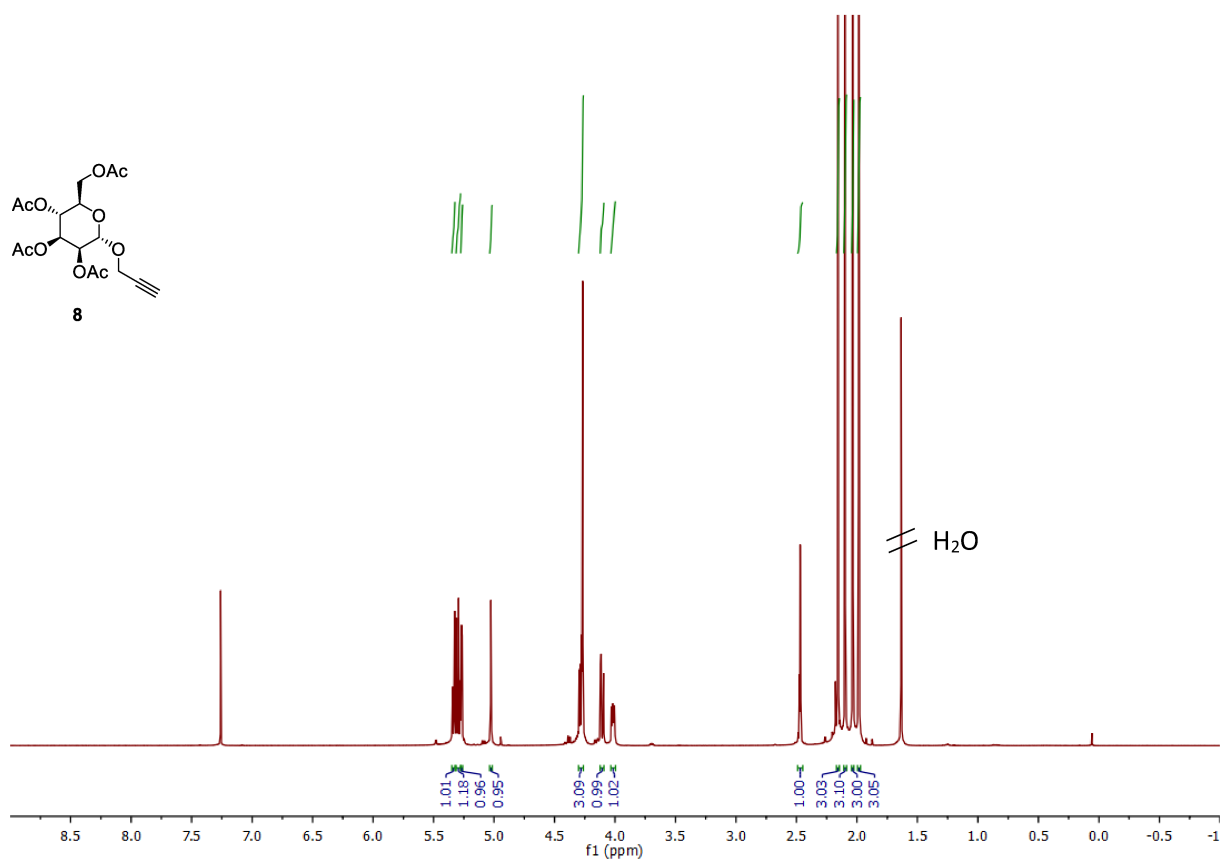
Figure S23: ^{1}H-NMR (600 MHz, CDCl$_3$) of compound **8.**
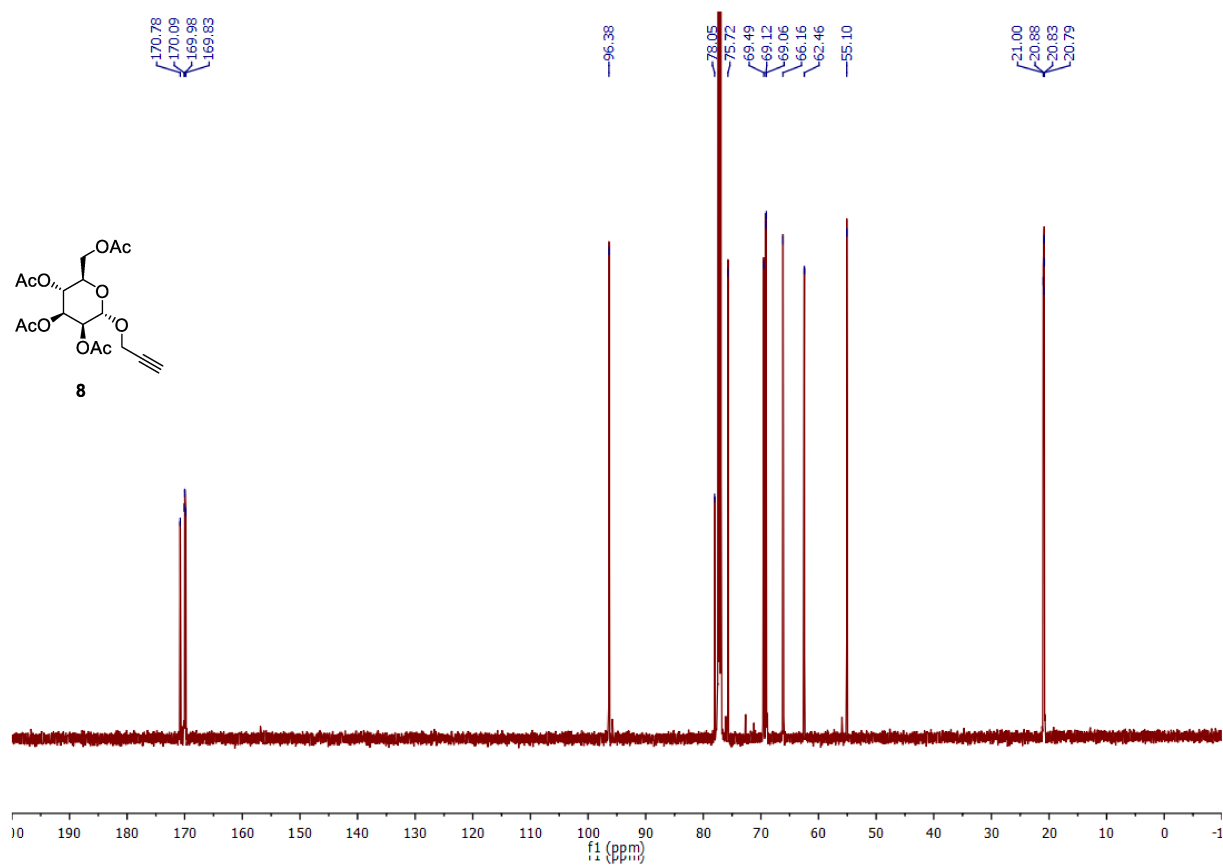
Figure S24: ^{13}C-NMR (75 MHz, CDCl$_3$) of compound **8**.
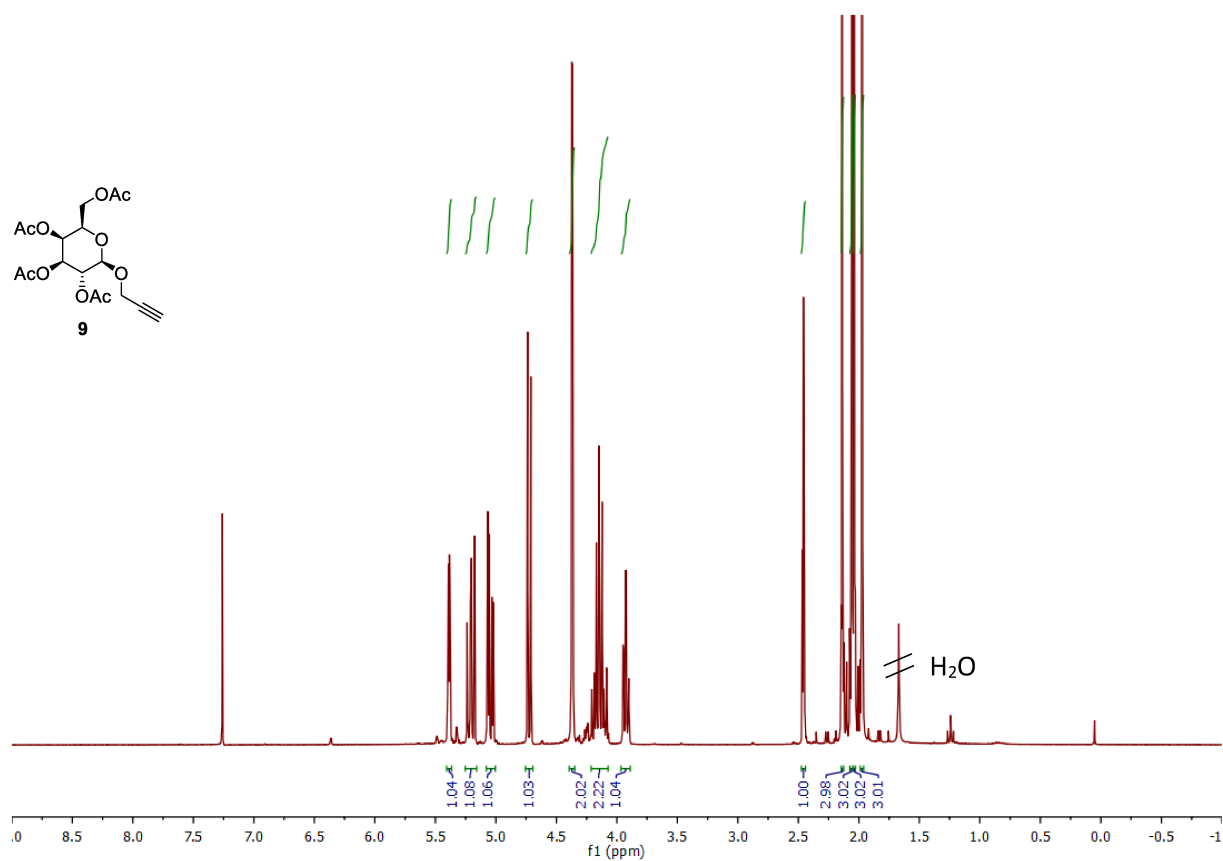
Figure S25: ^{1}H-NMR (600 MHz, CDCl$_3$) of compound **9**.
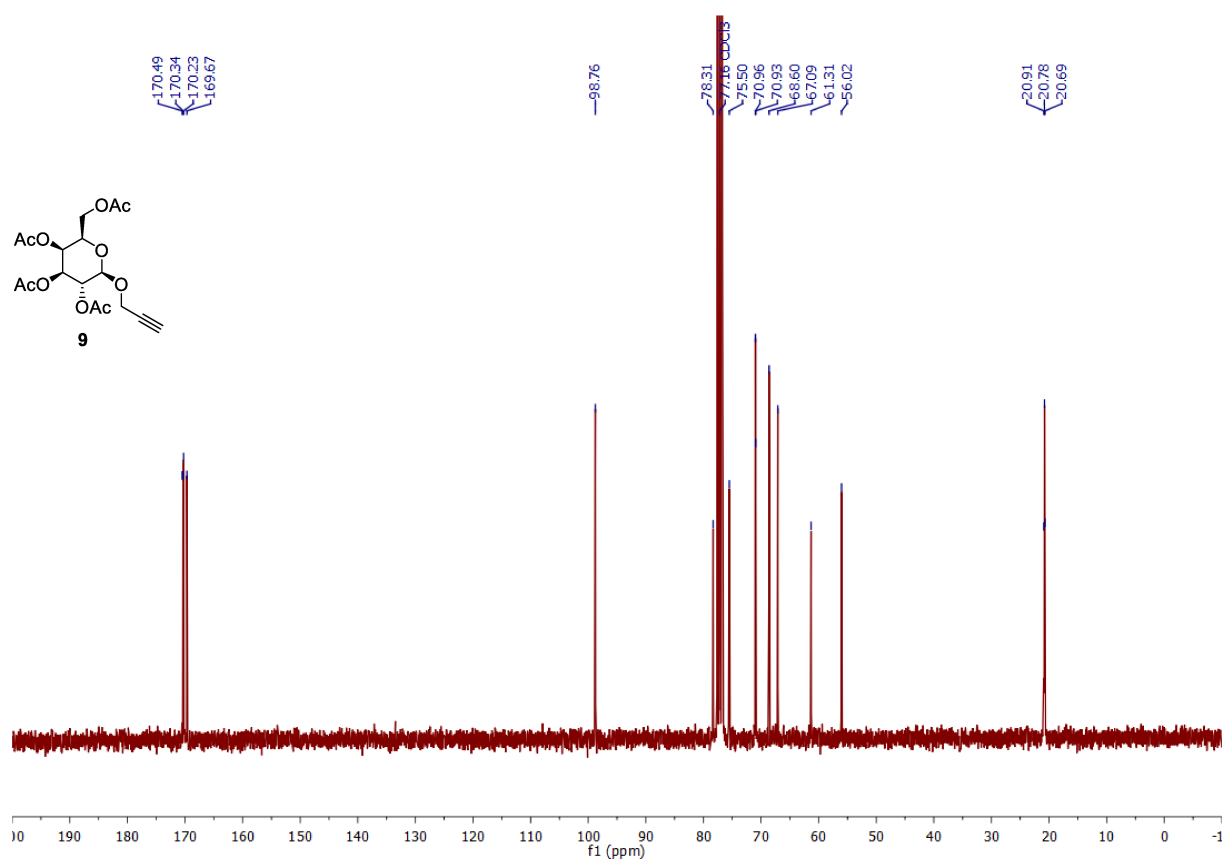
Figure S26: ^{13}C-NMR (75 MHz, CDCl$_3$) of compound **9.**

Kinetic studies of the TFA deprotection of the BADS building block

General procedure:

The compounds were given to the mixture of water, methanol and potassium carbonate under rigorous stirring. The reaction was monitored with RP-HPLC (linear gradient from 0 - 50 % eluent B in 17 min at 25°C) of the crude mixture after specific intervals. The relative UV absorption integrals of both the starting material and the products were summed up and normalized to one.
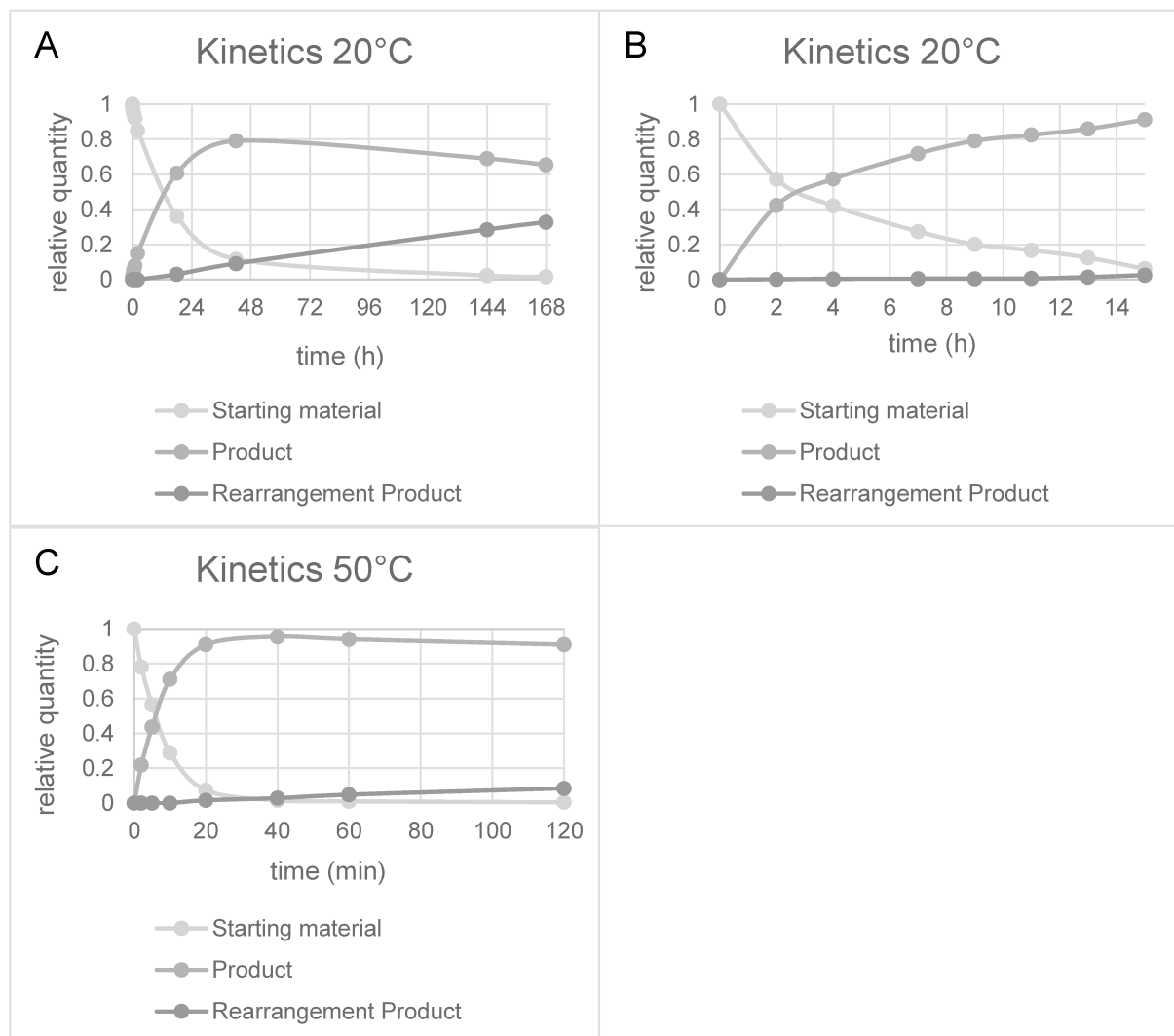
Figure S27: Kinetic studies of the BADS Building Block. A) TFA deprotection of compound **3** at 20°C; B) TFA deprotection of compound **6** at 20°C; C) TFA deprotection of compound **6** at 50°C.

Coupling efficiency determination of the BADS building block

General procedure:

A 50 µmol batch size of Tentagel SRAM was used and the three building blocks BADS, EDS and BADS were iteratively coupled. The Fmoc deprotection solution (20% piperidin in DMF) of each Fmoc deprotection was collected in a 100 mL volumetric flask and filled up with 20% piperidin in DMF. 1 mL of the solution was diluted to a third with deprotection solution and measured in a 10 mm silica UV cell in a spectrophotometer. Duplicates mere measured and the absorption at 290 nm of both measurements was averaged.

#	Time (min)	Area (%)	m/z (z) (+H$^+$/+Na$^+$)	composition
1	9.57	1.24	592/614 (1)	M-BADS-Ac
2	12.56	0.24	634/656 (1)	M-BADS
3	15.27	<0.1	-	-
4	16.13	1.26	953 (1)	M-N$_2$
5	16.83	93.9	978/1000 (1)	M
6	18.75	1.96	978/1000 (1)	M
7	19.57	0.50	662/683 (2)	M+BADS
8	20.74	0.22	-	-
9	22.62	0.58	517 (2)/1055 (1)	M-Ac+TFA
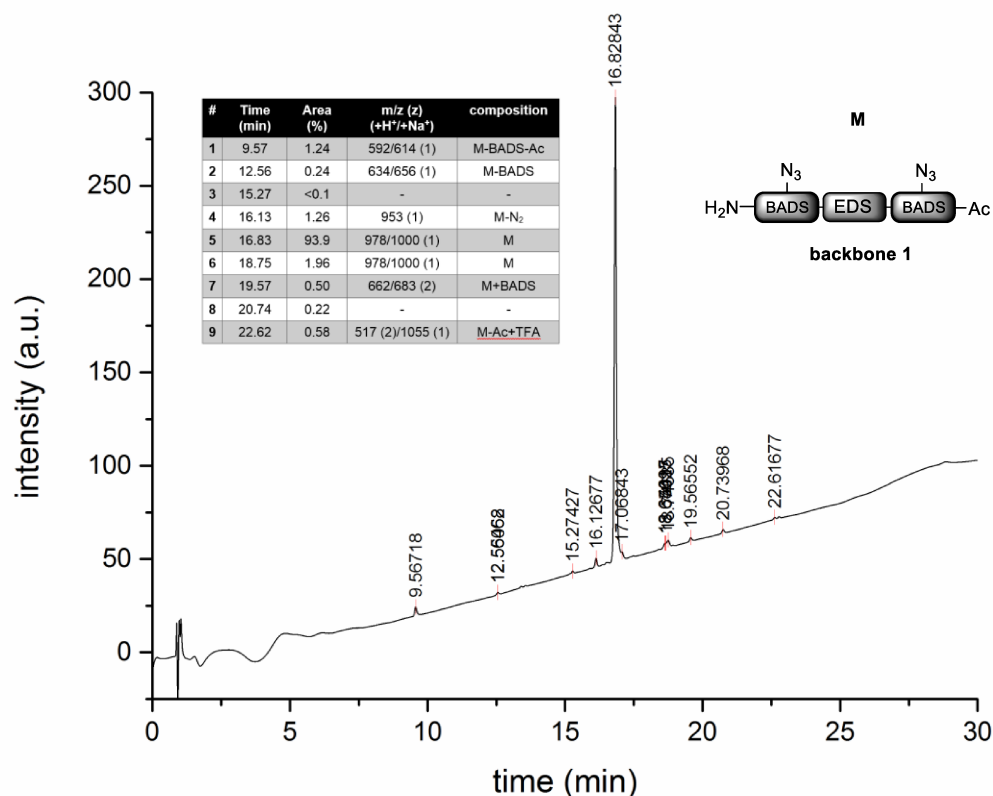
Figure S28: RP-HPLC (linear gradient from 0 - 50% eluent B in 30 min at 25°C) from the test oligomer sequence BADS-EDS-BADS, which after acetylation corresponds to the further used **scaffold 1**. Determined purity: 93.9%.
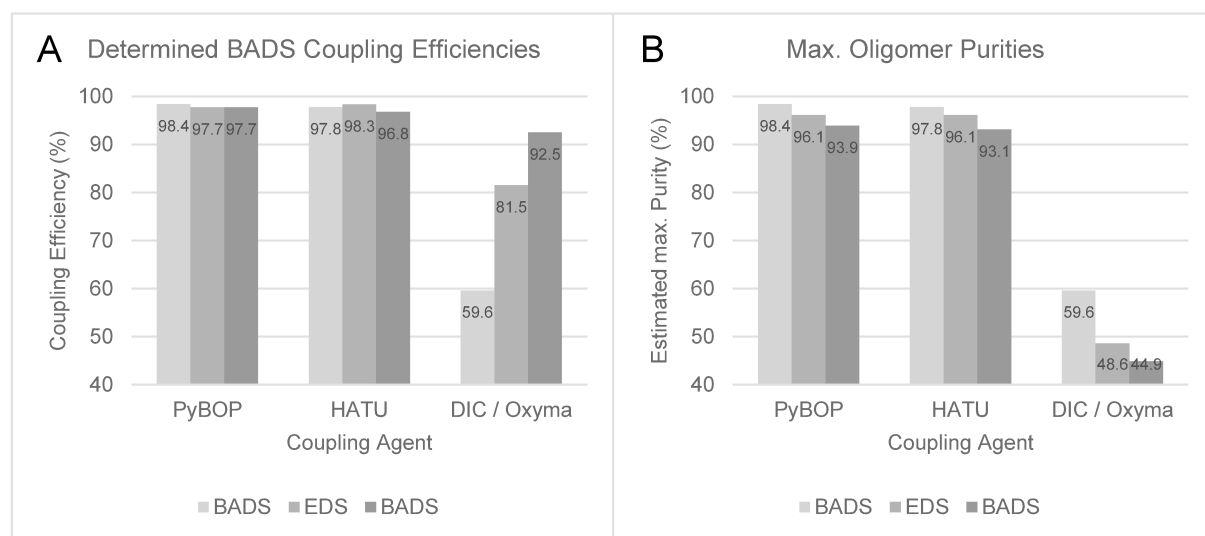
Figure S29: Determined BADS coupling efficiencies (A) and calculated maximum Oligomer purities (B) of the test oligomer sequence BADS-EDS-BADS. The use of PyBOP leads to the highest possible purity of 93.9%.

Solid phase synthesis of oligomer arms

Monovalent arm Man(1)-BADS-EDS-PA (arm 1)
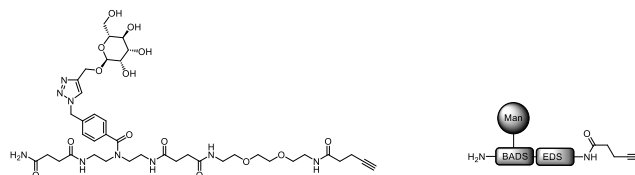
Arm 1 was synthesized in a 250 μmol scale. 114.5 mg (129 μmol, 51%) of a white and foamy solid were obtained after purification with preparative HPLC. For solid phase synthesis protocol see general methods.

^{1}H NMR (600 MHz, D_2O) δ 8.15 – 8.14 (s, 1H, *triazole-H*), 7.44 (d, ^3J = 7.9 Hz, 2H, *aryl-H*), 7.40 (d, ^3J = 8.1 Hz, 2H, *aryl-H*), 5.70 (s, 2H, *aryl-CH₂-aryl*), 4.98 – 4.97 (m, 1H, *Man-H1*), 4.84 (d, ^2J = 12.6, 1H, *propargyl-H*), 4.73 (d, ^2J = 12.6 Hz, 1H, *propargyl-H*), 3.94 – 3.91 (m, 1H, *Man-H2*), 3.80 – 3.49 (m, 20H, *7x CH₂, Man-H3-7, alkyne-H*), 3.42 – 3.34 (m, 4H, *all CH₂*), 3.23 (t, ^3J = 5.6 Hz, 2H, *CH₂*), 2.59 – 2.50 (m, 4H, *succinyl-CH₂*), 2.50 – 2.42 (m, 4H, *pentinyl-CH₂*), 2.42 – 2.33 (m, 4H, *succinyl-CH₂*).

^{13}C NMR (151 MHz, D_2O) δ 177.38, 174.87, 174.67, 174.63, 174.42, 173.89, 143.91, 136.73, 135.14, 128.34, 127.31, 125.43, 99.58, 83.31, 72.90, 70.44, 70.11, 69.94, 69.45, 69.43, 68.87, 68.81, 68.79, 66.60, 60.74, 59.85, 48.60, 44.44, 38.91, 37.13, 36.82, 34.37, 31.04, 30.95, 30.90, 30.83, 30.75, 30.71, 30.20, 30.01, 14.51.

HRMS for $C_{40}H_{59}N_9O_{14}$ (ESI-TOF) *m/z*: [M + H$^+$] calc.: 890.4254; found: 890.4245.

MS for $C_{40}H_{59}N_9O_{14}$ (ESI) *m/z*: [M + Na$^+$]$^+$ calc.: 912.41; found: 912., [M + H$^+$]$^+$ calc.: 890.42; found: 890.35, [M + 2H$^+$]$^{2+}$ calc.: 445.72; found: 445.80, [M + 2H$^+$-($C_6H_{11}O_5$ = Mannose)]$^{2+}$ calc.: 364.19; found: 364.80.

RP-HPLC (linear gradient from 0 – 50% eluent B in 30 min at 25°C): t_R = 10.6 min. Determined purity: 96%.
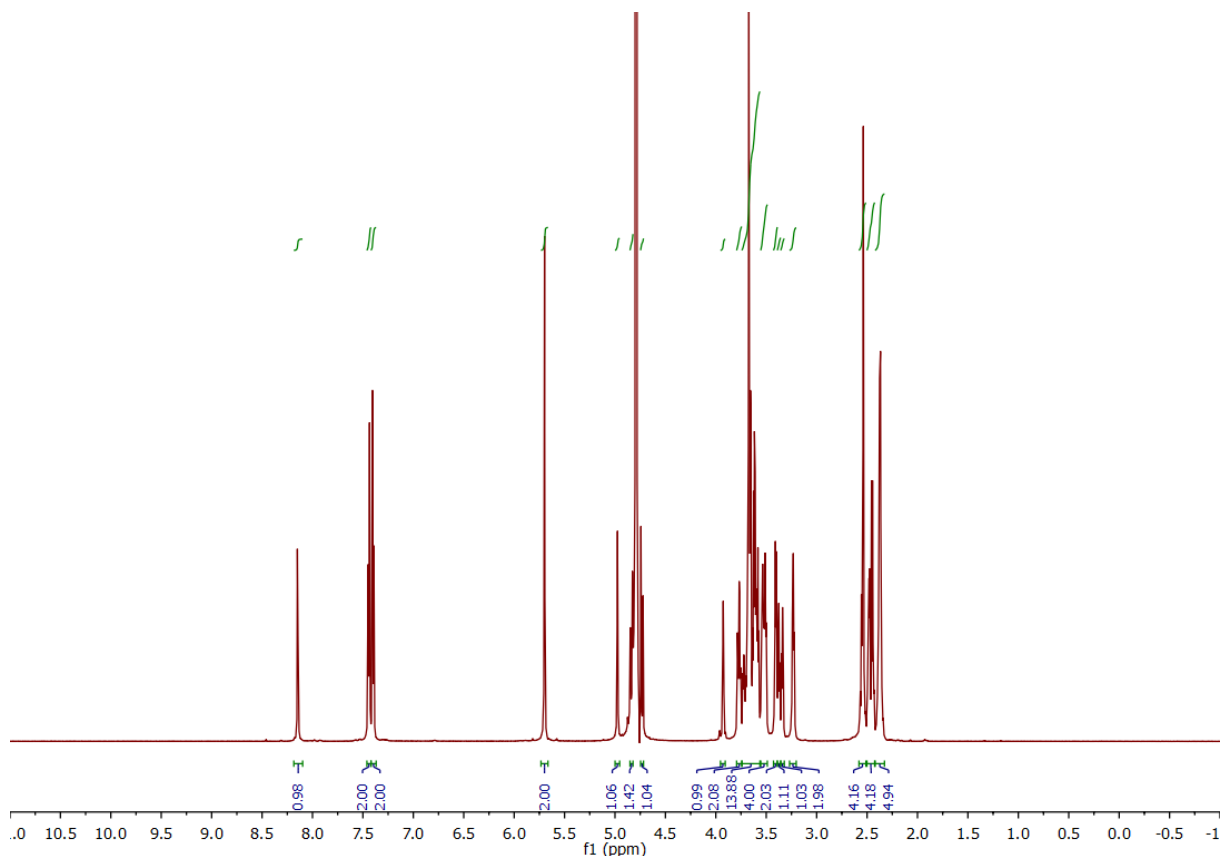
Figure S30. ^{1}H-NMR (600 MHz, D_2O) of monovalent **arm 1.**
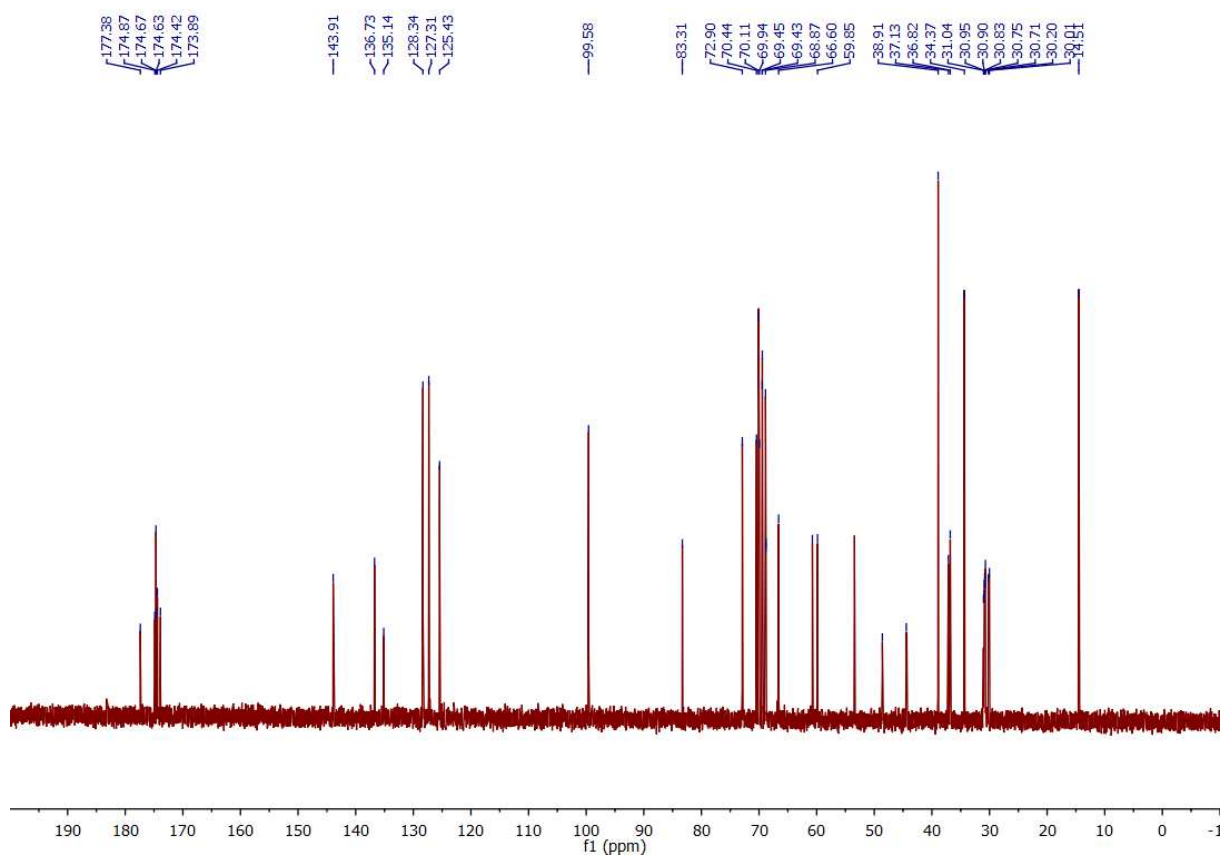
Figure S31. ^{13}C-NMR (151 MHz, D$_2$O) of monovalent **arm 1.**
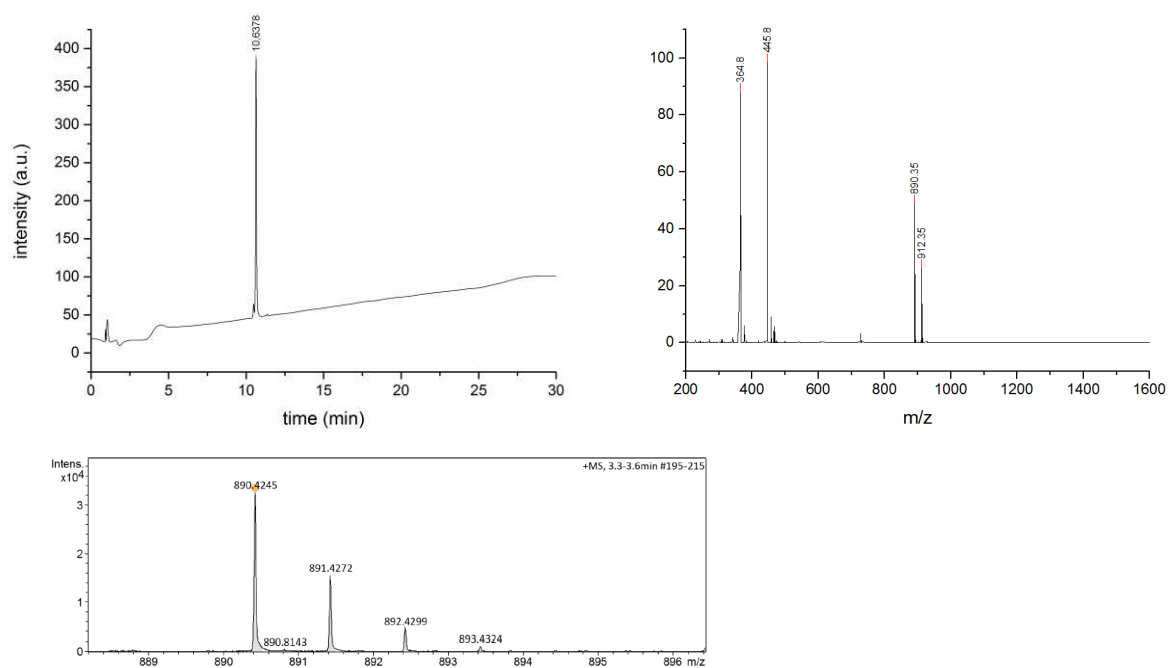
Figure S32. RP-HPLC (linear gradient from 0 - 50% eluent B in 30 min at 25°C), ESI-MS (positive mode) and HR-MS (ESI+ Q-TOF, positive mode) of **arm 1**.

Divalent arm Man(1,3)-[BADS-EDS]₂-PA (arm 2)
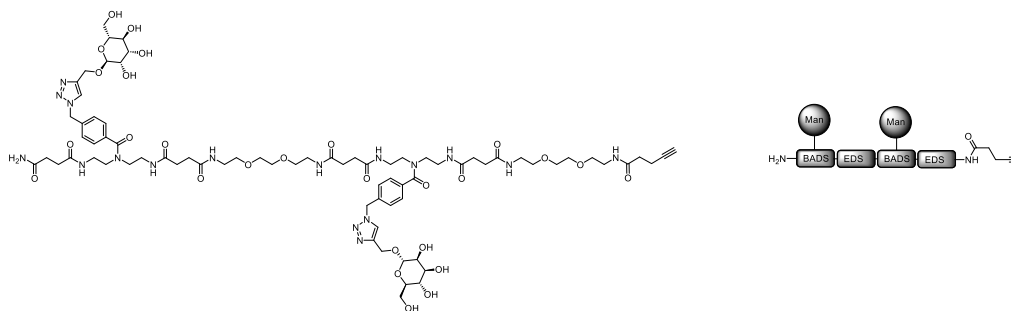
Arm 2 was synthesized in a 500 µmol scale. 520.9 mg (309 µmol, 62%) of a white and foamy solid were obtained after purification with preparative HPLC. For solid phase synthesis protocol see general methods.

^{1}H NMR (600 MHz, D₂O) δ 8.16 – 8.11 (m, 2H, *triazole-H*), 7.43 (d, ^3J = 7.3 Hz, 4H, *aryl-H*), 7.39 (d, ^3J = 8.0 Hz, 4H, *aryl-H*), 5.68 (s, 4H, *aryl-CH₂-aryl*), 4.97 (d, ^3J = 1.9 Hz, 2H, *Man-H1*), 4.83 (d, ^2J = 12.7 Hz, 2H, *propargyl-H*), 4.72 (d, ^2J = 12.5 Hz, 2H, *propargyl-H*), 3.93 – 3.90 (m, 2H, *Man-H2*), 3.80 – 3.46 (m, 39H, *14x CH₂, 2x Man-H3-7, alkyne-H*), 3.42 – 3.31 (m, 8H, *all CH₂*), 3.22 (m, 4H, *all CH₂*), 2.57 – 2.51 (m, 8H, *succinyl-CH₂*), 2.49 – 2.42 (m, 4H, *pentinyl-CH₂*), 2.40 – 2.33 (m, 8H, *succinyl-CH₂*).

HRMS for C₇₅H₁₁₁N₁₇O₂₇ (ESI-TOF) *m/z*: [M + 2H⁺]²⁺ calc.: 841.8990; found: 841.8995.

MS for C₇₅H₁₁₁N₁₇O₂₇ (ESI) *m/z*: [M + 2Na⁺]²⁺ calc.: 863.88; found: 863.90, [M + 2H⁺]²⁺ calc.: 841.90; found: 842.05, [M + 3H⁺]³⁺ calc.: 561.60; found: 561.75, [M + 3H⁺-(C₆H₁₁O₅ = Mannose)]³⁺ calc.: 507.25; found: 507.80, [M + 3H⁺-2(C₆H₁₁O₅ = Mannose)]³⁺ calc.: 452.89; found: 453.75.

RP-HPLC (linear gradient from 0 – 50% eluent B in 30 min at 25°C): t_R = 12.1 min. Determined purity: 98%.
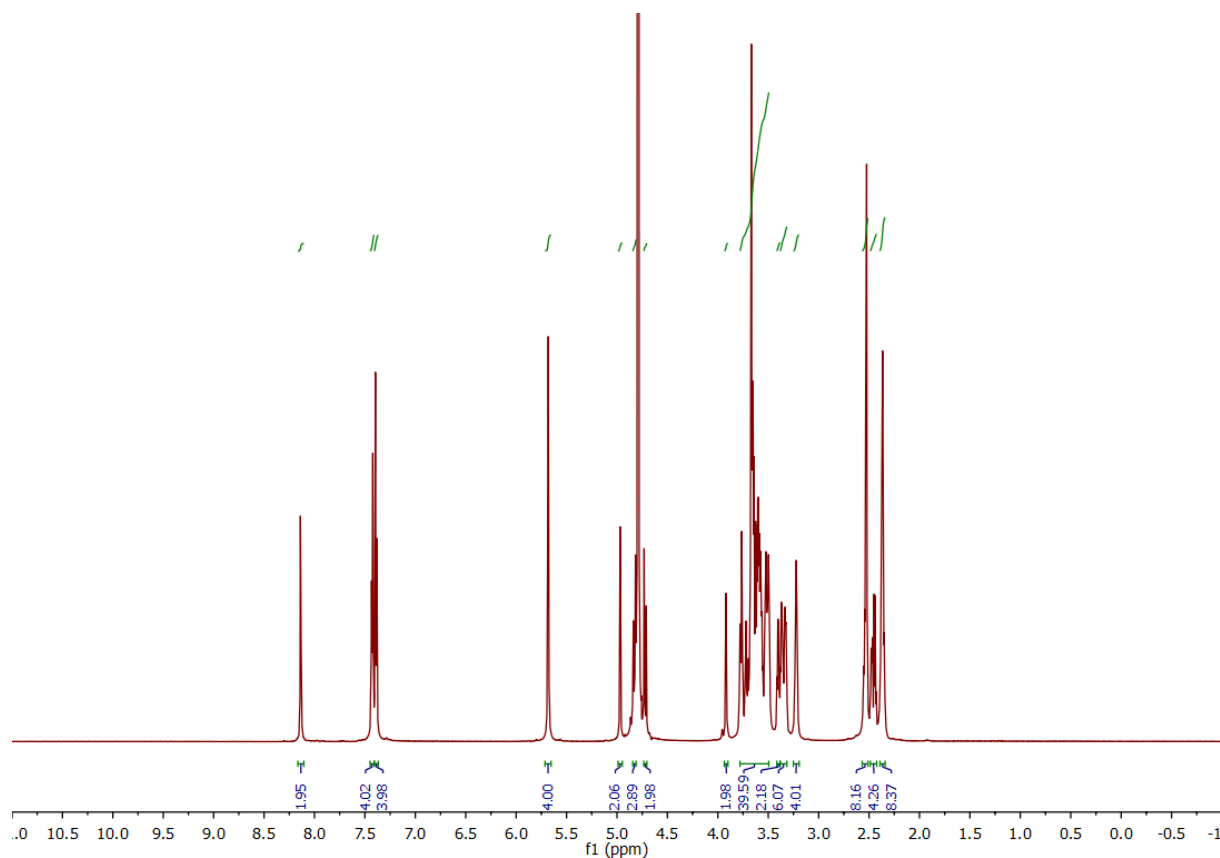
Figure S33. ^{1}H-NMR (600 MHz, D₂O) of divalent **arm 2.**
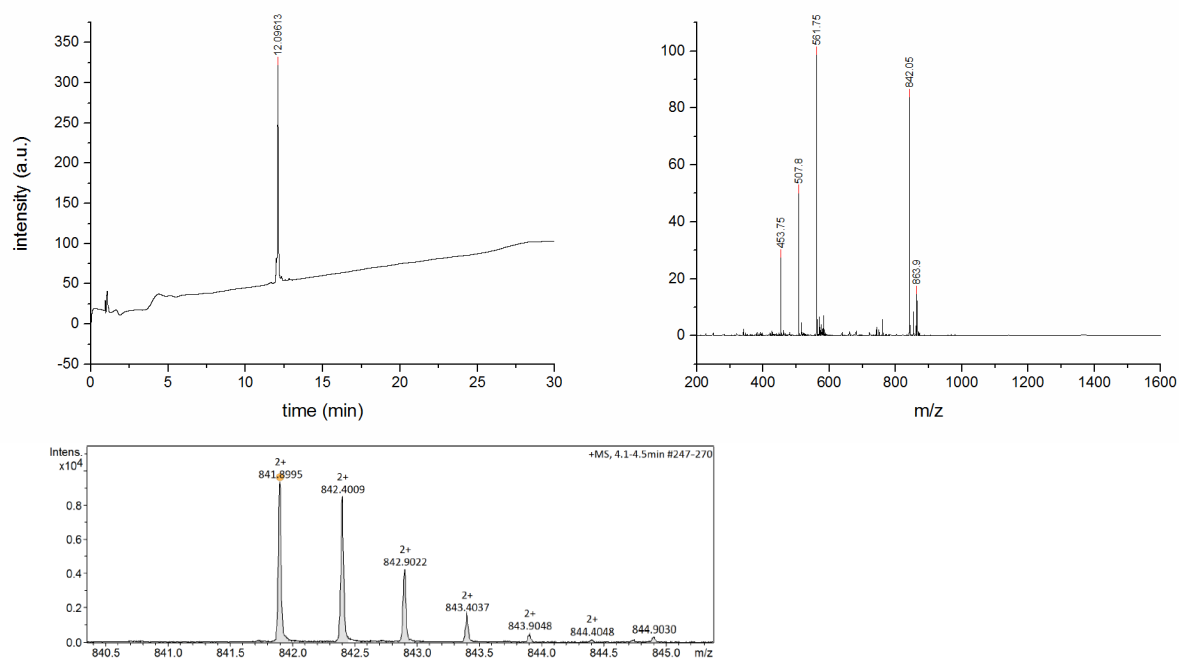
Figure S34. RP-HPLC (linear gradient from 0 - 50% eluent B in 30 min at 25°C), ESI-MS (positive mode) and HR-MS (ESI+ Q-TOF, positive mode) of **arm 2**.

Trivalent arm Man(1,3,5)-[BADS-EDS]₃-PA (arm 3)
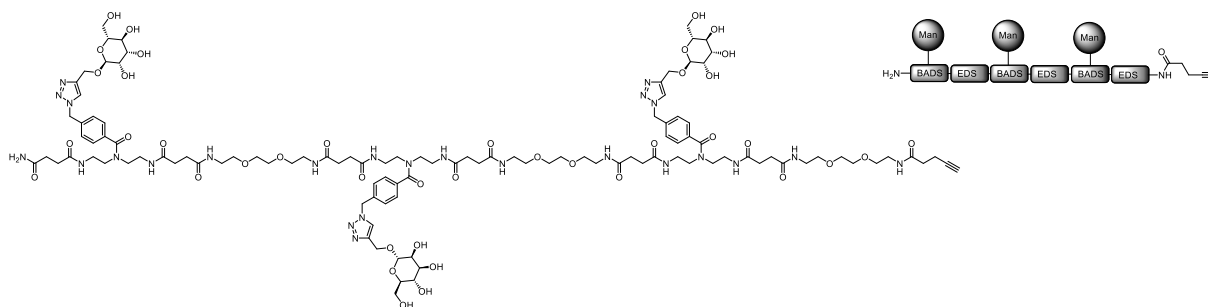
Arm 3 was synthesized in a 200 µmol scale. 202.8 mg (81.9 µmol, 41%) of a white and foamy solid were obtained after purification with preparative HPLC. For solid phase synthesis protocol see general methods.

^{1}H NMR (600 MHz, D_2O) δ 8.15 – 8.12 (m, 3H, *triazole-H*), 7.45 – 7.36 (m, 12H, *aryl-H*), 5.71 – 5.62 (m, 6H, *aryl-CH₂-aryl*), 4.98 – 4.96 (m, 3H, *Man-H1*), 4.87 – 4.82 (m, 3H, *propargyl-H*), 4.71 (m, 3H, *propargyl-H*), 3.96 – 3.89 (m, 3H, *Man-H2*), 3.79 – 3.47 (m, 76H, *30x CH₂, 3x Man-H3-7, alkyne-H*), 3.42 – 3.31 (m, 12H, *all CH₂*), 3.24 – 3.20 (m, 6H, *all CH₂*), 2.56 – 2.50 (m, 12H, *succinyl-CH₂*), 2.49 – 2.42 (m, 4H, *pentinyl-CH₂*), 2.40 – 2.34 (m, *J* = 3.7 Hz, 12H, *succinyl-CH₂*).

HRMS for $C_{110}H_{163}N_{25}O_{40}$ (ESI-TOF) *m/z*: $[M + 3H^+]^{3+}$ calc.: 826.0580; found: 826.0578.

MS for $C_{110}H_{163}N_{25}O_{40}$ (ESI) *m/z*: $[M + 3H^+]^{3+}$ calc.: 826.06; found: 825.95, $[M + 4H^+]^{4+}$ calc.: 619.80; found: 619.75, $[M + 4H^+-(C_6H_{11}O_5 =$ Mannose)$]^{4+}$ calc.: 579.03; found: 579.2.

RP-HPLC (linear gradient from 0 – 50% eluent B in 30 min at 25°C): t_R = 12.7 min. Determined purity: 96%.
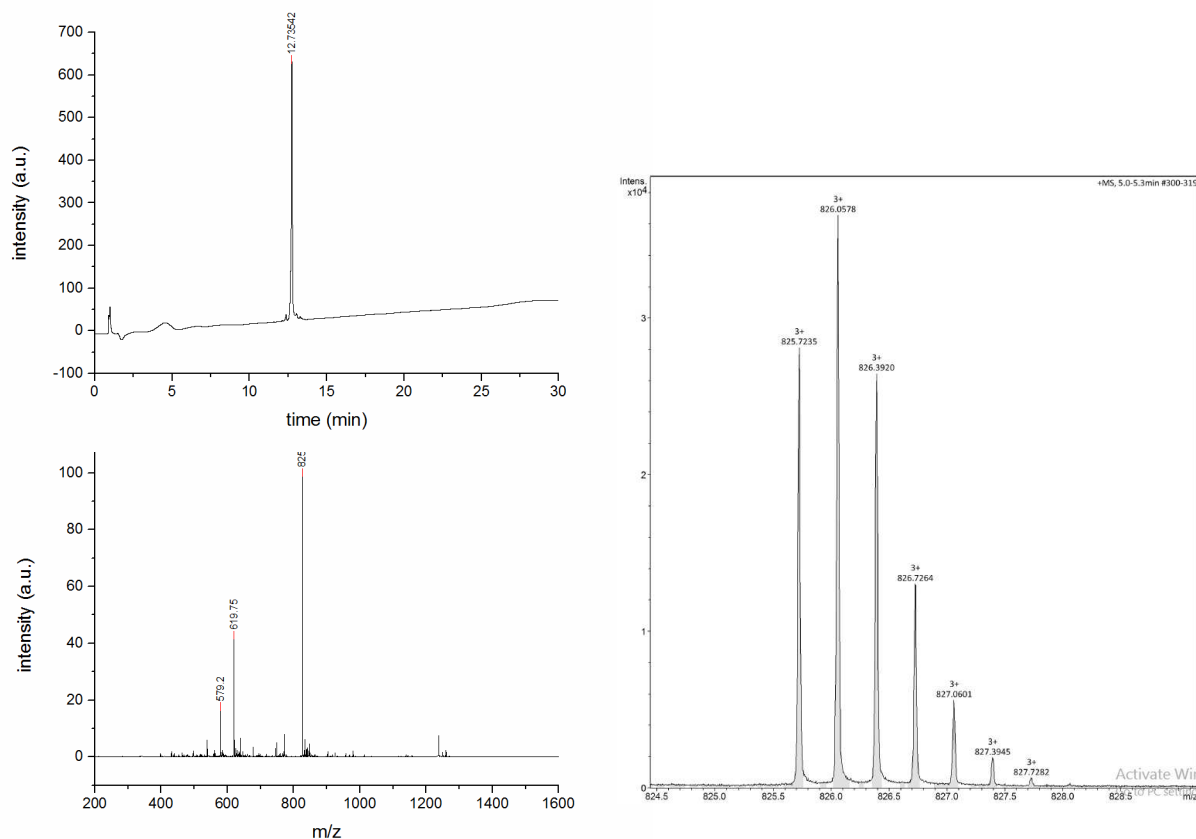
Figure S35. RP-HPLC (linear gradient from 0 - 50% eluent B in 30 min at 25°C), ESI-MS (positive mode) and HR-MS (ESI+ Q-TOF, positive mode) of **arm 3**.

Divalent arm Gal(1,3)-[BADS-EDS]₂-PA (arm 4)
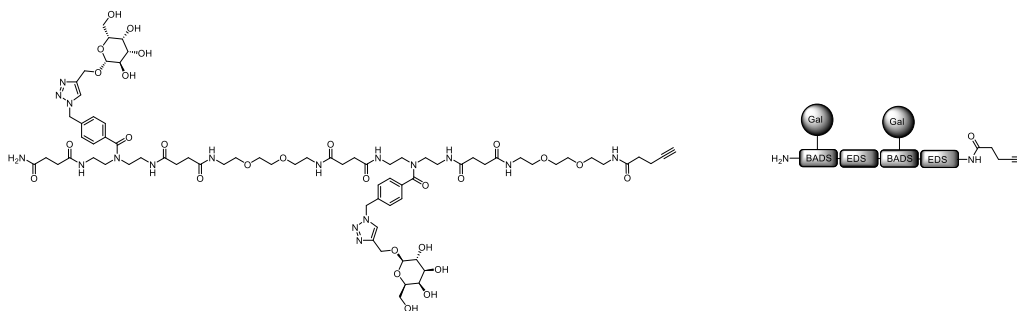
Arm 4 was synthesized in a 100 µmol scale. 143.2 mg (85.1 µmol, 85%) of a white and foamy solid were obtained after purification with preparative HPLC. For solid phase synthesis protocol see general methods.

^{1}H NMR (600 MHz, D₂O) δ 8.15 – 8.12 (m, 2H, *triazole-H*), 7.43 (d, ^3J = 7.3 Hz, 4H, *aryl-H*), 7.39 (d, ^3J = 8.3 Hz, 4H, *aryl-H*), 5.69 (s, 4H, *aryl-CH₂-aryl*), 5.01 (d, ^2J = 12.6 Hz, 2H, *propargyl-H*), 4.87 (d, ^2J = 12.6 Hz, 2H, *propargyl-H*), 4.49 (m, 2H, *Gal-H1*), 3.94 – 3.91 (m, 2H, *Gal-H2*), 3.77 – 3.48 (m, 39H, *14x CH₂, 2x Gal-H3-7, alkyne-H*), 3.42 – 3.31 (m, 8H, *all CH₂*), 3.22 (m, 4H, *all CH₂*), 2.56 – 2.51 (m, 8H, *succinyl-CH₂*), 2.50 – 2.43 (m, 4H, *pentinyl-CH₂*), 2.40 – 2.33 (m, 8H, *succinyl-CH₂*).

HRMS for C₇₅H₁₁₁N₁₇O₂₇ (ESI-TOF) *m/z*: [M + 2H⁺]²⁺ calc.: 841.8990; found: 841.8995.

MS for C₇₅H₁₁₁N₁₇O₂₇ (ESI) *m/z*: [M + 2Na⁺]²⁺ calc.: 863.88; found: 864.05, [M + 2H⁺]²⁺ calc.: 841.90; found: 842.00, [M + 3H⁺]³⁺ calc.: 561.60; found: 561.80, [M + 3H⁺-(C₆H₁₁O₅ = Galactose)]³⁺ calc.: 507.25; found: 507.80, [M + 3H⁺-2(C₆H₁₁O₅ = Galactose)]³⁺ calc.: 452.89; found: 453.70.

RP-HPLC (linear gradient from 0 – 50% eluent B in 30 min at 25°C): t_R = 11.8 min. Determined purity: 97%.
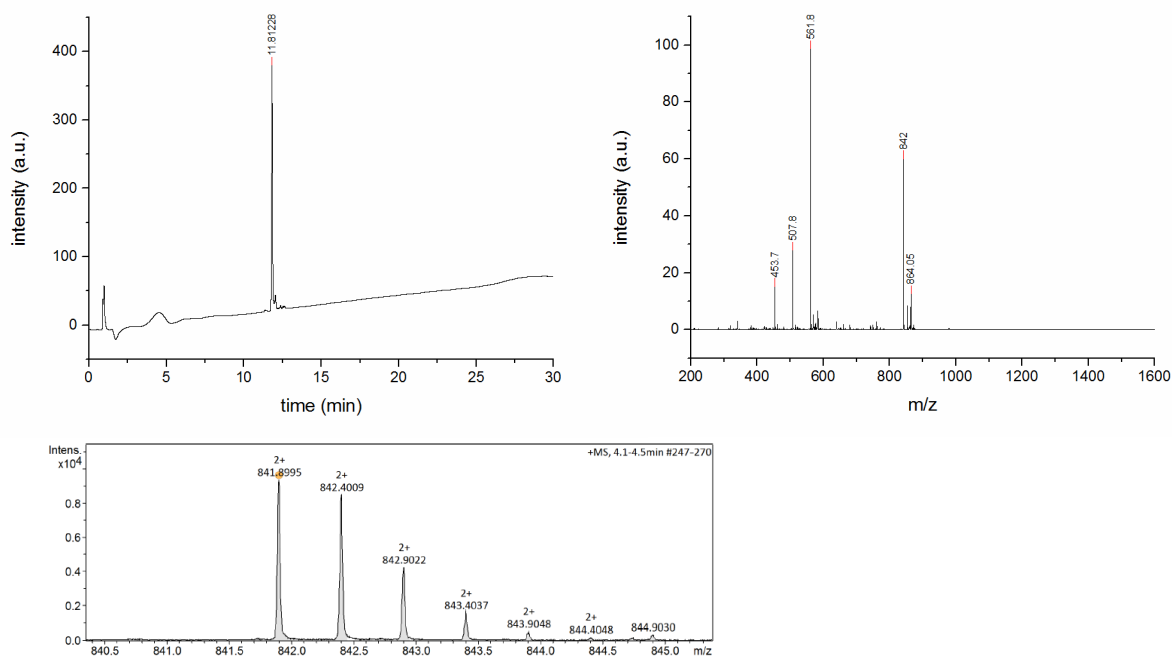
Figure S36. RP-HPLC (linear gradient from 0 - 50% eluent B in 30 min at 25°C), ESI-MS (positive mode) and HR-MS (ESI+ Q-TOF, positive mode) of **arm 4**.

Solid phase synthesis of branched oligomers

Man-2X1, (Man(1)-BADS-EDS-PA)(1,3)-BADS-EDS-BADS (13)
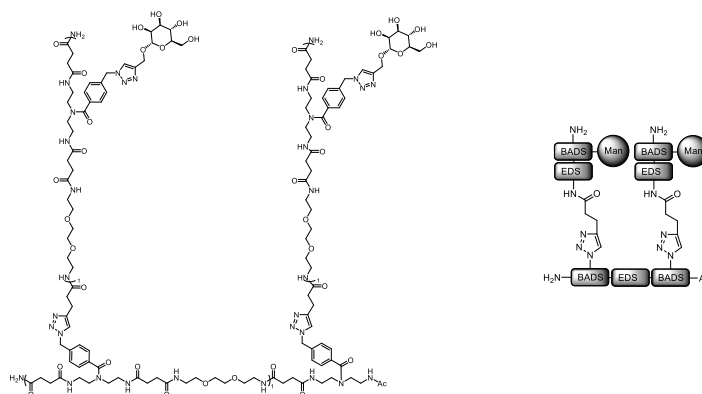
Man-2X1 was synthesized in a 20 µmol scale. 37.1 mg (13.5 µmol, 68%) of a white and foamy solid were obtained after purification with preparative HPLC. For solid phase synthesis protocol see general methods.

^{1}H NMR (600 MHz, D_2O) δ 8.14 – 8.10 (m, 2H, *triazole-H*), 7.83 (s, 2H, *triazole-H*), 7.43 – 7.34 (m, 16H, *aryl-H*), 5.66 (s, 4H, *aryl-CH₂-aryl*), 5.60 (s, 4H, *aryl-CH₂-aryl*), 4.97 – 4.95 (m, 2H, *Man-H1*), 4.83 (m, 2H, *propargyl-H*), 4.71 (d, [2]*J* = 12.5 Hz, 2H, *propargyl-H*), 3.92 – 3.89 (m, 2H, *Man-H2*), 3.80 – 3.44 (m, 58H, *24x CH₂, 2x Man-H3-7*), 3.37 – 3.17 (m, 20H, *all CH₂*), 2.98 (t, [3]*J* = 7.1 Hz, 4H, *pentinyl-CH₂*), 2.59 (t, [3]*J* = 6.9 Hz, 4H, *pentinyl-CH₂*), 2.55 – 2.49 (m, 14H, *succinyl-CH₂*), 2.39 – 2.32 (m, 14H, *succinyl-CH₂*), 1.98 – 1.78 (m, 3H, *acetyl-CH₃*).

HRMS for $C_{124}H_{181}N_{33}O_{39}$ (ESI-TOF) *m/z*: [M + 4H[+]][4+] calc.: 690.3380; found: 690.3381.

MS for $C_{124}H_{181}N_{33}O_{39}$ (ESI) *m/z*: [M + 3Na[+]][3+] calc.: 942.10; found: 942.05, [M + 3H[+]][3+] calc.: 920.11; found: 920.00, [M + 4H[+]][4+] calc.: 690.34; found: 690.30, [M + 5H[+]][5+] calc.: 552.47; found: 552.55.

RP-HPLC (linear gradient from 0 – 50% eluent B in 30 min at 25°C): t$_R$ = 12.8 min. Determined purity: 98%.

PDI (GPC-RI-LS, 50 mM NaH_2PO_4, 150 mM NaCl, 250 ppm NaN_3 (pH 7.2), 30% ACN. Flow rate: 1 mL/min): 1.03.
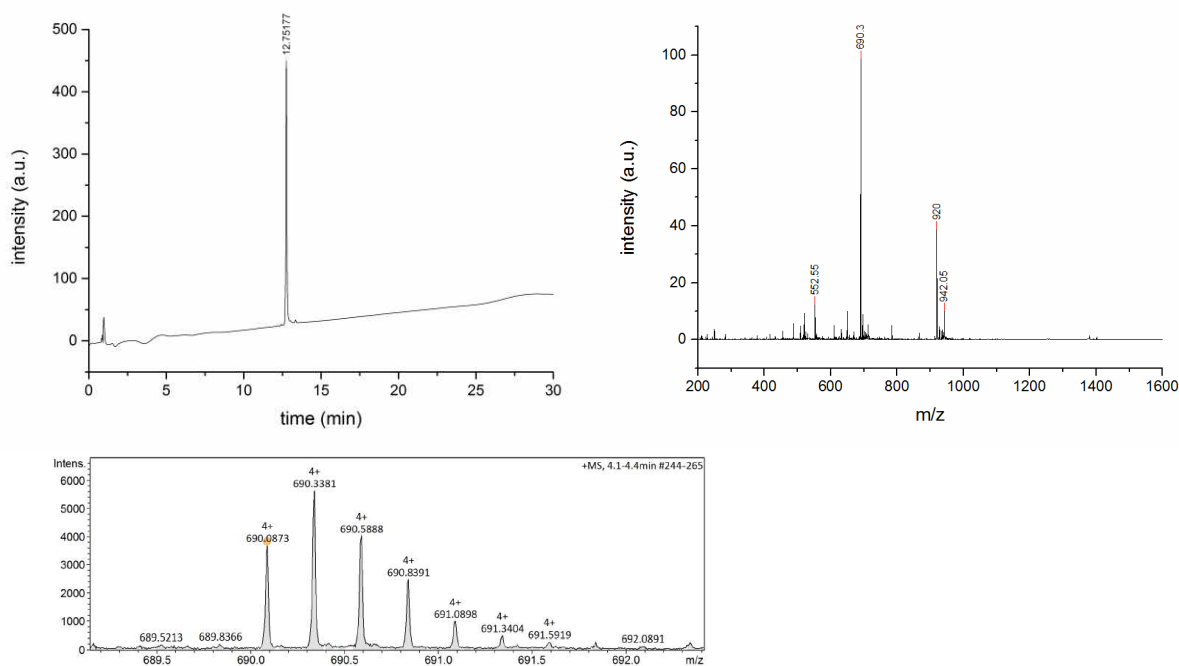
Figure S37. RP-HPLC (linear gradient from 0 - 50% eluent B in 30 min at 25°C), ESI-MS (positive mode) and HR-MS (ESI+ Q-TOF, positive mode) of compound **13**.
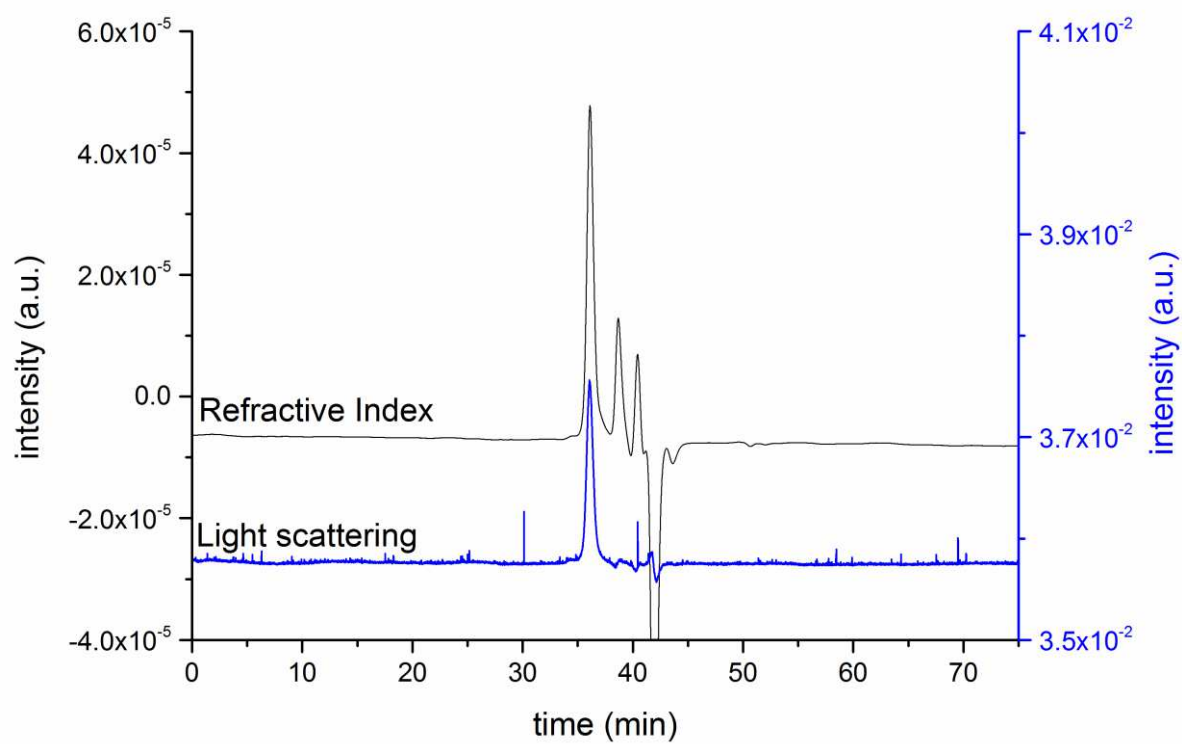
Figure S38. GPC (RI and LS) of compound **13**.

Man-2X2, (Man(1,3)-[BADS-EDS]₂-PA)(1,3)-BADS-EDS-BADS (14)
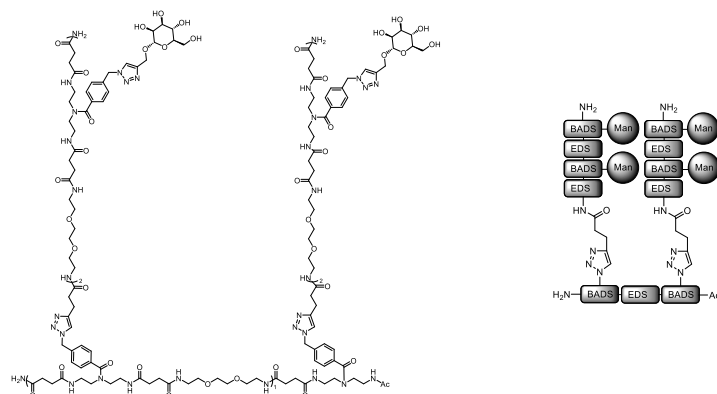
Man-2X2 was synthesized in a 20 µmol scale. 66.5 mg (15.3 µmol, 77%) of a white and foamy solid were obtained after purification with preparative HPLC. For solid phase synthesis protocol see general methods.

^{1}H NMR (600 MHz, D$_2$O) δ 8.16 – 8.09 (m, 4H, *triazole-H*), 7.83 (s, 2H, *triazole-H*), 7.48 – 7.32 (m, 24H, *aryl-H*), 5.70 – 5.56 (m, 12H, *aryl-CH$_2$-aryl*), 4.96 (s, 4H, *Man-H1*), 4.86 – 4.82 (m, 4H, *propargyl-H*), 4.71 (d, ^2J = 12.8 Hz, 4H, *propargyl-H*), 3.93 – 3.89 (m, 4H, *Man-H2*), 3.80 – 3.44 (m, 96H, *38x CH$_2$, 4x Man-H3-7*), 3.38 – 3.17 (m, 32H, *all CH$_2$*), 2.98 (t, ^3J = 7.2 Hz, 4H, *pentinyl-CH$_2$*), 2.59 (t, ^3J = 7.5 Hz, 4H, *pentinyl-CH$_2$*), 2.56 – 2.48 (m, 22H, *succinyl-CH$_2$*), 2.40 – 2.31 (m, 22H, *succinyl-CH$_2$*), 2.03 – 1.75 (m, 3H, *acetyl-CH$_3$*).

MS for C$_{194}$H$_{285}$N$_{49}$O$_{65}$ (ESI) *m/z*: [M + 6H$^+$]$^{6+}$ calc.: 724.9; found: 724.8, [M + 5H$^+$]$^{5+}$ calc.: 869.6; found: 869.5, [M + 4H$^+$]$^{4+}$ calc.: 1086.8; found: 1086.8, [M + 3H$^+$]$^{3+}$ calc.: 1448.7; found: 1448.6.

RP-HPLC (linear gradient from 0 – 50% eluent B in 30 min at 25°C): t$_R$ = 13.1 min. Determined purity (value shown correspond to the main peak, value in brackets refer to the sum of all peaks which show the same mass): 94% (98%).

PDI (GPC-RI-LS, 50 mᴍ NaH$_2$PO$_4$, 150 mᴍ NaCl, 250 ppm NaN$_3$ (pH 7.2), 30% ACN. Flow rate: 1 mL/min): 1.03.
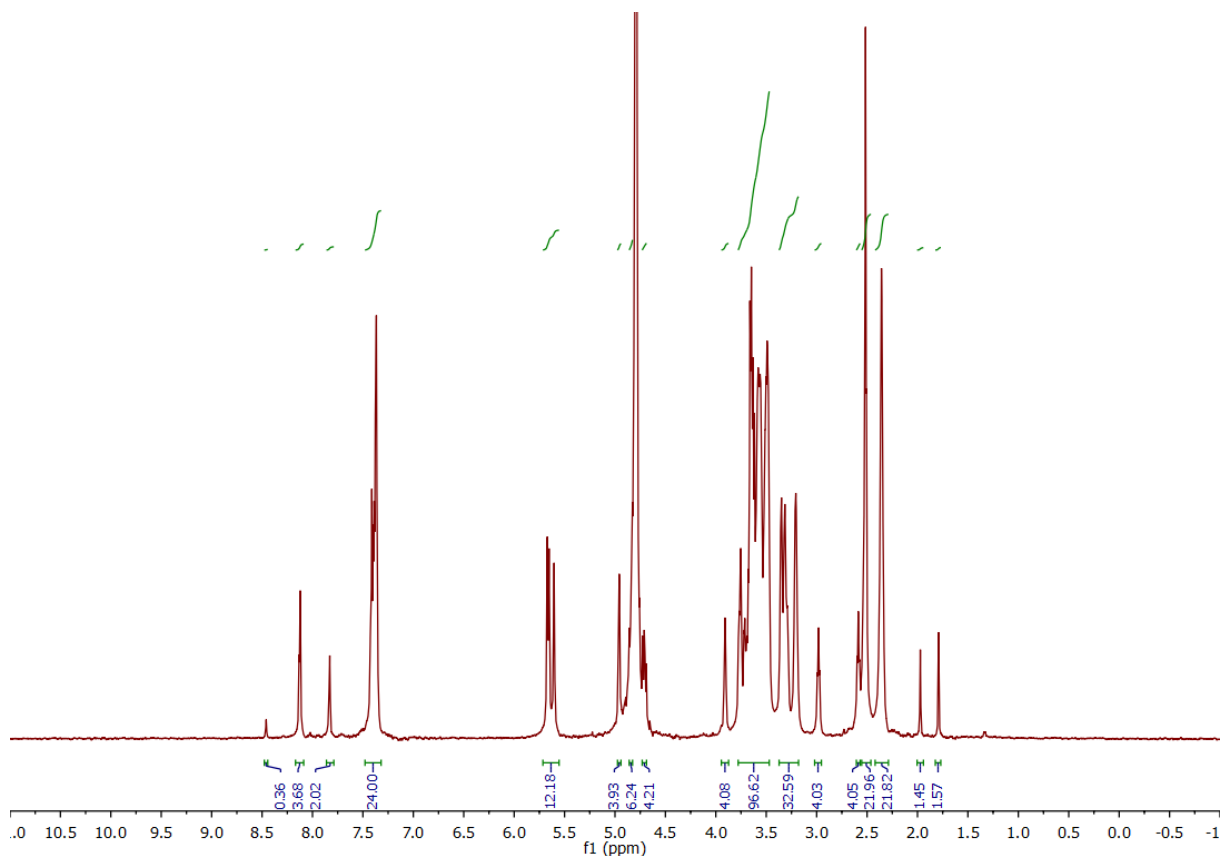
Figure S39. ^{1}H-NMR (600 MHz, D$_2$O) of compound **14**.
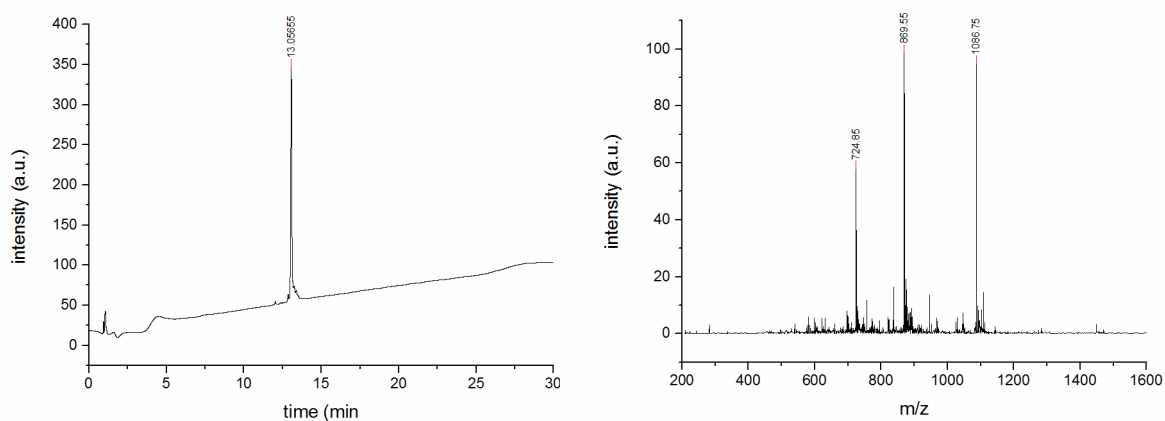
Figure S40. RP-HPLC (linear gradient from 0 - 50% eluent B in 30 min at 25°C) and ESI-MS (positive mode) of compound **14**.
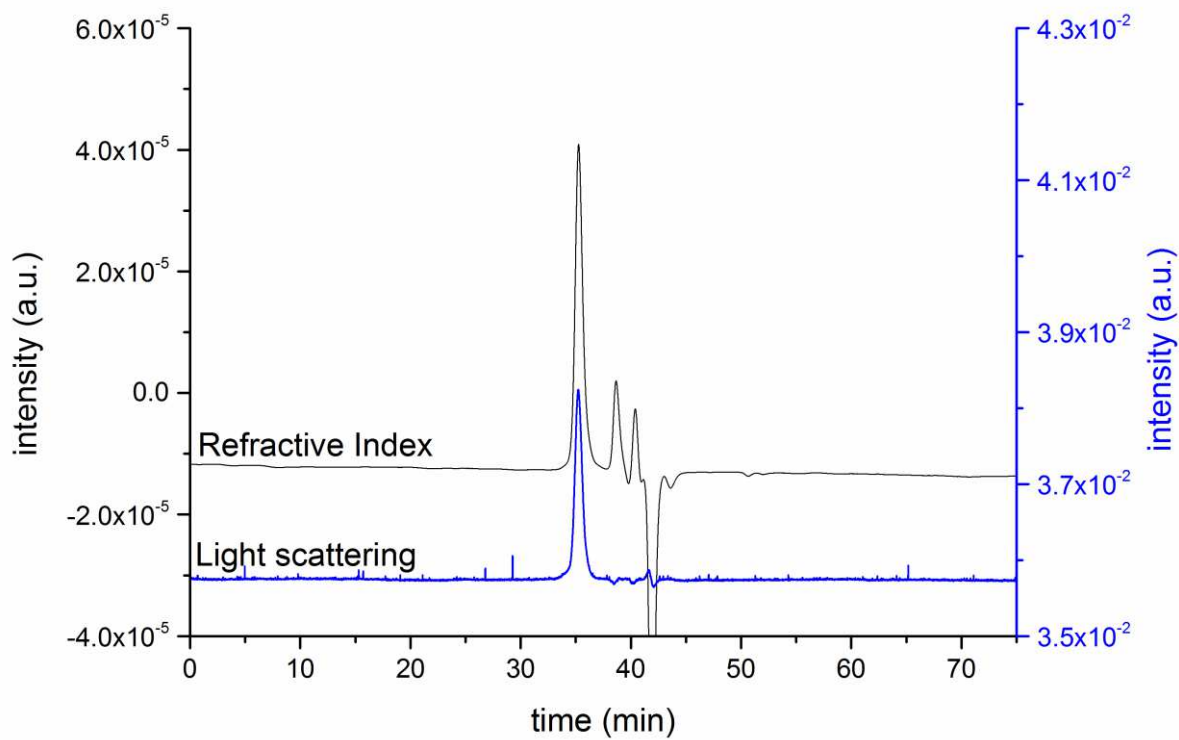
Figure S41. GPC (RI and LS) of compound **14**.

Man-2X3, (Man(1,3,5)-[BADS-EDS]₃-PA)(1,3)-BADS-EDS-BADS (15)
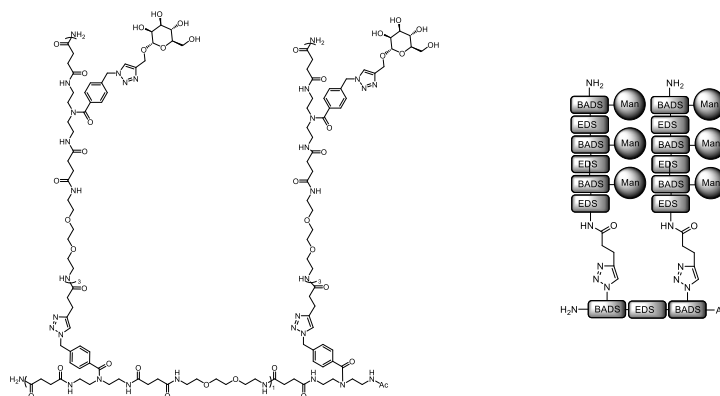
Man-2X3 was synthesized in a 10 µmol scale. 18.5 mg (3.12 µmol, 32%) of a white and foamy solid were obtained after purification with preparative HPLC. For solid phase synthesis protocol see general methods.

^{1}H NMR (600 MHz, D_2O) δ 8.17 – 8.08 (m, 6H, *triazole-H*), 7.83 (s, 2H, *triazole-H*), 7.46 – 7.33 (m, 32H, *aryl-H*), 5.71 – 5.56 (m, 16H, *aryl-CH$_2$-aryl*), 4.98 – 4.94 (m, 6H, *Man-H1*), 4.85 – 4.82 (m, 6H, *propargyl-H*), 4.73 – 4.68 (m, 6H, *propargyl-H*), 3.93 – 3.89 (m, 6H, *Man-H2*), 3.79 – 3.45 (m, 134H, *52x CH$_2$, 6x Man-H3-7*), 3.40 – 3.17 (m, 44H, *all CH$_2$*), 2.98 (t, ^3J = 7.2 Hz, 4H, *pentinyl-CH$_2$*), 2.59 (t, ^3J = 7.0 Hz, 4H, *pentinyl-CH$_2$*), 2.55 – 2.49 (m, 30H, *succinyl-CH$_2$*), 2.40 – 2.32 (m, 30H, *succinyl-CH$_2$*), 2.00 – 1.76 (m, 3H, *acetyl-CH$_3$*).

MS for $C_{264}H_{385}N_{65}O_{91}$ (ESI) *m/z*: [M + 7H$^+$]$^{7+}$ calc.: 847.8; found: 848.0, [M + 6H$^+$]$^{6+}$ calc.: 989.0; found: 989.2, [M + 5H$^+$]$^{5+}$ calc.: 1186.7; found: 1186.6, [M + 4H$^+$]$^{4+}$ calc.: 1483.0; found: 1482.8.

RP-HPLC (linear gradient from 0 – 50% eluent B in 30 min at 25°C): t_R = 13.4 min. Determined purity (value shown correspond to the main peak, value in brackets refer to the sum of all peaks which show the same mass): 88% (98%).

PDI (GPC-RI-LS, 50 mM NaH_2PO_4, 150 mM NaCl, 250 ppm NaN_3 (pH 7.2), 30% ACN. Flow rate: 1 mL/min): 1.05.
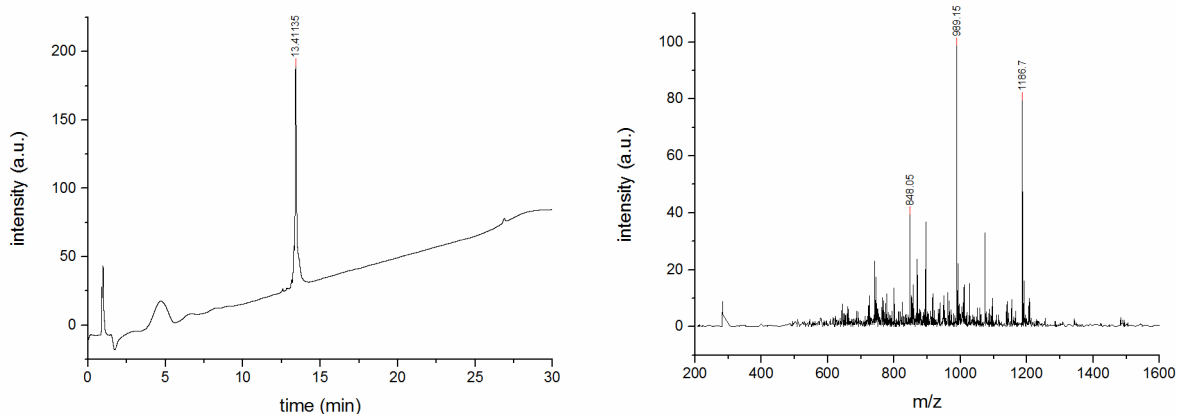
Figure S42. RP-HPLC (linear gradient from 0 - 50% eluent B in 30 min at 25°C) and ESI-MS (positve mode) of compound **15**.
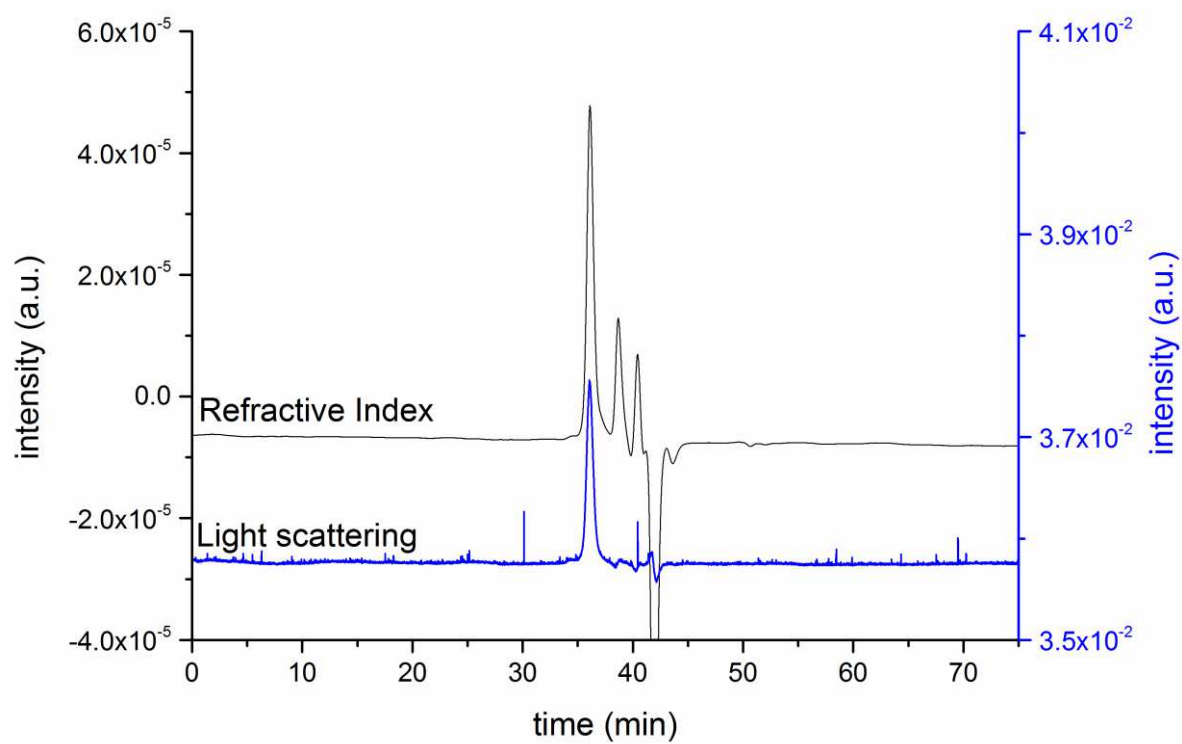
Figure S43. GPC (RI and LS) of compound **15**.

Man-3X1, (Man(1)-BADS-EDS-PA)(1,3,5)-[BADS-EDS]₂-BADS (16)
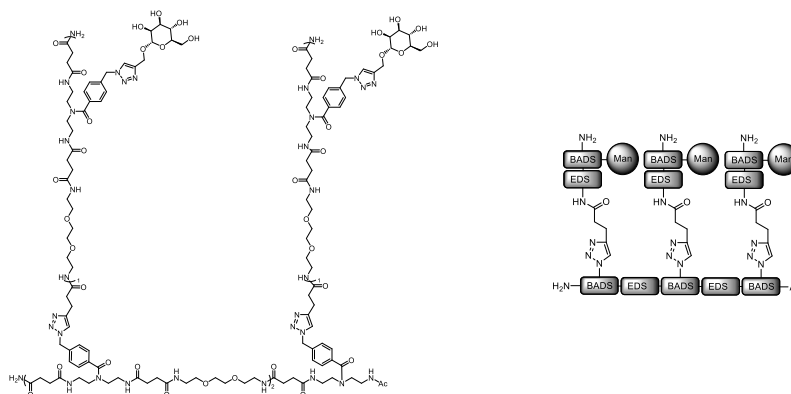
Man-3X1 was synthesized in a 15 μmol scale. 36.6 mg (8.67 μmol, 58%) of a white and foamy solid were obtained after purification with preparative HPLC. For solid phase synthesis protocol see general methods.

^{1}H NMR (600 MHz, D$_2$O) δ 8.14 – 8.09 (m, 3H, *triazole-H*), 7.83 (s, 3H, *triazole-H*), 7.43 – 7.34 (m, 24H, *aryl-H*), 5.70 – 5.54 (m, 12H, *aryl-CH$_2$-aryl*), 4.97 – 4.94 (m, 3H, *Man-H1*), 4.86 – 4.82 (m, 3H, *propargyl-H*), 4.71 (d, ^2J = 12.5 Hz, 3H, *propargyl-H*), 3.91 (m, 3H, *Man-H2*), 3.78 – 3.45 (m, 91H, *38x CH$_2$, 3x Man-H3-7*), 3.37 – 3.16 (m, 32H, *all CH$_2$*), 3.00 – 2.96 (m, 6H, *pentinyl-CH$_2$*), 2.61 – 2.56 (m, 6H, *pentinyl-CH$_2$*), 2.56 – 2.48 (m, 22H, *succinyl-CH$_2$*), 2.41 – 2.31 (m, 22H, *succinyl-CH$_2$*), 1.99 – 1.77 (m, 3H, *acetyl-CH$_3$*); *CH$_2$*).

MS for C$_{190}$H$_{278}$N$_{50}$O$_{60}$ (ESI) *m/z*: [M + 5H$^+$]$^{5+}$ calc.: 845.4; found: 845.5, [M + 4H$^+$]$^{4+}$ calc.: 1056.5; found: 1056.5, [M + 3H$^+$]$^{3+}$ calc.: 1408.4; found: 1408.4.

RP-HPLC (linear gradient from 0 – 50% eluent B in 30 min at 25°C): t$_R$ = 13.7 min. Determined purity (value shown correspond to the main peak, value in brackets refer to the sum of all peaks which show the same mass): 83% (92%).

PDI (GPC-RI-LS, 50 mM NaH$_2$PO$_4$, 150 mM NaCl, 250 ppm NaN$_3$ (pH 7.2), 30% ACN. Flow rate: 1 mL/min): 1.04.
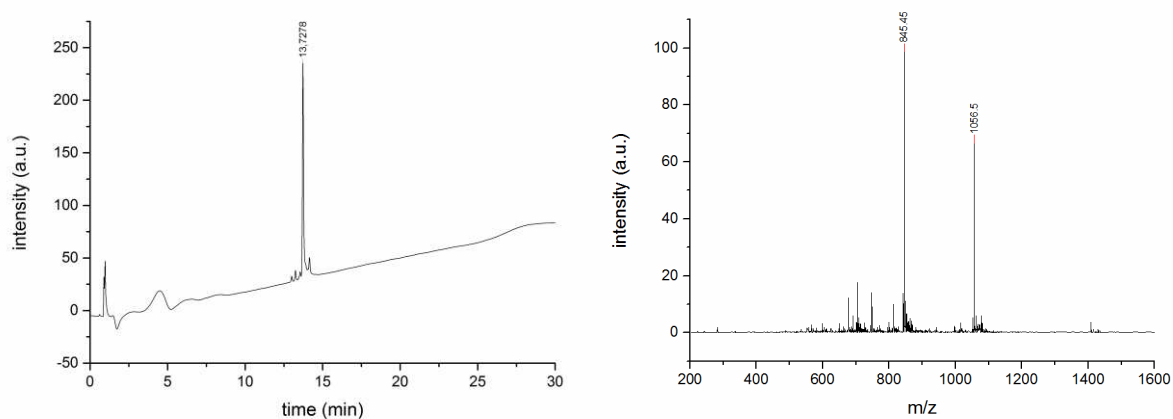
Figure S44. RP-HPLC (linear gradient from 0 - 50% eluent B in 30 min at 25°C) and ESI-MS (positve mode) of compound **16.**
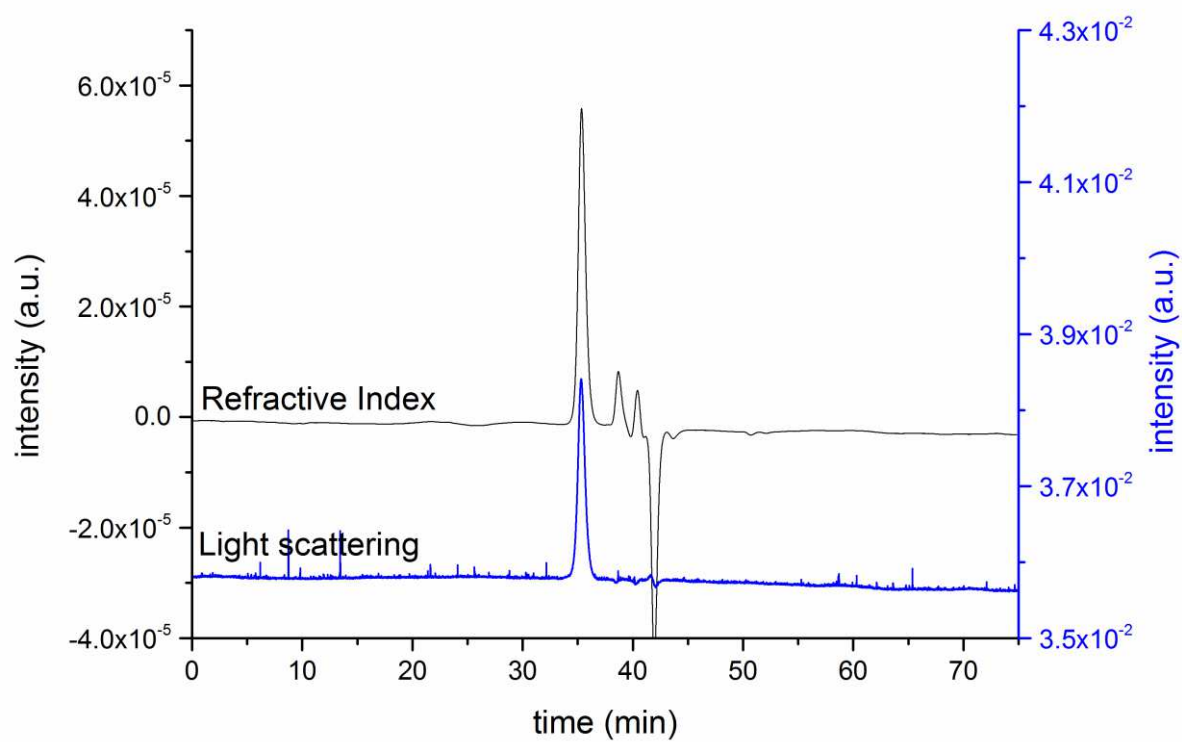
Figure S45. GPC (RI and LS) of compound **16**.

Man-3X2, (Man(1,3)-[BADS-EDS]₂-PA)(1,3,5)-[BADS-EDS]₂-BADS (17)
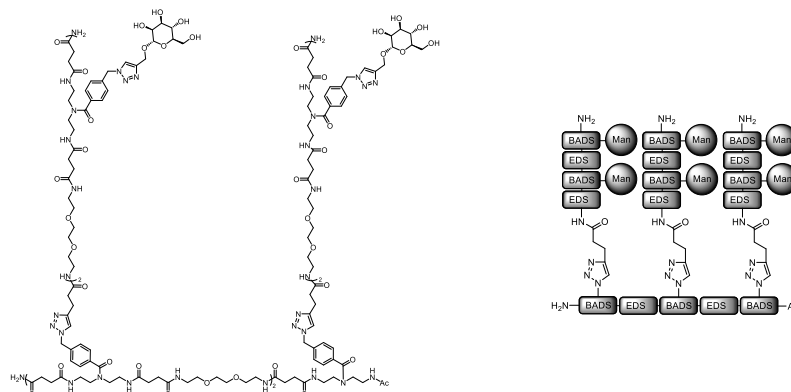
Man-3X2 was synthesized in a 10 µmol scale. 44.2 mg (6.70 µmol, 67%) of a white and foamy solid were obtained after purification with preparative HPLC. For solid phase synthesis protocol see general methods.

^{1}H NMR (600 MHz, D$_2$O) δ 8.14 – 8.11 (m, 6H, *triazole-H*), 7.83 (s, 3H, *triazole-H*), 7.44 – 7.33 (m, 36H, *aryl-H*), 5.68 – 5.58 (m, 18H, *aryl-CH₂-aryl*), 4.98 – 4.94 (m, 6H, *Man-H1*), 4.86 – 4.82 (m, 6H, *propargyl-H*), 4.70 (d, ^2J = 12.6 Hz, 6H, *propargyl-H*), 3.93 – 3.89 (m, 6H, *Man-H2*), 3.79 – 3.43 (m, 148H, *59x CH₂, 6x Man-H3-7*), 3.38 – 3.18 (m, 50H, *all CH₂*), 3.01 – 2.94 (m, 6H, *pentinyl-CH₂*), 2.58 (t, ^3J = 7.1 Hz, 6H, *pentinyl-CH₂*), 2.55 – 2.48 (m, 34H, *succinyl-CH₂*), 2.40 – 2.31 (m, 34H, *succinyl-CH₂*), 2.00 – 1.76 (m, 3H, *acetyl-CH₃*).

MS for C$_{295}$H$_{434}$N$_{74}$O$_{99}$ (ESI) *m/z*: [M + 7H$^+$]$^{7+}$ calc.: 943.9; found: 943.8, [M + 6H$^+$]$^{6+}$ calc.: 1100.9; found: 1101.1, [M + 5H$^+$]$^{5+}$ calc.: 1321.0; found: 1321.0.

RP-HPLC (linear gradient from 0 – 50 % eluent B in 30 min at 25° C): t$_R$ = 13.6 min. Determined purity: 96%.

PDI (GPC-RI-LS, 50 mM NaH$_2$PO$_4$, 150 mM NaCl, 250 ppm NaN$_3$ (pH 7.2), 30% ACN. Flow rate: 1 mL/min): 1.03.
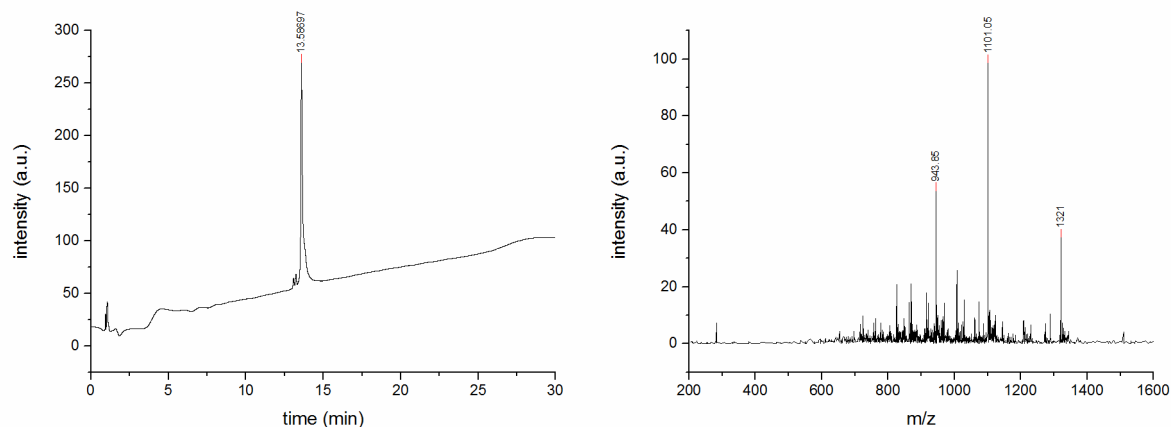
Figure S46. RP-HPLC (linear gradient from 0 - 50% eluent B in 30 min at 25°C) and ESI-MS (positve mode) of compound **17**.
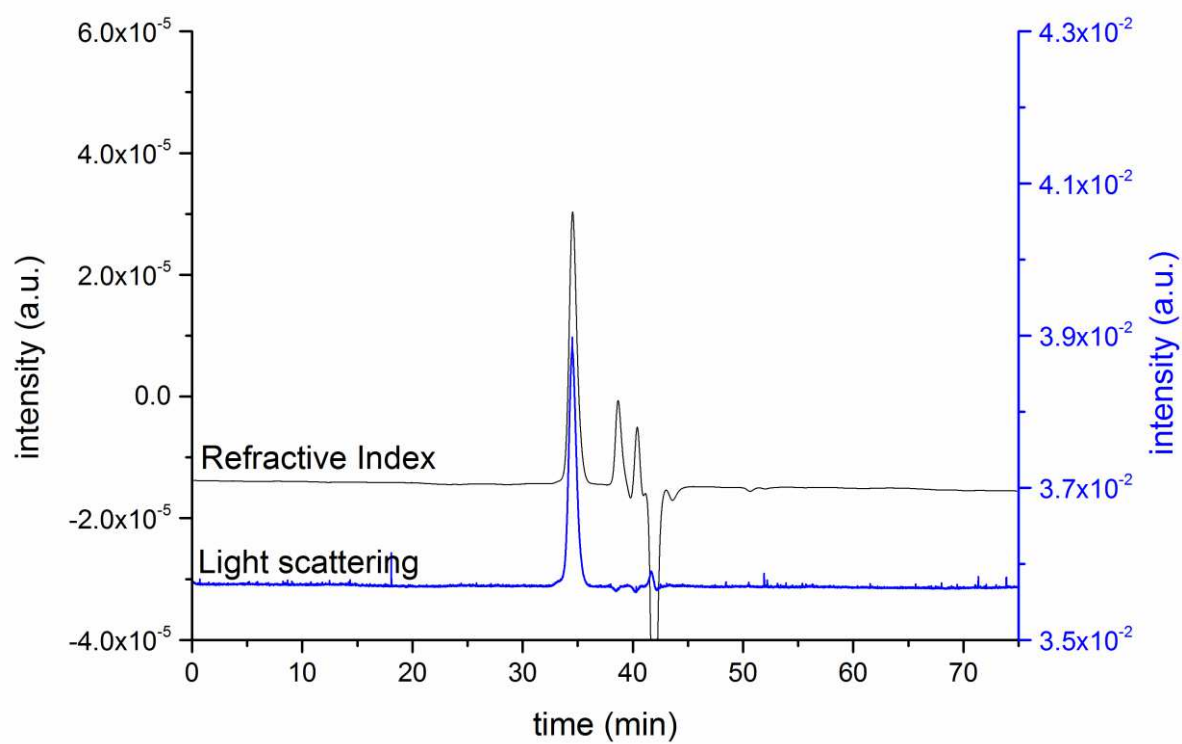
Figure S47. GPC (RI and LS) of compound **17**.

Gal-2X2, (Gal(1,3)-[BADS-EDS]₂-PA)(1,3)-BADS-EDS-BADS (18)
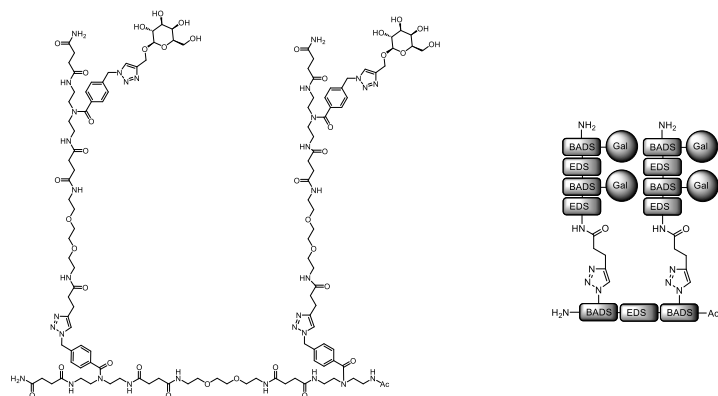
Gal-2X2 was synthesized in a 15 µmol scale. 40.8 mg (9.39 µmol, 63%) of a white and foamy solid were obtained after purification with preparative HPLC. For solid phase synthesis protocol see general methods.

^{1}H NMR (600 MHz, Deuterium Oxide) δ 8.17 – 8.10 (m, 4H, *triazole-H*), 7.83 (s, 2H, *triazole-H*), 7.46 – 7.32 (m, 24H, *aryl-H*), 5.73 – 5.57 (m, 12H, *aryl-CH₂-aryl*), 5.02 – 4.96 (m, 4H, *propargyl-H*), 4.88 – 4.84 (m, 4H, *propargyl-H*), 4.50 – 4.47 (m, 4H, *Gal-H1*), 3.94 – 3.90 (m, 4H, *Gal-H2*), 3.77 – 3.45 (m, 96H, *38x CH₂, 4x Gal-H3-7*), 3.39 – 3.17 (m, 32H, *all CH₂*), 2.98 (t, ^3J = 7.3 Hz, 4H, *pentinyl-CH₂*), 2.59 (t, ^3J = 7.3 Hz, 4H, *pentinyl-CH₂*), 2.56 – 2.48 (m, 22H, *succinyl-CH₂*), 2.40 – 2.32 (m, 22H, *succinyl-CH₂*), 2.00 – 1.76 (m, 3H, *acetyl-CH₃*).

MS for C₁₉₄H₂₈₅N₄₉O₆₅ (ESI) *m/z*: [M + 6H⁺]⁶⁺ calc.: 724.9; found: 725.0, [M + 5H⁺]⁵⁺ calc.: 869.6; found: 869.7, [M + 4H⁺]⁴⁺ calc.: 1086.8; found: 1086.8.

RP-HPLC (linear gradient from 0 – 50% eluent B in 30 min at 25°C): t_R = 13.0 min. Determined purity (value shown correspond to the main peak, value in brackets refer to the sum of all peaks which show the same mass): 87% (98%).

PDI (GPC-RI-LS, 50 mM NaH₂PO₄, 150 mM NaCl, 250 ppm NaN₃ (pH 7.2), 30% ACN. Flow rate: 1 mL/min): 1.06.
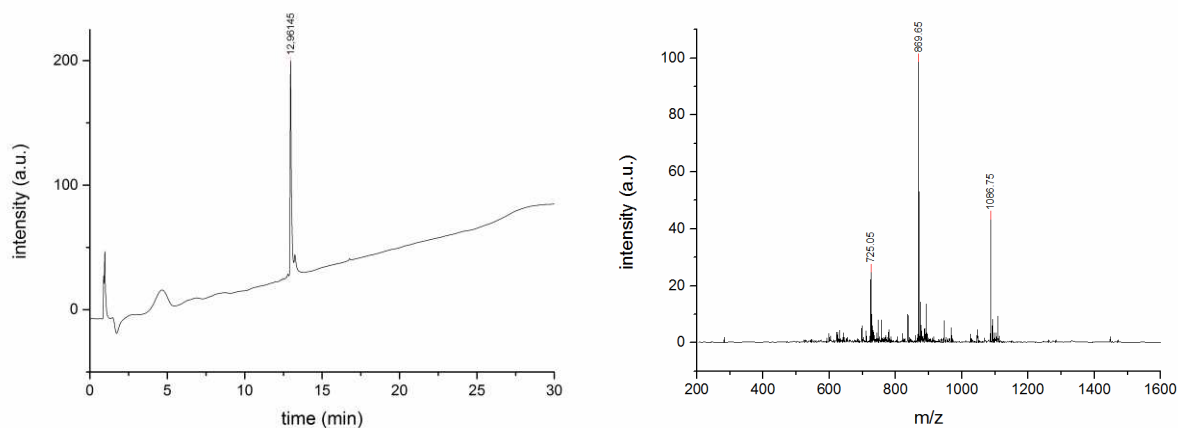
Figure S48. RP-HPLC (linear gradient from 0 - 50 % eluent B in 30 min at 25° C) and ESI-MS (positve mode) of compound **18.**
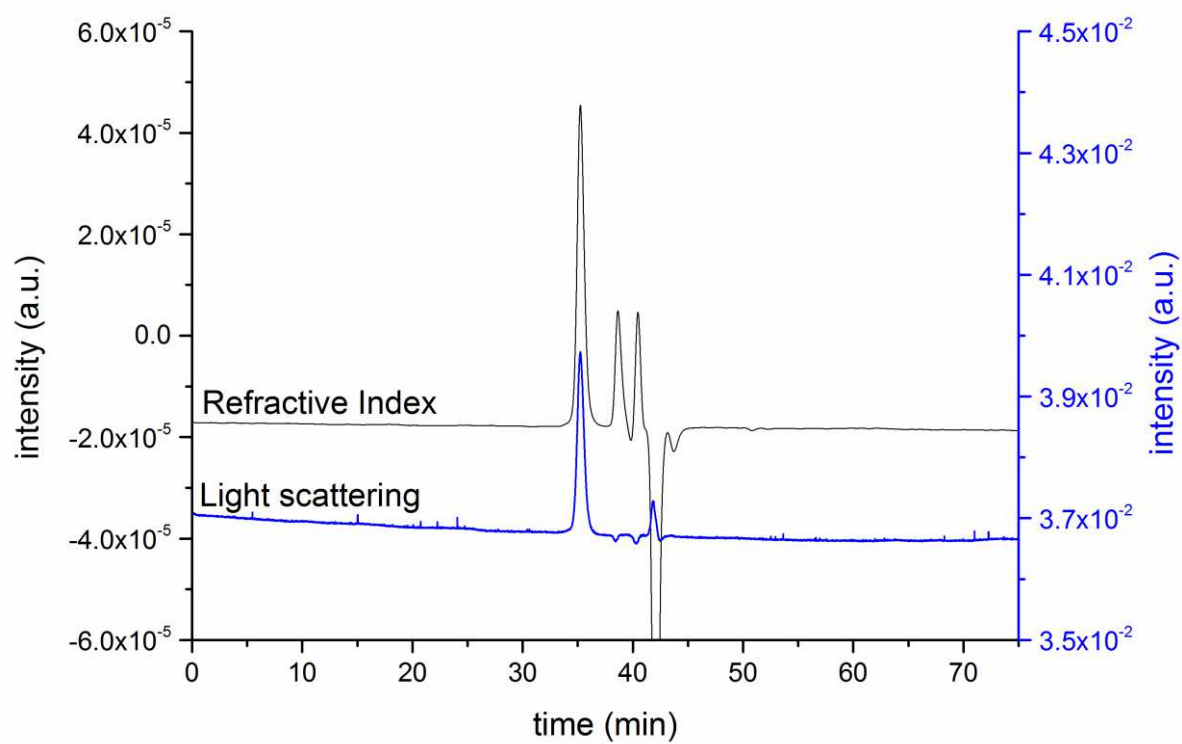
Figure S49. GPC (RI and LS) of compound **18**.

Surface plasmon resonance measurements

SPR sensograms
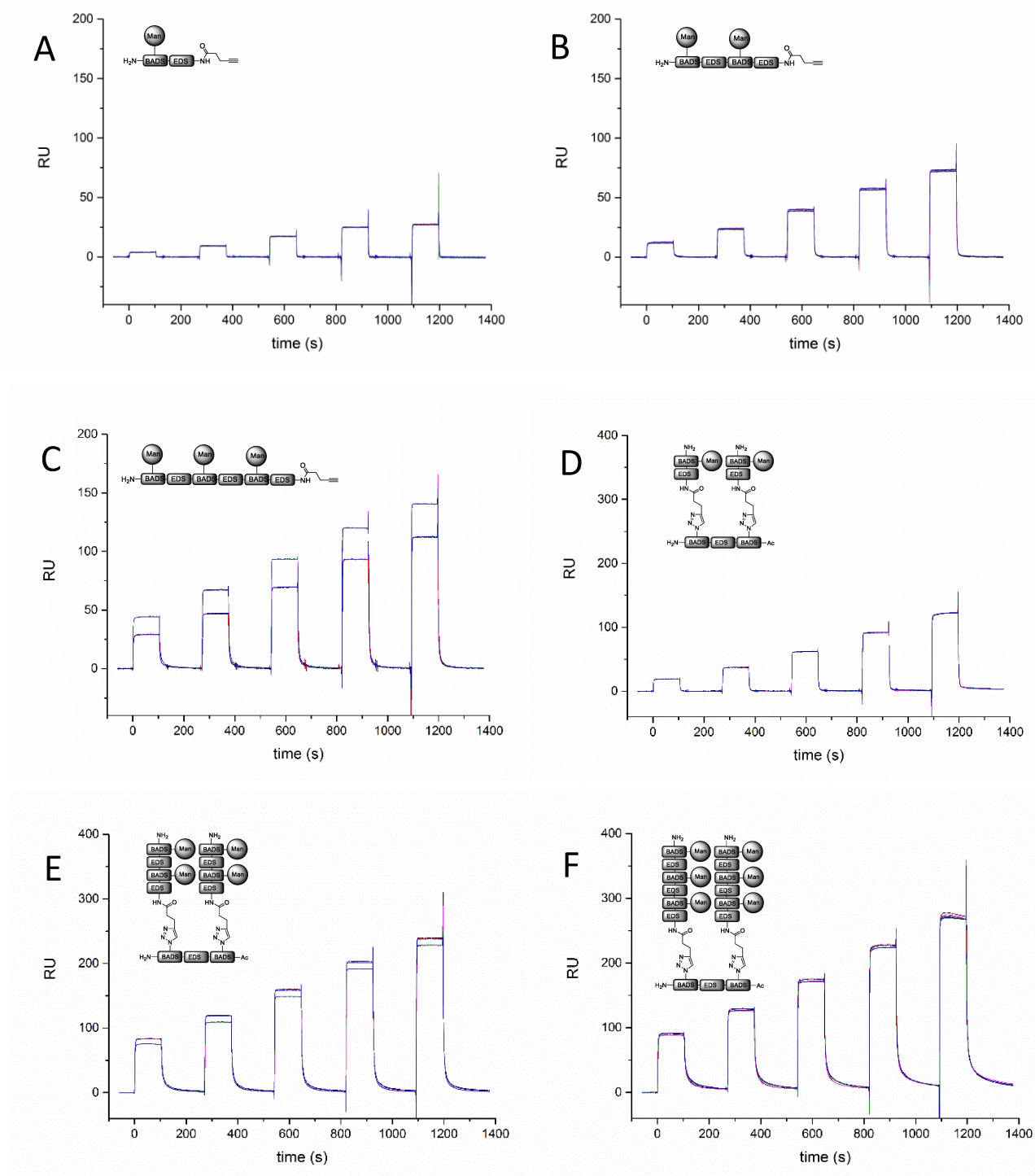
Figure S50: SPR sensograms from the compounds **arm** 1 (**A**), **arm 2** (**B**) and **arm 3** (**C**), **Man-2X1** (**D**), **Man-2X2** (**E**) and **Man-2X3** (**F**). The sensograms were measured in 2 series of 3 cycles, at least one day between the series. The compounds were injected at concentrations of 20, 60, 180, 540 and 1620 μM for arm 1 and 6.67, 20, 60, 180, 540 μM for all remaining compounds.
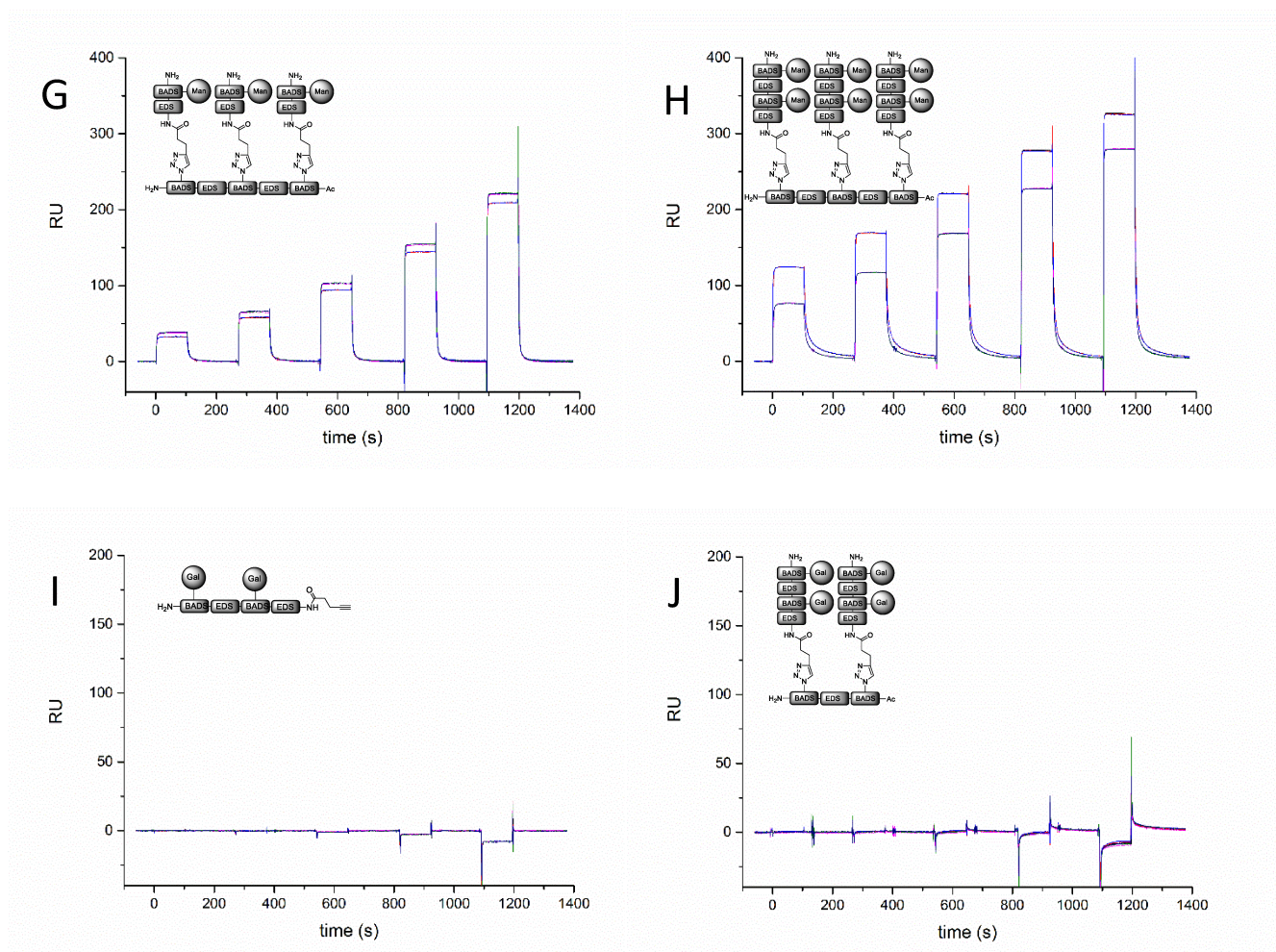
Figure S51: SPR sensograms from the compounds **Man-3X1** (**G**), **Man-3X2** (**H**), **Arm 4** (**I**) and **Gal-2X2** (**J**). The sensograms were measured in 2 series of 3 cycles, at least one day between the series. The compounds were injected at concentrations of 6.67, 20, 60, 180, 540 µM for all compounds. **Arm 4** (**I**) and **Gal-2X2** (**J**) do not show any binding.

SPR data

Table S1. Kinetic data obtained from SPR measurements of all glycomacromolecules using a two state reaction model.[23] The sensograms were measured in 2 series of 3 cycles, at least one day between the series. K_D values were obtained as mean values calculated as the arithmetic mean of two series of measurements.

group	compound	valency	k_{on1} [10^3 $M^{-1}s^{-1}$]	k_{off1} [10^{-1} s^{-1}]	K_{D1} [10^{-6} M^{-1}]	K_{D1} Man [10^{-5} M^{-1}]	k_{on2} [10^{-4} s^{-1}]	k_{off2} [10^{-3} s^{-1}]	K_{D2}	K_{D2} Man [M^{-1}]	K_{Dtotal} [10^{-6} M^{-1}]	R_{max} [RU]	X^2 [RU^2]
Arm 1	Arm 1[a]	1	-	-	-	-	-	-	-	-	-	-	-
	2X1	2	1.71 ± 0.06	5.52 ± 0.23	323.70 ± 24.00	64.74 ± 4.80	5.50 ± 0.07	5.58 ± 0.13	10.14 ± 0.36	20.28 ± 0.71	295.28 ± 21.5	211 ± 12	2.69 ± 0.74
	3X1	3	9.89 ± 0.93	4.10 ± 0.17	41.38 ± 5.56	12.42 ± 1.67	31.11 ± 11.17	36.38 ± 11.89	11.70 ± 8.04	35.09 ± 24.12	38.65 ± 5.15	163 ± 18	4.42 ± 0.86
Arm 2	Arm 2	2	7.32 ± 0.02	5.67 ± 0.38	77.41 ± 5.28	15.55 ± 1.06	8.79 ± 0.19	21.91 ± 0.50	24.93 ± 1.09	49.85 ± 2.19	74.42 ± 4.90	74 ± 3	0.77 ± 0.10
	2X2	4	18.95 ± 2.45	2.59 ± 0.01	13.66 ± 1.82	5.46 ± 0.73	25.75 ± 0.65	16.77 ± 2.15	6.51 ± 0.94	26.05 ± 3.78	12.04 ± 1.65	167 ± 1	15.60 ± 0.00
	3X2	6	26.52 ± 0.27	2.25 ± 0.18	8.49 ± 0.78	5.10 ± 0.47	30.95 ± 1.05	13.09 ± 0.75	4.23 ± 0.39	25.37 ± 2.32	6.88 ± 0.74	224 ± 15	31.35 ± 4.05
Arm 3	Arm 3	3	11.75 ± 0.35	3.53 ± 0.14	30.01 ± 2.04	9.00 ± 0.61	18.65 ± 0.25	23.27 ± 0.10	12.48 ± 0.22	37.44 ± 0.66	27.78 ± 0.20	111 ± 8	4.20 ± 2.57
	2X3	6	16.05 ± 3.25	2.43 ± 0.34	15.10 ± 5.14	9.06 ± 3.09	31.85 ± 0.25	9.27 ± 0.11	2.91 ± 0.056	17.44 ± 0.33	11.38 ± 0.70	192 ± 7	27.10 ± 1.50
Gal	Arm 4[b]	2	-	-	-	-	-	-	-	-	-	-	-
	2X2Gal[b]	4	-	-	-	-	-	-	-	-	-	-	-

[a] The monovalent compound **arm 1** could not be fitted to the two state reaction model. [b] Galactose containing molecules did not show any binding in the assay.

5.2. Divalent Sialylated Precision Glycooligomers Binding to Polyomaviruses and the Effect of Different Linkers

Authors: **Mischa Baier**, Nils H. Rustmeier, Joachim Harr, Norbert Cyrus, Dr. Guido J. Reiss, Dr. Andrea Grafmüller, Dr. Bärbel S. Blaum, Prof. Dr. Thilo Stehle, Prof. Dr. Laura Hartmann

1st author contribution:

Collaborative design of structures. Synthesis of functionalized sialic acid derivatives and synthesis of functional 3'-sialyllactose according to known methods. Single crystal production of two sialic acid derivatives. Synthesis of all building blocks by known methods. Elaboration of a new synthesis route for the already known building block TDS by applying pentynoic acid chloride was supported by Mr. Norbert Cyrus within his bachelor thesis. Solid phase assisted synthesis of divalent sialylated glycooligomers, their isolation and complete analysis. Collaborative writing of the manuscript.

Divalent Sialylated Precision Glycooligomers Binding to Polyomaviruses and the Effect of Different Linkers

Mischa Baier, Nils H. Rustmeier, Joachim Harr, Norbert Cyrus, Guido J. Reiss, Andrea Grafmüller, Bärbel S. Blaum, Thilo Stehle, and Laura Hartmann*

Divalent precision glycooligomers terminating in *N*-acetylneuraminic acid (Neu5Ac) or 3′-sialyllactose (3′-SL) with varying linkers between scaffold and the glycan portions are synthesized via solid phase synthesis for co-crystallization studies with the sialic acid-binding major capsid protein VP1 of human *Trichodysplasia spinulosa*-associated Polyomavirus. High-resolution crystal structures of complexes demonstrate that the compounds bind to VP1 depending on the favorable combination of carbohydrate ligand and linker. It is found that artificial linkers can replace portions of natural carbohydrate linkers as long as they meet certain requirements such as size or flexibility to optimize contact area between ligand and receptor binding sites. The obtained results will influence the design of future high affinity ligands based on the structures presented here, and they can serve as a blueprint to develop multivalent glycooligomers as inhibitors of viral adhesion.

Viral infections occur first by the attachment of a virion to the outer cell envelope prior to penetration of the cell, which is covered with a dense layer of carbohydrates, the so-called glycocalyx. Many types of viruses, enveloped such as influenza viruses and non-enveloped such as polyomaviruses, use terminal sialylated glycans as docking sites to which they bind multivalently. The multivalent presentation of individually low affinity ligands on

M. Baier, N. Cyrus, Prof. L. Hartmann
Institute of Organic and Macromolecular Chemistry
Heinrich-Heine-University Duesseldorf
Universitaetsstrasse 1, 40225 Duesseldorf, Germany
E-mail: laura.hartmann@uni-duesseldorf.de
N. H. Rustmeier, J. Harr, Dr. B. S. Blaum, Prof. T. Stehle
Interfaculty Institute of Biochemistry
University of Tuebingen
Hoppe-Seyler-Strasse 4, 72076 Tuebingen, Germany
Dr. G. J. Reiss
Institute of Inorganic and Structural Chemistry
Heinrich-Heine-University Duesseldorf
Universitaetsstrasse 1, 40225 Duesseldorf, Germany
Dr. A. Grafmüller
Max Planck Institute of Colloids and Interfaces
Am Muehlenberg 1, 14476 Potsdam, Germany
Prof. T. Stehle
Vanderbilt University School of Medicine
Nashville, Tennessee 37232, USA

 The ORCID identification number(s) for the author(s) of this article can be found under https://doi.org/10.1002/mabi.201800426.

an artificial scaffold can lead to an increase in binding affinity and has been successfully shown for various carbohydrate ligands and a multitude of artificial scaffolds, such as peptides, polymers, and dendrimers.[1] In the 1990s, Whitesides and co-workers introduced inhibitors of viral hemagglutination made of polyacrylamide scaffolds presenting high numbers of sialic acid ligands.[2] Today, a large variety of different sialylated scaffolds has been shown and tested for binding,[3] mostly to influenza viruses but to a much lesser extent to other viruses binding sialylated glycans such as the polyomaviruses. Polyomaviruses are small, non-enveloped DNA viruses that cause persistent asymptomatic infections in various species, and can, upon activation to productive infection, lead to serious diseases in immunocompromised individuals.[4] The polyomavirus outer capsid consists of 72 pentameric capsomers formed by the major capsid protein virus protein 1 (VP1). These VP1 capsomers typically contain five identical, shallow binding sites for sialylated glycans.[5] Individual binding affinities are weak, but the engagement of multiple binding sites on the virus capsid allows for high avidity, making polyomavirus VP1 an excellent target to develop multivalent ligands.

Previously we have introduced the synthesis of so-called precision glycomacromolecules and demonstrated their use in developing multivalent glycomimetic ligands targeting bacterial and viral lectins.[6] Through the solid phase assembly of tailor-made building blocks we can control the number, position, and kind of carbohydrate ligands to be placed on an oligoamide scaffold. Furthermore, we can vary the architecture of the scaffold from linear to branched, change hydrophobicity, and introduce different linker moieties to systematically investigate the effect of such structural parameters on the resulting binding properties, for example, in terms of their affinity or inhibitory potentials. Recently, and in accordance with similar studies on other scaffolds, we could show that changing the linker between carbohydrate ligand and scaffold strongly influences binding to the protein.[7] It seems that flexibility, length, and the chemical composition of the linker play important roles.

However, so far it has been difficult to visualize detailed interactions of our ligands by structural methods, which are challenged because of the high molecular weight and flexibility of our scaffolds. Nevertheless, especially when looking at effects of the scaffold in the close vicinity of the carbohydrate

**ADVANCED
SCIENCE NEWS**

www.advancedsciencenews.com

**Macromolecular
Bioscience**

www.mbs-journal.de

ligand, such as the variation of linkers, it would be highly relevant to obtain such structural information. Therefore, here we make use of our synthetic platform to create divalent sialylated glycooligomers with different linkers and look at their binding properties in co-crystallization experiments with the major capsid protein VP1 of human *Trichodysplasia spinulosa*-associated Polyomavirus (TSPyV). These oligomers with lower valency and lower molecular weight can be considered as components of more complex glycomacromolecules to be synthesized in the future for generating high affinity (or avidity) ligands of VP1. They can furthermore serve as useful templates to guide the development of other glycomimetic ligands.

Based on the previously presented solid phase assembly of tailor-made building blocks for the synthesis of precision glycomacromolecules, here a series of divalent sialylated oligomers with selected variations of the linker between scaffold and carbohydrate ligand were targeted. Specifically, we used previously established building blocks introducing either an azide or alkyne functionality in the side chain of the oligomeric scaffold, which allow for functionalization with different sialic acid derivatives via copper(I)-catalyzed azide-alkyne cycloaddition

(CuAAC).[6a,8] For on-resin attachment of sialic acid derivatives to oligoamide scaffolds presenting either azide or alkyne side chains, functionalized Neu5Ac derivatives Neu5Ac-Prop (**1**) and Neu5Ac-N$_3$ (**2**) were first synthesized following established protocols.[9] 3'-SL-Prop (**3**) was obtained following our previously reported protocol.[8] Although the chemical shifts of the ^{1}H-NMR signals of the sialic acid derivatives **1** and **2** are in line with already published data for α-anomer compounds, some uncertainty about the absolute configuration of the synthesized molecules remains. Due to the absence of hydrogen on the C2 atom, it is not possible to determine the configuration from the angle-dependent vicinal ^3J-coupling to H3 compared to hexoses. Reference is made only to the typical shift of the hydrogen signals at C3 of the sialic acid, wherein the influence of the azide in case of **2** was never discussed.[9a,10] However, we were able to grow crystals of both derivatives **1** and **2**, allowing a structural analysis. Thus, to the best of our knowledge, for the first-time crystal structures of C2-functionalized methyl 4, 7, 8, 9-tetra-*O*-acetyl-*N*-acetyl-α-D-neuraminates were determined, the results of which confirm the successful synthesis of the α-anomers (**Scheme 1**, see the Supporting Information for further details).
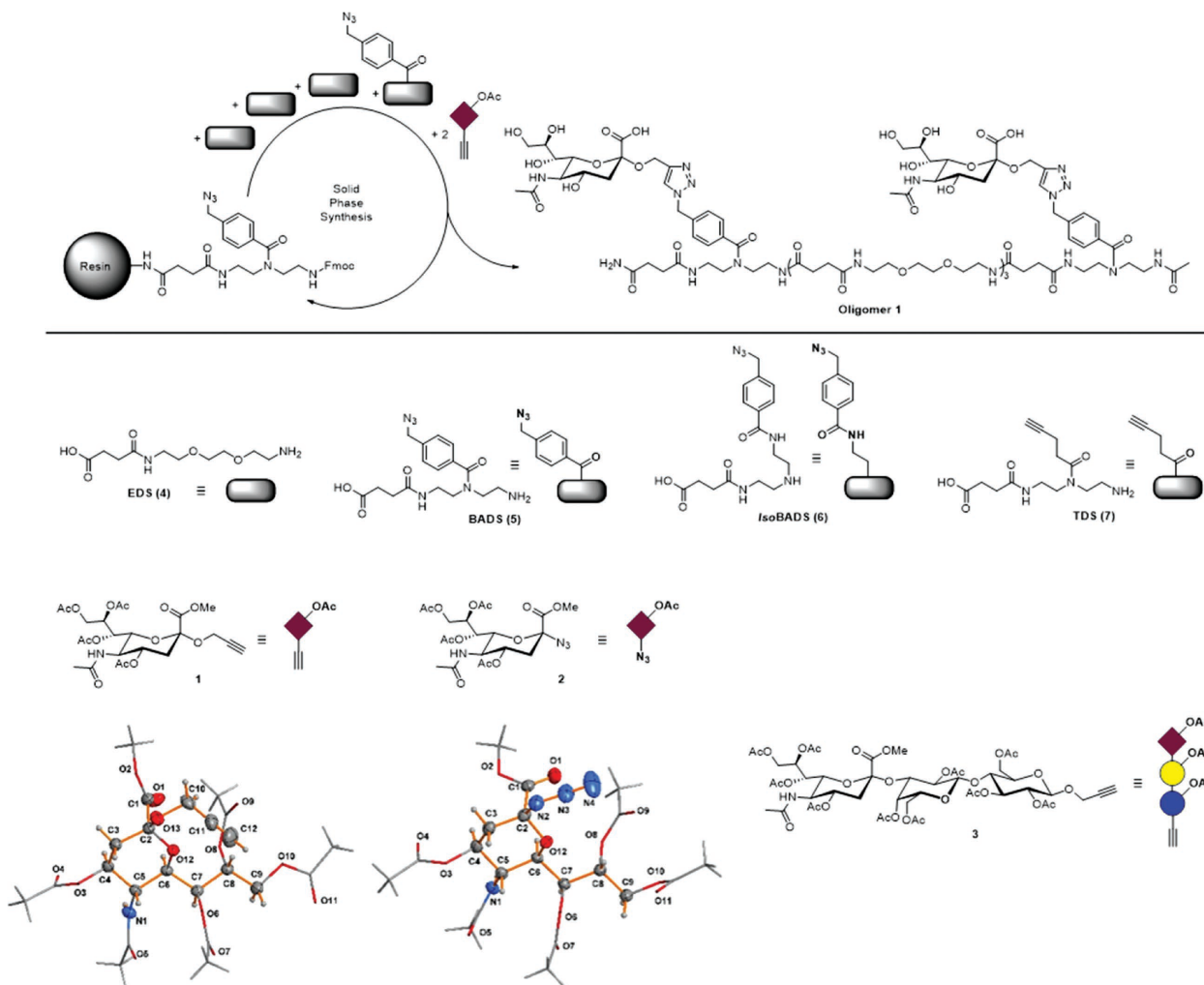
Scheme 1. Building blocks for solid phase assembly of precision glycooligomers, crystal structures obtained for Neu5Ac-derivatives **1** and **2**, and exemplary structure of glycofunctionalized ligand **O1**.

The synthesis of sialylated glycooligomers followed previously established protocols utilizing standard Fmoc-coupling conditions and tailor-made building blocks on solid support.[6] In short, all building blocks are equipped with free carboxy- and Fmoc-protected amine-groups, allowing for iterative deprotection and coupling steps to give the oligoamide scaffold. By choosing the sequence of building blocks during coupling, functional azide and alkyne side chains are positioned along the backbone. Functionalization of these side chains with the according glycoligands followed by cleavage from solid support, chromatographic purification and deprotection yields the final constructs.[6a,7f]

Four divalent glycooligomers were synthesized, three carrying Neu5Ac (**O1-O3**) and one carrying 3′SL side chains (**O4**) (**Table 1**).

As spacer building block constituting the backbone, the previously established EDS ((ethylendioxy)bis(ethylamine) succinic acid amide (**4**) was used.[11] Overall, glycooligomers present selected variations of two structural parameters: type of ligand and composition of linker. It has been shown before that the linker can influence ligand-receptor interactions not

only as an additional means of changing the overall spacing but also through secondary interactions, for example, via aromatic moieties introduced in close proximity of the carbohydrate ligand.[7,12] Here, we applied three different building blocks giving three different linkers. Since ligand conjugation is performed in all cases via CuAAC, all linker contain a 1, 2, 3-triazole unit (Scheme 1). Oligomers **O1** and **O4** were prepared using previously presented BADS ((azidomethyl)benzamido diethylenetriamine succinic acid amide) (**5**) as functional building block introducing azide side chains that allow for conjugation with both propargyl functionalized Neu5Ac (**1**) and 3′-SL (**3**) resulting in a linker incorporating a 1, 2, 3-triazole and a phenyl motif.[7f] Compound **O2** was prepared using the constitutional isomer of BADS (*Iso*BADS, **6**), thereby varying the linker between Neu5Ac and the scaffold by increase of one ethyl unit.[7f] **O3**, in turn, was obtained using alkyne-functionalized building block TDS[6a] (triple-bond functionalized diethylenetriamine succinic acid amide, **7**, see the Supporting Information for improved protocol)[13] that was functionalized with Neu5Ac-N$_3$ (**2**) resulting in a structurally different linker between **2** and the scaffold consisting only of a 1, 2, 3-triazole

Table 1. Synthesized sialylated precision glycooligomers.

Oligomer [#]	Structure	Building Blocks	Molecular weight [Da]	Relative Purity[a] [%]	Neu5Ac distance[b]/ stokes diameter[c] [Å]
O1		2*BADS (5), 3*EDS (4), 2*Neu5Ac-Prop (1)	2133.3	91 αα, 8 αβ, 1 ββ	7–23[b]
O2		2*IsoBADS (6), 3*EDS (4), 2*Neu5Ac-Prop (1)	2133.3	96 αα	27 ± 0.4[c]
O3		2*TDS (7), 3*EDS (4), 2*Neu5Ac-N$_3$ (2)	1949.1	90 αα, 8 unknown	21 ± 0.8[c]
O4		2*BADS (5), 3*EDS (4), 2*3′-SL-Prop (3)	2781.8	87 ββ, 12 αβ	17–30[b]

[a] Purities were determined by integration of UV signals in RP-HPLC (ACN in H$_2$O, linear gradient from 0–25% eluent B in 30 min); [b] Determined as the distance between the centers of mass of the Neu5Ac rings by molecular dynamics simulations; [c] Determined by dynamic light scattering (DLS).

positioned directly on the carbohydrate. Cleavage from solid support, purification via preparative HPLC, deprotection, and ion exchange gave the final compounds **O1-O3** in $\alpha\alpha$- and **O4** in $\beta\beta$-purities varying from 87–96% and yields up to 39%. All compounds were analyzed by ^{1}H-NMR, RP-HPLC-MS, and HR-ESI-MS (see the Supporting Information). Since neither 100% α-Neu5Ac nor 100% β-3′-SL was used, anomeric mixtures were expected. Anomeric ratios for all glycooligomers are given in Table 1.

Neu5Ac and 3′-SL were chosen as ligands since they were previously found to act as functional receptors for many polyomaviruses.[5a,14] The *Trichodysplasia spinulosa*-associated Polyomavirus (TSPyV) uses sialylated, lipid-linked glycans as cell-attachment receptors.[11,14c] The virus engages Neu5Ac as its minimal binding motif in a shallow, exposed binding site, and it binds Neu5Ac in the context of α2,3 as well as α2,6 linkages. Here, we explore the effect of covalent attachment at the Neu5Ac minimal binding epitopes on TSPyV VP1 binding. From previous studies investigating the conformation of glycooligomers of similar compositions, for example, via fluorescence correlation spectroscopy and dynamic light scattering,[6b,e] we hypothesize that the scaffolds adopt a coiled conformation in solution. This is supported by molecular dynamics (MD) simulations of the current series of Neu5Ac- and 3′-SL-functionalized glycooligomers (see the Supporting Information).

The distribution of ligand distances between the centers of mass of the sugar rings in the glycooligomers was measured. In glycooligomer **O1**, Neu5Ac rings are spaced by 7-23 Å (RMS) and in 3′-SL-functionalized glycooligomer **O4**, the distance of the terminal Neu5Ac increases to 17–30 Å. The specification of a maximum of the distribution function is hampered by the occurrence of multimodal distributions (Supporting Information). The results are supported by dynamic light scattering experiments showing hydrodynamic radii for glycooligomers **O2** and **O3** of 27 ± 0.4 and 21 ± 0.7 Å, respectively (see Table 1 and the Supporting Information). The spacing between different binding sites on the TSPyV VP1 pentamer was measured as the distances between Neu5Ac in the crystal structure (PDB ID 4U60). The smallest spacing is 35 Å between adjacent binding sites, and a larger spacing of 57 Å connects two sites that are located diagonally from each other (**Figure 1**).

Based on our information from modelling and light scattering, we predict that the Neu5Ac motifs in the 3′-SL-based glycooligomer **O4** could reach two adjacent binding sites also in the predicted coiled conformation; however, for other glycooligomers **O1 – O3** stretching of the backbone would have to occur for two carbohydrate motifs to bind simultaneously.

Previous structural analyses of TSPyV VP1 in complex with monovalent sialylated glycans showed that Neu5Ac is the minimal required motif for binding events between the protein and the respective cell attachment factors.[14c] It was further shown that the carbohydrate part of GM1 as larger glycan motif can also accommodate the TSPyV binding site.[14c] However, little is known on how the attachment of artificial linkers or scaffolds influences glycan binding to TSPyV. In this part of the work, we focused on investigating potential interactions of the glycooligomers **O1**, **O3**, and **O4** with TSPyV VP1.

Figure 1. Depiction of binding site distances on top of the *Trichodysplasia spinulosa*-associated Polyomavirus (TSPyV) major capsid protein VP1 pentamer. The protein is colored in grey with bound Neu5Ac shown as purple sticks. The measured distances are represented as dashed lines and distance values are given in Ångström.

TSPyV VP1 crystallization was performed as previously described.[14c] Complexes with glycooligomers were prepared by soaking or co-crystallization. Diffraction experiments were conducted at cryogenic temperatures at the X06DA and X06SA beamlines at the Swiss Light Source (PSI, Villigen). The terminal ends of **O1** and **O4** were clearly identifiable in unbiased Fo-Fc omit electron density maps (see the Supporting Information) after phase determination by molecular replacement and initial rounds of refinement. The visible portions of the ligands were incorporated into the model. The resulting binding modes of Neu5Ac correspond to the published glycan complex structures of TSPyV VP1,[14c] with the Neu5Ac forming interactions to the BC2 and the counter-clockwise DE loops of the protein surface (**Figure 2**).

For **O1**, all ten possible binding sites in the asymmetric unit (which contains two VP1 pentamers) are occupied by Neu5Ac. At one site, electron density for the glycooligomer linker is visible up to the phenyl ring (Scheme 1), indicating that this part of the linker mediates van-der-Waals contacts with an adjacent VP1 chain. For **O4**, six out of the ten possible binding sites are occupied. Electron density of all three sugar moieties of the 3′-SL are present at two of the six sites, where they also mediate crystal contacts with adjacent protein chains. The binding mode of **O3** could not be determined as soaking led to disintegration of the crystals and co-crystallization attempts were unsuccessful.

For **O1** and **O4**, the Neu5Ac interacts with the TSPyV VP1 protein in the same fashion that was previously described for the sialylated glycans that were used as cell receptor fragments.[14c] For both complex structures, additional electron

**ADVANCED
SCIENCE NEWS**

www.advancedsciencenews.com

**Macromolecular
Bioscience**

www.mbs-journal.de
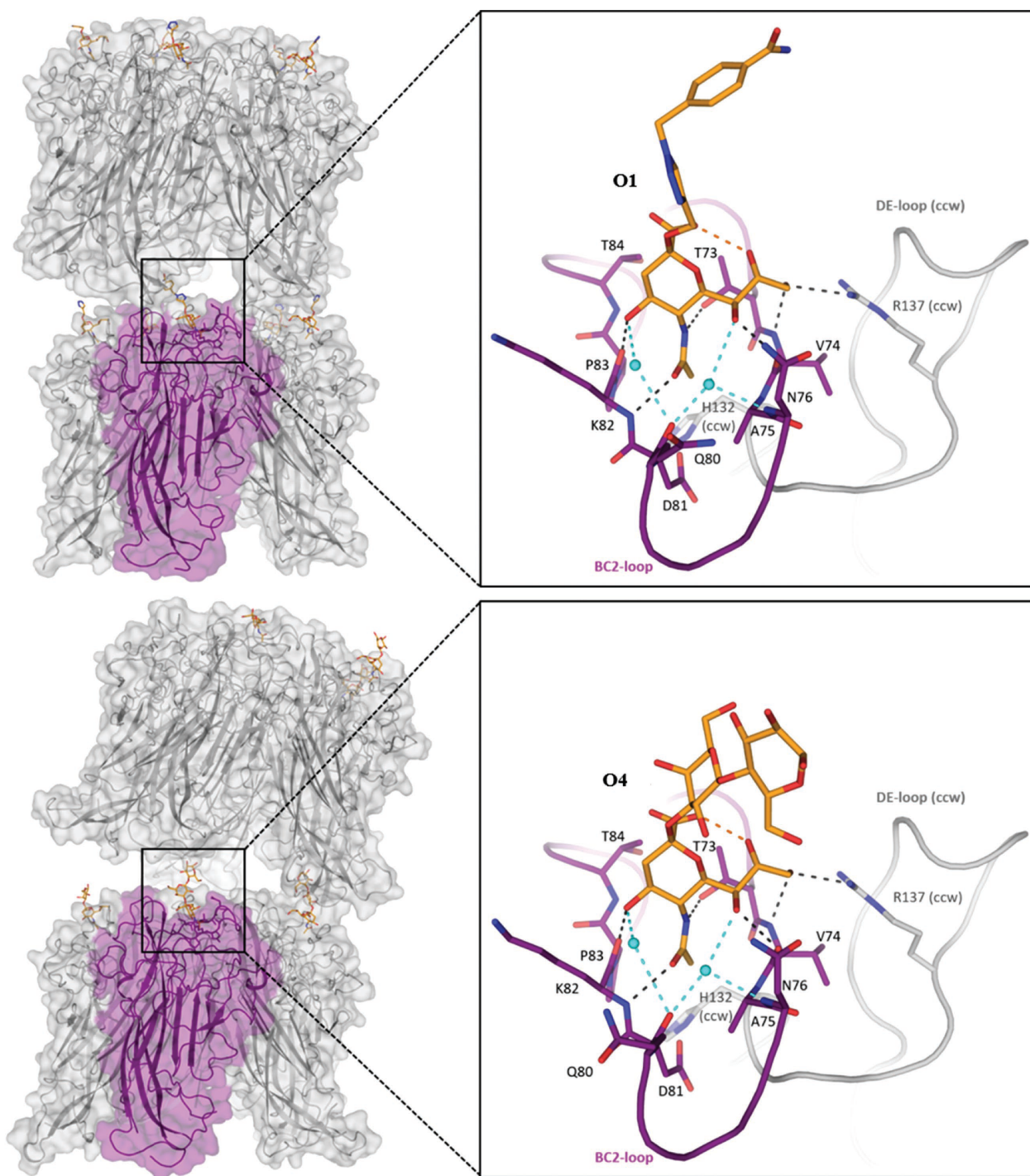
Figure 2. Structure of the glycooligomer—TSPyV VP1 complexes. Models on the top depict the complexed **O1**, the lower ones **O4**. Left: The structure of the bound ligand is shown in the context of the crystallographic asymmetric unit, with VP1 drawn in cartoon representation and as a transparent surface, with one chain colored in purple. Glycooligomer moieties are drawn as sticks with carbon atoms colored in orange, nitrogens in blue and oxygens in red. Right: Close-up view of the binding sites. In both cases the Neu5Ac part of the glycooligomer is recognized by residues of the VP1 surface loops BC2 and DE (ccw). Hydrogen bonds are represented as dashed lines. They are colored in dark grey for interactions between the compounds and protein residues, in cyan for interactions involving water (cyan spheres) and in orange for interactions within the compounds.

density allowed for modelling of the linker beyond the Neu5Ac part, validating that the linker participates in binding. Due to the high flexibility of the glycooligomers, the scaffold could not be built, and so we cannot experimentally confirm that glycooli-

gomers explicitly bridge more than one binding site. However, our findings show that the longer and aromatic linker of the BADS building block used in glycooligomer **O1** allows for similar occupation of the VP1 binding site compared to the larger

glycan motif of 3′-SL. Co-crystallization experiments with a shorter linker presenting Neu5Ac in O3 were not successful, suggesting that this linker might be unfavorable for binding of the glycan, possibly due to steric restraints.

We successfully synthesized a first series of divalent sialylated glycooligomers, selectively varying the ligand and linker structure to investigate the influence on addressing previously identified binding sites in TSPyV. Using X-ray crystallography, we could show how the linker between ligand and scaffold can participate in binding, replacing parts of the natural ligand in the binding site, as seen for compound **O1** in comparison to **O4**. On the other hand, as shown for **O3**, a short and rigid linker between the scaffold and minimal binding epitope did not yield a co-crystal structure, indicating that this kind of ligand-linker combination is unfavorable for binding site occupation.

Based on these findings we will now synthesize higher valent analogues of the sialylated glycooligomers with favorable linker–ligand combinations featuring an additional phenyl motif in the linker. As shown in the case of the inhibition of sialic acid-binding adenoviruses through trivalent glycan mimetics,[15] such glycomacromolecules could then benefit from both, optimized binding of linker and ligand as well as increase in avidity through multivalent binding.

Experimental Section

Materials and methods, as well as experimental details are provided in the Supporting Information.

Supporting Information

Supporting Information is available from the Wiley Online Library or from the authors.

Conflict of Interest

The authors declare no conflict of interest.

[1] For exemplary reviews on multivalency and use of different scaffolds for multivalent glycomimetics see: a) J. D. Badjic, A. Nelson, S. J. Cantrill, W. B. Turnbull, J. F. Stoddart, *Acc. Chem. Res.* **2005**, *38*, 723; b) C. Fasting, C. A. Schalley, M. Weber, O. Seitz, S. Hecht, B. Koksch, J. Dernedde, C. Graf, E. W. Knapp, R. Haag, *Angew. Chem., Int. Ed.* **2012**, *51*, 10472; c) Y. M. Chabre, R. Roy, *Curr. Top. Med. Chem.* **2008**, *8*, 1237; d) M. C. Galan, P. Dumy, O. Renaudet, *Chem. Soc. Rev.* **2013**, *42*, 4599; e) Y. Abdouni, G. Yilmaz, C. R. Becer, *Macromol. Rapid Commun.* **2017**, *38*, 1700212.

[2] a) J. E. Kingery-Wood, K. W. Williams, G. B. Sigal, G. M. Whitesides, *J. Am. Chem. Soc.* **1992**, *114*, 7303; b) M. Mammen, G. Dahmann, G. M. Whitesides, *J. Med. Chem.* **1995**, *38*, 4179; c) G. B. Sigal, M. Mammen, G. Dahmann, G. M. Whitesides, *J. Am. Chem. Soc.* **1996**, *118*, 3789.

[3] For selected examples see: a) R. Roy, D. Zanini, S. J. Meunier, A. Romanowska, *J. Chem. Soc., Chem. Commun.* **1993**, *0*, 1869; b) K. Hidari, T. Murata, K. Yoshida, Y. Takahashi, Y. Minamijima, Y. Miwa, S. Adachi, M. Ogata, T. Usui, Y. Suzuki, T. Suzuki, *Glycobiology* **2008**, *18*, 779; c) A. Nazemi, S. M. M. Haeryfar, E. R. Gillies, *Langmuir* **2013**, *29*, 6420; d) G. L. Hendricks, K. L. Weirich, K. Viswanathan, J. Li, Z. H. Shriver, J. Ashour, H. L. Ploegh, E. A. Kurt-Jones, D. K. Fygenson, R. W. Finberg, J. C. Comolli, J. P. Wang, *J. Biol. Chem.* **2013**, *288*, 8061; e) H. Wang, W. Huang, J. Orwenyo, A. Banerjee, G. R. Vasta, L. X. Wang, *Bioorg. Med. Chem.* **2013**, *21*, 2037; f) M. Ogata, S. Umemura, N. Sugiyama, N. Kuwano, A. Koizumi, T. Sawada, M. Yanase, T. Takaha, J. Kadokawa, T. Usuif, *Carbohydr. Polym.* **2016**, *153*, 96.

[4] T. Dalianis, H. H. Hirsch, *Virology* **2013**, *437*, 63.

[5] a) U. Neu, J. Bauer, T. Stehle, *Curr. Opin. Virol.* **2011**, *21*, 610; b) S. D. O'Hara, T. Stehle, R. Garcea, *Curr. Opin. Virol.* **2014**, *7*, 73; c) L. J. Ströh, T. Stehle, *Annu. Rev. Virol.* **2014**, *1*, 285.

[6] a) D. Ponader, F. Wojcik, F. Beceren-Braun, J. Dernedde, L. Hartmann, *Biomacromolecules* **2012**, *13*, 1845; b) D. Ponader, P. Maffre, J. Aretz, D. Pussak, N. M. Ninnemann, S. Schmidt, P. H. Seeberger, C. Rademacher, G. U. Nienhaus, L. Hartmann, *J. Am. Chem. Soc.* **2014**, *136*, 2008; c) S. Boden, K. Wagner, M. Karg, L. Hartmann, *Polymers* **2017**, *9*, 716; d) K. S. Bucher, N. Babic, T. Freichel, F. Kovacic, L. Hartmann, *Macromol. Biosci.* **2018**, *18*, 1800337; e) K. S. Bucher, H. Yan, R. Creutznacher, K. Ruoff, A. Mallagaray, A. Grafmuller, J. S. Dirks, T. Kilic, S. Weickert, A. Rubailo, M. Drescher, S. Schmidt, G. Hansman, T. Peters, C. Uetrecht, L. Hartmann, *Biomacromolecules* **2018**, *19*, 3714.

[7] a) S. Igde, S. Röblitz, A. Müller, K. Kolbe, S. Boden, C. Fessele, T. K. Lindhorst, M. Weber, L. Hartmann, *Macromol. Biosci.* **2017**, *17*, 1700198; b) S. J. Richards, M. W. Jones, M. Hunaban, D. M. Haddleton, M. I. Gibson, *Angew. Chem., Int. Ed.* **2012**, *51*, 7812; c) M. W. Jones, L. Otten, S. J. Richards, R. Lowery, D. J. Phillips, D. M. Haddleton, M. I. Gibson, *Chem. Sci.* **2014**, *5*, 1611; d) G. Yilmaz, V. Uzunova, M. Hartweg, V. Beyer, R. Napier, C. R. Becer, *Polym. Chem.* **2018**, *9*, 611; e) L. E. Wilkins, N. Badi, F. Du Prez, M. I. Gibson, *ACS Macro Lett..* **2018**, *7*, 1498; f) M. Baier, M. Giesler, L. Hartmann, *Chem. - Eur. J.* **2018**, *24*, 1619.

[8] M. Baier, J. L. Ruppertz, M. M. Pfleiderer, B. S. Blaum, L. Hartmann, *Chem. Commun.* **2018**, *54*, 10487.

[9] a) F. D. Tropper, F. O. Andersson, S. Braun, R. Roy, *Synthesis* **1992**, *1992*, 618; b) R. Šardzík, G. T. Noble, M. J. Weissenborn, A. Martin, S. J. Webb, S. L. Flitsch, *Beilstein J. Org. Chem.* **2010**, *6*, 699.

[10] H. Paulsen, U. Vondeessen, *Carbohydr. Res.* **1986**, *146*, 147.

[11] M. F. Ebbesen, C. Gerke, P. Hartwig, L. Hartmann, *Polym. Chem.* **2016**, *7*, 7086.

[12] K. L. Hudson, G. J. Bartlett, R. C. Diehl, J. Agirre, T. Gallagher, L. L. Kiessling, D. N. Woolfson, *J. Am. Chem. Soc.* **2015**, *137*, 15152.

[13] K. Crossey, M. E. Migaud, *Chem. Commun.* **2015**, *51*, 11088.

[14] a) U. Neu, H. Hengel, B. S. Blaum, R. M. Schowalter, D. Macejak, M. Gilbert, W. W. Wakarchuk, A. Imamura, H. Ando, M. Kiso, *PLoS Pathog.* **2012**, *8*, e1002738; b) U. Neu, S.-A. A. Allen, B. S. Blaum, Y. Liu, M. Frank, A. S. Palma, L. J. Ströh, T. Feizi, T. Peters, W. J. Atwood, T. Stehle, *PLoS Pathog.* **2013**, *9*, e1003688; c) L. J. Ströh, G. V. Gee, B. S. Blaum, A. S. Dugan, M. C. W. Feltkamp, W. J. Atwood, T. Stehle, *PLoS Pathog.* **2015**, *11*, e1005112.

[15] a) E. C. Nilsson, R. J. Storm, J. Bauer, S. M. C. Johansson, A. Lookene, J. Angstrom, M. Hedenstrom, T. L. Eriksson, L. Frangsmyr, S. Rinaldi, H. J. Willison, F. P. Domellof, T. Stehle, N. Arnberg, *Nat. Med.* **2011**, *17*, 105; b) R. Caraballo, M. Saleeb, J. Bauer, A. M. Liaci, N. Chandra, R. J. Storm, L. Frangsmyr, W. X. Qian, T. Stehle, N. Arnberg, M. Elofsson, *Org. Biomol. Chem.* **2015**, *13*, 9194.

Supporting Information

Divalent Sialylated Precision Glycooligomers Binding to Polyomaviruses and the Effect of Different Linkers

Mischa Baier, Nils H. Rustmeier, Joachim Harr, Norbert Cyrus, Guido J. Reiss, Andrea Grafmüller, Bärbel S. Blaum, Thilo Stehle, and Laura Hartmann*

Supporting Information

Divalent Sialylated Precision Glycooligomers Binding to Polyomaviruses and the Effect of Different Linkers

Mischa Baier, Nils H. Rustmeier, Joachim Harr, Norbert Cyrus, Guido J. Reiss, Andrea Grafmüller, Bärbel S. Blaum, Thilo Stehle, and Laura Hartmann[*]

Mischa Baier, Norbert Cyrus, Prof. Dr. Laura Hartmann
Institute of Organic and Macromolecular Chemistry, Heinrich-Heine-University Duesseldorf, Universitaetsstrasse 1, 40225 Duesseldorf, Germany.
E-mail: laura.hartmann@uni-duesseldorf.de.
Nils H. Rustmeier, Joachim Harr, Dr. Bärbel S. Blaum, Prof. Dr. Thilo Stehle
Interfaculty Institute of Biochemistry, University of Tuebingen, Hoppe-Seyler-Strasse 4, 72076 Tuebingen, Germany.
Dr. Guido J. Reiss
Institute of Inorganic and Structural Chemistry, Heinrich-Heine-University Duesseldorf, Universitaetsstrasse 1, 40225 Duesseldorf, Germany.
Dr. Andrea Grafmüller
Max Planck Institute of Colloids and Interfaces, Am Muehlenberg 1, 14476 Potsdam, Germany.
Prof. Dr. Thilo Stehle
Vanderbilt University School of Medicine, Nashville, Tennessee 37232, USA.

Table of Contents

Materials and Methods

Materials

N-Acetylneuraminic acid (>98%), 3'-Sialyllactose sodium salt (>98%) were purchased from Carbosynth. 2, 2′-(Ethylenedioxy)bis(ethylamine) (98%), Propargyl alcohol (99%), Succinic anhydride (>99%), Triethylsilane (99%), Triisopropylsilane (98%), (+)-Sodium-L-ascorbate (>99.0%), Amberlite® IR 120 H$^+$ were purchased from Merck (former Sigma Aldrich). Ion-exchange resin (AG® 1-X8 acetate-form) was purchased from Bio-Rad. 4-Pentynoic acid (95%) was purchased from Aldrich. Trityl chloride (98%), *p*-Toluic acid (98%), Piperidine (99%), Copper (II) sulfate (98%) were purchased from Acros Organics. Oxalyl dichloride (95%), *p*-Toluenesulfonic acid monohydrate (98%), Boron trifluoride diethyl etherate (>98%), Acetyl chloride (98%) were purchased from Alfa Aesar. *N*-Bromosuccinimide (99%) was purchased from Merck. Sodium azide (99%), Sodium diethyl dithiocarbamate (99%) were purchased from Applichem. PyBOP (Benzotriazole-1-yl-oxy-tris-pyrrolidino-phosphonium hexafluorophosphat) was obtained from Iris Biotech. Silver carbonate (>99%) was obtained from Strem Chemicals. Acetic anhydride (99%), Formic acid (>99%), Magnesium sulfate anhydrous (>99.5% min), Sodium chloride (>99.5%), Sodium hydrogen carbonate (>99.7%) were purchased from VWR. Lithium hydroxide monohydrate (>99%) was purchased from Janssen chimica. 9-Fluorenylmethyl chloroformate (Fmoc-Cl, 98%) was purchased from Chempur. *N, N*-Diisopropylethylamine (99%) was obtained from Roth. Trifluoroacetic acid (TFA, 99%) was purchased from Fluorochem. Tentagel® S RAM (Rink Amide) resin (Capacity 0.25 mmol/g) was purchased from Rapp Polymere. Peptide synthesis grade *N, N*-Dimethylformamide was used for solid phase synthesis. All solvents were of *p.a.* reagent grade.

Instrumentation

Nuclear Magnetic Resonance spectroscopy (NMR)
^{1}H-NMR (300 MHz) spectra were recorded on a Bruker AVANCE III - 300. ^{1}H-NMR (600 MHz) spectra were recorded on a Bruker AVANCE III - 600. Chemical shifts of all NMR spectra were reported in delta (δ) expressed in parts per million (ppm). For 1H-NMR the residual, non-deuterated solvent was used as internal standard. The following abbreviations are used to indicate the multiplicities: s, singlet; d, doublet; t triplet; m multiplet.

Attenuated Total Reflectance Fourier Transform Infrared Spectroscopy (ATR FTIR)
IR spectra were recorded with a Nicolet 6700, attenuated total reflectance Fourier transform infrared spectroscopy (ATR FTIR) spectrometer from Thermo Scientific and spectra analyzed using Omnic software 7.4.

Reversed Phase - High Performance Liquid Chromatography - Mass Spectrometry (RP-HPLC-MS)
Measurements were performed on an Agilent 1260 Infinity instrument coupled to a variable wavelength detector (VWD) (set to 214 nm) and a 6120 Quadrupole LC/MS containing an Electrospray Ionization (ESI) source (operated in positive ionization mode in a m/z range of 200 to 2000). As HPLC column a Poroshell 120 EC-C18 (3.0×50 mm, 2.5 μm) RP column from Agilent was used. The mobile phases A and B were H$_2$O/ACN (95/5) and H$_2$O/ACN (5/95), respectively. Both mobile phases contained 0.1% of formic acid. Samples were analyzed at a flow rate of 0.4 mL/min using a linear gradient starting with 100% mobile phase A reaching 50% mobile phase B within 30 min. The temperature of the column compartment was set to 25 °C. UV and MS spectral analysis was done within the OpenLab ChemStation software for LC/MS from Agilent Technologies.

Ultra High Resolution - Mass Spectrometry (UHR-MS)
UHR-MS measurements were performed with a Bruker UHR-QTOF maXis 4G instrument with a direct inlet via syringe pump, an ESI source and a quadrupole followed by a Time Of Flight (QTOF) mass analyzer.

Freeze dryer
The final oligomers were freeze dried with an Alpha 1-4 LD plus instrument from Martin Christ Freeze Dryers GmbH. The main drying method was set to -55 °C and 0.1 mbar.

Crystal structure determination
Crystal structures were collected using a Bruker D8 three-circle diffractometer equipped with a APEX II CCD detector and an Incoatec microfocus source Iμs 1.0 (Cu-radiation).[16] The data were integrated with SAINT.[16] The structure was solved by SHELXT [17] and refined against all data by full-matrix least-squares methods on F^2.[18]

Dynamic Light Scattering (DLS)

DLS experiments were performed on a Nikomp 380 DLS apparatus. Data were evaluated using the integrated CW388 software. Samples were measured at a concentration of 1 mM in triplicates in lectin binding buffer (LBB).

General Methods

(based on previously published methods)[7f]

Solid phase synthesis protocols

The batch sizes for synthesizing the oligomers using solid phase synthesis varied from 15 μmol to 150 μmol.

Fmoc cleavage

The Fmoc protecting group of the resin as well as the coupled building blocks were cleaved by the addition of a solution of 25% piperidine in DMF. The deprotection was performed twice for 10 min. After that, the resin was washed 10 times with DMF.

General coupling protocol

Commercially available Tentagel S RAM (Rink Amide) resin was used as resin for solid phase synthesis. As an example, 100 μmol of the resin were swollen in 10 mL of DCM for 20 min and subsequently washed five times with 10 mL of DMF. The Fmoc protecting group of the Tentagel S RAM resin was removed following the Fmoc cleavage protocol. A building block was coupled to the resin using a mixture of 0.5 mmol (5 eq.) of building block and 0.5 mmol PyBOP (5 eq.) dissolved in 4 mL of DMF to which 1 mmol (10 eq.) of DIPEA was added. The mixture was shaken for 30 s under a nitrogen stream for activation and subsequently added to the resin. The resin with the coupling mixture was shaken for 1 h. After that, the resin was washed from excessive reagent 5 times with 10 mL of DMF.

Capping of *N*-terminal primary amine

After successful assembly of the desired number of building blocks on solid phase, the *N*-terminal site was capped with an acetyl group. Therefore, 10 mL acetic anhydride were shaken twice with the resin for 30 min.

General CuAAC protocol

To 100 μmol of resin loaded with the oligomeric structure, 200 μmol (2 eq.) of protected sialic acid derivatives (**1**, **2**) per azide or alkyne group, dissolved in 1.5 mL DMF, were added. When propargylated sialic acid (**1**) was used, 100 mg (0.4 mmol) of $CuSO_4$ and 100 mg (0.5 mmol) of sodium ascorbate were used and dissolved each in 0.75 mL of water and added to the resin. When sialic acid azide (**2**) was coupled, 50 mg (0.2 mmol) of $CuSO_4$ and 50 mg (0.25 mmol) of sodium ascorbate were used and dissolved each in 0.75 mL of water. The mixture was shaken for 24 h and subsequently washed extensively with water, a 23 mM solution of sodium diethyldithiocarbamate in 50 vol.% DMF : H_2O, DMF and DCM. Propargylated 3'sialyllactose (**3**) was used in a 1.5-fold excess per functional group with 20 mg (80 μmol) of $CuSO_4$ and 20 mg (100 μmol) of sodium ascorbate.

Cleavage from solid phase

13 mL of a mixture of 95% TFA, 2.5% of TIPS and 2.5% of DCM (all vol%) were added to the resin and shaken for 1 h. The filtrate was poured into 60 mL cold diethyl ether. The resin was washed with an additional 5 mL of the cleavage mixture which were also added to the cold ether. The resulting precipitate was centrifuged three times and the ether decanted. The crude product was dried over a stream of nitrogen, dissolved in 6 mL of H_2O and lyophilized twice.

General ion exchange protocol

All glycooligomers were further purified by ion exchange chromatography. Therefore, compounds were dissolved in 2 mL of Milli-Q water to which 1 g AG® 1-X8 acetate-form resin was added, before the mixture was shaken for 10 min. Finally, the resin was filtered off by using a syringe filter before the compound was lyophilized again.

General preparative purification protocol of the oligomers

Final glycooligomers were purified by preparative reversed phase - high performance liquid chromatography on an Agilent 1260 Infinity instrument coupled to a variable wavelength detector (VWD) (set to 214 nm). As HPLC column a UG80 C18 (20mml.D.×250 mm, 5 μm) RP column from Shiseido was used. The mobile phases A and B were H_2O and ACN to which 0.1 % formic acid were added, respectively. Samples were purified at a flow rate of 20 mL/min using a linear gradient starting with 100% mobile phase A reaching 50% mobile phase B within 15 min. The temperature of the column compartment was room temperature (18-23° C). UV analysis was done within the OpenLab ChemStation software for LC/MS from Agilent Technologies.

Protective groups deprotection protocol

In order to remove both the acetyl and methyl protective groups of the carbohydrate moieties, 3 mL of a 0.1 M solution of lithium hydroxide monohydrate in a mixture of 50 vol.% MeOH : H_2O were added to the compound and shaken for 3 h at room temperature (18-23° C) (the pH needs to be set to 13 during the deprotection). Subsequently the dissolved and deprotected compound was treated with Amberlite® IR 120 H^+ ion exchange resin until pH 4-5 was reached. A neutralized mixture was dried in *vacuo* at a temperature not higher than 25 °C and finally lyophilized in order to give final deprotected compound.

General crystallization protocol for crystal structure elucidation of Neu5Ac-derivatives 1 and 2.

Neu5Ac-derivatives **1** and **2** were crystallized to elucidate their crystal structures and giving additional proof of their anomeric form. Both compounds were therefore first purified by preparative HPLC (20-80% eluent B in 10 min), before they were dissolved approximately in a $w_{Neu5Ac} = 10\%$ ratio (1 g in 10 mL) in ethyl acetate in a closed flask and placed at room temperature in a calm place. At one-day intervals, 1 mL of *n*-hexane was added until clear needles started growing, which continued growing when increasing the *n*-hexane concentration. Once the desired size of the crystals was achieved, they were carefully removed from the solution and rinsed briefly with diethyl ether before being dried at room temperature and atmospheric pressure for one day.

General method for determining crystal structures

Crystals suitable for X-ray diffraction were mounted (glued) on a thin fibre. The data of Neu5Ac-Prop (**1**) and Neu5Ac-N_3 (**2**) were collected at room temperature. All non-hydrogen atoms in the crystal structures of **1** and **2** were refined with anisotropic displacement parameters. The hydrogen atoms in crystal structure of **1** and **2** were placed in calculated positions and refined using a riding model.

Experimental Data

Neu5Ac derivatives

Neu5Ac-Prop (**1**) and Neu5Ac-N$_3$ (**2**) were synthesized by previously reported methods. Since single-crystal structure analyses of these structures is shown in this work, obtained analytical data for the verification of the structure is given below.

3'-SL-Prop (**3**) was synthesized and characterized according to Baier et al., *manuscript submitted (see SI for review only)*:

Methyl 2-(propargyl)-4,7,8,9-tetra-*O*-acetyl-*N*-acetyl-α-D-neuraminate (1)
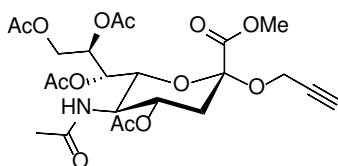
Synthesis was performed according to Šardzík *et al*, [9b] and Ebbesen *et al.* [19]

^{1}H-NMR (600 MHz, CDCl$_3$) δ 5.40 (ddd, ^3J = 8.6, 5.8, 2.8 Hz, 1H, *H8*), 5.30 (dd, ^3J = 8.6, 1.7 Hz, 1H, *H9'*), 5.22 – 5.18 (m, 1H, *-NH*), 4.86 (ddd, ^3J = 12.4, 9.6, 4.7 Hz, 1H, *H4*), 4.39 (dd, ^2J = 15.7, ^4J = 2.5 Hz, 1H, *propargyl-CH'*H), 4.28 (dd, ^3J = 12.4, 2.8 Hz, 1H, *H7*), 4.15 (dd, ^2J = 15.7, ^4J = 2.4 Hz, 1H, *propargyl-CHH''*), 4.10 – 4.02 (m, 3H, *H5, 6, 9''*), 3.80 (s, 3H, *-OCH$_3$*), 2.62 (dd, ^2J = 12.8, ^3J = 4.6 Hz, 1H, *H3eq.*), 2.43 (t, ^4J = 2.4 Hz, 1H, *propargyl-CH*), 2.14 – 2.02 (4s, 4x 3H, 4x *Ac*), 1.97 (dd, ^2J = 12.5 Hz, ^3J = 12.5 Hz, 1H, *H3ax.*), 1.87 (s, 3H, *Ac*) ppm.

^{13}C-NMR (151 MHz, CDCl$_3$) δ 171.10, 170.76, 170.33, 170.24, 170.20, 167.91, 98.21, 79.07, 74.62, 72.74, 68.96, 68.39, 67.30, 62.53, 52.98 (2C), 49.48, 38.01, 23.31, 21.25, 20.98, 20.95, 20.89 ppm.

IR (ATR) $\tilde{\nu}_{max}$: 3318 (w), 3252 (w), 2957 (w), 1748 (s), 1733 (s), 1648 (m), 1547 (m), 1369 (m), 1207 (s), 1037 (s), 620 (m), 602 (m) cm^{-1}.

MS for C$_{23}$H$_{31}$NO$_{13}$ (ESI, pos.) m/z: [M + Na$^+$]$^+$ calc.: 552.17; found 552.20, [M + H$^+$]$^+$ calc.: 530.19; found 530.20, [M – C$_3$H$_4$O + H$^+$]$^+$ calc.: 474.16; found 474.25, [M – C$_3$H$_4$O – AcOH + H$^+$]$^+$ calc.: 414.14; found 414.25.

HRMS for C$_{23}$H$_{31}$NO$_{13}$ (ESI-TOF) *m/z*: [M + H$^+$]$^+$ calc.: 530.1874; found: 530.1872.

Crystal structure: The asymmetric unit of the crystal structure contains one molecule only. The Flack-Parsons parameter verifies the chirality at all chiral centers independently (Table S1).
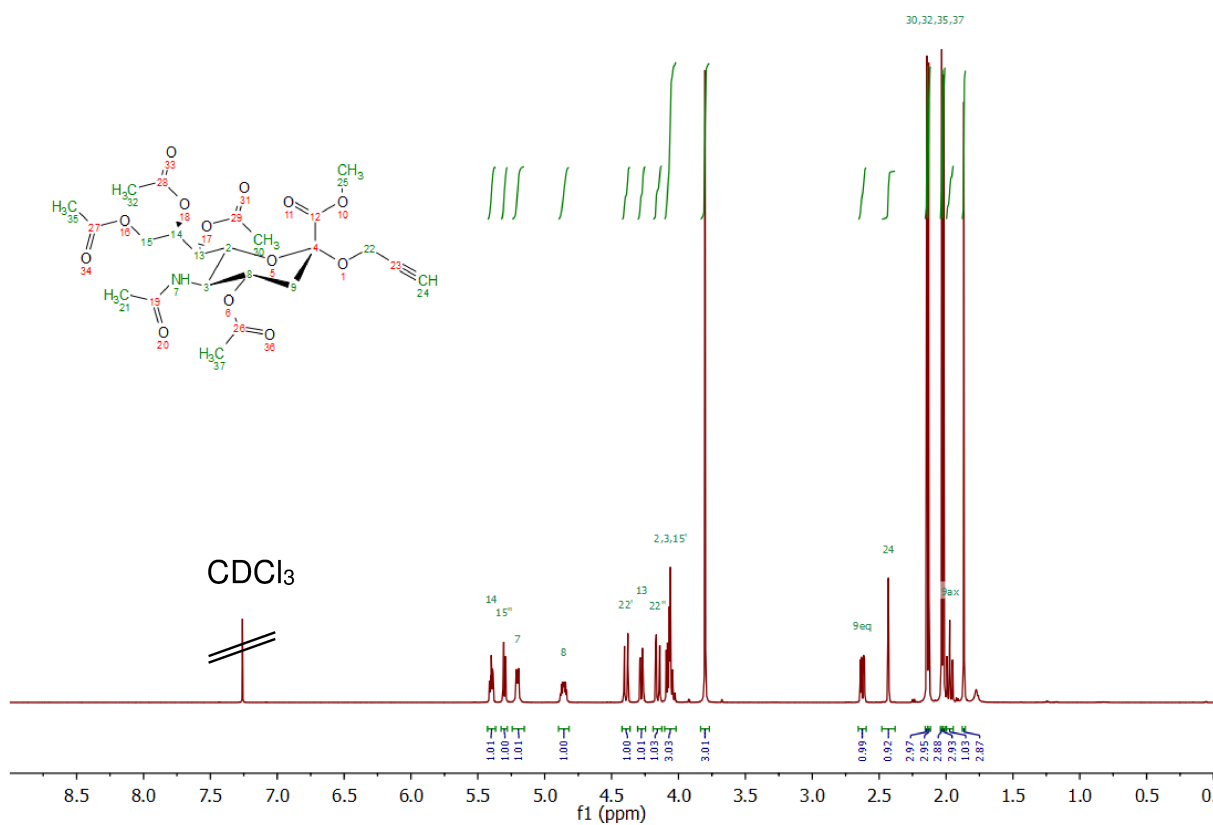
Figure S1: ¹H-NMR (600 MHz, CDCl₃) of compound 1.
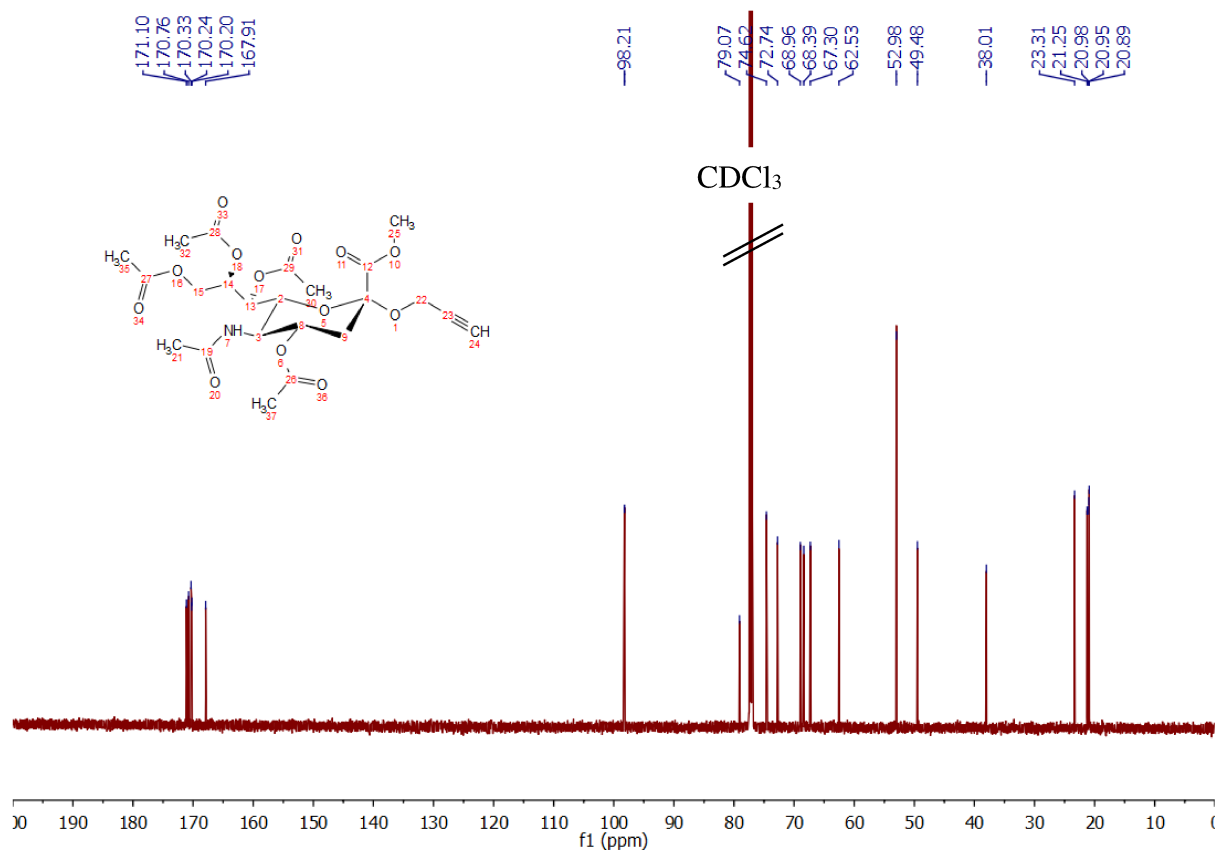
Figure S2: ¹³C-NMR (151 MHz, CDCl₃) of compound 1.
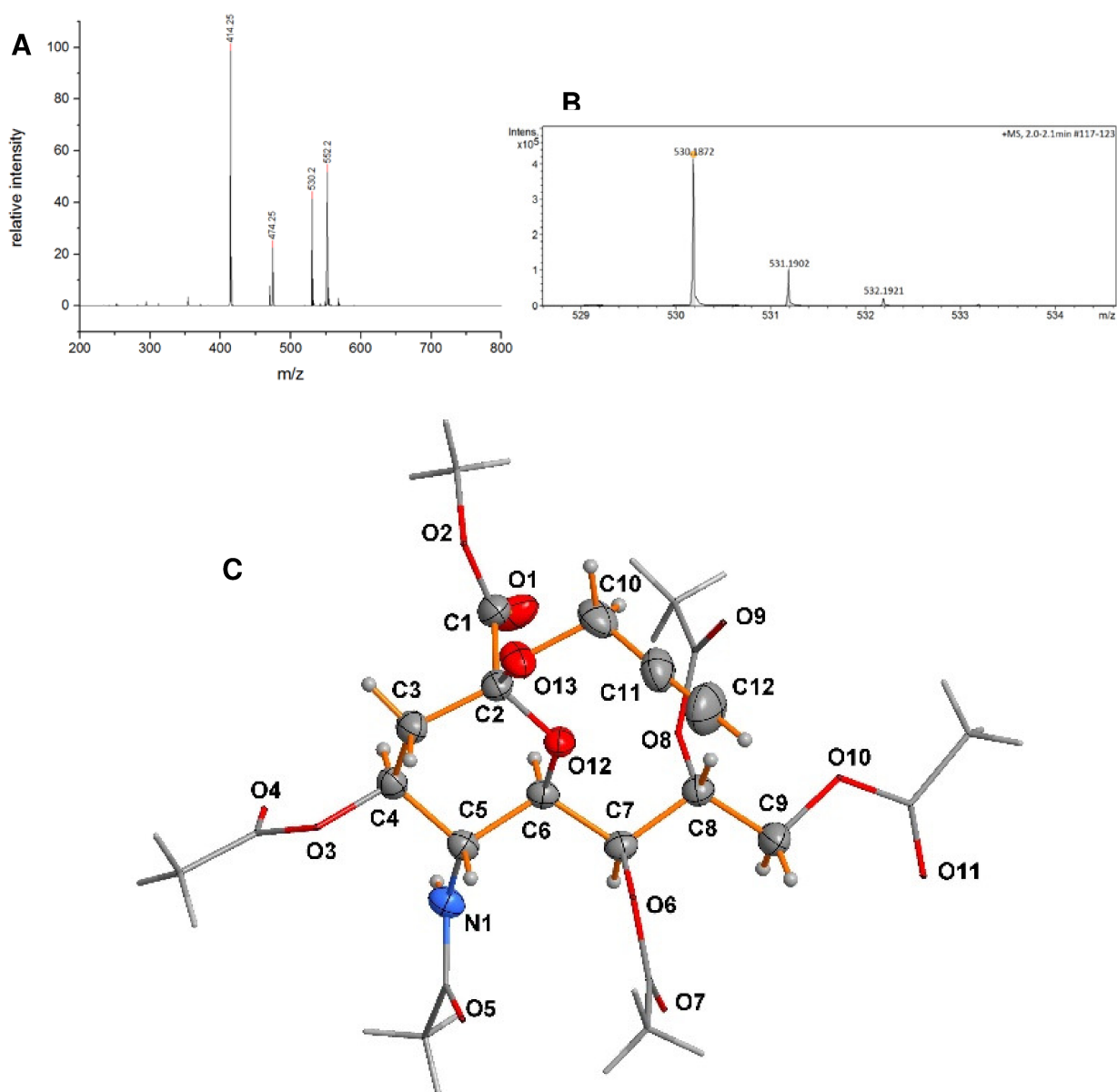
*Figure S3: **A**: ESI-MS (positive mode), **B**: HR-MS (ESI+ Q-TOF, positive mode) and DIAMOND [20] plot **C** of compound **1** forming the crystal structure.*

Methyl 2-azido-4,7,8,9-tetra-*O*-acetyl-*N*-acetyl-α-D-neuraminate (2)
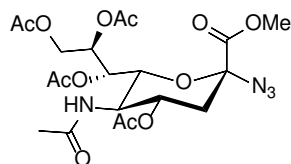
Synthesis was performed according to Tropper *et al.*[9a]

^{1}H-NMR (600 MHz, CDCl$_3$) δ 5.37 (d, ^3J = 10.0 Hz, 1H, *-NH*), 5.32 (s, 2H, *H8, 9'*), 5.04 (ddd, ^3J = 11.9, 10.1, 4.7 Hz, 1H, *H4*), 4.35 (dd, ^3J = 12.4, 1.7 Hz, 1H, *H7*), 4.15 – 4.09 (m, 1H, *H9''*), 4.05 (ddd, ^3J = 10.3 Hz, 1H, *H5*), 3.89 (d, ^3J = 10.8 Hz, 1H, *H6*), 3.87 (s, 3H, *-OCH$_3$*), 2.55 (dd, ^2J = 13.1, ^3J = 4.8 Hz, 1H, *H3eq.*), 2.14 – 1.87 (5s, 5x 3H, 5x *Ac*), 1.83 (dd, ^2J = 13.2, ^3J = 11.7 Hz, 1H, *H3ax.*) ppm.

^{13}C-NMR (151 MHz, CDCl$_3$) δ 170.96, 170.75, 170.46, 170.20, 170.18, 167.26, 89.15, 74.12, 69.71, 68.93, 67.62, 62.29, 53.62, 49.39, 36.68, 23.29, 21.16, 20.95, 20.88, 20.86 ppm.
IR (ATR) $\tilde{v}_{max}$: 3273 (w), 2121 (m), 1745 (s), 1661 (m), 1559 (m), 1440 (m), 1371 (m), 1207 (s), 1034 (s), 605 (m) cm^{-1}.

MS for C$_{20}$H$_{28}$N$_4$O$_{12}$ (ESI, pos.) m/z: [M + Na$^+$]$^+$ calc.: 539.16; found 539.30, [M + H$^+$]$^+$ calc.: 517.18; found 517.25, [M – HN$_3$ – AcOH + H$^+$]$^+$ calc.: 414.14; found 414.20.

HRMS for C$_{20}$H$_{28}$N$_4$O$_{12}$ (ESI-TOF) *m/z*: [M + H$^+$]$^+$ calc.: 517.1776; found: 517.1778.

Crystal structure: The asymmetric unit of the crystal structure contains two molecules of **2** and one additional molecule of water. A slight disorder in one of the two sugar molecules was refined using a restrained split model. Both crystallographically independent organic molecules display the same chirality at all chiral centers. The molecule exhibiting no disorder problem is shown below. The Flack-Parsons parameter verifies the chirality at all chiral centers independently (Table S1).
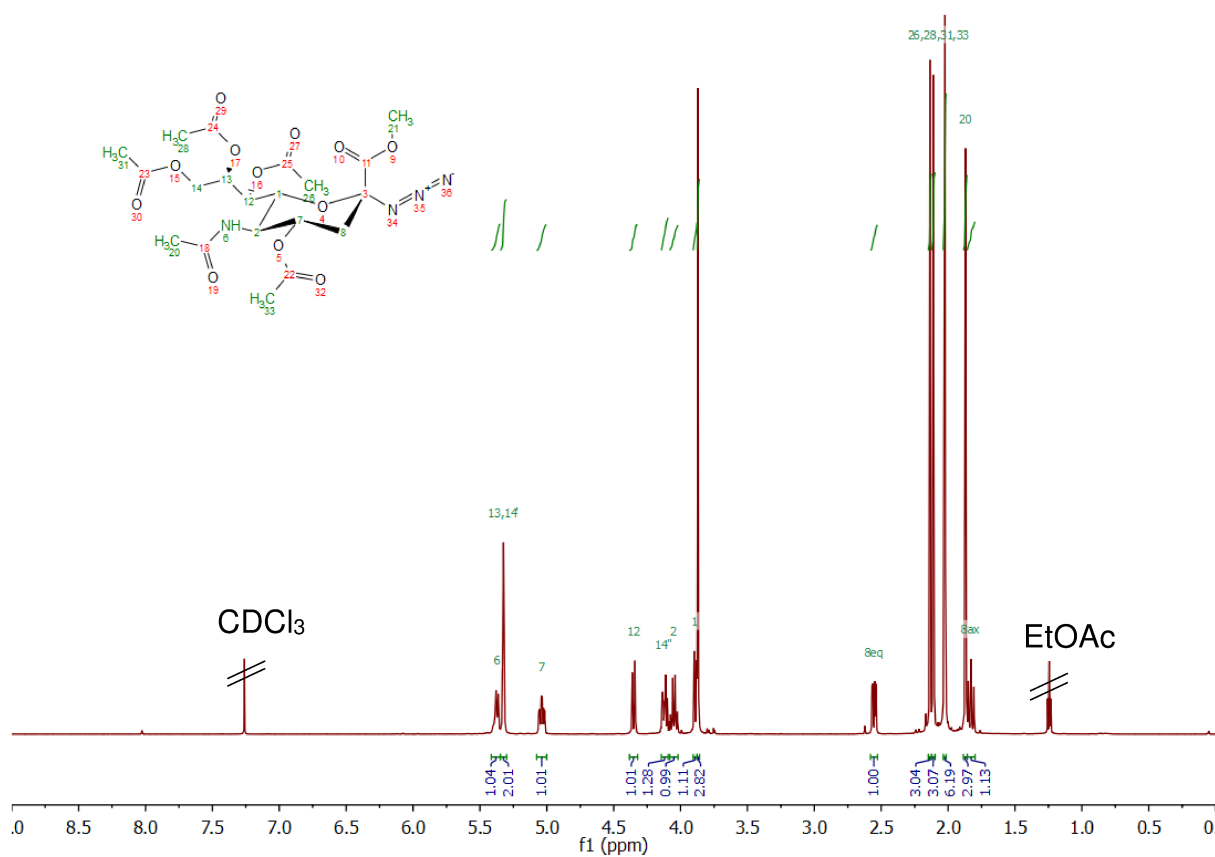
Figure S4: ^{1}H-NMR (600 MHz, CDCl$_3$) of compound **2.**
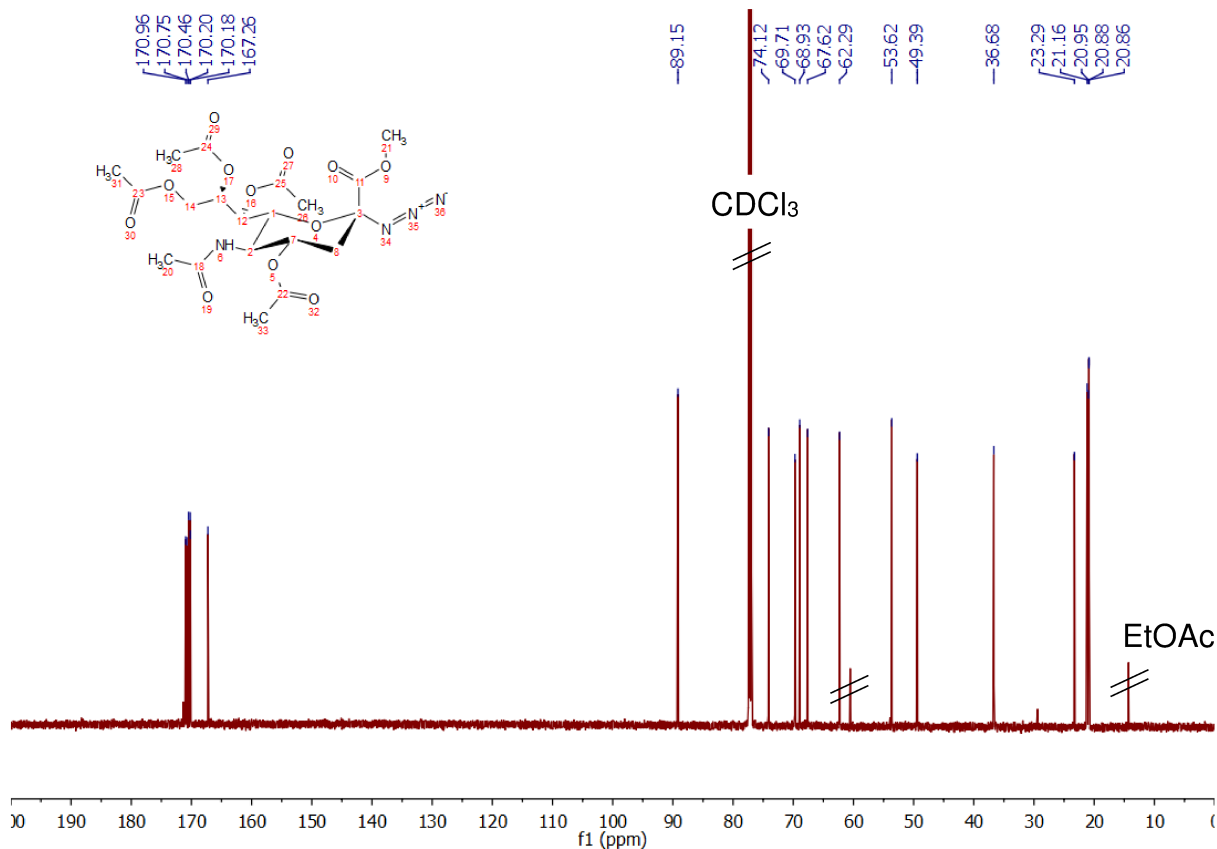
Figure S5: ^{13}C-NMR (151 MHz, CDCl$_3$) of compound **2.**
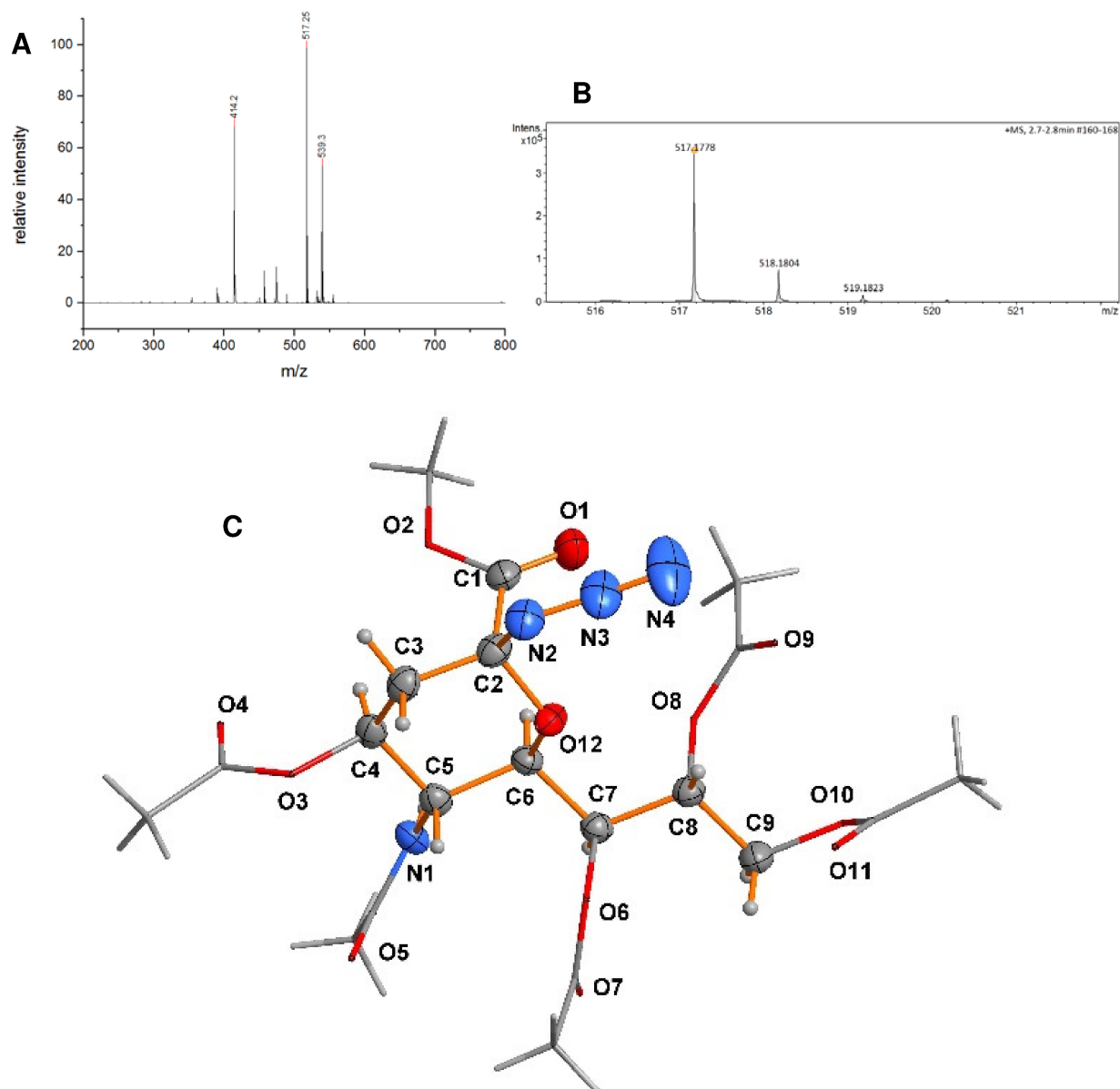
*Figure S6: **A**: ESI-MS (positive mode), **B**: HR-MS (ESI+ Q-TOF, positive mode) and DIAMOND [20] plot **C** of one of the two crystallographically independent molecules of **2** in the crystal structure.*

Crystal structure data for Neu5Ac-Prop and Neu5Ac-N₃

Table S1. Crystal structure data for Neu5Ac-Prop (1) and Neu5Ac-N₃ (2)

Compound	Neu5Ac-Prop (1)	Neu5Ac-N₃ (2)
Deposition number	**CCDC 1848409**	**CCDC 1848410**
Formula	$C_{23}H_{31}NO_{13}$	$2\,(C_{20}\,H_{28}\,N_4\,O_{12}) \bullet H_2O$
M_r	529.49	525.47
Cryst. size, mm^3	0.30 x 0.27 x 0.25	0.15 x 0.12 x 0.03
Crystal system	orthorhombic	orthorhombic
Space group	$P2_12_12_1$	$P2_12_12_1$
a, Å	8.4877(2)	11.8928(8)
b, Å	14.8501(3)	12.1066(8)
c, Å	21.0467(4)	37.186(3)
V, Å^3	2652.79(10)	5354.1(6)
Z	4	8[*]
D_{calcd}, g cm^{-3}	1.33	1.30
$\mu(CuK_a)$, mm^{-1}	0.94	0.94
$F(000)$, e	1120	2216
T, K	293	293
λ, Å	1.54178	1.54178
Θ_{max}, deg	69.0	67.5
Completeness, %	>98%	>99%
Measured / indep. refl.	46329 / 4953	62490 / 9547
Obeserved unique refl.	4943	9080
R_{int}	0.0265	0.0376
Ref. parameters / restraints	342 / 0	688 / 27
$R\,[F \geq 4\sigma(F)]$	0.0271	0.0498
$R\,(F$, all refl.)	0.0272	0.0514
$wR\,(F^2$, all refl.)	0.0565	0.1105
Flack-Parsons parameter	0.050(14) (2121 quotients)	0.05(8) (3697 quotients)
$S\,(GooF$, all refl.)	1.021	1.093
$\Delta\rho_{min\,/\,max}$, e Å^{-3}	-0.096 / 0.128	-0.15 / 0.77

[*] A Z of 8 instead of 4 was chosen for **2** to keep the basic formula of the basic carbohydrate comparable to **1**.

Improved synthesis conditions for TDS building block

Previously, TDS building block was synthesized coupling pentynoic acid via activation using PyBOP, HOBt and DIPEA to the key intermediate **a**.[6a] Here, an improved method using 4-pentynoic acid chloride **c** not requiring additional activation was used giving an overall higher yield of 86%.
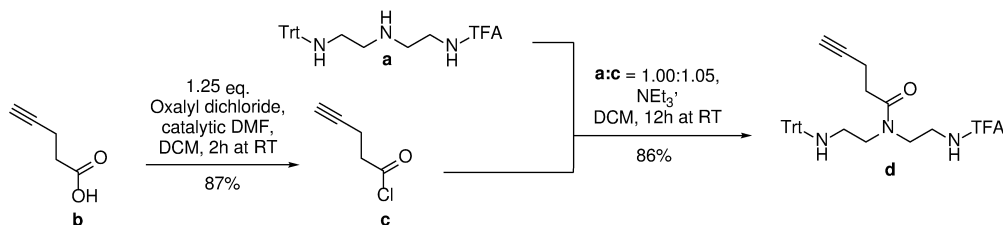
*Scheme S1: Synthesis of the TDS intermediate **d** using 4-pentynoic acid chloride **c** as intermediate resulting in an improved yield of 86%.*

4-Pentynoic acid chloride (c) was synthesized in a 40 mmol batch size according to the method described by Crossey *et al.*[13] After successful synthesis and distillation (45 °C, 30 mbar), pure **c** was obtained as transparent oil in a yield of 87%.

^{1}H-NMR (600 MHz, CDCl$_3$) δ 3.13 (t, ^3J = 7.1 Hz, 2H, CO-CH_2), 2.57 (td, ^3J = 7.1, ^4J = 2.7 Hz, 2H, CH_2), 2.04 (t, ^4J = 2.7 Hz, 1H, CH) ppm.

^{13}C-NMR (151 MHz, CDCl3) δ 172.31, 80.55, 70.43, 45.79, 14.86 ppm.

MS for C$_5$H$_5$ClO (ESI, pos.) m/z: [M + H$^+$]$^+$ calc.: 117.01; found 117.6.

TDS intermediate ***N*-(2-(2,2,2-trifluoroacetamido)ethyl)-*N'*-(2-(tritylamino)ethyl) pent-4-ynamide (c)** was synthesized in a 33 mmol scale using 1.00 equivalent of amine **a** (14.6 g, 33.0 mmol), and 1.05 equivalents of acid chloride **c** (4.06 g, 34.8 mmol). **a** and triethylamine (14 mL, 100 mmol) were dissolved in dichloromethane (150 mL) and cooled to 0 °C in an ice bath before **c**, dissolved in dichloromethane (50 mL) was added dropwise over a period of 30 min. After additional 12 h the mixture was washed with water (3x 30 mL) and sat. sodium bicarbonate solution (30 mL), dried over magnesium sulfate and concentrated under reduced pressure. Recrystallization from diethyl ether gave 15.8 g (30.3 mmol) of pure **d** (^{1}H-NMR and ^{13}C-NMR).

^{1}H-NMR (600 MHz, CDCl$_3$) δ 7.95 (s, 1H, *NH-TFA*), 7.44 – 7.41 (m, 6H, *aryl-H*), 7.32 – 7.27 (m, 6H, *aryl-H*), 7.23 – 7.19 (m, 3H, *aryl-H*), 3.56 – 3.52 (m, 2H, CH_2-NHTFA), 3.43 – 3.38 (m, 4H, CH_2-N-CH_2), 2.69 (t, ^3J = 7.3 Hz, 2H, CO-CH_2), 2.55 (td, ^3J = 7.3, ^4J = 2.7 Hz, 2H, CH_2-CCH), 2.36 (t, ^3J = 6.3 Hz, 2H, CH_2-NH-Trt), 1.94 (t, ^4J = 2.6 Hz, 1H, *alkyne-H*), 1.66 (s, 1H, *NH-Trt*).

^{13}C-NMR (151 MHz, CDCl$_3$) δ 174.21 (*CO*), 145.50 (3x *aryl-C*), 128.48 (6x *aryl-C*), 128.24 (6x *aryl-C*), 126.80 (3x *aryl-C*), 100.11 (*CF$_3$*), 82.96 (CH$_2$-*CC*-H), 71.22 (*C(Ph)$_3$*), 69.18 (CH$_2$-C*C*-H), 49.26, 44.96, 42.55, 40.47, 32.24, 14.84 (6C, 6x *CH$_2$*), -*CO*-CF$_3$ not visible.

*Figure S8: ¹H-NMR (600 MHz, CDCl₃) of compound **c**.*

*Figure S7: ¹³C-NMR (151 MHz, CDCl₃) of compound **c**.*
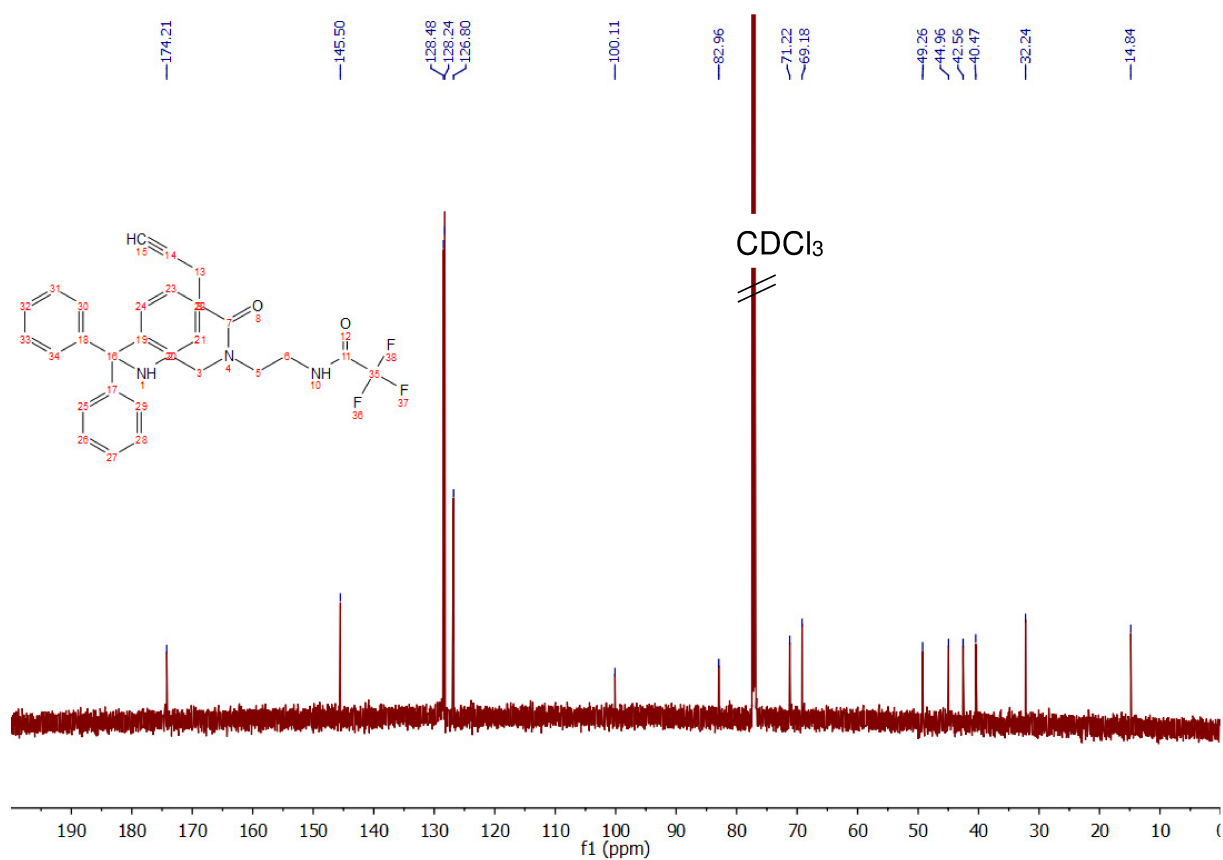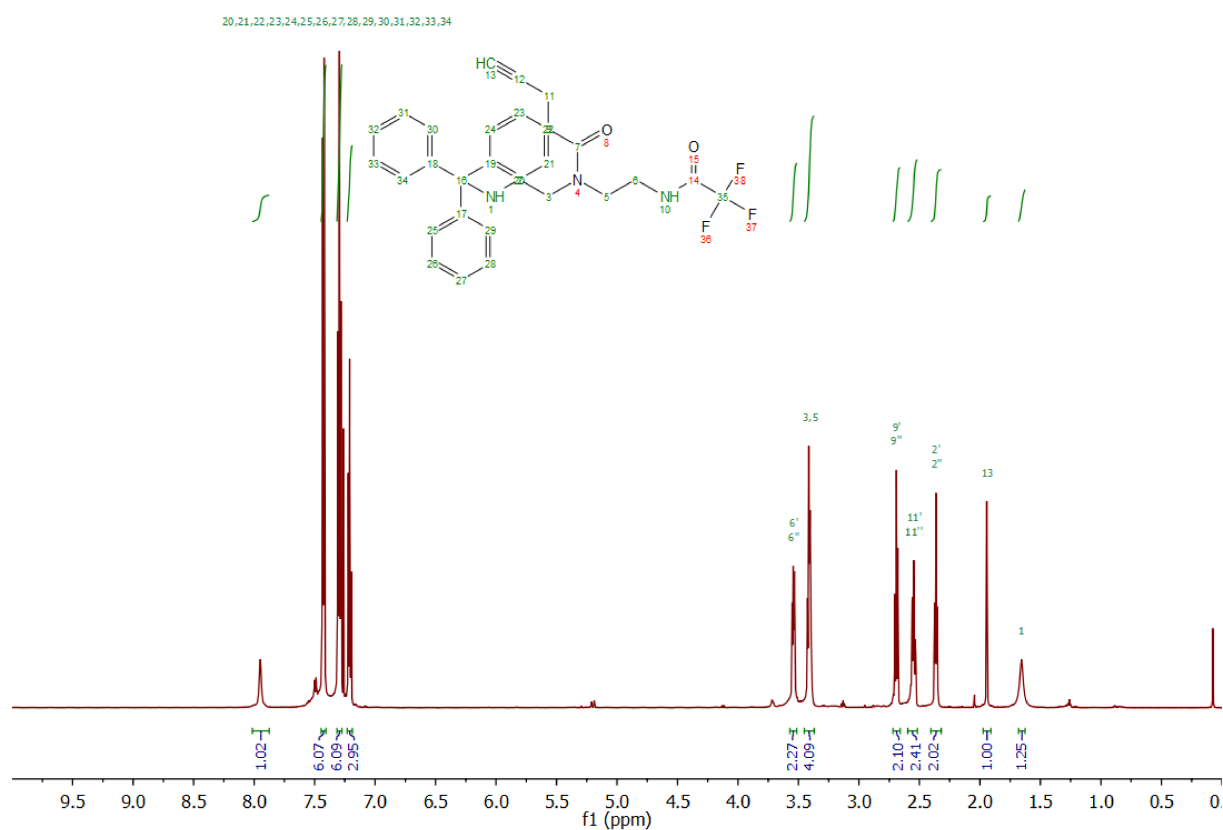
Solid phase synthesis based oligomers

Neu5Ac(1,5)-5-BADS (O1)
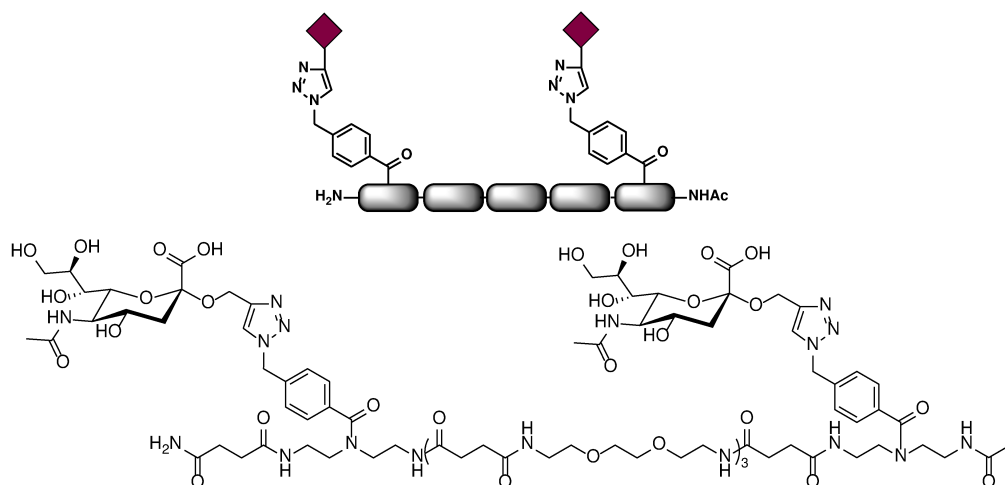
Neu5Ac(1,5)-5 was synthesized in a 50 µmol scale. 25.0 mg (11.7 µmol, 24%) of a white and foamy solid were obtained after purification with preparative HPLC, full deprotection and ion exchange. For solid phase synthesis and workup protocols see general methods.

^{1}H-NMR (600 MHz, D$_2$O) δ 8.10 (s, 2H, *triazole-H),* 7.42 – 7.39 (m, 8H, *aryl-H*), 5.69 (s, 4H, 2x *aryl-CH$_2$-aryl*), 4.93 (d, ^2J = 12.1 Hz, 2H, *propargyl-CH*), 4.69 (d, ^2J = 12.0 Hz, 2H, *propargyl-CH*), 3.90 – 3.80 (m, 8H, *2x (Neu5Ac-H5, 6, 8, 9')),* 3.75 (ddd, ^3J = 11.9, 9.7, 4.6 Hz, 2H, *2x Neu5Ac-H4*), 3.70 – 3.49 (m, 42H, *2x (Neu5Ac-H7, 9''), 12x O-CH$_2$ 7x N-CH$_2$)*, 3.39 – 3.31 (m, 10H, *5x N-CH$_2$*), 3.25 – 3.20 (m, 4H, *2x N-CH$_2$*), 2.73 (dd, ^2J = 12.5, ^3J = 4.6 Hz, 2H, *2x Neu5Ac-H3eq.*), 2.57 – 2.49 (m, 14H, *7x succinyl-CH$_2$*), 2.40 – 2.32 (m, 6H, *3x succinyl-CH$_2$*), 2.04 (s, 6H, *2x Neu5Ac-Ac*), 2.00 – 1.79 (m, 3H, *backbone-Ac*), 1.75 (dd, ^2J = 12.2, ^3J = 12.2 Hz, 2H, *Neu5Ac-H3ax.*) ppm.

RP-HPLC-MS (linear gradient from 0 – 50% eluent B in 30 min at 25° C): t_R = 17.64 min. Determined purity: 91% αα, 8% αβ, 1% ββ.

MS for C$_{92}$H$_{141}$N$_{21}$O$_{37}$ (ESI, pos.) *m/z*: [M + 2H$^+$]$^{2+}$ calc.: 1067.00; found: 1067.15, [M + 3H$^+$]$^{3+}$ calc.: 711.67; found: 711.90, [M + 4H$^+$]$^{4+}$ calc.: 534.00; found: 534.25.

MS for C$_{92}$H$_{141}$N$_{21}$O$_{37}$ (ESI, neg.) *m/z*: [M - 2H$^+$]$^{2-}$ calc.: 1064.98; found: 1065.30.

HRMS for C$_{92}$H$_{141}$N$_{21}$O$_{37}$ (ESI-TOF) *m/z*: [M + 3H$^+$]$^{3+}$ calc.: 711.6672; found: 711.6672.
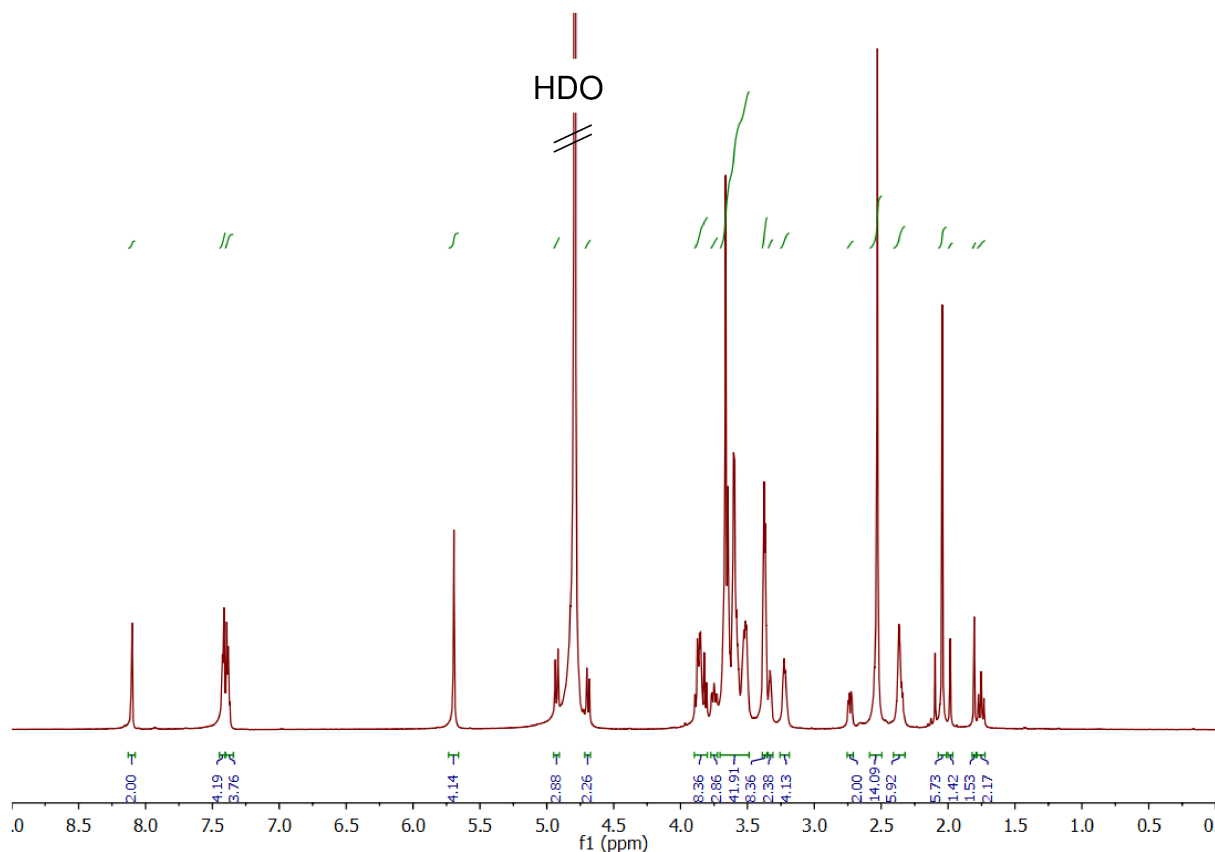
*Figure S9: ^{1}H-NMR (600 MHz, D_2O) of compound **O2**.*
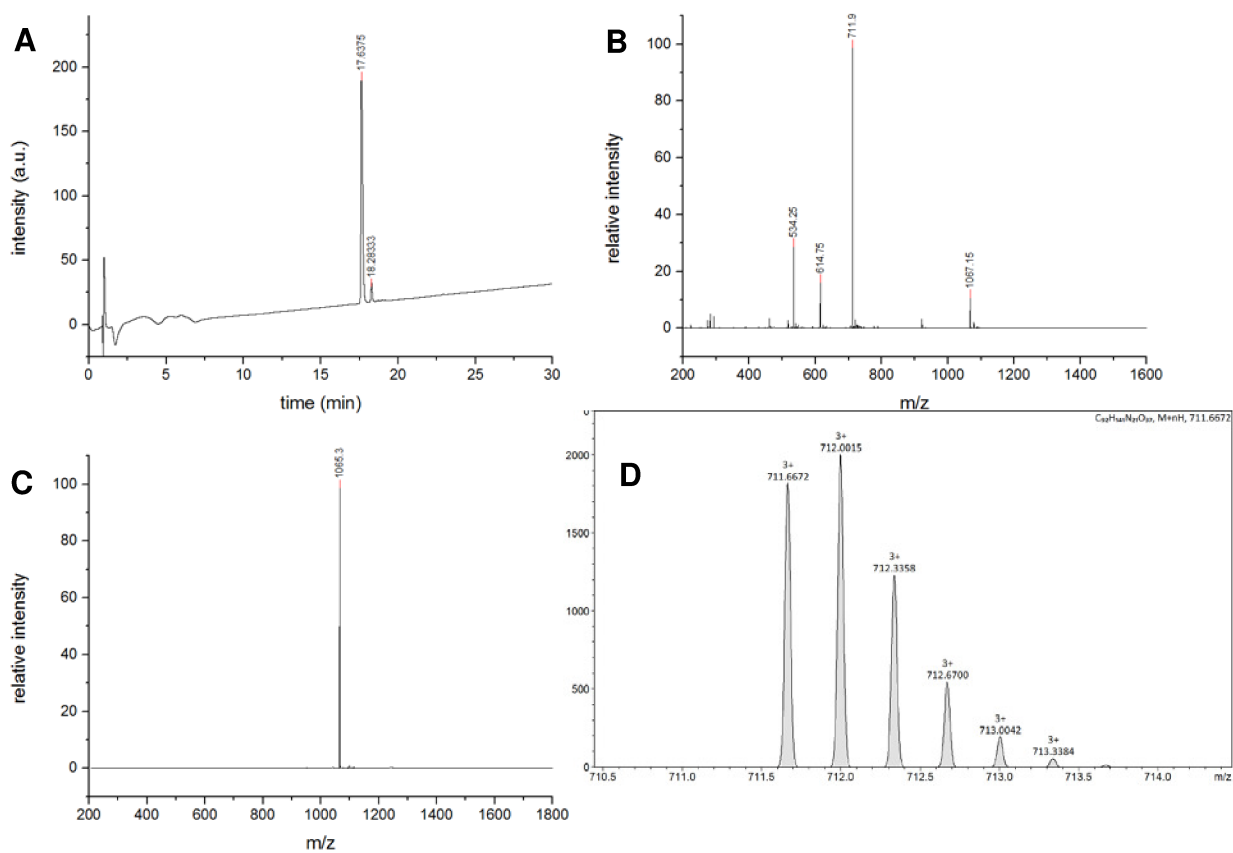
*Figure S10: **A**: RP-HPLC (linear gradient from 0 - 50% eluent B in 30 min at 25 °C), **B**: ESI-MS (positive mode), **C**: ESI-MS (negative mode), **D**: HR-MS (ESI+ Q-TOF, positive mode) of compound **O2**.*

Neu5Ac(1,5)-5-*Iso*BADS (O2)
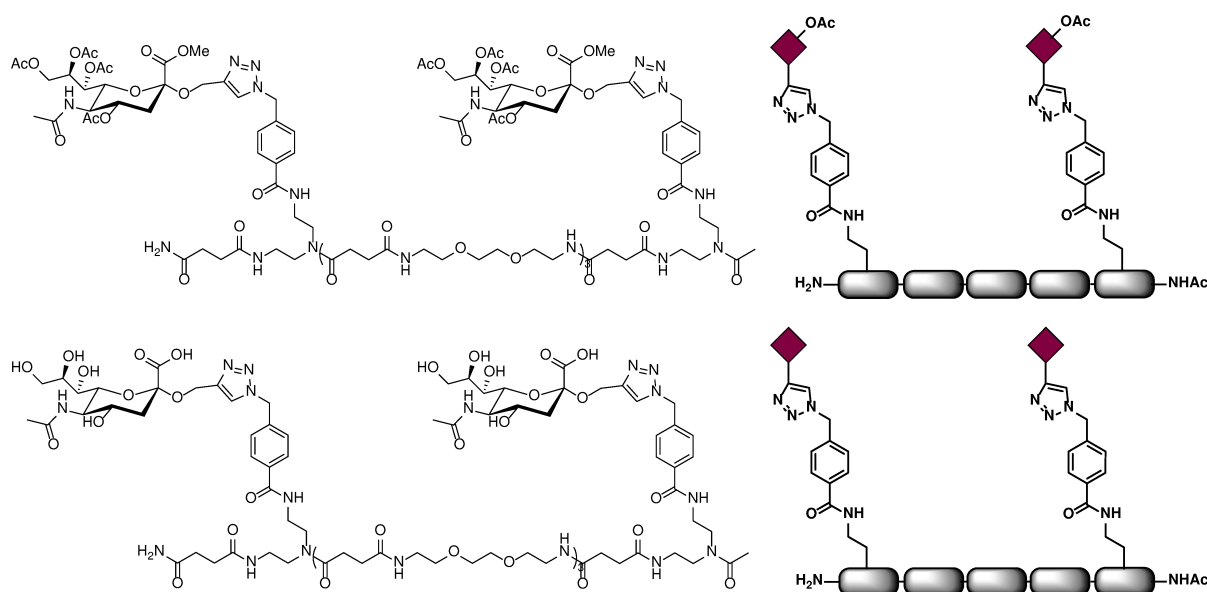
Neu5Ac(1,5)-5-*Iso*BADS was synthesized in a 100 µmol scale. 85.2 mg (34.1 µmol, 35%) of a white and foamy solid were obtained after purification with preparative HPLC. 48.5 mg (19.4 µmol) of the protected compound were deprotected applying the deprotection and ion exchange protocols. 37.8 mg (17.7 µmol, 92%) of the deprotected compound were finally isolated. For solid phase synthesis and work up protocols see general methods.

^{1}H-NMR (600 MHz, D$_2$O) δ 8.10 – 8.04 (m, 2H, *triazole-H*), 7.76 – 7.68 (m, 4H, *aryl-H*), 7.45 – 7.35 (m, 4H, *aryl-H*), 5.67 (m, 4H, *2x aryl-CH$_2$-aryl*), 4.90 (d, ^3J = 12.1 Hz, 2H, *propargyl-CH*), 4.66 (d, ^3J = 12.1 Hz, 2H, *propargyl-CH*), 3.89 – 3.78 (m, 8H, *2x (Neu5Ac-H5, 6, 8, 9')*), 3.74 (ddd, ^3J = 12.1, 6.2, 3.4 Hz, 2H, *2x Neu5Ac-H4*), 3.66 – 3.52 (m, 36H, *2x (Neu5Ac-H7, 9''), 12x O-CH$_2$, 4x N-CH$_2$*), 3.49 (m, 4H, *2x N-CH$_2$*), 3.41 (m, 2H, *N-CH$_2$*), 3.38 – 3.32 (m, 12H, *6x N-CH$_2$*), 3.28 (t, ^3J = 5.5 Hz, 1H, *N-CH*), 3.21 (t, ^3J = 5.4 Hz, 1H, *N-CH*), 2.72 (dd, ^2J = 12.6, ^3J = 3.9 Hz, 2H, *2x Neu5Ac-H3eq.*), 2.70 – 2.64 (m, 4H, *2x succinyl-CH$_2$*), 2.53 – 2.44 (m, 16H, *8x succinyl-CH$_2$*), 2.04 (s, 6H, *2x Neu5Ac-Ac*), 1.98 – 1.92 (m, 3H, *backbone-Ac*), 1.73 (dd, ^2J = 12.2, ^3J = 12.2 Hz, 2H, *2x Neu5Ac-H3ax.*) ppm.

(protected) RP-HPLC-MS (linear gradient from 0 – 75% eluent B in 30 min at 25° C): t$_R$ = 15.70 min. Determined purity: 96%.

(protected) MS for C$_{110}$H$_{161}$N$_{21}$O$_{45}$ (ESI, pos.) *m/z*: [M + 2H$^+$]$^{2+}$ calc.: 1249.56; found: 1249.35, [M + 3H$^+$]$^{3+}$ calc.: 833.37; found: 833.35, [M + 4H$^+$]$^{4+}$ calc.: 625.28; found: 625.20.

RP-HPLC-MS (linear gradient from 0 – 50% eluent B in 30 min at 25° C): t$_R$ = 12.26 min. Determined purity: 96%.

MS for C$_{92}$H$_{141}$N$_{21}$O$_{37}$ (ESI, pos.) *m/z*: [M + 2H$^+$]$^{2+}$ calc.: 1067.00; found: 1067.15, [M + 3H$^+$]$^{3+}$ calc.: 711.67; found: 711.95, [M + 4H$^+$]$^{4+}$ calc.: 534.00; found: 534.25.

MS for C$_{92}$H$_{141}$N$_{21}$O$_{37}$ (ESI, neg.) *m/z*: [M - 2H$^+$]$^{2-}$ calc.: 1064.98; found: 1065.15.

HRMS for C$_{92}$H$_{141}$N$_{21}$O$_{37}$ (ESI-TOF) *m/z*: [M + 3H$^+$]$^{3+}$ calc.: 711.6672; found: 711.6672.
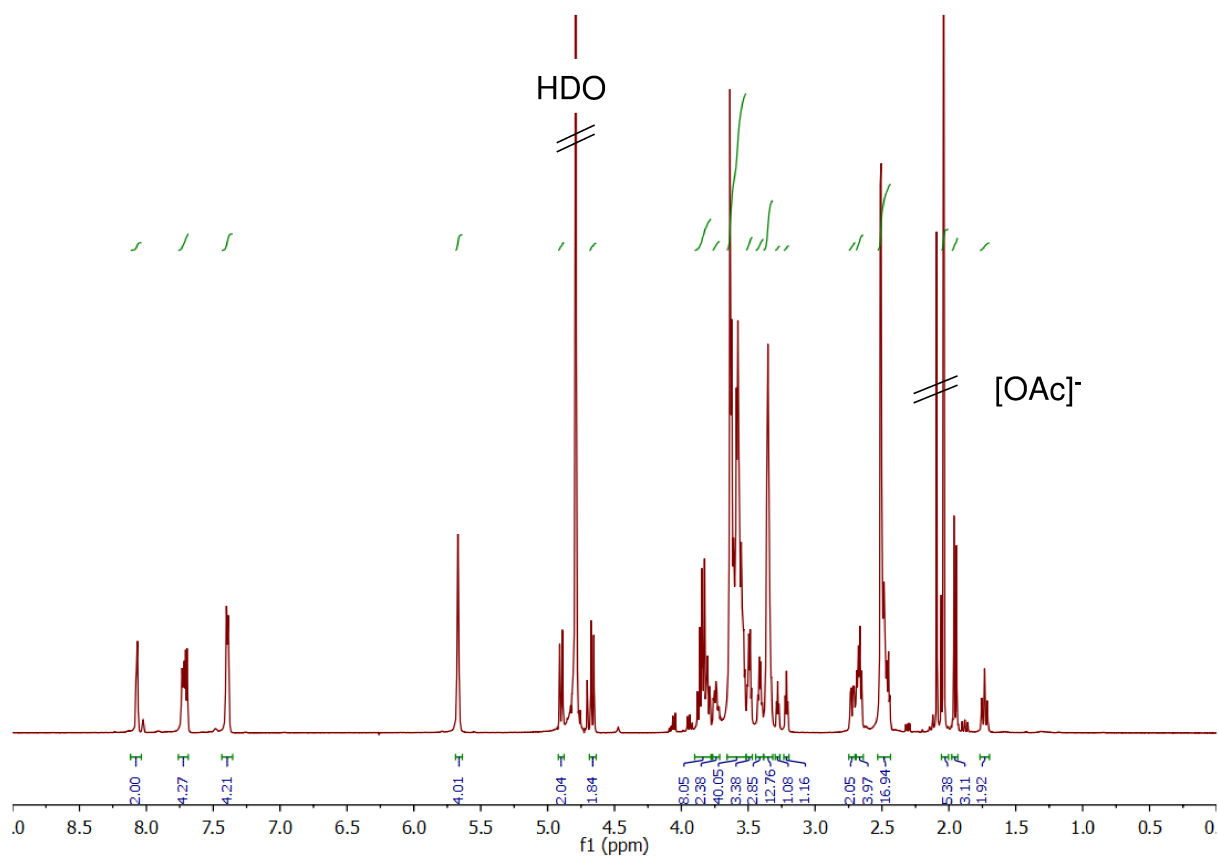
*Figure S11: ^{1}H-NMR (600 MHz, D_2O) of compound **O3**.*
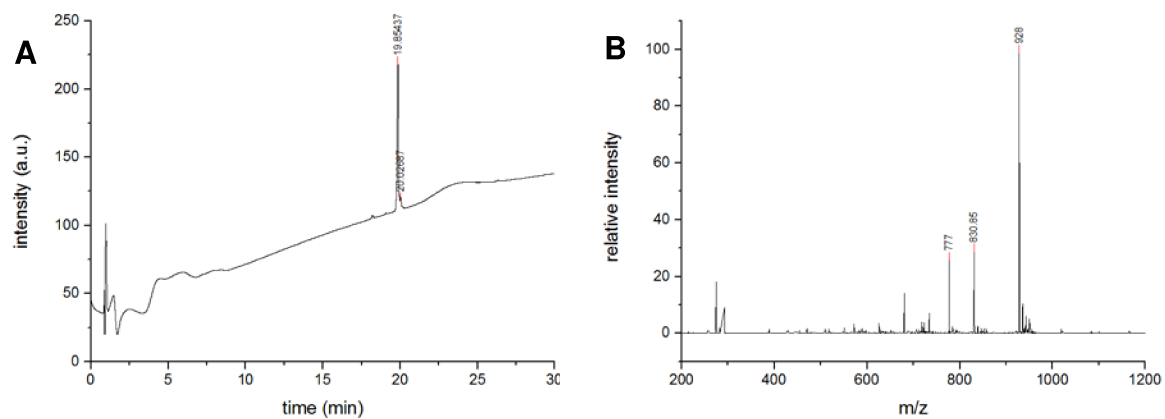
*Figure S12: **A**: RP-HPLC (linear gradient from 0 - 75% eluent B in 30 min at 25 °C), **B**: ESI-MS (positive mode) of compound **O3** in its protected form.*
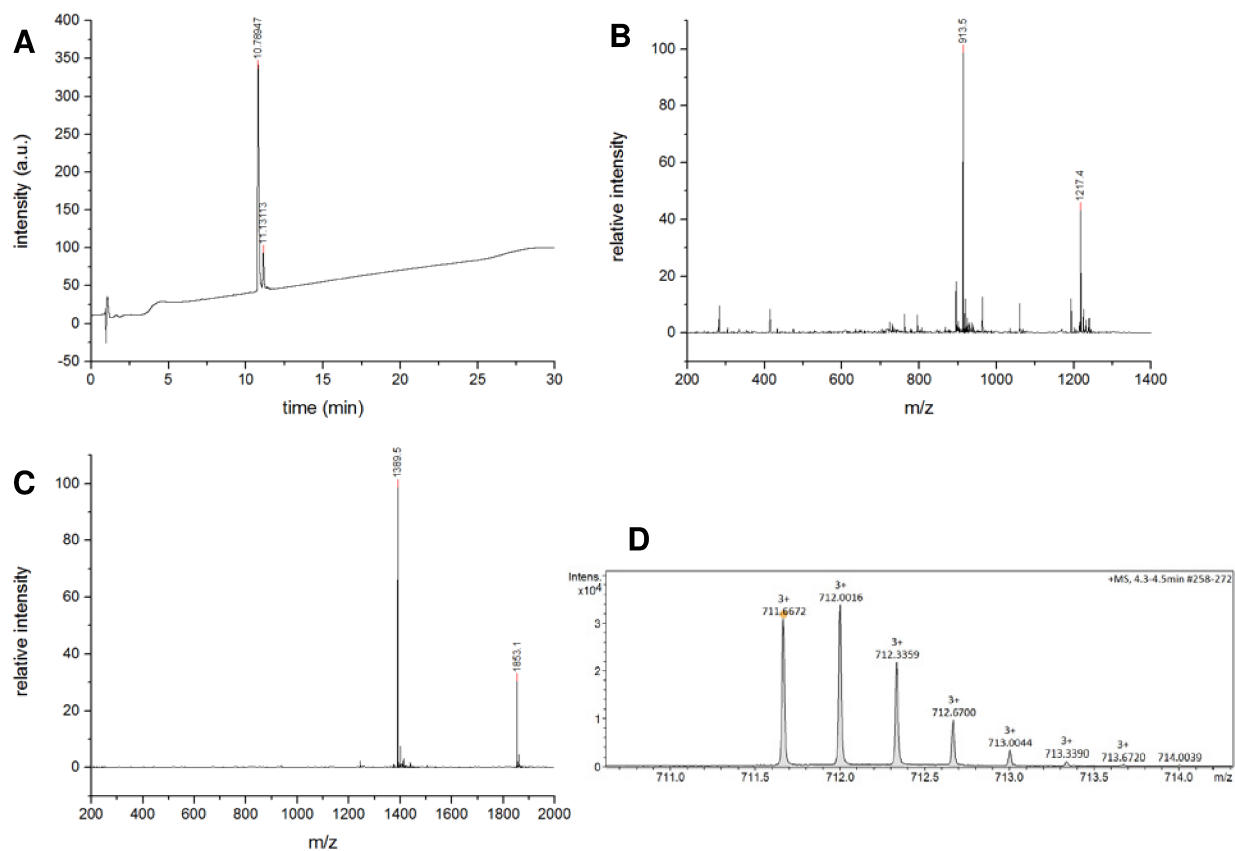
*Figure S13: **A**: RP-HPLC (linear gradient from 0 - 50% eluent B in 30 min at 25 °C), **B**: ESI-MS (positive mode), **C**: ESI-MS (negative mode), **D**: HR-MS (ESI+ Q-TOF, positive mode) of compound **O3**.*

Neu5Ac(1,5)-5-TDS (O3)
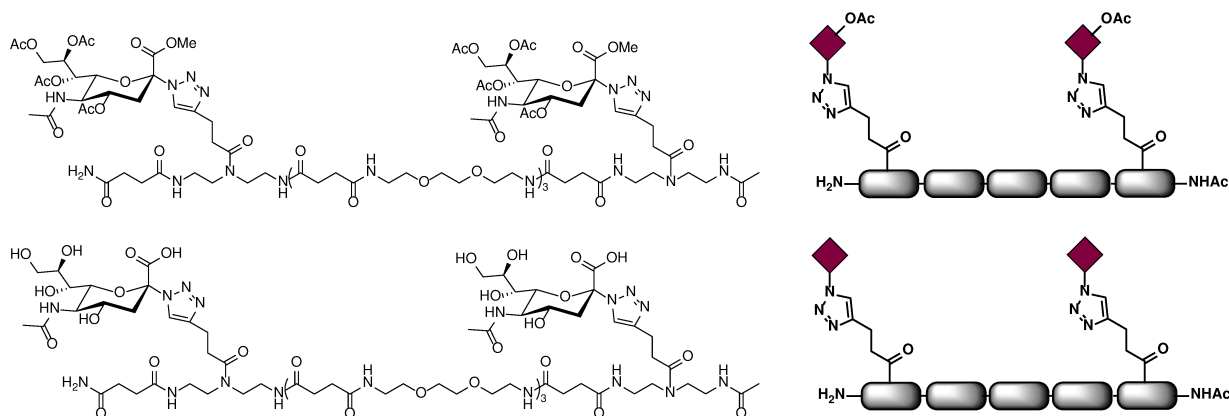
Neu5Ac(1,5)-5-TDS was synthesized in a 150 μmol scale. 101.3 mg (43.8 μmol, 30%) of a white and foamy solid were obtained after purification with preparative HPLC. 58.7 mg (25.4 μmol) of the protected compound were deprotected applying the deprotection and ion exchange protocols. 37.8 mg (22.3 μmol, 88%) of the deprotected compound were finally isolated. For solid phase synthesis and work up protocols see general methods.

^{1}H-NMR (600 MHz, D$_2$O) δ 8.01 – 7.98 (m, 2H, *triazole-H*), 4.02 – 3.84 (m, 10H, *2x (Neu5Ac-H4, 5, 6, 8, 9')*), 3.69 – 3.59 (m, 28H, *2x (Neu5Ac-H7, 9'')*, 12x *O-CH$_2$*), 3.48 – 3.42 (m, 8H, 4x *N-CH$_2$*), 3.41 – 3.29 (m, 20H, 10x *N-CH$_2$*), 3.26 (dd, ^2J = 12.5, ^3J = 4.3 Hz, 2H, *2x Neu5Ac-H3eq.*), 3.02 (t, ^3J = 7.2 Hz, 4H, *2x linker-CH$_2$*), 2.82 – 2.75 (m, 4H, *2x linker-CH$_2$*), 2.57 – 2.44 (m, 20H, 10x *succinyl-CH$_2$*), 2.23 (dd, ^3J = 11.7, 11.7 Hz, 2H, *2x Neu5Ac-H3ax.*), 2.06 (s, 6H, *2x Neu5Ac-Ac*), 1.95 – 1.89 (m, 3H, *backbone-Ac*) ppm.

(protected) RP-HPLC-MS (linear gradient from 0 – 75% eluent B in 30 min at 25° C): t$_R$ = 14.12 min. Determined purity: 94%, due to deacetylation (6%).

(protected) MS for C$_{98}$H$_{153}$N$_{21}$O$_{43}$ (ESI, pos.) *m/z*: [M + 2H$^+$]$^{2+}$ calc.: 1157.53; found: 1157.30, [M + 3H$^+$]$^{3+}$ calc.: 772.02; found: 771.90.

RP-HPLC-MS (linear gradient from 0 – 50 % eluent B in 30 min at 25° C): t$_R$ = 10.03 min. Determined purity: 90% αα, 8% unknown.

MS for C$_{80}$H$_{133}$N$_{21}$O$_{35}$ (ESI, pos.) *m/z*: [M + 2H$^+$]$^{2+}$ calc.: 974.97; found: 975.50, [M + 2H$^+$ - C$_{11}$H$_{17}$NO$_8$ (Neu5Ac)]$^{2+}$ calc.: 829.42; found: 829.50, [M + 2H$^+$ - 2(C$_{11}$H$_{17}$NO$_8$) (2Neu5Ac)]$^{2+}$ calc.: 683.88; found: 683.90, [M + 3H$^+$]$^{3+}$ calc.: 650.32; found: 650.50, [M + 3H$^+$ - C$_{11}$H$_{17}$NO$_8$ (Neu5Ac)]$^{3+}$ calc.: 553.28; found: 553.45, [M + 3H$^+$ - 2(C$_{11}$H$_{17}$NO$_8$) (2Neu5Ac)]$^{3+}$ calc.: 456.25; found: 456.40.

MS for C$_{80}$H$_{133}$N$_{21}$O$_{35}$ (ESI, neg.) *m/z*: [M - H$^+$]$^-$ calc.: 1946.92; found: 1946.70, [M - 2H$^+$]$^{2-}$ calc.: 972.96; found: 973.10.

HRMS for C$_{80}$H$_{133}$N$_{21}$O$_{35}$ (ESI-TOF) *m/z*: [M + 3H$^+$]$^{3+}$ calc.: 650.3164; found: 650.3173.
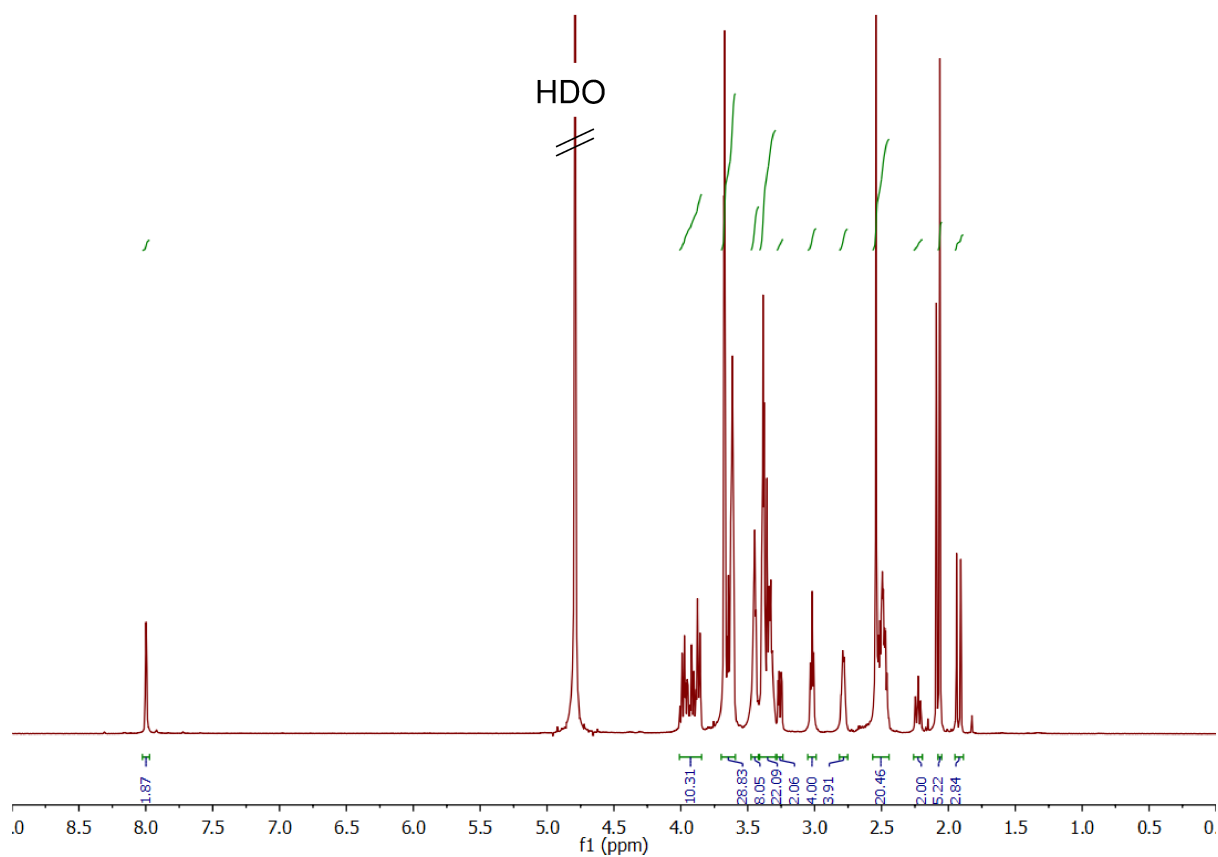
*Figure S14: ^{1}H-NMR (600 MHz, D$_2$O) of compound **O4**.*
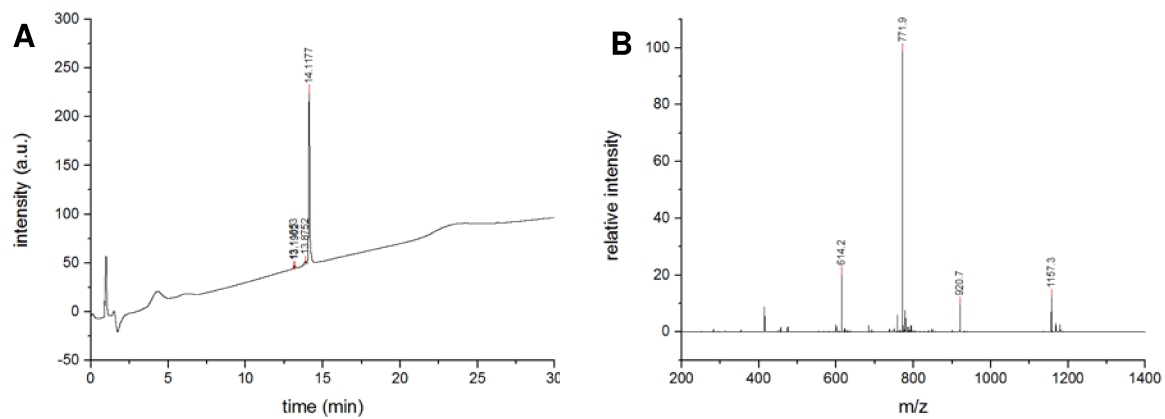
*Figure S15: **A**: RP-HPLC (linear gradient from 0 - 75% eluent B in 30 min at 25 °C), **B**: ESI-MS (positive mode) of compound **O4** in its protected form.*
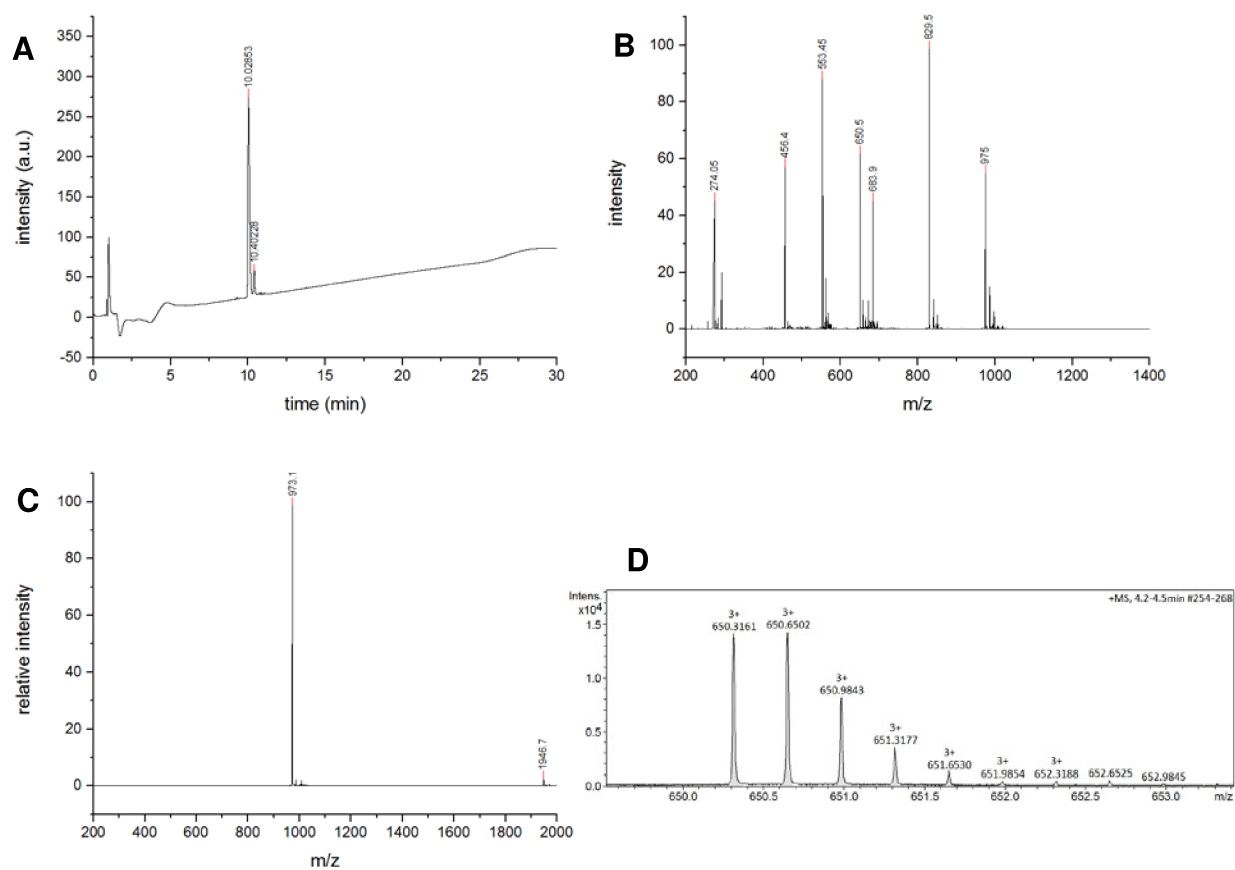
Figure S16: **A**: *RP-HPLC (linear gradient from 0 - 50% eluent B in 30 min at 25 °C),* **B**: *ESI-MS (positive mode),* **C**: *ESI-MS (negative mode),* **D**: *HR-MS (ESI+ Q-TOF, positive mode) of compound* **O4**.

3'Sialyllactose(1,5)-5-BADS (O4)
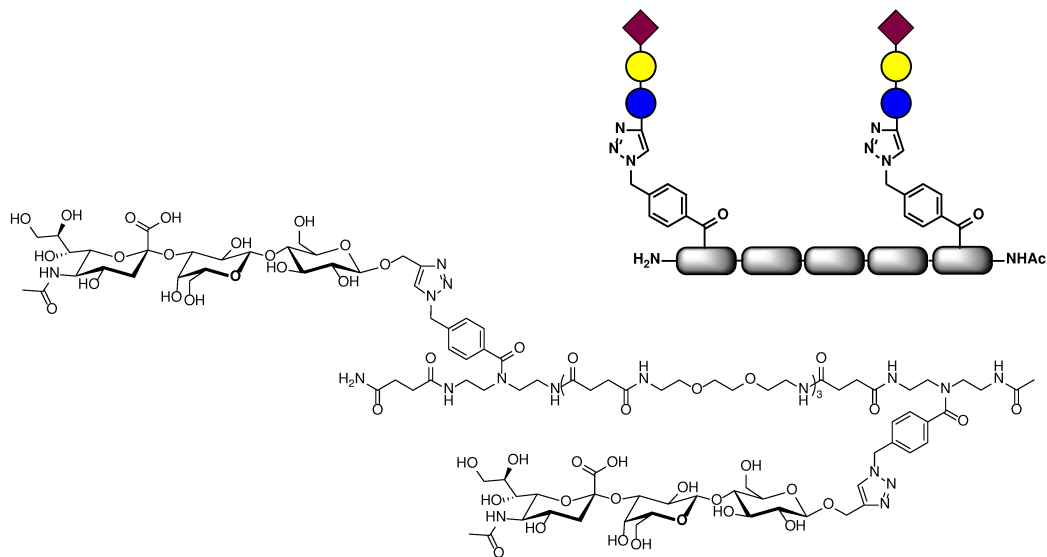
3'Sialyllactose(1,5)-5-BADS was synthesized in a 15 µmol scale. 16.1 mg (5.79 µmol, 39%) of a white and foamy solid were obtained after purification with preparative HPLC, full deprotection and ion exchange. For solid phase synthesis and workup protocols see general methods.

^{1}H-NMR (600 MHz, D$_2$O) δ 8.17 – 8.12 (m, 2H, *triazole-H*), 7.46 – 7.35 (m, 8H, *aryl-H*), 5.70 (s, 4H, 2x *aryl-CH$_2$-aryl*), 5.03 – 4.97 (m, 2H, *propargyl-CH*), 4.89 (d, ^3J = 12.6 Hz, 2H, *propargyl-CH*), 4.58 (d, ^3J = 7.9 Hz, 2H, 2x *Glc-H1*), 4.53 (d, ^3J = 7.9 Hz, 2H, 2x *Gal-H1*), 4.13 (dd, ^3J = 9.8, 3.2 Hz, 2H, 2x *Neu5Ac-H9'*), 3.99 – 3.79 (m, 16H, 2x *(3'-SL-8xH)*), 3.78 – 3.48 (m, 54H, 2x *(3'-SL-10xH)*, 12x *O-CH$_2$*, 5x *N-CH$_2$*), 3.42 – 3.30 (m, 14H, 7x *N-CH$_2$*), 3.22 (m, 4H, 2x *N-CH$_2$*), 2.76 (dd, ^2J = 12.5, ^3J = 4.6 Hz, 2H, 2x *Neu5Ac-H3eq.*), 2.53 (m, 14H, 7x *succinyl-CH$_2$*), 2.39 – 2.33 (m, 6H, 3x *succinyl-CH$_2$*), 2.04 (s, 6H, *2x Neu5Ac-Ac*), 1.99 (s, 1H, *backbone-Ac(1H)*), 1.85 – 1.80 (m, 4H, 2x *Neu5Ac-H3ax., backbone-Ac(2H)*) ppm.

(protected) RP-HPLC-MS (linear gradient from 0 – 75% eluent B in 30 min at 25° C): t$_R$ = 19.58 min. Determined purity: 86% due to deacetylation (9%).

(protected) MS for C$_{158}$H$_{225}$N$_{21}$O$_{77}$ (ESI, pos.) *m/z*: [M + 3H$^+$]$^{3+}$ calc.: 1217.49; found: 1217.40, [M + 4H$^+$]$^{4+}$ calc.: 913.37; found: 913.50.

RP-HPLC-MS (linear gradient from 0 – 50% eluent B in 30 min at 25° C): t$_R$ = 10.79 min. Determined purity: 87% ββ, 12% αβ.

MS for C$_{116}$H$_{181}$N$_{21}$O$_{57}$ (ESI, pos.) *m/z*: [M + 3H$^+$]$^{3+}$ calc.: 928.07; found: 928.00, [M + 3H$^+$ - C$_{11}$H$_{18}$NO$_8$ (Neu5Ac)]$^{3+}$ calc.: 831.04; found: 830.85, [M + 3H$^+$ - C$_{17}$H$_{27}$NO$_{13}$ (Neu5AcGal)]$^{3+}$ calc.: 777.02; found: 777.00.

MS for C$_{116}$H$_{181}$N$_{21}$O$_{57}$ (ESI, neg.) *m/z*: [2M - 3H$^+$]$^{3-}$ calc.: 1853.12; found: 1853.10, [M - 2H$^+$]$^{2-}$ calc.: 1389.59; found: 1389.50.

HRMS for C$_{116}$H$_{181}$N$_{21}$O$_{57}$ (ESI-TOF) *m/z*: [M + 3H$^+$]$^{3+}$ calc.: 928.0721; found: 928.0710.
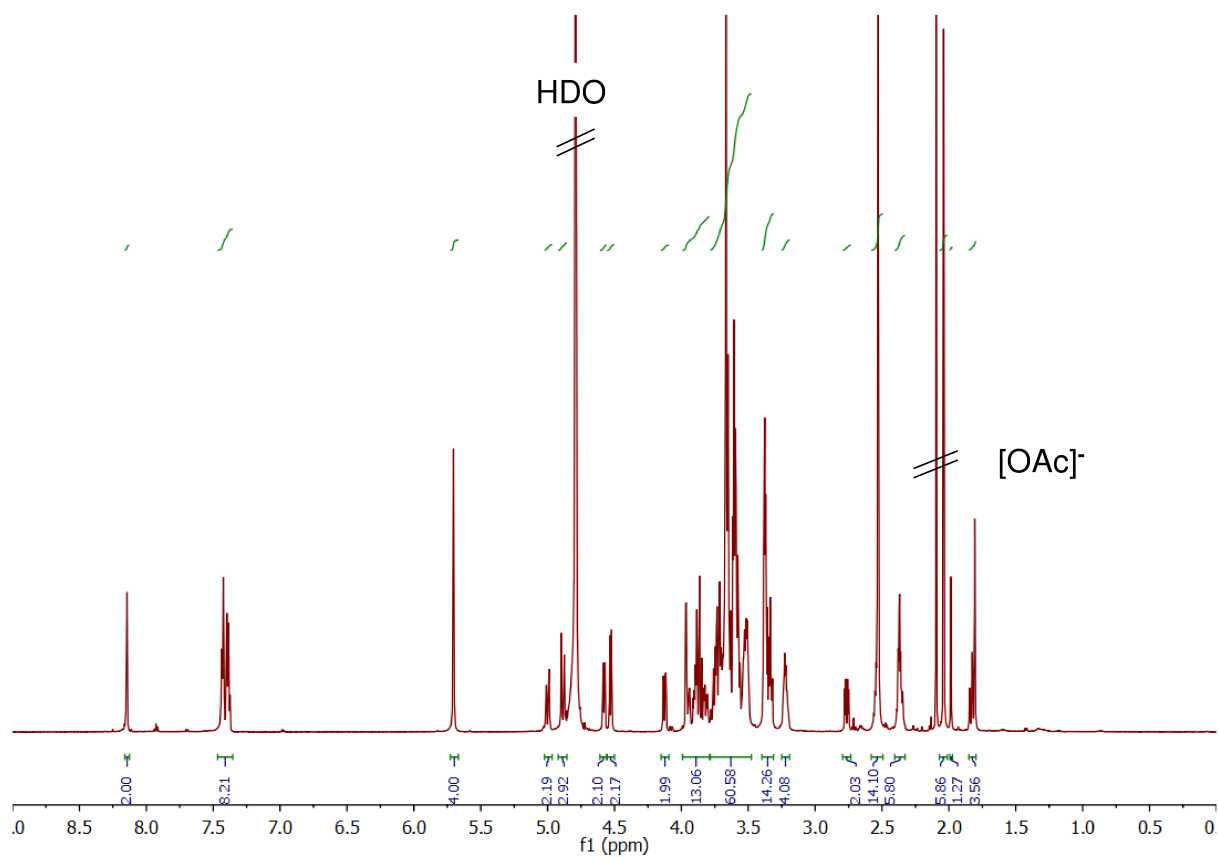
*Figure S17: ^{1}H-NMR (600 MHz, D$_2$O) of compound **O6**.*
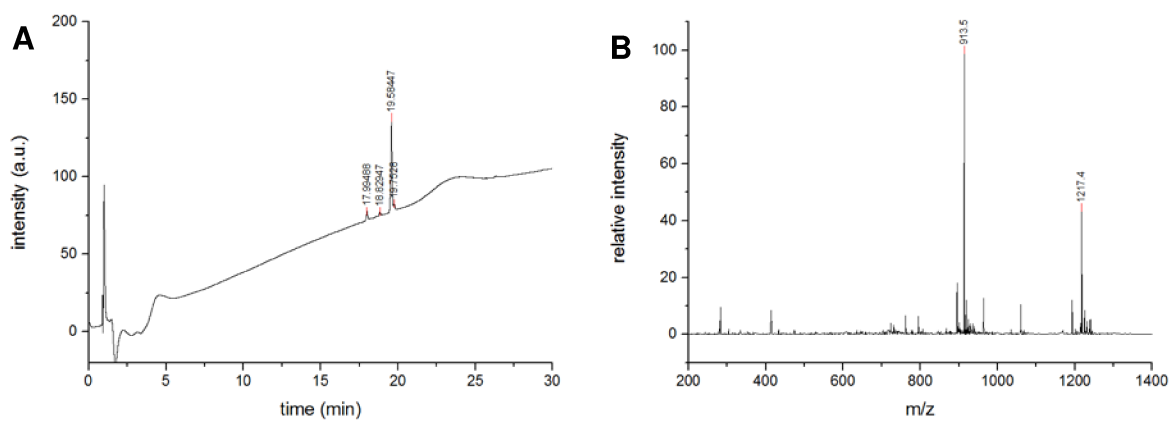
*Figure S18: **A**: RP-HPLC (linear gradient from 0 - 75% eluent B in 30 min at 25 °C), **B**: ESI-MS (positive mode) of compound **O3** in its protected form.*
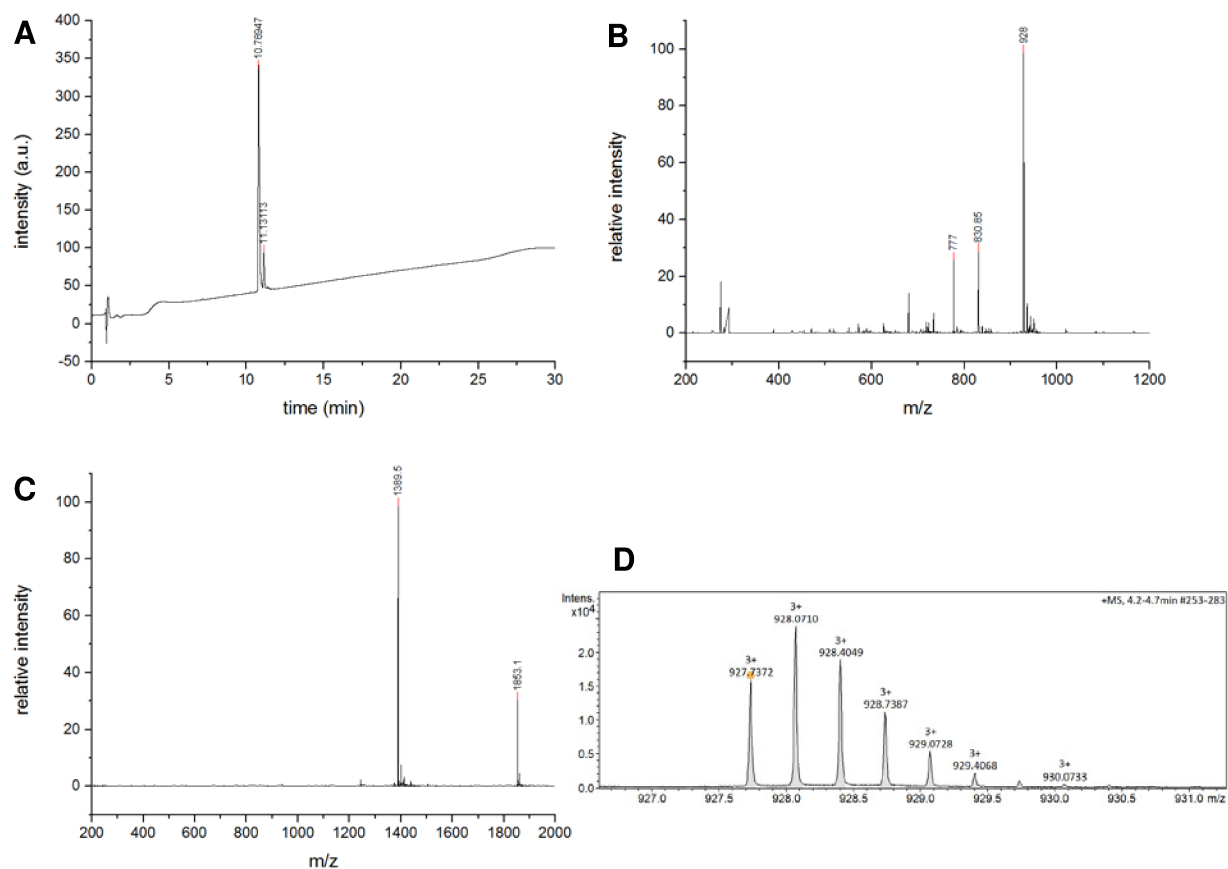
*Figure S19: **A**: RP-HPLC (linear gradient from 0 - 50% eluent B in 30 min at 25 °C), **B**: ESI-MS (positive mode), **C**: ESI-MS (negative mode), **D**: HR-MS (ESI+ Q-TOF, positive mode) of compound **O6**.*

Molecular Dynamic Simulations of Glycooligomers

Molecular Dynamics simulations were performed at a constant temperature of 310 °K and constant pressure of 1 bar using gromacs 4.5.5.[21] Each molecule was simulated for 500 ns after a 20 ns equilibration run. Electrostatics were calculated using the particle mesh Ewald method,[22] water molecules were kept rigid with SETTLE.[23] Interaction parameters for the building blocks of the oligomers were obtained from the amber SB99 force field [24] for the backbone and the general amber force field [25] for the 1,2,3-triazole linker and partial charges were derived using the R.E.D. tools scripts.[26] Structure optimization for the charge derivation was performed with Gaussian at the HF/6-31G* level of theory. The final set of charges for each molecular fragment was obtained from an ensemble average of 50 structures generated from 20 ns MD trajectories. The carbohydrate ligands were modelled using the GLYCAM6$_{OSMO,14}$ force field,[27] and the system was solvated with TIP5P water molecules [28] to avoid excessive interactions between the ligands. In figure 20 the distances of the terminal Neu5Ac and Glc (first and last sugars of the 3'-SL-motif) moieties are displayed.
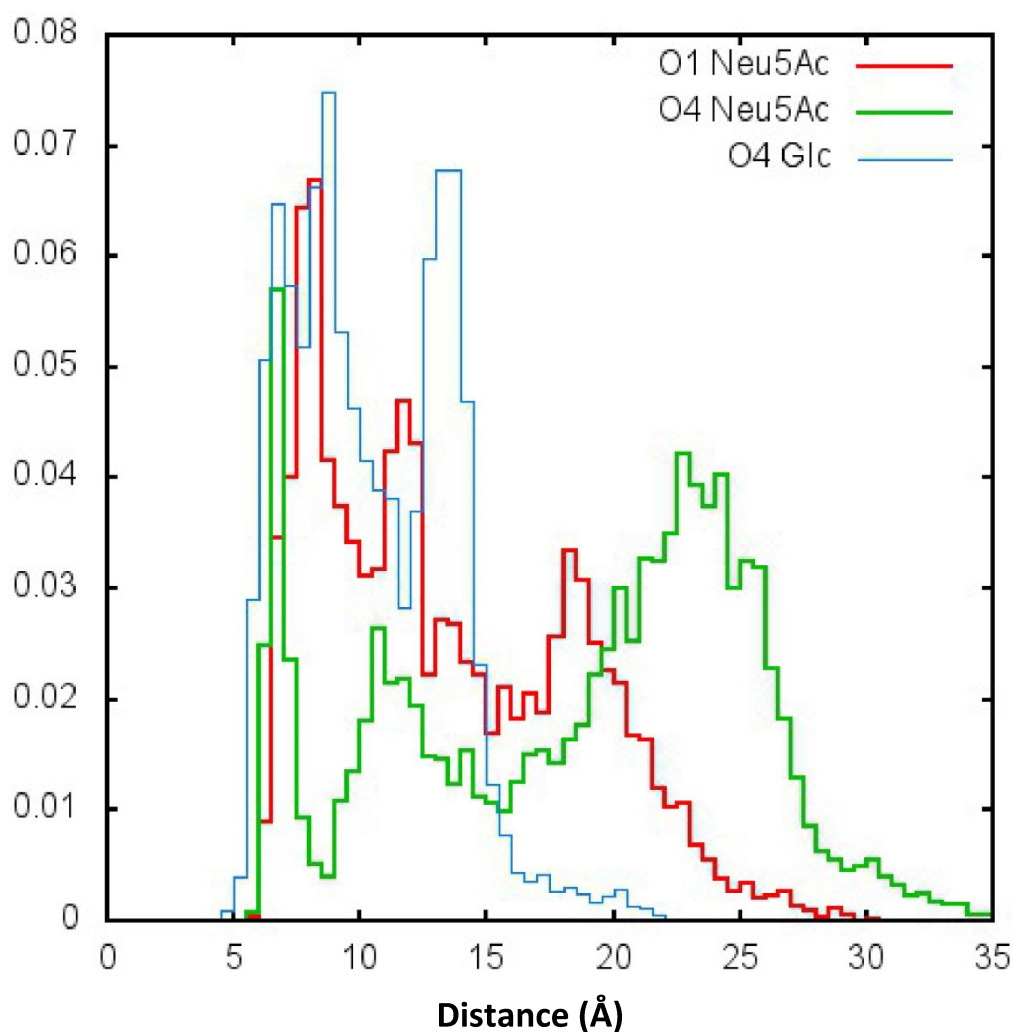
*Figure S20: Glycooligomersimulations: Distribution of distances between terminal Neu5Ac and Glc (first sugar of the 3'-Sl-motif) moieties. **O1** (red), **O4** (green), **O4-Glc** (blue).*

Dynamic Light Scattering experiments of Glycooligomers
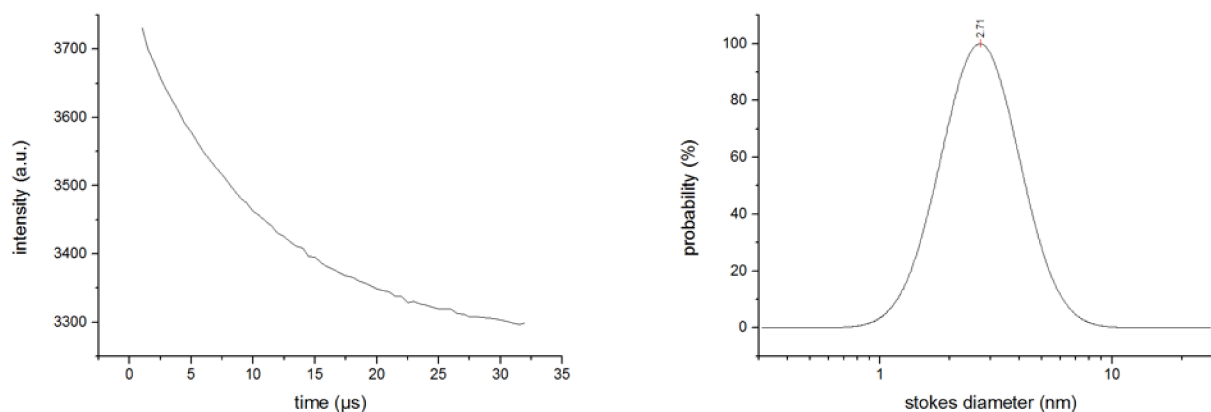
*Figure S21: Exemplary autocorrelation and size distribution of compound **O2**.*

Coefficient values ± one standard deviation for compound O2

y0   = 0.0019363 ± 0.00416

A   = 100 ± 0.0101

x0   = 2.7004 ± 0.000115

width   = 0.54296 ± 6.83e-005
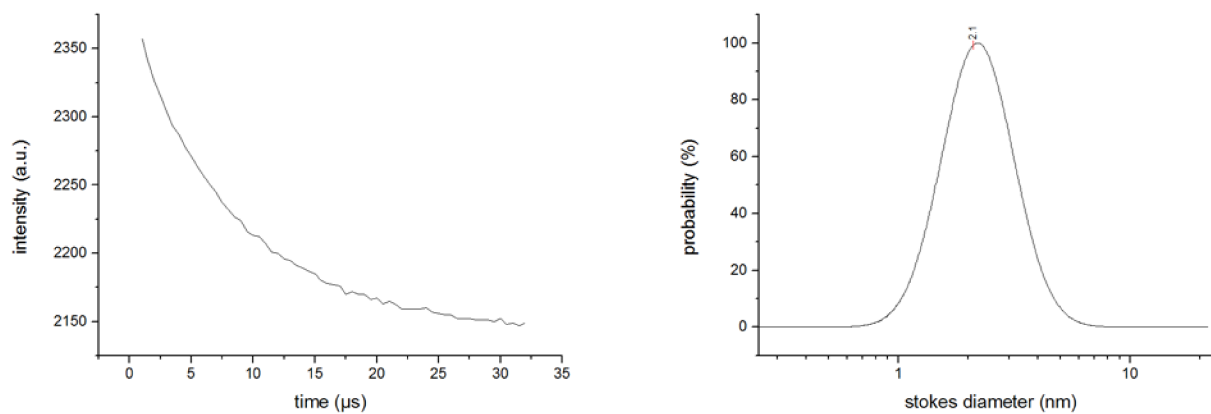
*Figure S22: Exemplary autocorrelation and size distribution of compound **O3**.*

Coefficient values ± one standard deviation for compound O3

y0   = 0.00022304 ± 0.00487

A   = 100 ± 0.0126

x0   = 2.197 ± 0.000109

width   = 0.50055 ± 7.8e-005

Glycooligomers – TSPyV VP1 complexes

TSPyV VP1 crystallization was performed as previously described.[14c] For **O1**, VP1 crystals were derivatized by soaking in crystallization solution supplemented with 5 mM of the compound for two hours. For **O4**, crystals were co-crystallized in the same condition but in the presence of the compound (5 mM) for five days. For **O3** both aforementioned approaches were tested from 3 to 5 mM compound concentration. For cryoprotection of the crystals, the respective solutions were supplemented with 25 % glycerol. After flash freezing in liquid nitrogen, diffraction experiments were conducted at cryogenic temperatures at the X06DA and X06SA beamlines at the Swiss Light Source (PSI, Villigen).

Data processing was carried out using XDS.[29] Molecular replacement was performed in Phaser (ccp4)[30] using a single unliganded TSPyV VP1 pentamer as search model (PDB ID 4U5Z). Structure refinement and modelling was carried out by alternating rounds of Refmac5 (ccp4)[31] and Coot.[32] Ligand models and restraints for **O1** were prepared in Coot and eLBOW (Phenix).[33] For **O4** no additional restraints were necessary.
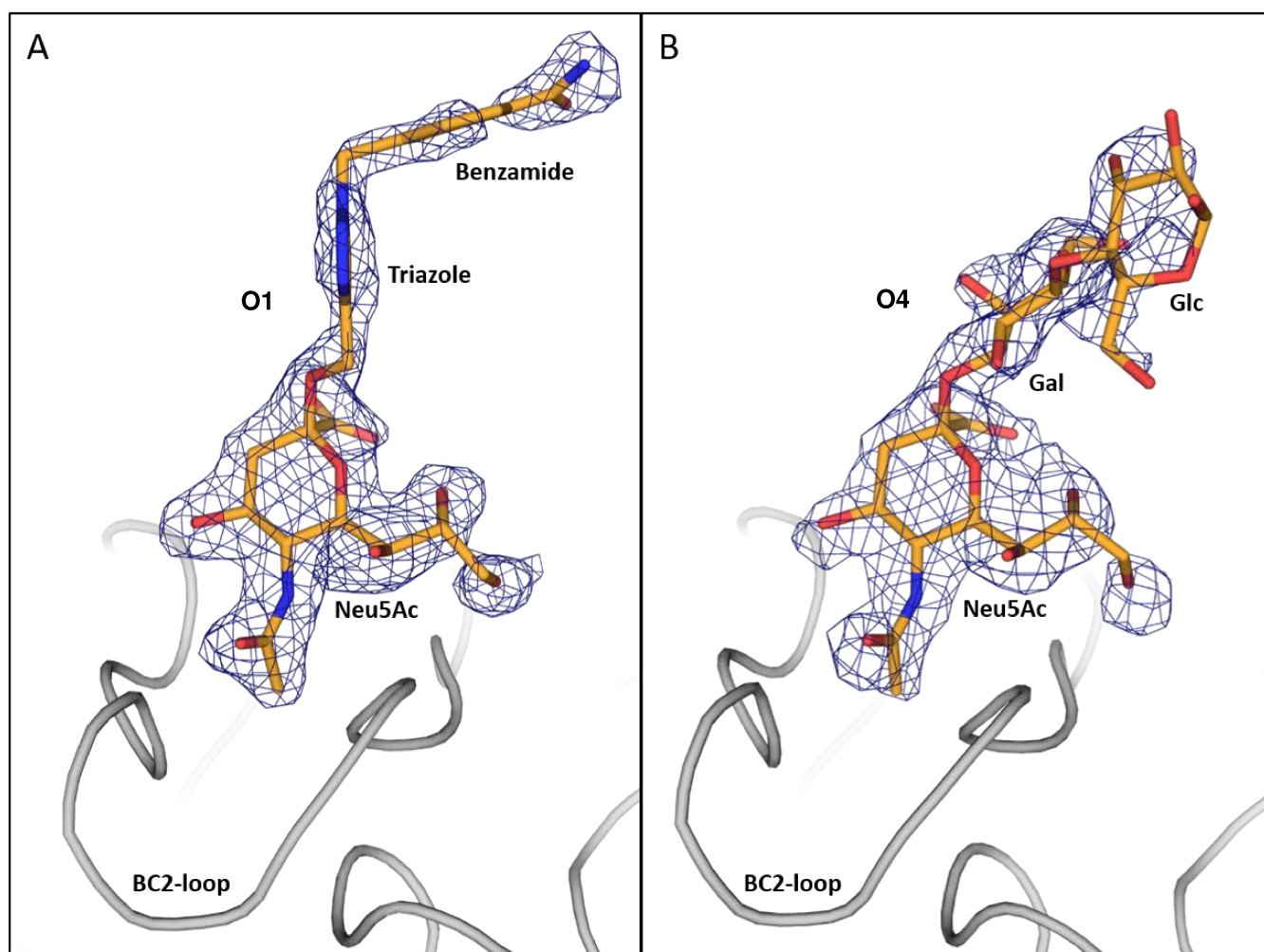
*Figure S23: Structures of the glycooligomer – TSPyV VP1 complexes after simulated annealing omit refinement for **O1** (A) and **O4** (B). The resulting electron density difference maps are shown as a blue mesh at a contouring level of 2.5 σ and with a radius of 2 Å around the glycooligomer models. VP1 is shown in cartoon representation (grey), the ligands are depicted as sticks with coloring according to the atom type, with carbons in orange, nitrogens in blue and oxygens in red.*

Table S2. Crystallographic data procession and refinement statistics for the major capsid protein VP1 of Trichodysplasia spinulosa-associated Polyomavirus (TSPyV) in complex with glycooligomers.

	TSPyV VP1 + O1 (1)	TSPyV VP1 + O4 (2)
PDB code	**6HKV**	**6HKU**
Data collection		
Space group	$P2_12_12_1$	$P2_12_12_1$
Unit cell		
a, b, c (Å)	138.40, 145.70, 149.46	139.06, 145.93, 150.16
Resolution (Å)	47.95 – 1.82 (1.93 – 1.82)	48.98 - 2.00 (2.12 - 2.00)
Unique reflections	269'084 (42'823)	205'830 (32'533)
Total reflections	2'411'269 (392'328)	2'156'049 (348'721)
Rmeas (%)	10.1 (108.3)	28.9 (149.3)
I/σI	17.85 (1.95)	8.71 (1.84)
$CC_{1/2}$	99.9 (71.1)	99.5 (64.7)
Completeness (%)	99.8 (99.1)	99.7 (98.4)
Wilson B factor (Å^2)	32.12	28.34
Refinement		
R_{work}/R_{free} [%]	17.3/21.0	18.3/23.7
No. of atoms		
Protein	20'776	20'806
Glycooligomer	266	203
Water	2'309	1'436
Ions	3	-
Average B factors (Å^2)		
Protein	28.8	27.5
Glycooligomer	41.2	47.2 (Neu5Ac), 64.4 (Gal), 63.4 (Glc)
Water	34.5	28.0
Ions	34.6	-
RMSD		
Bond length (Å)	0.011	0.011
Bond angles (°)	1.55	1.53
Ramachandran plot		
Favored (%)	96.7	96.3
Allowed (%)	2.6	3.0

Values for the highest resolution shell are given in parentheses. The R_{free} was calculated with 2.5 % (1) and 5 % (2) of the total reflections. RMSD – root mean square deviation.

References

[16]   Bruker, APEX2, SAINT, *Bruker AXS Inc., Madison, Wisconsin, USA* **2009**.

[17]   G. Sheldrick, *Acta Cryst.* **2015**, *A71*, 3.

[18]   G. Sheldrick, *Acta Cryst.* **2015**, *C71*, 3.

[19]   M. F. Ebbesen, D. Itskalov, M. Baier, L. Hartmann, *ACS Macro Lett.* **2017**, *6*, 399.

[20]   aS. Parsons, H. D. Flack, T. Wagner, *Acta Cryst.* **2013**, *B69*, 249; bBrandenburg, *Diamond - Crystal and Molecular Structure Visualization, Dr. H. Putz & Dr. K. Brandenburg GbR* **2018**.

[21]   D. van der Spoel, E. Lindahl, B. Hess, G. Groenhof, A. E. Mark, H. J. C. Berendsen, *J. Comput. Chem.* **2005**, *26*, 1701.

[22]   T. Darden, D. York, L. Pedersen, *J. Chem. Phys.* **1993**, *98*, 10089.

[23]   S. Miyamoto, P. A. Kollman, *J. Comput. Chem.* **1992**, *13*, 952.

[24]   aJ. Wang, P. Cieplak, P. A. Kollman, *J. Comput. Chem.* **2000**, *21*, 1049; bV. Hornak, R. Abel, A. Okur, B. Strockbine, A. Roitberg, C. Simmerling, *Proteins* **2006**, *65*, 712.

[25]   J. Wang, R. M. Wolf, J. W. Caldwell, P. A. Kollman, D. A. Case, *J. Comput. Chem.* **2004**, *25*, 1157.

[26]   F.-Y. Dupradeau, A. Pigache, T. Zaffran, C. Savineau, R. Lelong, N. Grivel, D. Lelong, W. Rosanski, P. Cieplak, *Phys. Chem. Chem. Phsy.* **2010**, *12*, 7821.

[27]   aK. N. Kirschner, A. B. Yongye, S. M. Tschampel, J. Gonzalez-Outeirino, C. R. Daniels, B. L. Foley, R. J. Woods, *J. Comput. Chem.* **2008**, *29*, 622; bJ. Sauter, A. Grafmüller, *J. Chem. Theory Comput.* **2016**, *12*, 4375.

[28]   M. W. Mahoney, W. L. Jorgensen, *J. Chem. Phys.* **2000**, *112*, 8910.

[29]   W. Kabsch, *Acta Cryst.* **2010**, *D66*, 125.

[30]   A. J. McCoy, R. W. Grosse-Kunstleve, P. D. Adams, M. D. Winn, L. C. Storoni, R. J. Read, *J. Appl. Cryst.* **2007**, *40*, 658.

[31]   G. N. Murshudov, A. A. Vagin, E. J. Dodson, *Acta Cryst.* **1997**, *B53*, 240.

[32]   P. Emsley, B. Lohkamp, W. G. Scott, K. Cowtan, *Acta Cryst.* **2010**, *D66*, 486.

[33]   P. D. Adams, P. V. Afonine, G. Bunkóczi, V. B. Chen, I. W. Davis, N. Echols, J. J. Headd, L.-W. Hung, G. J. Kapral, R. W. Grosse-Kunstleve, *Acta Cryst.* **2010**, *D66*, 213.

5.3. Synthesis of highly controlled carbohydrate-polymer based hybrid structures by combining heparin fragments and sialic acid derivatives, and solid phase polymer synthesis

1st author contribution:

Collaborative design of structures. Synthesis of all building blocks including propargylated sialic acid according to known methods and 3'-sialyllactose *via* a Fisher glycosylation as well as isolation of Fondaparinux® from ready-to-use units. Synthesis of an unprotected glucuronic acid derivative and optimization of coupling conditions thereof in aqueous mixtures to resin-bound macromolecules using DMTMM as coupling reagent was supported by Ms. Jana Ruppertz within her bachelor thesis. Synthesis of all hybrid glycomacromolecules in solution, isolation and analysis of these *via* NMR and LC-MS experiments. Evaluation of the results except the saturation difference transfer NMR measurements. Collaborative writing of manuscript.

Check for updates

Synthesis of highly controlled carbohydrate–polymer based hybrid structures by combining heparin fragments and sialic acid derivatives, and solid phase polymer synthesis†

Mischa Baier, [a] Jana L. Ruppertz, [a] Moritz M. Pfleiderer, [b] Bärbel S. Blaum *[b] and Laura Hartmann *[a]

Heparin is a polymeric carbohydrate with a variety of biomedical applications that is particularly challenging from a synthetic point of view. Here, we present the synthesis of carbohydrate–polymer based hybrid structures by combining defined heparin fragments with monodisperse, sequence-controlled glycooligo(amidoamines) suitable as glycan mimetic model compounds of heparin as demonstrated by STD-NMR binding studies with viral capsids.

Glycosaminoglycans (GAGs) are a class of long, unbranched polydisperse glycooligomers consisting of repeating units of selectively sulfated disaccharides, generally an amino sugar alternating with an uronic acid.[1] They are important components of the extracellular matrix and the glycocalyx, a dense layer of carbohydrates decorating almost all eukaryotic cells.[2] Heparin, which is a secreted GAG, shows the highest degree of sulfation of all GAGs and is widely used as an anticoagulant.[3] Structurally, it is closely related to heparan sulfate (HS), which is present on proteoglycans and acts as a co-receptor for numerous viruses, such as the human tumor viruses papillomavirus 16 (HPV16) and Merkel cell polyomavirus (MCPyV). Thus, heparin/HS-containing compounds have the potential to act as antivirals[3b,c,4] for papilloma- and polyomaviruses.[5] Since natural GAGs are chemically heterogeneous compounds, it is often difficult to study whether specific structural requirements exist for individual virus–GAG interactions, such as the GAG chain length or specific sulfation patterns.[6] While defined GAG fragments can be obtained *e.g. via* enzymatic degradation of the natural polysaccharides[7] or chemical synthesis[8] it is also highly interesting to create glycan mimetic structures as model compounds for systematic structure–property correlation studies. An important class of such glycan

mimetics are the glycopolymers, using a polymeric scaffold for the multivalent presentation of carbohydrate motifs. While such glycan mimetics can be used to investigate the effects of the overall length and sulfation patterns of heparin-mimicking systems,[9] they also offer an opportunity to study the interplay of heparin and other components of the glycocalyx, such as sialic acid (Neu5Ac) containing oligosaccharides. An interesting example is MCPyV as it was shown to utilize both GAGs of the heparin/HS-type as well as sialylated glycans as cellular attachment factors or entry receptors.[10]

Recently, we introduced the so-called solid phase polymer synthesis (SPPoS) to access structurally and sequentially defined glycomacromolecules as a novel class of glycan mimetics. In short, tailor-made building blocks carrying a carboxylic acid as well as a Fmoc-protected amine terminus are assembled stepwise on a solid support using standard peptide coupling chemistry. Different functional side chain or main chain motifs can be positioned within the resulting oligo(amidoamine) scaffold and used for conjugation of specific oligosaccharides.[11] These precise glycomacromolecules have been successfully applied as model compounds in various binding studies and have shown their potential as glycan mimetic structures in different biotechnological and biomedical applications.[11a,c,12]

Here, we now extend this concept by applying, for the first time, heparin fragments as carbohydrate moieties, demonstrating the potential of our synthetic approach to create a variety of GAG-mimetic structures. Heparin fragments can be accessed *via* chemical synthesis,[8,13] but the challenging synthesis and limited amounts available through such approaches prompted us to choose enzymatic degradation of unfractionated heparin, providing the defined heparin dp2 fragment on a suitable scale.[7] A pentasaccharide fragment, Fondaparinux®, used as an anticoagulant and commercially available, is applied here as well.[14]

The conjugation of heparin fragments, in principle, can be accomplished at the non-reducing end and at the reducing end,[15] as well as at the uronic acid carboxylic acids and amino sugar amines.[16] Here, we chose the carboxylic acids of the uronic acids as anchor points for straightforward combination

[a] *Institute of Organic and Macromolecular Chemistry, Heinrich-Heine-University Duesseldorf, Universitaetsstrasse 1, Duesseldorf 40225, Germany.*
  E-mail: laura.hartmann@hhu.de
[b] *Interfaculty Institute of Biochemistry, University of Tuebingen, Hoppe-Seyler-Strasse 4, Tuebingen 72076, Germany*
† Electronic supplementary information (ESI) available: Materials, methods and experimental data. See DOI: 10.1039/c8cc04898c
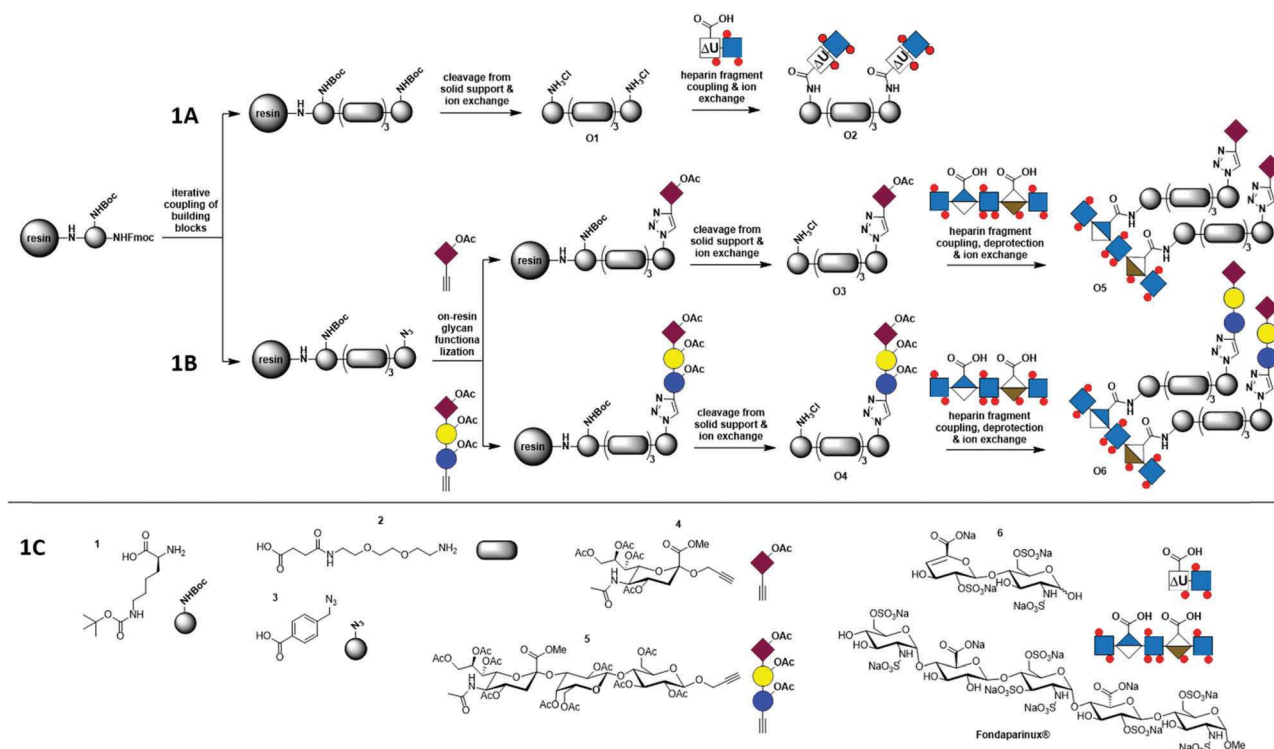
Fig. 1 Synthesis of oligo(amidoamine)–heparin fragment conjugates. (1A) Homovalent dp2-adduct; (1B) homomultivalent Fondaparinux-adducts; (1C) applied building blocks.

with our oligoamide-based scaffolds. It has been shown that DMTMM ((4-(4,6-dimethoxy-1,3,5-triazin-2-yl)-4-methyl-morpholinium chloride)) is promising as a coupling reagent for the synthesis of GAG-adducts.[16a,17] In general, following our previously introduced concept, conjugation of heparin fragments in the side chains of oligo(amidoamine) scaffolds leads to multivalent glycan mimetics. Our toolbox of building blocks also gives us the flexibility to use the heparin fragment itself as a scaffold and attach multiple copies of another ligand, e.g. Neu5Ac moieties (Fig. 1). This is the first example of a GAG fragment used as a scaffold to multivalently present glycan motifs and generate a novel class of heteromultivalent glycan mimetics.

For both classes of molecules, Fmoc-Lys(Boc)-OH (**1**) was used for the introduction of primary amine groups and subsequent conjugation to the uronic acid carboxylic acids of heparin fragments. Fmoc-based amino acids are easily combined with our tailor-made building blocks.[18] Following the first approach, oligomer **1** (**O1**) consisting of two lysines spaced by three ethylene-glycol based building blocks EDS[18a] (**2**) was synthesized on a TentaGel® S RAM resin. **O1** was isolated after cleavage from a solid support also removing Boc protecting groups and ion exchange to chloride as a counter-ion (Fig. 1A). DMTMM promoted coupling parameters were taken from test couplings of an unprotected glucuronic acid derivative to a resin-bound oligo(amidoamine) following protocols developed by Falchi et al.[19] (see the ESI† for experimental set-up and spectra). Although the ideal conditions in the solid phase do not reflect the ideal conditions in solution, attachment of two heparin dp2-fragments (**6**) to **O1** proceeded smoothly in a 9:1

mixture of DMF and phosphate buffer with pH 6.5. Fully dp2-conjugated glycomacromolecule **O2** was obtained with 81% purity after dialysis and ion exchange as determined by UV integration of signals in RP-HPLC (see the ESI†). Here, impurities can partially be attributed to different glucosamine pyranose forms and partial loss and re-addition of sulfates during synthesis and workup (see the ESI†).

Following our second approach, we inversed the conjugation scheme and first synthesized carbohydrate-functionalized oligo(amidoamines) that should then be conjugated onto a larger heparin fragment, here the pentasaccharide Fondaparinux®. Such non-natural heteromultivalent glycan mimetics can then be used as model structures to investigate the interplay of different GAG and non-GAG fragments e.g. on the adhesion of MCPyV. For this purpose, an oligo(amidoamine) scaffold introducing first a lysine followed by three EDS and an azide functionalized building block[12b] (**3**) was synthesized (Fig. 1B). Following previously established protocols, copper(i)-catalyzed alkyne-azide cycloaddition (CuAAC) of propargyl-functionalized Neu5Ac (**4**)[20a,b] or propargyl-functionalized 3′-sialyllactose (3′-SL, **5**) was performed. In the case of propargyl-functionalized Neu5Ac **4**, instead of 0.1 equivalents of copper(ii) sulfate, 2 equivalents were required for full conjugation. Potentially, propargyl-functionalized Neu5Ac is capable of complexing copper ions to some degree and thereby reducing coupling efficiency. After cleavage from the support and in situ deprotection of lysine side chains, glycomacromolecules **O3** and **O4** were purified via preparative RP-HPLC and ion exchange to give the final structures as hydrochloride salts in high purities as determined by ^{1}H NMR, RP-HPLC-MS and HR-MS (see the ESI†). In the

second step, **O3** and **O4** were then used to functionalize the two carboxylic acid moieties of Fondaparinux® (Fig. 1B). This was accomplished using 1.5 equivalents of **O3** and 10 equivalents of DMTMM per carboxylic acid; full conversion was accomplished as shown by RP-HPLC-MS. The product was deprotected with lithium hydroxide and isolated after dialysis and ion exchange. Fig. 2 shows the ¹H NMR spectra of Fondaparinux®, glycomacromolecule **O3** and the resulting adduct **O5**, demonstrating successful synthesis of the fully conjugated heparin fragment. Characteristic signals of both carbohydrate ligands as well as from the oligo(amidoamine) backbone are clearly visible and allow for quantification of the degree of conjugation. When coupling the 3′-SL-functionalized glycomacromolecule **O4** even 1.15 equivalents per carboxylic acid were sufficient to give the fully conjugated product in a high yield of 86%. Mono-substituted products and excessive reagents were easily removed by dialysis. The final conjugate **O6** was obtained in high purity after deprotection, dialysis and ion exchange as determined by RP-HPLC-MS, SAX-HPLC and ¹H NMR (see the ESI†). All macromolecules are listed in Table 1.

First insights into the applicability of the synthesized compounds as glycan mimetics were gained in saturation transfer difference NMR (STD-NMR) experiments using the MCPyV capsid, which binds to unmodified heparin dp2, Fondaparinux®, and 3′-SL. STD-NMR provides spectra from which the proximity of individual ligand protons to protein protons in the binding site can be delineated.[11b,21] For **O2**, we observed saturation transfer to protons of the unsaturated uronic acid as well as to the GlcNS anomeric proton (see the ESI†). Saturation transfer to the aliphatic lysine chains was also detected and, to a lesser degree, to the succinic acid CH₂-groups. For **O6**, we observed saturation transfer to a set of 3′-SL protons previously shown to constitute the MCPyV Neu5Ac binding epitope (see the ESI†).[22] However, in this compound, no signature protons of the Fondaparinux scaffold were detected, suggesting that only the exposed Neu5Ac binding site on the capsid's

Table 1 Overview of the oligomers obtained, molecular weights, purities determined *via* RP-HPLC and SAX-HPLC, and yields

#	Structure	M_W [Da]	Purity[a] (RP-HPLC) [%]	Purity[a] (SAX-HPLC) [%]	Yield [%]
O1		1079	97	—[b]	36
O2		2257	81	85	21
O3		1561	>99	—[b]	25
O4		2138	97 β	—[b]	27
O5		4377	98	88	74
O6		5026	90 ββ, 6 αβ/ βα, < 4% αα[c]	87	86

[a] Purities determined by integration of UV-signals in RP-HPLC (see the ESI for spectra and conditions). [b] Not determined. [c] Anomeric mixtures were expected since an anomeric mixture of **5** was used.

apical loops engages with compound **O6**. An optimized linker length may be necessary to bridge the Neu5Ac and GAG binding sites on the capsid. Nevertheless, our NMR experiments demonstrate that GAG and sialic acid units can, in principle, engage in lectin binding in the context of the investigated glycomacromolecules.
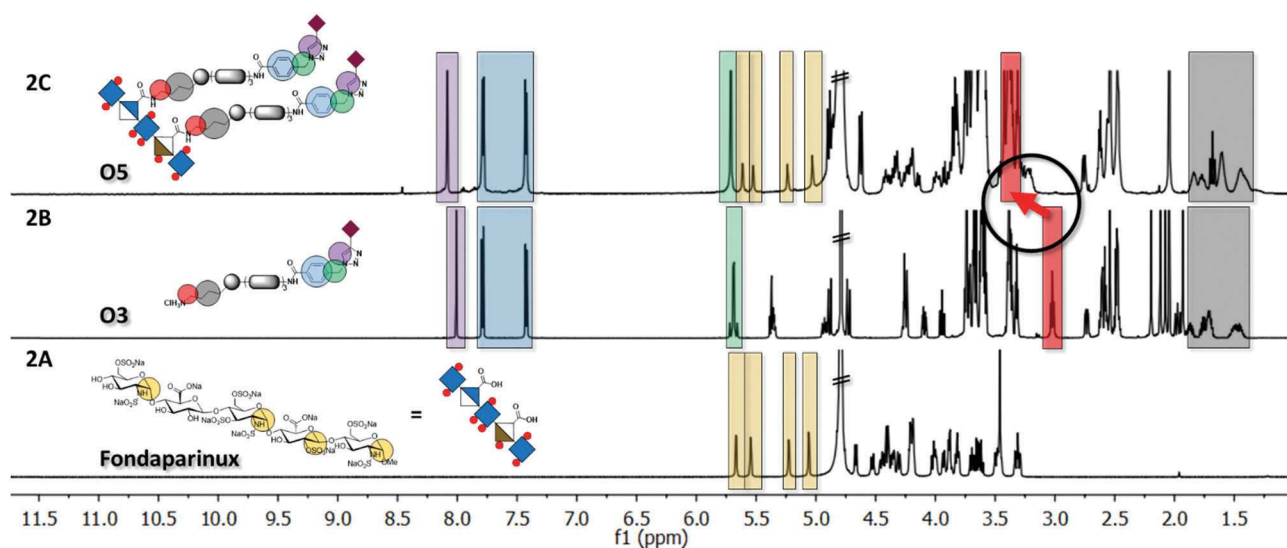
Fig. 2 ¹H NMR (D₂O) of Fondaparinux® (2A), compounds **O3** (2B) and **O5** (2C). Product **O5** shows all the ¹H-signals of Fondaparinux® as well as the aromatic signals, the sialic acid signals and the signals of the aliphatic lysine chain. Downfield shifting of the −ε-CH₂− signal in front of the ζ-NH₂ of lysine can be seen (see red arrow).

In conclusion, we have demonstrated the synthesis of glycomimetic conjugates of heparin fragments using our toolbox of oligo(amidoamines), also introducing Neu5Ac and 3′-SL ligands. In the first approach we followed the concept of conjugating carbohydrate ligands as pending side chains onto an oligo(amidoamine) scaffold for the first time using heparin dp2-fragments. Furthermore, we introduced an inverse strategy towards oligo(amidoamine)-based glycan mimetics where solid-phase derived glycomacromolecules are used as side chains for conjugation onto larger heparin fragments. We have used this strategy to create conjugates of multiple Neu5Ac or 3′-SL ligands bound to a heparin fragment. First binding studies probing the interaction of glycomacromolecules with the MCPyV capsid proved their potential as glycan mimetics targeting papilloma- and polyomaviruses. In general, this approach is applicable for the conjugation of oligo(amidoamine) side chains onto various oligo- and polysaccharides, such as hyaluronic or colominic acid giving access to novel carbohydrate–polymer based hybrid materials with potential applications in biotechnology and biomedicine.

Conflicts of interest

There are no conflicts to declare.

References

1 J. Esko, K. Kimata and U. Lindahl, in *Essentials of Glycobiology.*, ed. A. Varki, 2nd edn, 2009.
2 (*a*) A. Varki, *Glycobiology*, 1993, **3**, 97–130; (*b*) K. Kato and A. Ishiwa, *Trop. Med. Int. Health*, 2015, **43**, 41–52.
3 (*a*) B. Mulloy, E. Gray and T. W. Barrowcliffe, *Thromb. Heamost.*, 2000, **84**, 1052–1056; (*b*) I. Capila and R. J. Linhardt, *Angew. Chem., Int. Ed.*, 2002, **41**, 391–412; (*c*) I. Capila and R. J. Linhardt, *Angew. Chem.*, 2002, **114**, 426–450; (*d*) R. J. Linhardt, *J. Med. Chem.*, 2003, **46**, 2551–2564.
4 (*a*) R. S. Aquino, E. S. Lee and P. W. Park, in *Glycosaminoglycans in Development, Health and Disease*, ed. L. Zhang, 1st edn, 2010; (*b*) R. S. Aquino and P. W. Park, *Front. Biosci.*, 2016, **21**, 1260–1277.
5 (*a*) P. M. Day and M. Schelhaas, *Curr. Opin. Virol.*, 2014, **4**, 24–31; (*b*) J. Guan, S. M. Bywaters, S. A. Brendle, R. E. Ashley, A. M. Makhov, J. F. Conway, N. D. Christensen and S. Hafenstein, *Structure*, 2017, **25**, 253–263.
6 (*a*) J. Dasgupta, M. Bienkowska-Haba, M. E. Ortega, H. D. Patel, S. Bodevin, D. Spillmann, B. Bishop, M. Sapp and X. S. Chen, *J. Biol. Chem.*, 2011, **286**, 2617–2624; (*b*) C. Cerqueira, Y. Liu, L. Kuhling, W. G. Chai, W. Hafezi, T. H. van Kuppevelt, J. E. Kuhn, T. Feizi and M. Schelhaas, *Cell. Microbiol.*, 2013, **15**, 1818–1836.
7 (*a*) R. J. Linhardt, K. G. Rice, Y. S. Kim, D. L. Lohse, H. M. Wang and D. Loganathan, *Biochem. J.*, 1988, **254**, 781–787; (*b*) D. Ruhela, K. Riviere and F. C. Szoka, *Bioconjugate Chem.*, 2006, **17**, 1360–1363.
8 (*a*) M. F. Haller and G. J. Boons, *Eur. J. Org. Chem.*, 2002, 2033–2038; (*b*) S. Arungundram, K. Al-Mafraji, J. Asong, F. E. Leach, I. J. Amster, A. Venot, J. E. Turnbull and G.-J. Boons, *J. Am. Chem. Soc.*, 2009, **131**, 17394–17405; (*c*) P. Liu, L. Chen, J. K. C. Toh, Y. L. Ang, J.-E. Jee, J. Lim, S. S. Lee and S.-G. Lee, *Chem. Sci.*, 2015, **6**, 450–456.
9 (*a*) C. I. Gama, S. E. Tully, N. Sotogaku, P. M. Clark, M. Rawat, N. Vaidehi, W. A. Goddard Iii, A. Nishi and L. C. Hsieh-Wilson, *Nat. Chem. Biol.*, 2006, **2**, 467; (*b*) G. J. Sheng, Y. I. Oh, S.-K. Chang and L. C. Hsieh-Wilson, *J. Am. Chem. Soc.*, 2013, **135**, 10898–10901; (*c*) Y. I. Oh, G. J. Sheng, S.-K. Chang and L. C. Hsieh-Wilson, *Angew. Chem., Int. Ed.*, 2013, **52**, 11796–11799; (*d*) L. Fu, M. Suflita and R. J. Linhardt, *Adv. Drug Delivery Rev.*, 2016, **97**, 237–249.
10 R. M. Schowalter, D. V. Pastrana and C. B. Buck, *PLoS Pathog.*, 2011, **7**, e1002161.
11 (*a*) D. Ponader, F. Wojcik, F. Beceren-Braun, J. Dernedde and L. Hartmann, *Biomacromolecules*, 2012, **13**, 1845–1852; (*b*) D. Ponader, P. Maffre, J. Aretz, D. Pussak, N. M. Ninnemann, S. Schmidt, P. H. Seeberger, C. Rademacher, G. U. Nienhaus and L. Hartmann, *J. Am. Chem. Soc.*, 2014, **136**, 2008–2016; (*c*) S. Igde, S. Röblitz, A. Müller, K. Kolbe, S. Boden, C. Fessele, T. K. Lindhorst, M. Weber and L. Hartmann, *Macromol. Biosci.*, 2017, **17**, 1700198.
12 (*a*) F. Broecker, J. Hanske, C. E. Martin, J. Y. Baek, A. Wahlbrink, F. Wojcik, L. Hartmann, C. Rademacher, C. Anish and P. H. Seeberger, *Nat. Commun.*, 2016, **7**; (*b*) M. Baier, M. Giesler and L. Hartmann, *Chem. – Eur. J.*, 2018, **24**, 1619–1630.
13 (*a*) C. Zong, A. Venot, O. Dhamale and G.-J. Boons, *Org. Lett.*, 2013, **15**, 342–345; (*b*) O. P. Dhamale, C. Zong, K. Al-Mafraji and G.-J. Boons, *Org. Biomol. Chem.*, 2014, **12**, 2087–2098.
14 (*a*) J. Choay, M. Petitou, J. C. Lormeau, P. Sinaÿ, B. Casu and G. Gatti, *Biochem. Biophys. Res. Commun.*, 1983, **116**, 492–499; (*b*) H. Bounameaux and T. Perneger, *Lancet*, 2002, **359**, 1710–1711.
15 (*a*) S. Masuko, K. Higashi, Z. Wang, U. Bhaskar, A. M. Hickey, F. Zhang, T. Toida, J. S. Dordick and R. J. Linhardt, *Carbohydr. Res.*, 2011, **346**, 1962–1966; (*b*) Z. Q. Wang, C. Shi, X. R. Wu and Y. J. Chen, *Chem. Commun.*, 2014, **50**, 7004–7006.
16 (*a*) E. Gemma, A. N. Hulme, A. Jahnke, L. Jin, M. Lyon, R. M. Muller and D. Uhrin, *Chem. Commun.*, 2007, 2686–2688; (*b*) D. Tebbe, R. Thull and U. Gbureck, *Biomed. Eng.*, 2007, **6**, 31.
17 (*a*) P. Farkaš, A. Čížová, S. Bekešová and S. Bystrický, *Int. J. Biol. Macromol.*, 2013, **60**, 325–327; (*b*) M. D'Este, D. Eglin and M. Alini, *Carbohydr. Polym.*, 2014, **108**, 239–246.
18 (*a*) M. F. Ebbesen, C. Gerke, P. Hartwig and L. Hartmann, *Polym. Chem.*, 2016, **7**, 7086–7093; (*b*) C. Gerke, M. F. Ebbesen, D. Jansen, S. Boden, T. Freichel and L. Hartmann, *Biomacromolecules*, 2017, **18**, 787–796; (*c*) S. Boden, K. Wagner, M. Karg and L. Hartmann, *Polymers*, 2017, **9**, 716; (*d*) T. Freichel, S. Eierhoff, N. L. Snyder and L. Hartmann, *J. Org. Chem.*, 2017, **82**, 9400–9409.
19 A. Falchi, G. Giacomelli, A. Porcheddu and M. Taddei, *Synlett*, 2000, 275–277.
20 (*a*) R. Šardzík, G. T. Noble, M. J. Weissenborn, A. Martin, S. J. Webb and S. L. Flitsch, *Beilstein J. Org. Chem.*, 2010, **6**, 699–703; (*b*) M. F. Ebbesen, D. Itskalov, M. Baier and L. Hartmann, *ACS Macro Lett.*, 2017, **6**, 399–403.
21 (*a*) M. Mayer and B. Meyer, *Angew. Chem., Int. Ed.*, 1999, **38**, 1784–1788; (*b*) M. Mayer and B. Meyer, *J. Am. Chem. Soc.*, 2001, **123**, 6108–6117; (*c*) B. S. Blaum, U. Neu, T. Peters and T. Stehle, *Acta Crystallogr., Sect. F: Struct. Biol. Commun.*, 2018, **74**, 451–462; (*d*) K. S. Bücher, H. Yan, R. Creutznacher, K. Ruoff, A. Mallagaray, A. Grafmüller, J. S. Dirks, T. Kilic, S. Weickert, A. Rubailo, M. Drescher, S. Schmidt, G. Hansman, T. Peters, C. Uetrecht and L. Hartmann, *Biomacromolecules*, 2018, DOI: 10.1021/acs.biomac.8b00829.
22 U. Neu, H. Hengel, B. S. Blaum, R. M. Schowalter, D. Macejak, M. Gilbert, W. W. Wakarchuk, A. Imamura, H. Ando, M. Kiso, N. Arnberg, R. L. Garcea, T. Peters, C. B. Buck and T. Stehle, *PLoS Pathog.*, 2012, **8**, e1002738.

Electronic Supplementary Information

Synthesis of highly controlled carbohydrate-polymer based hybrid structures by combining heparin fragments, sialic acid derivatives, and solid phase polymer synthesis

Mischa Baier,[a] Jana L. Ruppertz,[a] Moritz M. Pfleiderer,[b] Bärbel S. Blaum*[b] and Laura Hartmann*[a]

---

[a]. Institute of Organic and Macromolecular Chemistry, Heinrich-Heine-University Düsseldorf, Universitätsstrasse 1, 40225 Düsseldorf, Germany
     E-mail: laura.hartmann@hhu.de

[b]. Interfaculty Institute of Biochemistry, University of Tübingen, Hoppe-Seyler-Strasse 4, 72076 Tübingen, Germany

Table of Contents

Materials and Methods

Materials

N-Acetylneuraminic acid (>98%), 3'-Sialyllactose sodium salt (>98%), Methyl-α-D-glucopyranoside (>98%) were purchased from Carbosynth. 2, 2'-(Ethylenedioxy)bis(ethylamine) (98%), Propargyl alcohol (99%), Succinic anhydride (>99%), Triethylsilane (99%), Triisopropylsilane (98%), (+)-Sodium-L-ascorbate (>99.0%), Amberlite® IR 120 H$^+$, Amberlite® IR 120 Na$^+$, Dowex® 1X4 Cl$^-$, Bovine Serum Albumin (BSA) were purchased from Merck (former Sigma Aldrich). Trityl chloride (98%), *p*-Toluic acid (98%), Piperidine (99%), Copper (II) sulfate (98%) were purchased from Acros Organics. *P*-Toluenesulfonic acid monohydrate (98%), Boron trifluoride diethyl etherate (>98%), Acetyl chloride (98%) were purchased from Alfa Aesar. *N*-Bromosuccinimide (99%) was purchased from Merck. Sodium azide (99%) diethyl dithiocarbamate (99%) were purchased from Applichem. PyBOP (Benzotriazole-1-yl-oxy-tris-pyrrolidino-phosphonium hexafluorophosphat), Fmoc-Lysine(Boc)-OH (>98%) were obtained from Iris Biotech. Silver carbonate (>99%) was obtained from Strem Chemicals. Sodium hypochloride solution (13%) was obtained from Hoesch. Sodium bromide (>99.5%), (2,2,6,6-tetramethylpiperidinyl) oxyl radical (TEMPO, >99%) were purchased from Fisher scientific (former Fluka). Acetic anhydride (99%), Formic acid (>99%), Magnesium sulfate anhydrous (>99.5% min), Sodium chloride (>99.5%), Sodiumhydrogen carbonate (>99.7%), Disodiumhydrogen phosphate dihydrate (>99%), Potassiumdihydrogen phosphate (>99%), Tris(hydroxymethyl)aminoethan (TRIS, >99.9%), Calcium chloride anhydrous (>96%) were purchased from VWR. Lithium hydroxide monohydrate (>99%) was purchased from Janssen chimica. 9-Fluorenylmethyl chloroformate (Fmoc-Cl, 98%) was purchased from Chempur. *N, N*-Diisopropylethylamine (99%) was obtained from Roth. Trifluoroacetic acid (TFA, 99%), 4-(4,6-Dimethoxy-1,3,5-triazin-2-yl)-4-methylmorpholinium chloride (DMTMM, 97%) were purchased from Fluorochem. Tentagel® S RAM (Rink Amide) resin (Capacity 0.25 mmol/g) was purchased from Rapp Polymere. Porcine sodium heparin (MW 15-19 kDa) was purchased from Bioiberica. Heparinase I from Flavobacterium heparinum was purchased from Iduron. Fondaparinux®-sodium was purchased as Arixtra® at a concentration of 10 mg / 0.8 mL from the Aspen Pharma Trading Limited as ready-to-use syringes. Peptide synthesis grade *N, N*-Dimethylformamide was used for solid phase synthesis. All solvents were of *p.a.* reagent grade. Phosphate buffer pH 6.5 was prepared according Sörensen's buffer: 68.7 vol.% (66.7 mM KH_2PO_4 in Milli-Q) and 31.3 vol.% (66.7 mM Na_2HPO_4*2 H_2O in Milli-Q). Vivaspin® MWCO 2000 and MWCO 3000 units were purchased from Sartorius. Spectra/Por® Float-a-Lyzer® G2 MWCO 0.1 – 0.5 kDa and 0.5 – 1.0 kDa were obtained from Spectrum Labs.

Instrumentation

Nuclear Magnetic Resonance spectroscopy (NMR)
^{1}H-NMR (300 MHz) spectra were recorded on a Bruker AVANCE III - 300. ^{1}H-NMR (600 MHz) spectra were recorded on a Bruker AVANCE III - 600. Chemical shifts of all NMR spectra were reported in delta (δ) expressed in parts per million (ppm). For ^{1}H-NMR the residual, non-deuterated solvent was used as internal standard. The following abbreviations are used to indicate the multiplicities: s, singlet; d, doublet; t triplet; m multiplet.

Attenuated Total Reflectance Fourier Transform Infrared Spectroscopy (ATR FTIR)
IR spectra were recorded with a Nicolet 6700, attenuated total reflectance Fourier transform infrared spectroscopy (ATR FTIR) spectrometer from Thermo Scientific and spectra analyzed using Omnic software 7.4.

Reversed Phase - High Performance Liquid Chromatography - Mass Spectrometry (RP-HPLC-MS)
Measurements were performed on an Agilent 1260 Infinity instrument coupled to a variable wavelength detector (VWD) (set to 214 nm) and a 6120 Quadrupole LC/MS containing an Electrospray Ionization (ESI) source (operated in positive or negative ionization mode in a m/z range of 200 to 2000). As HPLC column a Poroshell 120 EC-C18 (3.0 × 50 mm, 2.5 μm) RP column from Agilent was used. The mobile phases A and B were H_2O/ACN (95/5) and H_2O/ACN (5/95), respectively. Both mobile phases contained 0.1% of formic acid. Samples were analyzed at a flow rate of 0.4 mL/min using a linear gradient starting with 100% mobile phase A reaching 25, 50 or 75 % mobile phase B within 30 min. The temperature of the column compartment was set to 25 °C. UV and MS spectral analysis was done within the OpenLab ChemStation software for LC/MS from Agilent Technologies.

Strong Anion Exchange - High Performance Liquid Chromatography (SAX-HPLC)
Measurements were performed on an Agilent 1200 instrument coupled to a variable wavelength detector (VWD) (set to 214 nm). As SAX-HPLC column a Zobrax (4.6 x 250 mm, 5.0 μm) column from Agilent was used. The mobile phases A and B were A: 50 mM NaH_2PO_4, pH 7 in Milli-Q water, B: 50 mM NaH_2PO_4, 800 mM NaCl, pH 7 in Milli-Q water / ACN = 70% : 30%. Samples were analyzed at a flow rate of 1.0 mL/min using the following gradient within 60 min: 0 → 5 min: 95% A, 5% B; 5

→ 40 min: 5 → 100% B; 40 → 60 min: 100% B. The temperature of the column compartment was set to 25 °C. UV spectral analysis was done within the OpenLab ChemStation software for HPLC from Agilent Technologies.

Ultra High Resolution - Mass Spectrometry (UHR-MS)
UHR-MS measurements were performed with a Bruker UHR-QTOF maXis 4G instrument with a direct inlet via syringe pump, an ESI source and a quadrupole followed by a Time Of Flight (QTOF) mass analyzer.

Freeze dryer
The final oligomers were freeze dried with an Alpha 1-4 LD plus instrument from Martin Christ Freeze Dryers GmbH. The main drying method was set to -55 °C and 0.1 mbar.

General Methods
All general methods follow procedures as previously presented for solid phase polymer synthesis[1]

Solid phase synthesis protocols
The batch sizes for synthesizing the oligomers using solid phase synthesis varied from 15 μmol to 400 μmol.

Fmoc cleavage
The Fmoc protecting group of the resin as well as from the coupled building blocks or amino acid were cleaved by the addition of a solution of 25% piperidine in DMF. The deprotection was performed twice for 10 min. After that, the resin was washed thoroughly 10 times with DMF.

General coupling protocol
Commercially available Tentagel S RAM (Rink Amide) resin was used as resin for solid phase synthesis. As an example 100 μmol of the resin were swollen in 10 mL of DCM for 20 min and subsequently washed five times with 10 mL of DMF. The Fmoc protecting group of the Tentagel S RAM resin was removed following the Fmoc cleavage protocol. A building block was coupled to the resin using a mixture of 0.5 mmol (5 eq.) of building block and 0.5 mmol PyBOP (5 eq.) dissolved in 4 mL of DMF to which 1 mmol (10 eq.) of DIPEA was added. The mixture was shaken for 30 s under a nitrogen stream for activation and subsequently added to the resin. The resin with the coupling mixture was shaken for 1 h. After that, the resin was washed from excessive reagent 5 times with 10 mL of DMF.

Capping of *N*-terminal primary amine
After successful assembly of the desired number of building blocks on solid phase, the *N*-terminal site was capped with an acetyl group. Therefore, 10 mL acetic anhydride were shaken twice with the resin for 30 min.

General CuAAC protocol
To 100 μmol of the resin loaded with the oligomeric structure, 200 μmol (2 eq.) of protected sialic acid or sialyllactose derivative (**2**, **3**) per azide group, dissolved in 1.5 mL DMF, were added. When propargylated sialic acid (**2**) was used, a flat rate of 100 mg (0.4 mmol) of $CuSO_4$ and 100 mg (0.5 mmol) of sodium ascorbate were used and dissolved each in 0.75 mL of water and also added to the resin. When propargylated sialyllactose (**3**) was used, a flat rate of 50 mg (0.2 mmol) of $CuSO_4$ and 50 mg (0.25 mmol) of sodium ascorbate were used and dissolved each in 0.75 mL. This mixture was shaken for 24 h and subsequently washed extensively with water, a 23 mM solution of sodium diethyldithiocarbamate in DMF : H_2O = 1 : 1, DMF and DCM.

Cleavage from solid phase
13 mL of a mixture of 95% TFA, 2.5% of TIPS and 2.5% of DCM were added to the resin and shaken for 1 h. The filtrate was poured into 60 mL cold diethyl ether. The resin was washed with an additional 5 mL of the cleavage mixture which were also added to the cold ether. The resulting precipitate was centrifuged three times and the ether decanted. The crude product was dried over a stream of nitrogen, dissolved in 6 mL of H_2O and lyophilized twice.

General preparative purification protocol of the oligomers
The oligomers were purified by preparative Reversed Phase - High Performance Liquid Chromatography on an Agilent 1260 Infinity instrument coupled to a variable wavelength detector (VWD) (set to 214 nm). As HPLC column a UG80 C18 (20mmI.D.×250 mm, 5 μm) RP column from Shiseido was used. The mobile phases A and B were H_2O and ACN to which 0.1% formic acid were added, respectively. Samples were purified at a flow rate of 20 mL/min using a linear gradient starting with 100% mobile phase A reaching 50% mobile phase B within 15 min. The temperature of the column compartment was room

temperature (18-23° C). UV analysis was done within the OpenLab ChemStation software for LC/MS from Agilent Technologies.

Protective groups deprotection protocol
In order to remove both the acetyl and methyl protective groups of the carbohydrate moieties, 3 mL of a 0.1 M solution of lithium hydroxide monohydrate in a mixture of MeOH : H_2O = 1 : 1 were added to the compound and shaken for 3 h at room temperature (18-23° C) (the pH needs to be checked and has to be at 13 during the deprotection). Subsequently the dissolved and deprotected compound was treated with Amberlite® IR 120 H⁺ ion exchange resin until pH 4-5 was reached. Then the neutralized mixture was dried in *vacuo* at a temperature not higher than 25 °C and finally lyophilized in order to give final deprotected compound.

General ion exchange protocol
Compounds were dissolved in 2 mL of Milli-Q water to which 1 g DOWEX® 1X4 Cl⁻ was added and the mixture was shaken for 10 min. Finally, the resin was filtered off using a 0.45 μm PTFE syringe filter and the product was isolated by lyophilization.

MCPyV capsid production
MCPyV capsids were produced using the established 293 TT cell culture system for virus-like-particle production of papilloma- and polyomaviruses.[2] Briefly, 293 TT cells cultured in the presence of Hygromycin for SV40 T-antigen expression were transfected with codon-optimized VP1 or VP1- and VP2-coding plasmids[2b] (pwM and ph2m) and harvested 48 hours post-transfection. Cells were lysed with Triton X-100 and lysates incubated over night at 37 °C for particle maturation. MCPyV particles were purified via salt extraction, followed by CsCl velocity and equilibrium centrifugation steps and ion exchange chromatography (a manuscript containing a detailed description of an optimized purification protocol will be published elsewhere). Integrity of the ca. 50 nm diameter capsid was verified by negative stain transmission electron microscopy (TEM) and dynamic light scattering (DLS).

NMR experiments
For STD-NMR, capsids were buffer-exchanged to pure D_2O-buffer (99.5 %, Cortecnet) containing 150 mM NaCl, 1 mM $CaCl_2$, pH 6.3 using 500 kDa MWCO dialysis devices made from cellulose ester (Spectra Por). The same buffer was used to dissolve compounds **O2** and **O6** to yield 15 mM and 22.5 mM stock solutions, respectively. NMR samples contained 27.1 nM of MCPyV capsids (9.8 μM with respect to the major capsid protein VP1) and 1.5 mM of **O2** or 30.5 nM of MCPyV capsids (11.0 μM of VP1) and 1.1 mM of **O6**, respectively. NMR spectra were recorded at 283 K using 3 mm I.D. MATCH tubes (with 200 μL final sample volume) on a Bruker AVIII-600 spectrometer equipped with a room temperature probe head. For STD-NMR spectra the off- and on-resonance irradiation frequencies were set to -30 ppm and -0.5 ppm, respectively. The irradiation power of the selective pulses was 57 Hz, the saturation time 2 s and the total relaxation delay 3 s. A 50 ms continuous-wave spin-lock pulse at 3.2 kHz was employed and a total number of 1024 scans were recorded. A total of 12 k points was recorded, and spectra were multiplied with a Gaussian window function prior to Fourier transformation using TOPSPIN 3.0 (Bruker).

Experimental Data

Functionalized sialic acid synthesis

*Propargyl-functionalized Neu5Ac (**4**) was prepared according to previously published protocols by Šardzík[3] and Ebbesen.[4]*
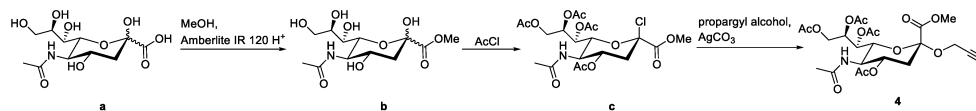
Scheme 1: Synthesis sequence of propargylated Neu5Ac.

N-acetyl neuraminic acid methyl ester (b)

30.9 g (100 mmol) of *N*-acetyl neuraminic acid (**a**) were stirred with 6 g of Amberlite® IR120 H⁺ in 400 ml of dry methanol at r.t. until all starting material was consumed. The resin was filtered off and removal of the solvent at reduced pressure afforded methyl ester (**b**) as a white solid in a quantitative yield.

^{1}H NMR (300 MHz, Deuterium oxide) δ 4.00 − 3.89 (m, 2H, *H4, 6*), 3.85 − 3.76 (m, 1H, *H5*), 3.75 − 3.68 (m, 4H, -*OCH₃, 9'*), 3.61 (ddd, ^3J = 8.9, 6.2, 2.5 Hz, 1H, *H8*), 3.49 (dd, ^3J = 11.7, 6.2 Hz, 1H, *H9''*), 3.43 (dd, ^3J = 9.2, 1.2 Hz, 1H, *H7*), 2.19 (dd, ^3J = 13.1, 4.8 Hz, 1H, *H3eq.*), 1.93 (s, 3H, *Ac*), 1.79 (dd, ^3J = 13.1, 11.5 Hz, 1H, *H3ax.*).

^{13}C NMR (75 MHz, D₂O) δ 174.75, 171.33, 95.27, 70.27, 70.02, 68.11, 66.60, 63.07, 53.41, 51.97, 38.58, 21.99.

MS for $C_{12}H_{21}NO_9$ (ESI, pos.) m/z: [M + Na⁺]⁺ calc.: 346.11; found 346.00, [M + H⁺]⁺ calc.: 324.13; found 324.00, [M - OH⁻]⁺ calc.: 306.11; found 306.20, [M + OH⁻ - H₂O]⁺ calc.: 288.11; found 288.10.

IR (ATR) $\tilde{v}_{max}$: 3322 (br), 2937 (w), 1767 (m), 1633 (m), 1541 (m), 1429 (m), 1371 (m), 1275 (m), 1124 (m), 1028 (s), 894 (m), 575 (s).
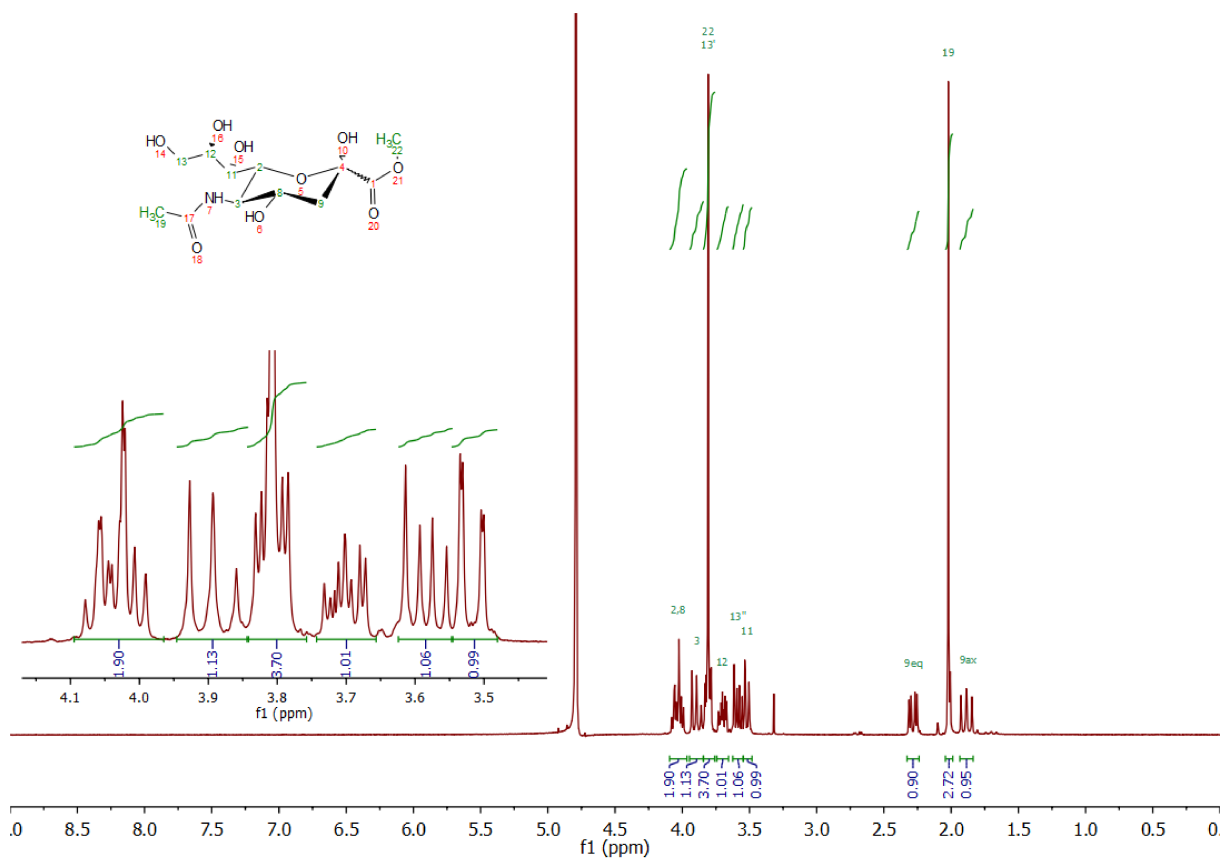
*Figure 1: ¹H NMR (300 MHz, Deuterium oxide) of compound **b**.*
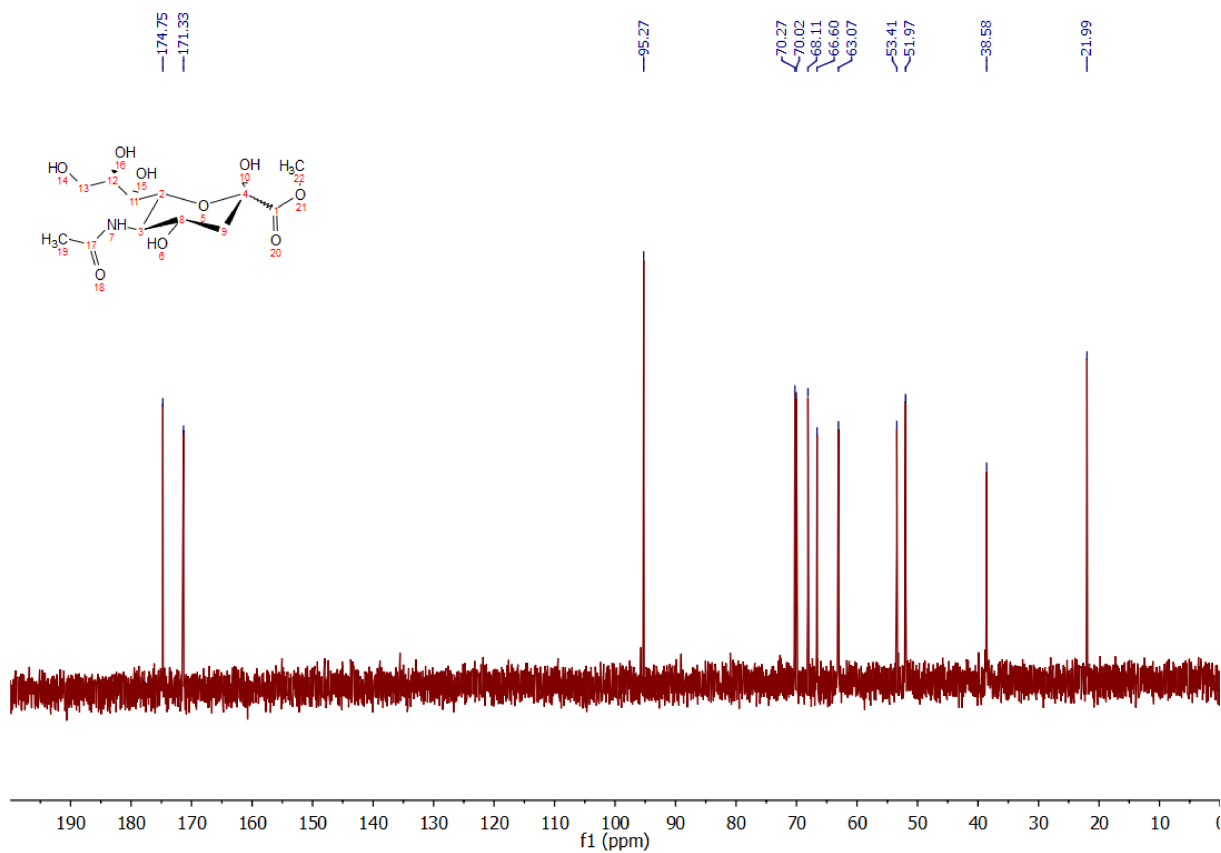
*Figure 2: ¹³C NMR (75 MHz, Deuterium oxide) of compound **b**.*
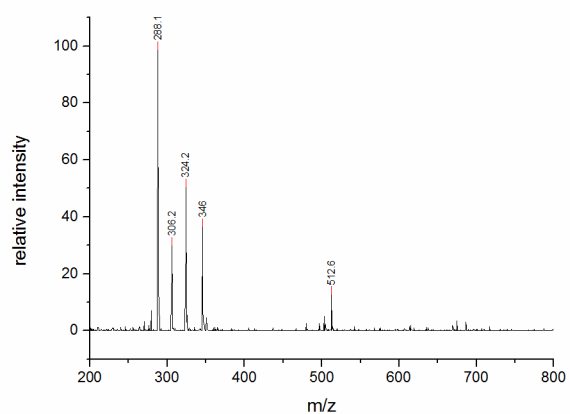
*Figure 3: ESI-MS (positive mode) of compound **b**.*

Methyl 2-chloro-4,7,8,9-tetra-*O*-acetyl-*N*-acetyl-β-D-neuraminate (c)

50 ml of freshly distilled and ice cold (0°C) acetyl chloride were given to 5 g (15.5 mmol) of *N*-acetyl neuraminic acid methyl ester (**b**) in an ice bath under moderate stirring equipped with a gas discharge tube, which leads to a saturated sodium bicarbonate solution. After consumption of the starting material, the remaining acetyl chloride was distilled off at reduced pressure by keeping the temperature not higher than 40 °C to afford the peracetylated and chlorinated intermediate **c** in a quantitative yield. **c** was used without further purification.

^{1}H NMR (300 MHz, Chloroform-*d*) δ 5.61 (d, ^3J = 10.1 Hz, 1H, *-NH*), 5.47 (dd, ^3J = 6.9, 2.4 Hz, 1H, *H7*), 5.39 (ddd, ^3J = 11.1, 4.9 Hz, 1H, *H4*), 5.17 (ddd, ^3J = 6.8, 6.0, 2.7 Hz, 1H, *H8*), 4.43 (dd, ^2J = 12.5, ^3J = 2.7 Hz, 1H, *H9'*), 4.35 (dd, ^3J = 10.8, 2.4 Hz, 1H, *H6*), 4.20 (ddd, ^3J = 10.3 Hz, 1H, *H5*), 4.06 (dd, ^2J = 12.5, ^3J = 5.9 Hz, 1H, *H9''*), 3.87 (s, 3H, *-OCH$_3$*), 2.78 (dd, ^2J = 13.9, ^3J = 4.8 Hz, 1H, *H3eq.*), 2.27 (dd, ^2J = 14.0, ^3J = 11.2 Hz, 1H, *H3ax.*), 2.11 – 1.91 (5s, 5x 3H, 5x *Ac*).

^{13}C NMR (75 MHz, CDCl$_3$) δ 171.17, 170.81, 170.73, 170.12, 169.87, 165.75, 96.71, 77.36, 74.00, 70.10, 68.90, 67.01, 62.20, 53.93, 48.90, 40.76, 23.22, 21.06, 20.91, 20.77.

MS for C$_{20}$H$_{28}$ClNO$_{12}$ (ESI, pos.) m/z: [M + H$^+$]$^+$ calc.: 510.14; found 510.00, [M – Cl$^-$ + H$_2$O]$^+$ calc.: 492.17; found 492.20, [M – Cl$^-$]$^+$ calc.: 474.16; found 474.00, [M - Cl$^-$ - AcOH]$^+$ calc.: 414.14; found 414.20.

IR (ATR) $\tilde{v}_{max}$: 2960 (w), 1739 (s), 1658 (m), 1549 (m), 1435 (m), 1370 (m), 1209 (ss), 1031 (s), 599 (m).
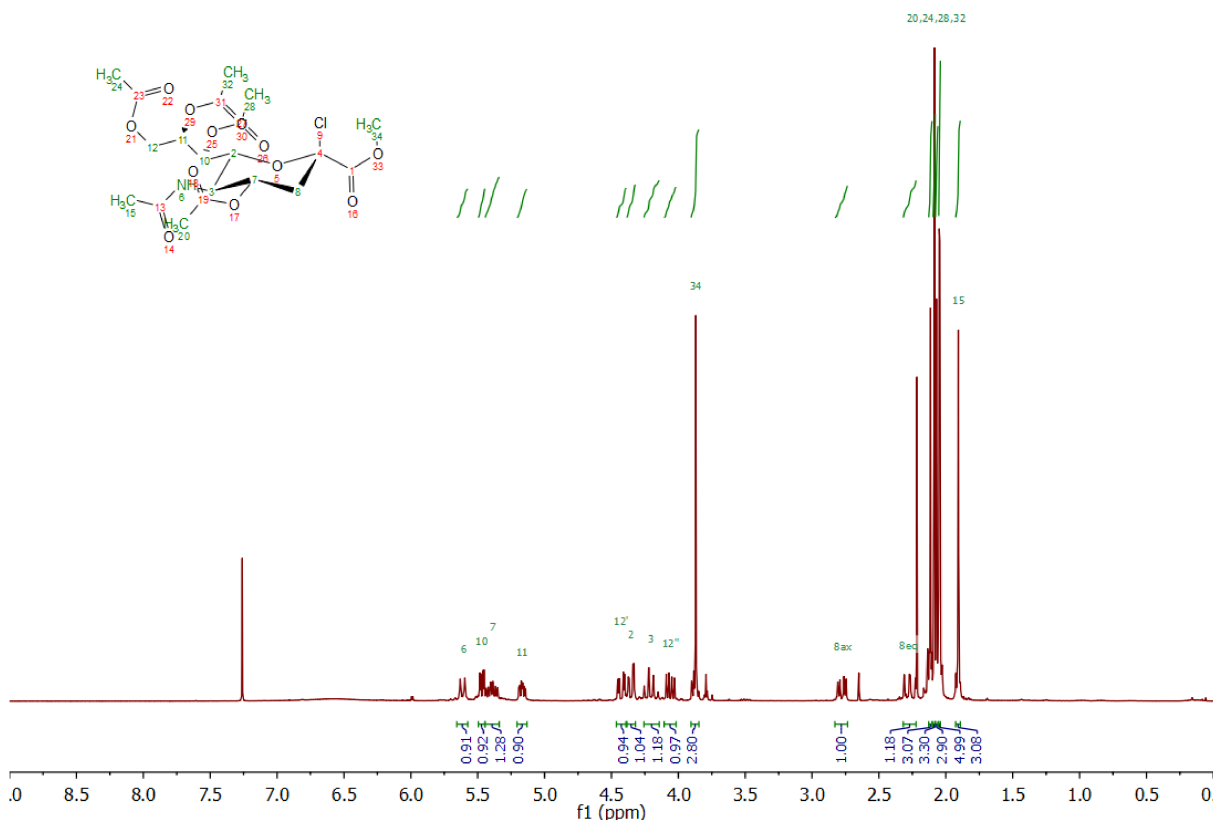
*Figure 4: ^{1}H NMR (300 MHz, Chloroform-d) of compound **c**.*
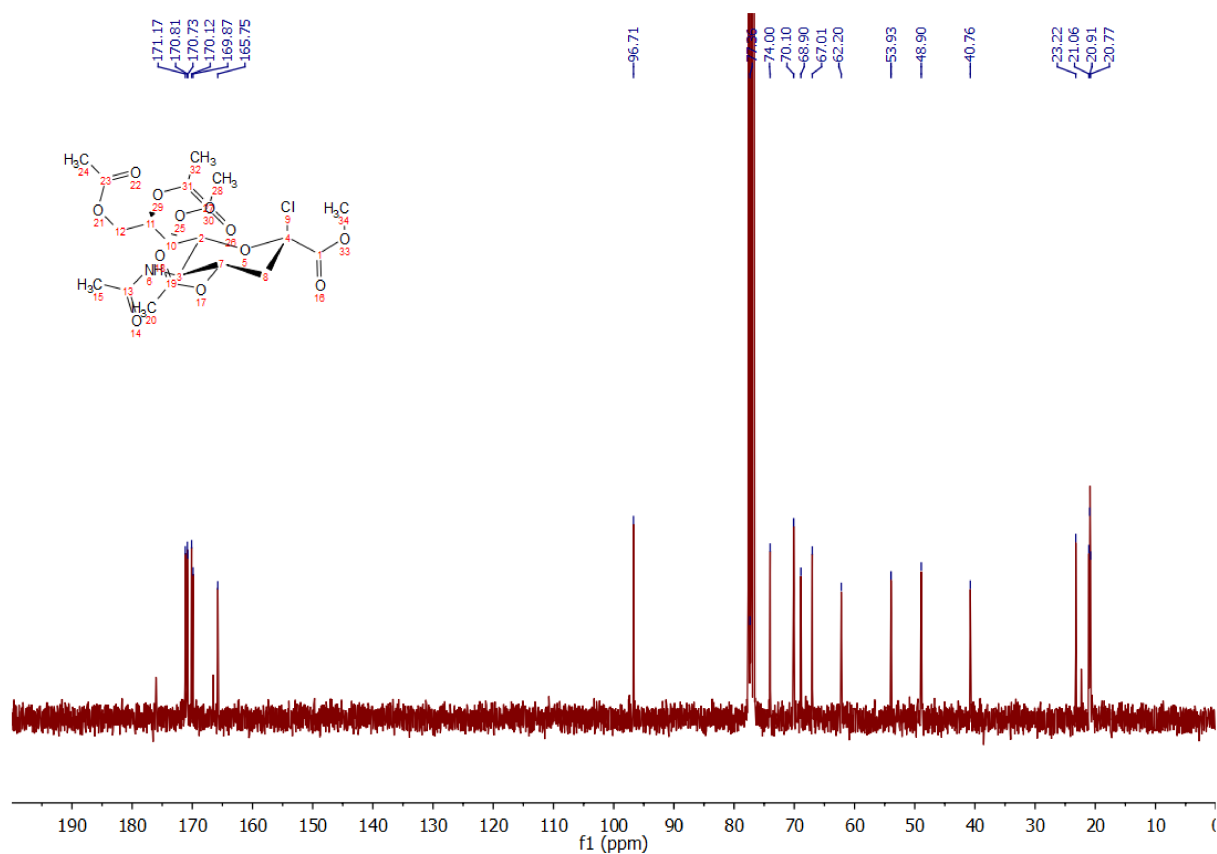
*Figure 5: ^{13}C NMR (75 MHz, Chloroform-d) of compound **c**.*
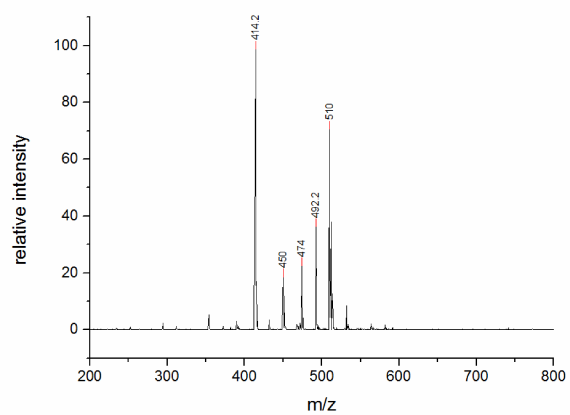
*Figure 6: ESI-MS (positive mode) of compound **c**.*

Methyl 2-(propargyl)-4,7,8,9-tetra-*O*-acetyl-*N*-acetyl-α-D-neuraminate (4)

7.90 g (15.5 mmol) of **c** were dissolved in 50 ml of freshly distilled propargylic alcohol at r.t., then 2 eq. (8.53 g, 30.9 mmol) of Ag$_2$CO$_3$ were added in one portion under rigorous stirring. After 16 h the reaction was stopped by filtering off all solids via vacuum filtration using a pore size 3 frit. The filter cake was washed twice (2x 50 ml) with dichloromethane. The combined organic layers were washed three times with deionized water (3x 100 ml), once with brine (100 ml), dried over MgSO$_4$ and concentrated under reduced pressure in order to give 3.63 g (6.86 mmol, 45%) of the raw product as a slightly yellow foam (α : β = 5 : 1, based on ^{1}H NMR). The raw product was purified via column chromatography (elution gradient EtOAc : nHex = 1 : 1 → pure EtOAc. R$_f$ (EtOAc) = 0.5) in order to afford 2.23 g (4.21 mmol, 28%) of a transparent white foam, which consisted mainly of the α-anomer. Recrystallization from EtOH afforded 1.65 g (3.12 mmol, 20%) of the α-form (**4**) as white crystals.

^{1}H NMR (600 MHz, Chloroform-*d*) δ 5.40 (ddd, ^3J = 8.6, 5.8, 2.8 Hz, 1H, *H8*), 5.30 (dd, ^3J = 8.6, 1.7 Hz, 1H, *H9'*), 5.22 – 5.18 (m, 1H, *-NH*), 4.86 (ddd, ^3J = 12.4, 9.6, 4.7 Hz, 1H, *H4*), 4.39 (dd, ^2J = 15.7, ^4J = 2.5 Hz, 1H, *propargyl-CH'H*), 4.28 (dd, ^3J = 12.4, 2.8 Hz, 1H, *H7*), 4.15 (dd, ^2J = 15.7, ^4J = 2.4 Hz, 1H, *propargyl-CHH''*), 4.10 – 4.02 (m, 3H, *H5, 6, 9''*), 3.80 (s, 3H, *-OCH$_3$*), 2.62 (dd, ^2J = 12.8, ^3J = 4.6 Hz, 1H, *H3eq*.), 2.43 (t, ^4J = 2.4 Hz, 1H, *propargyl-CH*), 2.14 – 2.02 (4s, 4x 3H, 4x *Ac*), 1.97 (dd, ^2J = 12.5 Hz, ^3J = 12.5 Hz, 1H, *H3ax*.), 1.87 (s, 3H, *Ac*).

^{13}C NMR (151 MHz, CDCl$_3$) δ 171.10, 170.76, 170.33, 170.24, 170.20, 167.91, 98.21, 79.07, 74.62, 72.74, 68.96, 68.39, 67.30, 62.53, 52.98 (2), 49.48, 38.01, 23.31, 21.25, 20.98, 20.95, 20.89.

MS for C$_{23}$H$_{31}$NO$_{13}$ (ESI, pos.) m/z: [M + Na$^+$]$^+$ calc.: 552.17; found 552.20, [M + H$^+$]$^+$ calc.: 530.19; found 530.20, [M − C$_3$H$_4$O + H$^+$]$^+$ calc.: 474.16; found 474.25, [M − C$_3$H$_4$O − AcOH + H$^+$]$^+$ calc.: 414.14; found 414.25.

HRMS for C$_{23}$H$_{31}$NO$_{13}$ (ESI-TOF) *m/z*: [M + H$^+$]$^+$ calc.: 530.1874; found: 530.1872.

IR (ATR) $\tilde{v}_{max}$: 3318 (w), 3252 (w), 2957 (w), 1748 (s), 1733 (s), 1648 (m), 1547 (m), 1369 (m), 1207 (s), 1037 (s), 620 (m), 602 (m).
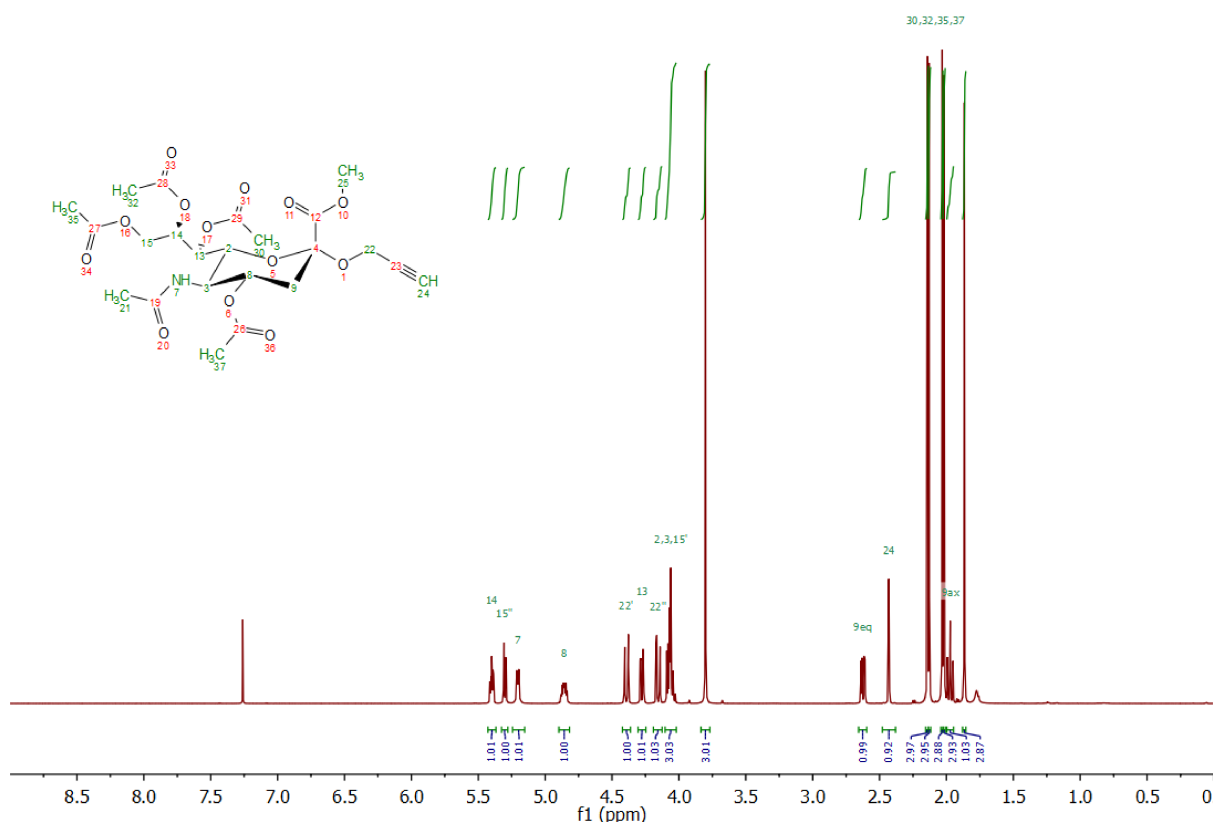
*Figure 7: ^{1}H NMR (600 MHz, Chloroform-d) of compound **4**.*
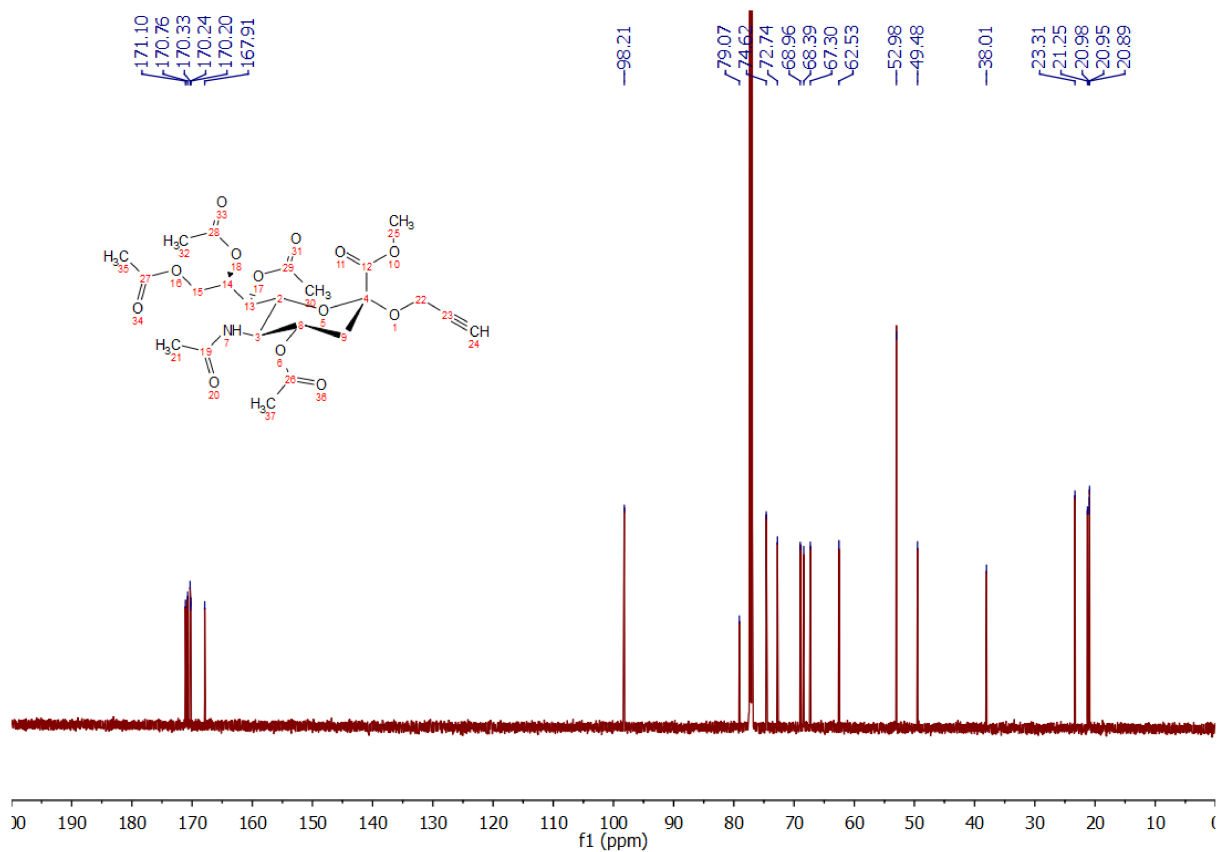
*Figure 8: ^{13}C NMR (151 MHz, Chloroform-d) of compound **4**.*
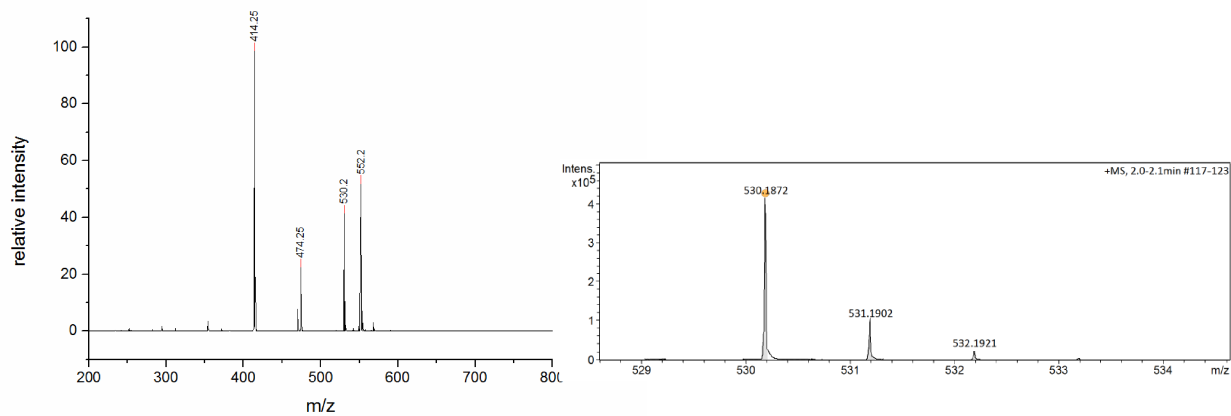
*Figure 9: ESI-MS (positive mode), HR-MS (ESI+ Q-TOF, positive mode) of compound **4**.*

Functionalized 3'-sialyllactose synthesis
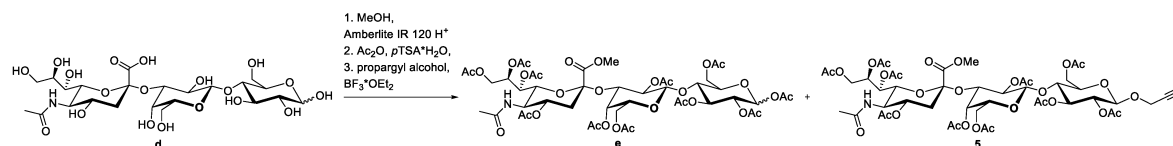
Scheme 2: Synthesis sequence of propargylated 3'-sialyllactose.

500 mg (763 μmol) of 3'sialyllactose sodium salt (**d**) were suspended in 50 mL of methanol before 0.5 g of Amberlite IR 120 H⁺ were added. After 2 days the esterification was complete (monitored by ESI-MS). Then the resin was filtered off and the solution was dried under reduced pressure. To the raw and non-purified product 50 mL of acetonitrile were added, before 3 eq. per alcohol group (3 x 11 x 763 μmol = 25 mmol, 2.4 mL) of acetic anhydride and 0.1 eq. per alcohol of *p*-toluenesulfonic acid monohydrate (0.8 mmol, 160 mg) were added while stirring. The reaction was stirred at 40 °C until the ester was completely dissolved and converted. After the solvent was removed under reduced pressure, the product was redissolved in 50 mL of ethyl acetate and 50 mL of water, washed with 50 mL of sat. sodium bicarbonate solution, twice with water (2 x 50 mL) and 50 mL of brine, dried over magnesium sulfate and concentrated to dryness. 855 mg of the raw product were obtained, which were used without further purification. The obtained, peracetylated raw product was dissolved in 50 mL of dichloromethane before 0.5 mL of propargyl alcohol (8.7 mmol, 11.4 eq.) and 0.3 mL of boron trifluoride diethyl etherate (2.4 mmol, 3.1 eq.) were added. After 3 days the reaction was stopped by the addition of 50 mL of water before the product was washed with water, sat. sodium bicarbonate solution, brine (50 mL each), dried over magnesium sulfate and concentrated in *vacuo*. The product was purified via preparative RP-HPLC (20-80% ACN in water, 0.1% formic acid). 123 mg (111 μmol, 14.6%) of the desired, propargyl functionalized **Methyl 1-(propargyl)-deca-*O*-acetyl-β-3'sialyllactoside (5)** was obtained in an α : β ratio of 10% : 90% (based on ¹H NMR) and 130 mg (117 mg, 15.3 %) of the unconverted **Methyl α,β-undeca-*O*-acetyl-3'sialyllactoate (e)** was obtained in an α : β ratio of about 70% : 30% (based on ¹H NMR).

Methyl α,β-undeca-*O*-acetyl-3'-Sialyllactoate (e)

(Methyl (4,7,8,9-tetra-*O*-acetyl-*N*-actetyl-neuraminate)yl-(2→3)-2,4,6-tri-*O*-acetyl-β-galactopyranosyl-(1→4) - 1,2,3,6-tetra-*O*-acetyl-α,β-glucopyranose (e)

¹H NMR (600 MHz, Chloroform-*d*) δ **Glc:** 6.23 (d, ³*J* = 3.6 Hz, 1H, *H1*), 5.00 (dd, ³*J* = 10.3, 3.7 Hz, 1H, *H2*), 5.44 (dd, ³*J* = 10.3, 9.2 Hz, 1H, *H3*), 3.89 (dd, ³*J* = 10.1, 9.2 Hz, 1H, *H4*), 3.85 − 3.83 (m, 1H, *H5*), 4.19 (dd, ²*J* = 12.1, ³*J* = 4.5 Hz, 1H, *H6'*), 4.37 (dd, ²*J* = 12.1, ³*J* = 2.2 Hz, 1H, *H6''*); **Gal:** 4.63 (d, ³*J* = 8.0 Hz, 1H, *H1*), 4.92 (dd, ³*J* = 10.2, 7.9 Hz, 1H, *H2*), 4.50 (dd, ³*J* = 10.2, 3.5 Hz, 1H, *H3*), 4.90 − 4.84 (m, 1H, *H4*), 4.05 − 3.95 (m, 1H, *H5*), 4.05 − 3.95 (m, 2H, *H6', 6''*); **Neu5Ac:** 3.83 (s, 3H, -*OCH₃*), 1.78 (dd, ²*J* = 13.9 Hz, ³*J* = 11.5, 0.23H, β-*H3ax.*), 1.66 (dd, ²*J* = 12.4 Hz, ³*J* = 12.4 Hz, 0.77H, α-*H3ax.*), 2.56 (dd, ²*J* = 12.7, ³*J* = 4.6 Hz, 0.68H, α-*H3eq.*), 2.44 (dd, ²*J* = 13.7, ³*J* = 5.2 Hz, 0.32H, β-*H3eq.*), 4.90 − 4.84 (m, 1H, *H4*), 4.05 − 3.95 (m, 1H, *H5*), 5.17 (d, *J* = 10.2 Hz, 1H, -*NH*), 3.62 (dd, ³*J* = 10.8, 2.8 Hz, 1H, *H6*), 5.39 (dd, ³*J* = 9.4, 2.8 Hz, 1H, *H7*), 5.48 (ddd, ³*J* = 9.4, 4.6, 2.8 Hz, 1H, *H8*), 4.41 (dd, ²*J* = 12.8, ³*J* = 2.8 Hz, 1H, *H9'*), 4.05 − 3.95 (m, 1H, *H9''*), 2.23 − 1.84 (12s, 12x 3H, 12x *Ac*).

¹³C NMR (151 MHz, Chloroform-*d*) δ 170.98, 170.77, 170.77, 170.54, 170.54, 170.42, 170.35, 170.11, 169.76, 169.71, 169.67, 169.15, 168.05, 101.19, 96.87, 89.17, 75.89, 72.12, 71.50, 70.82, 70.61, 70.09, 70.05, 69.62, 69.42, 67.90, 67.37, 66.88, 62.15, 61.87, 61.68, 53.28, 49.24, 37.51, 23.28, 21.65, 21.11, 21.08, 20.95, 20.91, 20.89, 20.86, 20.84, 20.81, 20.74, 20.64.

RP-HPLC-MS (linear gradient from 0 − 75% eluent B in 30 min at 25° C): t_R = 21.00 min.

MS for $C_{46}H_{63}NO_{30}$ (ESI, pos.) *m/z*: [M + Na⁺]⁺ calc.: 1132.33; found: 1132.25, [M - $C_{14}H_{19}O_{10}$ (Glc)⁻]⁺ calc.: 762.25; found: 762.20. HRMS for $C_{46}H_{63}NO_{30}$ (ESI-TOF) *m/z*: [M + H⁺]⁺ calc.: 1110.3508; found: 1110.3500.
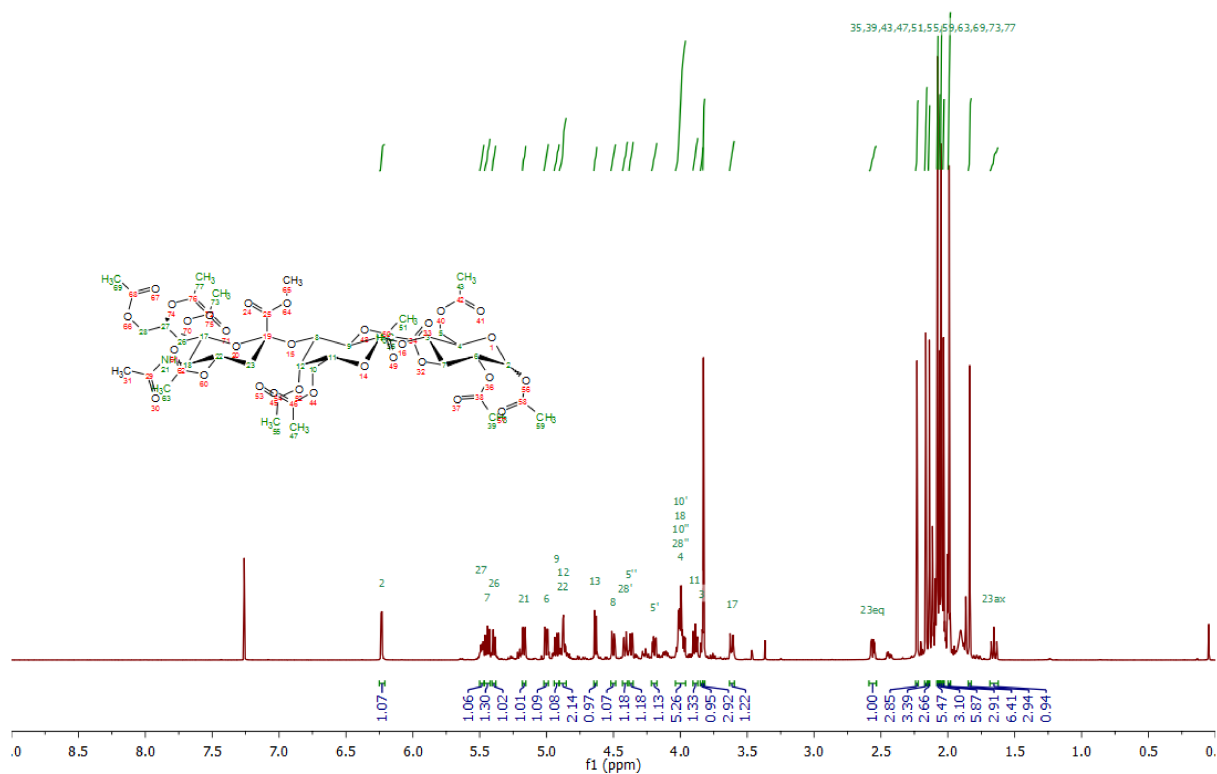
*Figure 10: ^{1}H NMR (600 MHz, Chloroform-d) of compound **e**.*
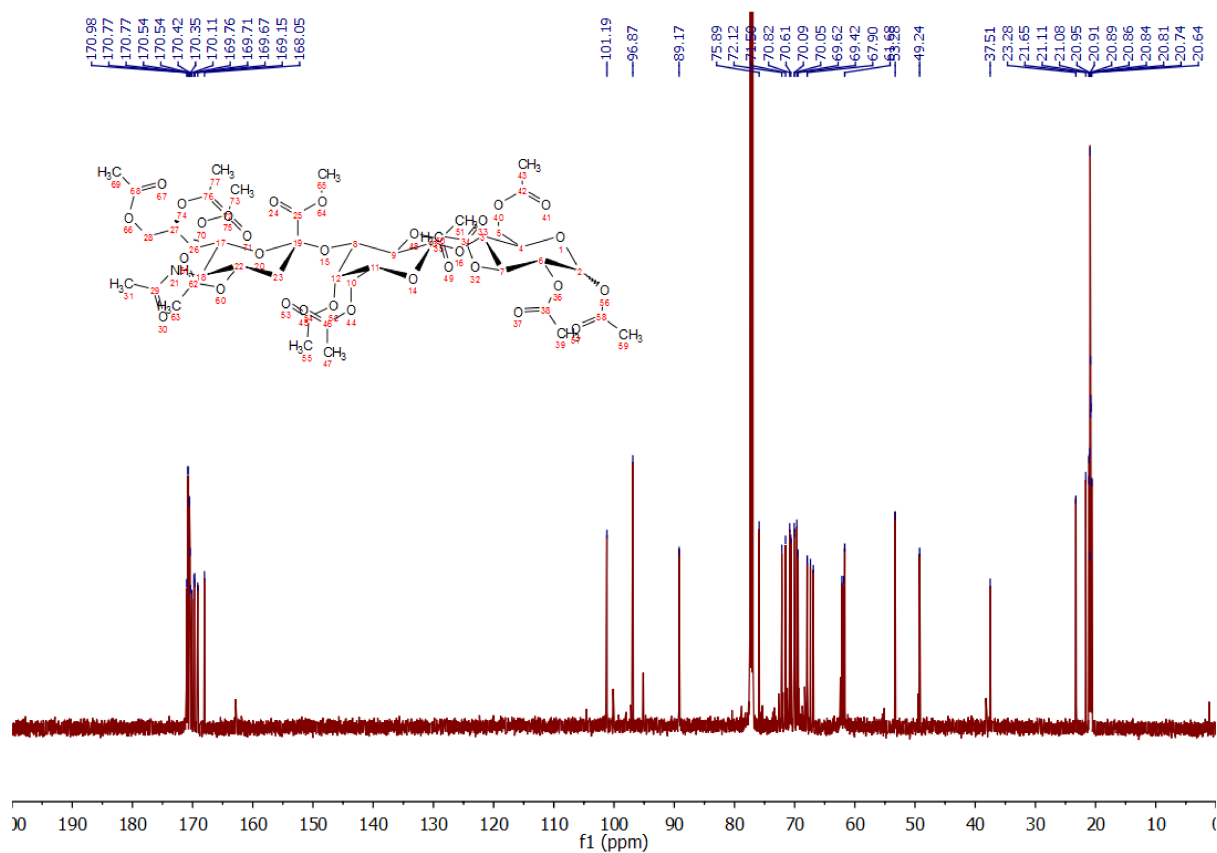
*Figure 11: ^{13}C NMR (151 MHz, Chloroform-d) of compound **e**.*
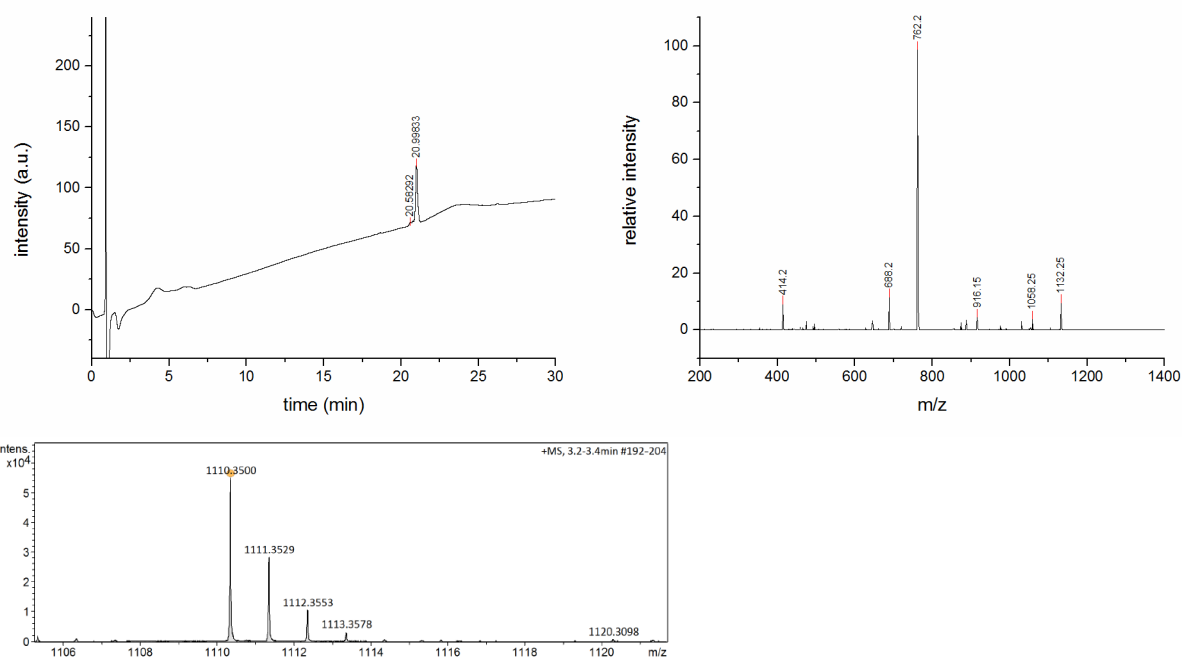
*Figure 12: RP-HPLC (linear gradient from 0 - 75% eluent B in 30 min at 25°C), ESI-MS (positive mode), HR-MS (ESI+ Q-TOF, positive mode) of compound **e**.*

Methyl 1-(propargyl)-deca-*O*-acetyl-β-3'Sialyllactoside (5)

(Methyl (4,7,8,9-tetra-*O*-acetyl-*N*-actetyl-neuraminate)yl-(2→3)-2,4,6-tri-*O*-acetyl-β-galactopyranosyl-(1→4) -1-(propargyl)-(2,3,6-tri-*O*-acetyl-β-glucopyranoside (5)

¹H NMR (600 MHz, Chloroform-*d*) δ **Propargyl:** 4.33 (d, ^4J = 2.5 Hz, 2H, *propargyl-CH₂*), 2.45 (t, ^4J = 2.4 Hz, 0.9H, *β-propargyl-CH*), 2.42 (t, ^4J = 2.4 Hz, 0.1H, *α-propargyl-CH*); **Glc:** 4.73 (d, ^3J = 7.9 Hz, 1H, *H1*), 4.94 – 4.89 (m, 1H, *H2*), 5.20 (dd, ^3J = 9.3, 9.3 Hz, 1H, *H3*), 3.85 – 3.80 (m, 1H, *H4*), 4.04 – 3.95 (m, 1H, *H5*), 4.45 (dd, ^2J = 12.1, ^3J = 2.1 Hz, 1H, *H6'*), 4.18 (dd, ^2J = 12.1, ^3J = 5.3 Hz, 1H, *H6''*); **Gal:** 4.65 (d, ^3J = 8.0 Hz, 1H, *H1*), 4.94 – 4.89 (m, 1H, *H2*), 4.50 (dd, ^3J = 10.2, 3.3 Hz, 1H, *H3*), 4.88 – 4.85 (m, 1H, *H4*), 3.91 – 3.86 (m, 1H, *H5*), 4.04 – 3.95 (m, 4H, *H6', 6''*); **Neu5Ac:** 3.83 (s, 3H, *OCH₃*), 1.66 (dd, ^2J = 12.4 Hz, ^3J = 12.4 Hz, 1H, *H3ax.*), 2.56 (dd, ^2J = 12.6, ^3J = 4.6 Hz, 1H, *H3eq.*), 4.88 – 4.85 (m, 1H, *H4*), 4.04 – 3.95 (m, 1H, *H5*), 5.15 (d, ^3J = 10.3 Hz, 1H, *-NH*), 3.66 – 3.60 (m, 1H, *H6*), 5.38 (dd, ^3J = 9.3, 2.8 Hz, 1H, *H7*), 5.52 (ddd, ^3J = 9.4, 5.1, 2.8 Hz, 1H, *H8*), 4.40 (dd, ^2J = 12.7, ^3J = 2.8 Hz, 1H, *H9'*), 4.04 – 3.95 (m, 1H, *H9''*), 2.23 – 1.84 (11s, 11x 3H, 11x *Ac*).

¹³C NMR (151 MHz, Chloroform-*d*) δ 171.00, 170.77, 170.76, 170.61, 170.53, 170.45, 170.37, 169.96, 169.90, 169.75, 169.68, 168.05, 101.06, 98.04, 96.89, 78.29, 76.23, 75.52, 73.35, 72.91, 72.12, 71.52, 71.49, 70.60, 70.02, 69.43, 67.88, 67.42, 66.99, 62.31, 62.24, 61.67, 56.02, 53.28, 49.22, 37.51, 23.29, 21.65, 21.07, 20.96, 20.91, 20.88, 20.82, 20.80, 20.77, 20.75, 20.63.

RP-HPLC-MS (linear gradient from 0 – 75% eluent B in 30 min at 25° C): t_R = 21.63 min.

MS for $C_{47}H_{63}NO_{29}$ (ESI, pos.) *m/z*: $[M + Na^+]^+$ calc.: 1128.34; found: 1128.15, $[M - C_{14}H_{19}O_{10}\ (Glc)^-]^+$ calc.: 762.25; found: 762.20.

HRMS for $C_{47}H_{63}NO_{29}$ (ESI-TOF) *m/z*: $[M + H^+]^+$ calc.: 1106.3559; found: 1106.3552.
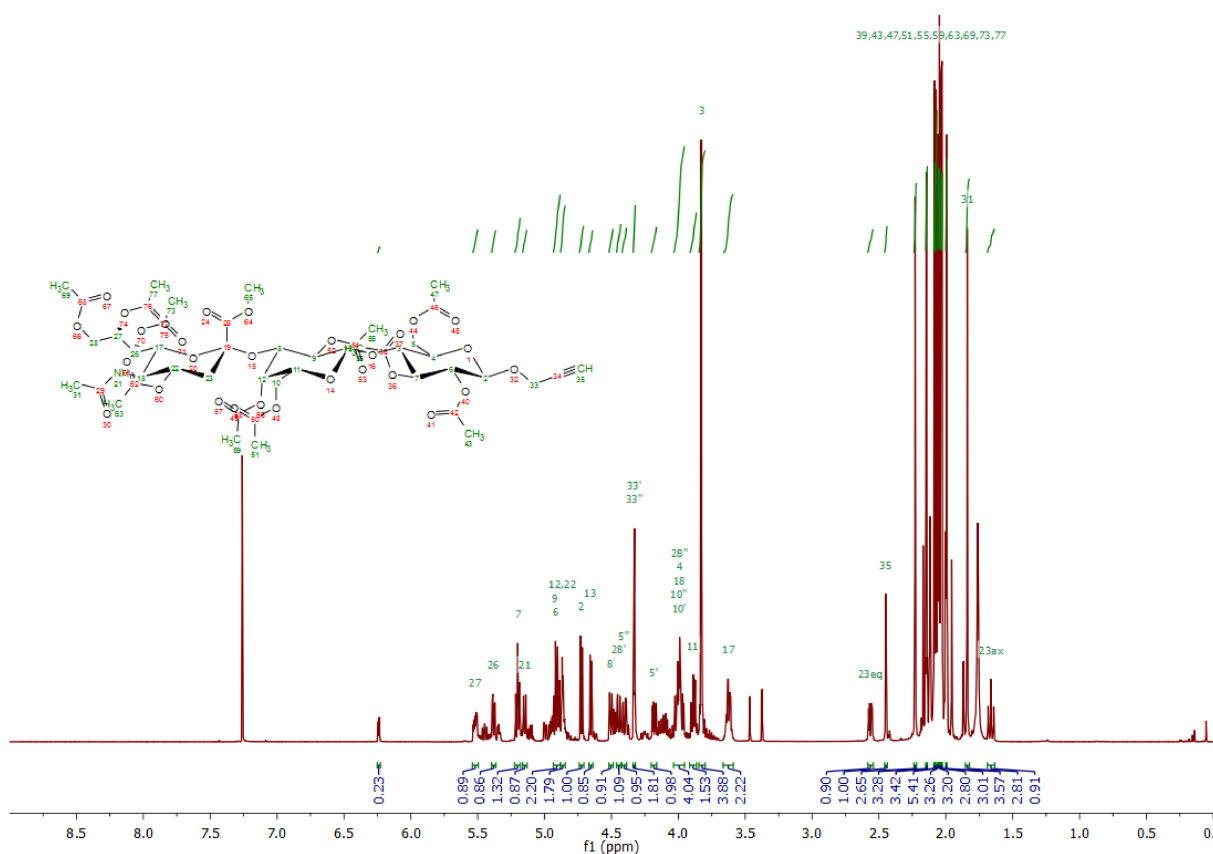
*Figure 13: ¹H NMR (600 MHz, Chloroform-d) of compound **5**.*
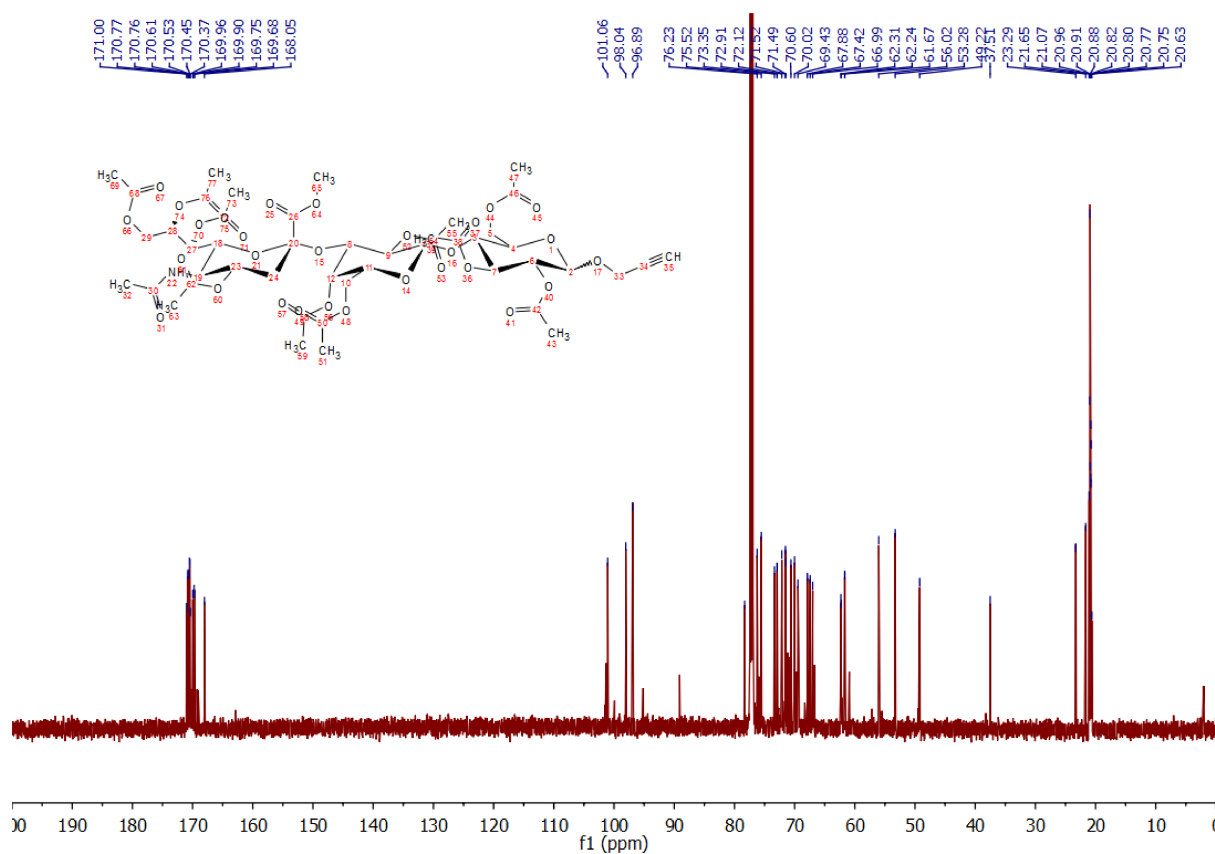
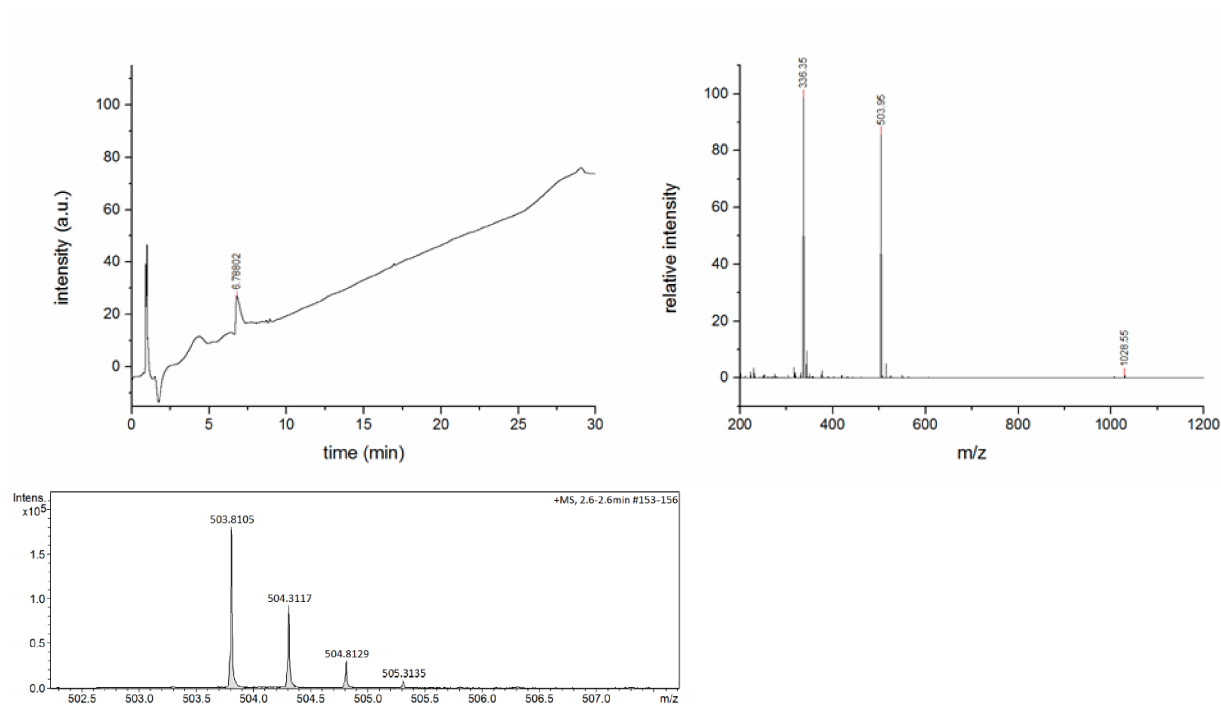*Figure 14: ^{13}C NMR (151 MHz, Chloroform-d) of compound **5**.*
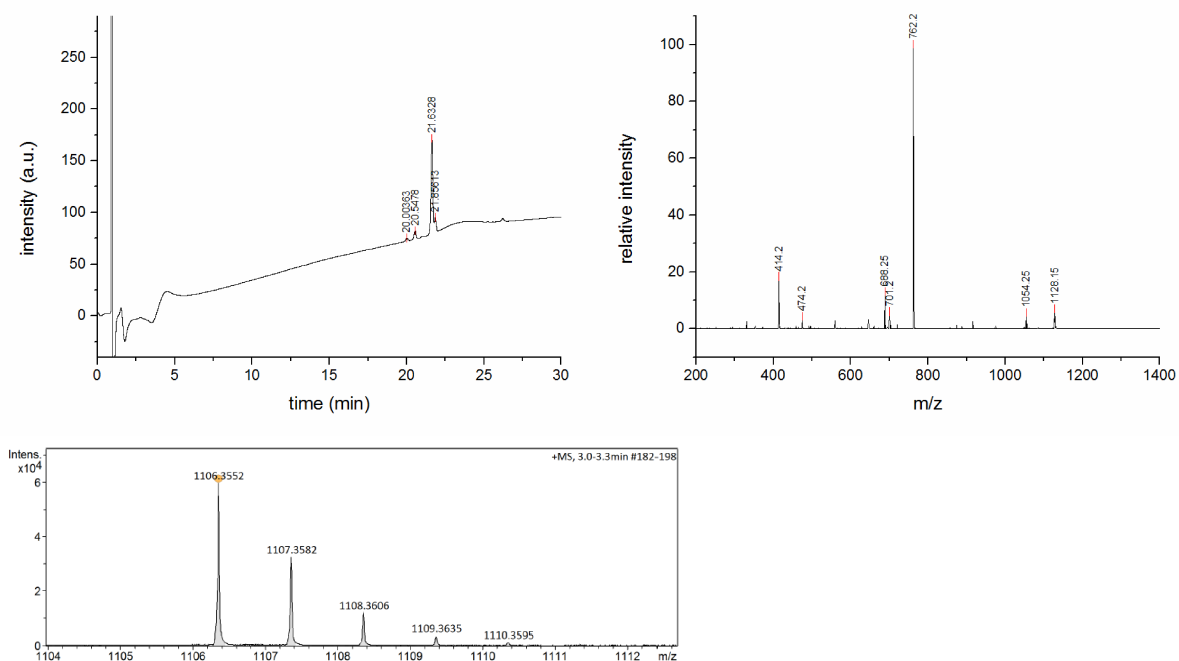
Figure 15: RP-HPLC (linear gradient from 0 - 75% eluent B in 30 min at 25°C), ESI-MS (positive mode), HR-MS (ESI+ Q-TOF, positive mode) of compound 5.

Heparin fragments

Heparin-dp2 (6)
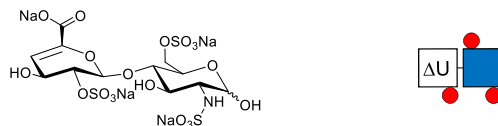
5 g of porcine sodium heparin (MW 15-19 kDa) were dissolved in 50 mM TRIS pH 7.5, 5 mM $CaCl_2$, 100 mM NaCl, with bovine serum albumin added to 5 mg/mL in a final volume of 40 mL. Heparinase I from *Flavobacterium heparinum* was added to 0.26 I.U. per gram of sodium heparin and the reaction was incubated for several days at 37 °C. The reaction progress was followed at different time points by applying 5-20 μL of the reaction mixture onto analytical gel filtration column (Superdex Peptide 10/300 GL, GE Healthcare) and monitoring the UV absorption at 232 nm. After four days, the cleavage reaction was heat-inactivated and 2 mL of the reaction mixture were filtered at 0.2 μm and loaded onto a self-cast preparative gel filtration column (Bio-Gel P-10 superfine 2.6 cm x 170 cm, Bio-Rad) equilibrated with 50 mM TRIS at pH 7.5, 5 mM $CaCl_2$, 100 mM NaCl, 0.02 (w/v) % sodium azide. The flow rate was set to 0.2 mL/min, the absorbance at 232 nm was monitored, and 5 mL fractions were collected. Dp2-containing fractions were pooled and freeze-dried. For desalting, the freeze-dried material was dissolved in deionized water, filtered and applied to a HiPrep Desalting 26/10 column (Sephadex G-25 superfine resin, GE Healthcare) using deionized water as running buffer and monitoring the absorbance at 280 nm. Both chromatography steps were conducted at 4 °C. Desalted dp2 was again freeze-dried and stored at -20 °C. Approximately 210 mg (326 μmol, 4.2%, residual sodium chloride) of the Heparin-dp2 fragment were obtained in a purity greater than 99% (SAX-HPLC)

^{1}H NMR (600 MHz, Deuterium Oxide) δ 5.99 (dd, ^3J = 4.6, ^4J = 1.2 Hz, 1H, *ΔUA-H4*), 5.54 (dd, ^3J = 3.6 Hz, ^4J = 1.1 Hz, 1H, *ΔUA -H1*), 5.47 (d, ^3J = 3.6 Hz, 1H, *GlcN-H1*), 4.63 (ddd, ^3J = 3.1, ^3J = 2.9, ^4J = 1.3 Hz, 1H, *ΔUA -H2*), 4.41 − 4.28 (m, 2H, *ΔUA -H3, GlcN-H6'*), 4.24 (dd, ^2J = 11.2, ^3J = 2.2 Hz, 1H, *GlcN-H6''*), 4.18 (ddd, ^3J = 10.2, 3.7, 2.0 Hz, 1H, *GlcN-H5*), 3.89 (dd, ^3J = 9.9, 8.6 Hz, *GlcN-H4*), 3.81 − 3.75 (m, 1H, *GlcN-H3*), 3.30 (dd, ^3J = 10.4, 3.6 Hz, 1H, *GlcN-H2*). ^{13}C NMR (151 MHz, ACN-*d3*) δ 168.15, 143.86, 105.55, 96.00, 90.19, 77.67, 74.04, 68.13, 67.07, 65.74, 62.41, 56.81.

SAX – HPLC (isocratic elution in 40 mM Na_2HPO_4, 25 mM KH_2PO_4 in Milli-Q water in 20 min at 25° C): t_R = 9.93 min. Determined purity: > 99%.

MS for $C_{12}H_{15}NNa_4O_{19}S_3$ (ESI, neg.) m/z: $[M - 2Na^+ + H^+]^-$ calc.: 619.93; found 619.90, $[M - 3Na^+ + 2H^+]^-$ calc.: 597.95; found 597.85, $[M - 4Na^+ + 3H^+]^-$ calc.: 575.96; found 575.85, $[M - 3Na^+ + 2H^+ - SO_3]^-$ calc.: 517.99; found 517.90, $[M - 4Na^+ + 3H^+ - SO_3]^-$ calc.: 496.01; found 496.00.IR

IR (ATR) $\tilde{v}_{max}$: 3185 (s), 2384 (m), 1610 (m), 1402 (m), 1222 (s), 1040 (s), 994 (s), 583 (s).
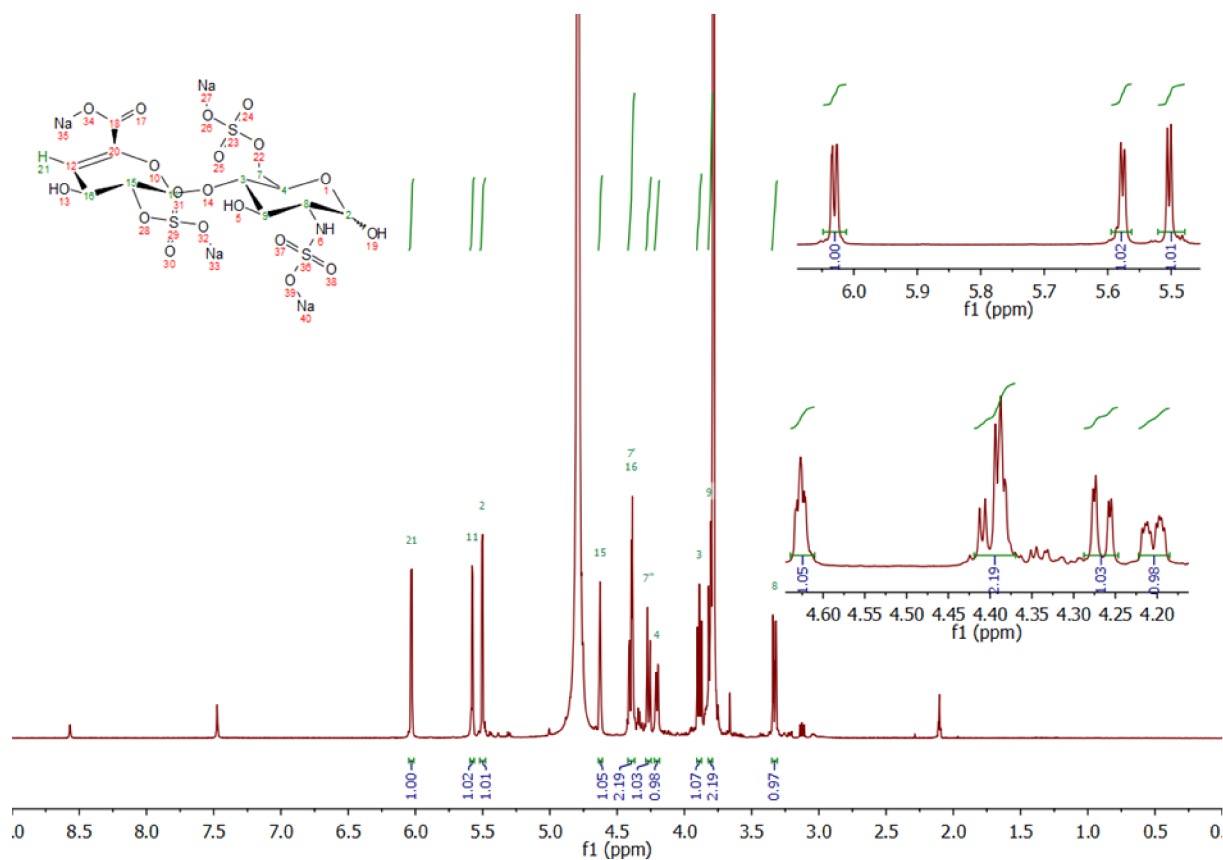
Figure 16: *H NMR (600 MHz, Deuterium oxide) of compound **Heparin-dp2**.*
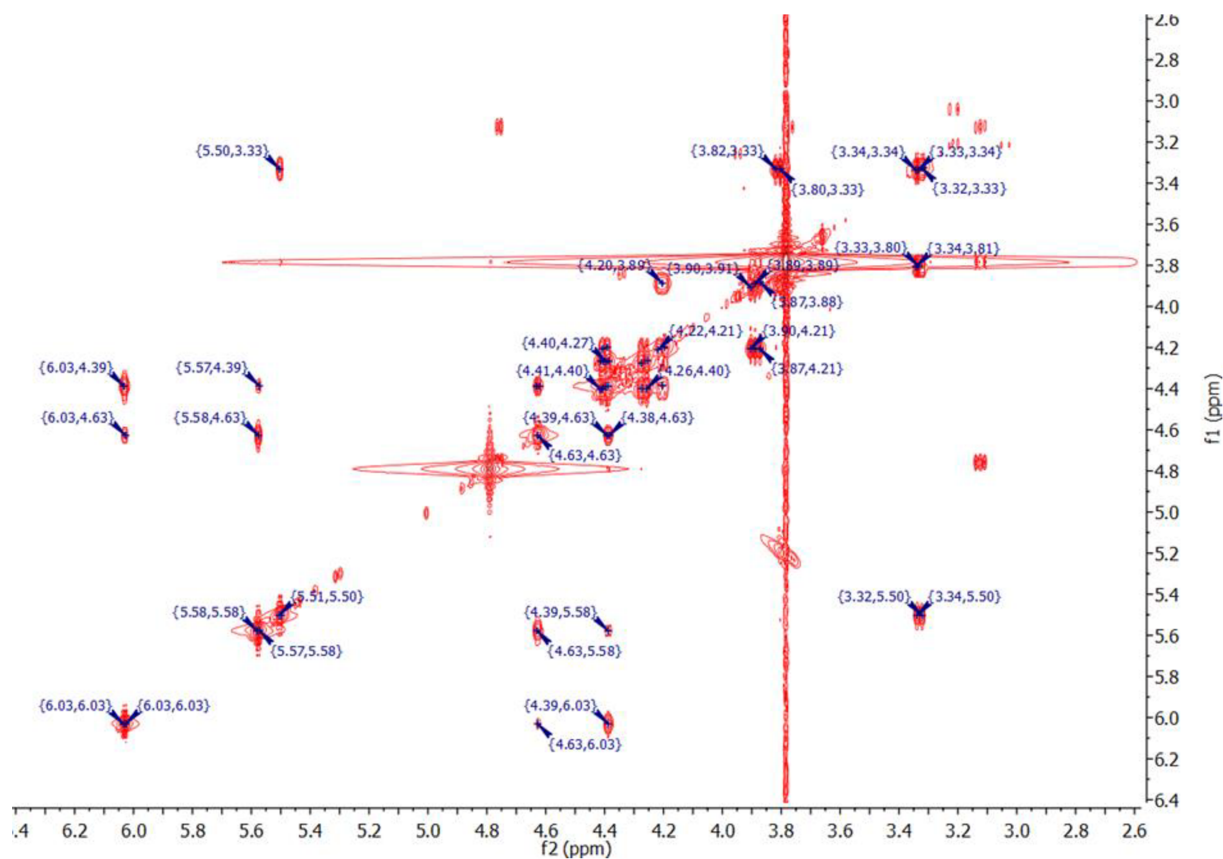
Figure 17: *H COSY NMR (600 MHz, Deuterium oxide) of compound **Heparin-dp2**.*
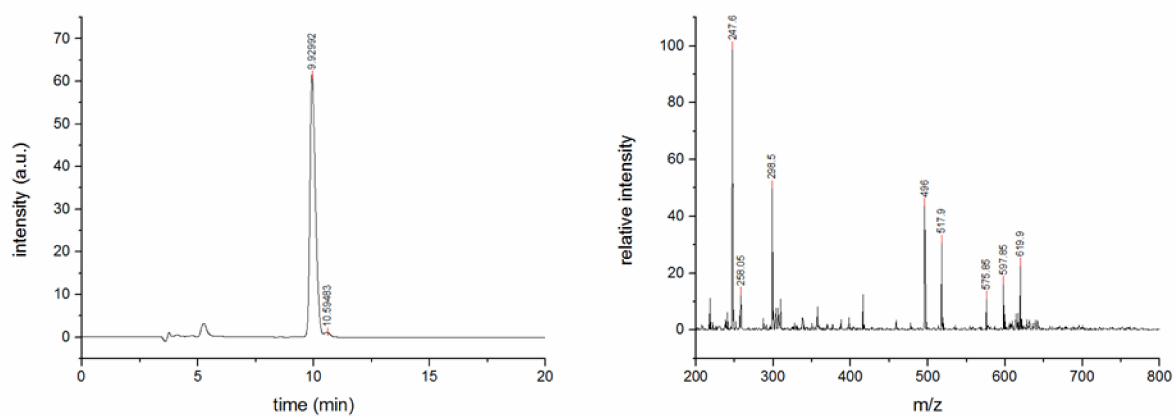
*Figure 18: SAX-HPLC (isocratic elution in 40 mM Na$_2$HPO$_4$, 25 mM KH$_2$PO$_4$ in Milli-Q water in 20 min at 25° C), ESI-MS (negative mode) of compound **O3**.*

Fondaparinux®-sodium
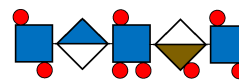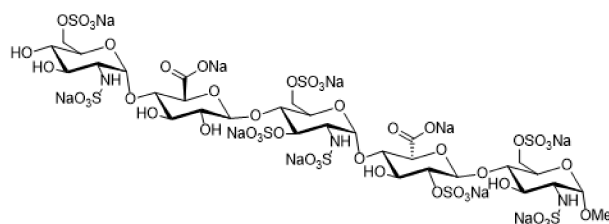
Fondaparinux-sodium was purchased as Arixtra® at a concentration of 10 mg / 0.8 mL from the Aspen Pharma Trading Limited as ready-to-use syringes. The content of 10 syringes (each of them containing 10 mg Fondaparinux-sodium in 0.8 mL of sodium chloride solution) was dialyzed by the use of a Spectra/Por® Float-A-Lyzer® G2 10 mL unit with a MWCO of 0.1 – 0.5 kDa in order to remove excess of sodium chloride. 98.8 mg (57.1 μmol, 99%) of Fondaparinux were isolated and further analysed.

^{1}H NMR (600 MHz, Deuterium Oxide) δ 5.67 (d, ^3J = 3.8 Hz, 1H, A_S^{nr}-H1), 5.54 (d, ^3J = 3.5 Hz, 1H, A_S^*-H1), 5.23 (d, ^3J = 3.8 Hz, 1H, I_S-H1), 5.06 (d, ^3J = 3.6 Hz, 1H, A_S^r-H1), 4.77 – 4.76 (m, 1H, I_S-H5), 4.67 (d, ^3J = 7.9 Hz, 1H, G-H1), 4.53 (d, ^3J = 10.0 Hz, 1H, A_S^*-H3), 4.45 – 4.31 (m, 6H, A_S^{nr}-H6', A_S^*-H6', 6'', I_S-H2, A_S^r-H6', 6''), 4.24 – 4.16 (m, 4H, A_S^{nr}-H6'', A_S^*-H5, I_S-H3, 4), 4.05 – 3.97 (m, 2H, A_S^*-H4, A_S^r-H5), 3.96 – 3.84 (m, 3H, A_S^{nr}-H5, G-H3, 4), 3.81 (m, 2H, G-H5, A_S^*-H4), 3.69 (dd, ^3J = 10.6, 9.0 Hz, 1H, A_S^r-H3), 3.69 – 3.58 (m, 2H, A_S^{nr}-H3, 4), 3.49 (dd, ^3J = 10.7, 3.4 Hz, 1H, A_S^*-H2), 3.46 (s, 4H, G-H2, -OMe), 3.31 (2dd, ^3J = 14.0, 10.3, 3.7 Hz, 2H, A_S^{nr}-H2, A_S^r-H2).

MS for $C_{31}H_{43}N_3Na_{10}O_{49}S_8$ (ESI, neg.) m/z: [M - 2Na$^+$]$^{2-}$ calc.: 840.40; found 840.30, [M - 3Na$^+$ + H$^+$]$^{2-}$ calc.: 829.41; found 829.35, [M - 4Na$^+$ + 2H$^+$]$^{2-}$ calc.: 818.41; found 818.40, [M - 5Na$^+$ + 3H$^+$]$^{2-}$ calc.: 807.42; found 807.55, [M - 6Na$^+$ + 4H$^+$]$^{2-}$ calc.: 796.43; found 796.40, [M - 7Na$^+$ + 5H$^+$]$^{2-}$ calc.: 785.44; found 785.6.

IR (ATR) $\tilde{v}_{max}$: 3413 (br), 1615 (m), 1419 (m), 1222 (s), 1097 (s), 992 (s), 817 (m), 580 (s).
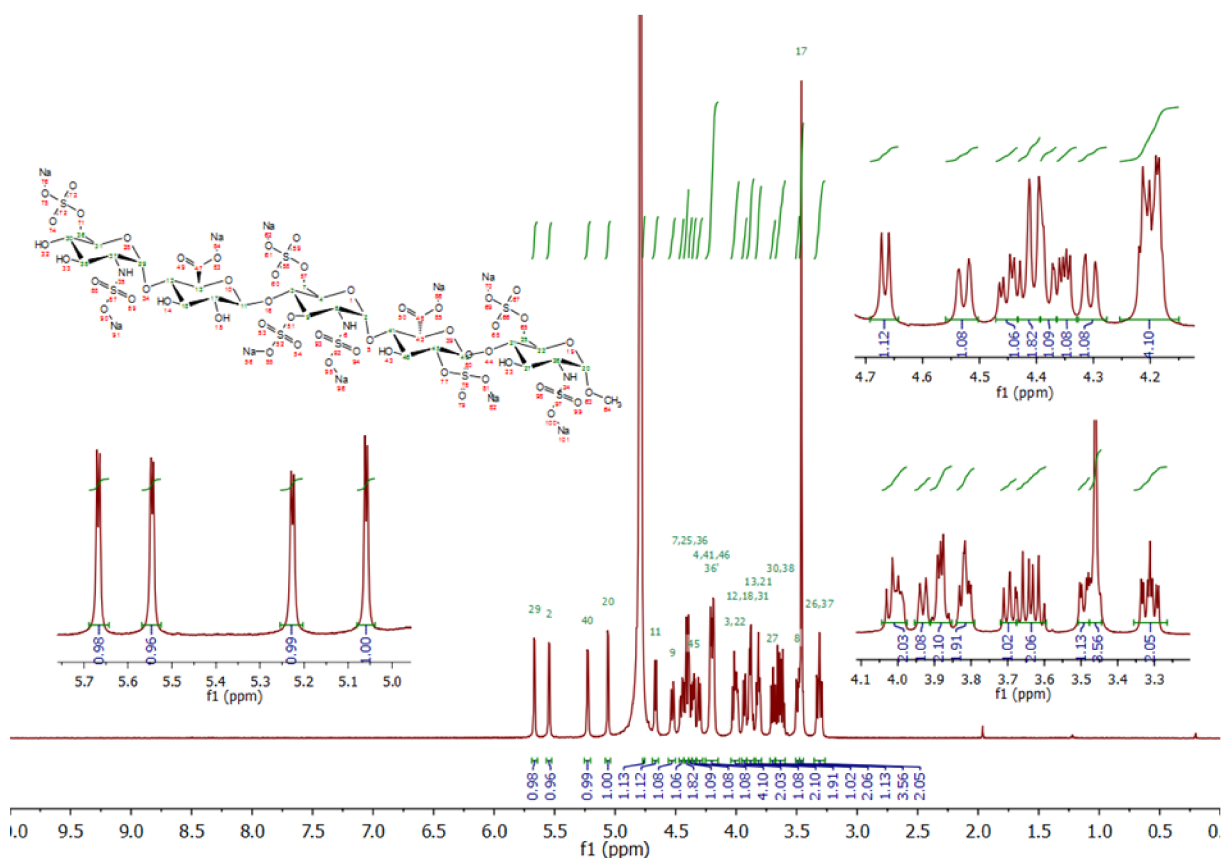
*Figure 19: ^{1}H NMR (600 MHz, Deuterium oxide) of compound **Fondaparinux® sodium**.*
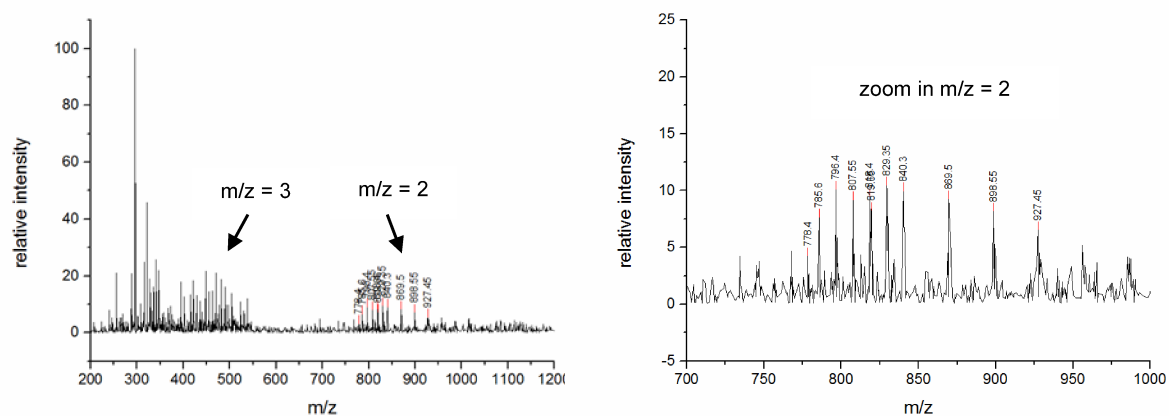
Figure 20: ESI-MS (negative mode) of compound **Fondaparinux®-sodium.** The m/z = 2 area was analysed.

Solid phase synthesis approach for coupling of unprotected glucuronic acid
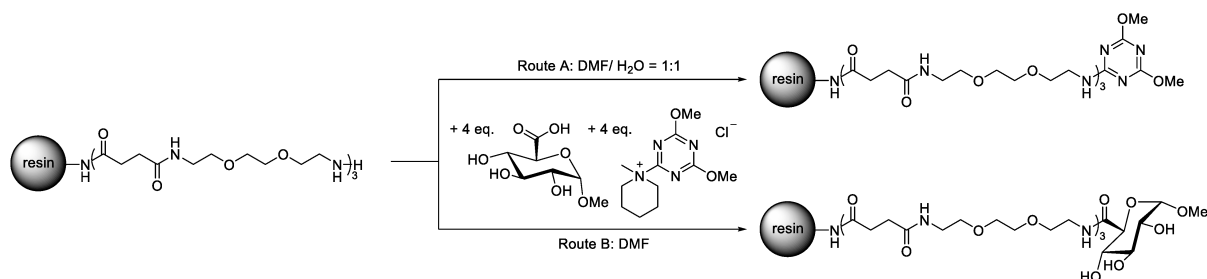
Scheme 3: Synthesis scheme of the DMTMM mediated coupling of unprotected GlcA to a resin-bound oligomer.
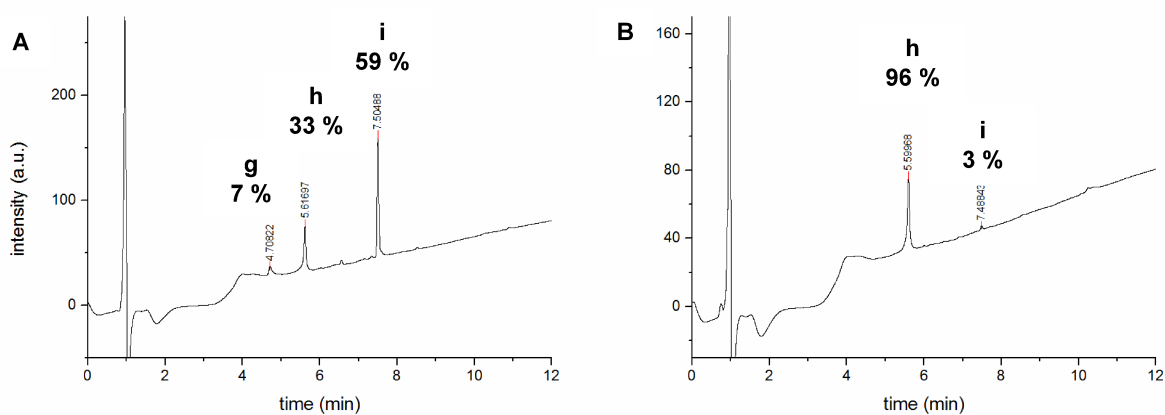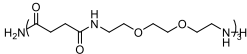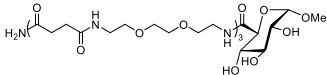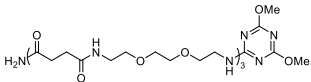
Figure 21: RP-HPLC (linear gradient from 0 – 50% eluent B in 12 min at 25° C) of the investigated Oligomer-GlcA Amide conjugates.

The resin-bound oligomeric sequence (EDS)₃ was synthesized in a 40 μmol batch size according the standard solid phase synthesis protocol using Tentagel® S RAM for test purposes. Microcleavage showed a purity of 98% (data not shown) before further conversion. The test batch was split into two, then methyl-α-D-glucuronic acid (**f**) was coupled using either a 1:1 mixture of DMF and water (**Route A**) or using pure DMF (**Route B**). Four equivalents of the carbohydrate and the coupling agent were used and double coupling was performed. GlcA was preactivated for 60 min with DMTMM in the appropriate solvent before the mixture was given to the resin-bound amine and shaken for another 60 min. Microcleavage was performed and analyzed via RP-HPLC-MS. The use of a 1:1 mixture of DMF and water led primarily to the formation of the amine-triazine product **i**, whereby the choice of pure DMF as solvent led to nearly full conversion to the desired oligoamidoamine-GlcA adduct **h**.

Table 1. Observed products after the conversion of the resin-bound oligomer -(EDS)$_3$- with methyl-α-D-glucuronic acid (**f**) using a 1:1 mixture of DMF and water (**A**) or pure DMF (**B**)

Product[a] [#]	Structure	Retention time [min]	MW[b] [Da]	Product Composition Route A[c] [%]	Product Composition Route B[c] [%]
g		4.71	calc.: 708.41, found: 708.40.	7	0
h		5.61	calc.: 898.46, found: 898.50.	33	96
i		7.49	calc.: 847.45, found: 847.40.	59	3

[a] Products were identified via RP-HPLC-MS; [b] Monoisotopic mass detected as [M + H$^+$]$^+$; [c] Based on the absorption integrals after microcleavage, test batch was not isolated quantitatively, non-normalized data.

Methyl-α-D-glucuronic acid (f)
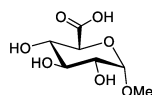
Methyl-α-D-glucuronic acid (f) was synthesized according the method described by Adorjan *et al.*[5]

5.00 g (25.75 mmol) of methyl α-D-glucopyranoside, 1.32 g (12.9 mmol) of sodium bromide and 40 mg (0.256 mmol) of TEMPO ((2,2,6,6-tetramethylpiperidinyl) oxyl radical) were dissolved in 250 ml distilled water and cooled to 0°C. Sodium hypochloride solution (60 ml, 13%, 105 mmol) was added dropwise while keeping the pH within 10-11 with sodium hydroxide solution (0.5 M). The reaction mixture was stirred overnight. Excess of sodium hypochloride was deactivated by addition of methanol (50 ml) before the solvent was removed under diminished pressure to half volume. Salts (sodium chloride, sodium bromide), which crystallized by cooling were filtered off. The yellowish supernatant was pipetted off and adjusted to pH 3 with concentrated hydrochloric acid. Hereafter it was precipitated in diethyl ether to remove remaining salts. The solvent was removed under reduced pressure and the product was lyophilized from 60 ml distilled water. 2.65 g (11.55 mmol, 45%) of the product **f** were obtained as yellow powder.

^{1}H NMR (600 MHz, Deuterium Oxide) δ 4.89 (d, ^3J = 3.7 Hz, 1H, *H1)*, 3.96 (d, ^3J = 10.1 Hz, 1H, *H5)*, 3.75 (dd, ^3J= 9.4, 9.4, 1H, *H3)*, 3.67 (dd, ^3J= 3.8, 9.8, 1H, *H2)*, 3.56 (dd, ^3J = 10.1, 9.0, 1H, *H4)*, 3.49 (s, 3H, *-OCH₃)* ppm.

^{13}C NMR (151 MHz, D$_2$O) δ 176.69 (*Carbonyl-C*), 99.37 (*Acetal-C*), 72.94, 72.03, 71.99, 71.09, 55.30 (*CH₃*).

MS for C$_7$H$_{12}$O$_7$ (ESI, pos.) m/z: [2M+Na$^+$]$^+$: calc.: 439.10; found: 439.00, [M + Na$^+$]$^+$: calc.: 231.08; found: 231.00.

IR (ATR) $\tilde{v}_{max}$: 3270 (b), 2912 (b), 2862 (w), 1604 (υ, (s), 1417 (s), 1038 (s).
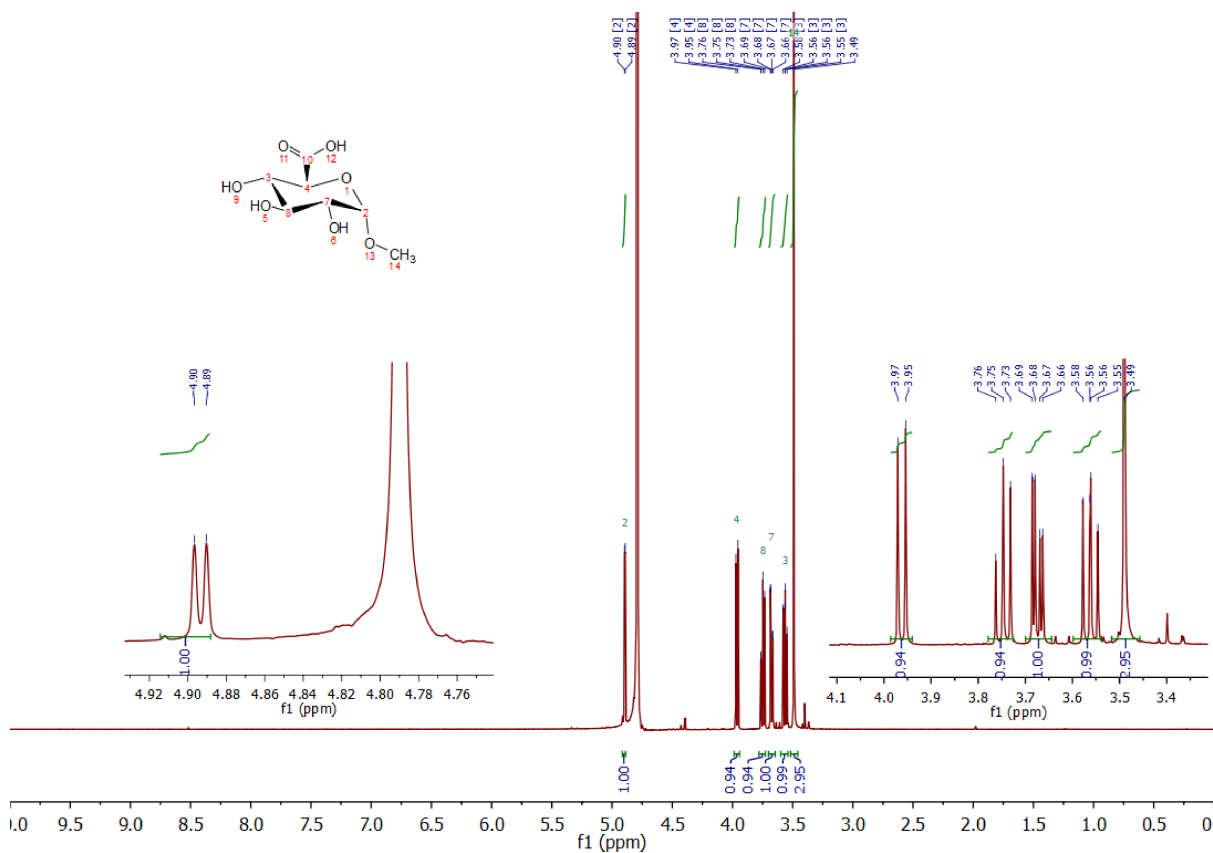
Figure 22: ^{1}H NMR (600 MHz, Deuterium oxide) of compound f.
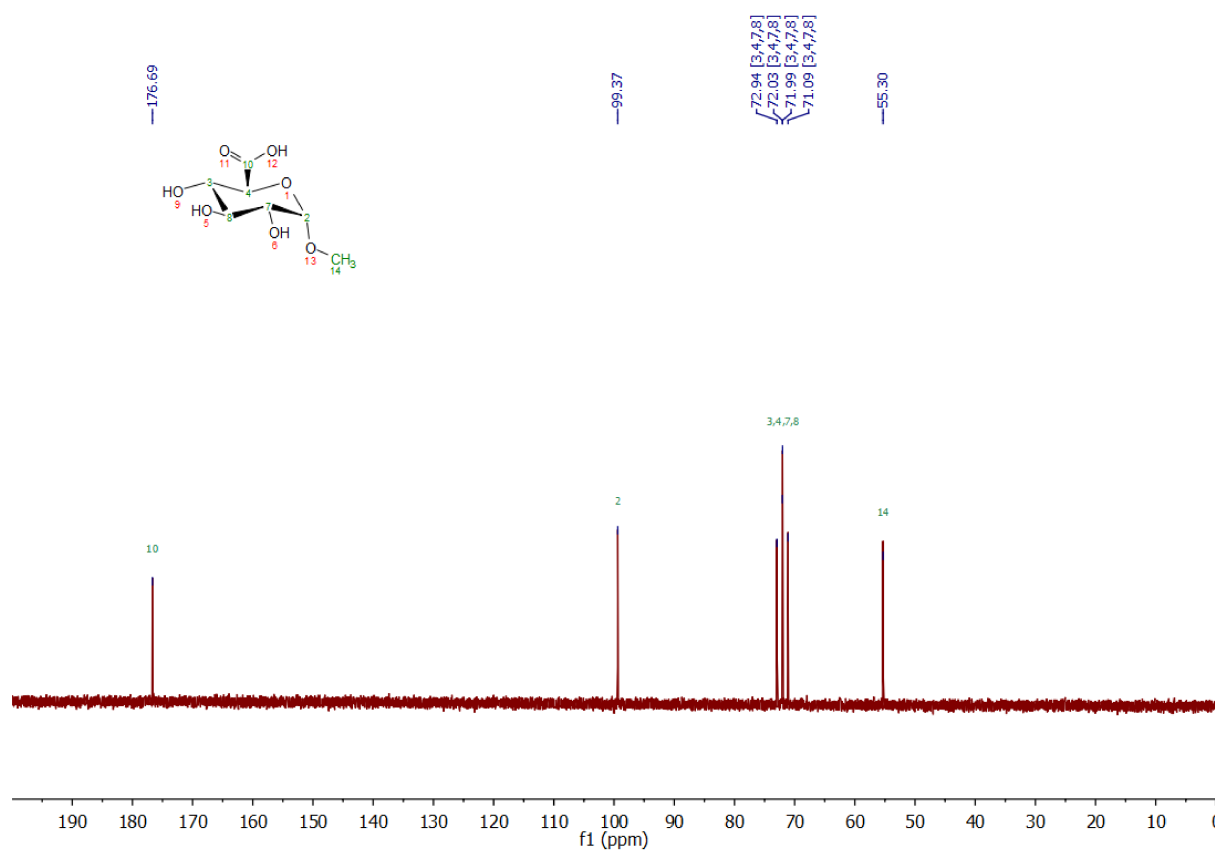
Figure 23: ^{13}C NMR (151 MHz, Deuterium oxide) of compound f.
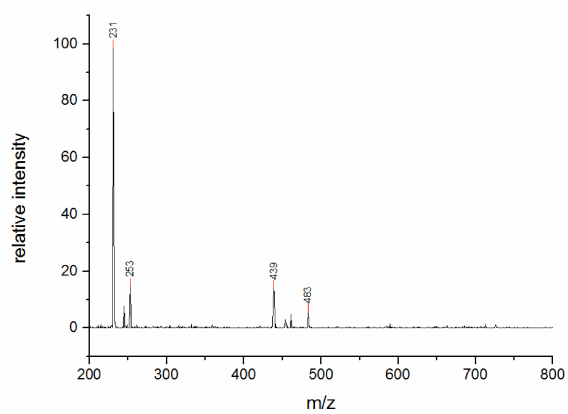
Figure 24: ESI-MS (positive mode) of compound f.

(EDS)₃-GlcA amide (h)
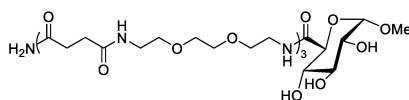
(EDS)₃-GlcA amide (**h**) was synthesized in a 200 µmol scale. Methyl-α-D-glucuronic acid was coupled twice in a four-fold excess with DMTMM as coupling agent to the resin-bound oligomeric sequence -(EDS)₃-. The carbohydrate was preactivated for 60 min with DMTMM before the suspension was given to the resin-bound amine and shaken for another 60 min. The compound was purified by ion exchange. For solid phase synthesis and workup protocols see general methods.72.82 mg (81.1 µmol, 41%) of a white and foamy solid were obtained.

^{1}H NMR (600 MHz, Deuterium Oxide) δ 4.86 (d, ^3J = 3.7 Hz, 1H, *GlcA-H1)*, 4.05 (d, ^3J = 9.9 Hz, 1H, *GlcA-H5)*, 3.69 – 3.67 (m, 15H, *GlcA-H2; GlcA-H3*; *3x -O-CH₂-CH₂-O-*), 3.63 – 3.60 (m, 12H, *6x O-CH₂*), 3.57 (dd, ^3J = 9.08, 9.94 Hz, 1H, *Glc-H4*), 3.47 (m, 2H, *CH₂-N-GlcA*), 3.42 (s, 3H, *GlcA-OCH₃*), 3.39 (m, 10H, *5x N-CH₂*), 2.56 – 2.53 (m, 12H, *6x succinyl CH₂*)

RP-HPLC-MS (linear gradient from 0 – 50 % eluent B in 30 min at 25° C): t_R = 9.87 min. Determined purity: 96%.

MS for C₄₇H₆₃NO₂₉ (ESI, pos.) *m/z*: [M + Na⁺]⁺ calc.: 920.44; found: 920.40, [M + H⁺]⁺ calc.: 898.46; found: 898.35, [M + 2H⁺]²⁺ calc.: 449.73; found: 449.80.
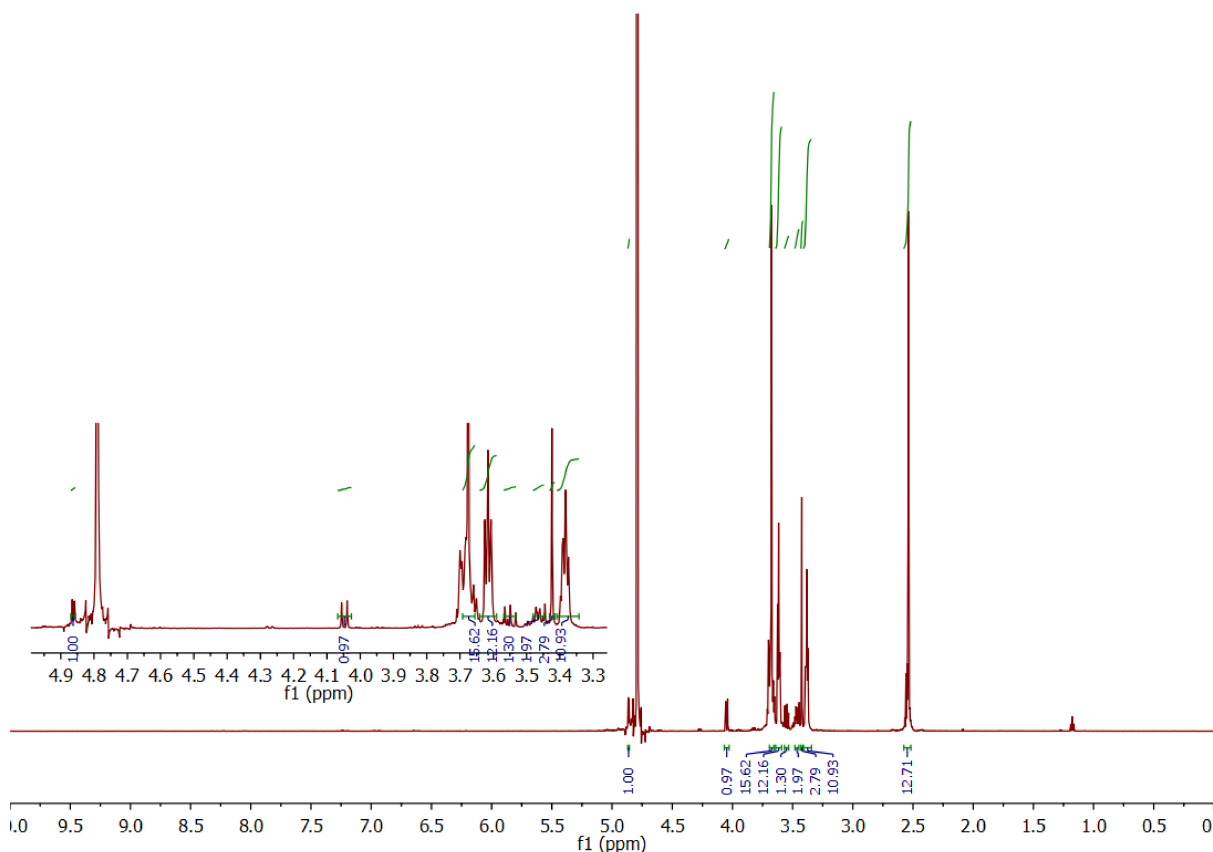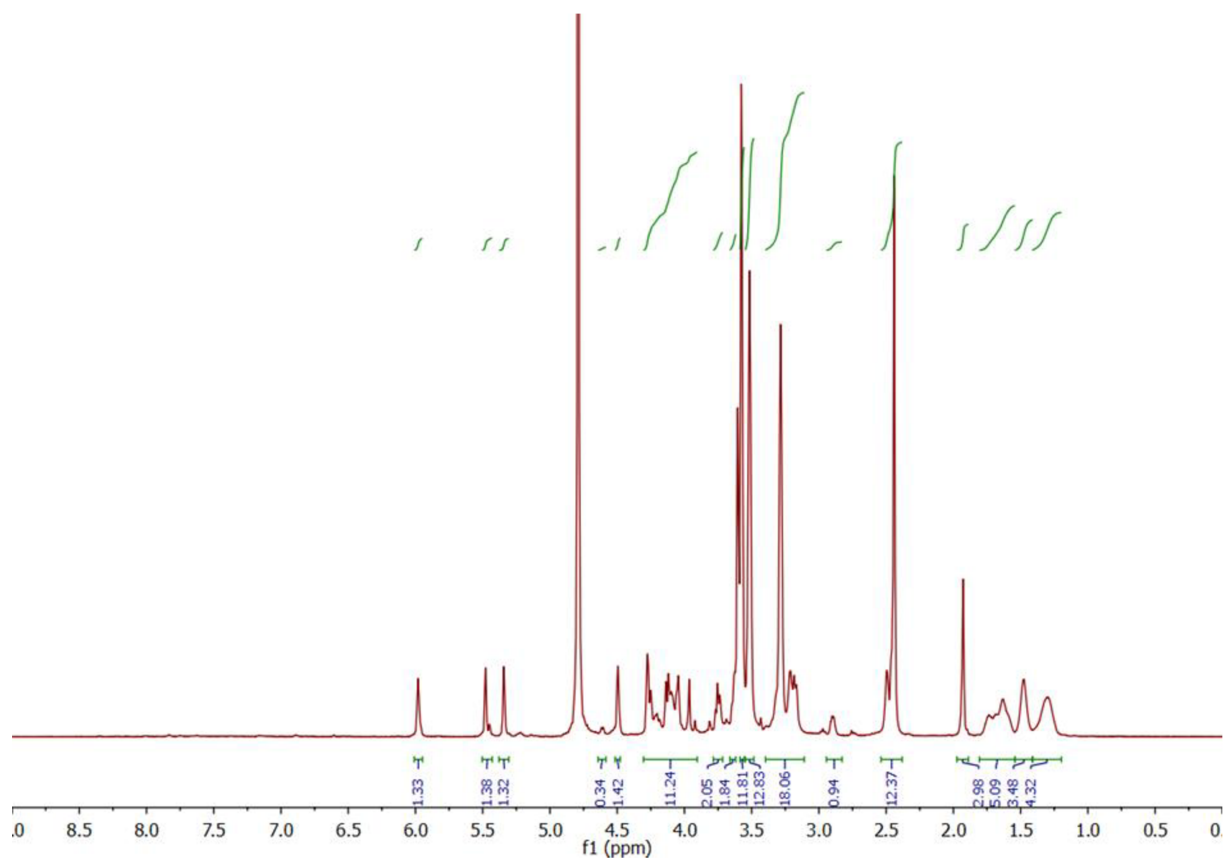

*Figure 25: ^{1}H NMR (600 MHz, Deuterium oxide) of compound **h**.*
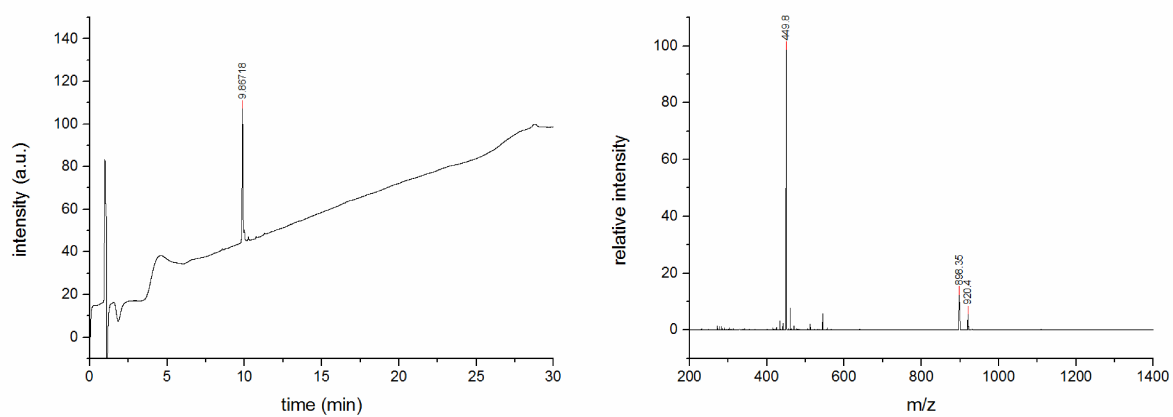
*Figure 26: RP-HPLC (linear gradient from 0 - 50% eluent B in 30 min at 25°C), ESI-MS (positive mode) of compound **h**.*

Solid phase synthesis derived oligomers

N_ϵ(HCl)Lys(1,5)-5 (O1)
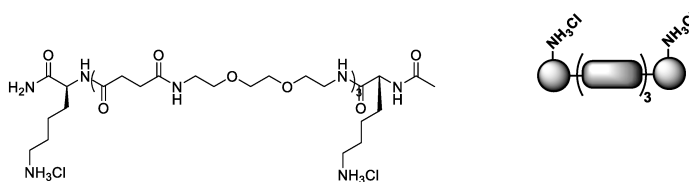
N_ϵ(HCl)Lys(1,5)-5 was synthesized in a 400 µmol scale. 154.2 mg (143 µmol, 36%) of a slightly yellow foamy solid were obtained. The compound was purified by ion exchange. For solid phase synthesis and workup protocols see general methods.

^{1}H NMR (600 MHz, Deuterium Oxide) δ 4.25 (2t, ^3J = 5.3 Hz, 2H, 2x *Lys-CH*), 3.69 – 3.67 (m, 12H, 3x O-*CH$_2$-CH$_2$*-O), 3.63 (t, ^3J = 5.5 Hz, 12H, 6x O-*CH$_2$*-CH$_2$-N), 3.44 – 3.36 (m, 12H, 6x O-CH$_2$-*CH$_2$*-N), 3.01 (2t, ^3J = 7.4, 4H, 2x *Lys-N-CH$_2$*), 2.63 – 2.52 (m, 12H, 6x *succinyl-CH$_2$*), 2.05 (s, 3H, *backbone-Ac*), 1.90 – 1.46 (2m, 12H, 6x *Lys-CH$_2$*).

RP-HPLC-MS (linear gradient from 0 – 50% eluent B in 30 min at 25° C): t_R = 6.79 min. Determined purity: 97%.

MS for $C_{44}H_{85}Cl_2N_{11}O_{15}$ (ESI, pos.) *m/z*: [M + Na$^+$ - 2 HCl]$^+$ calc.: 1028.60; found: 1028.55, [M + 2H$^+$ - 2HCl]$^{2+}$ calc.: 503.81; found: 503.95, [M + 3H$^+$ - 2HCl]$^{3+}$ calc.: 336.21; found: 336.35.

HRMS for $C_{44}H_{85}Cl_2N_{11}O_{15}$ (ESI-TOF) *m/z*: [M + 2H$^+$ - 2HCl]$^{2+}$ calc.: 503.8108; found: 503.8105.
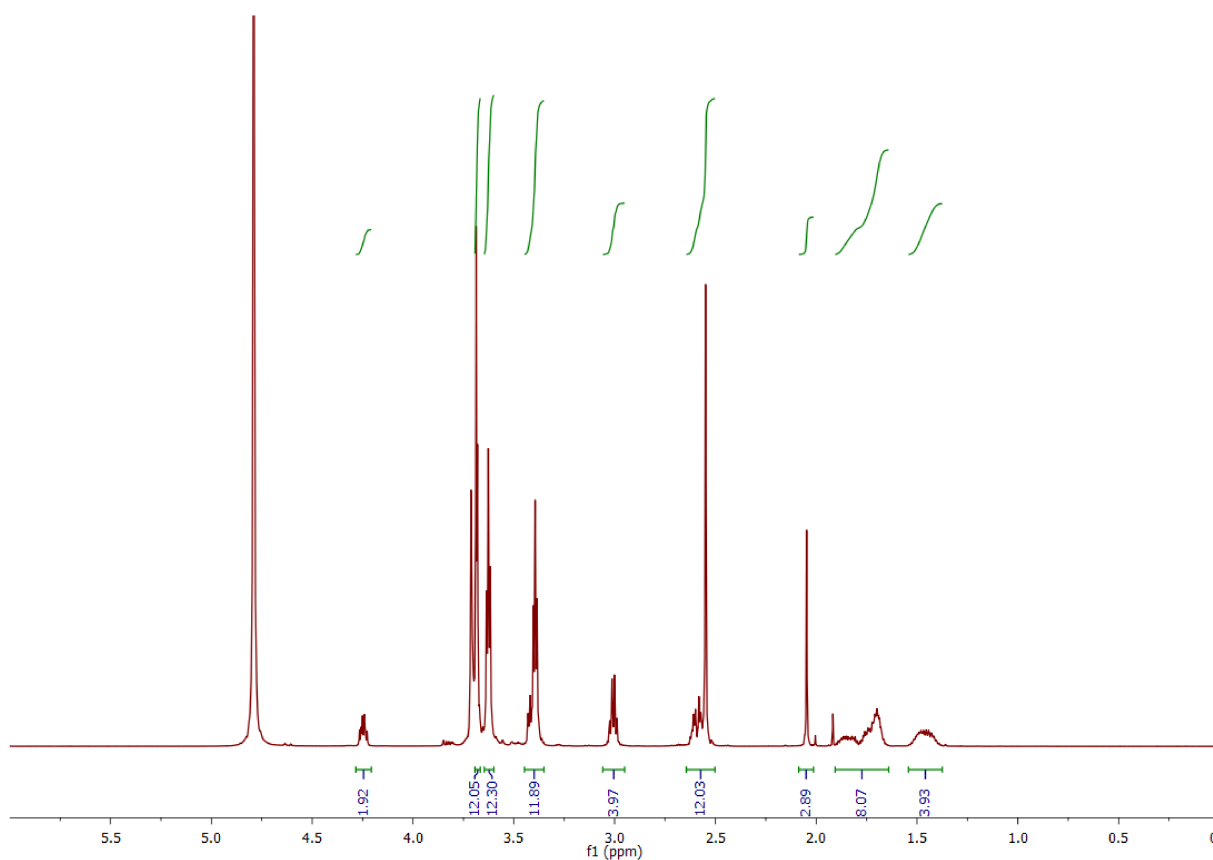
Figure 27: ^{1}H NMR (600 MHz, Deuterium oxide) of compound $O1$.

*Figure 28: RP-HPLC (linear gradient from 0 - 50% eluent B in 30 min at 25°C), ESI-MS (positive mode), HR-MS (ESI+ Q-TOF, positive mode) of compound **O1**.*

_N_ε(HCl)Lys(1)-4-Neu5Ac (protected) (O3)
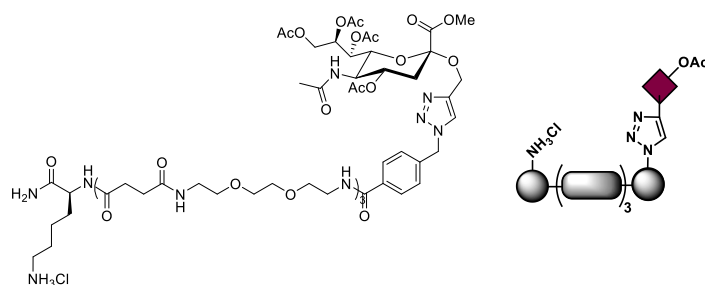
_N_ε(HCl)Lys(1)-4-Neu5Ac was synthesized in a 100 µmol scale. 38.9 mg (24.9 µmol, 25%) of a white and foamy solid were obtained after purification by preparative HPLC and ion exchange. For solid phase synthesis and workup protocols see general methods.

^{1}H NMR (600 MHz, Deuterium Oxide) δ 8.01 (s, 1H, *triazole-H*), 7.79 (d, ^3J = 8.3 Hz, 2H, *aryl-H*), 7.42 (d, ^3J = 8.3 Hz, 2H, *aryl-H*), 5.73 – 5.64 (m, 2H, *aryl-CH$_2$-aryl*), 5.38 (dd, ^3J = 8.9, 1.8 Hz, 1H, *Neu5Ac-H9'*), 5.35 (ddd, ^3J = 8.9, 4.5, 2.5 Hz, 1H, *Neu5Ac-H8*), 4.92 (ddd, ^3J = 11.8, 10.2, 4.8 Hz, 1H, *Neu5Ac-H4*), 4.88 (d, ^2J = 13.0 Hz, 1H, *propargyl-H*), 4.73 (d, ^2J = 12.9 Hz, 1H, *propargyl-H*), 4.28 – 4.23 (m, 3H, *Lys-CH, Neu5Ac-H6, 9''*), 4.09 (dd, ^3J = 12.7, 4.5 Hz, 1H, *Neu5Ac-H7*), 3.94 (dd, ^3J = 10.5 Hz, 1H, *Neu5Ac-H5*), 3.76 – 3.70 (m, 7H, *Neu5Ac-OCH$_3$, 2x O-CH$_2$*), 3.68 (s, 6H, 3x *O-CH$_2$*), 3.66 (s, 4H, 2x *O-CH$_2$*), 3.63 – 3.57 (m, 12H, 5x *O-CH$_2$, N-CH$_2$*), 3.41 – 3.35 (m, 8H, 4x *N-CH$_2$*), 3.32 (t, ^3J = 5.4 Hz, 2H, *N-CH$_2$*), 3.02 (td, ^3J = 7.8, ^2J = 1.7 Hz, 2H, *Lys-N-CH$_2$*), 2.73 (dd, ^2J = 13.0, ^3J = 4.8 Hz, 1H, *Neu5Ac-H3eq.*), 2.63 – 2.45 (m, 12H, 6x *succinyl-CH$_2$*), 2.20 – 2.04 (4s, 4x 3H, 4x *Neu5Ac-Ac*), 1.97 (dd, ^2J = 13.1, ^3J = 11.7 Hz, 1H, *Neu5Ac-H3ax.*), 1.93 (s, 3H, Neu5Ac-*Ac*), 1.91 – 1.39 (3m, 6H, 3x *Lys-CH$_2$*).

RP-HPLC-MS (linear gradient from 0 – 50% eluent B in 30 min at 25° C): t_R = 16.50 min. Determined purity: > 99%.

MS for C$_{67}$H$_{106}$ClN$_{13}$O$_{27}$ (ESI, pos.) *m/z*: [M + 2H$^+$ - HCl]$^{2+}$ calc.: 762.87; found: 763.00, [M + 3H$^+$ - HCl]$^{3+}$ calc.: 508.92; found: 509.00.

HRMS for C$_{67}$H$_{106}$ClN$_{13}$O$_{27}$ (ESI-TOF) *m/z*: [M + 2H$^+$- HCl]$^{2+}$ calc.: 762.8694; found: 762.8682.
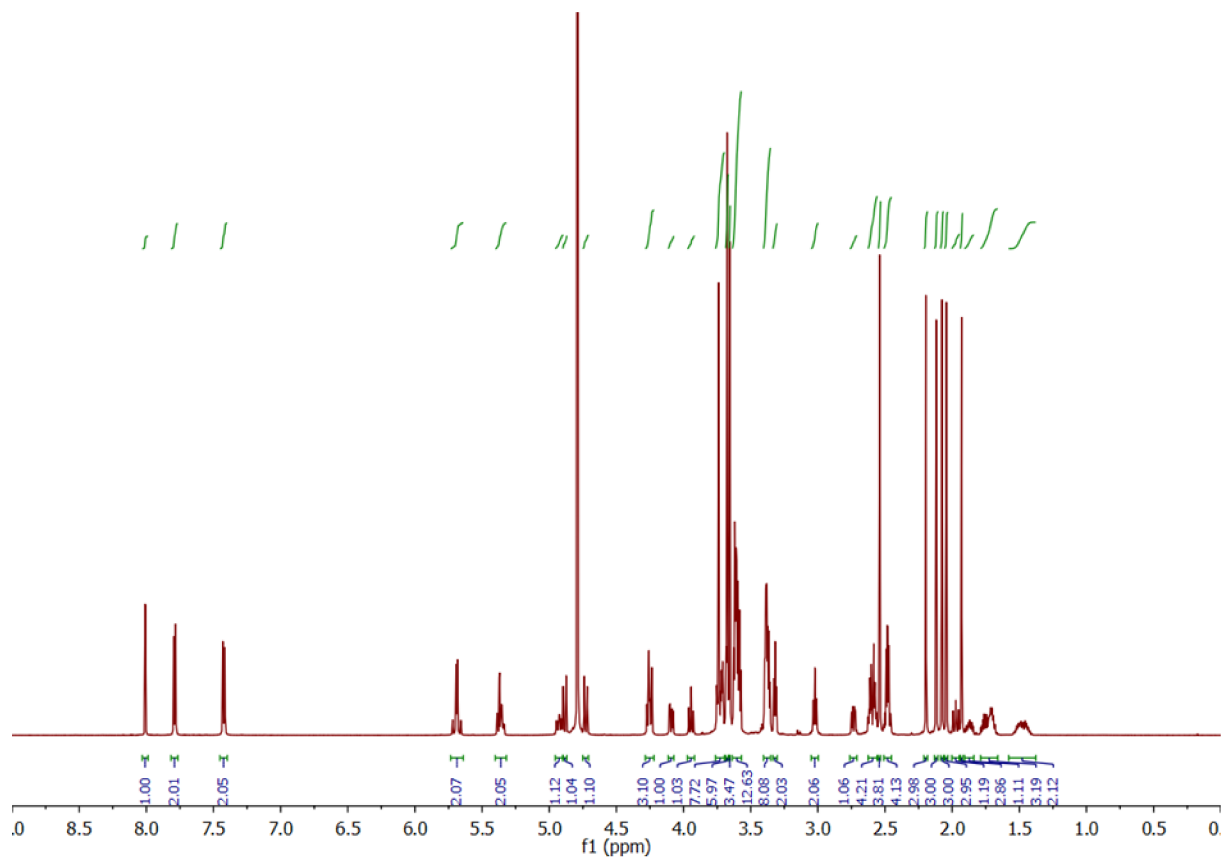
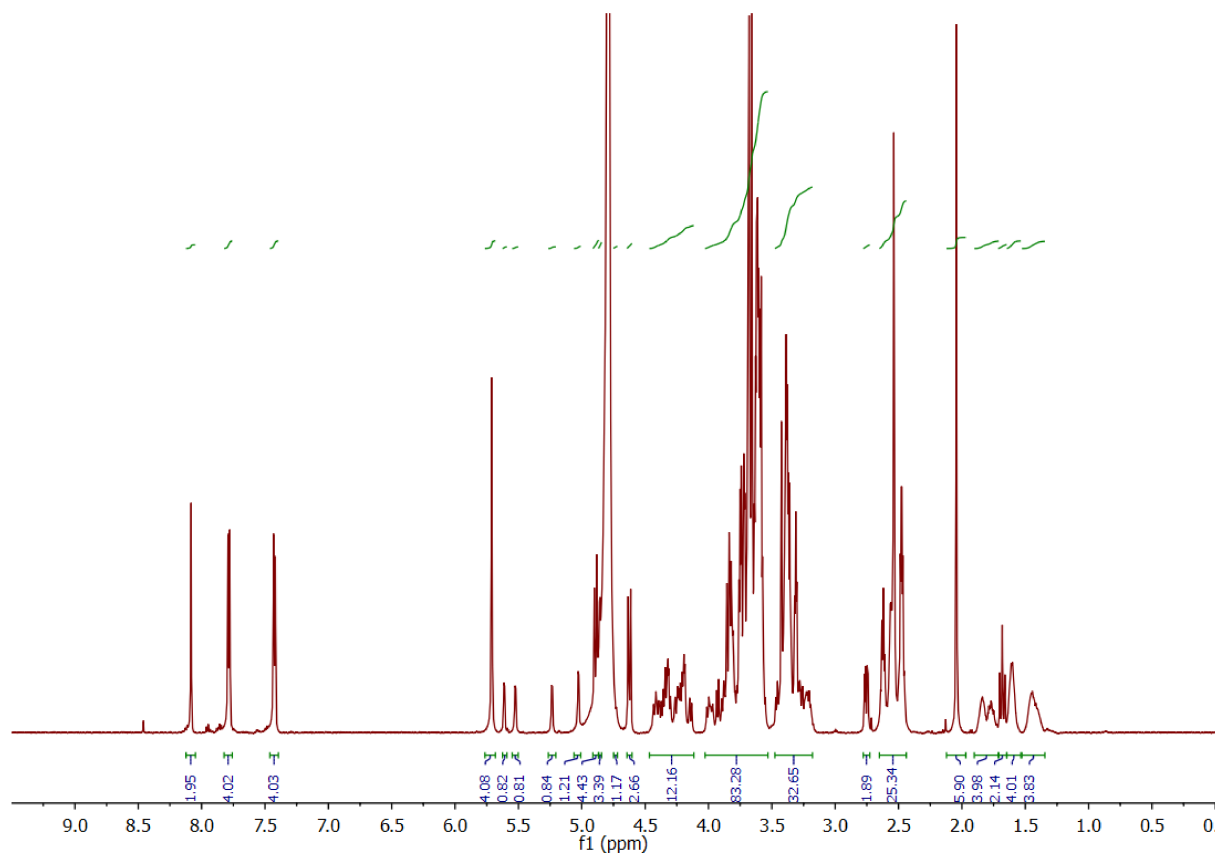*Figure 29: ^{1}H NMR (600 MHz, Deuterium oxide) of compound **O3**.*
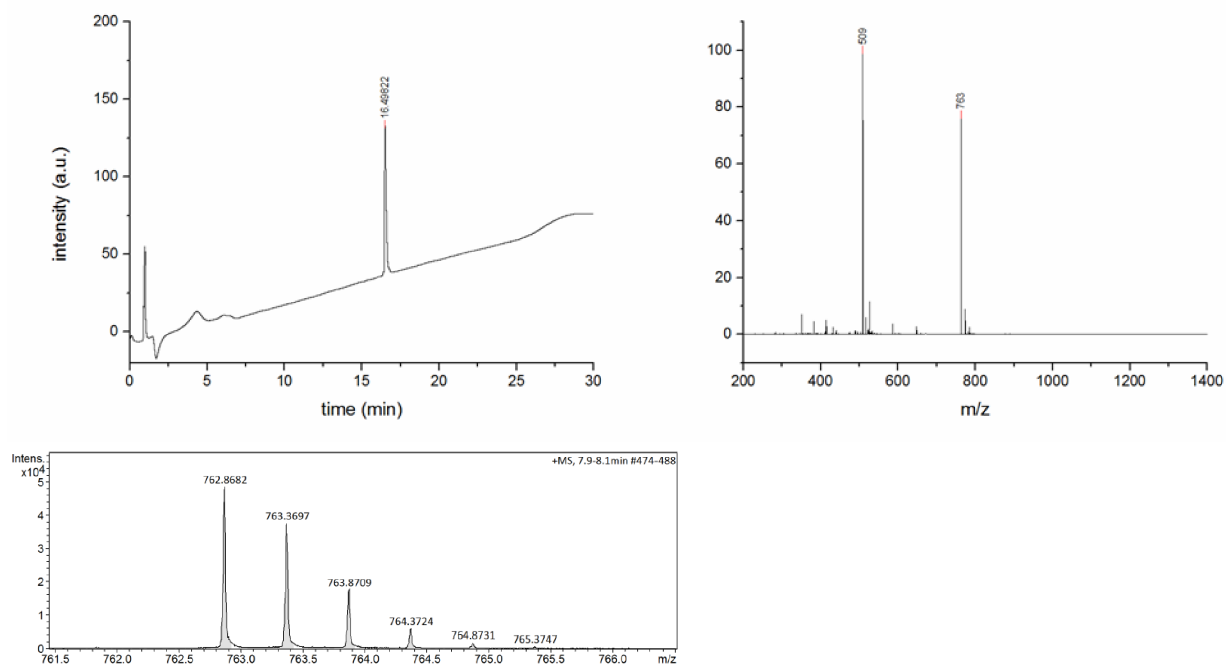
*Figure 30: RP-HPLC (linear gradient from 0 - 50% eluent B in 30 min at 25°C), ESI-MS (positive mode), HR-MS (ESI+ Q-TOF, positive mode) of compound **O3**.*

N_ε(HCl)Lys(1)-4-3'Sialyllactose (protected) (O4)
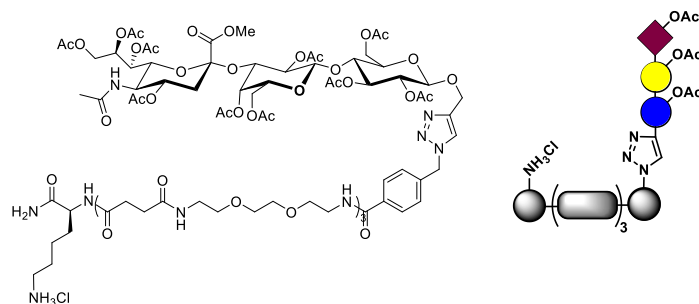
N_ε(HCl)Lys(1)-4-3'Sialyllactose was synthesized in a 25 μmol scale. 14.3 mg (6.69 μmol, 27%) of a white and foamy solid were obtained after purification by preparative HPLC and ion exchange. For solid phase synthesis and workup protocols see general methods.

^{1}H NMR (600 MHz, Deuterium Oxide) δ 8.11 (s, 1H, *triazole-H*), 7.78 (d, ^3J = 8.2 Hz, 2H, *aryl-H*), 8.04 (d, ^3J = 8.0 Hz, 2H, *aryl-H*), 5.70 (s, 2H, *aryl-CH$_2$-aryl*), 5.52 − 5.44 (m, 2H), 5.42 − 5.22 (m, 1H), 5.19 − 5.08 (m, 1H), 5.01 (d, ^3J = 3.2 Hz, 1H), 4.96 (ddd, ^3J = 11.9, 10.1, 4.8 Hz, 1H, *Neu5Ac-H4*), 4.92 (d, ^2J = 13.0 Hz, 1H, *propargyl-H*), 4.87 − 4.81 (m, 4H), 4.71 (d, ^3J = 8.0 Hz, 1H, *Gal-H1*), 4.59 (dd, ^3J = 10.2, 3.3 Hz, 1H, *Gal-H3*), 4.56 − 4.46 (m, 1H), 4.40 (dd, ^2J = 12.9, ^3J = 2.6 Hz, 1H, *Glc-H6'*), 4.25 (dd, ^2J = 9.2, ^3J = 5.1 Hz, 1H, *Lys-CH*), 4.22 − 4.09 (m, 4H), 4.06 − 3.99 (m, 1H), 3.96 − 3.91 (m, 1H), 3.90 (s, 3H, *Neu5Ac-OCH$_3$*), 3.87 (m, 2H), 3.77 − 3.56 (m, 26H, 12x *O-CH$_2$, N-CH$_2$*), 3.41 − 3.34 (m, 8H, 4x *N-CH$_2$*), 3.30 (t, ^3J = 5.4 Hz, 2H, *N-CH$_2$*), 3.04 − 2.99 (m, 2H, *Lys-N-CH$_2$*), 2.67 (dd, ^2J = 12.7, ^3J = 4.7 Hz, 1H, *Neu5Ac-H3eq.*), 2.62 − 2.45 (m, 12H, 6x *succinyl-CH$_2$*), 2.35 − 1.81 (11s, 11x 3H, 11x *Ac*), 1.60 (dd, ^2J = 12.3, ^3J = 12.3 Hz, 1H, *Neu5Ac-H3ax.*), 1.89 − 1.39 (3m, 6H, 3x *Lys-CH$_2$*).

RP-HPLC-MS (linear gradient from 0 − 50% eluent B in 30 min at 25° C): t_R = 21.57 min. Determined purity: 97%.

MS for $C_{91}H_{138}ClN_{13}O_{43}$ (ESI, pos.) *m/z*: [M + 2H$^+$ - HCl]$^{2+}$ calc.: 1050.95; found: 1051.25, [M + 3H$^+$ - HCl]$^{3+}$ calc.: 700.97; found: 701.25.

HRMS for $C_{91}H_{138}ClN_{13}O_{43}$ (ESI-TOF) *m/z*: [M + 2H$^+$- HCl]$^{2+}$ calc.: 1050.9539; found: 1050.9531.
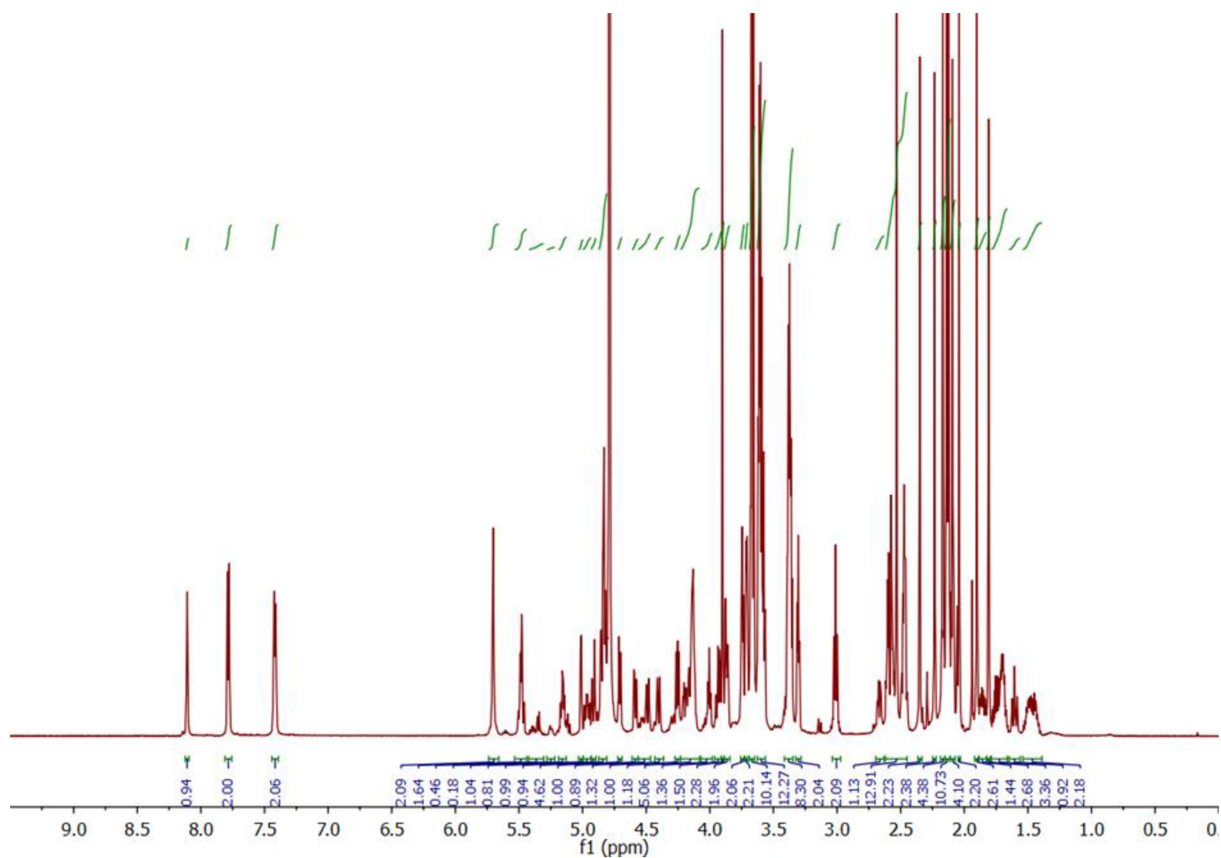
*Figure 31: ^{1}H NMR (600 MHz, Deuterium oxide) of compound **O4**.*
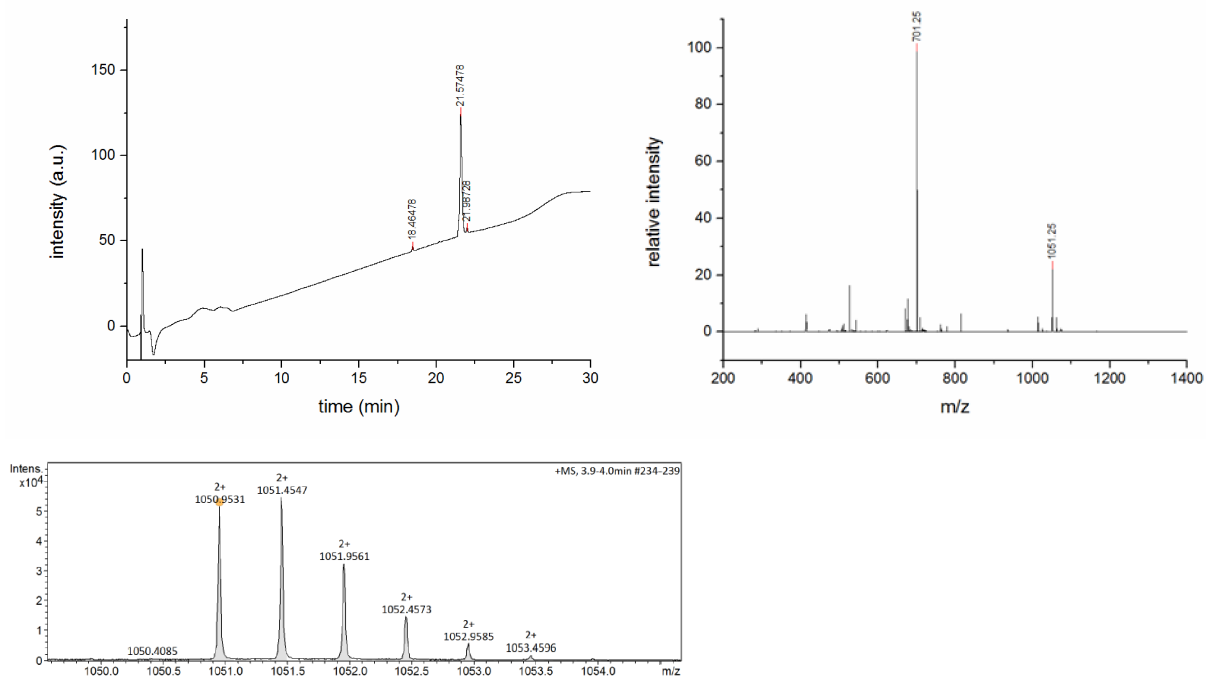
*Figure 32: RP-HPLC (linear gradient from 0 - 50% eluent B in 30 min at 25°C), ESI-MS (positive mode), HR-MS (ESI+ Q-TOF, positive mode) of compound **O4**.*

Coupling of oligo(amidoamines) and heparin fragments

N_ε(dp2)Lys(1,5)-5 (O2)
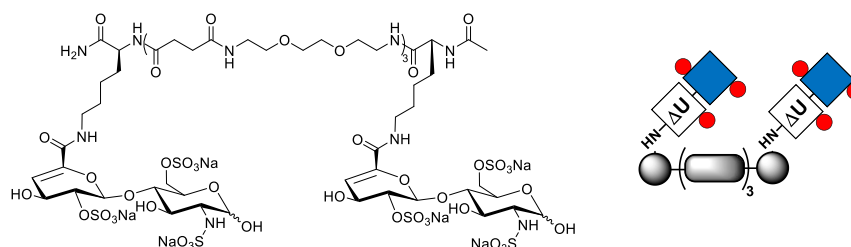
31.9 mg (29.6 µmol) of **N_ε(HCl)Lys(1,5)-5**, 83.26 mg (125 µmol, 4.2 eq.) of **Heparin-dp2** and 170 mg (614 µmol, 4.9 eq. based on Heparin-dp2) of DMTMM were mixed in a 1 mL glass vial, before 1 mL of a mixture of 0.9 mL dimethylformamide and 0.1 mL phosphate-buffer pH 6.5 were added. The mixture was shaken at room temperature for 24 h, diluted to 5 mL with Milli-Q water and dialyzed using a Vivaspin® MWCO 2000 2 ml unit. Separation from mono-substituted product was not to quantitative (analysed by HPLC, data not shown) so dialysis was performed again using a MWCO 3000 unit. After ion exchange with Amberlite® IR 120 Na$^+$ and lyophilisation, 13.9 mg (6.16 µmol, 21%) of the desired product were obtained as a white and foamy solid with a purity of 81% (HPLC)-85% (SAX-HPLC). Side products stem from different glucosamine pyranose forms and partial loss and readdition of sulphates during synthesis and workup, either by hydrolysis and condensation or elimination and addition, respectively. Mono-substituted product were removed completely by dialysis.

^{1}H NMR (600 MHz, Deuterium Oxide) δ 6.00 – 5.94 (m, 2H, 2x *ΔUA-H4*), 5.50 – 5.43 (m, 2H, 2x *ΔUA-H1*), 5.36 – 5.31 (m, 2H, 2x *GlcN-H1*), 4.52 – 4.47 (m, 2H, 2x *ΔUA-H2*), 4.30 – 3.92 (m, 10H, 2x (*ΔUA-H3, GlcN-H5, 6′, 6′′),* 2x *Lys-CH*), 3.79 – 3.71 (m, 2H, 2x *GlcN-H4*), 3.66 – 3.62 (m, 2H, 2x *GlcN-H3*), 3.59 – 3.56 (m, 12H, 3x O-*CH$_2$-CH$_2$*-O), 3.53 – 3.49 (m, 12H, 6x O-*CH$_2$*-CH$_2$-N), 3.39 – 3.13 (m, 17H, 6x O-CH$_2$-*CH$_2$*-N, 1.5x *Lys-N-CH$_2$*), 2.93 – 2.84 (m, 1H, 0.5x *Lys-N-CH$_2$*), 2.52 – 2.41 (m, 12H, 6x *succinyl-CH$_2$*), 1.96 – 1.90 (m, 3H, *backbone-Ac*), 1.79 – 1.22 (3m, 12H, 6x *Lys-CH$_2$*).

RP-HPLC-MS (linear gradient from 0 – 25% eluent B in 30 min at 25° C): t_R = 10.05 min. Determined purity: 81%.

SAX-HPLC (0 → 5 min: 95% A, 5% B; 5 → 40 min: 5 → 100% B; 40 → 60 min: 100% B at 25 °C): t_R = 12.75 + 13.21 min. Determined purity: 85%

MS for $C_{68}H_{111}N_{13}Na_6O_{51}S_6$ (ESI, neg.) *m/z*: [M − 6Na$^+$ + 4H$^+$]$^{2-}$ calc.: 1060.75; found: 1060.95, [M − 6Na$^+$ + 4H$^+$ - SO$_3$]$^{2-}$ calc.: 1020.78; found: 1021.05, [M − 6Na$^+$ + 4H$^+$ - SO$_3$ - OH]$^{2-}$ calc.: 1012.28; found: 1011.95, [M − 6Na$^+$ + 4H$^+$ - 2SO$_3$]$^{2-}$ calc.: 980.80; found: 980.95, [M − 6Na$^+$ + 3H$^+$]$^{3-}$ calc.: 706.84; found: 706.95, [M − 6Na$^+$ + 3H$^+$ - SO$_3$]$^{3-}$ calc.: 680.18; found: 680.40, [M − 6Na$^+$ + 3H$^+$ - 2SO$_3$]$^{3-}$ calc.: 653.53; found: 653.60, [M − 6Na$^+$ + 2H$^+$]$^{4-}$ calc.: 529.87; found: 530.10, [M − 6Na$^+$ + 2H$^+$ - SO$_3$]$^{4-}$ calc.: 509.89; found: 509.95, [M − 6Na$^+$ + 2H$^+$ - 2SO$_3$]$^{4-}$ calc.: 489.90; found: 490.00.

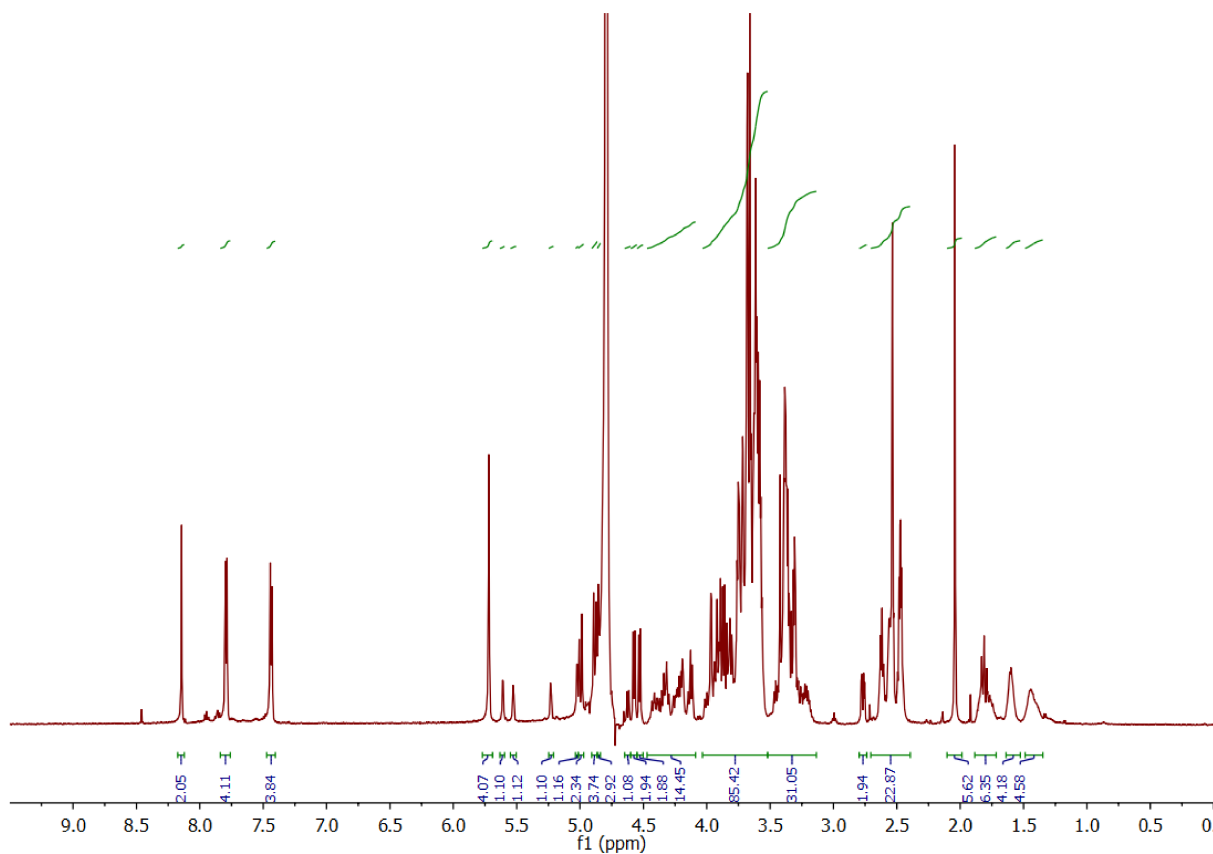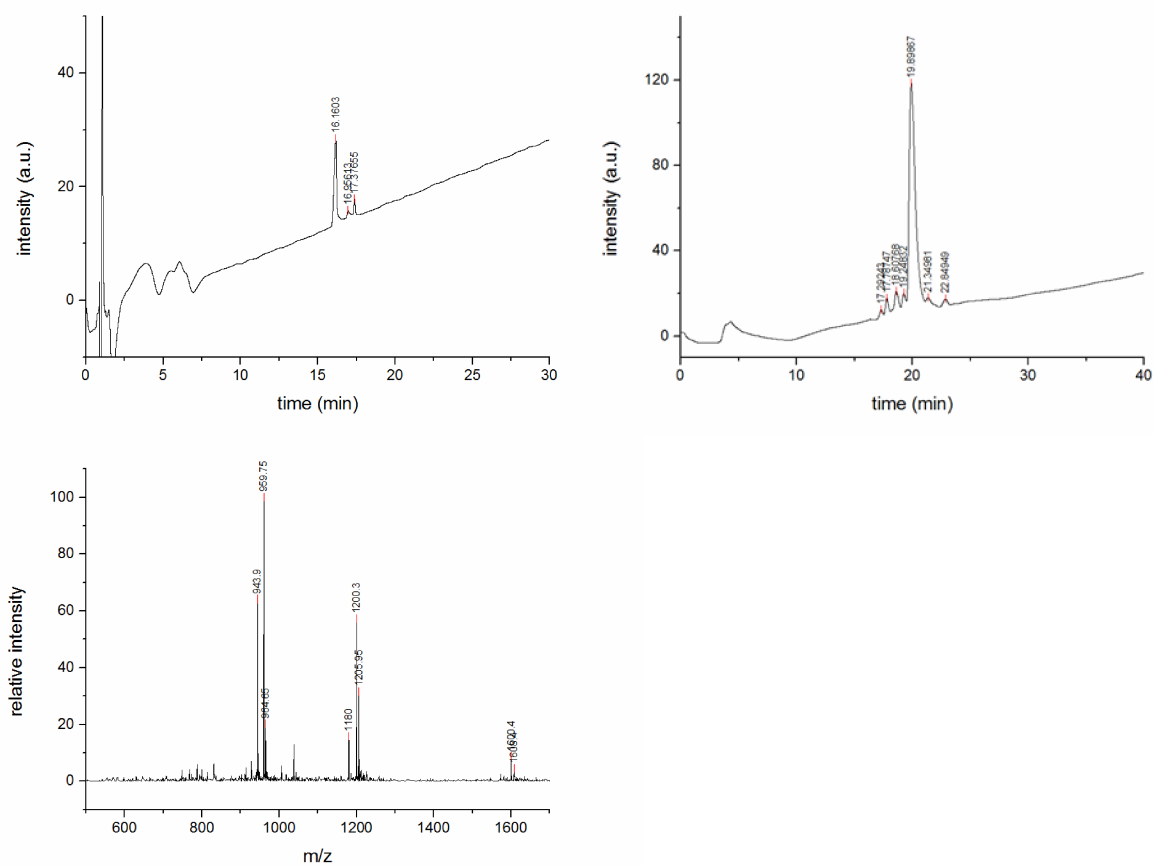*Figure 33: ^{1}H NMR (600 MHz, Deuterium oxide) of compound **O2**.*
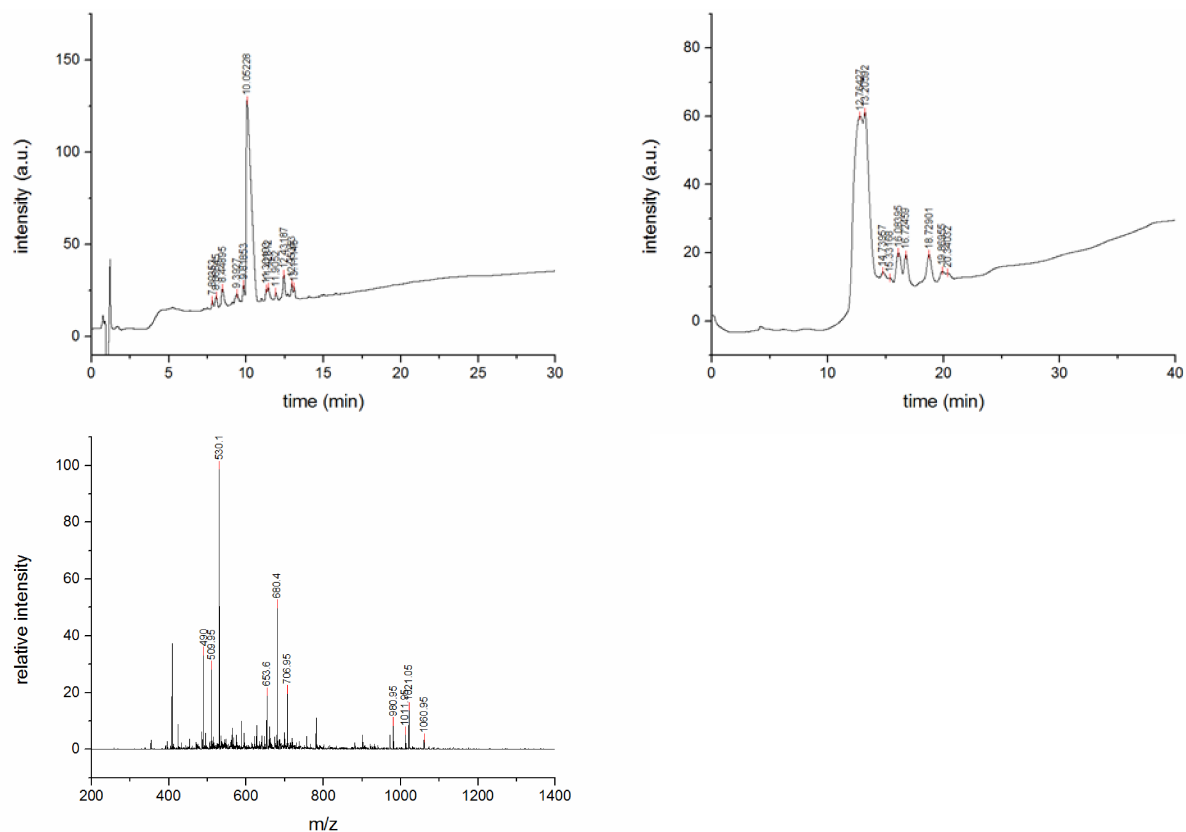
*Figure 34: RP-HPLC (linear gradient from 0 – 25% eluent B in 30 min at 25° C), SAX-HPLC (0 → 5 min: 95% A, 5% B; 5 → 40 min: 5 → 100% B; 40 → 60 min: 100% B at 25 °C), ESI-MS (negative mode) of compound **O2.***

GlcA, IdoA-(NεLys(1)-4-Neu5Ac)-Fondaparinux (O5) synthesis

R =
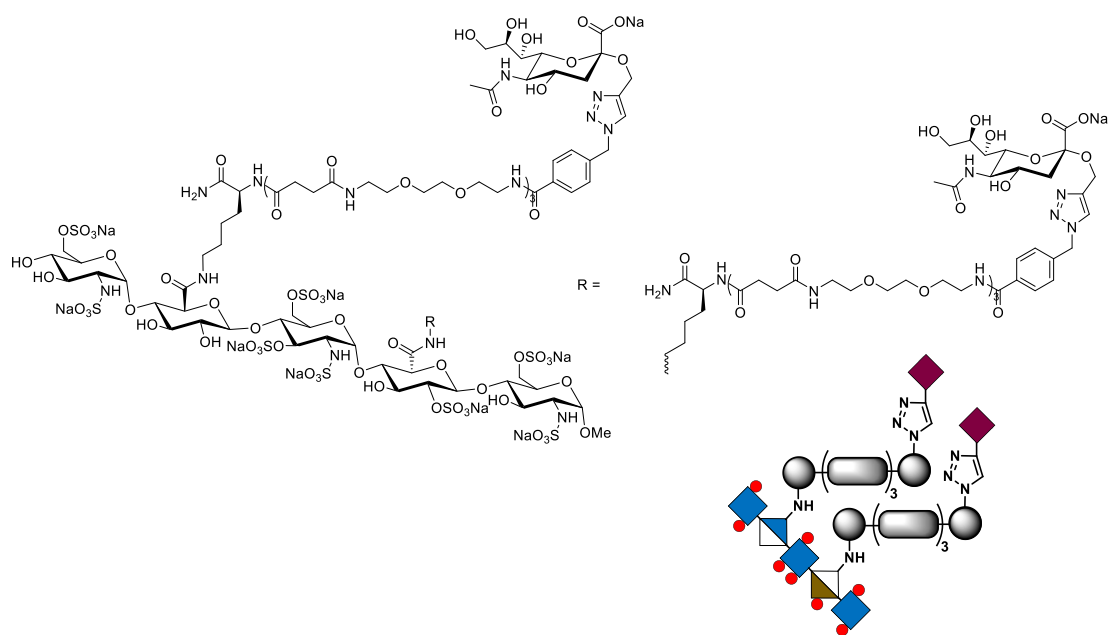
5.02 mg **Fondaparinux** (2.91 µmol), 13.6 mg (8.71 µmol, 3 eq.) **Nε(HCl)Lys(1)-4-Neu5Ac (O3)** and 16.0 mg (57.8 µmol, 20 eq.) DMTMM were combined in a 1 mL glass vial and dissolved in 0.5 ml of a mixture of 0.45 mL dimethylformamide and 0.05 mL phosphate-buffer pH 6.5. The mixture was shaken at room temperature for 24 h, before it was diluted to 5 mL with Milli-Q water and dialyzed using a Vivaspin® MWCO 2000 2 ml unit. After lyophilisation the mixture was dissolved in 3 mL of a 0.1 M lithium hydroxide solution (methanol : water = 1 : 1) and shaken for 4 h. The resulting, fully deprotected compound was separated from its protecting groups and excessive lithium hydroxide by dialysis using a Vivaspin® MWCO 2000 2 ml unit and finally isolated after ion exchange with Amberlite® IR 120 Na+ and lyophilisation. 9.4 mg (2.15 µmol, 74%) of the desired product were obtained as a white and foamy solid in a purity of 88% (SAX-HPLC) and 98% (RP-HPLC).

^{1}H NMR (600 MHz, Deuterium Oxide) δ 8.08 (s, 2H, *triazole-H*), 7.78 (d, ^3J = 8.4 Hz, 4H, *aryl-H*), 7.42 (d, $_3J$ = 8.4 Hz, 4H, *aryl-H*), 5.71 (s, 4H, 2x *aryl-CH$_2$-aryl*), 5.61 (d, ^3J = 3.7 Hz, 1H, A_S^{nr}*-H1*), 5.52 (d, ^3J = 3.3 Hz, 1H, A_S*-H1*), 5.23 (d, ^3J = 3.7 Hz, 1H, I_S-*H1*), 5.03 (d, ^3J = 3.7 Hz, 1H, A_S^r*-H1*), 4.89 (d, ^2J = 12.0 Hz, 2H, 2x *propargyl-H*), 4.87 – 4.83 (m, 2H, 2x *Neu5Ac-H4*), 4.75 – 4.71 (m, 1H, I_S-*H5*), 4.62 (d, ^2J = 11.8 Hz, 2H, 2x *propargyl-H*), 4.47 – 4.09 (m, 12H, 10x *Fondaparinux-H*, 2x *Lys-CH*), 4.03 – 3.53 (m, 76H, 10x *Fondaparinux-H*, 24x *O-CH$_2$*, 2x *N-CH$_2$*, 2x *(Neu5Ac-H4, 5, 6, 7, 8, 9', 9'')*), 3.51 – 3.16 (m, 31H, 3x A_S-*H2, G-H2, A_S^r-OCH$_3$*, 2x *Lys-N-CH$_2$*, 10x *N-CH$_2$*), 2.75 (dd, ^2J = 12.4, ^3J = 4.8 Hz, 2H, 2x *Neu5Ac-H3eq.*), 2.65 – 2.44 (m, 24H, 12x *succinyl-CH$_2$*), 2.04 (s, 6H, 2x *Neu5Ac-Ac*), 1.90 – 1.45 (3m, 12H, 6x *Lys-CH$_2$*), 1.68 (dd, ^2J = 12.2, ^3J = 12.2 Hz, 2H, 2x *Neu5Ac-H3ax.*).

RP-HPLC-MS (linear gradient from 0 – 25% eluent B in 30 min at 25° C): t_R = 16.94 min. Determined purity: 98%.

SAX-HPLC (0 → 5 min: 95% A, 5% B; 5 → 40 min: 5 → 100% B; 40 → 60 min: 100% B at 25 °C): t_R = 20.64 min. Determined purity: 88%

MS for $C_{147}H_{229}N_{29}Na_{10}O_{93}S_8$ (ESI, neg.) *m/z*: [M − 9Na+ + 6H+]$^{3-}$ calc.: 1391.41; found: 1391.95, [M − 10Na+ + 7H+]$^{3-}$ calc.: 1384.08; found: 1384.40, [M − 9Na+ + 5H+]$^{4-}$ calc.: 1043.30; found: 1043.95, [M − 10Na+ + 6H+]$^{4-}$ calc.: 1037.81; found: 1037.95, [M − 10Na+ + 6H+ -SO$_3$]$^{4-}$ calc.: 1017.82; found: 1018.25, [M − 9Na+ + 4H+]$^{5-}$ calc.: 834.44; found: 834.90, [M − 10Na+ + 5H+]$^{5-}$ calc.: 830.05; found: 830.25, [M − 10Na+ + 5H+ - SO$_3$]$^{5-}$ calc.: 814.05; found: 814.00, [M − 10Na+ + 5H+]$^{5-}$ calc.: 798.06; found: 798.00.

Figure 35: ^{1}H NMR (600 MHz, Deuterium oxide) of compound **O5**.
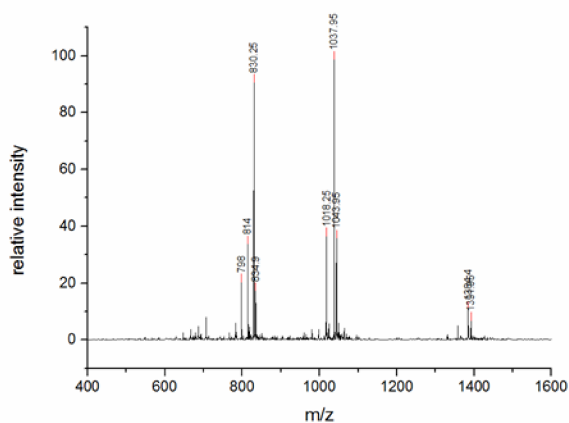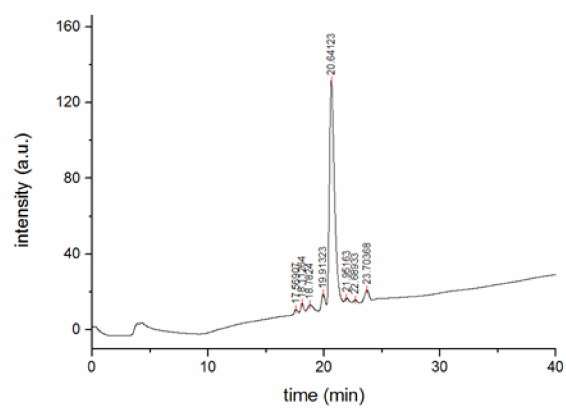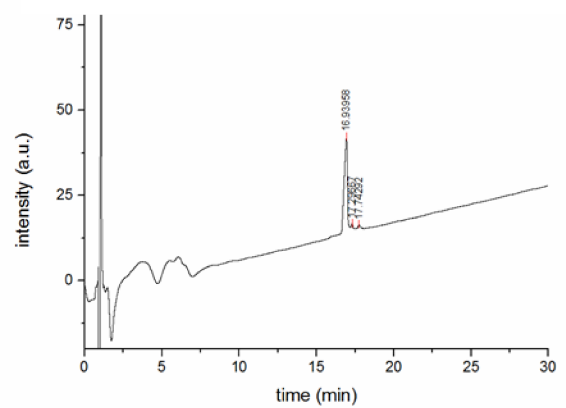
Figure 36: RP-HPLC (linear gradient from 0 – 25% eluent B in 30 min at 25° C), SAX-HPLC (0 → 5 min: 95% A, 5% B; 5 → 40 min: 5 → 100% B; 40 → 60 min: 100% B at 25 °C), ESI-MS (negative mode) of compound **O5.**

GlcA, IdoA-(N_ϵLys(1)-4-3'Sialyllactose)-Fondaparinux (O6)
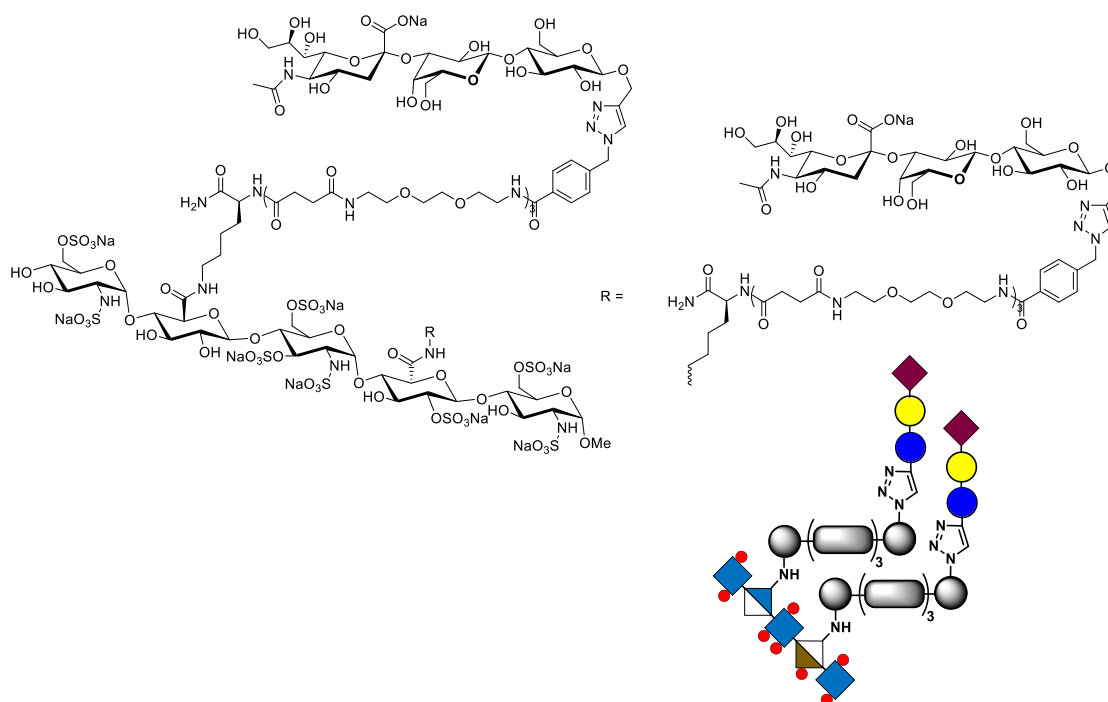
3.09 mg **Fondaparinux** (1.79 μmol), 8.76 mg (4.10 μmol, 2.3 eq.) **N_ϵ(HCl)Lys(1)-4-3'Sialyllactose (O4)** and 10.8 mg (39.0 μmol, 22 eq.) DMTMM were combined in a 1 mL glass vial and dissolved in 0.5 ml of a mixture of 0.45 mL dimethylformamide and 0.05 mL phosphate-buffer pH 6.5. The mixture was shaken at room temperature for 24 h, before it was diluted to 5 mL with Milli-Q water and dialyzed using a Vivaspin® MWCO 2000 2 ml unit. After lyophilisation the mixture was dissolved in 3 mL of a 0.1 M lithium hydroxide solution (methanol : water = 1 : 1) and shaken for 4 h. The resulting, fully deprotected compound was separated from its protecting groups and excessive lithium hydroxide by dialysis using a Vivaspin® MWCO 2000 2 ml unit and finally isolated after ion exchange with Amberlite® IR 120 Na⁺ and lyophilisation. 7.7 mg (1.53 μmol, 86%) of the desired product were obtained as a white and foamy solid in a purity of 90% ββ (RP-HPLC) and 87% (SAX-HPLC).

^{1}H NMR (600 MHz, Deuterium Oxide) δ 8.14 (s, 2H, *triazole-H*), 7.79 (d, ^3J = 8.3 Hz, 4H, *aryl-H*), 7.44 (d, ^3J = 8.2 Hz, 4H, *aryl-H*), 5.72 (s, 4H, 2x *aryl-CH$_2$-aryl*), 5.61 (d, ^3J = 3.7 Hz, 1H, $A_S{}^{nr}$*-H1*), 5.53 (d, ^3J = 3.4 Hz, 1H, A_S*-H1*), 5.23 (d, ^3J = 3.8 Hz, 1H, I_S-*H1*), 5.02 (d, ^3J = 3.7 Hz, 1H, $A_S{}^r$-*H1*), 5.00 (d, ^2J = 12.7 Hz, 2H, 2x *propargyl-H*), 4.88 (d, ^2J = 12.6 Hz, 2H, 2x *propargyl-H*), 4.86 – 4.84 (m, 2H, 2x *Neu5Ac-H4*), 4.62 (d, ^2J = 7.8 Hz, 1H, I_S-*H5*), 4.57 (d, ^3J = 8.0 Hz, 2H, 2x *Glc-H1*), 4.53 (d, ^3J = 7.8 Hz, 2H, 2x *Gal-H1*), 4.46 – 4.09 (m, 12H, 10x *Fondaparinux-H*, 2x *Lys-CH*), 4.03 – 3.53 (m, 100H, 10x *Fondaparinux-H*, 24x *O-CH$_2$*, 2x *N-CH$_2$*, 2x *(3'SL-19xH)*), 3.49 – 3.15 (m, 31H, 3x A_S-*H2*, G-*H2*, $A_S{}^r$-*OCH$_3$*, 2x *Lys-N-CH$_2$*, 10x *N-CH$_2$*), 2.77 (dd, ^2J = 12.4, ^3J = 4.6 Hz, 2H, 2x *Neu5Ac-H3eq.*), 2.67 – 2.41 (m, 24H, 12x *succinyl-CH$_2$*), 2.04 (s, 6H, 2x *Neu5Ac-Ac*), 1.88 – 1.44 (3m, 12H, 6x *Lys-CH$_2$*), 1.60 (dd, ^2J = 12.3, ^3J = 12.3 Hz, 2H, 2x *Neu5Ac-H3ax.*).

RP-HPLC-MS (linear gradient from 0 – 25 % eluent B in 30 min at 25° C): t_R = 16.16 min. Determined purity: 90% ββ, 6% αβ/βα, < 4% αα.

SAX-HPLC (0 → 5 min: 95% A, 5% B; 5 → 40 min: 5 → 100% B; 40 → 60 min: 100% B at 25 °C): t_R = 19.90 min. Determined purity: 87%

MS for $C_{171}H_{269}N_{29}Na_{10}O_{113}S_8$ (ESI, neg.) *m/z*: [M − 9Na⁺ + 6H⁺]³⁻ calc.: 1607.48; found: 1608.40, [M − 10Na⁺ + 7H⁺]³⁻ calc.: 1600.15; found: 1600.40, [M − 9Na⁺ + 5H⁺]⁴⁻ calc.: 1205.36; found: 1205.95, [M − 10Na⁺ + 6H⁺]⁴⁻ calc.: 1199.86; found: 1200.30, [M − 10Na⁺ + 6H⁺ -SO$_3$]⁴⁻ calc.: 1180.00; found: 1179.87, [M − 9Na⁺ + 4H⁺]⁵⁻ calc.: 964.08; found: 964.65, [M − 10Na⁺ + 5H⁺]⁵⁻ calc.: 959.69; found: 959.75, [M − 10Na⁺ + 5H⁺ - SO$_3$]⁵⁻ calc.: 943.70; found: 943.90.

*Figure 37: ¹H NMR (600 MHz, Deuterium oxide) of compound **O6**.*

*Figure 38: RP-HPLC (linear gradient from 0 – 25% eluent B in 30 min at 25° C), SAX-HPLC (0 → 5 min: 95% A, 5% B; 5 → 40 min: 5 → 100% B; 40 → 60 min: 100% B at 25 °C), ESI-MS (negative mode) of compound **O6.***

Saturation transfer difference NMR studies
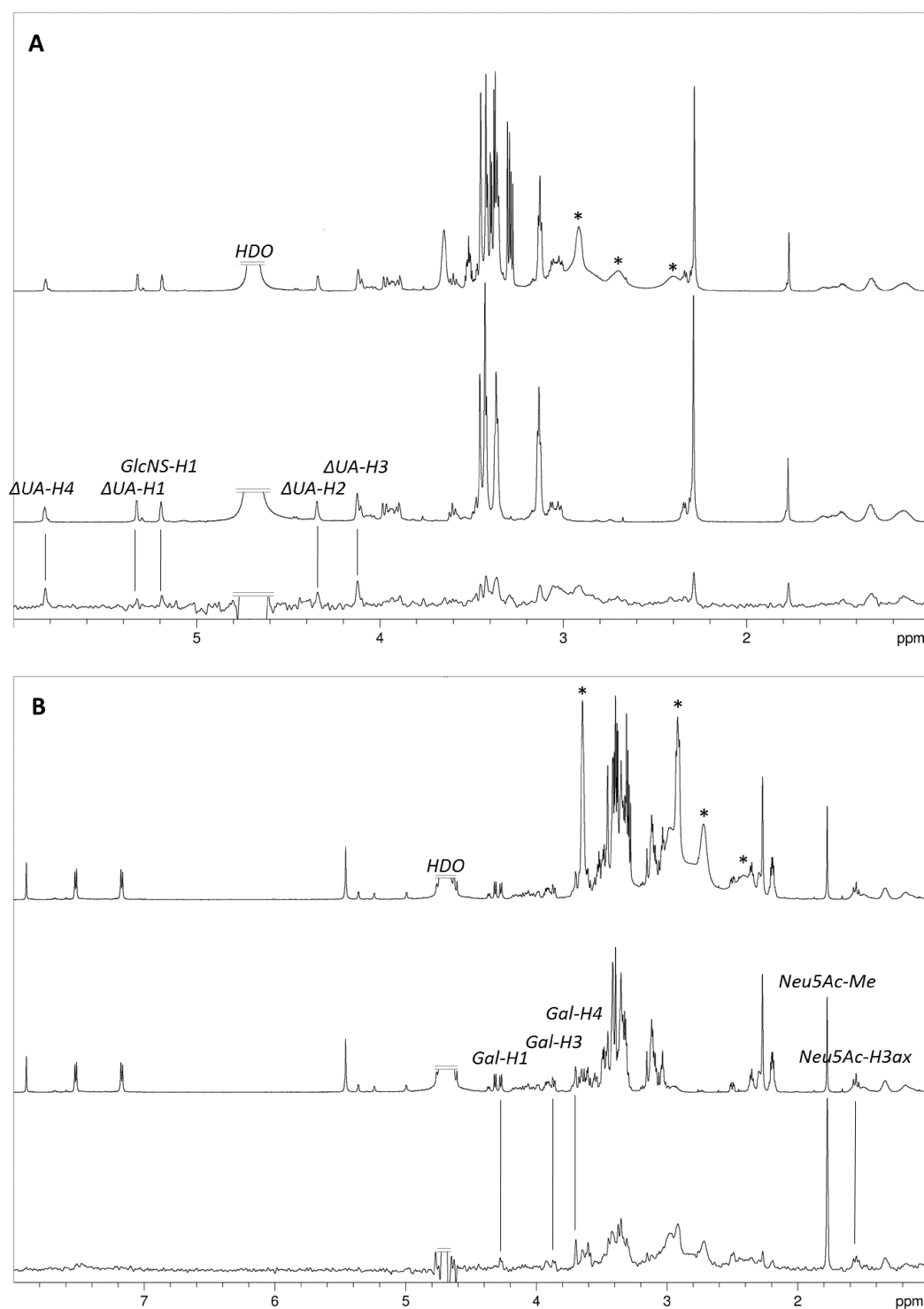
Figure 39: NMR spectra of MCPyV capsids interacting with compounds **O2** and **O6**. **A)** Top: ^{1}H NMR spectrum of MCPyV capsids with **O2**, 2nd from top: ^{1}H NMR spectrum of **O2**, bottom: STD-NMR difference spectrum of MCPyV capsids with **O2**. **B)** Top: ^{1}H NMR spectrum of MCPyV capsids with **O6**, 2nd from top: ^{1}H NMR spectrum of **O6**, bottom: STD-NMR difference spectrum of MCPyV capsids with **O6**. All spectra were recorded at 283 K in D_2O-buffer containing 150 mM NaCl, 1 mM $CaCl_2$, pH 6.3. HDO signals were truncated in each spectrum for the sake of clarity. Unidentified impurities that appear bound to the capsids due to their broad line shape are highlighted with asterisks.

References

1. M. Baier, M. Giesler and L. Hartmann, *Chem. Eur. J.*, 2018, **24**, 1619-1630.
2. aC. B. Buck, D. V. Pastrana, D. R. Lowy and J. T. Schiller, *Journal of virology*, 2004, **78**, 751-757; bD. V. Pastrana, Y. L. Tolstov, J. C. Becker, P. S. Moore, Y. Chang and C. B. Buck, *PLOS Path.*, 2009, **5**, e1000578.
3. R. Šardzík, G. T. Noble, M. J. Weissenborn, A. Martin, S. J. Webb and S. L. Flitsch, *Beilstein J. Org. Chem.*, 2010, **6**, 699-703.
4. M. F. Ebbesen, D. Itskalov, M. Baier and L. Hartmann, *ACS Macro Lett.*, 2017, **6**, 399-403.
5. I. Adorjan, A.-S. Jääskeläinen and T. Vuorinen, *Carbohydr. Res.*, 2006, **341**, 2439-2443.

6. Appendix

6.1. Abbreviations

Building Blocks

Abbreviation	Definition
ADS	Alloc-functionalized diethylenetriamine succinic acid amide
BADS	Benzylazide-functionalized diethylenetriamine succinic acid amide
*Iso*BADS	Isomeric Benzylazide-functionalized diethylenetriamine succinic acid amide
BDS	Boc-functionalized diethylenetriamine succinic acid amide
DDS	Doublebond-functionalized diethylenetriamine succinic acid amide
EDS	(Ethylenedioxy)bis(ethylamine) succinic acid amide
MDS	Methylsuccinyl-functionalized diethylenetriamine succinic acid amide
ODS	Octanediamine succinic acid amide
SDS	Short ethylenediamine succinic acid amide
TDS	Triplebond-functionalized diethylenetriamine succinic acid amide

Carbohydrates

Abbreviation	Definition
CMP	Cytidine Monophosphate
dp2 (Heparin)	Shortest Heparin disaccharide unit
Fuc	Fucose
GAG	Glycosaminoglycan
Gal	Galactose
GalNAc	*N*-Acetyl-Galactosamine
Glc	Glucose
GlcA	Glucuronic acid
GlcNAc	*N*-Acetyl-Glucosamine
HBGA	Histo-blood group antigen
HS	Heparan sulfate
IdoA	Iduronc acid
Man	Mannose
Neu5Ac	*N*-Acetyl neuraminic acid (Sialic acid)
3'-SL	3'-Sialyllactose
6'-SL	6'-Sialyllactose

Appendix

Biological abbreviations

Abbreviation	Definition
Con A	Concanavalin A
CRD	Carbohydrate recognition domain
DGL	*Dioclea grandiflora* lectin
DNA	Deoxyribonucleic acid
HIV	Humane Immunodeficiency Virus
HPV 16	Humane Papillomavirus Type 16
HSV	Herpes Simplex Virus
MCPyV	Merkel Cell Polyomavirus
NCAM	Neutral Cell Adhesion Molecule
PA-IL	*Pseudomonas Aeruginosa* IL
PNA	Peanut agglutinin
RNA	Ribonucleic acid
TSPyV	*Trichodysplasia Spinulosa* associated Polyomavirus
VP 1	Virus Particle 1 (surface protein pentamer)
VVA	*Vicia villose agglutinin*

Chemicals

Abbreviation	Definition
Alloc	Allyloxycarbonyl protecting group
Boc	*tert*. Butyloxycarbonyl protecting group
Cys	Cysteine
D_2O	Deuterium oxide
DCC	*N, N'*-Dicyclohexylcarbodiimide
DCM	Dichloromethane
DIC	*N, N'*-Diisopropylcarbodiimide
DIPEA	*N, N*-Diisopropylethylamine
DMF	*N, N*-Dimethylformamide
DMSO	Dimethyl sulfoxide
DMTMM	(4-(4,6- Dimethoxy-1,3,5-triazin-2-yl)-4-methyl-morpholinium chloride)
EDC	1-Ethyl-3-(3-dimethylaminopropyl)carbodiimide
EtOAc	Ethyl acetate
Fmoc	Fluorenylmethoxycarbonyl protecting group
H_2O	Water
HATU	(1-[Bis(dimethylamino)methylene]-1H-1,2,3-triazolo[4,5-b]pyridinium 3-oxid hexafluorophosphate)
HOAt	Hydroxyazabenzotriazole
HOBt	Hydroxybenzotriazole
LBB	Lectin binding buffer
Lys	Lysine
MeOH	Methanol

*n*Hex	*n*-Hexane
NHS	*N*-Hydroxy succinimide
OxymaPure®	Ethyl (hydroxyimino) cyanoacetate
PyBOP	(Benzotriazol-1-yl-oxytripyrrolidinophosphonium hexafluorophosphate)
PyOxim®	(Ethyl cyano(hydroxyimino)acetate-O^2]tri-1-pyrrolidinylphosphonium hexafluorophosphate)
*t*BuOH	*tert.* Butanol
TentaGel® SRAM	TentaGel® S with Rink-Amide linker
TFA	Trifluoracetic acid/Trifluoroacetamide
Trt	Trityl/Triphenylmethane

Methods and Instrumentation

Abbreviation	*Definition*
ATR	Attenuated total reflection
^{13}C	Carbon with 13 atomic mass units
COSY	Correlation spectroscopy
CuAAC	Copper(I)-catalyzed alkyne-azide cycloaddition
DLS	Dynamic light scattering
ELLA	Enzyme-linked lectin assay
ESI	Electrospray-Ionization
GPC-RI-LS	Gel permeation chromatography coupled to a refractive index and light scattering detector
^{1}H	Hydrogen with one atomic mass unit
HRMS	High-resolution mass spectrometry
IR	Infrared spectroscopy
ITC	Isothermal titration calorimetry
LC-MS	Liquid chromatography coupled to mass spectrometry
MD	Molecular dynamics
NMR	Nuclear magnetic resonance
Q-TOF	Quadrupole coupled to Time-of-Flight spectrometry
RP-HPLC	Reverse phase high performance liquid chromatography
RU	Response units
SCP RICM	Soft colloidal probe reflection interference contrast microscopy
SAX HPLC	Strong anion exchange high performance liquid chromatography
SPAAC	Strain promoted alkyne-azide cycloaddition
SPPS	Solid Phase peptide synthesis
SPPoS	Solid phase polymer synthesis
SPR	Surface plasmon resonance
SPS	Solid phase synthesis
STD-NMR	Saturation transfer difference Nuclear magnetic resonance spectroscopy
TEC	Thiol-ene-click
TLC	Thin layer chromatography
UV-Vis	Ultraviolet-visible spectrophotometry

6.2. List of figures

values (black bars) and K_{Atotal} values (blue bars) obtained from the two-state reaction for all analyzed compounds. (**B**) Mannose normalized K_{A1} values (black bars) and K_{Atotal} values (orange bars) obtained from the two-state reaction for all analyzed compounds. Constructs of higher valency bind multivalently better than constructs of lower valency; constructs with more branches are relatively superior to compound with less branches. Figure taken from Baier *et al., Chem. Eur. J.* **2018**, *24*, 1619-1630. ... 30

6.3. List of schemes

7. Acknowledgements

XX